

**University of Alberta**

**Cross-conjugated Enyne Oligomers: Synthesis, Properties,  
and Nonlinear Optical Investigations**

by

Yuming Zhao ©

A thesis submitted to the Faculty of Graduate Studies and Research in partial fulfillment  
of the requirement of the degree of Doctor of Philosophy

Department of Chemistry

Edmonton, Alberta

Fall, 2002



National Library  
of Canada

Acquisitions and  
Bibliographic Services

395 Wellington Street  
Ottawa ON K1A 0N4  
Canada

Bibliothèque nationale  
du Canada

Acquisitions et  
services bibliographiques

395, rue Wellington  
Ottawa ON K1A 0N4  
Canada

*Your file Votre référence*

*Our file Notre référence*

The author has granted a non-exclusive licence allowing the National Library of Canada to reproduce, loan, distribute or sell copies of this thesis in microform, paper or electronic formats.

The author retains ownership of the copyright in this thesis. Neither the thesis nor substantial extracts from it may be printed or otherwise reproduced without the author's permission.

L'auteur a accordé une licence non exclusive permettant à la Bibliothèque nationale du Canada de reproduire, prêter, distribuer ou vendre des copies de cette thèse sous la forme de microfiche/film, de reproduction sur papier ou sur format électronique.

L'auteur conserve la propriété du droit d'auteur qui protège cette thèse. Ni la thèse ni des extraits substantiels de celle-ci ne doivent être imprimés ou autrement reproduits sans son autorisation.

0-612-81292-8

**Canada**

# University of Alberta

## Library Release Form

**Name of Author:** Yuming Zhao

**Title of Thesis:** Cross-conjugated Enyne Oligomers: Synthesis,  
Characterization, and Nolinear Optical Investigations

**Degree:** Doctor of Philosophy

**Year this Degree Granted:** 2002

Permission is hereby granted to the University of Alberta Library to reproduce single copies of this thesis and to lend or sell such copies for private, scholarly or scientific research purpose only.

The author reserves all other publication and other rights in association with the copyright in the thesis, and except as herein before provided, neither the thesis nor any substantial portion thereof may be printed or otherwise reproduced in any material form whatever without the author's prior written permission.



Apt 3 10638-83 Av

Edmonton, AB T6E 2E2, CANADA

July 18, 2002

*What chemistry!*

*That the winds are really not infectious,*

*That this is no cheat, this transparent green-wash of the sea which  
is so amorous after me,*

*That it is safe to allow it to lick my naked body all over with its  
tongues,*

*That it will not endanger me with the fevers that have deposited  
themselves in it,*

*That all is clean forever and forever, ...*

**–Walt Whitman**

**University of Alberta**

**Faculty of Graduate Studies and Research**

The undersigned certify that they have read, and recommend to the Faculty of Graduate Studies and Research for acceptance, a thesis entitled Cross-conjugated Enyne Oligomers: Synthesis, Properties and Nonlinear Optical Investigations by Yuming Zhao in partial fulfillment of the requirements for the degree of Doctor of Philosophy.



Dr. R. R. Tykwinski, Assistant Professor of Chemistry



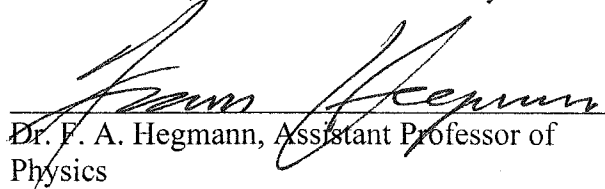
Dr. D. G. Hall, Assistant Professor of Chemistry



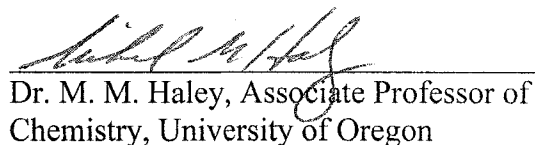
Dr. D. L. J. Clive, Professor of Chemistry



Dr. M. Cowie, Professor of Chemistry



Dr. F. A. Hegmann, Assistant Professor of Physics



Dr. M. M. Haley, Associate Professor of Chemistry, University of Oregon

July 17, 2002

## Abstract

This thesis focuses on the synthesis of monodisperse cross-conjugated enyne oligomers, the study of their unique  $\pi$ -electron systems, and their potential as nonlinear optical (NLO) materials.

The first class of oligomers, namely *iso*-polydiacetylenes (*iso*-PDAs), was assembled iteratively up to the length of nonamer, using a protideprotection/Pd-catalyzed cross-coupling protocol. Structural and electronic properties were investigated using X-ray crystallographic and UV-vis spectroscopic methods. The results confirmed the existence of electronic communication across the oligomeric backbones, and this effect saturates at the nonameric stage.

To improve the stability and solubility of *iso*-PDAs, a series of perphenylated *iso*-PDA oligomers were synthesized in a similar iterative manner. X-ray crystallographic and electronic absorption and emission spectroscopic methods have been used to elucidate the properties of these oligomers. NLO characteristics, in particular, second hyperpolarizability  $\gamma$ , were evaluated by differential optical Kerr effect (DOKE) experiments. The results showed that the second hyperpolarizability increases superlinearly with increasing chain length. Additionally, the perphenylated *iso*-PDA oligomers also show interesting conformational preference in the solution state, which has been investigated by spectroscopic analyses.

A third series of monodisperse cross-conjugated oligomers was assembled, based on the *iso*-polytriacetylene backbone (*iso*-PTAs). Using Pd-catalyzed cross-coupling of vinyl triflates with terminal alkynes, *iso*-PTAs were assembled in a divergent, iterative manner up to the pentamer. Moreover, Cu-mediated oxidative homocoupling of these *iso*-PTA oligomers provided an efficient route to hybrid, tetrayne-based enyne oligomers. Electronic absorption spectral analysis showed that extension of linearly conjugated segment reduced the electronic communication dramatically across the cross-conjugated segments.

Utilizing a sequence of Pd-catalyzed cross-coupling/Cu-catalyzed homocoupling reactions, cross-conjugated tetraynes with various functionality have been synthesized. Electronic absorption analyses show that the pendant functionality has little electronic

influence on the absorption characteristics of the central tetrayne structure. X-ray crystallographic analyses reveal the possibility for solid-state topochemical polymerization in 1,6-addition manner for two derivatives. The polymerization behavior of these tetraynes has been characterized by thermal (DSC and TGA), UV-vis, and solid-state CP-MAS  $^{13}\text{C}$  NMR spectroscopies.

Additional and related work on cross-conjugated molecules and theoretical studies of expanded radialenes have been outlined in the final chapter of this thesis.

## Acknowledgements

I would like first to thank my supervisor, Dr. Rik R. Tykwinski. Being the first student joining in his group as a Ph.D. student in the spring of 1998, I have witnessed his contagious enthusiasm and remarkable achievements in the field of materials chemistry, in particular, the chemistry of acetylenes. I thank him for shaping my knowledge of chemistry and attitude toward research, for his encouragement and support when I felt depressed with my project(s), and for generously offering me opportunities to attend conferences and getting our work published. I thank you, Rik, for opening the “door of chemistry” in front of me, which will benefit my whole life. I would also like to thank Dr. Frank A. Hegmann who has provided wonderful collaborations on the projects of nonlinear optical characterization. My thanks also go to Dr. Roderick E. Wasilyshen, who has warmly supported and cooperated on the project of solid-state  $^{13}\text{C}$  NMR spectroscopic characterization.

I would like to acknowledge the work of my physicist friend, Aaron D. Slepov, who has done so many amazing studies on the nonlinear optical experiments. Aaron, you never let me down whenever I desperately need your help. Thank you very much for your sense of humor turning the tedious measurements into a joyful experience. I would like to thank my colleague, Dr. Guy Bernard, who has done all the solid-state  $^{13}\text{C}$  NMR spectroscopic experiments in this thesis. Guy, a super nice guy, has always cordially assisted my research. I am also indebted to Dr. Robert McDonald for his remarkable work on X-ray crystallographic analyses. My thanks also go to Dr. Randy M. Whittal and Angelina Morales-Izquierdo for their work on the MS characterizations. I would also

like to thank the staff of the spectroscopic services for their help in my daily work, Dr. Tom Nakashima, Darlene Mahlow, and Andrea Dunn. Moreover, I must necessarily acknowledge the contributions of my group members, without whom I would not have completed the work here and elsewhere; Sorin C. Ciulei, Joon Cho, Sara Eisler, Katie Campbell, Trent Rankin, Colin Vitols, Annabelle Shi Shun, Clement Akoto, have provided friendly assistances and collaborations during my four year study. I also thank the undergraduates in my group: Darren Bykowski, Erin Chernick, and Erin Elliott, for cheering me up and making me feel young again.

I am grateful for the supports from my parents who have enlightened me so much in the discipline of chemistry. Finally, I would like to give my special thanks to my beloved my wife, Lidan Tao. I particularly thank her wholehearted support of my study, and taking care of my life. My dear Lidan, without you I wouldn't have been so successful in my career.

Financial supports were generously provided by NSERC, the University of Alberta, and PetroCanada.

## Table of Contents

<b>Chapter 1 Introduction.....</b>	<b>1</b>
1.1 A Brief Historical Review on Polymer Science.....	1
1.2 The Significances, Synthesis and Applications of Monodisperse Oligomers.....	4
1.2.1 <i>The Importance of Monodisperse Oligomers.....</i>	<i>5</i>
1.2.2 <i>General Synthetic Strategies towards Monodisperse Oligomers.....</i>	<i>7</i>
1.2.3 <i>The Effective Conjugation Length in <math>\pi</math>-Conjugated System.....</i>	<i>11</i>
1.2.4 <i>The Applications of <math>\pi</math>-Conjugated Oligomers.....</i>	<i>14</i>
1.3 Nonlinear Optical Properties of Oligomers.....	21
1.3.1 <i>Physical Background of Nonlinear Optical Phenomena.....</i>	<i>22</i>
1.3.2 <i>Measurement Techniques and Theories on Third-Order Optical Nonlinearity.....</i>	<i>23</i>
1.4 Cross Conjugation and Why Cross-conjugated Molecules.....	29
1.5 Survey on Monodisperse $\pi$ -Conjugated Oligomers.....	31
1.5.1 <i><math>\pi</math>-Conjugated Oligomers Containing Nonaromatic Backbones.....</i>	<i>31</i>
1.5.2 <i><math>\pi</math>-Conjugated Oligomers Containing Aromatic Backbones.....</i>	<i>51</i>
1.5.3 <i>Cross-conjugated Oligomers.....</i>	<i>62</i>
1.6 Conclusions.....	69
1.7 References and Notes.....	70
<b>Chapter 2 Synthesis and Characterization of <i>iso</i>-Polydiacetylenes.....</b>	<b>93</b>
2.1 Introduction.....	93

2.2 Results and Discussion.....	95
2.2.1 <i>Synthesis</i> .....	95
2.2.2 <i>Physical Characteristics</i> .....	101
2.2.3 <i>Solid-State Structures</i> .....	102
2.2.4 <i>Electronic Properties</i> .....	104
2.3 Conclusions.....	112
2.4 References and Notes.....	113
<b>Chapter 3 Synthesis, Characterization, and Nonlinear Optical Studies of Perphenylated <i>iso</i>-Polydiacetylenes.....</b>	<b>115</b>
3.1 Introduction.....	115
3.2 Results and Discussion.....	118
3.2.1 <i>Synthesis</i> .....	118
3.2.2 <i>Physical Characteristics</i> .....	124
3.2.3 <i>Solid-State Structures</i> .....	125
3.2.4 <i>Electronic Absorption and Emission Properties</i> .....	132
3.2.5 <i>Nonlinear Optical Properties</i> .....	144
3.2.6 <i>Conformational Studies</i> .....	148
3.3 Conclusions.....	153
3.4 References and Notes.....	153
<b>Chapter 4 Synthesis and Characterization of <i>iso</i>-Polytriacetylenes and Related Oligoenynes.....</b>	<b>156</b>

4.1 Introduction.....	156
4.2 Results and Discussion.....	157
4.2.1 <i>Synthesis and Characterization of iso-PTAs</i> .....	157
4.2.2 <i>Synthesis and Characterization of Expanded Enynes</i> .....	162
4.2.3 <i>Solid-State Properties of Cross-conjugated iso-PTA 156 and Tetrayne 160</i> .....	164
4.2.4 <i>Electronic Characteristics of Cross-conjugated Oligoenynes</i> .....	170
4.3 Conclusions.....	172
4.4 References and Notes.....	173
<b>Chapter 5 Synthesis, Characterization, and Solid-State Polymerization of Cross-conjugated Tetraynes.....</b>	<b>175</b>
5.1 Introduction.....	175
5.2 Results and Discussion.....	178
5.2.1 <i>Synthesis</i> .....	178
5.2.2 <i>Physical Properties</i> .....	181
5.2.3 <i>Electronic Properties</i> .....	183
5.2.4 <i>Solid-State Properties and Topochemical Polymerization</i> .....	186
5.3 Conclusions.....	200
5.4 References and Notes.....	201
<b>Chapter 6 Other Related Work and Theoretical Studies.....</b>	<b>205</b>
6.1 Introduction.....	205

6.2	Synthesis.....	206
6.2.1	<i>Synthetic Efforts on Modification of Vinyl Triflate Building Blocks.....</i>	206
6.2.2	<i>Synthesis of Precursors to Strained Cross-conjugated Tetraynes.....</i>	210
6.2.3	<i>Synthesis of Donor/Acceptor Functionalized Cross-conjugated Enynes.....</i>	212
6.2.4	<i>Synthesis of Cross-conjugated Macrocycles.....</i>	215
6.3	Results and Discussion.....	218
6.3.1	<i>Physical Characteristics.....</i>	218
6.3.2	<i>Solid-State Structures.....</i>	220
6.3.3	<i>Electronic Properties.....</i>	224
6.4	Density Functional Theory (DFT) Studies of Expanded Radialenes.....	227
6.4.1	<i>Structural and Electronic Properties.....</i>	230
6.4.2	<i>Aromaticity Studies Based on NICS Calculations.....</i>	233
6.5	Conclusions.....	236
6.6	References and Notes.....	236
<b>Chapter 7</b>	<b>Conclusions.....</b>	<b>240</b>
<b>Chapter 8</b>	<b>Experimental.....</b>	<b>244</b>
<b>Appendix</b>	<b>Selected <sup>1</sup>H and <sup>13</sup>C NMR Spectra.....</b>	<b>319</b>

## List of Figures

<b>Fig. 1.1</b> Schematic outline of the differential optical Kerr effect (DOKE) detection setup. .....	26
<b>Fig. 1.2</b> Progression of linearly $\pi$ -conjugated all-carbon backbones from <i>trans</i> -polyacetylene to carbyne. ....	32
<b>Fig. 1.3</b> Resonance structures of <b>27</b> , with the polymethine form shown in the middle. .....	40
<b>Fig. 2.1</b> Proposed assembly of <i>iso</i> -PDAs. ....	95
<b>Fig. 2.2</b> ORTEP drawing (20% probability level) of <b>99</b> (molecule A). ....	103
<b>Fig. 2.3</b> ORTEP drawing (20% probability level) of <b>101</b> . ....	104
<b>Fig. 2.4</b> Orthogonal $\pi$ -systems in <i>iso</i> -PDAs. ....	105
<b>Fig. 2.5</b> (a) Electronic absorption spectra ( $\epsilon$ [L mol <sup>-1</sup> cm <sup>-1</sup> ]) in CHCl <sub>3</sub> comparing the effects of oligomer length between TIPS-endcapped <i>iso</i> -PDA oligomers. (b) Electronic absorption spectra ( $\epsilon$ [L mol <sup>-1</sup> cm <sup>-1</sup> ]) in CHCl <sub>3</sub> comparing the effects of oligomer length between TMS-endcapped <i>iso</i> -PDA oligomers. ....	106
<b>Fig. 2.6</b> Plot of estimated optical band gap ( $E_g$ ) versus reciprocal number of monomer units ( $1/n$ ) of TIPS and TMS endcapped <i>iso</i> -PDAs via method A ( $\circ$ , TMS; $\diamond$ , TIPS) and method B ( $\bullet$ , TMS; $\blacklozenge$ , TIPS). ....	108
<b>Fig. 2.7</b> Plot of calculated band gap ( $E_g$ ) versus reciprocal number of monomer units ( $1/n$ ) of unsubstituted <i>iso</i> -PDAs <b>78</b> . ....	109

<b>Fig. 2.8</b> Electronic absorption spectra ( $\epsilon$ [ $\text{L mol}^{-1} \text{cm}^{-1}$ ]) of <b>108</b> in various solvents. .....	110
<b>Fig. 2.9</b> Electronic absorption spectra of <b>102</b> at various concentrations. The absorption scale has been normalized to facilitate comparison. ....	111
<b>Fig. 2.10</b> Electronic absorption spectra for thin films of <b>101</b> , <b>103</b> , <b>108</b> , and <b>111</b> . ....	112
<b>Fig. 3.1</b> Proposed oxygen ene reaction at the allylic position of cyclohexylvinylidene <i>iso</i> -PDA. ....	117
<b>Fig. 3.2</b> Proposed assembly of perphenylated <i>iso</i> -PDAs. ....	118
<b>Fig. 3.3</b> ORTEP drawing (20% probability level) of <b>134</b> . ....	126
<b>Fig. 3.4</b> (a) ORTEP drawing (20% probability level) of <b>136b</b> . (b) Crystal packing diagram of <b>136b</b> . ....	129
<b>Fig. 3.5</b> ORTEP drawing (20% probability level) of <b>138</b> . ....	130
<b>Fig. 3.6</b> ORTEP drawing (20% probability level) of <b>137a</b> . ....	131
<b>Fig. 3.7</b> (a) Crystal packing diagram of <b>137a</b> viewed along <i>b</i> -axis. (b) Geometry parameters: $\Phi = 34.7^\circ$ , $R_{1,4} = 6.14 \text{ \AA}$ , $d = 8.56 \text{ \AA}$ . Optimal parameters for 1,4-addition are: $\Phi = 45^\circ$ , $R_{1,4} = 3.5 \text{ \AA}$ , $d = 5.0 \text{ \AA}$ . ....	132
<b>Fig. 3.8</b> Electronic absorption spectra ( $\epsilon$ [ $\text{L mol}^{-1} \text{cm}^{-1}$ ]) in $\text{CHCl}_3$ comparing the effects of oligomer chain length between <b>136b</b> , <b>138–144</b> . ....	134
<b>Fig. 3.9</b> Plot of estimated optical band gap ( $E_g$ ) versus reciprocal number of monomer unit ( $1/n$ ) of perphenylated <i>iso</i> -PDAs via method A (■) and method B (●). ....	135

<b>Fig. 3.10</b> Electronic absorption spectra of <b>141</b> in various solvents. ....	136
<b>Fig. 3.11</b> Electronic absorption spectra ( $\epsilon$ [ $\text{L mol}^{-1} \text{cm}^{-1}$ ]) in acetonitrile comparing the effects of oligomer chain length between <b>136b</b> , <b>138–142</b> . ....	137
<b>Fig. 3.12</b> Electronic absorption spectra of <b>140</b> (Fig. A) and <b>141</b> (Fig. B) in $\text{CHCl}_3$ at various concentrations. The absorption scale has been normalized to facilitate comparison. ....	138
<b>Fig. 3.13</b> Electronic absorption spectra for thin films of <b>136b</b> , <b>138–144</b> . ....	139
<b>Fig. 3.14</b> Plot of relative maximum emission intensity versus concentration in $\text{CHCl}_3$ for <b>139</b> (Fig. A) and <b>141</b> (Fig. B) (Maximum emission intensity at 501 nm for <b>139</b> and 504 nm for <b>141</b> ). ....	141
<b>Fig. 3.15</b> Emission spectra in $\text{CHCl}_3$ for <i>iso</i> -PDA series of <b>136b</b> , <b>138–144</b> . ....	142
<b>Fig. 3.16</b> Emission spectra of <b>141</b> in $\text{CHCl}_3$ comparing the effects of concentrations, whereas the relative emission intensities are normalized. ....	143
<b>Fig. 3.17</b> Emission spectra in acetonitrile of <i>iso</i> -PDA series <b>136b</b> , <b>138–142</b> . (A) Spectra in range of 400–700 nm. (B) Expansion spectra in range of 400–450 nm. ....	144
<b>Fig. 3.18</b> Molecular second hyperpolarizability of perphenylated <i>iso</i> -PDAs, $\gamma_s$ , relative to the absolute THF hyperpolarizability, $\gamma_{\text{THF}}$ , as a function of monomer repeat units, $n$ . ....	145
<b>Fig. 3.19</b> Correlation of relative molecular second hyperpolarizabilities ( $\gamma_s/\gamma_{\text{THF}}$ ) as a function of oligomer length $n$ . (a) Linear fit ( $n = 1–15$ ). (b) Two linear fits ( $n = 2–9$ and $n = 9–15$ ). (c) Exponential fit ( $n = 2–15$ ). ....	147

<b>Fig. 3.20</b> Schematic illustration of pseudo- <i>trans</i> and pseudo- <i>cis</i> perphenylated <i>iso</i> -PDA. .....	149
<b>Fig. 3.21</b> Minimized structure of tridecameric <i>iso</i> -PDA using MM3* force field parameters. Only backbone carbons are displayed as space-filling representation for clarity. (A) View from side. (B) View from top. ....	149
<b>Fig. 3.22</b> Plot of absorbance ratio $A_{378}/A_{323}$ vs. chain length ( $n$ ) in $\text{CHCl}_3$ (●) and acetonitrile (■). $A_{378}$ denotes the absorbance intensity at 378 nm, and $A_{323}$ denotes the absorbance intensity at 323 nm. ....	150
<b>Fig. 3.23</b> Zoom in on hump in <i>iso</i> -PDA series Kerr response. Signals have been normalized to monomer concentration and THF peak signals. Data series have been averaged. ....	152
<b>Fig. 4.1</b> Proposed synthesis of <i>iso</i> -PTAs. ....	156
<b>Fig. 4.2</b> ORTEP drawings (20% probability level) of <b>156</b> . ....	166
<b>Fig. 4.3</b> ORTEP drawings (20% probability level) of <b>157</b> . ....	168
<b>Fig. 4.4</b> (a) Crystal packing diagram of structure A of <b>157</b> , as viewed along $a$ -axis. (b) Crystal packing diagram of structure B of <b>157</b> , as viewed along $a$ -axis. .....	169
<b>Fig. 4.5</b> (a) Electronic absorption spectra ( $\epsilon$ [ $\text{L} \cdot \text{mol}^{-1} \cdot \text{cm}^{-1}$ ]) in $\text{CHCl}_3$ comparing <b>148</b> , <b>149</b> , <b>154</b> , and <b>156</b> . (b) Electronic absorption spectra ( $\epsilon$ [ $\text{L} \cdot \text{mol}^{-1} \cdot \text{cm}^{-1}$ ]) in $\text{CHCl}_3$ comparing dimers <b>151</b> , <b>154</b> , and <b>156</b> . ....	171

<b>Fig. 4.6</b> Electronic absorption spectra ( $\epsilon$ [ $\text{L} \cdot \text{mol}^{-1} \cdot \text{cm}^{-1}$ ]) in $\text{CHCl}_3$ comparing <b>157–160</b> . .....	172
<b>Fig. 5.1</b> Solid-state topochemical polymerization of tetrynes in 1,6-addition fashion .....	175
<b>Fig. 5.2</b> Solid-state topochemical polymerization of tetrynes in 1,4-addition fashion .....	176
<b>Fig. 5.3</b> Electronic absorption spectra ( $\epsilon$ [ $\text{L} \cdot \text{mol}^{-1} \cdot \text{cm}^{-1}$ ]) in $\text{CHCl}_3$ for <b>163a</b> , <b>163c</b> , <b>163i</b> , and <b>164</b> . .....	184
<b>Fig. 5.4</b> Electronic absorption spectra ( $\epsilon$ [ $\text{L} \cdot \text{mol}^{-1} \cdot \text{cm}^{-1}$ ]) in $\text{CHCl}_3$ for <b>163d</b> , <b>163e</b> , <b>163f</b> and <b>163h</b> . .....	185
<b>Fig. 5.5</b> Electronic absorption spectra ( $\epsilon$ [ $\text{L} \cdot \text{mol}^{-1} \cdot \text{cm}^{-1}$ ]) in $\text{CHCl}_3$ for <b>163j</b> and <b>163k</b> . .....	186
<b>Fig. 5.6</b> Crystal packing diagram of <b>157</b> (polymorph A). (a) views along <i>b</i> -axis. (b) geometry parameters: $\Phi = 28^\circ$ , $R_{1,6} = 3.6 \text{ \AA}$ , $R_{1,8} = 4.2 \text{ \AA}$ , $d = 7.5 \text{ \AA}$ . .....	187
<b>Fig. 5.7</b> (a) ORTEP drawing (20% probability level) of <b>163k</b> . (b) Crystal packing diagram as viewed along <i>b</i> -axis. (c) Geometry parameters: $\Phi = 31^\circ$ , $R_{1,6} = 3.7 \text{ \AA}$ , $R_{1,4} = 4.5 \text{ \AA}$ , $R_{1,8} = 4.5 \text{ \AA}$ , $d = 7.4 \text{ \AA}$ . .....	189
<b>Fig. 5.8</b> DSC spectrum for <b>163d</b> scanned from 50 to 400 °C at a rate of 5 °C/min (the heat flow fluctuation at 120 °C is due to the instrumental errors). .....	191
<b>Fig. 5.9</b> DSC spectrum for <b>163k</b> scanned from 50 to 400 °C at a rate of 5 °C/min. .....	192

<b>Fig. 5.10</b> DSC spectrum for <b>163j</b> scanned from 50 to 400 °C at a rate of 5 °C/min. .....	192
<b>Fig. 5.11</b> TGA spectrum for <b>163k</b> scanned from 50 to 600 °C at a rate of 5 °C/min. .....	193
<b>Fig. 5.12</b> DSC isothermal scanning spectra for <b>163k</b> at various temperatures. ....	194
<b>Fig. 5.13</b> Correlation of $\ln(\tau)$ versus $1/T$ obtained from isothermal analysis of <b>163k</b> . .....	195
<b>Fig. 5.14</b> Solid-state UV-vis spectra for <b>163k</b> comparing the effect of heating. ....	196
<b>Fig. 5.15</b> Solid-state $^{13}\text{C}$ NMR spectra for <b>163d</b> recorded before and after heating at 160 °C for 3 h. ....	197
<b>Fig. 5.16</b> Solid-state $^{13}\text{C}$ NMR spectra for <b>163j</b> recorded before and after heating at 100 °C for shown times. ....	199
<b>Fig. 5.17</b> Solid-state $^{13}\text{C}$ NMR spectra for <b>163k</b> recorded before and after heating at 150 °C for shown times. ....	200
<b>Fig. 6.1</b> ORTEP drawings (20% probability level) of two crystallographically independent molecules of <b>193a</b> . ....	222
<b>Fig 6.2</b> ORTEP drawings (20% probability level) of <b>197a</b> . ....	222
<b>Fig. 6.3</b> ORTEP drawings (20% probability level) of <b>197b</b> . ....	223
<b>Fig. 6.4</b> Electronic absorption spectra ( $\epsilon$ [ $\text{L mol}^{-1} \text{cm}^{-1}$ ]) in $\text{CHCl}_3$ for <b>191a</b> and <b>191b</b> . .....	224

<b>Fig. 6.5</b> Electronic absorption spectra ( $\epsilon$ [ $\text{L mol}^{-1} \text{cm}^{-1}$ ]) in $\text{CHCl}_3$ for <b>193a</b> and <b>193b</b> . .....	225
<b>Fig. 6.6</b> Electronic absorption spectra ( $\epsilon$ [ $\text{L mol}^{-1} \text{cm}^{-1}$ ]) in $\text{CHCl}_3$ for <b>190b</b> and <b>197a–b</b> . .....	226
<b>Fig. 6.7</b> Electronic absorption spectra ( $\epsilon$ [ $\text{L mol}^{-1} \text{cm}^{-1}$ ]) in $\text{CHCl}_3$ for <b>199</b> . .....	226
<b>Fig. 6.8</b> Orthogonal $\pi$ -systems in expanded radialene. ....	228
<b>Fig. 6.9</b> Optimized structures of <b>204–207</b> by B3LYP/6-311G**. ....	231
<b>Fig. 6.10</b> Frontier MOs of <b>204–207</b> plotted at isocontour of 0.01000 a.u. ....	232
<b>Fig. 6.11</b> Plots of $-\text{NICS}$ values versus the distances from ring center, where a positive Gaussian-shape curve denotes aromaticity, and a negative Gaussian-shape curve denotes antiaromaticity. (a) <b>204</b> . (b) <b>205</b> . (c) <b>206</b> . (d) <b>207</b> . ....	235
<b>Fig. A-1</b> $^1\text{H}$ and $^{13}\text{C}$ NMR spectra of compound <b>101</b> . ....	319
<b>Fig. A-2</b> $^1\text{H}$ and $^{13}\text{C}$ NMR spectra of compound <b>103</b> . ....	320
<b>Fig. A-3</b> $^1\text{H}$ and $^{13}\text{C}$ NMR spectra of compound <b>105</b> . ....	321
<b>Fig. A-4</b> $^1\text{H}$ and $^{13}\text{C}$ NMR spectra of compound <b>107</b> . ....	322
<b>Fig. A-5</b> $^1\text{H}$ and $^{13}\text{C}$ NMR spectra of compound <b>108</b> . ....	323
<b>Fig. A-6</b> $^1\text{H}$ and $^{13}\text{C}$ NMR spectra of compound <b>111</b> . ....	324

<b>Fig. A-7</b> $^1\text{H}$ and $^{13}\text{C}$ NMR spectra of compound <b>138</b> .	.....325
<b>Fig. A-8</b> $^1\text{H}$ and $^{13}\text{C}$ NMR spectra of compound <b>139</b> .	.....326
<b>Fig. A-8</b> $^1\text{H}$ and $^{13}\text{C}$ NMR spectra of compound <b>140</b> .	.....327
<b>Fig. A-10</b> $^1\text{H}$ and $^{13}\text{C}$ NMR spectra of compound <b>141</b> .	.....328
<b>Fig. A-11</b> $^1\text{H}$ and $^{13}\text{C}$ NMR spectra of compound <b>142</b> .	.....329
<b>Fig. A-12</b> $^1\text{H}$ and $^{13}\text{C}$ NMR spectra of compound <b>143</b> .	.....330
<b>Fig. A-13</b> $^1\text{H}$ and $^{13}\text{C}$ NMR spectra of compound <b>144</b> .	.....331
<b>Fig. A-14</b> $^1\text{H}$ and $^{13}\text{C}$ NMR spectra of compound <b>147a</b> .	.....332
<b>Fig. A-15</b> $^1\text{H}$ and $^{13}\text{C}$ NMR spectra of compound <b>149</b> .	.....333
<b>Fig. A-16</b> $^1\text{H}$ and $^{13}\text{C}$ NMR spectra of compound <b>153</b> .	.....334
<b>Fig. A-17</b> $^1\text{H}$ and $^{13}\text{C}$ NMR spectra of compound <b>154</b> .	.....335
<b>Fig. A-18</b> $^1\text{H}$ and $^{13}\text{C}$ NMR spectra of compound <b>156</b> .	.....336
<b>Fig. A-19</b> $^1\text{H}$ and $^{13}\text{C}$ NMR spectra of compound <b>159</b> .	.....337
<b>Fig. A-20</b> $^1\text{H}$ and $^{13}\text{C}$ NMR spectra of compound <b>163b</b> .	.....338
<b>Fig. A-21</b> $^1\text{H}$ and $^{13}\text{C}$ NMR spectra of compound <b>163d</b> .	.....339
<b>Fig. A-22</b> $^1\text{H}$ and $^{13}\text{C}$ NMR spectra of compound <b>163j</b> .	.....340

<b>Fig. A-23</b> $^1\text{H}$ and $^{13}\text{C}$ NMR spectra of compound <b>163k</b> . .....	341
<b>Fig. A-24</b> $^1\text{H}$ and $^{13}\text{C}$ NMR spectra of compound <b>191a</b> . .....	342
<b>Fig. A-25</b> $^1\text{H}$ and $^{13}\text{C}$ NMR spectra of compound <b>191b</b> . .....	343
<b>Fig. A-26</b> $^1\text{H}$ and $^{13}\text{C}$ NMR spectra of compound <b>193a</b> . .....	344
<b>Fig. A-27</b> $^1\text{H}$ and $^{13}\text{C}$ NMR spectra of compound <b>193b</b> . .....	345
<b>Fig. A-28</b> $^1\text{H}$ and $^{13}\text{C}$ NMR spectra of compound <b>197a</b> . .....	346
<b>Fig. A-29</b> $^1\text{H}$ and $^{13}\text{C}$ NMR spectra of compound <b>197b</b> . .....	347
<b>Fig. A-30</b> $^1\text{H}$ and $^{13}\text{C}$ NMR spectra of compound <b>199</b> . .....	348

## List of Schemes

<b>Scheme 1.1</b> (a) Iterative divergent synthetic protocol. M = monomer unit. i) is the step that deprotects or activates the protection group A, yielding A*. iii) Coupling reaction. (b) Binomial reaction protocol. i) and ii) are steps that deprotect or activate the protection groups A and B, yielding A* and B*, respectively. iii) Coupling reaction. (c) Homocoupling of a monomer building block in the presence of an end-capping unit E. The polydisperse mixture obtained has subsequently to be purified, e.g., by chromatographic methods. (c) Solid-phase supported reaction scheme. iv) Coupling reaction. ....	7
<b>Scheme 1.2</b> A representative selection of cross-conjugated molecules. ....	29
<b>Scheme 2.1</b> .....	97
<b>Scheme 2.2</b> .....	101
<b>Scheme 3.1</b> Synthesis of pentamers <b>118</b> and <b>119</b> . ....	116
<b>Scheme 3.2</b> Synthesis of adamantanylidene <i>iso</i> -PDAs. ....	117
<b>Scheme 3.3</b> .....	119
<b>Scheme 3.4</b> .....	122
<b>Scheme 3.5</b> .....	123
<b>Scheme 4.1</b> .....	158
<b>Scheme 4.2</b> .....	158

<b>Scheme 4.3</b>	.....	160
<b>Scheme 4.4</b>	.....	161
<b>Scheme 4.5</b>	.....	163
<b>Scheme 4.6</b>	.....	164
<b>Scheme 5.1</b>	.....	178
<b>Scheme 5.2</b>	.....	179
<b>Scheme 5.3</b>	.....	180
<b>Scheme 6.1</b>	.....	206
<b>Scheme 6.2</b>	.....	206
<b>Scheme 6.3</b>	.....	209
<b>Scheme 6.4</b>	.....	210
<b>Scheme 6.5</b>	.....	211
<b>Scheme 6.6</b>	.....	213
<b>Scheme 6.7</b>	.....	214
<b>Scheme 6.8</b>	.....	215
<b>Scheme 6.9</b>	.....	216

<b>Scheme 6.10</b>	.....	218
--------------------	-------	-----

## List of Equations

<b>Eq. 1.1</b>	.....	12
<b>Eq. 1.2</b>	.....	22
<b>Eq. 1.3</b>	.....	22
<b>Eq. 1.4</b>	.....	22
<b>Eq. 1.5</b>	.....	24
<b>Eq. 1.6</b>	.....	25
<b>Eq. 1.7</b>	.....	25
<b>Eq. 1.8</b>	.....	27
<b>Eq. 1.9</b>	.....	27
<b>Eq. 1.10</b>	.....	28
<b>Eq. 1.11</b>	.....	28
<b>Eq. 1.12</b>	.....	28
<b>Eq. 1.13</b>	.....	29
<b>Eq. 2.1</b>	.....	96

<b>Eq. 2.2</b>	.....	100
<b>Eq. 3.1</b>	.....	120
<b>Eq. 4.1</b>	.....	160
<b>Eq. 6.1</b>	.....	212
<b>Eq. 6.2</b>	.....	213
<b>Eq. 6.3</b>	.....	213
<b>Eq. 6.4</b>	.....	217

## List of Tables

<b>Table 1.1</b> Summarization of Algorithms predicting the ECL in $\pi$ -conjugated systems. .....	13
<b>Table 2.1</b> Semi-empirical calculation results for <i>iso</i> -PDA oligomers <b>78</b> ( $n = 2-10$ ). .....	109
<b>Table 3.1</b> Summary of results for the <i>iso</i> -polydiacetylene oligomer series. $\gamma_s$ and $\gamma_{\text{THF}}$ are the second hyperpolarizabilities of the oligomer samples and THF reference, respectively. $n$ is the number of repeat units in the oligomer. ....	145
<b>Table 5.1</b> Synthesis of enetriyne monomers <b>162a-k</b> . ....	180
<b>Table 5.2</b> Synthesis of cross-conjugated tetraynes <b>163a-k</b> . ....	181
<b>Table 6.1</b> Total Energies and frontier MO energies for <b>204-207</b> . ....	233

## List of Symbols

$\text{\AA}$	angstrom
$\beta$	quadratic hyperpolarizability
$\beta_0$	first hyperpolarizability at zero field
$\delta$	chemical shift
$\epsilon$	molar extinction coefficient
$H$	enthalpy
$\gamma$	second hyperpolarizability
$\lambda_{\max}$	wavelength of maximum absorption
$\mu$	field effect mobility
$\omega$	frequency of waves
$\chi$	nonlinear optical susceptibility coefficient
$\bar{E}$	electrical field strength
$\bar{P}$	macroscopic polarization of a medium

## List of Abbreviations

A	acceptor
Ac	acetyl
Aq	aqueous
AM1	Austin model one
BLA	bond length alternation
Bu	butyl
CL	confinement length
cm	centimeter
CP-MAS	cross-polarization/magic-angle spinning
CV	cyclic voltammogram
d	doublet
D	donor
DEE	<i>trans</i> -1,2-diethynylethene
DFWM	degenerate four wave mixing
DFT	density functional theory
DL	delocalization length
DMAP	4- <i>N,N</i> -dimethylaminopyridine
DMF	<i>N,N</i> -dimethylformamide
DNA	deoxyribonucleic acid
DOKE	differential optical Kerr effect
DP	decomposition point

DSC	differential scanning calorimetry
$E_g$	band gap
ECL	effective conjugation length
EFISH	electronic field induced second harmonic generation
EI-MS	electron impact mass spectroscopy
EL	electroluminescence
Et	ethyl
ESI	electrospray ionization
eV	electronvolt
Fc	ferrocenyl
FET	field-effect transistor
g	gram(s)
GED	gas-phase electron diffraction
GIAO	gauge-invariant atomic orbital
GPC	gel permeation chromatography
h	hour(s)
HF	Hatree-Fock
HOMO	highest occupied molecular orbital
HRMS	high resolution mass spectrometry
Hz	hertz
<i>i</i>	iso
IR	infrared
LDA	lithium diisopropylamide, $\text{LiN}(i\text{-C}_3\text{H}_7)_2$

LEC	light-emitting electro-chemical cell
LED	light emitting diode
LOP	ladder-type oligophenylenes
LUMO	lowest unoccupied molecular orbital
m	multiplet
M	molar
MALDI-TOF	matrix assisted laser desorption ionization-time of flight
Me	methyl
mg	milligram(s)
MHz	megahertz
mL	milliliter
mmol	millimole
mol	mole
Mp	melting point
MS	mass spectrometry
<i>m/z</i>	mass-to-charge ratio
n	normal
NICS	nuclear independent chemical shielding
NLO	nonlinear optical (optics)
nm	nanometer(s)
NMR	nuclear magnetic resonance
OHD-OKE	optical heterodyne detection-optical Kerr effect
OLED	organic polymer-based light-emitting device

ORTEP	oak ridge thermal ellipsoid plot
PA	polyacetylene
PDA	polydiacetylene
Ph	phenyl
PP	polyphenylene
PPE	poly(phenylene ethynylene)
PPHT	poly(1,4-phenylenehexa-1,3,5-trienylene)
ppm	parts per million
PPP	poly( <i>p</i> -phenylene)
PPV	poly(phenylene vinylene)
Pr	propyl
ps	picosecond(s)
PTA	polytriacetylene
q	quartet
ROM	ring opening metathesis
ROMP	ring opening metathesis polymerization
rt	room temperature
s	singlet
SEC	size-exclusion chromatography
soln	solution
STM	scanning-tunneling microscopy
t	triplet
TBAF	tetrabutylammonium fluoride

TEE	tetraethynylethene
TES	triethylsilyl
TGA	thermogravimetric analysis
THF	tetrahydrofuran
THG	third harmonic generation
TIPS	triisopropylsilyl
TLC	thin layer chromatography
TMEDA	<i>N,N,N',N'</i> -tetramethylethylenediamine ( $\text{Me}_2\text{NCH}_2\text{CH}_2\text{NMe}_2$ )
TMS	trimethylsilyl
TPP	tetraphenyl porphyrin
TsOH	<i>p</i> -toluenesulfonic acid
TTF	tetrathiofulvalene
UV	ultraviolet
UV-vis	ultraviolet-visible
VEH	valence effective Hamiltonian
vs	versus

## Chapter 1 Introduction

### 1.1 A Brief Historical Review on Polymer Science

Although the idea that atoms clump to form *molecules* can be traced back to Ancient Greece 2000 years ago in a philosopher's imagination, it is within the past two hundred years that these small entities have been experimentally identified and determined as real, discrete physical objects.<sup>1,2</sup> Since then, scientists have recognized that many things around us (wood, cloth, food, our bodies themselves, etc.) are made of *macromolecules* or *polymers*, as we call them now. However, the concept of macromolecules emerged very slowly, and it was only after the pioneering work of Staudinger that, by beginning of the 1930s,<sup>3</sup> the concept of the chain structure of macromolecules became generally established. Like other scientific ideas, the concept of macromolecules has grown very rapidly from a dubious seed into a well-studied giant tree. Furthermore, the emergence of molecular biology also makes this area of significant value in understanding biomacromolecules and their function in complex biological systems.<sup>4</sup>

The term polymer refers to molecules that consist of many parts or units, where the many units are joined to each other through chemical bonds in a repeating manner. By convention, a polymer usually consists of more than 1000 atoms (or a molecular weight of at least 10,000).<sup>3,5</sup> On the other hand, it can also be argued that a polymer is a molecule containing the number of repeat units where a physical properties reaches saturation. The latter definition, however, suggests a much looser criterion for a polymer, in which the molecular weight is not necessarily significant (e.g., a molecular weight of a

polymer can be even in the thousands). The longest known polymer—both natural and synthetic—is the deoxyribonucleic acid (DNA) molecule, where the number of monomer units can easily reach a million.<sup>5</sup> The elucidation of the chemical structure of the giant molecules of living systems, DNA, RNA, proteins, as well as their biological relationships, is so important that it has become one of the pillars of modern biological chemistry.<sup>6</sup> It is certainly not an exaggeration to state that all life on earth depends on the interplay between the two classes of biomacromolecules: nucleic acids and proteins. Nearly all chemical reactions in organisms such as the generation of energy or the synthesis of new cell structures are catalyzed by specific proteins called enzymes. Besides these two outstanding classes of biopolymers that carry out an astonishing range of biological functions, there are many other polymers that are widespread in nature. For example, oligo- and polysaccharides play a tremendously important biological role and show properties of great technical and commercial value.

In addition to the omnipresent biomacromolecules in biological world, over the last 60 years, a plethora of artificial polymers and plastics have been synthesized and introduced into the market.<sup>7</sup> However, in the early stage of synthetic polymers, they were no more than common plastics, such as plastic bags. In 1960, with the advent of light-amplification by stimulated emission of radiation (laser) technology,<sup>8</sup> a new era of polymer chemistry began: the search for new materials with unusual optical properties. The manner in which these high-tech  $\pi$ -conjugated polymers manipulate light can be used to build “active” optical devices for switching, amplifying, and storage of light signals just as silicon-based devices operated with electrical signals. Another important discovery, by Shirakawa, Heeger and MacDiarmid,<sup>9-11</sup> was the finding in the late 1960s

that polyacetylene, after doping with iodine, exhibits an electrical conductivity up to  $10^5$  S cm<sup>-1</sup>, similar to that of copper.<sup>12,13</sup> A vigorous search for purely organic-based conductors began, and many other doped-conducting  $\pi$ -polymers, so-called “synthetic metals”, soon appeared, e.g., poly(*p*-phenylene), poly(*p*-phenylene sulfide), and poly(pyrrole). In 1990 Holmes and co-workers discovered that poly(*p*-phenylene vinylene) and related polymers can be used as active component in organic polymer-based light-emitting devices (OLEDs), and this has become one of the most important landmark works in the history of polymer chemistry.<sup>14</sup> This breakthrough in the field of  $\pi$ -conjugated polymers soon inspired an intense worldwide search for organic semiconductors that combine the optical and electronic properties of classical inorganic semiconductors (e.g., Si, Ge) used for photonic devices with the well-known processing advantage and mechanical properties of organic polymers. Since these pioneering days, considerable progress has been made in both the development of emissive materials for display purposes, and the fabrication of large-area, ultra-lightweight, comfortable, high-resolution, full-color flat panel displays. It is not merely a dream that, in the near future, the manufacture of computers, laptops, TV-screens with low power consumption will approach reality. Meanwhile, the potential for discovery and practical applications in this area still seems unlimited.

During the past decade, the number of  $\pi$ -conjugated organic materials and polymers being explored as advanced materials for electronic and photonic applications has developed rapidly and witnessed an ever increasing interest from both academic and industrial research laboratories. Nowadays, this area represents a topic of extreme significance and practicability, due to their inherent synthetic flexibility, potential ease of

processing, and the possibility of tailoring materials characteristics to suit a desired property. The versatility in applications has made organic polymers very promising candidates in materials science and many other areas of modern chemistry and physics.

## 1.2 The Significance, Synthesis, and Applications of Monodisperse Oligomers

The oldest study on the preparation of oligomers can be traced back to the 1860s, when Lourenco first reported the synthesis of a series of ethynylene glycol oligomers, from monomer to hexamer.<sup>15,16</sup> The term *oligomer* generally refers to the compounds containing only a few monomeric units (usually up to 20); however, the boundary between oligomer and polymer is still vague. With the ever growing importance of  $\pi$ -conjugated polymers in materials science and many other areas of modern chemistry and physics, the studies of oligomers with precisely defined length and constitution soon became an important tool to reveal the correlation of physical properties to chemical structures. To date, a great number of homologous series of monodisperse oligomers have been synthesized and investigated, which have shown profound utility in both theoretical and experimental perspectives.

A second interest in monodisperse  $\pi$ -conjugated oligomers of defined length and constitution arises from their potential to act as molecular wires in molecular scale electronics and nanotechnological devices,<sup>12,17</sup> which have attracted extensive interest in the experimental and theoretical study of such mesoscopic devices. Nanostructures are assemblies of bonded atoms that have dimensions in the range of 1 to 100 nm with  $10^3$ – $10^9$  atoms and a molecular mass of  $10^4$ – $10^{10}$  Da.<sup>90</sup> Whereas in nature larger structures are built up from smaller building blocks, either through formation of covalent

bonds or supramolecular assemblies, today's technology has focused over the last years in optimizing the fabrication of electronic components from the macroscopic level downward, reaching ultimately the nanoscopic level. This steadily increasing miniaturization of micro-patterned structures has opened up new and exciting perspectives for the realization of quantum-effect and single-electron solid-state devices. With state-of-the-art photolithographic techniques, the current resolution limit for micro-structure manufacturing has reached the 10 nm mark,<sup>18,19</sup> which is in the range of molecular scale wires that are now synthetically accessible owing to the remarkable progress over the past years in synthetic chemistry. First proposed by Aviram and Ratner in 1974,<sup>20</sup> the idea of constructing useful devices at the molecular level has expeditiously become the most intriguing and fascinating overture toward the highly challenging goals in nanotechnology. One of the many examples based on this newly developed technique is the ultimate realization of a molecular-leveled computational system in terms of information storage density and speed.<sup>21,22</sup> So far, it is widely accepted that future nanoelectronic or nanophotonic processes will likely require monodisperse  $\pi$ -conjugated molecular rods of defined length as key components for ultradense and ultrafast information transportation, processing, and storage.<sup>23-25</sup> However, the question of addressing large arrays of ordered molecular scale devices still remains a major problem that has yet to be attained.

### ***1.2.1 The Importance of Monodisperse Oligomers***

Investigation of extended  $\pi$ -chain polymers is often persecuted by their insolubility in common organic solvent, and the presence of structural defects can severely hamper sound physical characterization. Hence, monodisperse oligomers serve

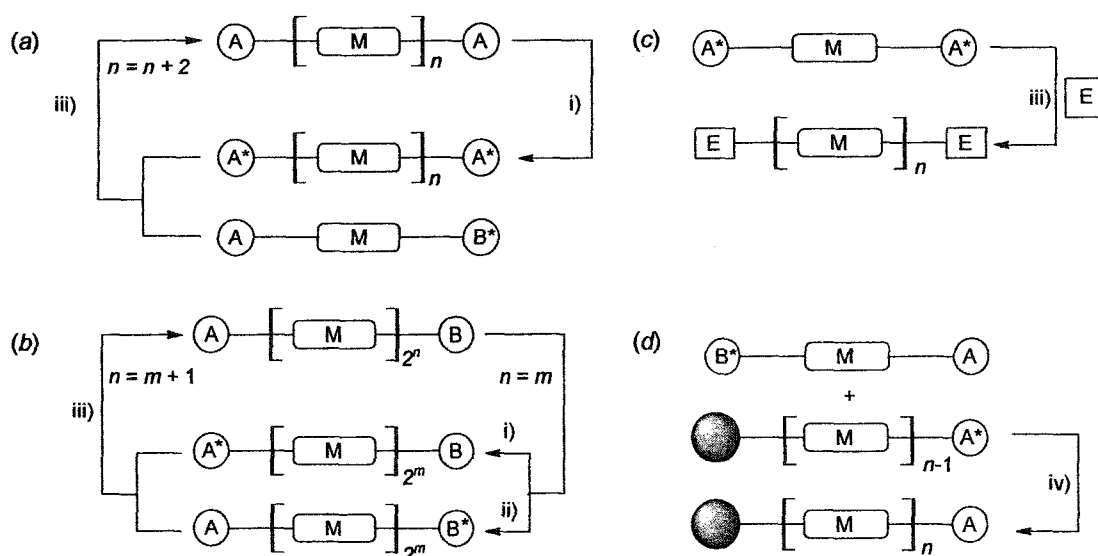
as excellent models to provide specific information concerning the solution, electronic, photonic, thermal, and morphological properties of their polydisperse macromolecular analogs.<sup>17,26</sup> Furthermore, they have also been used as model compounds for interpreting structural and conformational properties of polymers. As Tour recently pointed out,<sup>25</sup> the following questions are likely to be answered by the careful study of model oligomers: 1) When does an oligomer begin behaving like a polymer for a specific function: the wavelength of maximum absorption ( $\lambda_{\max}$ ), the optical band gap ( $E_g$ ), redox, or nonlinear optical (NLO) properties? 2) By building a series of oligomers with increasing chain-length and determining their physical trends, can we assess the required minimum degree of polymerization needed to attain a desired response from a polymer? 3) How do chain-length and conformation relate to physical, electronic, and optical phenomena? 4) Can we learn about polymer conformations in solution by studying the response of a family of well-defined smaller structures? 5) What is the mean value of monomer units becoming charged upon doping in a conjugated system? In fact, numerous publications over the last years have convincingly proved that such questions (and certainly many more) can indeed be answered by careful analysis of precisely defined oligomers.

Meanwhile, the characterization of oligomers with defined length and molecular structure is often far easier than the characterization of their polydisperse homologs. For example, NMR spectroscopic details of a monodisperse oligomer sample can be more easily elucidated than those of the randomly distributed polymers. Although the “oligomer approach” does provide a powerful tool to solve many problems for polymeric systems, it is not a universal answer to all questions raised. In fact, it is not necessarily true that all physical or chemical properties can be extrapolated to a high molecular

weight polymer. For instance, macromolecules differ from small molecules both in their solution properties and bulk effects, and these properties are not likely to be simulated by their low molecular counterparts.

### 1.2.2 General Synthetic Strategies towards Monodisperse Oligomers

One of the most striking challenges in studying monodisperse oligomers is their often difficult synthesis and purification. For the synthesis of well-defined  $\pi$ -conjugated oligomers, several approaches have emerged over the last years.<sup>17,25-27</sup> The most common methods used will be briefly discussed as following (as outlined in Scheme 1.1).



**Scheme 1.1** (a) Iterative divergent synthetic protocol. M = monomer unit. i) is the step that deprotects or activates the protection group A, yielding A\*. iii) Coupling reaction. (b) Binomial reaction protocol. i) and ii) are steps that deprotect or activate the protection groups A and B, yielding A\* and B\*, respectively. iii) Coupling reaction. (c) Homocoupling of a monomer building block in the presence of an end-capping unit E. The polydisperse mixture obtained has subsequently to be purified, e.g., by chromatographic methods. (d) Solid-phase supported reaction scheme. iv) Coupling reaction.

The first strategy towards a series of monodisperse oligomers is an “iterative divergent/convergent synthesis”, which is a commonly used method in the realization of many oligomeric species (Scheme 1.1a). The essential prerequisites for the iteration are: 1) bis-protected monomer with protection group A that can be deprotected or activated to A\*, 2) mono-protected monomer building block with an already activated group B\*, and 3) high-yielding cross-coupling using modern organic and organometallic methodologies, together with an easy isolation of respective product. The most noteworthy feature of this protocol is that the oligomeric chain increases by two units in each iteration. In addition, it can also be envisaged that using a “bigger” building block can result in a more rapid and efficient elongation of oligomers; however, extra efforts must be made on the assembly of such a building block.

The most elegant and efficient way for the direct acquisition of long oligomers, is certainly a “binomial strategy” (Scheme 1b). For such an approach, three essential requirements have to be met: 1) two orthogonal protection groups A and B must allow selective deprotection or activation to A\* and B\*, respectively, 2) the cross-coupling reaction must be selective and high-yielding, and 3) each reaction product should be easily separable from the by-products and the starting materials.<sup>28-31</sup> This reaction sequence also allows, in principle, the coupling of oligomers with different length, giving rise to the synthesis of oligomers with an odd number of repeating units (e.g., coupling of a hexamer with a monomer unit to a heptamer).<sup>32,33</sup>

The third possible strategy is homocoupling of a symmetrical monomer (Scheme 1.1c), which is eventually terminated by the addition of an end-capping agent that will irreversibly block the end of the chains, preventing any further reaction. This “one-pot-

synthesis” approach generally prevents control of oligo-selectivity, and such a statistical polymerization often yields very small amounts of each particular oligomer. Nevertheless, this reaction protocol can be useful in case where high-yielding cross-coupling reactions<sup>34</sup> are simply not available or where rapid access to an entire series of monodisperse oligomers is desirable, and a subsequent chromatographic separation is applicable. For instance, the oxidative Hay<sup>35</sup> or Eglinton<sup>36,37</sup> acetylenic coupling methods are typical examples for this strategy and have been widely used for the synthesis of oligomers with a polytriacetylene backbone.<sup>38-43</sup> Careful choice of reaction conditions (e.g., solvent, temperature, and time) usually allows optimization of the formation of a desired oligomer range.

The practical limitation of three methods mentioned above often lies in the difficulties encountered during chromatographic separation, e.g., size-exclusion chromatography (SEC) of intermediates or products with relatively low differences in molecular weight. This problem may be circumvented by using higher oligomers as the “monomer” in the synthetic reaction scheme and thus the oligomeric chain can grow by several monomer units per iteration. The second limitation for the construction of larger, well-defined oligomers from this method results from the low solubility of rigid structures, which often precludes facile separation. To provide solubility, the attachment of suitable side-chains to each repeating unit is an essential design criterion that has to be met at a very early stage of synthesis-planning. Furthermore, appropriate side-chains can also provide stability and aid in the tuning of electronic properties of the oligomer in a desirable way. High-yielding and clean reactions are, however, critical in every case, as structural defects seldom can be “corrected” afterwards by removal of a side-product.<sup>44</sup>

In principle, one could also start with polymeric material and carry out a degradation process, which for non-conjugated polymers has reached some importance.<sup>45</sup> This strategy, however, also reaches its limit when the differences in molecular weight between subsequent oligomers are not sufficient to permit chromatographic separation.

The last strategy, outlined in Scheme 1.1d, was initially designed for the synthesis of peptides: the solid-phase synthesis method introduced by Merrifield in 1963.<sup>46,47</sup> In this stepwise approach, the monomer units are covalently anchored to an insoluble polymer resin (e.g., poly(*p*-chloromethyl styrene)). After transformation or activation of the free end-group, a monomer unit that is dissolved in a suspension of the polymer-supported material is coupled. After an eventual washing step, the end-group can be reactivated and coupled to a new monomer. The primary advantage of this solid-phase supported method lies in the vast excess of coupling units that can be added to help force each reaction step to completion, which is essential for the formation of pure products. In the last step, low molecular weight compounds are removed by filtration and washing of the resin, and the completed oligomers are then cleaved from the polymer support. A strategy to overcome the main shortcoming of this process, that not all activated end-groups have reacted during the reaction, is to use a second reagent as a capping agent that irreversibly blocks the unreacted ends of the chain, since subsequent purification is far easier with compounds of large size difference. Several aspects of the design and synthesis of  $\pi$ -conjugated molecules, as well as detailed discussion of the synthetic methods presented herein, have previously been reviewed.<sup>17,21,25,48</sup>

Finally, it should be pointed out that the rapid progress in the synthesis of  $\pi$ -conjugated molecules has been spurred by marked developments and improvements in

other fields of science. Complex and sophisticated analytical and materials characterization methods like high molecular weight mass spectrometry, for instance electrospray ionization mass spectrometry (ESI-MS) and matrix-assisted laser-desorption-ionization time-of-flight mass spectrometry (MALDI-TOF-MS), have uniquely contributed to our understanding of high molecular weight oligomers and polymers.

### ***1.2.3 The Effective Conjugation Length in $\pi$ -Conjugated Systems***

The knowledge of the number of repeat or monomer units in a  $\pi$ -conjugated oligomer required to furnish size-independent properties that correspond to those of the related infinite-chain polymer is of greatly practical and theoretical interest.<sup>44</sup> For instance, if a  $\pi$ -conjugated material with a saturated property is targeted, an intractable high molecular weight polymer could be replaced with shorter oligomers that have reached convergence of their physical properties and display better processability.

Initially, “conjugation without end” was thought to be an idealized concept. It soon turned out, however, that an effective conjugation length (ECL),<sup>49</sup> confinement length (CL), or delocalization length (DL)<sup>50</sup> exists even in very long  $\pi$ -conjugated chain or ladder polymers (excluding structural defects). Albeit, the effective  $\pi$ -electron delocalization length is a value that is not directly accessible by physical measurement. The idea of “conjugation length” or “effective conjugation length” has evolved to one of the central concepts in the theoretical and experimental understanding of many properties of conjugated polymers.<sup>51</sup> The usefulness of homologous series of oligomers for the experimental determination of the effective conjugation length has been widely demonstrated.<sup>51-54</sup>

The fact that  $\pi$ -conjugated polymers exhibit a converging limit for certain physical properties (e.g.,  $\lambda_{\max}$ , redox potentials, first and second hyperpolarizabilities) often arises from mutual distortions from planarity of the conjugated backbone, for instance, by rotation about single bonds. This results in reduced  $\pi$ -overlap, and thus the conjugation exhibits a limited extension. In systems containing aromatic building blocks, resonance stabilization is another factor reducing the mobility of the  $\pi$ -electrons. Furthermore, electron-electron correlations, which are often negligible in short  $\pi$ -systems, become relevant in molecules containing large numbers of  $\pi$ -electrons.

The dependence of the energy gap between the highest occupied molecular orbital (HOMO) and the lowest unoccupied molecular orbital (LUMO) on the oligomer length and geometry of the molecule is not only of fundamental interest, but it is the key issue to be considered in designing new oligomeric and polymeric materials, in particular, those with large optical nonlinearities.<sup>55,56</sup> One of the simplest theoretical models that can be used to describe changes in physical properties as a function of chain-length follows the description of a “particle in a box” as shown in Eq. (1.1), where  $n$  stands for the quantum number,  $h$  for the Planck constant,  $m$  for the mass of the electron or particle,  $L$  for the length of the box, and  $E$  for the energy of the particle.<sup>57</sup> Although this classical model contains no correction for electron-electron correlation effects, it has been proved to have significant predicting power at both the qualitative and quantitative levels.

$$E = \frac{n^2 h^2}{8mL^2} \quad (1.1)$$

**Table 1.1** Summarization of Algorithms predicting the ECL in  $\pi$ -conjugated systems.

Wenz <i>et al.</i> <sup>58</sup>	$E = V_0 + \left( \frac{h^2}{4mL_0^2} - \frac{V_0}{4} \right) \frac{1}{N+1/2}$	Based on Kuhn's 'Free Electron Gas Model'. Successfully applied in estimation of polydiacetylene and polytriacetylene series.
Lewis and Calvin <sup>59</sup>	$\lambda^2 = kn$	Based on the harmonic oscillator. Shows excellent results in the linear range for polyynes.
Hirayama <sup>60-63</sup>	$\lambda_{\max}^2 = A - BC^N$	Modification of Lewis and Calvin's equation.
Meier <i>et al.</i> <sup>49</sup>	$E_i(n) = E_{i,\infty} + (E_{i,l} - E_{i,\infty})e^{-a_i(n-1)}$ $\lambda_i(n) = \lambda_{i,\infty} + (\lambda_{i,l} - \lambda_{i,\infty})e^{-b_i(n-1)}$	A reliable method accurately predicting the ECL in a large variety of different $\pi$ -conjugated systems.

To evaluate the ECL, various algorithms have been discussed in the literature. One simple way is to plot a relevant physical property (e.g.,  $\lambda_{\max}$  or  $E_g$ ) against the inverse number of monomer units  $1/n$ . Extrapolation to infinite chain length yields  $n_{\text{ECL}}$ , the number of repeat units in an oligomer at which saturation of a property occurs. Usually, this linear correlation of a homologous series of oligomers yields reasonable results in cases where no obvious deviation (e.g., saturation) occurs. In fact, the estimation of convergence values by extrapolation can often only afford a rough approximation and sometimes results in misleading conclusions.<sup>49</sup> However, satisfactory results can be obtained in cases where higher oligomers or polydisperse polymers are available that already show saturation of the physical property. In such cases, the crossing point of the linear regression line obtained from the oligomer series with that of

the horizontal saturation level line for the polymer allows a good estimation of the ECL.<sup>38</sup> Based on a variety of theoretical hypotheses, several mathematic models have been elegantly elaborated and successfully applied in prediction of ECL for different types of  $\pi$ -conjugated oligomeric systems, as briefly summarized in Table 1.1.

The definition of the ECL is by no means restricted to UV-vis spectroscopy. Many data from various other spectroscopic methods like vibrational spectroscopy (e.g., Raman, IR), electrochemical methods, and nonlinear optical spectroscopy also display saturation effects above a critical value.

#### ***1.2.4 The Applications of $\pi$ -Conjugated Oligomers***

The extended  $\pi$ -systems of conjugated oligomers qualify them as chromophores with a broad range of optical properties, and as electrophores with the ability to accept or donate charge. Many physical properties relevant to materials science are related to the initiation, transport, annihilation, or storage of charge. Generally, there are two main reasons for studying oligomers of conjugated polymers: 1) Oligomers represent model systems for understanding the fundamental electronic properties of the corresponding polymer. Oligomers can be synthesized with a well-defined molecular length. They therefore have been recognized for some time as model systems for extrapolating physical properties of the corresponding ideal polymer of infinite length. In marked contrast, real conjugated polymers exhibit a distribution of lengths, along which  $\pi$ -conjugation is effective. The coherent conjugated segments of the polymer chain are interrupted by defects, which may be of a conformational nature (e.g., twisting of the chain so that it is no longer planar) or of a chemical nature, such as a saturated  $sp^3$ -hybridized carbon atom located somewhere along the chain. Furthermore, oligomers are

well-defined systems of monodisperse molecules, with a greatly reduced occurrence of defects within the molecular chains, in comparison with polymers. They therefore offer the possibility of better ordering of the molecules and consequently more well-defined optical properties. This renders them particularly appealing for both theoretical and experimental investigations into a number of issues, which cannot be so readily assessed in polymeric systems. 2) In some cases, oligomers have already been shown to exhibit characteristics superior to those currently found in many conjugated polymers. For instance, oligothiophenes show high field-effect mobilities for thin film transistors due to very effective intermolecular charge transport.<sup>23</sup> Another example is employing short oligomers to achieve blue electroluminescence devices (e.g., blue emitting LEDs) due to their more confined band gaps that lead to blue emission. In this section, discussion will be mainly emphasized on optical and electronic applications using  $\pi$ -conjugated oligomers.

**Light emitting diodes based on  $\pi$ -conjugated oligomers.** In the mid-1950s, electroluminescence (EL) was reported from cellulose film doped with organic dye molecules.<sup>64,65</sup> Since then, dramatic progress has been made in this area. Recently, light emitting diodes (LEDs) have been fabricated with  $\pi$ -conjugated oligomers, such as oligothiophenes, oligophenylenes, and oligo(phenylene vinylene)s,<sup>66</sup> in single-layer devices, as well as in bilayer and multilayer devices. However, electroluminescence (EL) efficiencies, referring to the ratio of emitted photons to injected electrons, generally remain much lower than those of polymeric devices. The first reported single-layer thin-film oligothiophene LEDs were fabricated by Geiger *et al.*<sup>67</sup> using spin-coated films of cycloalkane end-capped oligothiophenes. The efficiency of these LEDs was low

( $10^{-2}$ – $10^{-3}$ %) and decreased for longer chain lengths. Uchiyama *et al.*<sup>68</sup> later reported electroluminescence from single layer devices with highly crystalline films of  $\alpha,\omega$ -dimethylsexithiophene deposited under ultrahigh vacuum. Although high rectification ratios were obtained (1500 at  $\pm 10$ V) and onset voltages for electroluminescence were low (4V), very low quantum efficiencies (ca.  $3 \times 10^{-7}$ %) were obtained. They were able to increase the electroluminescence by a factor of up to 1000 by fabricating a bilayer device in which a shorter oligomer (of higher energy gap) is inserted between the sexithiophene layer and the aluminum electrode in order to block holes and enhance recombination at the heterojunction. Horowitz *et al.*<sup>69</sup> have prepared bilayer LEDs using a combination of unsubstituted sexithiophene and substituted derivatives, either with two decyl side-chain or with triisopropylsilyl end-groups. The quantum yield of these bilayer LEDs can be thus increased by three or four orders of magnitude.

Garten *et al.*<sup>70,71</sup> reported the preparation of an efficient blue LED based on a novel partially conjugated co-polymer (SiPPV). In single-layer devices based on SiPPV, the high barrier at the aluminum top electrode limits efficient electron-injection into the device. In double-layer structures with an evaporated polymer film at the cathodic side, electron and hole currents are much more balanced, resulting in an internal quantum efficiency of 3.2%. The average turn-on field of a double-layer device is reduced compared to a single-layer LED.

Zhu and co-workers<sup>72</sup> recently investigated new a cyano-containing polymer, namely CN-P3PV, which is a CN-PPV derivative with two less vinylene linkages for every four vinylene groups. The oligomers of CN-P3PV were synthesized via the Suzuki coupling, and a double-layer LED was fabricated and characterized. This device showed

high electron transporting ability and good EL performance with the emission of bright orange light.<sup>72</sup>

**Photoconductive and photovoltaic devices based on  $\pi$ -conjugated oligomers.**

Photoconductivity was first observed in anthracene by Pochettino<sup>73</sup> and Volmer<sup>74</sup> almost a century ago. Interest in using organic materials for xerography began in the 1950s and 1960s. Now small organic semiconductors have found widespread applications in xerography and laser printing. The principal advantages of using organic materials are that they can be prepared as flexible layers, suitable for coating cylindrical drums and belts, at relatively low cost, with spectral sensitivity throughout the visible region and into the near infra-red by the use of a mixture of photoreceptors of different semiconductor gaps, and with lower toxicity than the chalcogenide alloys, which they have largely replaced. Although the small organic semiconductors used in xerography can often be viewed as oligomers, e.g., tetracene, pentacene, and derivatives, there have been to date relatively few reported investigations of the photoconductive and photovoltaic properties of oligomers of conjugated polymers. Recent studies of photoconductive properties of sexithiophene thin films suggested that the stacked layer structure play an important role in photoconductivity.

A related application is in the use of organic semiconductors is solar cells.<sup>75</sup> The advantages of organic semiconductors include the facile deposition of large area films from solution at low cost, as well as the possibility of selecting molecules of a variety of energy gaps and chemical modifications in order to make most efficient use of the solar spectrum. A major breakthrough in the use of organic semiconductors in solar cells was the report by Tang<sup>76</sup> and Panayotatos<sup>77,78</sup> concerning of efficient two-layer photovoltaic

cells. Recently, Noma *et al.*<sup>79</sup> have used a similar bi-layer strategy with the oligomer octathiophene, which achieved a fill factor of 0.5 and a conversion efficiency of ca. 0.6% under white light illumination at 105 mW cm<sup>2</sup>. Studies on ladder-type oligophenylenes (LOP) by Köhler *et al.*<sup>80</sup> indicated that absorption into aggregate states may be highly efficient for the generation of photocurrent, leading to increased quantum yields by two orders of magnitude, compared with intramolecular excitation. The deliberate use of materials which undergo aggregation may therefore offer an important strategy for improving organic solar cell. Furthermore, as emphasized by Karl *et al.*,<sup>81</sup> the power conversion of organic solar cell is often low, due to a high internal cell resistance, because the mobility of many organic semiconductors is low. To solve this problem, they advocated the use of more crystalline materials with strong intermolecular  $\pi$ -electron interactions and high mobilities, as might yet be achieved with suitable oriented sublimed films of conjugated oligomers. Recent studies also show that oligomer/fullerene bilayer devices are of particular interest in photovoltaic applications owing to the electron donor-acceptor systems.<sup>82</sup> Green *et al.* investigated a 5-ring *n*-octyloxy-substituted PPV oligomer and C<sub>60</sub> bilayer devices as an organic solar cell, which delivered external quantum efficiencies up to 60–70% in the UV-vis spectrum.<sup>83</sup> Alivisatos and co-workers<sup>84</sup> recently successfully prepared a photovoltaic device consisting of 7 nm by 60-nm CdSe nanorods and conjugated polymer poly(3-hexylthiophene), which was assembled from solution with an external quantum efficiency of over 54% and a monochromatic power conversion efficiency of 6.9% under 0.1 mW cm<sup>-2</sup> illumination at 515 nm.<sup>84</sup>

**Field-effect transistors based on  $\pi$ -conjugated oligomers.** First work on organic semiconductors, such as polyacenes, started in the early 1950s and were mainly devoted to the fundamental aspect of charge transport. Later, in the early 1970s, energy problems highlighted the potential interests of organic-based devices. The ease of processing organic materials held out the hope of developing low cost and large area photovoltaic devices, which stimulated active research in the field of organic semiconductors. In the 1980s, conjugated polymers emerged in this field as a new class of organic materials with promising electrical properties. Intensive research, devoted both to the conducting and the semiconducting states of these conjugated materials, was thus carried out aimed at understanding their charge-transport properties in terms of chemical structure and structural organization. A new class of well-defined materials, conjugated oligomers, arrived on the scene in the mid-1980s and have continued to attract interest, both as model compounds for their parent polymers and also for their particular characteristics. Field-effect transistors (FETs) have been studied with a long term aim to develop a new area of organic electronics, and oligothiophenes and fullerenes have recently been shown to reach characteristics close to those of hydrogenated amorphous silicon. These achievements open the perspectives of low cost and large area FET devices.

Many conjugated materials have been analyzed concerning their semiconducting properties, through the characterization of FETs made from these materials. Two main classes can be distinguished, macromolecular materials (i.e., conjugated polymers) and molecular materials (i.e., conjugated oligomers and  $\pi$ -electron rich molecules). Conjugated oligomers have been proposed as active layers in FETs, and those most

studied are the thiophene oligomers,<sup>85-88</sup> either unsubstituted or alkyl substituted with pendent group in the  $\beta$ -position or as the end groups in the  $\alpha,\alpha'$ -positions. Unsubstituted oligothiophenes, from terthiophene to octithiophene, as well as  $\alpha,\alpha'$ -dialkyl substituted oligothiophenes, from dialkylterthiophene to dialkyloctithiophene, have been deposited by vacuum evaporation, owing to their very low solubility. When substituted in the  $\beta$ -position, these oligomers become more soluble, such as  $\beta$ -didecyldodecithiophene, and  $\beta$ -tetradecyldodecithiophene, and have thus been deposited by spin coating.

Early work on conjugated oligomers has revealed a significant increase in field-effect mobility, the first results on sexithiophene showing values of  $2 \times 10^{-3} \text{ cm}^2 \text{ V}^{-1} \text{ s}^{-1}$ .<sup>89</sup> Furthermore, thiophene oligomers ranging from the trimer to octamer have been subsequently characterized concerning their conductivity and field mobility in the regard of understanding the role of effective conjugation length.<sup>23,91-92</sup> It has been found that the conductivity indeed increased with the increasing conjugation length as generally observed in conjugated materials. However, the field-effect mobility increases much faster, up to the hexamer (sexithiophene), and then decreases slightly. Nevertheless, the decrease is not significant and can be attributed to chemical impurities. These data show that, on the basis of conjugation length, one of the most interesting candidates for FET devices is the hexamer, sexithiophene, where future work is being focused. Another marked progress in organic FET was recently accomplished by Bao and co-workers,<sup>88,93-95</sup> using solution-processed self-organized<sup>96</sup> conjugated polymers, such as poly(3-hexylthiophene), as an active material. This well-formed poly(3-hexylthiophene) shows a high charge carrier mobility of  $0.05\text{--}0.1 \text{ cm}^2 \text{ V}^{-1} \text{ s}^{-1}$  at room temperature. At low

temperature (ca. 2.35 K), interestingly, this film becomes superconducting owing to the self-assembly properties of the polymer.<sup>88</sup>

### 1.3 Nonlinear Optical Properties of $\pi$ -Conjugated Oligomers

Perhaps one of the most intriguing aspects of  $\pi$ -conjugated oligomers are their nonlinear optical (NLO) properties.<sup>97</sup> The development of materials with large optical nonlinearities is a key to controlling the propagation of light beams by optical means. The control of light by light requires that photons can strongly interact with the medium. This is only possible in media where the optical properties, such as the refractive index, depend on the light intensity. The availability of appropriate materials for this purpose could revolutionize information technology in a similar manner to the development of materials for semiconductor electronics.

Optical materials with a sufficiently large intensity-dependent refractive index, which could play a similar role to silicon in electronics, have not so far been identified. Currently, this field is still at the stage of basic research, where strong efforts are devoted to an understanding of the fundamental relations between molecular structure and optical nonlinearities. It is clear, however, that materials with a highly polarizable electron system are interesting candidates for achieving strong polarizations of the medium, which respond to the electric field of the lightwave in a nonlinear manner. Therefore, organic materials with a delocalized  $\pi$ -electron system have attracted much interest, and large nonlinearities for one-dimensional conjugated polymers have been reported.<sup>98,99</sup> As the optical properties of conjugated polymers are determined largely by the extent of electron delocalization, the corresponding conjugated oligomers have a key role in the study of the

scaling of the linear and nonlinear optical properties with the size of the system. It will be seen that the size of the delocalized electron systems and electron correlation effects primarily determine the optical nonlinearities of oligomers. In this section, discussion will mainly focus on third-order optical nonlinearity, because this can lead to an intensity-dependent refractive index, and relevant work will be addressed in later chapters.

### 1.3.1 Physical Background of Nonlinear Optical Phenomena

When a medium is subject to an intense electric field  $\vec{E}$  such as that due to an intense laser pulse, the polarization response  $\vec{P}$  of the material no longer follows the electric field linearly due to an anharmonic motion and response of the bound electrons. Therefore,  $\vec{P}$  is usually described as a power series expansion as Eq. (1.2):

$$\vec{P} = \chi^{(1)}\vec{E} + \chi^{(2)}\vec{E}^2 + \chi^{(3)}\vec{E}^3 + \dots \quad (1.2)$$

$\chi^{(n)}$  stands for the optical susceptibilities of order  $n$ . The manifestation of nonlinear optical behavior can be seen by substituting a sinusoidal field equation into to the polarization expansion of Eq. (1.2), and thus gives

$$\vec{P} = \chi^{(1)}\vec{E}_0 \cos(\omega t - kz) + \chi^{(2)}\vec{E}_0^2 \cos^2(\omega t - kz) + \chi^{(3)}\vec{E}_0^3 \cos^3(\omega t - kz) \quad (1.3)$$

and using appropriate trigonometric identities for  $\cos^2 \theta$  and  $\cos^3 \theta$  gives

$$\begin{aligned} \vec{P} = & \chi^{(1)}\vec{E}_0 \cos(\omega t - kz) + \frac{1}{2}\chi^{(2)}\vec{E}_0^2 [1 + \cos(2\omega t - 2kz)] \\ & + \chi^{(3)}\vec{E}_0^3 \left[ \frac{3}{4}\cos(\omega t - kz) + \frac{1}{4}\cos(3\omega t - 3kz) \right] \end{aligned} \quad (1.4)$$

Equation (1.4) clearly shows the presence of new frequency components due to the nonlinear polarization. The second-order term gives a frequency independent contribution as well as one at  $2\omega$  (the second harmonic), whereas the third term indicates

a frequency response at the frequency of the optical field  $\omega$  as well as a response at  $3\omega$  (the third harmonic).

At this point, it can simply be noted that contribution from the second- and third-order terms to the nonlinear polarization are predicated from different symmetry properties of the medium. A contribution from  $\chi^{(2)}$  can come from only noncentrosymmetric media, whereas  $\chi^{(3)}$  can arise from any medium regardless of symmetry.

Another manifestation of nonlinear optics is the so-called nonlinear index of refraction of the medium. In fact, almost all of the nonlinear effects can be deemed as arising from field-induced modulation of the refractive index. Second-order nonlinear optical effects can be visualized as a three-wave mixing process where the waves exchange energy with one another through the intercession of the nonlinear medium. Similarly, third-order nonlinear optical effects can be described as four-wave mixing process where waves at frequencies  $\omega_1, \omega_2, \omega_3$  interact to produce  $\omega_4$ . In general, the waves can be at any combination of frequencies that satisfies the momentum conservation requirement. This coefficient is usually represented as  $\chi^{(3)}(-\omega_4; \omega_1, \omega_2, \omega_3)$ . For third-harmonic generation (THG), for instance, it becomes  $\chi^{(3)}(-3\omega; \omega_1, \omega_2, \omega_3)$ .

### ***1.3.2 Measurement Techniques and Theories on Third-Order Optical Nonlinearity***

The third-order nonlinear optical interactions give rise to a large number of phenomena, any of which can be monitored to obtain information on third-order optical nonlinearity. Experimental probes generally employed to measure  $\chi^{(3)}$  are based on the following effects: 1) third-harmonic generation (THG), 2) electric field-induced second-harmonic generation (EFISH), 3) degenerate four-wave mixing (DFWM), 4) optical Kerr

gate, and 5) self-focusing (Z-scan). Detailed explanations of these techniques can be readily obtained from the relevant literature.<sup>23,97,99,100</sup> Herein, we describe a newly established technique, namely differential optical Kerr effect (DOKE) detection, the full details of which have been published in a recent collaborative paper. The details of this technique are explained as following (cited from the original paper).<sup>101</sup>

The optical Kerr effect (OKE) is an optically induced birefringence in an isotropic medium.<sup>102</sup> In a standard homodyne Kerr gate,<sup>103-108</sup> an intense, linearly polarized pump pulse, polarized, for example, at 45° to the horizontal, excites a birefringence in an isotropic medium. The change in the index of refraction induced by the pump pulse,  $\delta n = \delta n_{//} - \delta n_{\perp}$ , between the parallel and perpendicular axes to the pump polarization can be probed by a weaker probe pulse that is polarized horizontally. The induced birefringence,  $\delta n$ , manifests itself as retardation in the probe beam polarization and may be detected by a post-sample analyzer. Furthermore, the probe beam may be time-delayed with respect to the pump pulse, yielding a temporal profile of the induced birefringence. When the pump pulse arrives well before the probe pulse, there is no induced birefringence and no probe light passes through the crossed polarizers. When the two pulses arrive simultaneously at a sample dominated by an ultrafast electronic nonlinearity, the probe beam experiences the maximum rotation in polarization given by

$$\phi = \frac{2\pi d}{\lambda} n_2 I_{pump}, \quad (1.5)$$

where  $n_2$  is the nonlinear index of refraction and is proportional to  $\chi^{(3)}$ ,  $\lambda$  is the wavelength,  $d$  is the sample length, and  $I_{pump}$  is the pump intensity in units of W/m<sup>2</sup>. The quantity  $n_2$  can be considered as a modification to the linear index of refraction such that

the total index of refraction is given by  $n = n_0 + n_2 I_{\text{pump}}$ ;  $n_0$  being the linear index of refraction.  $\chi^{(3)}$  is obtained from  $n_2$  by

$$n_2 \left( \frac{\text{m}^2}{\text{W}} \right) = \frac{3.9 \times 10^{-6}}{n_0^2} \chi^{(3)} (\text{esu}), \quad (1.6)$$

where  $n_2$  is in units of  $\text{m}^2 \text{W}^{-1}$  and  $\chi^{(3)}$  is in esu, the respective units currently in favour.

The molecular second hyperpolarizability,  $\gamma$ , may be approximated by

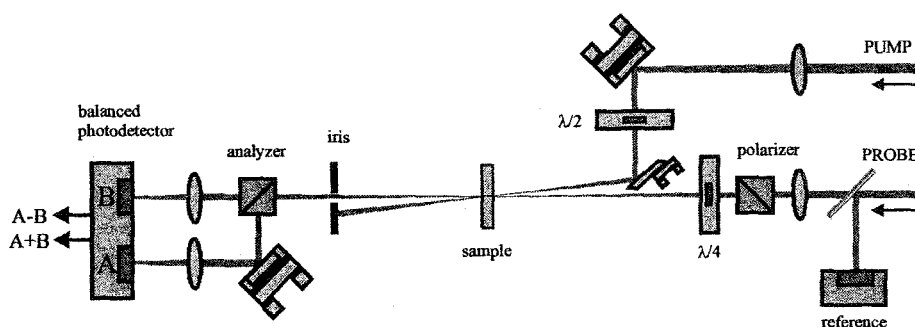
$$\gamma = \frac{\chi^{(3)}}{N_c L^4}, \quad (1.7)$$

where  $N_c$  is the molecular number density in  $\text{cm}^{-3}$  and  $L^4$  is the Lorentz field-factor which may be approximated by  $[(n_0^2 + 2)/3]^4$  for isotropic liquid media.

To separate the real and imaginary components of  $\chi^{(3)}$  and to obtain larger signals, optical heterodyne detection (OHD-OKE) is used by many groups. In OHD-OKE, a quarter-wave plate ( $\lambda/4$ ) is placed between the probe polarizer and sample such that the fast axis of the quarter-wave plate is parallel to the polarizer. By slightly rotating the polarizer axis,  $\pi/2$  out-of-phase light is added to the probe beam, and this technique can provide the real (third-order nonlinear susceptibility) or imaginary (two-photon absorption) components of the nonlinear response directly from the Kerr signal. This scheme is restricted to the regime where the transmitted signal is linear with pump intensity.

The DOKE setup (shown in Fig. 1.1)<sup>101</sup> uses pump and probe pulses generated by an amplified Ti:sapphire laser, producing 800 nm, 100 fs pulses at a 1 kHz repetition rate. A computer-controlled stage is used to vary the delay between the pump and probe pulses. The pump pulse is polarized 45° to the horizontal before being focused onto a 1

mm sample path-length quartz cuvette filled with a sample solution. The weaker probe beam is initially polarized vertically by a Glan-laser polarizer and then passes through a quarter-wave plate oriented to produce circular polarized light. Typical pump and probe powers at the sample location are between 0.5–6 mW for the pump beam and 50–80  $\mu$ W for the probe beam. The probe light is focused to overlap in the sample with the pump beam at a near coincident angle,  $\theta < 5^\circ$ . Typical spot sizes for the pump and probe beams are 500  $\mu$ m and 240  $\mu$ m, respectively. The pump beam is blocked post-sample while the probe light is allowed to travel to a second Glan-laser polarizer acting as the analyzer. Here, the transmitted and rejected beams are separated and directed to a pair of balanced photodiodes. Photodiode “A” receives the rejected beam, and photodiode “B” receives the transmitted beam. The pump beam is chopped at 125 Hz, and lock-in detection is used to monitor the  $A - B$  signal. The  $A + B$  signal is detected at 1 kHz using a separate lock-in amplifier. Finally, these signals are sent to a computer used for data acquisition



and delay-stage control.

Fig. 1.1 Schematic outline of the differential optical Kerr effect (DOKE) detection setup.

The key feature of the DOKE setup is that the  $A - B$  detection acts as our Kerr effect signal. If  $\text{Im}(\chi^{(3)})$  is small,  $A + B$  acts as a probe beam reference. In the presence of nonlinear absorption such as two-photon absorption, the  $A + B$  signal provides

independent detection of the  $\text{Im}(\chi^{(3)})$  processes. The photodiodes are calibrated in such a way that in the absence of any birefringence, A and B signals are equal and  $A - B$  is zero.

Consider a vertically polarized probe beam and a sample with an induced birefringence of  $\phi = \phi' + i\phi''$ , where  $\phi'$  and  $\phi''$  are the real and imaginary components of the phase retardation, respectively. If after passing through a quarter-wave plate set with fast axis at  $45^\circ$ , the beam is incident on the sample, the detected signal ratio is given by

$$\frac{A - B}{A + B} = \frac{\sin \phi'}{\cosh \phi''} \quad (1.8)$$

This relationship is valid when the pump and probe beams are initially polarized at  $45^\circ$  with respect to each other. In the absence of nonlinear absorption,  $\phi'' = 0$ , and Eq. 1.8 is reduced to Eq. 1.9, a purely real response:

$$\frac{A - B}{A + B} = \sin \phi' \quad (1.9)$$

Much like the heterodyne scheme, DOKE detection obtains signals that are linear with pump and probe intensity. The DOKE technique affords a larger dynamic range of linear signal than the typical heterodyne scheme. We have also observed that the DOKE signals are larger, in comparison to OHD-OKE, making detection easier.

In the study of third-order polarizabilities of long-chain molecules, experimental results of conjugated systems like oligoenes show a strong superlinear increase of  $\gamma$  with the chain length. This behavior is explained due to the delocalization of  $\pi$ -electron along the conjugated chain. Furthermore, it was noted that the increase of  $\gamma$  follows a power law dependent on the size of the conjugated system. Therefore, the study of oligomers

with extended  $\pi$ -electron conjugation gives a means to elucidate the influence of the chain length  $n$  and on the magnitude of  $\gamma$ .

The theoretical explanation of this superlinear increase of  $\gamma$  with the conjugation length still remains challenging. A variety of theoretical models and calculation methods (e.g., free electron in box, Hückel, PPP, SCF CI, *ab initio* HF, SOS, etc.) have been employed by different researchers,<sup>23</sup> yielding power laws of the form

$$\gamma \sim n^\mu \quad (1.10)$$

for the limit of very small conjugated systems (less than ca. 2 nm). In these various theories,  $n$  denotes the number of repeat units or the number of atomic or molecular sites. Although the complexity and accuracy of these theories differ considerably, they accordingly lead to exponent  $\mu$  around 4 to 5 in the limit of short chains. Clearly, this result cannot go on indefinitely. At a characteristic, critical length, the  $\pi$ -electrons are no longer correlated. Loosely speaking, they start to respond independently to the external optical fields and, consequently, the microscopic polarization  $\alpha(\omega, \omega)$  and  $\gamma$  increase linearly with the size of the system, commonly called saturation of polarizabilities.<sup>23</sup>

For polymers with a 1D conjugated  $\pi$ -electron system, Flytzanis *et al.*<sup>109</sup> used the one-electron Hückel approximation to derive a universal behavior between  $\chi^{(3)}$  and the  $\pi$ -electron delocalization length  $L_d$ . Their theory yields the simple but general relationships

$$\chi^{(1)} \sim L_d^2 \quad (1.11)$$

and

$$\chi^{(3)} \sim L_d^6 \quad (1.12)$$

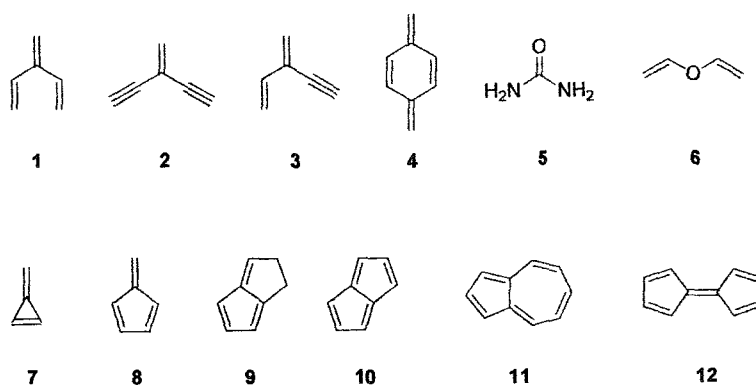
As well, it can be also express by

$$\chi^{(3)} \sim \lambda_{\max}^6 \quad (1.13)$$

This so-called “scaling law” has become very popular and frequently used to interpret the third-order nonlinearities of conjugated systems. Recently, a final experimental test of its validity has also been accomplished.<sup>110</sup>

#### 1.4 Cross Conjugation and Why Cross-conjugated Molecules

In addition to the most extensively studied linear conjugation, there is another type of conjugation, namely cross conjugation,<sup>111</sup> which has attracted an ever-growing interest. Originally, the term cross-conjugated referred to systems possessing three unsaturated groups, two of which, although conjugated to a third center, are not conjugated to each other. The word “conjugated” is used in the classical sense of describing a system of alternating single and double bonds. A representative selection of cross-conjugated molecules is listed in Scheme 1.2.



**Scheme 1.2** A representative selection of cross-conjugated molecules.

Although the term “cross conjugation” has been employed in many publications, its concept still remains rather unclear. This is evidenced by the fact that even a clear definition of which compounds should be classified as cross-conjugating is lacking. One requirement mentioned above is that there must be two unsaturated bonds in conjugation with a third one, but not in a linear arrangement. For instance, the simplest representative is 3-methylene-1,4-pentadiene **1**, which can be seen as an ethene disubstituted geminally with two vinyl groups. However, this definition can not be applied on its cyclic analog fulvene **8**, as well as molecules like pentalene **10** and azulene **11**, where the two double bonds on the cyclic ring are also conjugated with each other. Therefore, the concept of cross conjugation generally extends to: there are (at least) two unsaturated bonds conjugated with a “central” unsaturated bond in such a way that the  $\pi$ -electron systems form a bifurcation. In addition, the cross conjugation can also be used in other conjugated motifs such as heteroatoms with lone pairs (e.g., urea **5** and divinylether **6**).

As pointed out by Henning Hopf almost 20 years ago,<sup>112</sup> cross-conjugated molecules<sup>113-115</sup> have remained a neglected class of compounds, and compared to the extensively studied linearly  $\pi$ -conjugated species, cross-conjugated molecules still remain quite unexplored.<sup>116-126</sup> On the other hand, owing to their unique  $\pi$ -electron delocalization mode, interesting properties are expected to be generated with potential in applications to molecular optics and electronics. One of the most intriguing aspects of these species is the concept that they might be utilized as active optical materials (e.g., third-order nonlinear optics) with “electronic transparency”.

It has been demonstrated that the organic molecule with NLO activity generally requires a highly polarizable system, in other words, a highly  $\pi$ -conjugated structure.

However, for linearly conjugated molecules, the highly delocalized  $\pi$ -system can bring about a fatal drawback for optical applications, that is, the bathochromic shift of the maximum electronic absorption  $\lambda_{\max}$  with the increasing conjugation. Whenever the  $\lambda_{\max}$  shifts to visible region, the operating light beam of the optical devices will be blocked (absorbed at this frequency), as a result, making it useless for application. Nevertheless, by adopting the cross-conjugated systems, the aforementioned drawback can be potentially overcome due to the unique  $\pi$ -delocalization in cross conjugation. Since the  $\pi$ -electrons in such a system normally can not readily delocalize along the entire system, but delocalize in confined segments, it is obvious that a drastic bathochromic shift in  $\lambda_{\max}$  is not likely to occur, even in a long extended cross-conjugated system. Hence, the visible region can still remain fairly transparent, and the so-called “electronic transparency” is thus achieved.

## **1.5 Survey on Monodisperse $\pi$ -Conjugated Oligomers**

### ***1.5.1 $\pi$ -Conjugated Oligomers Containing Nonaromatic Backbones***

#### ***1.5.1.1 Oligoenes***

The major interest in linear oligo- and polyenes lies in their capability to serve as defect-free model compounds for electrically conducting materials such as polyacetylene (PA, Fig. 1.2). PA is the simplest conjugated polymer with a nonaromatic all-carbon backbone and a degenerated electronic state. As an ubiquitous species in both natural<sup>127</sup> and synthetic<sup>128</sup> compounds, PA and shorter oligomers have been extensively explored for years because of its interesting and promising properties, in particular for its high electrical conductivity (up to  $10^5 \text{ S cm}^{-1}$ ) upon doping.<sup>12,129-132</sup>

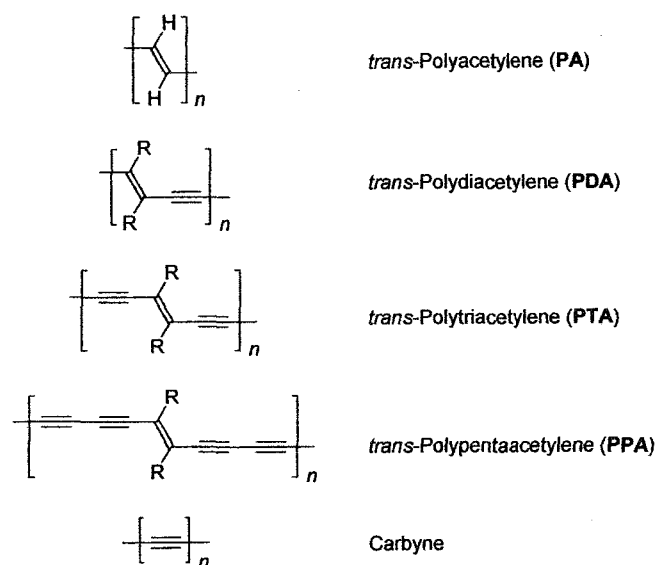


**Fig. 1.2** Progression of linearly  $\pi$ -conjugated all-carbon backbones from *trans*-polyacetylene to carbyne.

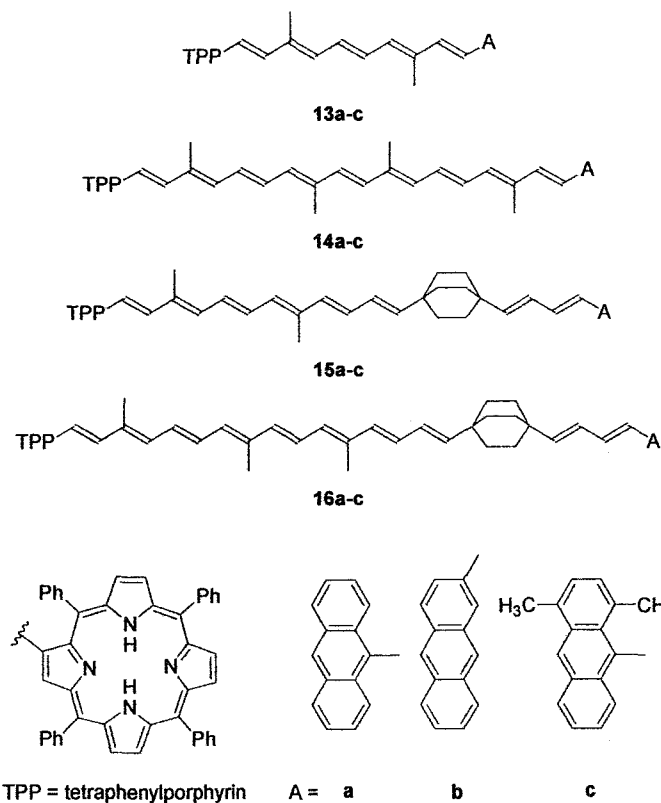
Polyene model compounds have played a dominant role in studying these processes.<sup>133</sup> It has recently been reported that highly conjugated ionic polyacetylene polymers may overcome some of the limitations of classical PA, and this area has regained considerable interest.<sup>133</sup> This high conjugation has been achieved by introducing one or two ionic charges into each PA repeat unit, resulting in polymers with one of the highest charge densities known and extended conformations owing to the electrostatic repulsion between subsequent segments.<sup>133</sup> Recent progress in the synthesis and characterization of PA as well as that of other conjugated polymers and oligomers has been reviewed.<sup>48</sup>

Unfortunately, PA is an intractable, insoluble, and infusible material and thus several attempts have been made to make PA more processible by attaching solubility-providing side-chains. However, severe steric interactions between adjacent side-groups, other than hydrogen, distort the  $\pi$ -conjugated backbone out of planarity resulting in loss

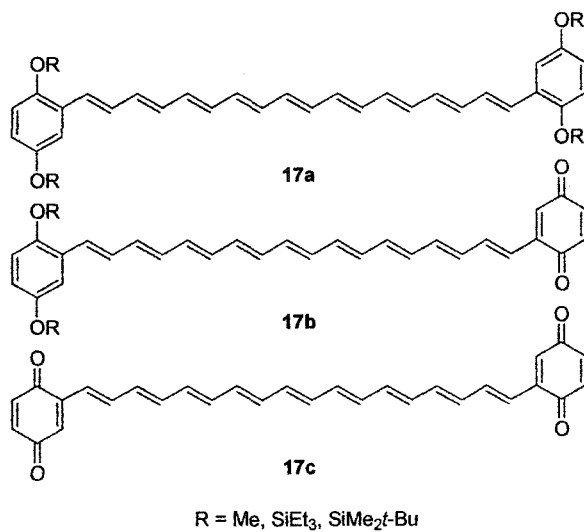
of conjugation. In polyenes with a carotenoid backbone this effect, known as allylic-1,3-strain, also plays a significant role owing to steric interactions of the methyl group and adjacent hydrogens.<sup>134</sup>

Various polyenes with terminally functionalized donor (D), acceptor (A), or redox-active groups have been synthesized with the aim of showing their energy transfer properties or exploring their use as molecular wires.<sup>17,21,25,135-137</sup> For instance, Lehn and co-workers demonstrated that  $\alpha,\omega$ -bis-pyridyl oligoenes, incorporated into vesicle bilayer membranes, function as a molecular wire mediating electron transfer from an external reducing phase to an internal oxidizing phase.<sup>138</sup>

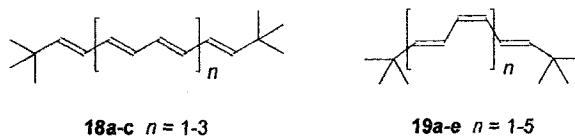
Effenberger and Wolf have synthesized the carotenoid polyenes **13a–16c** with different end-groups to study intramolecular energy transfer process. Interestingly, the interruption of the conjugation by a bicycloalkane unit in the oligomers **15a–16c** resulted in a modified, but still observable energy transfer as evidenced by fluorescence quantum yield measurements.<sup>139</sup>



Duhamel and co-workers have presented a short synthesis of the D-D, D-A, and A-A polyenes **17a-c**.<sup>135</sup> These polyenes, lacking any angular methyl or other groups, show potential as molecular wires for energy transfer and as nonlinear optical chromophores.



Müllen and co-workers have synthesized, via Stille coupling, a homologous series of stable polyenes **18a–c** to study the electron-transfer behavior by cyclic voltammetry.<sup>133</sup> The facility of this route opened up a versatile, alternative approach to the preparation of polyenes without using more conventional methods like the Wittig reaction.<sup>140,141</sup> The oligomers **18a–c** showed high redox activity, with **18c** displaying seven successive reversible charge-transfer events from the tetraanion to trication on the time-scale of cyclic voltammetry. A plot of the HOMO–LUMO energy difference  $\Delta E$  according to the electrochemical data yielded an extrapolated  $\Delta E$  value for PA of 1.7 eV, which is in agreement with the band gap determined experimentally and theoretically for PA itself.<sup>142</sup> A single crystal X-ray structural analysis of the dodecahexaene **18b** revealed a packing structure where the bulky *t*-butyl groups in the spaces between the layers are accommodated in such a way that each polyene chain is surrounded by six neighboring *t*-butyl groups. This arrangement shows a sub-cell structure very similar to that of *trans*-PA as obtained from X-ray diffraction and lattice packing calculations.<sup>143</sup> The authors therefore concluded that **18b** can be regarded as a model compound for the packing in *trans*-PA.



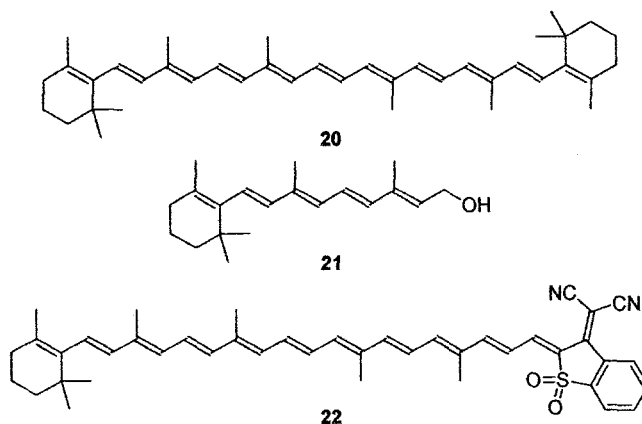
Furthermore, **18a–c** can serve as models for doped PA, since polyenes with six to ten or more double bonds are comparable to the regions of the PA chain becoming charged upon oxidation or reduction.<sup>144</sup> The nature of the electrical conductivity in PA was subject of tremendous experimental and theoretical efforts over recent years and has been addressed in several publications using polyene model oligomers.<sup>145-150</sup> Valence

effective Hamiltonian (VEH) calculations on oligomers of PA have been used to compute ionization potentials, optical transition energies, and electron affinities in PA.<sup>53</sup> These have been found to be in remarkably good accordance with experimentally observed values.

An elegant way to synthesize odd and even polyene oligomers has been presented by Knoll and Schrock.<sup>151</sup> Controlled ring-opening metathesis (ROM) gave access to poly-disperse mixtures of different polyene isomers end-capped by *t*-butyl groups, and those having as many as 13 double bonds were subsequently separated by flash chromatography on silica gel under nitrogen at  $-40\text{ }^{\circ}\text{C}$ . The *trans(cis,trans)*<sub>*n*</sub> series **19** as well as the odd and even series of all-*trans* oligomers containing up to nine double bonds were analyzed in more detail by UV-vis, and <sup>1</sup>H and <sup>13</sup>C NMR spectroscopies. Oligoenes above the heptadecamer (*n* = 17) were found to be rather unstable under the reaction and isolation conditions. Extrapolation by plotting UV-vis absorption data versus *1/n* revealed a HOMO–LUMO gap of 1.79–1.80 eV for an infinite all-*trans* PA chain. In a different study, the same oligomers containing 3–13 conjugated double bonds were then used as model compounds to study the doping process in PA by UV-vis spectroscopy.<sup>145</sup> The Negishi group recently reported a breakthrough work for the iterative construction of (*all-E*)-oligoenes via hydrozirconation-palladium-catalyzed cross-coupling reactions.<sup>152</sup> This method has provided an efficient, selective, and general route to various oligoene species.

*β*-Carotene **20** and vitamin **21** are naturally occurring polyene oligomers and thus were early targets for studying intramolecular energy transfer processes and first and second hyperpolarizabilities. For instance, large molecular third-order optical

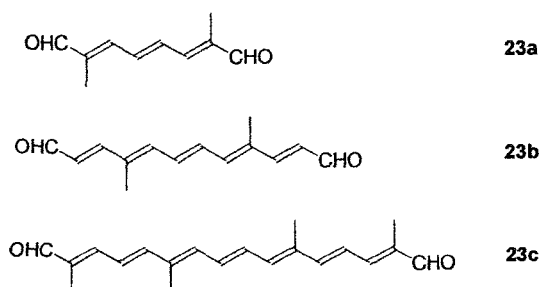
nonlinearities were measured in polarized carotenoids like **22**, displaying a 35-fold enhancement of the second hyperpolarizability  $\gamma$  relative to the symmetrical  $\beta$ -carotene **20**.<sup>153,154</sup> This dramatic increase in  $\gamma$  of **22** as compared with  $\beta$ -carotene, which itself has one of the largest third-order nonlinearities known, has been attributed to symmetry breaking and to the large difference in dipole moments between ground and excited states introduced by the strong terminal acceptor functionality.

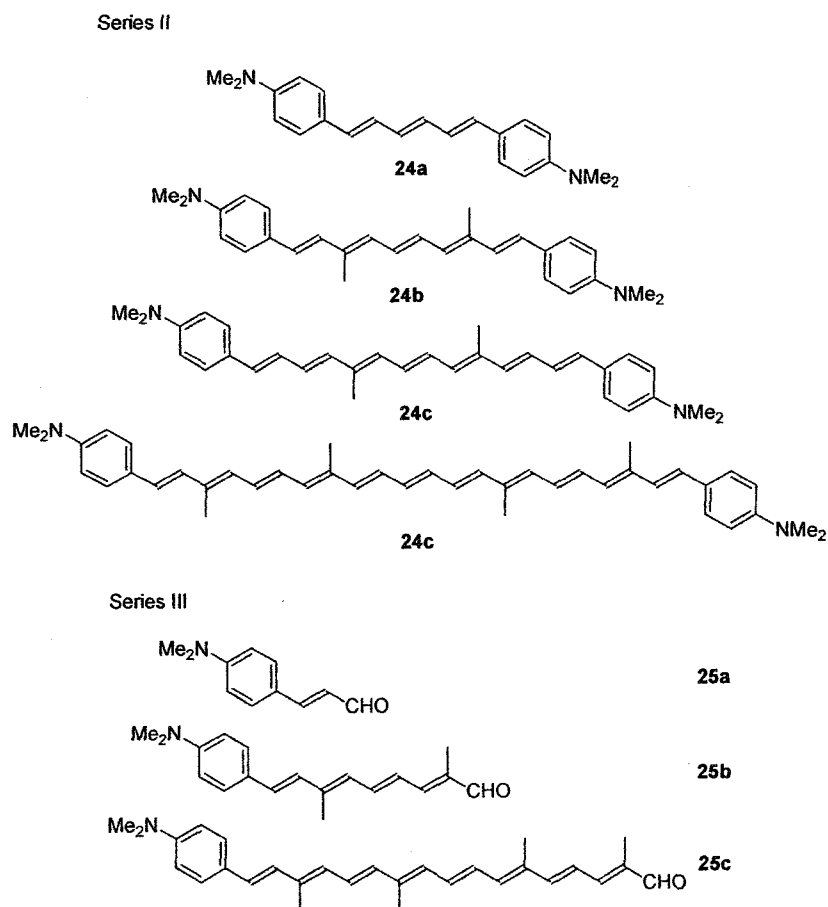


Oligoenes have also served as textbook examples for the correlation between various propounded theoretical models and experimentally observed parameters (e.g., particles in a box model, *vide supra*). Especially in nonlinear optics, combined experimental and theoretical studies have been made using both unsubstituted and D and/or A functionalized oligoenes for establishing design criteria towards conjugated organic molecules with enhanced nonlinear optical response.<sup>155-158</sup> The chain-length dependence on the third-order polarizability in three different series of  $\alpha,\omega$ -polyenes bearing electron-withdrawing (Series I: **23a–c**) or electron-donating end-groups (Series II: **24a–d**) and asymmetric D-A polyenes (Series III: **25a–c**) was systematically studied by Pucetti *et al.* revealing the following trend:<sup>159</sup> 1) In each series of homologous compounds, the lengthening of the conjugated chain induces hyperchromic and

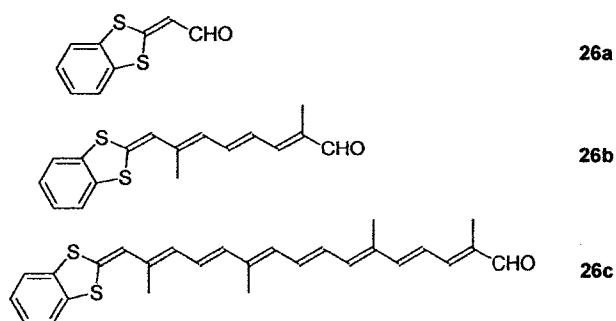
bathochromic shifts in the UV-vis absorption, and each series obeyed the linear dependence of  $\lambda_{\max}$  with the square root of the number of carbon-carbon double bonds as has been previously observed in the case of oligoenes. 2) Measurement of the first hyperpolarizability  $\beta$  by EFISH at 1.34  $\mu\text{m}$  and the second hyperpolarizability  $\gamma$  via THG at 1.91  $\mu\text{m}$  showed a sharp increase in the  $\gamma$  values in all three series of homologous compounds with increasing chain-length. A nonlinear fit according to the relationship  $\gamma = k \cdot n^{\alpha}$  of the  $\gamma$ -values obtained by THG against the number of monomer units  $n$  revealed an exponent of  $\alpha = 2.3$  for the bis-acceptor Series I (23a–c) and 3.0 for the bis-donor Series II (24a–d). 3) Exceptionally large  $\gamma$ -values were observed for the longest bis-donor polyenes and no saturation occurred up to 11 double bonds and for the D-A Series III (25a–d).

Series I





In a similar study using THG and EFISH techniques, the asymmetrically substituted  $\alpha,\omega$ -polyenes **26a-c** were investigated, and an increase in  $\gamma$  by about two orders of magnitude was observed for **26c** as compared with that for **26a**.<sup>160</sup> Experimental results disclosed that, for small numbers of double bonds  $n$ , a power law dependence  $\gamma = k \cdot n^a$  is suitable to approximate the theoretical results in all models, with an exponent  $a$  between 3 and 6. For larger values of  $n$ ,  $\gamma$  becomes linear in  $n$  and  $\gamma/n$  approaches a constant value. The saturation of  $\gamma/n$  in polyenes with very narrow polydispersities obtained by living polymerization techniques has been found by THG measurement (1.9  $\mu\text{m}$ ) to occur at approximately 120 double bonds<sup>161</sup> and thus at considerably longer chain-lengths than theoretically predicted.<sup>162</sup>



Utilizing D-A substituted oligoenes, specially polymethine dyes such as oligomers **27**, Marder and co-workers developed a bond length alternation model (BLA, defined as the difference between the average lengths of carbon-carbon single and double bonds in a polymethine chain) using both experimental and theoretical results to relate the magnitude of the second hyperpolarizability  $\gamma$  to the extent of changes in molecular geometry (Fig. 1.3).<sup>163-166</sup>

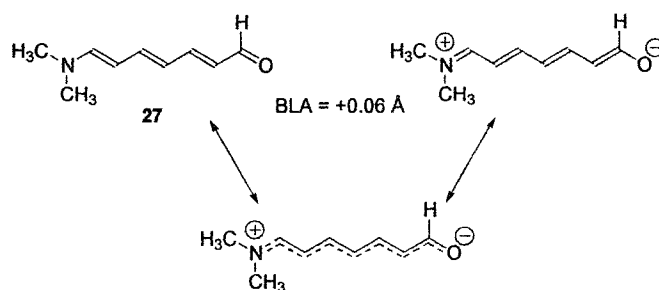


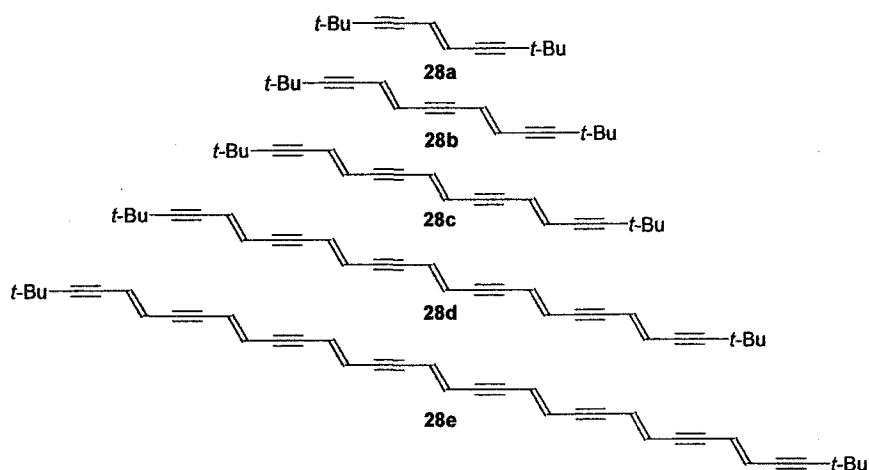
Fig. 1.3 Resonance structures of **27**, with the polymethine form shown in the middle.

By tuning the BLA through chromophoric structures, solvation effects, or an external electrical field,  $\gamma$  could be optimized in either a positive or negative sense for polymethine dyes of a given conjugation length.<sup>167</sup> These same studies, and others,<sup>168</sup> suggested a strong correlation between linear and nonlinear optical properties ( $\alpha$ ,  $\beta$ ,  $\gamma$ ) of conjugated organic molecules and predicted that as the first hyperpolarizability  $\beta$  is maximized for a given chromophore, the second hyperpolarizability  $\gamma$  should approach

zero, suggesting a limit to the ability of D-A substitution to increase  $\gamma$ -values. A more detailed overview on the recent experimental and theoretical progress in the field of nonlinear optics dealing with oligomeric and polymeric chromophores can be found in references.<sup>169-173</sup>

### 1.5.1.2 *Oligoenynes and Oligoenediynes*

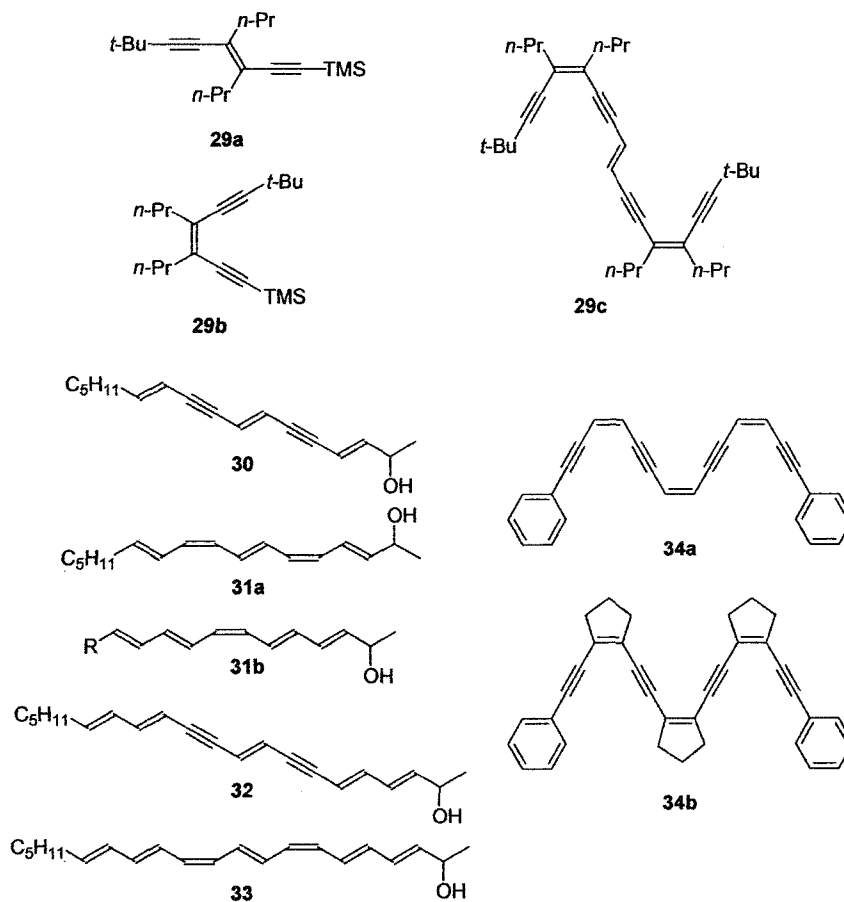
The second representatives in the progression of linearly  $\pi$ -conjugated all-carbon backbones that do not contain aromatic units are polydiacetylenes (PDAs, Fig. 1.2). They represent a unique class of conjugated polymers insofar as PDAs can be obtained as perfect macroscopic single crystals by topochemical solid-state polymerization of suitably pre-arranged and substituted butadiynes,<sup>174-183</sup> a requirement that also severely limits their accessibility. PDAs are not conducting upon doping but show large third-order nonlinear coefficients and are considerably more stable than PAs.<sup>99,184,185</sup> Polyenyne oligomers as model compounds for PDA have been much less investigated than oligoenes in the case of PA. The first systematic series of *trans*-enyne oligomers dates back to 1986 and was published by Wudl and Bitler.<sup>186</sup> They reported the synthesis of *t*-butyl-capped oligomers **28a–e** by a repetitive strategy applying transition-metal-mediated (Ni(0) and Pd(0)) cross-coupling reactions. With increasing chain-length, the color turns from white (**28a,b**) to deep yellow (**28e**) and solubility in *n*-hexane or benzene rapidly decreases.



The *t*-butyl end-caps were found to be essential for high thermal stability, and the oligomers displayed no particular sensitivity to air and light, as is generally observed on the case of oligoenes. Interestingly, **28d** doesn't react with iodine over a period > 24 h, which strongly contrasts the behavior of oligoenes with identical chain-length. In addition, attempts to n-dope a film of **28d** with sodium naphthalenide and 18-crown-6 in ether were unsuccessful.<sup>186</sup>

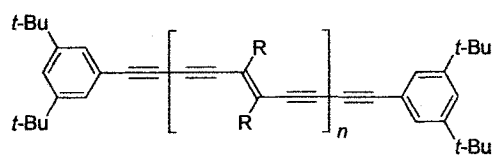
In an in depth study, Giesa and Schulz used the oligoenynes **28a–d** and the substituted compounds **29a–c** as model compounds for PDA and investigated their physical properties by UV-vis, Raman, <sup>1</sup>H and <sup>13</sup>C NMR spectroscopies, and secondary hyperpolarizability  $\gamma$  as a function of chain-length and geometry.<sup>187</sup> The ECL in PDAs was calculated to be around 10 monomer units, with an extrapolated optical absorption energy towards an infinite chain-length of  $V_0 = 2.25$  eV ( $\lambda_{\max} = 551$  nm, see Wenz's equation in Table 1.1).<sup>187</sup> The construction of stereo-defined oligomers **30–33** with double and triple bonds of limited conjugation length by Pd(0)-catalyzed reactions from readily available precursors has been reported by Crousse *et al.*<sup>188</sup> These compounds may help to generate a deeper insight into the influence of geometry (*Z/E*) or bond type

(double vs. triple bond) on various physical properties. A series of phenyl-terminated *cis*-oligodiacetylenes **34a-b** was constructed by Hirsch<sup>189</sup> and co-workers via an iterative approach using Pd-catalyzed Sonogashira coupling protocol. In the solution of oligomer **34a**, a clear *cis/trans* isomerization is observable in the <sup>1</sup>H NMR spectrum. To avoid such a drawback, a ring system was incorporated onto the ene moiety to yield a derivative **34b** that is stable in both solution and solid state. Furthermore, X-ray crystallographic analysis and computational investigation suggest that these oligoenynes prefer a helical conformation in solution.



Another linearly  $\pi$ -conjugated polymer without aromatic repeat units in the series that starts with PA and PDA is polytriacetylene (PTA, see Fig. 1.2). Whereas the chemistry and physical properties of PA and PDA oligomers and polymers had been

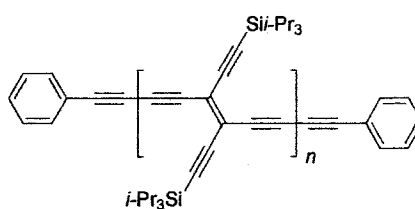
investigated for about two decades, much less is known about PTAs, which were reported for the first time in 1994.<sup>40,190</sup> Despite this late discovery, the synthetic accessibility of PTAs and functional derivatives by simple oxidative acetylenic coupling is more versatile than that of PAs and PDAs. Furthermore, the additional acetylenic moiety in each repeat unit of PTAs increases the spacing between laterally appended side chains. As a consequence, intramolecular steric repulsions that cause distortion of the linearly  $\pi$ -conjugated backbone from planarity are avoided. Similar to PDAs, PTA polymers such as **35** and **36** were not found to be conductive upon doping.<sup>190</sup>



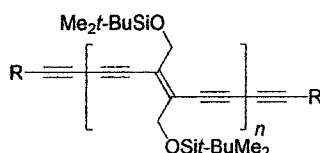
	R	$X_n$	$M_n$
<b>35</b>	$\text{C}\equiv\text{C}-\text{Si}i\text{-Pr}_3$	22	9600
<b>36a</b>	$\text{CH}_2\text{OSi}i\text{-BuMe}_2$	31	11300
<b>36b</b>	$\text{CH}_2\text{OSi}i\text{-BuMe}_2$	22	8000

The first series of monodisperse PTA oligomers (oligoenediynes) prepared were the phenylacetylene endcapped compounds **37a–e** that contained tetraethynylethene (TEE, 3,4-diethynylhex-3-ene-1,5-diyne) repeat units.<sup>40,42,190,191</sup> These compounds are highly colored and extended in length up to about 5 nm. Nevertheless, they are amazingly kinetically stable, high-melting materials that remain unchanged for months when exposed to air at ambient temperature. The X-ray crystal structure of **37b** displayed a perfectly planar  $\pi$ -conjugated backbone including the two terminal phenyl rings. The optical band gap for the series **37a–e** extrapolated to infinite chain length was estimated to be  $E_g = 2.3$  eV (536 nm), which is comparable to that of many PDAs ( $E_g = 2.1$  eV).<sup>40</sup> Electro-chemical analysis of these  $\pi$ -conjugated rods revealed interesting

redox properties. While none of the oligomers **37a–e** could be oxidized below +1.0 V in THF (versus Fc/Fc<sup>+</sup>), which helps to explain their amazingly high stability in air, they were all readily reduced with the number of reversible, one-electron reduction steps corresponding to the number of TEE moieties in each oligomer. Furthermore, the first electron transfer was strongly shifted to less negative potentials with increasing number of monomer units; thus, the first reduction of **37a** occurs at  $E^{\ominus} = -1.57$  eV (versus Fc/Fc<sup>+</sup>, in THF +0.1 M Bu<sub>4</sub>NPF<sub>6</sub>) whereas the first reduction of **37e** is much more facilitated and occurs at  $-1.07$  eV.<sup>40</sup>



**37a-e**  $n = 1-5$



**38a-f**  $n = 1-6$       R = SiMe<sub>3</sub>  
**39a-g**  $n = 1,2,4,6,8,12,16$       R = SiEt<sub>3</sub>

The Me<sub>3</sub>Si endcapped oligoenediynes **38a–f** with *trans*-1,2-diethynylethene (DEE, (*E*)-hex-3-en-1,5-diyne) repeat units displayed significantly enhanced solubility and processability relative to the tetraethynylethene oligomers **37a–e** as a consequence of the more flexible Me<sub>2</sub>*t*-BuSiOCH<sub>2</sub> side chains.<sup>38</sup> These compounds ranged from a 0.96 nm long monomeric to a 4.61 nm long hexameric rod and allowed for a comprehensive investigation of structure-property relationships in PTAs. By extrapolative evaluation of linear optical and nonresonant third-order nonlinear optical data, the ECL of PTAs was

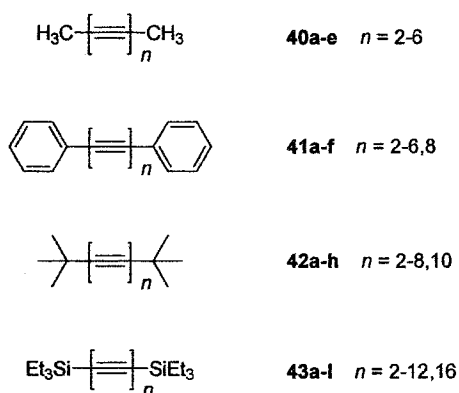
predicted to lie in the range of seven to ten monomer units, which corresponds to 21 or 30 conjugated double and triple bonds, respectively.<sup>38</sup> Furthermore, a plot of  $\gamma/n$  versus  $n$  for the PTA samples **38a–f** revealed an exponential correlation for  $\gamma$  with a fitted exponent  $a = 2.5 \pm 0.1$ .

For a direct determination of the ECL, the Et<sub>3</sub>Si-endcapped monodisperse oligomers **39a–g** containing  $n = 1, 2, 4, 6, 8, 12, 16$  monomeric units were prepared by a rapid and efficient statistical deprotection-oxidative oligomerization protocol.<sup>192</sup> Longer-chain monomers were used as starting materials for the preparation of the higher oligomers ( $n = 8, 12, 16$ ) in order to reduce separation problems by SEC. The gap between oligomer and polymer analysis was closed with the completion of this series of PTA oligomers. All compounds up to hexadecamer **39g** featured good solubility in apolar solvents, which allowed a direct determination of the ECL by means of UV-vis spectroscopy. This study revealed as accurate the previously predicted value of  $n_{\text{ECL}} = 10$ . Raman scattering studies of oligoenediyne **39a–g** showed an exponential decrease in the frequencies of carbon-carbon triple and double bond stretches respectively, with lengthening of the  $\pi$ -conjugated backbone, and plots of triple bond stretching frequencies as a function of  $n$  also revealed an ECL of ten monomer units. PTA monomers (TEEs and DEEs) and dimers substituted at the terminal alkynes with donor (D; *p*-*N,N*-dimethylaminophenyl) and/or acceptor (A; *p*-nitrophenyl) groups were found to display very high second hyperpolarizabilities  $\gamma$ , which were determined by THG measurement.<sup>170,193,194</sup> The second-order nonlinear optical properties of these compounds are also quite appealing.<sup>195</sup> Likewise, the photochemical *trans-cis* isomerization of such compounds was investigated comprehensively.<sup>196</sup> Their photochemical behavior differs

substantially from that of similarly substituted stilbenes and azobenzenes since, in contrast to the latter, both *cis* and *trans* isomers of the D/A-substituted TEEs display fully planar conjugated  $\pi$  chromophores.

### 1.5.1.3 Oligoynes

A challenging aspect of carbon chemistry is the preparation of infinite one-dimensional rods composed exclusively of alkyne units, which seem to be the ultimate prototype for carbon-based molecular wires.<sup>197</sup> The corresponding polymer, carbyne  $C_{\infty}$ , gained early interest as a hypothetical carbon allotrope which could behave as a novel electrical conductor.<sup>198</sup> The inability of attaching side-chains to oligoynes to provide solubility, stability, or for fine-tuning of physical properties is a significant drawback and severely limits the use of this oligomer class. Nevertheless, the intense synthetic activity in preparing oligoynes for predicting carbyne properties led to three series of oligomers, namely **40a-e**,<sup>199</sup> **41a-f**,<sup>200-202</sup> **42a-h**,<sup>203,204</sup> containing up to 20 linearly conjugated carbon atoms.

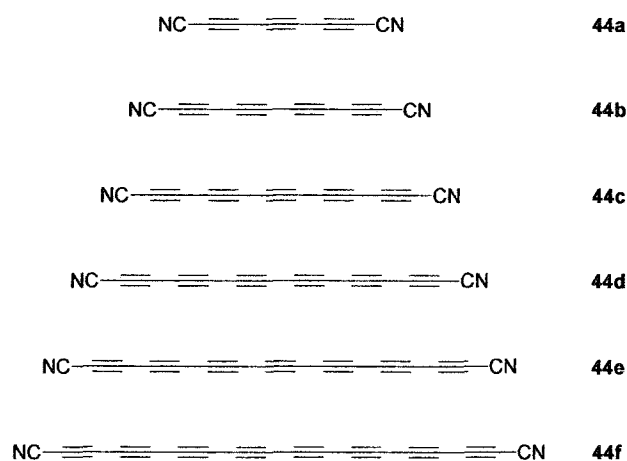


Walton and co-workers describe the bis-triethylsilyl-protected oligoynes series **43a-l**. Oligomer **43l**, which is composed of 16 conjugated  $\text{C}\equiv\text{C}$  units, represents the longest oligoyne reported so far, but has never been completely characterized.<sup>205</sup> The

oligomers **43a–l** were constructed by repeated oxidative Hay-coupling of mono-protected oligoynes, which were obtained by statistical deprotection with methanolic NaOH of the appropriate precursor and subsequent chromatographic separation. The authors measured not only the UV-vis spectra of the protected series **43a–l**, which displayed distinctive fine-structured absorption, but also of the corresponding deprotected oligomers up to the undecamer. The low solubility and chemical stability of the deprotected oligoynes allowed only operations under high dilution conditions and prevented accurate determination of extinction coefficients by UV-vis spectroscopy. The same group also reported the synthesis of asymmetrically substituted (*t*-butyl-, phenyl-, triethylsilyl-end-capped) oligoynes containing up to 6 C≡C units prepared by mixed oxidative Hay-coupling using one the reaction partners in huge excess.<sup>205</sup> An alternative way to access odd and asymmetrically substituted oligoynes utilizes the Cadiot-Chodkiewicz cross-coupling reaction. Eastmond and Walton applied this methodology to the synthesis of a mono-silylated triyne, bearing differently substituted phenyl groups.<sup>206</sup> In the same study, the germanium analogue of triethylsilylacetylene was utilized as a protecting group. The cleavage of the Ge-acetylene bond under acidic condition (unlike their silicon counterparts) may serve as an alternative protection scheme to base-sensitive oligoynes.<sup>207-210</sup>

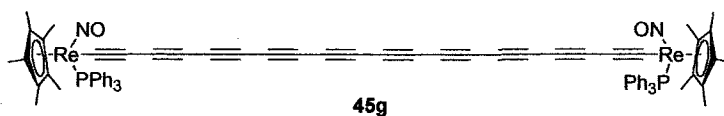
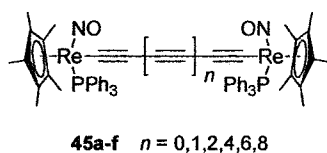
In a comprehensive study, Hirsh and co-workers presented the one-step synthesis, isolation, spectroscopic characterization (by UV-vis, IR, <sup>13</sup>C NMR spectroscopy, cyclic voltammetry), and computational investigation of the rod-shaped  $\alpha,\omega$ -dicyanopolyynes **44a–f**.<sup>211</sup> Together with the already known smaller representatives NC-CN, NC-C≡C-CN, and NC-C≡C≡C-CN,<sup>212</sup> oligomers **44a–f** form a continuous homologous series of

oligoynes. The compounds **44a–f** were prepared by vaporization of graphite under Krätschmer-Huffman condition in the presence of dicyan ((CN)<sub>2</sub>), allowing convenient access to the new oligomers and avoiding tedious successive acetylene couplings. Oligoynes of similar constitution to **44a–f** such as HC<sub>*n*</sub>N (*n* = 1,3,5,7) have been detected by Hare and Kroto as molecules in interstellar space.<sup>213</sup>

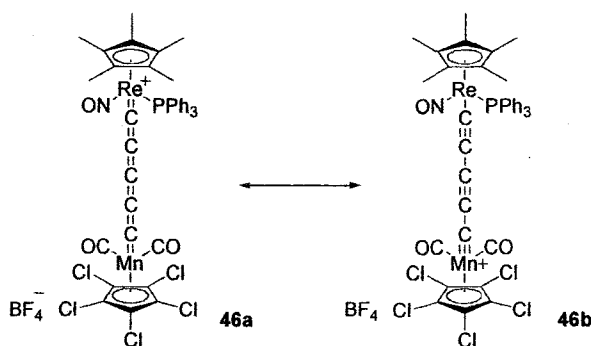


In order to explore charge transfer and electron delocalization process, Gladysz and co-workers have prepared the one-dimensional symmetrically metal end-capped molecular wires **45a–g** using a step-growth approach.<sup>214-217</sup> The dirhenium  $\mu$ -oligoynediyl complexes **45a–g** were synthesized by a combination of Cu-catalyzed oxidative and cross-coupling reactions and displayed a surprisingly high environmental stability which allowed an extensive investigation of their physical properties. The redox-active Re(I) end-groups undergo a reversible oxidation to the +2 state, with a potential separation of the two distinct oxidation events in **45a** of 0.53 V. As the conjugated spacer between the metal centers, and thus the “resistance” of the bridge increases, the two oxidations start to behave independently and merge to give a single—presumably two-electron—oxidation for **45g**, which represents with its C<sub>20</sub>-chain, the longest oligoyne between two terminal

metal centers reported so far. Surprisingly, as the carbon chain lengthens in this series, the first oxidation potential becomes thermodynamically less favorable.

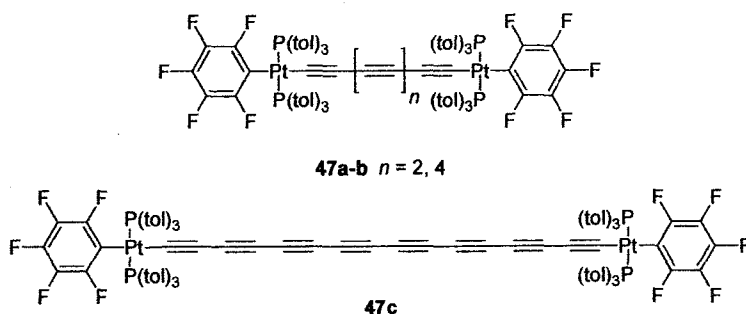


The same group reported on the asymmetrically substituted oligomer **46** with an odd number of carbon atoms between the two metal centers. This was found to be extremely light sensitive and decomposed on the time scale of hours in the dark at room temperature.<sup>218</sup> However, from IR measurement it became apparent that the cumulene resonance form **46a** dominated over the alternative acetylene resonance structure **46b** in such a type of complexes and absorptions at  $\lambda_{\text{max}} = 634$  nm in the UV-vis spectrum suggest appreciable rhenium-to-manganese charge transfer character.

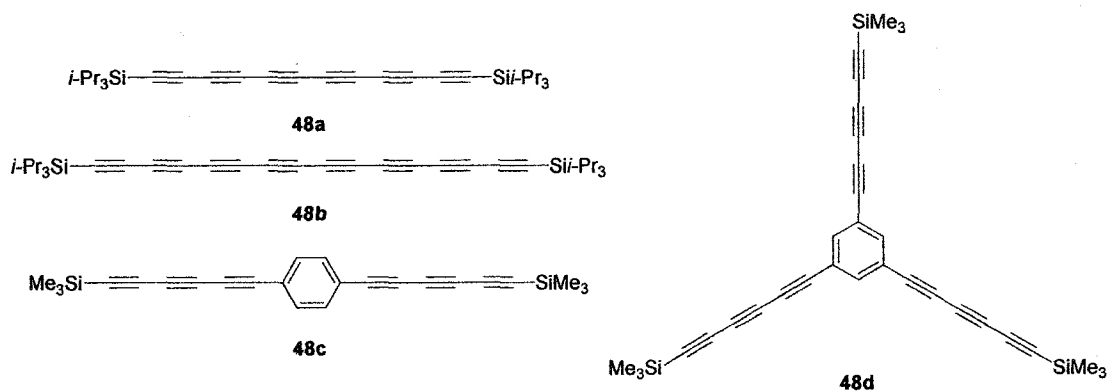


Gladysz and co-workers<sup>219</sup> has also successfully constructed platinum endcapped oligoynes **47a–b** through oxidative homocoupling reactions, and elucidated their solid-state structural properties by X-ray crystallography. Interestingly, a dramatic curvature shape was observed in the single crystal structure of hexayne **47b**, showing the most bent

feature for a polyynes to date. However, the longer-chain octayne **47c** shows a much straighter and slightly S-shaped geometry.



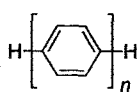
Tykwinski and Eisler<sup>220</sup> recently reported the synthesis of polyynes species using a modified Fritsch-Buttenberg-Wiechell method,<sup>221</sup> where an alkyne moiety migrated in a carbenoid pathway to generate the polyynes species. Triisopropylsilyl-end-capped hexayne **48a** and octayne **48b**<sup>222</sup> and phenyl-linked polyynes **48c-d** have been exemplified in their research, which were characterized by  $^1\text{H}$  and  $^{13}\text{C}$  NMR spectroscopy, and X-ray crystallography. Furthermore, this methodology has provided a high-yielding alternative way to obtain polyynes instead of the conventional Cu-based coupling reactions.



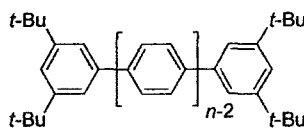
## 1.5.2 $\pi$ -Conjugated Oligomers Containing Aromatic Backbones

### 1.5.2.1 Oligo(p-phenylene)s

Poly(*p*-phenylene) (PPP) has gained considerable interest over the last years since it acts as an excellent organic conductor upon doping. Whereas the neutral form PPP is an insulator displaying conductivities down to  $10^{-12} \Omega^{-1} \text{ cm}^{-1}$ , doping raised its conductivity into the metallic region with values around  $500 \Omega^{-1} \text{ cm}^{-1}$ .<sup>223,224</sup> In addition, PPP polymers were also found to exhibit nonlinear optical activity.<sup>225</sup> It is therefore not surprising that PPPs have become one of the most widely investigated polymers as documented by several review articles,<sup>48,132,223,224,226-235</sup> which deal with their synthesis and various physical properties. The second interesting aspect of PPP materials comes from the fact that oligomers and polymers with PPP backbone and derivatives of PPP can be used as the active component in blue light-emitting devices (LEDs).<sup>66,233,236-239</sup> Although poly(*p*-phenylene)s often exhibit remarkable thermal stabilities, which make them attractive candidates for numerous applications requiring thermally robust  $\pi$ -conjugated organic materials, their low solubility and intractability still remain challenging for the commercial development of this polymer class.<sup>223</sup> The structurally related and more soluble oligomers like oligo(*p*-phenylene)s **49a–h** also show a rapid decrease in solubility with increasing chain-length,<sup>224,240,241</sup> but solubility can be slightly enhanced by addition of *t*-butyl groups on the terminal aryl rings like **50a–d**.<sup>242,243</sup> As expected, the ECL determined by linear absorption spectroscopy for both series **49a–h** and **50a–d** was found to be in good agreement yielding  $n = 9$  and 11, respectively.<sup>49</sup>



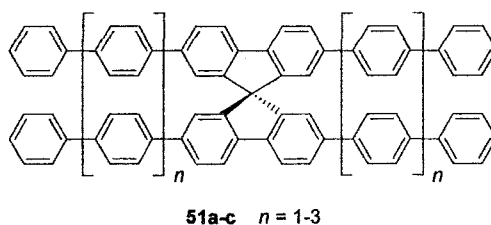
**49a–h**  $n = 1-8$



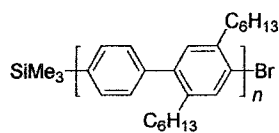
**50a–d**  $n = 2-5$

An interesting feature of oligo(*p*-phenylene)s has been reported by Yanagida and co-workers.<sup>244</sup> They studied oligomers **49c–f** as well-defined model compounds for PPP in a homogeneous photocatalysis process, which leads to the simultaneous formation of hydrogen and ethanol upon laser flash photolysis of **49c–f** in aqueous triethylamine in the presence of RuCl<sub>3</sub>.

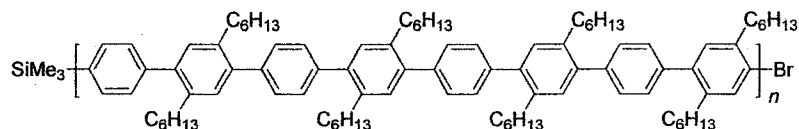
Spiro-linked oligo(*p*-phenylene)s like **51a–c** have been used as blue emitters in electroluminescent applications. They are soluble in common solvents, show glass transition temperatures up to 250 °C, and with their high photoluminescence quantum efficiencies in the solid state, present an alternative to high molecular weight PPP polymers.<sup>245</sup>



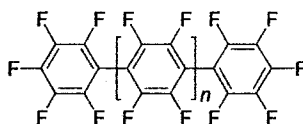
Using Suzuki cross-coupling reactions of boronic acids and aromatic halides under Pd(0)-catalysis, Schlüter and co-workers prepared in a repetitive sequence the rigid rods **52a–d** with up to 16 phenylene rings and orthogonal functional groups at both termini.<sup>246</sup> The substituted oligomers **52d** represents the longest monodisperse oligo(*p*-phenylene) reported so far. Recently, Heidenhain *et al.*<sup>247</sup> reported the synthesis of a class of perfluorinated PPP oligomers **52e–h**. Although these oligomers are insoluble in common organic solvents, they can be readily purified by train sublimation as colorless solids and used for characterization. Furthermore, OLED were fabricated using oligomers **52e–h** as electron transport layer, which have shown efficient n-type semiconducting properties and high electron mobilities.



**52a-b**  $n = 1,2$

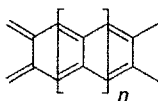


**52c-d**  $n = 1,2$

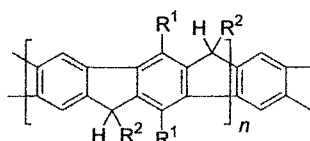


**52e-h**  $n = 3,4,5,6$

The planarization of oligo- and poly(*p*-phenylene)s to maximize the extent of conjugation by enhancing  $\pi$ -orbital overlap has been of interest for many years. One possible approach in pursuing this objective is the connection of adjacent aryl groups by 1,2-annulation rather than linear 1,4-connection as in the case of classical PPP. For instance, linear [*n*]acenes **53** were found to have low band gap energies, and thus are inherently sensitive towards oxidation and dimerization.<sup>248-250</sup> Another approach toward the planarization of the classical PPP backbone is to introduce  $\alpha,\alpha'$ -connected methylene bridges. This route has given the low band gap polymer **54**,<sup>251-255</sup> which is of theoretical interest owing to its electronic properties and the possibility of topological isomers. The ladder polymer **54**, and its functionalized derivatives, exhibit very attractive optical and electronic properties, such as extremely small Stoke shifts. They are also highly electroluminescent when used as the emitter materials in LEDs.<sup>256,257</sup>



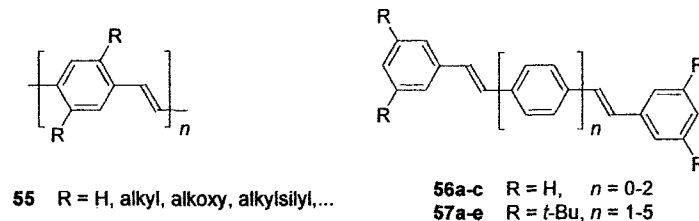
**53**



**54**  $R^1 = C_6H_{13}$ ,  $R^2 = -1,4-C_6H_4-C_{10}H_{21}$

### 1.5.2.2 Oligo(*p*-phenylene vinylene)s

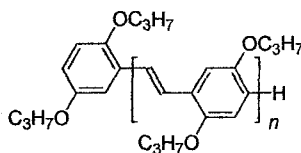
The report of Friend and Holmes<sup>14</sup> in 1990 that light-emitting devices can be constructed from poly(*p*-phenylene vinylene) (PPV, **55**) films has provided a highly stimulating impetus to the field of  $\pi$ -conjugated organic molecules, and polymers with the PPV backbone are now among the most extensively studied.<sup>233,236,258</sup> The physical and electronic properties of PPV and its substituted derivatives have attracted much attention both from experimental and theoretical scientists.<sup>259,260</sup> Molecular engineering has allowed the controlled manipulation of the HOMO–LUMO gap energy in PPV-based polymers, copolymers, and blends, allowing the manufacture of electroluminescent materials for the construction of LEDs<sup>237,261–268</sup> with light emission covering the whole visible spectrum, and light-emitting electro-chemical cells (LECs).<sup>269</sup> Even difficult to achieve blue light-emitter can be fabricated from PPV owing to polymers containing regions with limited conjugation length or short oligomers of the PPV type as side-chain chromophores.<sup>270,271</sup> In this respect, oligo(*p*-phenylene vinylene)s such as **56a–57e** have contribute to the drive to achieve a basic understanding of the optical properties of PPV polymers.<sup>49</sup> It is worth noting that PPVs as emitter materials could also be successfully applied to the fabrication of organic-based lasers.<sup>272</sup>



Several groups have studied the photoexcited state behavior of PPVs utilizing PPV oligomers of defined length and constitution in order to determine structure-property relations and to gain information about their decay behavior.<sup>273-277</sup> Recently, Yu and co-

workers<sup>278</sup> elegantly studied the LED performance as a function of conjugation length for an alkylated hexameric and decameric oligo(*p*-phenylene vinylene), which allowed uniform films to be obtained by spin-casting. Whereas UV-vis, photoluminescence, and electroluminescence spectra showed small shifts for the two oligomers, the decamer device displayed a lower turn-on voltage, a smaller operation current, and greater stability than the hexamer device. Furthermore, it has been demonstrated that oligo(*p*-phenylene vinylene)s can be vacuum evaporated to yield high purity thin films, which are studied in order to gain insight into solid-state structural aspects of conjugated materials.<sup>279</sup>

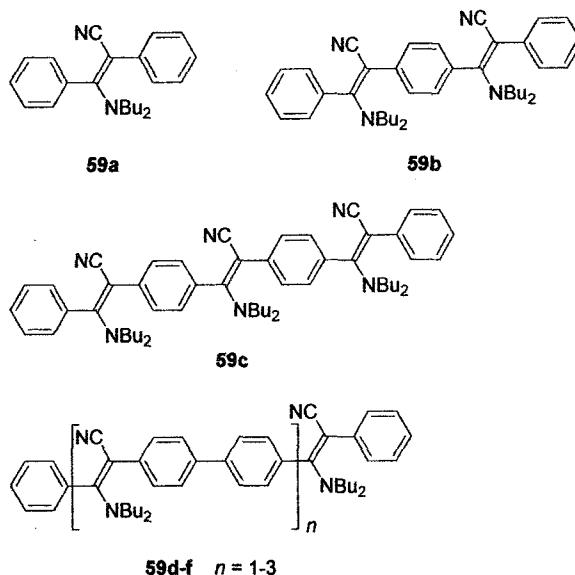
The ECL of the longest-wavelength absorption maximum  $\lambda_{\max}$  for the series **57a–e** was estimated to be  $n = 10$  monomer units and thus is in surprisingly good accordance with the value obtained for oligo(*p*-phenylene)s **50a–d** ( $n = 11$ ) considering the less sterical hinderance in the former system.<sup>280,281</sup> The longest monodisperse oligo(*p*-phenylene vinylene)s synthesized are the dialkoxy substituted oligomers **58a–h**.<sup>49,282</sup> With the longest oligomer **58h** ( $n = 15$ ) saturation of  $\lambda_{\max}$  was indeed attained, nicely conforming with the experimentally estimated ECL value of about  $n = 10$  monomer units found for the unsubstituted series **57a–e**. Oligomers and polymers of type **58** were also subject to a systematic investigation of their photoreactivity and photoconductivity in order to optimize the photoconducting properties of dialkoxy substituted PPVs.<sup>283</sup>



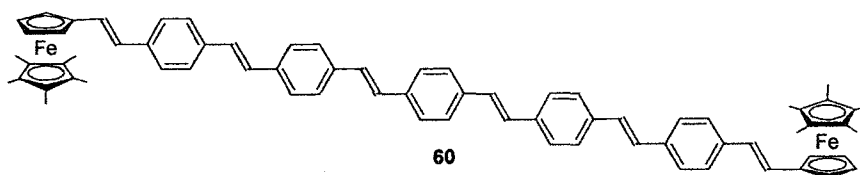
**58a–h**  $n = 1,2,3,4,6,8,11,15$

The third-order nonlinear optical susceptibility  $\chi^{(3)}$  of thin film of oligo- and poly(*p*-phenylene vinylene)s measured by THG using variable laser wavelengths from 900 to 1520 nm revealed general scaling laws for PPV and related oligomers, as well as other one-dimensional  $\pi$ -conjugated polymers.<sup>110</sup> For the scaling relationship  $\chi^{(3)}/\alpha_{\max} \sim \lambda_{\max}^x$ , where  $\alpha_{\max}$  and  $\lambda_{\max}$  denote the absorption coefficient and the wavelength of the lowest-energy absorption maximum, respectively, an exponent  $x = 10 \pm 1$  was found, which is much larger than the theoretically predicted value of  $x = 6$  by Hückel calculation.<sup>110</sup>

The donor/acceptor substituted oligo(*p*-phenylene vinylene)s **59a–f** were prepared by an elegant cation-anion coupling sequence, targeting NLO chromophores with enhanced hyperpolarizabilities owing to large lateral dipole moments.<sup>251</sup> In contrast to unsubstituted PPV, which possesses an ECL of about  $n = 10$  monomer units, convergence of the  $\lambda_{\max}$ -value occurs in the D-A systems **59a–f** after only 5–6 units. The fluorescence of the oligomers is effectively quenched, and the compounds stabilize, according to cyclic voltammetry measurement, both positive and negative charges equally well. However, configurational and conformational isomers and Coulombic repulsion between the individual dipole centers prevent a significant additivity of the individual dipoles (**59a**:  $\mu = 6.12$  D; **59f**:  $\mu = 9.35$  D).

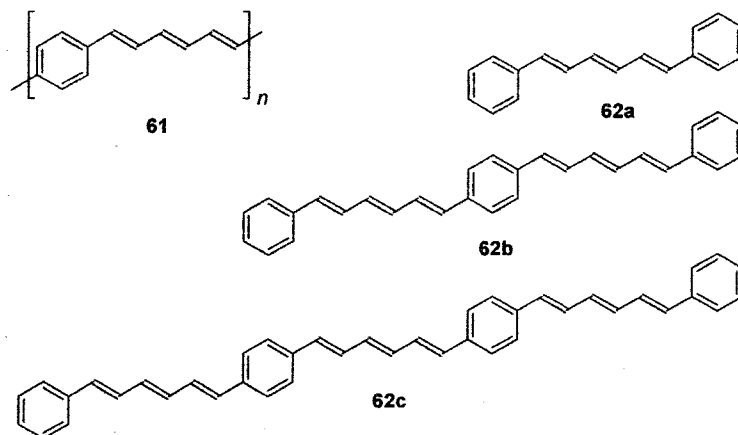


The *p*-phenylene vinylene molecular wire **60** with terminal ferrocenes and a metal-to-metal distance of 4 nm has been prepared by the groups of Bildstein, Schottenberger, and Launay.<sup>284</sup> The pentamethylated ferrocenes in **60** showed increased solubility in combination with enhanced stability of the oxidized states compared to the nonmethylated analogues. Therefore, compounds such as **60** are promising materials for studying electron transfer process across a conjugated  $\pi$ -chain. Another example for a model compound to study electron transfer process is the PPV hexamer terminated with porphyrin groups synthesized by Ono *et al.*<sup>285</sup>



An expanded version of PPV, poly(1,4-phenylenehexa-1,3,5-trienylene) (PPHT) **61** has been presented by Sonoda and Kaeriyama.<sup>286</sup> Preliminary investigations of the model oligomers **62a–c** showed that PPHT undergoes easily thermally induced *cis-trans*

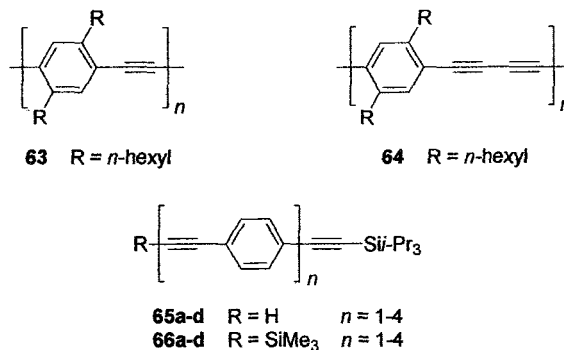
isomerization under iodine catalysis and displays a significant bathochromic shift in UV-vis absorption compared to PPV.



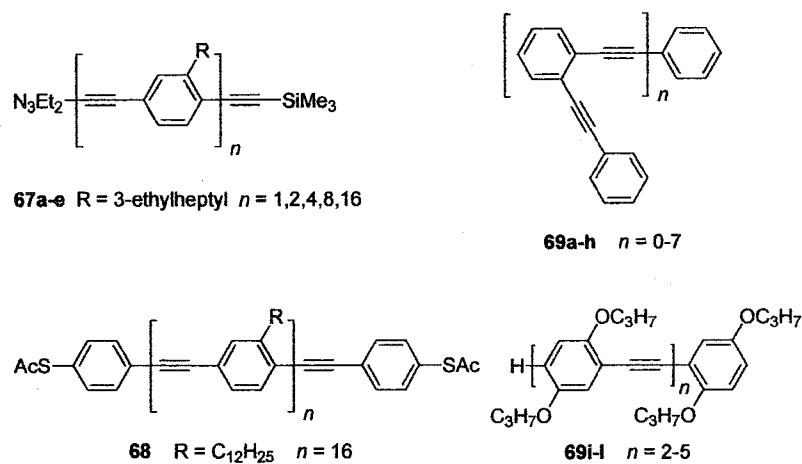
### 1.5.2.3 Oligo(*p*-phenylene ethynylene)s

The tremendous advances in the chemistry and physics of PPV over recent years have stimulated further interest in related types of structures, such as the poly(*p*-phenylene ethynylene) (PPE) polymers like **63**, which can be viewed as dehydrogenated PPVs, or the poly(*p*-phenylene butadiynylene) **64**.<sup>287,288</sup> Owing to their high degree of rigidity, PPEs exhibit large photoluminescence efficiencies both in solution and in the solid state and their extremely stiff, linear backbone enables maximum orientation, which is an important feature for the preparation of oriented films or blends. Their potential as photoluminescence materials in organic polymer based devices<sup>289,290</sup> or as fluorescent chemosensors<sup>291</sup> has already been demonstrated. Additionally, various oligo(*p*-phenylene ethynylene) spacers for the modular construction of organometallic nonlinear optical chromophores have been designed.<sup>292</sup> Furthermore, Moore and co-workers recently demonstrated that oligo(*m*-phenylene ethynylenes) can spontaneously adopt a stable helical conformation having a large cavity, and thus are valuable tools for studying folding processes in polymer systems.<sup>293</sup> Using palladium-copper-mediated cross-

coupling reactions, Dixneuf and co-workers prepared the two oligo(*p*-phenylene ethynylene) series **65a–d** and **66a–d**, which were characterized by IR and NMR spectroscopies, MS, and elemental analysis.<sup>294</sup>



In an attempt to span the lithographically-derived probe gaps of two gold electrodes with a single molecule or with small packets of molecules, the group of Tour has synthesized via an iterative divergent/convergent approach the 128 Å long oligo(*p*-phenylene ethynylene) **67e**.<sup>295,296</sup> As binding sites for adhesion to the gold surfaces in the longest known oligo(*p*-phenylene ethynylene) **68**<sup>297</sup> thiol ene-groups were used, protected as thioacetyl moieties which undergo cleavage under mildly basic conditions.<sup>298</sup> The whole series **67a–e** provided useful information about the optical properties of PPE polymers as a function of chain-length. Experimentally, Tour and co-workers observed saturation for the longest-wavelength absorption  $\lambda_{\text{max}}$  of compounds **67a–e** in the range of *n* = 10 monomer units.<sup>295</sup> Interestingly, Meier *et al.* predicted for exactly the same series a considerably lower ECL of *n* = 5 repeating monomers.<sup>49</sup>



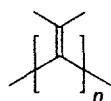
Bumm *et al.* used the recent developments in scanning-tunneling microscopy (STM) methodology to directly measure the conductivity through a single organic molecule.<sup>299</sup> They self-assembled a small number of short PPE oligomers into a monolayer film of non-conjugated thioalkanes on a gold surface, where the molecular “wire” protruded about 7 Å above the insulating layer. By searching on the top of the layer, a significantly enhanced current flow was found, when the STM probe tip was in contact with one of the conjugated molecules as compared to the insulating monolayer. In a different experimental set-up, using the mechanically controllable break junction, Tour and co-workers measured the conductance of a junction containing a single benzene-1,4-dithiol molecule.<sup>300</sup>

A set of conjugated *ortho*-linked oligo(*o*-phenylene ethynylene)s **69a-h** were synthesized by Grubbs and Kratz according to classical Pd(0)-mediated methodologies.<sup>301</sup> The white to slightly tan solids dissolve well in benzene and show no tendency for reduction under cyclic voltammetry conditions but rather undergo irreversible oxidations in CH<sub>2</sub>Cl<sub>2</sub>. Combined UV-vis spectroscopic and single X-ray crystal structure studies of **69c** and **69d** indicated that rotation about the C(sp)–C(sp<sup>2</sup>) bonds is facile, allowing for a helical orientation of the *o*-phenylene ethynylene moieties.

Meier and co-workers synthesized a series of oligo(1,4-phenyleneethynylene)s **69i-1** with solubilizing propoxy side chains using Hagihara-Sonogashira coupling reactions.<sup>302</sup> Electronic absorption spectral analysis of **69i-1** shows a bathochromic shift of  $\lambda_{\text{max}}$  with the increase of chain length  $n$ . Furthermore, a superlinear increase of the second hyperpolarizability  $\gamma$  against  $n$  is also obtained from THG measurements. These data demonstrated that the  $n_{\text{ECL}}$  is greater than 5.

### 1.5.3 Cross-conjugated Oligomers

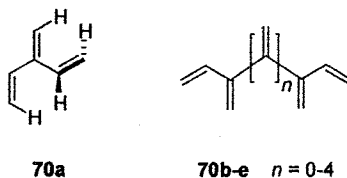
Cross-conjugated oligomers have potential for applications as electronic (e.g., organic conducting and semiconducting) and optical (third-order NLO) materials. However, compared to their linearly conjugated oligomers counterparts, this class of oligomers is still far less studied and understood. The first members of cross-conjugated oligomeric series are the  $[n]$ dendralenes,<sup>111,303</sup> the simplest acyclic cross-conjugated hydrocarbons.



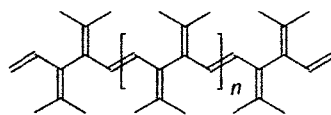
Dendralene

Almennnigen and co-workers<sup>115</sup> elucidated the structural properties of [3]dendralene **70a** by electron diffraction, vibrational, NMR and UV-vis spectroscopies. Rather than adopting a planar conformation to gain the maximum conjugation, an *anti-skew* conformation (as shown in **70a**) is found to be the most stable conformation for [3]dendralene **70a**. Originally, dendralenes, in particular [3]dendralene, drew attention for synthetic applications (e.g., as a tandem-annelating reagent or diene in Diels–Alder additions) rather than their unique  $\pi$ -electron delocalization mode. Although the endeavors to synthesize  $[n]$ dendralenes and their derivatives started many decades ago,

the first successful completion of the dendralene family **70a–e** was achieved by Sherburn and co-workers using an elegantly-designed 3-sulfolene masking-unmasking strategy.<sup>304</sup> The dendralene oligomers **70a–e** were fully characterized by IR, <sup>1</sup>H and <sup>13</sup>C NMR spectroscopies, and mass spectrometry. Their UV-vis spectra display a single maximum absorption  $\lambda_{\text{max}} = 219.8\text{--}232.2$  nm (whereas a butadiene shows  $\lambda_{\text{max}} = 217$  nm), confirming the nonplanar, nonconjugated arrangement of *s-trans*-1,3-butadiene and ethylene units in these molecules. This result is in accordance with the study by Davis and co-workers, where the molecular structures of [4]dendralene were investigated using gas-phase electron diffraction (GED) and *ab initio* computation methods.<sup>305</sup>

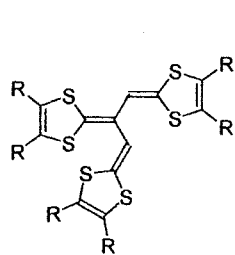


Grubbs and Swager<sup>306</sup> reported the synthesis of a cross-conjugated polymer **71**, containing a [3]dendralene repeating unit, using ring-opening olefin-metathesis polymerization (ROMP). This polymer possesses an average molecular weight between 12,000 and 51,000, with polydispersity being as low as 2.1. Despite the lack of delocalization due to its cross-conjugated nature, surprisingly, polymer **71** is quite easily oxidized and allows high carrier concentrations. Furthermore, modest conductivity (from  $10^{-3}\text{--}10^{-4}$  S  $\text{cm}^{-1}$ ) as well as paramagnetism can be achieved upon doping. The UV-vis spectrum of **71** displays a maximum absorption  $\lambda_{\text{max}} = 278$  nm, manifesting the fact that its  $\pi$ -system is segregated into triene segments, and a nonplanar backbone conformation is assumed owing to the presence of large steric interactions.

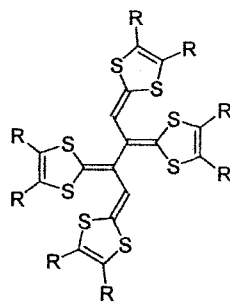


71

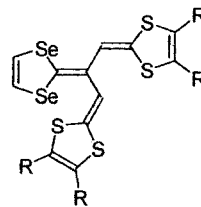
Beside the interest in its unique  $\pi$ -system, dendralenes can also be used as a cross-conjugated bridge to bear various functional molecules. For instance, the TTF substituted dendralenes **72a–c** and **73a–b** have been synthesized using Wittig reactions.<sup>307</sup> Recently, Cava and co-workers studied the electrochemistry behaviors of these dendralene-type TTF vinylogs **72** and **73**, as well as the 1,3-diselenole derivatives **74a–c**.<sup>307</sup> Cyclic voltammetric measurements of these compounds show three distinct redox potentials. Moreover, it is found that replacement of the sulfur by selenium lowered the oxidation potentials.<sup>307</sup>



**72a** R = COOMe  
**72b** R = H  
**72c** R = -(CH=CH)<sub>2</sub>



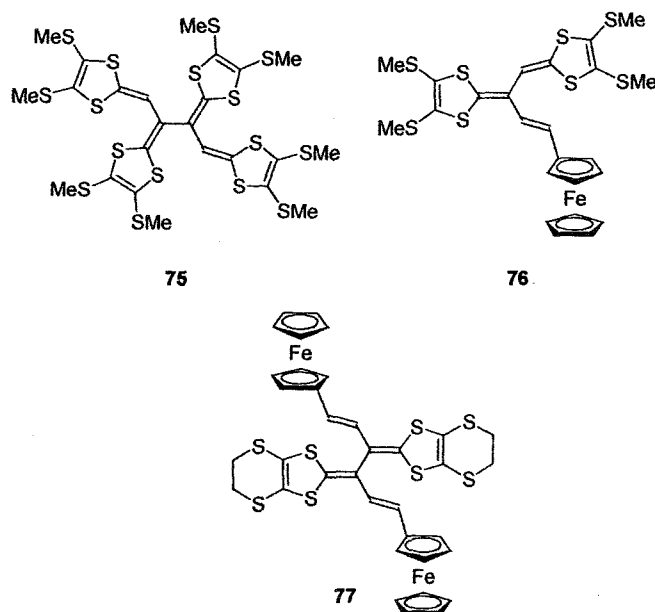
**73a** R = COOMe  
**73b** R = H



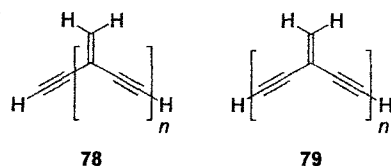
**74a** R = COOMe  
**74b** R = H  
**74c** R = -SCH<sub>2</sub>CH<sub>2</sub>S-

A similar series of the dithiole and ferrocenyl substituted dendralenes **75–77** were investigated by Bryce and co-workers<sup>308</sup> using cyclic voltammetry and X-ray crystallographic analysis. Solution state electrochemical data demonstrate that the dendralenes are strong  $\pi$ -electron donors, which give rise to dication, radical trication or tetracation species. Spectroelectrochemical studies of **75** suggest that the radical species are situated within the linear 1,2-ethynylenediylidene moieties, and a conformational

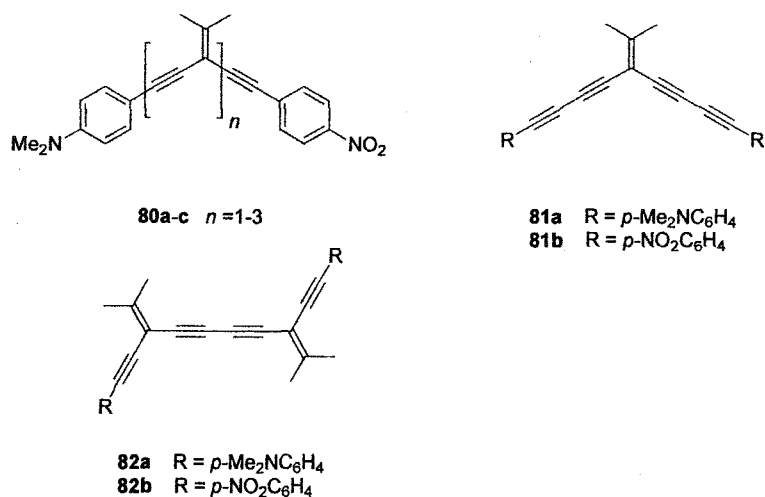
change may occur at the dication redox stage. UV-vis spectroscopic results are also in agreement with the nonplanar, cross-conjugated systems.



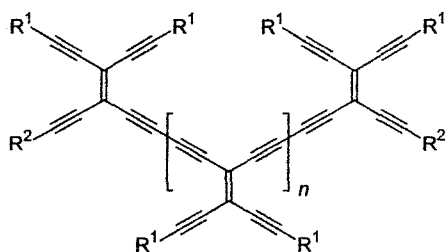
One solution to circumvent the nonplanarity of dendralene backbone caused by steric repulsion is to insert one or more carbon-carbon triple bond(s) between each vinylidene repeat unit; therefore, bringing out an alternative series of cross-conjugated oligoenynes, namely expanded dendralenes or, more specifically, *iso*-polydiacetylenes (*iso*-PDAs) **78**<sup>309,310</sup> and *iso*-polytriacetylenes (*iso*-PTAs) **79**.<sup>311</sup> These compounds have become one of the major research focuses in our group, and substantial progress on the synthesis of these cross-conjugated oligomers has been made during the last four years, utilizing the metal-mediated coupling protocols. A detailed description of the synthesis and characterization of these molecules will be related in later chapters.



In order to probe the influence by donor-acceptor (D-A) substitution on these cross-conjugated enyne frameworks, Ciulei and Tykwinski<sup>312</sup> recently reported the synthesis and characterization of a series of D-A substituted *iso*-polydiacetylene oligomers **80a–c**, as well as related D-A cross-conjugated enynes **81a–b** and **82a–b**.<sup>313</sup> UV-vis spectra of **80a–c** display similar absorption characteristic, however, with the notable exception that there is no lower energy absorption for the longer derivatives ( $n = 2–3$ ). It is evident by UV-vis spectroscopy that only monomer **80a** exhibits an observable influence from the incorporation of D-A groups.

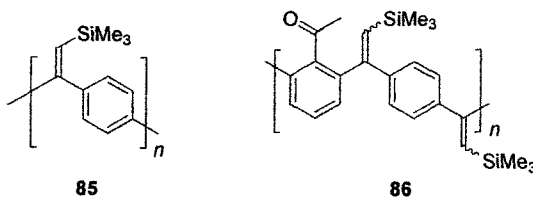


In addition to our efforts on *iso*-PTAs, other examples of *iso*-PTA oligomers **83a–c** and **84** containing the tetraethynylethene repeat unit have been synthesized and characterized by Diederich and co-workers.<sup>42</sup> The oligomeric series **83–84** was afforded in a one-pot oxidative homocoupling reaction, where the individual oligomers were then isolated via column chromatography.



**83a-c**  $n = 0-2$   $R^1 = R^2 = i\text{-Pr}_3\text{Si}$   
**84**  $n = 1$   $R^1 = i\text{-Pr}_3\text{Si}$   $R^2 = \text{Et}_3\text{Si}$

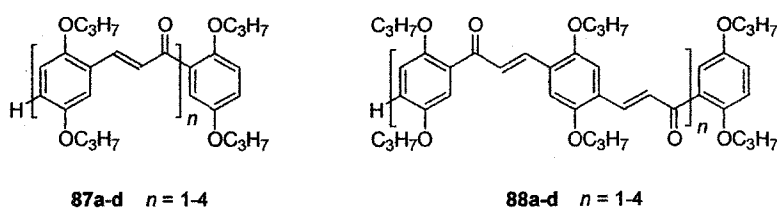
*Iso*-Polyphenylenevinylene (*iso*-PPV) is the constitutional isomer of its linearly conjugated counterpart PPV. It has also attracted attention and has been synthesized by several groups. Polymer **85** was reported by Tilley and Mao,<sup>314</sup> with a low average molecular weight ( $M_w/M_n = 2700/1700$ ). Moreover, a maximum absorption  $\lambda_{\text{max}} = 270$  nm is observed from its UV-vis spectrum, indicating that there is no dramatic bathochromic shift due to its cross-conjugated nature.



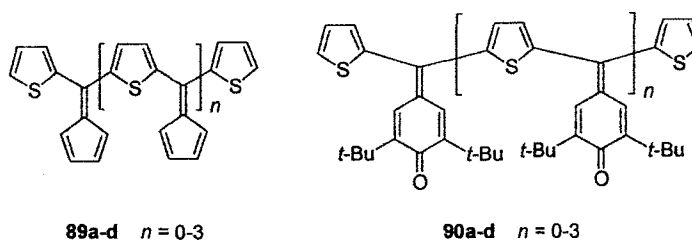
Londergan and co-workers<sup>315</sup> reported the synthesis of a cross-conjugated copoly(arylene/1,1-vinylene)s **86**, which has potential utility in a number of applications such as organic LEDs, using ruthenium catalyzed copolymerization of acetophenone and 1,4-(bis(trimethylsilylethynyl)benzene. This reaction involves regioselective catalytic addition of the *ortho* C-H bonds of acetophenone across the C≡C triple bonds of 1,4-bis(trimethylsilylethynyl)benzene such that the hydrogen becomes bonded to the carbon which bears the trimethylsilyl group. Gel permeation chromatography (GPC) and NMR integration gave two consistent  $M_n$  values equal to 5170 and 7460 respectively. The UV-

vis spectrum of **86** displays two maximum absorption peaks at  $\lambda_{\text{max}} = 240$  and  $284$  nm, and the fluorescence spectrum shows a maximum emission at  $\lambda_{\text{max}} = 420$  nm.

Meier *et al.* prepared two series of cross-conjugated oligomers **87a-d** and **88a-d** that contain the chalcone building block.<sup>316,317</sup> Bathochromic shifts can be observed in both UV-vis and fluorescence spectra, which are the result of the cross-conjugated ketone moiety present in the system. In addition, the ECL of oligomers **87a-d** and **88a-d** has been estimated as 6 and 14 chalcone building blocks, respectively.



Oda's group has reported the synthesis of two series of thiophene-containing cross-conjugated oligomers, oligo-6-(2-thienyl)pentafulvenes **89a-d** and thiophene bridged oligo(*p*-quinone methide)s **90a-d**.<sup>318,319</sup> The reduction of both oligomer series by Na-Hg has been investigated using NOE experiments and UV-vis spectroscopy, from which the possible geometries of reduced products were elucidated. Electrochemical studies via cyclic voltammetry show that oligomers **90a-d** possess much better stability and electron affinity than **89a-d**.



## 1.6 Conclusions

Conjugated oligomers, in particular, monodisperse oligomers play a central role in understanding the chemistry and physics of conjugated polymers, notably for optoelectronic properties. The synthesis of monodisperse conjugated oligomers can be achieved via a step-by-step synthesis, a modular synthesis, and/or a random synthesis followed by a chromatographic isolation. All strategies present their own advantages and disadvantages depending on target molecular architecture and the nature of the chemical reactions involved. In general, modern metal-mediated coupling reactions provide an efficient toolbox for the assembly of various conjugated oligomers. The rapidly developing synthetic techniques have also fueled research on the respective physical properties of monodisperse oligomers, such as electronic and/or optical properties as a function of chain length. Eventually, a reliable extrapolation to the corresponding polymer is thus achieved.

Practical applications of conjugated oligomers in electronic and optical devices have been discussed in this chapter, together with typical examples of recent investigations on monodisperse oligomers. Other than linearly conjugated oligomers, an alternative class of oligomers, namely cross-conjugated oligomers, has received more and more interest during the past decade due to their unique  $\pi$ -delocalization and properties derived from it. In our group, one motive to elaborate these cross-conjugated species has focused on third-order nonlinear optical (NLO) applications. A brief introduction on the NLO effects and relevant measurement techniques has also been discussed herein.

In this thesis, four major projects on cross-conjugated oligomers and molecules have been achieved as described in following chapters. In Chapter 2, investigations on a

series of model compounds, namely cross-conjugated *iso*-polydiacetylenes (*iso*-PDAs), will be discussed. A series of modified perphenylated *iso*-PDAs will be related in Chapter 3, together with a summary of third-order NLO and conformational studies. Chapter 4 details the study of a series of oligomers with expanded cross conjugation structures, namely cross-conjugated *iso*-polytriacetylenes (*iso*-PTAs) and related enyne oligomers. In Chapter 5, a class of cross-conjugated tetraynes and their solid-state properties (e.g., topochemical polymerization) are outlined. Other relevant, albeit less focused, work on cross-conjugated molecules will be summarized in Chapter 6.

### 1.7 References and Notes

- (1) Staudinger, H.; Fritschi, J. *Helv. Chim. Acta* **1922**, *5*, 785-806.
- (2) Grosberg, A. Y.; Khokhlov, A. R. *Giant Molecules-Here, There, and Everywhere...*; AIP press, 1996.
- (3) Staudinger, H. *Organische Kolloid Chemie*; Vieweg Verlag: Braunschweig, 1950.
- (4) Brooke, J. H. In *Recent Developments in the History of Chemistry*; Russell, C. A., Ed.; Royal Society of Chemistry: London, 1985, pp 97-152.
- (5) Uglea, C. V.; Dumitriu-Medvichi, C. *Medical Applications of Synthetic Oligomers, in Polymeric Biomaterials*; Marcel Dekker: New York, 1994.
- (6) Nelson, D. L.; Cox, M. M. *Lehninger Principles of Biochemistry*; Worth Publishers: New York, 2000.
- (7) Woodburn, J. *Opportunities in Chemistry*; National Academic Press: Washington, D. C., 1985.
- (8) Maiman, T. H. *Nature* **1960**, *187*, 493-494.

- (9) Shirakawa, H. *Angew. Chem. Int. Ed.* **2001**, *40*, 2574-2580.
- (10) MacDiarmid, A. G. *Angew. Chem. Int. Ed.* **2001**, *40*, 2581-2590.
- (11) Heeger, A. J. *Angew. Chem. Int. Ed.* **2001**, *40*, 2591-2611.
- (12) Chiang, C. K.; Finchner Jr., C. R.; Park, Y. W.; Heeger, A. J.; Shirakawa, H.; Louis, E. J.; Gau, S. C.; MacDiarmid, A. G. *Phys. Rev. Lett.* **1977**, *39*, 1098-1101.
- (13) Spangler, C. W.; Liu, P.-K.; Havelka, O. In *Molecular Electronics and Molecular Electronic Devices*; Sienicki, K., Ed.; CRC Press: New York, 1994; Vol. III, pp 97-115.
- (14) Burroughes, J. H.; Bradley, D. D. C.; Brown, A. R.; Marks, R. N.; MacKay, K.; Friend, R. H.; Burn, P. L.; Holmes, A. B. *Nature* **1990**, *347*, 539-541.
- (15) Lourenco, M. A.-V. *Comptes Rendus Acad. Sci.* **1860**, *67*, 365-367.
- (16) Lourenco, M. A.-V. *Ann. Chim. Phys.* **1863**, *67*, 257-339.
- (17) Tour, J. M. *Acc. Chem. Res.* **2000**, *33*, 791-804.
- (18) MacDonald, S. A.; Willson, C. G.; Fréchet, J. M. J. *Acc. Chem. Res.* **1994**, *27*, 151-158.
- (19) Van der Gaag, B. P.; Scherer, A.; Schiavone, L. M. *Microfabrication below 10 Nanometers*; SPIE (The International Society for Optical Engineering): San Diego, 1990; Vol. 1284.
- (20) Aviram, A.; Ratner, M. A. *Chem. Phys. Lett.* **1974**, *29*, 277-283.
- (21) Ward, M. D. *Chem. Ind. (London)* **1996**, 568-573.
- (22) Tour, J. M.; Rawlett, A. M.; Kozaki, M.; Yao, Y.; Jagessar, R. C.; Dirk, S. M.; Price, D. W.; Reed, M. A.; Zhou, C.-w.; Chen, J.; Wang, W.; Campbell, I. *Chem. Eur. J.* **2001**, *7*, 5118-5134.

- (23) Müllen, K.; Wegner, G., Eds. *Electronic Materials: The Oligomer Approach*; Wiley-VCH: Weinheim, 1997.
- (24) Jones II, L.; Pearson, D. L.; Schumm, J. S.; Tour, J. M. *Pure & Appl. Chem.* **1996**, *68*, 145-148.
- (25) Tour, J. M. *Chem. Rev.* **1996**, *96*, 537-553.
- (26) Müllen, K. *Pure & Appl. Chem.* **1993**, *65*, 89-96.
- (27) Feuerbacher, N.; Vögtle, F. *Top. Curr. Chem.* **1998**, *197*, 1-18.
- (28) Igner, E.; Paynter, O. I.; Simmonds, D. J.; Whiting, M. C. *J. Chem. Soc., Perkin Trans. 1* **1987**, 2447-2454.
- (29) Bidd, I.; Kelly, D. J.; Ottley, P. M.; Paynter, O. I.; Simmonds, D. J.; Whiting, M. C. *J. Chem. Soc., Perkin Trans. 1* **1983**, 1369-1372.
- (30) Zhang, J.; Moore, J. S.; Xu, Z.; Aguirrem, R. A. *J. Am. Chem. Soc.* **1992**, *114*, 2273-2274.
- (31) Xu, Z.; Moore, J. S. *Angew. Chem. Int. Ed. Engl.* **1993**, *32*, 1354-1357.
- (32) Pearson, D. L.; Tour, J. M. *J. Org. Chem.* **1997**, *62*, 1376-1387.
- (33) Pearson, D. L.; Schumm, J. S.; Tour, J. M. *Macromolecules* **1994**, *27*, 2348-2350.
- (34) Diederich, F.; Stang, P., Eds. *Metal-catalyzed Cross-coupling Reactions*; Wiley-VCH: Weinheim, 1998.
- (35) Hay, A. S. *J. Org. Chem.* **1962**, *27*, 3320-3321.
- (36) Eglinton, G.; Galbraith, A. R. *J. Chem. Soc.* **1959**, 889-896.
- (37) Eglinton, G.; McCrae, W. *Adv. Org. Chem.* **1963**, *4*, 225-328.
- (38) Martin, R. E.; Gubler, U.; Boudon, C.; Gramlich, V.; Bosshard, C.; Gisselbrecht, J.-P.; Günter, P.; Gross, M.; Diederich, F. *Chem. Eur. J.* **1997**, *3*, 1505-1512.

- (39) Schenning, A. P. H. J.; Martin, R. E.; Ito, M.; Diederich, F.; Boudon, C.; Gisselbrecht, J.-P.; Gross, M. *Chem. Commun.* **1998**, 1013-1014.
- (40) Anthony, J.; Boudon, C.; Diederich, F.; Gisselbrecht, J.-P.; Gramlich, V.; Gross, M.; Seiler, M. H. P. *Angew. Chem. Int. Ed. Engl.* **1994**, *33*, 763-766.
- (41) Anthony, J.; Boldi, A. M.; Rubin, Y.; Hobi, M.; Gramlich, V.; Knobber, C. B.; Seiler, P.; Diederich, F. *Helv. Chim. Acta* **1995**, *78*, 13-45.
- (42) Boldi, A. M.; Anthony, J.; Gramlich, V.; Knobler, C. B.; Boudon, C.; Gisselbrecht, J.-P.; Gross, M.; Diederich, F. *Helv. Chim. Acta* **1995**, *78*, 779-796.
- (43) Nierengarten, J.-F.; Guillon, D.; Heinrich, B.; Nicoud, J.-F. *Chem. Commun.* **1997**, 1233-1234.
- (44) Scherf, U.; Müllen, K. *Synthesis* **1992**, 23-28.
- (45) Tanaka, Y.; Boochathum, P.; Shimizu, M.; Mita, K. *Polymer* **1993**, *34*, 1098-1101.
- (46) Merrifield, R. B. *J. Am. Chem. Soc.* **1963**, *85*, 2149-2154.
- (47) Merrifield, R. B. *Life During a Golden Age of Peptide Chemistry. The Concept and Development of Solid-Phase Peptide Synthesis*; ACS: Washington, 1993.
- (48) Feast, W. J.; Tsibouklis, J.; Pouwer, K. L.; Groenendaal, L.; Meijer, E. W. *Polymer* **1996**, *37*, 5017-5047.
- (49) Meier, H.; Stalmach, U.; Kolshorn, H. *Acta Polym.* **1997**, *48*, 379-384.
- (50) Zerbi, G.; Galbiati, E.; Gallazzi, M. C.; Castiglioni, C.; Del Zoppo, M.; Schenk, R.; Müllen, K. *J. Chem. Phys.* **1996**, *106*, 2509-2516.
- (51) Jenekhe, S. A. *Macromolecules* **1990**, *23*, 2848-2854.

- (52) Grimme, J.; Kreyenschmidt, M.; Uckert, F.; Müllen, K.; Scherf, U. *Adv. Mater.* **1995**, *7*, 292-295.
- (53) Brédas, J. L.; Silbey, R.; Boudreaux, D. S.; Chance, R. R. *J. Am. Chem. Soc.* **1983**, *105*, 6555-6559.
- (54) Guay, J.; Kasai, P.; Diaz, A.; Wu, R.; Tour, J. M.; Dao, L. H. *Chem. Mater.* **1992**, *4*, 1097-1105.
- (55) Onipko, A.; Klymenko, Y.; Malysheva, L. *J. Chem. Phys.* **1997**, *107*, 7331-7344.
- (56) Brédas, J. L. In *Organic Materials for Photonics*; Zerbi, G., Ed.; Elsevier: Amsterdam, 1993, pp 127-153.
- (57) Alonso, M.; Finn, E. J. *Physics*; Addison-Wesley: MA, 1970.
- (58) Wenz, G.; Müller, M. A.; Schmidt, M.; Wegner, G. *Macromolecules* **1984**, *17*, 837-850.
- (59) Lewis, G. N.; Calvin, M. *Chem. Rev.* **1939**, *39*, 273-328.
- (60) Hirayama, K. *J. Am. Chem. Soc.* **1955**, *77*, 373-379.
- (61) Hirayama, K. *J. Am. Chem. Soc.* **1955**, *77*, 379-381.
- (62) Hirayama, K. *J. Am. Chem. Soc.* **1955**, *77*, 382-383.
- (63) Hirayama, K. *J. Am. Chem. Soc.* **1955**, *77*, 383-384.
- (64) Bernanose, A.; Vouaux, P. *J. Chim. Phys.* **1955**, *52*, 509.
- (65) Bernanose, A. *J. Chim. Phys.* **1955**, *52*, 396.
- (66) Segura, J. L. *Acta Polym.* **1998**, *49*, 319-344.
- (67) Geiger, F.; Stoldt, M.; Schweizer, H.; Bäuerle, P.; Umbach, E. *Adv. Mater.* **1993**, *5*, 922-925.

- (68) Uchiyama, K.; Akimichi, H.; Hotta, S.; Noge, H.; Sakaki, H. *Synth. Met.* **1994**, *63*, 57-59.
- (69) Horowitz, G.; Delannov, P.; Bouchriha, H. *Adv. Mater.* **1994**, *6*, 752-755.
- (70) Garten, F.; Hilberber, A.; Cacialli, F. J.; Esselink, F.; van Dam, Y.; Schlatmann, A. R.; Friend, R. H.; Klapwijk, T. M.; Hadziioannou, G. *Adv. Mater.* **1997**, *9*, 127-131.
- (71) Garten, F.; Hilberber, A.; Cacialli, F. J.; Esselink, F.; van Dam, Y.; Schlatmann, A. R.; Friend, R. H.; Klapwijk, T. M.; Hadziioannou, G. *Synth. Met.* **1997**, *85*, 1253-1254.
- (72) Wu, X.; Liu, Y.; Zhu, D. *J. Mater. Chem.* **2001**, *11*, 1327-1331.
- (73) Pochettino, A. *Acad. Lincei Rediconti* **1906**, *15*, 355.
- (74) Volmer, M. *Ann. Physik* **1913**, *40*, 775.
- (75) Chamberlain, G. A. *Solar Cells* **1983**, *8*, 47-83.
- (76) Tang, C. *Appl. Phys. Lett.* **1986**, *48*, 183.
- (77) Panayotatos, P.; Parikh, D.; Sauers, R.; Bird, G.; Piechowski, A.; Husain, S. *Solar Cells* **1986**, *18*, 71-84.
- (78) Panayotatos, P.; Bird, G.; Sauers, R.; Piechowski, A.; Husain, S. *Solar Cells* **1987**, *21*, 301-311.
- (79) Noma, N.; Tsuzuki, T.; Shirota, Y. *Adv. Mater.* **1995**, *7*, 647-648.
- (80) Köhler, A.; Grüner, J.; Friend, R. H.; Müllen, K.; Scherf, U. *Chem. Phys. Lett.* **1995**, *243*, 456-461.
- (81) Karl, N.; Bauer, A.; Holzäpfel, J.; Marktanner, J.; Möbus, M.; Stölzle, F. *Mol. Cryst. Liq. Cryst.* **1994**, *252*, 243-258.

- (82) Andreev, A. Y.; Matt, G.; Sitter, H.; Bradec, C. J.; Badt, D.; Neugebauer, H.; Sariciftci, N. S. *Synth. Met.* **2001**, *116*, 235-239.
- (83) Green, W.; Poortmans, J.; Jian, S. C.; Nijs, J.; Mertens, R.; Veenstra, S. C.; Krasnikov, V. V.; Hadziioannou, G. *Solar Energy Mater. & Solar Cell* **2000**, *61*, 43-51.
- (84) Huynh, W. U.; Dittmer, J. J.; Alivisatos, A. P. *Science* **2002**, *295*, 2425-2427.
- (85) Paloheimo, J.; Punkka, E.; Kuivalainen, P.; Stubb, H.; Vourimaa, E.; Yli-Lahti, P. *Acta Polytech. Scand., El. Eng. Ser.* **1989**, *64*, 178-185.
- (86) Tsumura, A.; Fuchigami, H.; Koezuka, H. *Synth. Met.* **1991**, *41*, 1181-1184.
- (87) Voss, K. F.; Braun, D.; Heeger, A. J. *Synth. Met.* **1991**, *41*, 1185-1188.
- (88) Schön, J. H.; Dodabalapur, A.; Bao, Z.; Kloc, C.; Schenker, O.; Batlogg, B. *Nature* **2001**, *410*, 189-192.
- (89) Horowitz, G.; Fichou, D.; Peng, X. Z.; Xu, Z.; Garnier, F. *Solid State Commun.* **1989**, *72*, 381-384.
- (90) Drexler, K. E. *Nanosystems: Molecular Machinery, Manufacturing, and Computation*; John Wiley & Sons, Inc.: New York, 1992.
- (91) Garnier, F.; Yaasar, A.; Hajlaoui, R.; Horowitz, G.; Deloffre, F.; Servet, B.; Ries, S.; Alnot, P. *J. Am. Chem. Soc.* **1993**, *115*, 8716-8721.
- (92) Servet, B.; Horowitz, G.; Ries, S.; Lagorsse, O.; Alnot, P.; Yaasar, A.; Deloffre, F.; Srivastava, P.; Hajlaoui, R.; Lang, P.; Garnier, F. *Chem. Mater.* **1994**, 1809-1815.
- (93) Bao, Z.; Dodabalapur, A.; Lovinger, A. J. *Appl. Phys. Lett.* **1996**, *69*, 4108-4110.

- (94) Bao, Z.; Feng, Y.; Dodabalapur, A.; Raju, V. R.; Lovinger, A. J. *Chem. Mater.* **1997**, *9*, 1299-1301.
- (95) Bao, Z.; Lovinger, A. J. *Chem. Mater.* **1999**, *11*, 2607-2612.
- (96) Sirringhaus, H.; Brown, P. J.; Friend, R. H.; Nielsen, M. M.; Bechgaard, K.; Langeveld-Voss, B. M. W.; Spiering, A. J. H.; Janssen, R. A. J.; Meijer, E. W.; Herwing, P.; de Leeuw, D. M. *Nature* **1999**, *401*, 685-688.
- (97) Prasad, P. N.; Williams, D. J. *Introduction to Nonlinear Optical Effects in Molecules and Polymers*; John Wiley & Sons, Inc.: New York, 1991.
- (98) *Conjugated Oligomers, Polymers, and Dendrimers: From Polyacetylene to DNA*; Brédas, J.-L., Ed.; De Boeck & Larcier s.a.: Paris, Bruxelles, 1999.
- (99) *Nonlinear Optics of Organic Molecules and Polymers*; Nalwa, H. S.; Miyata, S., Eds.; CRC Press, Inc.: Boca Raton, 1997.
- (100) *Characterization Techniques and Tabulations for Organic Nonlinear Optical Materials*; Kuzyk, M. G.; Dirk, C. W., Eds.; Marcel Dekker, Inc.: New York, 1998.
- (101) Slepikov, A. D.; Hegemann, F. A.; Zhao, Y.; Tykwinski, R. R.; Kamada, K. *J. Chem. Phys.* **2002**, *116*, 3834-3840.
- (102) Ho, P. P.; Alfano, R. R. *Phys. Rev. A* **1979**, *20*, 2170-2187.
- (103) Ho, P. P. In *Semiconductors Probed by Ultrafast Laser Spectroscopy*; Alfano, R. R., Ed.; Academic: New York, 1984; Vol. II, pp 409-493.
- (104) Guha, S.; Frazier, C. C.; Porter, P. L.; Kang, K.; Finberg, S. E. *Opt. Lett.* **1989**, *14*, 952-954.

- (105) Kuzyk, M. G.; Norwood, R. A.; Wu, J. W.; Garito, A. F. *J. Opt. Soc. Am. B* **1989**, *6*, 154-164.
- (106) Pang, Y.; Samoc, M.; Prasad, P. N. *J. Chem. Phys.* **1991**, *94*, 5282-5290.
- (107) Philippart, V.; Dumont, M.; Nunzi, J. M.; Charra, F. *Appl. Phys. A: Solids Surf.* **1993**, *56*, 29-34.
- (108) Vigil, S. R.; Kuzyk, M. G. *J. Opt. Soc. Am. B* **2001**, *18*, 679-691.
- (109) Agrawal, G. P.; Cojan, C.; Flytzanis, C. *Phys. Rev. B* **1978**, *17*, 776-789.
- (110) Mathy, A.; Ueberhofen, K.; Schenk, R.; Gregorius, H.; Garay, R.; Müllen, K.; Bubeck, C. *Phys. Rev. B* **1996**, *53*, 4367-4376.
- (111) Hopf, H. *Classics in Hydrocarbon Chemistry*; Wiley-VCH: Weinheim, 2000.
- (112) Hopf, H. *Angew. Chem. Int. Ed. Engl.* **1984**, *23*, 948-960.
- (113) Trætteberg, M.; Hopf, H. *Acta Chem. Scand.* **1994**, *48*, 989-993.
- (114) Phelan, N. F.; Orchin, M. J. *J. Chem. Ed.* **1968**, *45*, 633-637.
- (115) Almenningen, A.; Gatial, A.; Grace, D. S. B.; Hopf, H.; Klæboe, P.; Leirich, F.; Nielsen, C. J.; Powell, D. L.; Trætteberg, M. *Acta Chem. Scand.* **1988**, *A42*, 634-650.
- (116) Leirich, F.; Hopf, H. *Tetrahedron Lett.* **1987**, *28*, 2697-2700.
- (117) Misaki, Y.; Matsumura, Y.; Sugimoto, T.; Yoshida, Z. *Tetrahedron Lett.* **1989**, *30*, 5289-5292.
- (118) Yamauchi, J.; Aoyama, T.; Kanemoto, K.; Sasaki, S.; Iyoda, M. *J. Phys. Org. Chem.* **2000**, *13*, 197-202.
- (119) Schulz, D. A.; Gwaktney, K. P.; Lee, H. *J. Org. Chem.* **1998**, *63*, 4034-4038.

- (120) Nicoud, J.-F.; Serbutoviez, C.; Barrans, Y.; Chasseau, D.; Gautier-Luneau, I.; Ledoux, I.; Zyss, J. *Nonlinear Opt.* **1995**, *9*, 127-141.
- (121) Wang, W. L.; Helgeson, R.; Ma, B.; Wudl, F. *J. Org. Chem.* **2000**, *65*, 5862-5867.
- (122) Maertens, C.; Detrembleur, C.; Dubois, P.; Jerome, R.; Boutton, C.; Persoons, A.; Kogej, T.; Brédas, J.-L. *Chem. Eur. J.* **1999**, *5*, 369-380.
- (123) Gleiter, R.; Röckel, H.; Irgartinger, H.; Oeser, T. *Angew. Chem. Int. Ed. Engl.* **1994**, *33*, 1270-1272.
- (124) Song, Y.; Spencer, L.; Euler, W. B.; Rosen, W. *Org. Lett.* **1999**, *1*, 561-564.
- (125) Hopf, H.; Theurig, M.; Jones, P. G.; Bubenitschek, P. *Liebigs Ann.* **1996**, 1301-1311.
- (126) Faust, R.; Göbelt, B.; Weber, C.; Krieger, C.; Gross, M.; Gisselbrecht, J.-P.; Boudon, C. *Eur. J. Org. Chem.* **1999**, 205-214.
- (127) Thirsk, C.; Whiting, A. *J. Chem. Soc., Perkin Trans. 1* **2002**, 999-1023.
- (128) Rychnovsky, S. D. *Chem. Rev.* **1995**, *95*, 2021-2040.
- (129) Heeger, A. J.; McDiarmid, A. G. In *The Physics and Chemistry of Low-Dimensional Solids*; Alcacer, L., Ed.; Reidel: Dordrecht, 1980, pp 353-391.
- (130) Monkman, A. P. *Physics of Conductive Polymers*; Edward Arnold: London, 1995.
- (131) *Handbook of Conducting Polymers*; Skotheim, T. A., Ed.; Dekker: New York, 1986; Vol. 1,2.
- (132) *Handbook of Organic Conductive Molecules and Polymers*; Nalwa, H. S., Ed.; Wiley & Sons: Chichester, 1997; Vol. 1-4.
- (133) Kiehl, A.; Eberhardt, A.; Adam, M.; Enkelmann, V.; Müllen, K. *Angew. Chem. Int. Ed. Engl.* **1992**, *31*, 1588-1591.

- (134) Hoffmann, R. W. *Chem. Rev.* **1989**, *89*, 1841-1860.
- (135) Duhamel, L.; Duhamel, P.; Plé, G.; Ramondenc, Y. *Tetrahedron Lett.* **1993**, *34*, 7399-7400.
- (136) Effenberger, F.; Schlosser, H.; Bäuerle, P.; Maier, S.; Port, H.; Wolf, H. C. *Angew. Chem. Int. Ed. Engl.* **1988**, *27*, 281-284.
- (137) Tolbert, L. M.; Zhoa, X.; Ding, Y.; Bottomley, L. A. *J. Am. Chem. Soc.* **1995**, *117*, 12891-12892.
- (138) Kugimiya, S.-I.; Lazrak, T.; Blanchard-Desce, M.; Lehn, J.-M. *Chem. Commun.* **1991**, 1179-1182.
- (139) Effenberger, F.; Wolf, H. C. *New J. Chem.* **1991**, *15*, 117-123.
- (140) Spangler, C. W.; McCoy, R. K.; Dembek, A. A.; Sapochak, L. S.; Gates, B. D. *J. Chem. Soc., Perkin Trans. 1* **1989**, 151-154.
- (141) Spangler, C. W.; Liu, P.-K.; Dembek, A. A.; Havelka, O. *J. Chem. Soc., Perkin Trans. 1* **1991**, 799-802.
- (142) Lahti, P. M.; Obrzut, J.; Karasz, F. E. *Macromolecules* **1987**, *20*, 2023-2026.
- (143) Baughman, R. H.; Hsu, S. L.; Anderson, L. R.; Pez, G. P.; Signorelli, A. J. *Structural Perspectives for Polymeric Metals*; Plenum Press: New York, 1979.
- (144) Kuzmany, H.; Mehring, M.; Roth, S. *Electronic Properties of Polymers and Related Compounds (Springer Ser. Solid State Sci. 63)*; Springer: Berlin, 1985.
- (145) Bally, T.; Roth, K.; Tang, W.; Schrock, R. R.; Knoll, K.; Park, L. Y. *J. Am. Chem. Soc.* **1992**, *114*, 2440-2446.
- (146) Roth, S.; Bleier, H. *Adv. Phys.* **1987**, *36*, 385-462.

- (147) Heeger, A. J.; Kivelson, S.; Schrieffer, J. R.; Su, W.-P. *Rev. Mod. Phys.* **1988**, *60*, 781-850.
- (148) Gorman, C. B.; Ginsburg, E. J.; Grubbs, R. H. *J. Am. Chem. Soc.* **1993**, *115*, 1397-1409.
- (149) Leclerc, M.; Faïd, K. *Adv. Mater.* **1997**, *9*, 1087-1094.
- (150) Patil, A. O.; Heeger, A. J.; Wudl, F. *Chem. Rev.* **1988**, *88*, 183-200.
- (151) Knoll, K.; Schrock, R. R. *J. Am. Chem. Soc.* **1989**, *111*, 7989-8004.
- (152) Zeng, F.; Negishi, E. *Org. Lett.* **2002**, *4*, 703-706.
- (153) Marder, S. R.; Torruellas, W. E.; Blanchard-Desce, M.; Ricci, V.; Stegeman, G. I.; Gilmour, S.; Brédas, J.-L.; Li, J.; Bublitz, G. U.; Boxer, S. G. *Science* **1997**, *276*, 1233-1236.
- (154) Service, R. F. *Science* **1997**, *276*, 1195-1196.
- (155) Blanchard-Desce, M.; Alain, V.; Bedworth, P. V.; Marder, S. R.; Fort, A.; Runser, C.; Barzoukas, M.; Lebus, S.; Wortmann, R. *Chem. Eur. J.* **1997**, *3*, 1091-1104.
- (156) Meyers, F.; Brédas, J.-L.; Zyss, J. *J. Am. Chem. Soc.* **1992**, *114*, 2914-2921.
- (157) Albert, I. D. L.; Morley, J. O.; Pugh, D. *J. Phys. Chem. A* **1997**, *101*, 1763-1766.
- (158) Marder, S. R.; Gorman, C. B.; Tiemann, B. G.; Cheng, L.-T. *J. Am. Chem. Soc.* **1993**, *115*, 3006-3007.
- (159) Puccetti, G.; Blanchard-Desce, M.; Ledoux, I.; Lehn, J.-M.; Zyss, J. *J. Phys. Chem.* **1993**, *97*, 9385-9391.
- (160) Messier, J.; Kajzar, F.; Sentein, C.; Barzoukas, M.; Zyss, J.; Blanchard-Desce, M.; Lehn, J.-M. *Nonlinear Opt.* **1992**, *2*, 53-70.

- (161) Samuel, I. D. W.; Ledoux, I.; Dhenaut, C.; Zyss, J.; Fox, H. H.; Schrock, R. R.; Silbey, R. J. *Science* **1994**, *265*, 1070-1072.
- (162) Spano, F. C.; Soos, Z. G. *J. Chem. Phys.* **1993**, *99*, 9265-9271.
- (163) Gorman, C. B.; Marder, S. R. *Chem. Mater.* **1995**, *7*, 215-220.
- (164) Marder, S. R.; Gorman, C. B.; Meyers, F.; Perry, J. W.; Bourhill, G.; Brédas, J.-L.; Pierce, B. M. *Science* **1994**, *265*, 632-635.
- (165) Meyers, F.; Marder, S. R.; Pierce, B. M.; Brédas, J.-L. *J. Am. Chem. Soc.* **1994**, *116*, 10703-10714.
- (166) Marder, S. R.; Perry, J. W.; Bourhill, G.; Gorman, C. B.; Tiemann, B. G.; Mansour, K. *Science* **1993**, *261*, 186-189.
- (167) Dähne, S. *Chimia* **1991**, *45*, 288-296.
- (168) Lu, D.; Chen, G.; Perry, P. W.; Goddard III, W. A. *J. Am. Chem. Soc.* **1994**, *116*, 10679-10685.
- (169) Brédas, J. L.; Adant, C.; Tackx, P.; Persoons, A. *Chem. Rev.* **1994**, *94*, 243-278.
- (170) Tykwinski, R. R.; Gubler, U.; Martin, R. E.; Diederich, F.; Bosshard, C.; Günter, P. *J. Phys. Chem. B* **1998**, 4451-4465.
- (171) Reihardt, B. A. *Trend Polym. Sci.* **1993**, *1*, 4-9.
- (172) Kirtman, B.; Champagne, B. *Int. Rev. Phys. Chem.* **1997**, *16*, 389-420.
- (173) André, J.-M.; Delhalle, J. *Chem. Rev.* **1991**, *91*, 843-865.
- (174) Campbell, A. J.; Davies, C. K. L. *Polymer* **1994**, *35*, 4787-4793.
- (175) Bloor, D.; Chance, R. R., Eds. *Polydiacetylenes: Synthesis, Structure, and Electronic Properties*, 1989; Vol. Applied Science No. 102.
- (176) Bäessler, H. *Photopolymerization of Diacetylenes*; Springer: Berlin, 1984.

- (177) Wenz, G.; Müller, A.; Schmidt, M.; Wegner, G. *Macromolecules* **1984**, *17*, 837-850.
- (178) Bloor, D. *The Polymerization of Disubstituted Diacetylene Crystals*; Applied Science Publishers: London, 1982.
- (179) Baughman, R. H. *J. Polym. Sci., Polym. Phys. Ed.* **1974**, *12*, 1511-1535.
- (180) Baughman, R. H. *J. Appl. Phys.* **1972**, *43*, 4362-4370.
- (181) Wegner, G. *Makromol. Chem.* **1971**, *145*, 85-94.
- (182) Wegner, G. *Z. Naturforsch. B* **1969**, *24*, 824-832.
- (183) Fowler, F. W.; Lauher, J. W. *J. Phys. Org. Chem.* **2000**, *13*, 850-857.
- (184) Nalwa, H. S. *Adv. Mater.* **1993**, *5*, 341-358.
- (185) Gubler, U.; Bosshard, C. *Adv. Polym. Sci.* **2002**, *158*, 123-191.
- (186) Wudl, F.; Bitler, P. *J. Am. Chem. Soc.* **1986**, *108*, 4685-4687.
- (187) (a) Giesa, R.; Schulz, R. C. *Polym. Int.* **1994**, *33*, 43-60. (b) Byrne, H. J.; Blau, W.; Giesa, R.; Schulz, R. C. *Chem. Phys. Lett.* **1990**, *167*, 484-489.
- (188) Crousse, B.; Alami, M.; Linstumelle, G. *Tetrahedron Lett.* **1995**, *36*, 4245-4248.
- (189) Kosinski, C.; Hirsch, A.; Heinemann, F. W.; Hampel, F. *Eur. J. Org. Chem.* **2001**, 3879-3890.
- (190) Schreiber, M.; Anthony, J.; Diederich, F.; Spahr, M. E.; Nesper, R.; Hubrich, M.; Bommeli, F.; Degiorgo, L.; Wachter, P.; Kaatz, P.; Bosshard, C.; Günter, P.; Colussi, M.; Suter, U. W.; Boudon, F.; Gisselbrecht, J.-P.; Gross, M. *Adv. Mater.* **1994**, *6*, 786-790.
- (191) Diederich, F.; Gobbi, L. *Top. Curr. Chem.* **1998**, *201*, 43-79.

- (192) Martin, R. E.; Mäder, T.; Diederich, F. *Angew. Chem. Int. Ed. Engl.* **1999**, *38*, 817-821.
- (193) Bosshard, C.; Spreiter, R.; Günter, P.; Tykwinski, R. R.; Schreiber, M.; Diederich, F. *Adv. Mater.* **1996**, *8*, 231-234.
- (194) Gubler, U.; Spreiter, R.; Bosshard, C.; Günter, P.; Tykwinski, R. R.; Diederich, F. *Appl. Phys. Lett.* **1998**, *73*, 2396-2398.
- (195) Spreiter, R.; Bosshard, C.; Knöpfle, G.; Günter, P.; Tykwinski, R. R.; Schreiber, M.; Diederich, F. *J. Phys. Chem.* **1998**, *102*, 29-32.
- (196) Martin, R. E.; Bartek, J.; Diederich, F.; Tykwinski, R. R.; Meister, E. C.; Hilger, A.; Lüthi, H. P. *J. Chem. Soc., Perkin Trans. 2* **1998**, 233-241.
- (197) Diederich, F. In *Modern Acetylene Chemistry*; Stang, P. J., Diederich, F., Eds.; Wiley VCH: Weinheim, 1995, pp 443-471.
- (198) Smith, P. P. K.; Buseck, P. R. *Science* **1982**, *216*, 984-986.
- (199) Cook, C. L.; Jones, E. R. H.; Whiting, M. C. *J. Chem. Soc.* **1952**, 2883-2891.
- (200) Schlubach, H. H.; Franzen, V. *Liebigs Ann.* **1951**, *573*, 110-115.
- (201) Nakagawa, M. *Proc. Japan Acad. Sci.* **1950**, *26*, 43-47.
- (202) Armitage, J. B.; Entwistle, N.; Jones, E. R. H.; Whiting, M. C. *J. Chem. Soc.* **1954**, 147-154.
- (203) Bohlman, F. *Chem. Ber.* **1953**, *86*, 657-667.
- (204) Jones, E. R. H.; Lee, H. H.; Whiting, M. C. *J. Chem. Soc.* **1960**, 3483-3489.
- (205) Johnson, T. R.; Walton, D. R. M. *Tetrahedron* **1972**, *28*, 5221-5236.
- (206) Eastmond, R.; Walton, D. R. M. *Tetrahedron* **1972**, *28*, 4591-4599.
- (207) Ernst, A.; Gobbi, L.; Vasella, A. *Tetrahedron Lett.* **1996**, *37*, 7959-7962.

- (208) Ernst, A.; Vasella, A. *Helv. Chim. Acta* **1996**, *79*, 1279-1294.
- (209) Cai, C.; Vasella, A. *Helv. Chim. Acta* **1995**, *78*, 732-757.
- (210) Cai, C.; Vasella, A. *Helv. Chim. Acta* **1996**, *79*, 255-268.
- (211) Schermann, G.; Grösser, T.; Hampel, F.; Hirsch, A. *Chem. Eur. J.* **1997**, *3*, 1105-1112.
- (212) Hopf, H.; Witulski, B. In *Modern Acetylene Chemistry*; Stang, P. J., Diederich, F., Eds.; Wiley VCH: Weinheim, 1995, pp 33-66.
- (213) Hare, J. P.; Kroto, H. W. *Acc. Chem. Res.* **1992**, *25*, 106-112.
- (214) Brady, M.; Weng, W.; Gladysz, J. A. *Chem. Commun.* **1994**, 2655-2656.
- (215) Bartik, T.; Bartik, B.; Brady, M.; Dembinski, R.; Gladysz, J. A. *Angew. Chem. Int. Ed. Engl.* **1996**, *35*, 414-417.
- (216) Bunz, U. H. F. *Angew. Chem. Int. Ed. Engl.* **1996**, *35*, 969-971.
- (217) Weng, W.; Bartik, T.; Brady, M.; Bartik, B.; Ramsden, J. A.; Arif, A. M.; Gladysz, J. A. *J. Am. Chem. Soc.* **1995**, *117*, 11922-11931.
- (218) Weng, W.; Bartik, T.; Gladysz, J. A. *Angew. Chem. Int. Ed. Engl.* **1994**, *33*, 2199-2202.
- (219) Mohr, W.; Stahl, J.; Hampel, F.; Gladysz, J. A. *Inorg. Chem.* **2001**, *40*, 3263-3264.
- (220) Eisler, S.; Tykwinski, R. R. *J. Am. Chem. Soc.* **2000**, *122*, 10736-10737.
- (221) Chernick, E. T.; Eisler, S.; Tykwinski, R. R. *Tetrahedron Lett.* **2001**, *42*, 8575-8578.
- (222) Elliott, E.; Tykwinski, R. R. *Unpublished results*.
- (223) Tour, J. M. *Adv. Mater.* **1994**, *6*, 190-198.

- (224) Kovacic, P.; Lange, R. M. *J. Org. Chem.* **1964**, *29*, 2416-2420.
- (225) Taylor, D. K.; Samulski, E. T. *Macromolecules* **2000**, *33*, 2355-2358.
- (226) Kovacic, P.; Jones, M. B. *Chem. Rev.* **1987**, *87*, 357-359.
- (227) Novák, P.; Müller, K.; Santhanam, K. S. V.; Haas, O. *Chem. Rev.* **1997**, *97*, 207-281.
- (228) Norten, G. K.; Stille, J. K. *Macromol. Rev.* **1971**, *5*, 385-430.
- (229) Baughman, R. H.; Brédas, J. L.; Chance, R. R.; Elsenbaumer, R. L.; Shacklette, L. W. *Chem. Rev.* **1982**, *82*, 209-222.
- (230) Economy, J. In *Contemporary Topics in Polymer Science*; Vandenberg, E. J., Ed.; Plenum Press: New York, 1984; Vol. 5.
- (231) Schlüter, A.-D.; Wegner, G. *Acta Polym.* **1993**, *44*, 59-69.
- (232) Rau, I. U.; Rehahn, M. *Acta Polym.* **1994**, *45*, 3-13.
- (233) Kraft, A.; Grimsdale, A. C.; Holmes, A. B. *Angew. Chem. Int. Ed.* **1998**, *37*, 403-428.
- (234) Scherf, U. *Top. Curr. Chem.* **1999**, *201*, 163-222.
- (235) Berresheim, A. J.; Müller, M.; Müllen, K. *Chem. Rev.* **1999**, *99*, 1747-1785.
- (236) Hide, F.; Díaz-García, M. A.; Schwartz, B. J.; Heeger, A. J. *Acc. Chem. Res.* **1997**, *30*, 430-436.
- (237) Birgerson, J.; Kaeriyama, K.; Barta, P.; Bröms, P.; Fahlman, M.; Granlund, T.; Salaneck, W. R. *Adv. Mater.* **1996**, *8*, 982-985.
- (238) Grem, G.; Leditzky, G.; Ullrich, B.; Leising, G. *Adv. Mater.* **1992**, *4*, 36-37.
- (239) Grem, G.; Leditzky, G.; Ullrich, B.; Leising, G. *Synth. Met.* **1992**, *51*, 383-389.
- (240) Unroe, M. R.; Reinhardt, B. A. *Synthesis* **1987**, 981-986.

- (241) Pummerer, R.; Seligsberger, L. *Chem. Ber.* **1931**, *64*, 2477-2486.
- (242) Bohnen, A.; Heitz, W.; Müllen, K.; Räder, H.-J.; Schenk, R. *Makromol. Chem.* **1991**, *192*, 1679-1693.
- (243) Häfelinger, G.; Beyer, M. *Liebigs Ann. Chem.* **1980**, *12*, 2012-2020.
- (244) Matsuoka, S.; Fujii, H.; Yamada, T.; Pac, C.; Ishida, A.; Takamuku, S.; Kusaba, M.; Nakashima, N.; Yanagida, S.; Hashimoto, K.; Sakata, T. *J. Phys. Chem.* **1991**, *95*, 5802-5808.
- (245) Salbeck, J.; Weissörtel, F.; Bauer, J. *Macromol. Symp.* **1997**, *125*, 121-132.
- (246) Liess, P.; Hensel, V.; Schlüter, A.-D. *Liebigs Ann.* **1996**, 1037-1040.
- (247) Heidenhain, S. B.; Sakamoto, Y.; Suzuki, T.; Miura, A.; Fujikawa, H.; Mori, T.; Tokito, S.; Tag, Y. *J. Am. Chem. Soc.* **2000**, *122*, 10240-10241.
- (248) Müllen, K.; Scherf, U. *Makromol. Chem., Macromol. Symp.* **1993**, *69*, 23-33.
- (249) Horn, T.; Wegener, S.; Müllen, K. *Macromol. Chem. Phys.* **1995**, *196*, 2463-2474.
- (250) Wegener, S.; Müllen, K. *Macromolecules* **1993**, *26*, 3037-3040.
- (251) Klärner, G.; Former, C.; Yan, X.; Richert, R.; Müllen, K. *Adv. Mater.* **1996**, *8*, 932-935.
- (252) Scherf, U.; Müllen, K. *Makromol. Chem., Rapid Commun.* **1991**, *12*, 489-497.
- (253) Scherf, U.; Müllen, K. *Macromolecules* **1992**, *25*, 3546-3548.
- (254) Freund, T.; Müllen, K.; Scherf, U. *Macromolecules* **1995**, *28*, 547-551.
- (255) Fiesel, R.; Huber, J.; Scherf, U. *Angew. Chem. Int. Ed.* **1996**, *35*, 2111-2113.
- (256) Huber, J.; Müllen, K.; Salbeck, J.; Schenk, H.; Scherf, U.; Stehlin, T.; Stern, R. *Acta Polym.* **1994**, *45*, 244-247.

- (257) Grünter, J.; Hamer, P. J.; Friend, R. H.; Huber, H.-J.; Scherf, U.; Holmes, A. B. *Adv. Mater.* **1994**, *6*, 748-752.
- (258) Jin, S.-H.; Jang, M.-S.; Suh, H.-S.; Cho, H.-N.; Lee, J.-H.; Gal, Y.-S. *Chem. Mater.* **2002**, *14*, 643-650.
- (259) Fahlman, M.; Lögdlund, S.; Stafström, S.; Salaneck, W. R.; Friend, R. H.; Burn, P. L.; Holmes, A. B.; Kaeriyama, K.; Sonoda, Y.; Lhost, O.; Meyers, F.; Brédas, J. L. *Macromolecules* **1995**, *28*, 1959-1965.
- (260) Brédas, J. L. *Adv. Mater.* **1995**, *7*, 263-274.
- (261) Friend, R. H. In *Conjugated Polymers and Related Materials*; Salaneck, W. R., Lundström, I., Rånby, B., Eds.; Oxford University Press: Oxford, 1993, pp 285-323.
- (262) Burn, P. L.; Holmes, A. B.; Kraft, A.; Bradley, D. D. C.; Brown, A. R.; Friend, R. H.; Gymer, R. W. *Nature* **1992**, *356*, 47-49.
- (263) Greenham, N. C.; Moratti, S. C.; Bradley, D. D. C.; Friend, R. H.; Holmes, A. B. *Nature* **1993**, *365*, 628-630.
- (264) Hwang, D.-H.; Kim, S. T.; Shim, H.-K.; Holmes, A. B.; Moratti, S. C.; Friend, R. H. *Chem. Commun.* **1996**, 2241-2242.
- (265) Burn, P. L.; Kraft, A.; Baigent, D. R.; Bradley, D. D. C.; Brown, A. R.; Friend, R. H.; Gymer, R. W.; Holmes, A. B.; Jackson, R. W. *J. Am. Chem. Soc.* **1993**, *115*, 10117-10124.
- (266) Chung, S.-J.; Jin, J.-I.; Kim, K.-K. *Adv. Mater.* **1997**, *9*, 551-554.
- (267) Gao, M.; Richter, B.; Kirstein, S. *Adv. Mater.* **1997**, *9*, 802-805.
- (268) Tessler, N.; Harrison, N. T.; Friend, R. H. *Adv. Mater.* **1998**, *10*, 64-68.

- (269) Yu, G.; Cao, Y.; Anderson, M.; Gao, J.; Heeger, A. J. *Adv. Mater.* **1998**, *10*, 385-388.
- (270) Garten, F.; Hilberer, A.; Cacialli, F.; Esselink, E.; van Dam, Y.; Schlatmann, B.; Friend, R. H.; Klapwijk, T. M.; Hadziioannou, G. *Adv. Mater.* **1997**, *9*, 127-131.
- (271) Lee, J.-K.; Schrock, R. R.; Baigent, D. R.; Friend, R. H. *Macromolecules* **1995**, *28*, 1966-1971.
- (272) Berggrem, M.; Dodabalapur, A.; Bao, Z.; Slusher, R. E. *Adv. Mater.* **1997**, *9*, 968-971.
- (273) Klimoc, V. I.; McBranch, D. W.; Barashkov, N. N.; Ferraris, J. P. *Chem. Phys. Lett.* **1997**, *277*, 109-117.
- (274) Cornil, J.; Beljonne, D.; Shuai, Z.; Hagler, T. W.; Campbell, I.; Bradley, D. D. C.; Brédas, J. L.; Spangler, C. W.; Müllen, K. *Chem. Phys. Lett.* **1995**, *247*, 425-432.
- (275) Hennecke, M.; Damerau, T.; Müllen, K. *Macromolecules* **1993**, *26*, 3411-3418.
- (276) Colaneri, N. F.; Bradley, D. D. C.; Friend, R. H.; Burn, P. L.; Holmes, A. B.; Spangler, C. W. *Phys. Rev. B* **1990**, *42*, 11670-11681.
- (277) Xing, K. Z.; Johansson, N.; Beamson, G.; Clark, D. T.; Brédas, J. L.; Salaneck, W. R. *Adv. Mater.* **1997**, *9*, 1027-1031.
- (278) Goodson III, T.; Li, W.; Gharavi, A.; Yu, L. *Adv. Mater.* **1997**, *9*, 639-643.
- (279) Gill, R. E.; Hadziioannou, G.; Lang, P.; Garnier, F.; Wittmann, J. C. *Adv. Mater.* **1997**, *9*, 331-334.
- (280) Weitzel, H.-P.; Bohnen, A.; Müllen, K. *Makromol. Chem.* **1990**, *191*, 2815-2835.
- (281) Weitzel, H.-P.; Müllen, K. *Makromol. Chem.* **1990**, *191*, 2837-2851.
- (282) Stalmach, U.; Kolshorn, H.; Brehm, I.; Meier, H. *Liebigs Ann.* **1996**, 1449-1456.

- (283) (a) Meier, H.; Kretzschmann, H.; Lang, M.; Fraß, W.; Albrecht, C.; März, K. *J. Prakt. Chem.* **1994**, *336*, 297-302. (b) Meier, H.; Ickenroth, D. *Eur. J. Org. Chem.* **2002**, 1745-1749.
- (284) Hradsky, A.; Bildstein, B.; Schuler, N.; Schottenberger, H.; Jaitner, P.; Ongania, K.-H.; Wurst, K.; Launay, J.-P. *Organometallics* **1997**, *16*, 392-402.
- (285) Ono, N.; Tomita, H.; Maruyama, K. *J. Chem. Soc., Perkin Trans. 1* **1992**, 2453-2456.
- (286) Sonoda, Y.; Kaeriyama, K. *Polymer* **1992**, *33*, 2437-2442.
- (287) Mangel, T.; Eberhardt, A.; Scherf, U.; Bunz, U. H. F.; Müllen, K. *Makromol. Rapid Commun.* **1995**, *16*, 571-580.
- (288) Bunz, U. H. F. *Chem. Rev.* **2000**, *100*, 1605-1644.
- (289) Montali, A.; Bastiaansen, C.; Smith, P.; Weder, C. *Nature* **1998**, *392*, 261-264.
- (290) Weder, C.; Sarwa, C.; Bastiaansen, C.; Smith, P. *Adv. Mater.* **1997**, *9*, 1035-1039.
- (291) Zhou, Q.; Swager, T. M. *J. Am. Chem. Soc.* **1995**, *117*, 12593-12602.
- (292) Polin, J.; Buchmeiser, M.; Nock, H.; Schottenberger, H. *Mol. Cryst. Liq. Cryst.* **1997**, *293*, 287-307.
- (293) Nelson, J. C.; Saven, J. G.; Moore, J. S. *Science* **1997**, *277*, 1793-1796.
- (294) Lavastre, O.; Ollivier, L.; Dixneuf, P. H.; Sibandhit, S. *Tetrahedron* **1996**, *52*, 5495-5504.
- (295) Schumm, J. S.; Pearson, D. L.; Tour, J. M. *Angew. Chem., Int. Ed. Engl.* **1994**, *33*, 1360-1363.
- (296) Schumm, J. S.; Pearson, D. L.; Jones II, L.; Hara, R.; Tour, J. M. *Nanotechnology* **1996**, *7*, 430-433.

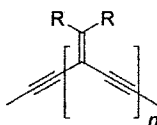
- (297) Young, J. K.; Nelson, J. C.; Moore, J. S. *J. Am. Chem. Soc.* **1994**, *116*, 10841-10842.
- (298) Tour, J. M.; Jones II, L.; Pearson, D. L.; Lamba, J. J. S.; Burgin, T. P.; Whitesides, G. M.; Allara, D. L.; Parikh, A. N.; Atre, S. V. *J. Am. Chem. Soc.* **1995**, *117*, 9529-9534.
- (299) Bumm, L. A.; Arnold, J. J.; Cygan, M. T.; Dunbar, T. D.; Burgin, T. P.; Jones II, L.; Allara, D. L.; Tour, J. M.; Weiss, P. S. *Science* **1996**, *271*, 1705-1707.
- (300) Reed, M. A.; Zhou, C.; Muller, C. J.; Burgin, T. P.; Tour, J. M. *Science* **1997**, *278*, 252-254.
- (301) Grubbs, R. H.; Kratz, D. *Chem. Ber.* **1993**, *126*, 149-157.
- (302) Meier, H.; Ickenroth, D.; Stalmach, U.; Koynov, K.; Bahtiar, A.; Bubeck, C. *Eur. J. Org. Chem.* **2001**, 4431-4443.
- (303) Hopf, H.; Maas, G. *Angew. Chem., Int. Ed. Engl.* **1992**, *31*, 931-954.
- (304) Fielder, S.; Rowan, D. D.; Sherburn, M. S. *Angew. Chem. Int. Ed.* **2000**, *39*, 4331.
- (305) Brain, P. T.; Smart, B. A.; Robertson, H. E.; Davis, M. J.; Rankin, D. W. H.; Henry, W. J.; Gosney, I. *J. Org. Chem.* **1997**, *62*, 2767-2773.
- (306) Swager, T. M.; Grubbs, R. H. *J. Am. Chem. Soc.* **1987**, *109*, 894-896.
- (307) Armaresh, R. A.; Liu, D.; Knonvalova, T.; Lakshmikantham, M. V.; Cava, M. P.; Kispert, L. D. *J. Org. Chem.* **2001**, *66*, 7757-7764.
- (308) Bryce, M. R.; Coffin, M. A.; Skabara, P. J.; Moore, A. J.; Batsanov, A. S.; Howard, J. A. K. *Chem. Eur. J.* **2000**, *6*, 1955-1962.
- (309) Zhao, Y.; Tykwinski, R. R. *J. Am. Chem. Soc.* **1999**, *121*, 458-459.
- (310) Zhao, Y.; Campbell, K.; Tykwinski, R. R. *J. Org. Chem.* **2002**, *67*, 336-344.

- (311) (a) Zhao, Y.; McDonald, R.; Tykwinski, R. R. *Chem. Commun.* **2000**, 77-78. (b)  
Zhao, Y.; McDonald, R.; Tykwinski, R. R. *J. Org. Chem.* **2002**, *67*, 2805-2812.
- (312) Ciulei, S. C.; Tykwinski, R. R. *Org. Lett.* **2000**, *2*, 3607-3610.
- (313) Zhao, Y.; Ciulei, S. C.; Tykwinski, R. R. *Tetrahedron Lett.* **2001**, *42*, 7721-7723.
- (314) Mao, S. S. H.; Tilley, T. D. *J. Organomet. Chem.* **1996**, *521*, 425-428.
- (315) Londergan, T. M.; You, Y. J.; Thompson, M. E.; Weber, W. P. *Macromolecules*  
**1998**, *31*, 2784-2788.
- (316) Meier, H.; Aust, H. *J. Prakt. Chem.* **1999**, *341*, 466-471.
- (317) Aust, H.; Ickenroth, D.; Meier, H. *J. Prakt. Chem.* **1999**, *341*, 523-528.
- (318) Kurata, H.; Kawase, T.; Oda, M. *Chem. Lett.* **1994**, 2219-2222.
- (319) Kurata, H.; Hisamitsu, A.; Oda, M. *Tetrahedron Lett.* **1997**, *38*, 8875-8878.

## Chapter 2 Synthesis and Characterization of *iso*-Polydiacetylenes

### 2.1 Introduction

As I started my Ph.D. studies in the area of acetylene chemistry in 1998, one fact had become of extreme interest in our group: cross-conjugated molecules had remained a neglected class of compounds compared with the extensively investigated linearly conjugated molecules. More importantly, the potential applications of oligomeric and polymeric materials with a fully cross-conjugated carbon backbone were quite unexplored.<sup>1</sup> This is not to say, however, that molecules with a cross-conjugated framework are rare. The situation is, in fact, quite the opposite. Cross conjugation can be found in a wide range of natural and non-natural molecules, including examples such as quinones, radialenes, fulvalenes and fused aromatics (*vide supra*). As for nonaromatic oligomers and polymers, however, there seems to be a definite void in the literature.



91 R = H, Me, alkyl, phenyl,...

As we were contemplating a series of model compounds for surveying cross-conjugated oligomers, *iso*-polydiacetylenes (*iso*-PDAs) **91** emerged as an ideal class of molecules to begin with.<sup>2</sup> Unlike that of dendralenes, the backbone of *iso*-PDAs **91** favors a planar conformation since the insertion of a C≡C triple bond supplies sufficient space to eliminate steric hindrance. Therefore, they can act satisfactorily as model compounds for the study of cross-conjugation effects in oligomeric systems. It is obvious that  $\pi$ -electron density in the cross-conjugated oligomers can not readily be delocalized

along the carbon framework in a manner analogous to that in their linearly conjugated counterparts. To a first approximation, it may be expected that electronic communication could be limited to segments composed of the longest linearly conjugated  $\pi$ -orbitals. As a consequence, an infinite, cross-conjugated system would then be approximated by the combined contributions of these segments. It seemed inappropriate, however, to predict the electronic properties of cross-conjugated oligomers based on this simple empirical model that could exclude weak electronic interaction between each cross-conjugated segment.

This, then, became the focus of our work in the area of enyne oligomers, as we sought to answer several questions: (1) Is the synthesis of monodisperse, enyne oligomer viable? (2) Would they be stable? (3) Could we find evidence of electronic communication via cross conjugation? (4) Could cross conjugation be used to provide fully conjugated polymers with significant transparency to function as nonlinear optical or electroluminescent materials?

Two major factors suggested that *iso*-PDAs would be an excellent class of molecules to target as we began our quest into the electronic effects of cross conjugation. First, we anticipated that *iso*-PDAs would be synthetically accessible via palladium-catalyzed cross-coupling reactions between vinyl triflates and terminal alkynes; methodology that could be used iteratively to provide monodisperse oligomers.<sup>3,4</sup> Second, the insertion of the alkynyl group into the dendralene skeleton would allow for coplanarity of the enyne repeat units (in the case of methylenidene and isopropylidene substitution), regardless of whether a cisoid or transoid conformation were assumed. In this way, electronic effects could be separated from steric effects.

The synthesis we envisioned for cross-conjugated enynes hinged essentially on the success of only two transformations. First, we need easy access to the vinyl triflate building blocks (e.g., **92**, Fig. 2.1). This part was easy, as Stang and co-workers had elegantly worked out the high-yielding methodology for numerous vinyl triflates during the 1980's.<sup>5-7</sup> Second, we needed to successfully apply palladium-catalyzed cross-coupling methods employing vinyl triflates and terminal alkynes toward highly conjugated systems. Although alkynyl cross-coupling reactions with vinyl triflates had been well documented in the literature,<sup>3,4</sup> they had not been used extensively for molecules and oligomers with such highly unsaturated frameworks.

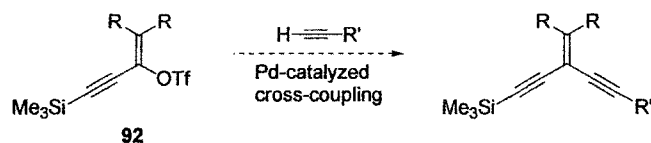


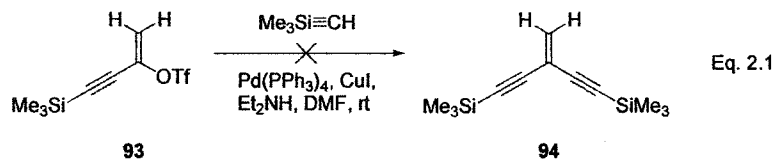
Fig. 2.1 Proposed assembly of *iso*-PDAs.

## 2.2 Results and Discussion

### 2.2.1 Synthesis

The reported procedure of Stang easily provided vinyl triflate **93** from corresponding ketone.<sup>6</sup> Targeting what we consider to be the parent *iso*-PDA series, with vinylidene subunits, attempts to apply palladium-catalyzed cross-coupling conditions to **93** were quite disappointing (Eq. 2.1). Using several different conditions including Pd(PPh<sub>3</sub>)<sub>4</sub> or PdCl<sub>2</sub>(PPh<sub>3</sub>)<sub>2</sub> catalysts, CuI co-catalyst, Et<sub>2</sub>NH, in THF or DMF, the results were consistently the same—an intractable black mass. These results, however, were not completely unexpected considering that Alberts had previously reported that enediyne **94** showed considerable instability and slowly polymerized at room temperature.<sup>8</sup>

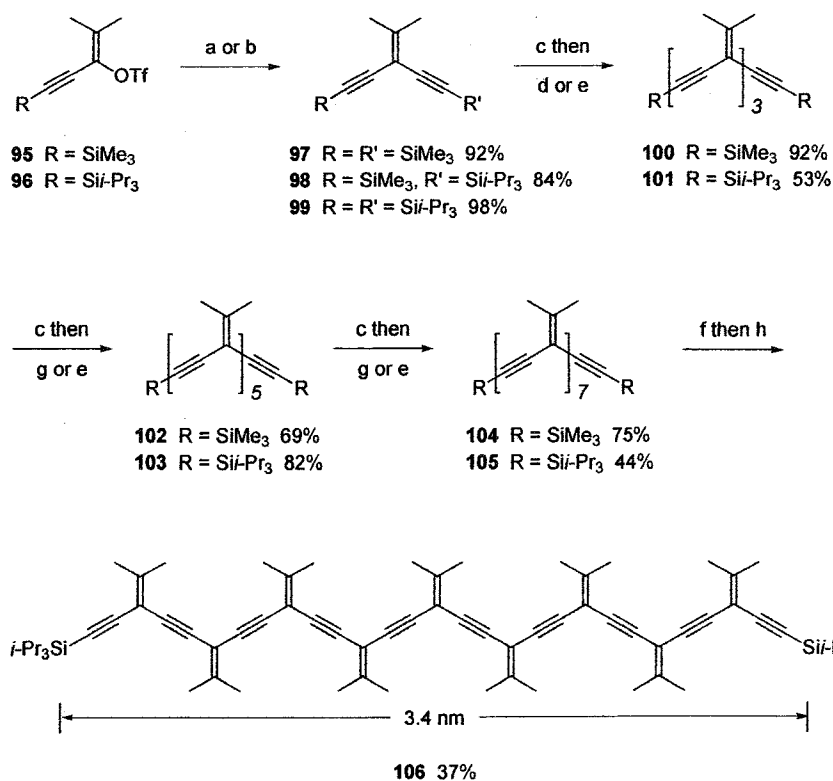
Furthermore, one can easily envision a number of competing processes under standard palladium coupling conditions, including alkyne formation via the elimination of triflic acid, as well as Heck chemistry at the vinylidene position.



Thus, we targeted the next higher analogue, which placed methyl groups at the vinylidene positions rather than the hydrogen of **94**, expecting that the methyl groups could provide additional stability to the system as well as, perhaps, solubility. A synthetic strategy was subsequently chosen, which included an iterative series of desilylation and cross-coupling steps such that the oligomeric chain lengths could be rapidly increased in a divergent manner from enediynes **97–99** (Scheme 2.1).<sup>9</sup>

The essential vinyl triflate building blocks **95** and **96** were readily obtained through the methods described by Stang *et al.* Triflates **95** and **96** were cross-coupled with trimethylsilylacetylene (TMSA) or triisopropylsilylacetylene (TIPSA) using PdCl<sub>2</sub>(PPh<sub>3</sub>)<sub>2</sub> catalyst, CuI co-catalyst, and *i*-Pr<sub>2</sub>NH base in THF at ambient temperature to give monomers **97**, **98**, and **99** respectively. Optimization of the cross-coupling conditions of these reactions showed that the choice of catalyst and solvent (THF or DMF) could be altered without significantly affecting the outcome of the coupling reaction. In most cases, the reactions were complete within 2 h as determined by thin layer chromatographic (TLC) analysis.

### Scheme 2.1



Reagents and conditions: (a) trimethylsilylacetylene, PdCl<sub>2</sub>(PPh<sub>3</sub>)<sub>2</sub>, CuI, *i*-Pr<sub>2</sub>NH, THF, rt. (b) triisopropylsilylacetylene, PdCl<sub>2</sub>(PPh<sub>3</sub>)<sub>2</sub>, CuI, *i*-Pr<sub>2</sub>NH, THF, rt. (c) K<sub>2</sub>CO<sub>3</sub>, wet MeOH/THF (1:1), rt. (d) **95**, Pd(PPh<sub>3</sub>)<sub>4</sub>, CuI, Et<sub>2</sub>NH, DMF, rt. (e) **96**, Pd(PPh<sub>3</sub>)<sub>4</sub>, CuI, Et<sub>2</sub>NH, DMF, rt. (f) TBAF, wet THF, rt. (g) **95**, Pd(PPh<sub>3</sub>)<sub>4</sub>, CuI, Et<sub>2</sub>NH, THF, rt. (h) **96**, Pd(PPh<sub>3</sub>)<sub>4</sub>, CuI, Et<sub>2</sub>NH, THF, rt.

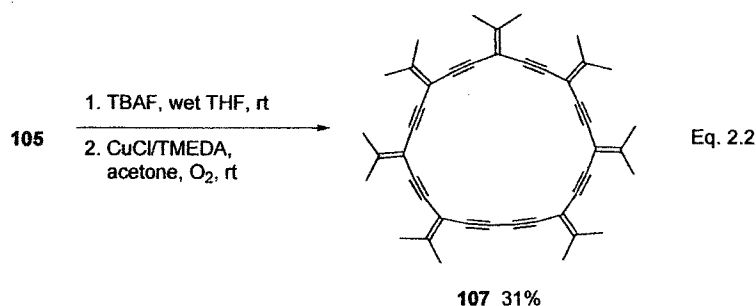
The first series of oligomers we targeted were end-capped with trimethylsilyl (TMS) groups, as it was anticipated that removal of this group in subsequent iterations would be more facile than the removal of the more robust triisopropylsilyl (TIPS) group. Thus, monomer **97** was protodesilylated in methanoic K<sub>2</sub>CO<sub>3</sub> to give, in essentially quantitative yield, the deprotected terminal diyne that may be used without further purification. The deprotected enediyne was cross-coupled with **95** to afford trimer **100**, which was isolated via flash chromatography as a colorless solid in 92% yield. A

subsequent iteration of the protidesilylation and cross-coupling sequence gave pentamer **102** in 69% yield, as a colorless solid that was still quite soluble in chlorinated organic solvents. Desilylation of **102** followed by cross-coupling in DMF, however, was problematic as both deprotected **102** and heptamer **104** were only sparingly soluble in this solvent. Performing the cross-coupling reaction of desilylated **102** with vinyl triflate **95** with THF as the solvent helped to solubilize the heptamer product **104** such that it could be isolated in 75% yield as a relatively insoluble, colorless solid. We were unable, however, to effect the next iteration with **104** toward the nonameric derivative due to insolubility. Intermolecular aggregation may contribute to this insolubility,<sup>10,11</sup> although dilution studies (*vide infra*) monitored by UV-vis spectroscopy as well as NMR data suggest that aggregation is not a major factor.

In the second series of *iso*-PDAs, the TIPS group was employed as an endcapping group, which was expected to enhance solubility of the products because of increased steric bulk that reduces the aggregation effects. Using the iterative sequence outlined above, the formation of the TIPS-protected series employed the respective TMS-endcapped precursors due to the more facile removal of this protecting group. Thus, protidesilylation of enediyne **97** followed directly by cross-coupling with TIPS-protected triflate **96** afforded trimer **101** in 53% yield. Desilylation of TMS-protected trimer **100** followed by cross-coupling with **96** gave pentamer **103** in 82% yield. Desilylation of pentamer **102** and cross-coupling with **96** afforded heptamer **105** as a stable colorless solid in a yield of 44%, which was gratifyingly soluble in most organic solvents. While the increased solubility of **105** circumvented the problem encountered with TMS-protected heptamer **104**, there was no way to enhance the solubility of the

deprotected heptamer (*vide supra*). Thus, toward the formation of nonamer **106**, the best conditions for deprotection of **104** utilized tetrabutylammonium fluoride (TBAF) in a dilute solution of THF, thus avoiding the less solubilizing MeOH used with K<sub>2</sub>CO<sub>3</sub>. After reaction of **104** with TBAF for ca. 15 min, the reaction mixture was diluted with a large volume of Et<sub>2</sub>O, and aqueous workup provided the terminal alkyne. Following concentration of the ethereal solution, and resolution with a minimal amount of THF, coupling to triflate **96** gave nonamer **106** in 37% yield. The reasonable solubility of **106** allowed for spectroscopic characterization of this nanometer-length oligomer, which measures 3.4 nm from Si to Si.<sup>12</sup> The <sup>1</sup>H NMR spectrum of **106** showed a resonance pattern and integration that is consistent with the proposed structure. The IR spectrum is also in good agreement with the structure of **106**, where no butadiyne vibrational peak is present. All attempts to obtain a meaningful mass spectral analysis (e.g., EI and ESI MS), however, have been unsuccessful. The reaction to produce **106** was always accompanied by the formation of macrocycle **107** (see Eq. 2.2), the result of copper-catalyzed, oxidative homocoupling of the two terminal alkynes. Prior to this point, the competing homocoupling reaction had not been problematic. Two factors likely contributed to its presence in current case: (1) a greater amount of O<sub>2</sub> (requisite for the homocoupling reaction) due to the increased amount of solvent employed to accommodate desilylated **104**, and (2) the higher dilution favoring an intramolecular reaction.<sup>13</sup> To provide sufficient quantities of expanded radialene **107** for characterization, it was synthesized via homocoupling of the deprotected heptamer using Hay catalysis<sup>14</sup> in dry acetone (Eq. 2.2). Although the solubility of both the precursor

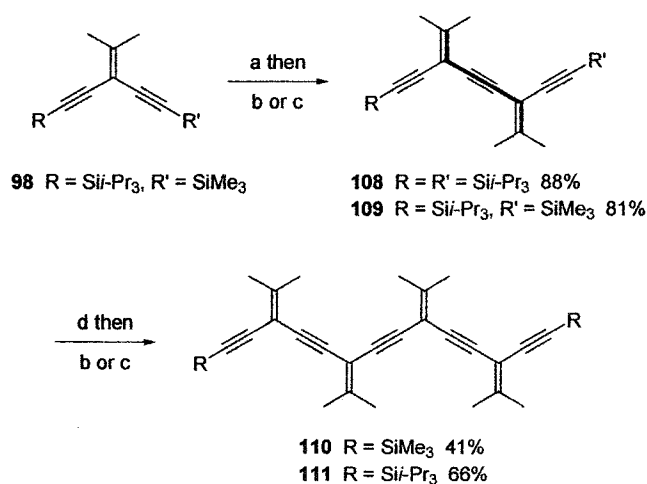
and product complicates this reaction, the cyclic enyne heptamer **107** could be isolated in 31% yield as a rather insoluble colorless solid.



To complete the series of oligomers, and for the purpose of comparison, *iso*-PDA oligomers with an even number of repeating units were assembled as outlined in Scheme 2.2. Treatment of differentially protected enediyne **98** with  $\text{K}_2\text{CO}_3$  in THF/MeOH (1:1) effected selective removal of the TMS group, while leaving the more robust TIPS group unaffected. Following workup, cross-coupling with either vinyl triflate **96** or vinyl triflate **95** gave dimer **108** and **109** in yields of 88% and 81%, respectively. Protodesilylation of **108** or **109** in a dilute THF solution using TBAF followed by cross-coupling with **95** or **96** led to tetramer **110** and **111** in yields of 41% and 66%, respectively.

Irrespective of TMS or TIPS protecting groups, the *iso*-PDA oligomers incorporating the isopropylidene building block show decreasing stability with increasing chain length. For oligomers longer than the pentamer, stability can vary from a couple days to several weeks under refrigeration, as evaluated by TLC and  $^1\text{H}$  NMR spectroscopic analysis. Storing the oligomers under an inert gas afforded better stability, but not substantially. Preliminary evidence<sup>15</sup> suggests that an oxygen ene reaction at the isopropylidene moiety is likely the primary decomposition pathway.<sup>16-18</sup>

## Scheme 2.2



Reagents and conditions: (a) K<sub>2</sub>CO<sub>3</sub>, wet MeOH/THF (1:1), rt. (b) **96**, Pd(PPh<sub>3</sub>)<sub>4</sub>, CuI, Et<sub>2</sub>NH, DMF, rt. (c) **95**, Pd(PPh<sub>3</sub>)<sub>4</sub>, CuI, Et<sub>2</sub>NH, DMF, rt. (d) TBAF, wet THF, rt.

### 2.2.2 Physical Characteristics

The spectroscopic data for the *iso*-PDA oligomers are consistent with their proposed structures. In the <sup>13</sup>C NMR spectra for members of this isopropylidene *iso*-PDA series, the resonances of the pendant methyl groups are observed in a range of 22–23 ppm. The vinylidene carbons outside of the main chain of the oligomers (C=CMe<sub>2</sub>) are quite deshielded, resonating in a range of 152–155 ppm. The other vinylidene carbons (C=CMe<sub>2</sub>) fall into the chemical shift of the acetylene carbons, from 88 to 104 ppm. Even at 125 MHz, significant chemical shift degeneracy is observed in the <sup>13</sup>C NMR spectroscopic analysis of the longest oligomer, nonamer **106**, for which only 11 of 20 unique sp and sp<sup>2</sup> carbon resonances are discernible. Nevertheless, all unique sp and sp<sup>2</sup> resonances for the pentameric species **102** and **103** are observed in the expected ranges.

All *iso*-PDAs show significant thermal stability. For the TMS-endcapped series, trimeric **100** melts at 136 °C, whereas pentameric **102** and heptameric **104** show only decomposition points at 196 and >170 °C, respectively. For TIPS derivatives, dimeric **108**, trimeric **101**, and tetrameric **111** show well-defined melting points at 65–66, 70–71, and 89–90 °C, respectively. This data suggests that, despite their highly unsaturated structures, longer oligomeric or polymeric *iso*-PDAs would also be expected to show reasonable thermal stability.

### 2.2.3 *Solid-State Structures*

To shed light on the solid-state structural properties of cross-conjugated enynes, single-crystal X-ray analyses of monomer **99** and trimer **101** were performed, and the respective ORTEP plots are shown in Fig. 2.2 and 2.3.<sup>19</sup> Single crystals of **99** were obtained by diffusion of MeOH into a CH<sub>2</sub>Cl<sub>2</sub> solution at 4 °C, and the X-ray crystal data were collected at low temperature (–80 °C). Two crystallographically independent molecules were present in the unit cell. Although disorder hampered refinement of the data, the structure of **99** is sufficient for an empirical analysis, as well as a point of comparison to the extended structure of trimer **101**. There are two notable features of the solid-state structure of **99**: (1) the vinylidene angle C(12)–C(13)–C(17) at 112.9(4)° (114.4(4)° for the other independent molecule), which is slightly less than the anticipated angle of 120° for an sp<sup>2</sup>-hybridized carbon center, and (2) the Si–C≡C bonds at 173°, which is distorted from linearity, presumably due to crystal packing effects.

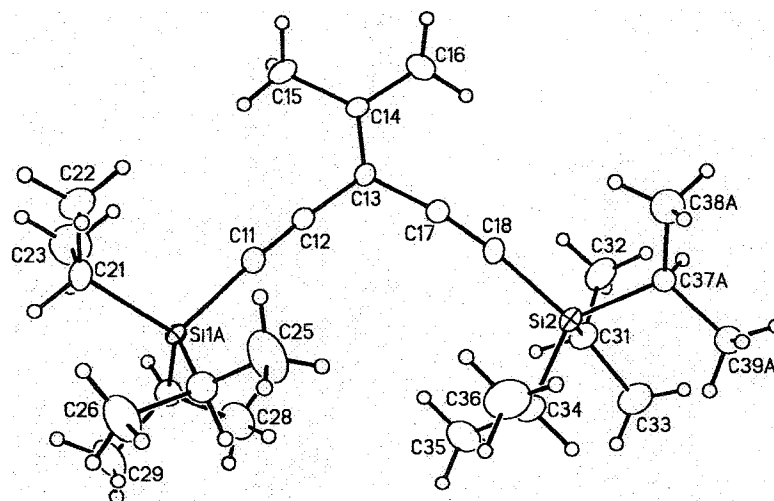


**Fig. 2.2** ORTEP drawing (20% probability level) of **99** (molecule A). Selected bond lengths (Å) and angles (°): C(11)–C(12) 1.191(6), C(12)–C(13) 1.440(6), C(13)–C(14) 1.347(6), C(13)–C(17) 1.448(7), C(17)–C(18) 1.215(6); Si(1A)–C(11)–C(12) 173.2(6), C(11)–C(12)–C(13) 176.0(5), C(12)–C(13)–C(14) 124.3(4), C(12)–C(13)–C(17) 112.9(4), C(13)–C(17)–C(18) 172.4(5), Si(2)–C(18)–C(17) 172.7(4).

In the same manner, single crystals of **101** were also obtained by diffusion of MeOH into a CH<sub>2</sub>Cl<sub>2</sub> solution at 4 °C, and the structural data were collected at low temperature. The C<sub>2v</sub> symmetrical structure of **101** is essentially planar with a maximum deviation from the least-squares plane of carbon and silicon framework (excluding the isopropyl groups) of 0.126(4) Å. Of three possible planar geometries, **101** assumes an all-transoid orientation of the olefins with respect to the acetylenic linkers. Unlike their linearly conjugated isomers, polydiacetylenes,<sup>20</sup> no observable reduction in bond length alternation is observed in the *iso*-PDA trimer. Single bonds of the conjugated framework, for example, C(3)–C(5) and C(6)–C(7) at 1.435(5) and 1.439(5) Å, respectively, are in the range expected for single bonds linking sp and sp<sup>2</sup> carbons.<sup>25</sup> The two C≡C bonds at 1.206(5) and 1.199(5) Å and the two C=C bonds at 1.347(5) and 1.349(5) Å are also in the range expected. Bond lengths for **101** are comparable to those

found in monomer **99**. The alkylidene bond angle C(2)–C(3)–C(5) at 115.4(3)° and C(6)–C(7)–C(6') at 115.5(5)° are also similar to the analogous angle of enediyne **99**.

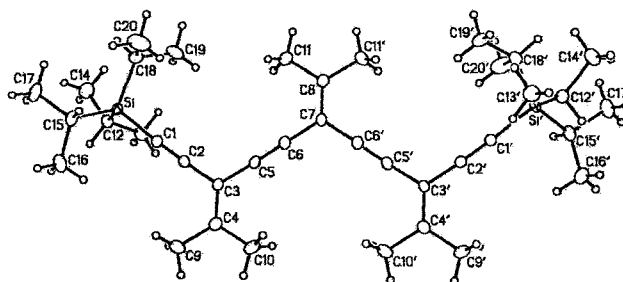


**Fig. 2.3** ORTEP drawing (20% probability level) of **101**. Selected bond lengths (Å) and angles (°): C(1)–C(2) 1.206(5), C(2)–C(3) 1.442(5), C(3)–C(4) 1.347(5), C(3)–C(5) 1.435(5), C(5)–C(6) 1.199(5), C(6)–C(7) 1.439(5), C(7)–C(8) 1.349(8); Si–C(1)–C(2) 177.1(3), C(1)–C(2)–C(3) 176.7(4), C(2)–C(3)–C(4) 123.1(3), C(2)–C(3)–C(5) 115.4(3), C(3)–C(5)–C(6) 177.4(4), C(5)–C(6)–C(7) 178.2(4), C(6)–C(7)–C(8) 122.2(2), C(6)–C(7)–C(6') 115.5(5).

#### 2.2.4 Electronic Properties

From our perspective, the most interesting feature of the *iso*-PDA oligomers is their unique cross-conjugated  $\pi$  framework. As demonstrated by the diagrams in Fig 2.4 for a cisoid *iso*-PDA dimer, two sets of orthogonal sp orbitals can potentially contribute to electron communication. The out-of-plane p orbitals (right) form the longest  $\pi$ -conjugated segment in an *iso*-PDA oligomer, and it is anticipated that the lowest-energy electronic absorption would be due to this sequence of  $sp^2$  and sp orbitals. Because of the nature of cross conjugation, the out-of-plane  $\pi$  electrons would be expected to be delocalized across the alkylidene segments only in the lowest-energy  $\pi$  orbital, that is, the fully symmetrical orbital as depicted in Fig. 2.4. The in-plane set of orbital (left) are essentially isolated, but could allow for a certain amount of overlap between each conjugated segment as a result of homoconjugation.<sup>21</sup>

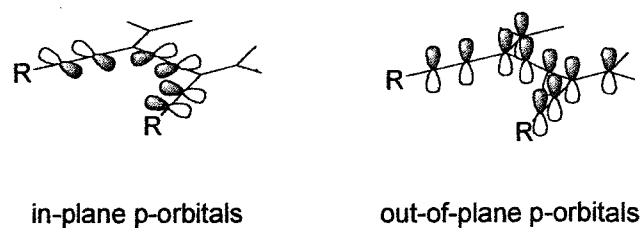
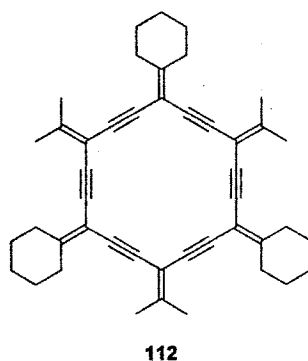


**Fig. 2.4** Orthogonal  $\pi$ -systems in *iso*-PDAs.

The UV-vis spectra in  $\text{CHCl}_3$  of the TMS- and TIPS-encapped oligomers ranging from trimer to heptamer and dimer to nonamer, respectively, are shown in Fig. 2.5. The predominant feature of the electronic absorption behavior of the *iso*-PDA oligomers is a steadily increasing molar absorptivity as the number of enyne monomer unit is increased. In the spectrum of dimer **108**, two distinct, low-energy absorptions are due to the  $\pi \rightarrow \pi^*$  transition from HOMO to LUMO. In the cisoid orientation ( $C_{2v}$ ), the HOMO to LUMO ( $A_1 \rightarrow B_1$ ) and HOMO to LUMO + 1 ( $A_1 \rightarrow A_1$ ) transitions are both symmetry-allowed. However, in the centrally symmetric transoid orientation ( $C_{2h}$ ), only the HOMO to LUMO ( $A_g \rightarrow B_u$ ) transition is symmetry-allowed, whereas the HOMO to LUMO + 1 ( $A_g \rightarrow A_g$ ) transition is symmetry forbidden. The low-energy absorption peak at 306 nm is ascribed to the HOMO to LUMO transition in the transoid orientation, whereas the higher-energy absorption peak seen at 291 nm likely corresponds to HOMO to LUMO or a combination of the HOMO to LUMO and HOMO to LUMO + 1 transitions of the cisoid orientation. This assignment is supported by UV-vis analysis of cyclic *iso*-PDA oligomers (expanded radialenes, e.g., **112**) which are constrained to a cisoid conformation. In the cyclic derivatives such as **112**, the analogous lower-energy absorbance at 305 nm is absent, whereas the higher energy absorption at 283 nm remains.



Unfortunately, the absence of a second, clear absorption band in the spectrum of **112** makes it impossible to distinguish between the HOMO to LUMO and HOMO to LUMO + 1 transitions in the spectra of either the cyclic or the acyclic *iso*-PDAs. As one progresses from the dimer **108** to longer oligomers, the absorption band broaden significantly due to an increasing number of rotational degrees of freedom, and beyond the stage of trimer **101**, only one broad, featureless absorption is observed. The spectra of TMS-encapped *iso*-PDAs showed similar characteristics.

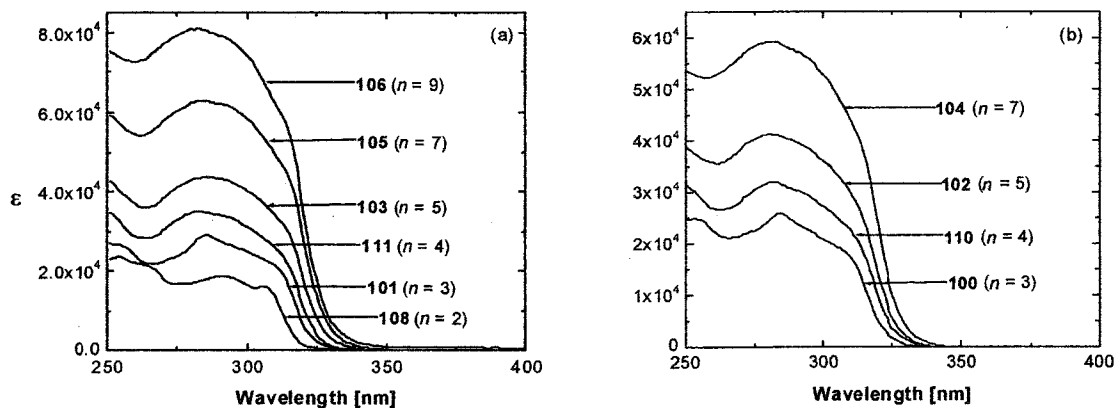


**Fig. 2.5** (a) Electronic absorption spectra ( $\epsilon$  [ $\text{L mol}^{-1} \text{cm}^{-1}$ ]) in  $\text{CHCl}_3$  comparing the effects of oligomer length between TIPS-encapped *iso*-PDA oligomers. (b) Electronic absorption spectra ( $\epsilon$  [ $\text{L mol}^{-1} \text{cm}^{-1}$ ]) in  $\text{CHCl}_3$  comparing the effects of oligomer length between TMS-encapped *iso*-PDA oligomers.

The framework of dimeric **108** and **109** contains the longest linearly conjugated segment found in any of the *iso*-PDAs, that is the ene-yne-ene sequence shown in bold (Scheme 2.2). In the absence of electronic contributions from cross conjugation, the absorbance spectrum of **108** or **109** should be representative of the longer *iso*-PDA oligomers. As can be seen in Fig. 2.5, however, a slight lowering of the cutoff energy for elongated oligomers is observed as one progresses from dimer **108** to nonamer **106**.

The solution state optical band gap  $E_g$  of the *iso*-PDA oligomers has been approximated by two methods: (a) from the intersection between the tangent passing through the turning point of the shoulder of the lowest-energy absorption band and the x axis, and (b) from maximal wavelength at one-half intensity of the maximal absorption. Fig. 2.6 shows that plots of estimated band gap ( $E_g$ ) versus the reciprocal of monomer unit numbers ( $1/n$ ) are similar for both methods. The band gap values decrease slightly with an increasing monomer unit number ( $n$ ) from dimer to heptamer, eventually reaching a constant at the stage of nonamer. By extrapolation, it is reasonable to suggest that any further extension of the oligomer chain length will not lower  $E_g$ ; that is, the band gap of a polymer containing an infinite number of monomer units would be the same as that of the nonamer, 3.75 eV (as measured by method A). As this value represents the  $\pi \rightarrow \pi^*$  transition, it is clear that  $\pi$ -electron communication along the *iso*-PDA framework (between adjacent cross-conjugated enyne subunits) quickly reaches saturation by the stage of the nonamer, and transparency should be preserved beyond this energy level. In other words, this result suggests an  $n_{\text{ECL}} = 9$  for the *iso*-PDA oligomeric systems.

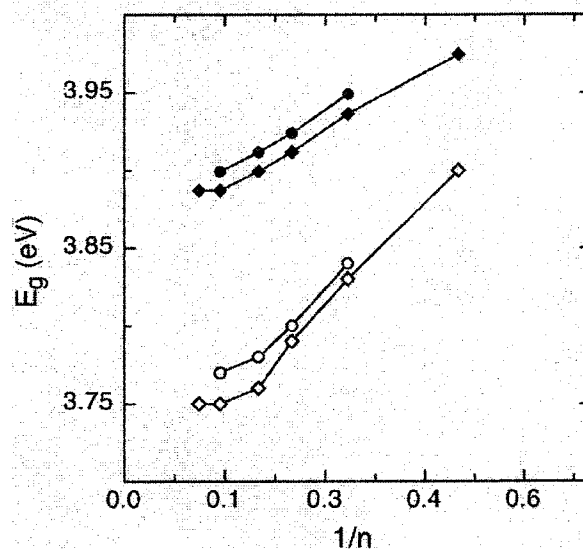


**Fig. 2.6** Plot of estimated optical band gap ( $E_g$ ) versus reciprocal number of monomer units ( $1/n$ ) of TIPS and TMS endcapped *iso*-PDAs via method A ( $\circ$ , TMS;  $\diamond$ , TIPS) and method B ( $\bullet$ , TMS;  $\blacklozenge$ , TIPS).

Furthermore, the experimental ECL of *iso*-PDAs obtained from UV-vis spectral analysis is, interestingly, in good agreement with the value from theoretical prediction. Semi-empirical calculations were accomplished for the series of *s-trans iso*-PDA oligomers ( $n = 2-10$ ) **78** (see page 65 for structure), where all the vinylidene substituents and endcapped groups were replaced by hydrogens to save computing time. The geometries optimization of this *iso*-PDA series as well as consequent single-point energy calculations were all performed using AM1 method.<sup>22</sup> The calculated results of the *iso*-PDAs **78**, ranging from dimer to dodecamer, are listed in Table 2.1. It is noteworthy that the calculated bandgaps of **78** in gas phase are dramatically greater than those measured in solution state ( $> 8$  eV), because the calculation did not take the solvation effect and other weak interactions into account. Additionally, a plot of band gap ( $E_g = E_{\text{LUMO}}$

–  $E_{\text{HOMO}}$ ) versus reciprocal number of monomer units ( $1/n$ ) (as shown in Fig. 2.7) also suggests an  $n_{\text{ECL}} = 9\sim 10$ , which is consistent with the experimental value.

**Table 2.1** Semi-empirical calculation results for *iso*-PDA oligomers **78** ( $n = 2\text{--}10$ ).<sup>a</sup>

$n$	$\Delta H_f$ (kcal/mol)	$E_{\text{LUMO}}$ (eV)	$E_{\text{HOMO}}$ (eV)	$E_g$ (eV)
2	193.2891	-0.3602	-9.08913	8.72893
3	262.4478	-0.51905	-8.95010	8.43105
4	331.6082	-0.59822	-8.89325	8.29503
5	400.7714	-0.64401	-8.86604	8.22203
6	469.9347	-0.67315	-8.85145	8.17830
7	539.0987	-0.69293	-8.84300	8.15007
8	608.2630	-0.70698	-8.83781	8.13083
9	677.4271	-0.71739	-8.83445	8.11706
10	746.5911	-0.72531	-8.83160	8.10629

<sup>a</sup> All oligomers were assumed adopting *s-trans* conformations. Optimization and single-point energy calculations were done at AM1 level using *MacSpartan Plus*.

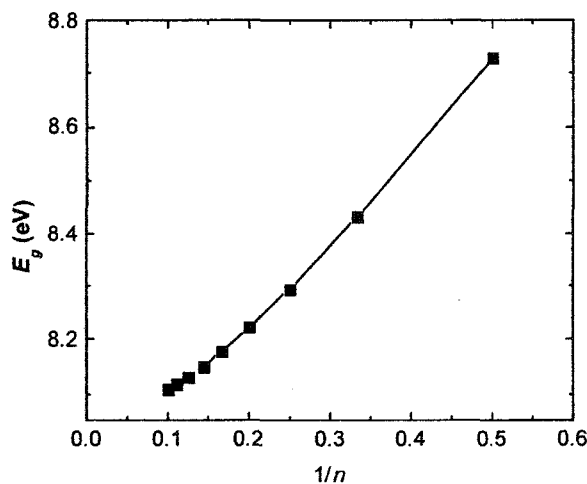


**Fig. 2.7** Plot of calculated band gap ( $E_g$ ) versus reciprocal number of monomer units ( $1/n$ ) of unsubstituted *iso*-PDAs **78**.

The influence of solvent polarity on the electronic absorption for dimeric **108** was investigated via spectroscopic measurement in  $\text{CHCl}_3$ , THF, benzene,  $\text{Et}_2\text{O}$ , and hexanes (Fig. 2.8). Spectra for **108** acquired in more polar solvents display a maximum absorption peak ( $\lambda_{\text{max}}$ ) slightly shifted to longer wavelengths. This shift, however, is rather small; it ranges from a minimum value in hexanes of 303 nm to a maximum value in THF or  $\text{CHCl}_3$  of 306 nm. The overall shape and molar absorptivities for the spectra are essentially independent of solvent.

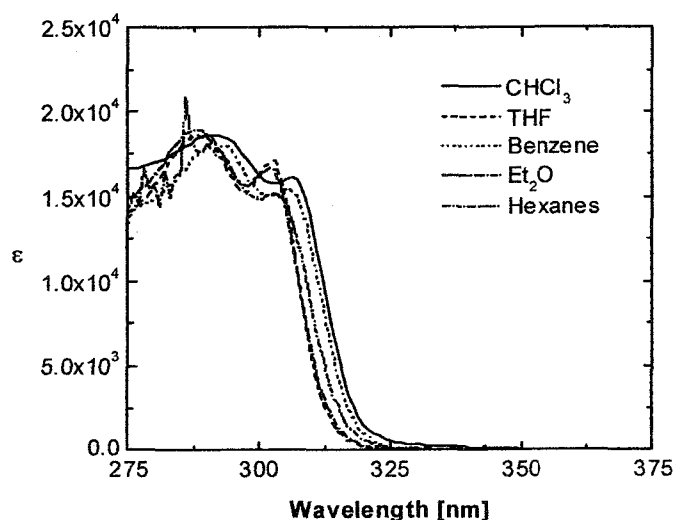
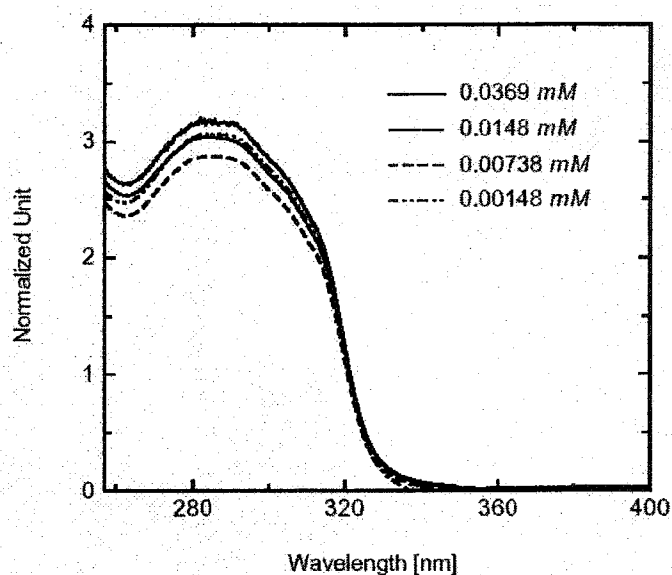


Fig. 2.8 Electronic absorption spectra ( $\epsilon$  [ $\text{L mol}^{-1} \text{cm}^{-1}$ ]) of **108** in various solvents.

The possible effects of intermolecular aggregation of the *iso*-PDA pentamer **102** were measured in  $\text{CHCl}_3$  at varying concentrations ranging from  $10^{-5}$  to  $10^{-8}$  M. The consistent profiles and molar absorptivity values observed at different concentrations suggest that aggregation is negligible for molecule **102** in  $\text{CHCl}_3$  for the concentration range accessible for UV-vis spectroscopic studies. Consistent line shapes and chemical shifts observed in  $^1\text{H}$  NMR spectroscopic analyses, regardless of concentration, also support the absence of aggregation in more concentrated solutions of **102**.



**Fig. 2.9** Electronic absorption spectra of **102** at various concentrations. The absorption scale has been normalized to facilitate comparison.

The absorption spectra of TIPS-encapped *iso*-PDAs as thin films cast from  $\text{CHCl}_3$  solutions onto quartz slides are shown in Fig. 2.10. The shorter oligomers with  $n = 2-4$  (**108**, **101**, and **111**) form reasonably decent films, and the absorption spectra are virtually identical to those measured in  $\text{CHCl}_3$ ; that is, no pronounced aggregation band is detected. Films of the longest oligomer to be measured, pentamer **103**, were less well behaved and showed considerable tailing to low energy. The films of **103**, however, reproducibly demonstrated a measurable red shift in the low-energy absorption to 331 nm that suggests aggregation may become a factor for longer oligomers in the solid state.<sup>23,24</sup>

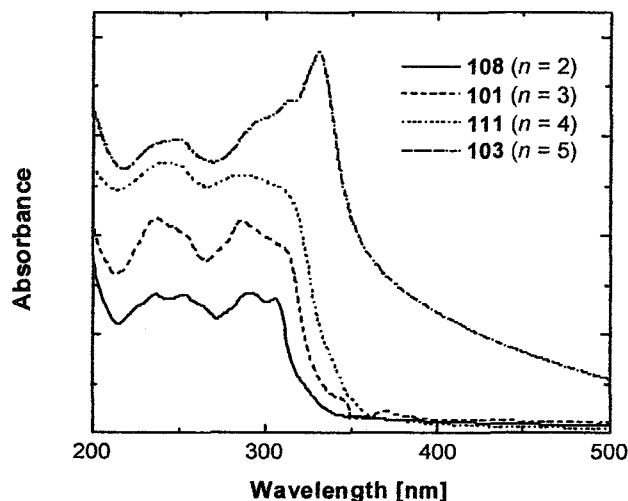


Fig. 2.10 Electronic absorption spectra for thin films of **101**, **103**, **108**, and **111**.

### 2.3 Conclusions

In this chapter, we have described an efficient synthesis for two series of monodisperse cross-conjugated oligomers: the *iso*-polydiacetylenes. These highly unsaturated materials can be isolated as reasonably stable solids, and all derivatives show substantial thermal stability. Solid-state analyses of two molecules, monomeric **99** and trimeric **101**, show that lengthening of the *iso*-PDA framework has little effect on bond lengths and angles for these derivatives. UV-vis spectroscopic analysis reveals that the predominant electronic features of the oligomers include a steadily broadening of *cis* and *trans* absorption bands due to increased rotational degrees of freedom as the chain length is increased. A slight lowering of the lower-energy absorption and absorption cutoff energies as a function of chain length is also observed, and these effects reach saturation by the stage of the nonamer, suggesting an  $n_{ECL} = 9$  for the *iso*-PDA oligomeric systems. This result is also supported by theoretical calculations at AM1 level.

## 2.4 References and Notes

- (1) For a comprehensive review on cross conjugation and cross-conjugated molecules, see references in Chapter 1.
- (2) Zhao, Y.; Tykwinski, R. R. *J. Am. Chem. Soc.* **1999**, *121*, 458-459.
- (3) Rossi, R.; Carpita, A.; Bellina, F. *Org. Prep. Proc. Int.* **1995**, *27*, 127-160.
- (4) *Metal-catalyzed Cross-coupling Reactions*; Diederich, F.; Stang, P., Eds.; Wiley-VCH: Weinheim, 1998.
- (5) Ladika, M.; Stang, P. J.; Schiavelli, M. D.; Hughey, M. R. *J. Org. Chem.* **1982**, *47*, 4563-4566.
- (6) Stang, P. J.; Fisk, T. E. *Synthesis* **1979**, 438-440.
- (7) Stang, P. J.; Treptow, W. *Synthesis* **1980**, 283-284.
- (8) Alberts, A. H. *J. Am. Chem. Soc.* **1989**, *111*, 3093-3094.
- (9) Feuerbacher, N.; Vögtle, F. In *Top. Curr. Chem.*; Springer Verlag: Berlin Heidelberg, 1998; Vol. 197, pp 1-18.
- (10) Prince, R. B.; Barnes, S. A.; Moore, J. S. *J. Am. Chem. Soc.* **2000**, *122*, 2758-2762.
- (11) Moore, J. S. *Curr. Opin. Colloid Interface Sci.* **1999**, *4*, 108-116.
- (12) *MacSpartan Plus*, Version 1.19; Wavefunction, Inc.: Irvine, CA, 1998
- (13) Siemsen, P.; Livingston, R. C.; Diederich, F. *Angew. Chem. Int. Ed.* **2000**, *39*, 2633-2657.
- (14) Hay, A. S. *J. Org. Chem.* **1962**, *27*, 3320-3321.
- (15) Eisler, S.; Tykwinski, R. R. *Angew. Chem. Int. Ed.* **1999**, *38*, 1940-1943.
- (16) Orfanopoulos, M.; Stratakis, M.; Elemes, Y. *Tetrahedron* **1989**, *30*, 4875-4878.

- (17) Clennam, E. L.; Chen, X.; Koola, J. J. *J. Am. Chem. Soc.* **1990**, *112*, 5193-5199.
- (18) Orfanopoulos, M.; Stratakis, M.; Elemen, Y. *J. Am. Chem. Soc.* **1990**, *112*, 6417-6419.
- (19) For the X-ray structures of other geminal enediynes, see: (a) Diederich, F. *Chem. Commun.* **2001**, 219-227. (b) Nikas, S.; Rodios, N. A.; Varvoglis, A.; Terzis, A.; Raptopoulou, C. P. *J. Heterocycl. Chem.* **1996**, *33*, 997-999. (c) Shultz, D. A.; Lee, H.; Kumar, R. K.; Gwaltney, K. P. *J. Org. Chem.* **1999**, *64*, 9124-9136.
- (20) Kawanami, H.; Okada, S.; Matsuda, H.; Doi, T.; Kabuto, C.; Oikawa, H.; Nakanishi, H. *Nonlinear Optics* **1995**, *14*, 97-102.
- (21) Eisler, S.; McDonald; Loppnow, G. R.; Tykwinski, R. R. *J. Am. Chem. Soc.* **2000**, *122*, 6917-6928.
- (22) Stewart, J. P. *J. Am. Chem. Soc.* **1985**, *107*, 3902-3909.
- (23) Pschirer, N. G.; Bunz, U. H. F. *Macromolecules* **2000**, *33*, 3961-3963.
- (24) Halkyard, C. E.; Rampey, M. E.; Kloppenburg, L.; Studder-Martinez, S. L.; Bunz, U. H. F. *Macromolecules* **1998**, *31*, 8655-8659.
- (25) Allen, F. H.; Kennard, O.; Waston, D. G.; Brammer, L.; Orpen, A. G.; Taylor, R. *J. Chem. Soc., Perkin Trans 2*, **1987**, S1-S19.

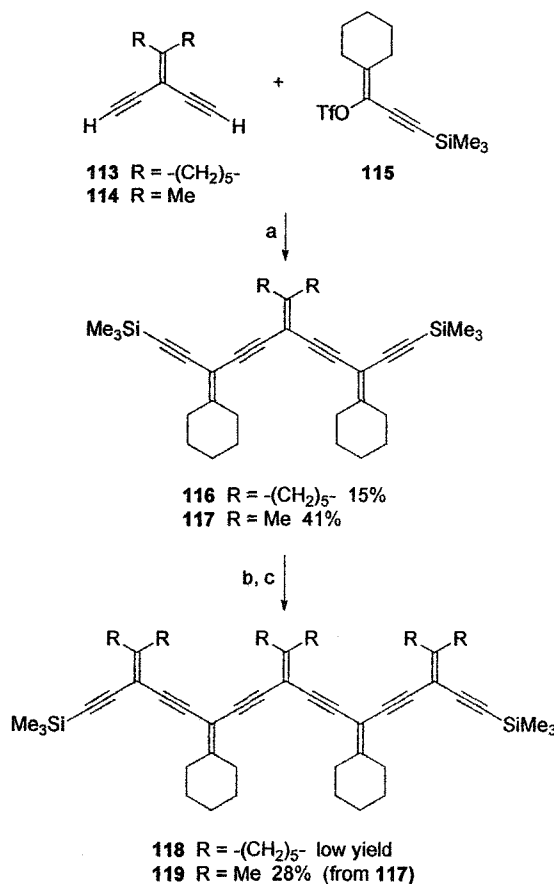
## Chapter 3 Synthesis, Characterization, and Nonlinear Optical Studies of Perphenylated *iso*-Polydiacetylenes

### 3.1 Introduction

Employing the sequence of protodesilylation and cross-coupling reactions outlined in Chapter 2, we have successfully synthesized the first class of isopropylidene substituted cross-conjugated *iso*-PDA oligomers ranging from dimer to nonamer. Although the shorter oligomers ( $n < 7$ ) show satisfactory stability and solubility, efforts to further extend the chain length had quickly become problematic because of limited stability and solubility. This drawback led us to the next rational step in the evolution of *iso*-PDAs; that is, to replace the methyl groups by larger alkyl substituents so as to improve the solubility such that we could extend the *iso*-PDAs beyond the length of nonamer. Meanwhile, we also targeted a potential candidate for practical use as a nonlinear optical (NLO) or electroluminescent (EL) material.

The first attempt, carried out by my colleague, Sara Eisler, targeted the cyclohexylvinylidene substituted *iso*-PDA series as outlined in Scheme 3.1, with the hope that the incorporation of cyclohexyl groups would help solublize the longer oligomers. The coupling of **113** and **115** was, however, problematic. While the formation of **116** appeared quite successful as the reaction proceeded under our standard cross-coupling conditions, this trimer turned out to be considerably less stable upon isolation. Furthermore, pentameric **118** was barely stable enough to isolate and characterize. Alternatively, attempts to produce trimeric **117** and **119** by alternating isopropylidene and cyclohexylvinylidene units, albeit still in low yields, gave much better results. It seemed

that partial inclusion of the isopropylidene functionality could provide sufficient stability for isolation and characterization, but their chemical stability meant that the usefulness of such derivatives would clearly be quite limited.



**Scheme 3.1** Synthesis of pentamers **118** and **119**. (a)  $\text{Pd}(\text{PPh}_3)_4$ ,  $\text{CuI}$ ,  $\text{Et}_2\text{NH}$ , DMF, rt. (b)  $\text{K}_2\text{CO}_3$ , wet MeOH/THF (1:1), rt, 2 h. (c) **115** or **95**,  $\text{Pd}(\text{PPh}_3)_4$ ,  $\text{CuI}$ ,  $\text{Et}_2\text{NH}$ , DMF, rt.

What was the source of the instability? A plausible answer is: the likely mode of decomposition would involve an oxygen ene reaction at the allylic position of the *iso*-PDAs (Fig. 3.1).<sup>1,2</sup> This situation would be exacerbated by the existence of the pseudo-axial protons of the cyclohexyl groups, which are perfectly localized in the  $\pi$ -plane for the ene reaction. The logical conclusion: all we had to do was to eliminate these protons and our problems would be over.

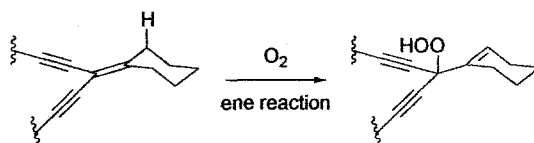
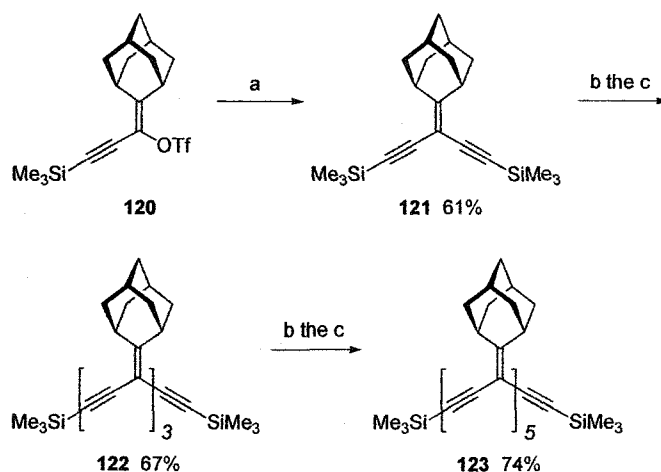


**Fig. 3.1** Proposed oxygen ene reaction at the allylic position of cyclohexylvinylidene *iso*-PDA.

A consequent attempt therefore addressed the adamantylidene derived *iso*-PDA oligomers. We anticipated that the problematic allylic protons, in this case, would be perpendicular to the  $\pi$ -plane and unavailable for an ene reaction. The efforts by my colleague, Katie Campbell, produced a series of adamantylidene oligomers, including monomer **121**, trimer **122**, and pentamer **123** (Scheme 3.2).<sup>3,4</sup> These derivatives were indeed considerably more stable in the presence of air, but solubility turned out to be an even worse problem than for the isopropylidene analogues. For this so called improved series of *iso*-PDAs, it was impossible to extend the chain length beyond that of even pentamer **123**.



**Scheme 3.2** Synthesis of adamantanylidene *iso*-PDAs. (a)  $\text{Me}_3\text{SiC}\equiv\text{CH}$ ,  $\text{Pd}(\text{PPh}_3)_4$ ,  $\text{CuI}$ ,  $\text{Et}_2\text{NH}$ ,  $\text{DMF}$ ,  $\text{rt}$ . (b)  $\text{TBAF}$ , wet  $\text{THF}$ ,  $\text{rt}$ . (c) **120**,  $\text{Pd}(\text{PPh}_3)_4$ ,  $\text{CuI}$ ,  $\text{Et}_2\text{NH}$ ,  $\text{DMF}$ ,  $\text{rt}$ .

Thus, we subsequently designed an alternative series of *iso*-PDA oligomers, the perphenylated *iso*-PDAs, with diphenylmethylidene as the substituent (Fig. 3.2). The rationale for incorporation of diphenylmethylidene groups onto the oligomer backbones lies in that: (a) the lack of an allylic proton would eliminate the possible decomposition under air; thereby, improving the stability, (b) the diphenyl groups were expected to improve solubility, and (c) the diphenyl groups would contribute somewhat to the  $\pi$ -conjugation; as a result, enhancing the properties for potential applications (e.g., NLO, electroluminescence).

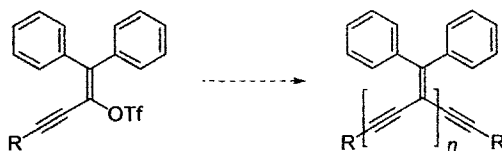


**Fig. 3.2** Proposed assembly of perphenylated *iso*-PDAs.

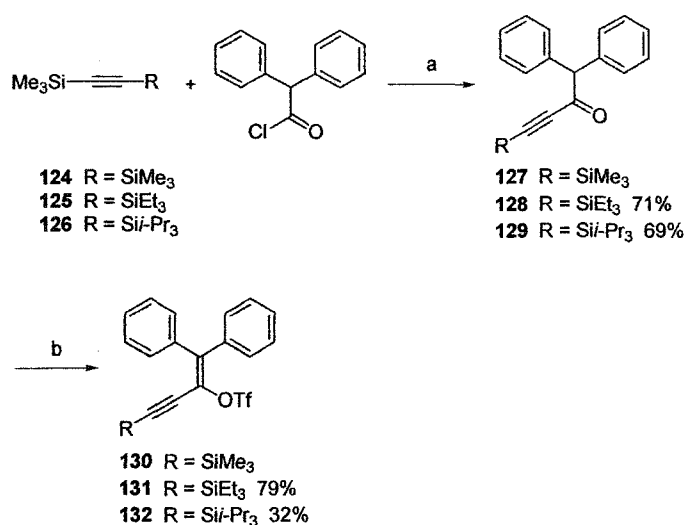
## 3.2 Results and Discussion

### 3.2.1 Synthesis

The essential synthetic building blocks (vinyl triflates **130**, **131**, and **132**), can be readily accessed via modification of the procedure described by Stang, as outlined in Scheme 3.3.<sup>5,6</sup> In the process of the Friedel–Crafts type acylation of silyl-protected acetylenes,<sup>7,8</sup> it was found that using the bistrimethylsilylacetylene **124** as starting material could result in a mixture of bis-acylated and mono-acylated products. As well, desilylation of the newly formed ketone under the reaction conditions was also observed. These side-reactions caused the subsequent isolation to be problematic. Replacement of one protecting group with a more robust silyl group, such as triethylsilyl (TES) or triisopropylsilyl (TIPS) groups, indeed reduced the unwanted side-reactions, alleviating

the purification problem. The ketones **127–129** showed limited stability even under conditions of inert gas environment and low temperature ( $-20\text{ }^{\circ}\text{C}$ ). Therefore, an immediate transformation into the corresponding vinyl triflates **130–132** was necessary. Triflation of **128** and **129** took place in the presence of an excess triflic anhydride and 2,6-di(*tert*-butyl)-4-methylpyridine in  $\text{CH}_2\text{Cl}_2$  at room temperature. Although the reaction normally took more than 3 days to complete, reasonable yields for triflation could be obtained as 79% for **131** and a lowered yield of 32% for **132**.

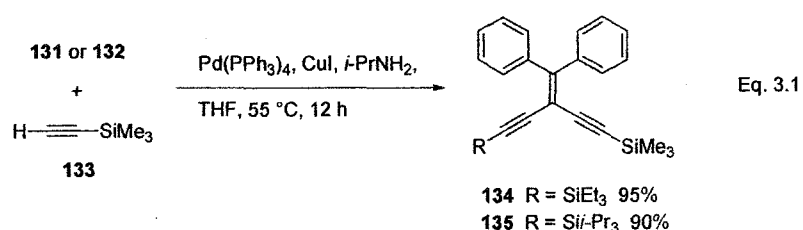
**Scheme 3.3**



Reagents and conditions: (a)  $\text{AlCl}_3$ ,  $\text{CH}_2\text{Cl}_2$ ,  $0\text{ }^{\circ}\text{C}$ . (b) triflic anhydride, 2,6-di(*t*-butyl)-4-methylpyridine,  $\text{CH}_2\text{Cl}_2$ , rt.

Next, synthesis of the diphenylmethylidene substituted enediyne **134** and **135** was accomplished under Pd-catalyzed cross-coupling conditions as described in the previous chapter. This reaction, unlike that of isopropylidene analogues, proceeded in an unbearably slow rate at room temperature in THF, possibly due to the increased steric demands of the two phenyl rings. Increasing the reaction temperature to  $65\text{ }^{\circ}\text{C}$  (i.e.,

refluxing THF) consequently led to a more rapid reaction (accomplished in ca. 12 h, Eq. 3.1). Employing either Pd(PPh<sub>3</sub>)<sub>4</sub> or PdCl<sub>2</sub>(PPh<sub>3</sub>)<sub>2</sub> as catalyst, CuI as co-catalyst and *i*-Pr<sub>2</sub>NH as base, under Ar-atmosphere, gave similar results. More homocoupled by-product, 1,4-bis(trimethylsilyl)butadiyne, however, was formed from the PdCl<sub>2</sub>(PPh<sub>3</sub>)<sub>2</sub> catalyzed reactions. After purification through a silica gel column, enediyne monomers **134** and **135** were isolated in pure form as colorless solids with defined melting points of 61–62 °C and 79–81 °C, respectively.



The first effort to iteratively elongate the perphenylated *iso*-PDA oligomer via Pd-catalyzed cross-coupling was directed at dimer **136a**. Monomer **135** was selectively desilylated by K<sub>2</sub>CO<sub>3</sub> in MeOH/THF (1:1) and cross-coupled with triflate **132** in the presence of PdCl<sub>2</sub>(PPh<sub>3</sub>)<sub>2</sub> as catalyst, CuI as co-catalyst, *i*-Pr<sub>2</sub>NH as base, in Ar-degassed THF (Scheme 3.4). The reaction proceeded at 50 °C overnight, under Ar-protection. Interestingly, this yielded exclusively the unexpected homocoupled by-product **137a** in 70% yield. This result is, however, not completely surprising since an analogous homocoupling methodology (using PdCl<sub>2</sub>(PPh<sub>3</sub>)<sub>2</sub> catalyst, CuI co-catalyst, Et<sub>3</sub>N base in DMF) has recently been reported by Roy and co-workers.<sup>9</sup>

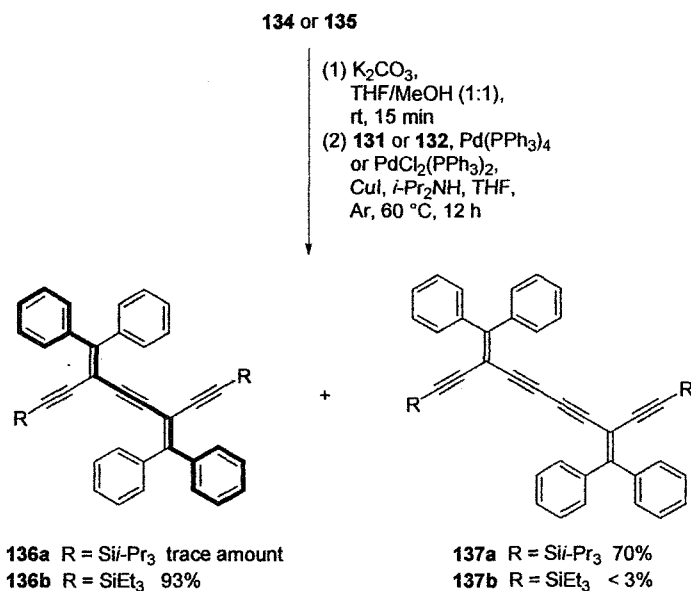
The second attempt to synthesize dimeric **136b** was initiated with TMS-TES-protected monomer **134**, where the TMS group could be removed readily by catalytic amount of K<sub>2</sub>CO<sub>3</sub> in MeOH/THF (1:1) while the TES group remained intact. The TES group, however, was also subject to desilylation at a much slower rate; therefore, a short

reaction time (usually less than 15 min) was crucial to the successful selective removal of the TMS group. After a brief workup, deprotected monomer **134** was directly cross-coupled with triflate **131** without further purification, yielding dimer **136b**. Although the reaction proceeded in a carefully Ar-degassed THF solvent, as well as under vigorous Ar-bubbling, substantial amount of oxidative homocoupled dimer **137b** was persistently formed in the case of PdCl<sub>2</sub>(PPh<sub>3</sub>)<sub>2</sub> as catalyst. Alternatively, using Pd(PPh<sub>3</sub>)<sub>4</sub> as catalyst, together with positive argon pressure over the reaction, as expected, reduced the yield of **137b** into trace amounts (ca. 3%). It was at this point that the cross-coupling reaction became sensitive to the Pd sources. It is believed that at high temperature Pd(II) can speed up the homocoupling reaction more dramatically than Pd(0); as a result, increasing the yield of homocoupled product. Accordingly, Pd(PPh<sub>3</sub>)<sub>4</sub> was utilized as catalyst rather than PdCl<sub>2</sub>(PPh<sub>3</sub>)<sub>2</sub> in all the subsequent cross-coupling reactions to reduce the unwanted homocoupling reaction. To date, the optimized cross-coupling conditions are: using Pd(PPh<sub>3</sub>)<sub>4</sub> as catalyst, CuI as co-catalyst, *i*-Pr<sub>2</sub>NH as base in THF under positive Ar-pressure, at 60 °C for at least 12 h.

Monomer **134** could also be bis-deprotected by 2 equiv. of tetrabutylammonium fluoride (TBAF) to give the bis-terminal alkyne, which was subsequently cross-coupled with triflate **131** to afford trimer **138**, using Pd(PPh<sub>3</sub>)<sub>4</sub> catalyst (Scheme 3.5). Purified through SiO<sub>2</sub> column chromatography, pure trimer **138** was isolated as a yellow solid in 81% yield. A small amount of the homocoupled by-product tetrameric **145** was separated in a yield of 8% from the main product via column chromatography. Repetition of the protideprotection and cross-coupling iteration from trimer **138** thus afforded pentamer **139** as a yellow solid in 72% yield. In the same manner, heptamer **140** was formed from

pentamer **139** as a yellow solid in a yield of 97%. Further iteration of heptamer **140** thus afforded nonamer **141** as a yellow solid.

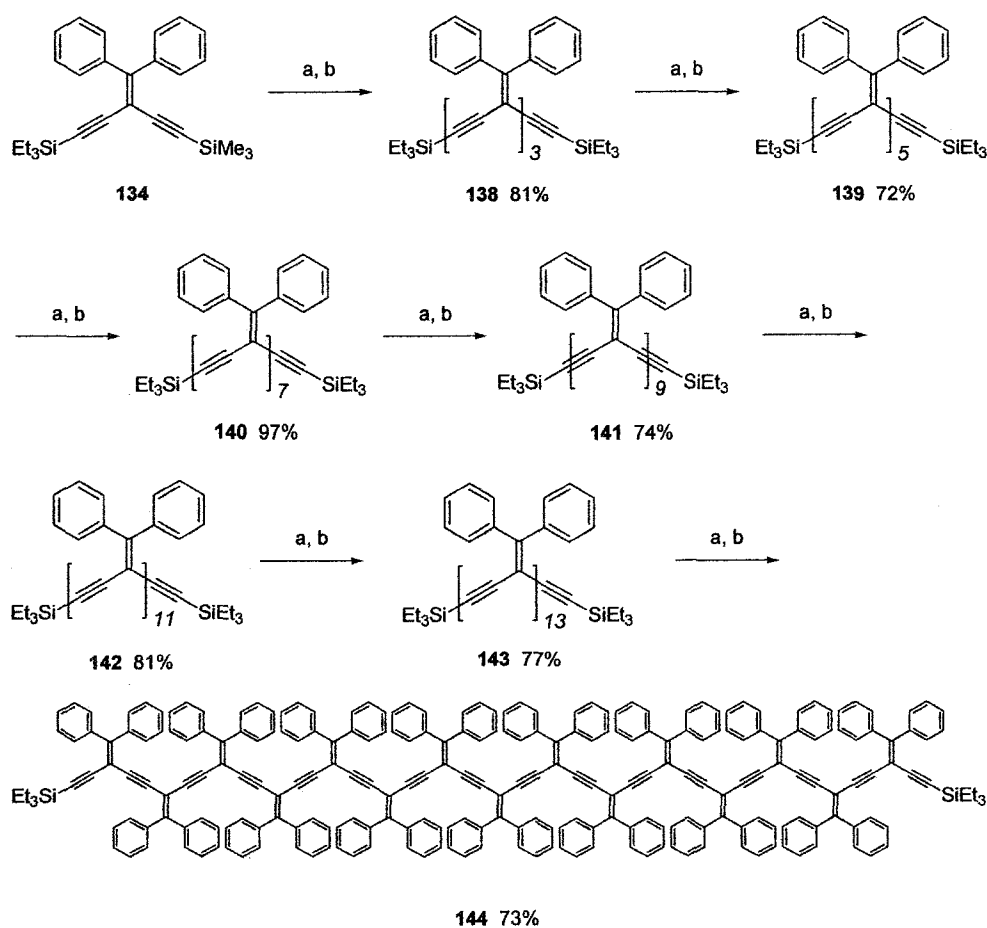
### Scheme 3.4



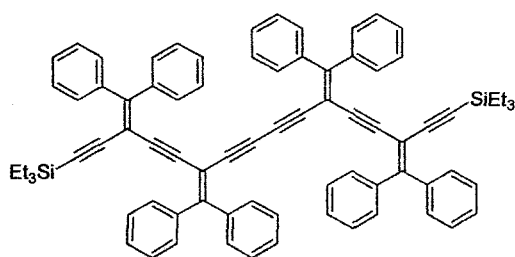
Although the nonamer **141** show decent solubility in organic solvents, purification through a SiO<sub>2</sub> column turned out to be problematic because of significant aggregation. Size-exclusion chromatography (SEC) proved to be invaluable in the purification of nonamer **141**, as well as longer oligomers. Nonamer **141** was isolated via SEC as a yellow solid in 74% yield. Performing the cross-coupling reaction of desilylated **141** with vinyl triflate **131** resulted in the undecamer **142** as a yellow solid in 81% yield. In the same manner, tridecamer **143** was obtained as a yellow solid in 77% yield. For the molecular mass characterization of this series of oligomers, ranging from trimer **138** to tridecamer **143**, electrospray mass spectrometry (ESI-MS) proved particularly beneficial. For instance, analysis (positive mode) of a MeOH/toluene (1:3) solution of **143** with added AgOTf provided a signal at  $m/z$  2991 expected for  $[M + Ag]^+$ , as silver

coordinates to an alkyne unit of the *iso*-PDA. To this point, all the perphenylated *iso*-PDA oligomers are sufficiently stable and soluble for meaningful NMR spectroscopic analysis. A further iteration of tridecamer **143** yielded the pentadecamer **144** ( $n = 15$ ) as a dark yellow solid in 73% yield. Compound **144** is the longest monodisperse *iso*-PDA oligomer ever synthesized to date by a divergently iterative method, and displays a cross-conjugated backbone constructed of 62  $sp-sp^2$  carbons. Again, ESI-MS proved efficient in identification of the molecular mass of **144**, where a signal peak at  $m/z$  3309 is observed as expected for  $[M + Na^+]^+$ .

**Scheme 3.5**



Reagents and conditions: (a) TBAF, wet THF, rt. (b) **131**, Pd(PPh<sub>3</sub>)<sub>4</sub>, CuI, *i*-Pr<sub>2</sub>NH, THF, 60 °C, 12 h.



**145** 8% from cross-coupling

### 3.2.2 Physical Characteristics

The perphenylated *iso*-PDA oligomers show superior stability and solubility in comparison to the isopropylidene substituted analogues. The spectroscopic data for these *iso*-PDA oligomers are consistent with their proposed structures. In the  $^{13}\text{C}$  NMR spectra of the diphenylmethylidene series, the resonances of the phenyl groups are observed in the range of 127–130 ppm for the tertiary carbons, and 139–140 ppm for the quaternary carbons, respectively. Like those of the isopropylidene series, the vinylidene carbons outside of the main chain ( $\text{Ph}_2\text{C}=\text{C}$ ) are quite deshielded, resonating at 154–157 ppm. For heptamer **140**, each of the four different types of these carbons are discernible at  $\delta$  154.9, 155.0, 155.4 and 156.9. For longer oligomers **141–144** chemical shift degeneracy of such carbons can be observed; for instance, 5 of 7 unique carbon resonances are distinguishable for tridecamer **143**, which are present at  $\delta$  155.8, 156.0, 156.1, 156.2, and 157.6, respectively. The in-chain vinylidene carbons ( $\text{Ph}_2\text{C}=\text{C}$ ) fall into the chemical shift range of the acetylenic carbons, from 90–104 ppm. At 125 MHz, dramatic chemical shift degeneracy occurs in the  $^{13}\text{C}$  NMR spectroscopic analysis even for pentamer **139**, where only 11 of 12 unique  $\text{sp}$  and  $\text{sp}^2$  carbon resonances (excluding the phenyl carbons) are discernible.

All *iso*-PDA oligomers show decently improved thermal stability. Dimeric **136b** shows a well defined melting point at 67–69 °C, whereas trimeric **138**, pentameric **139**, and heptameric **140** show well defined melting points at 60–61, 85–86, and 124–126 °C, respectively. Nonameric **141**, undecameric **142**, tridecameric **143**, and pentadecameric **144** decompose (shrinkage of the sample accompanied by discolorization) at 134–135, 140–142, 148–150, and 155–159 °C, respectively. Differential scanning calorimetry (DSC) measurements on **142**, **143**, and **144** were performed and also confirm the decompositions at these temperatures. Additionally, compared to isopropylidene *iso*-PDA series, all the perphenylated oligomers show substantially improved kinetic stability; for example, even when exposed to air at room temperature for weeks, no significant decomposition (such as the ene reaction in Fig. 3.1) can be observed by either TLC or NMR spectroscopic analyses.

### 3.2.3 *Solid-State Structures*

Single crystallographic X-ray analysis of *iso*-PDA monomer **134**, dimer **136b**, and trimer **138**, as well as the homocoupled dimer **137a** were performed to reveal the solid-state structural properties of these perphenylated *iso*-PDA oligomers. The respective ORTEP diagrams are found in Fig. 3.3–3.6. Single crystals of **134** were obtained by diffusion of MeOH into a CH<sub>2</sub>Cl<sub>2</sub> solution at –20 °C, and the X-ray crystal data were collected at low temperature (–80 °C). Disorder, particularly at the ethyl groups, hampered refinement of the data; however, the structure of **134** is sufficient enough for an empirical analysis and as a point of comparison to the other structures of oligomers.<sup>10-12</sup> It is notable that the vinylidene angle C(2)–C(3)–C(5) is 114.(3)°, which is comparable to the that of isopropylidene monomer **99** as 112.9(4)°. The other

vinylidene angle C(21)–C(4)–C(31) is observed at 116.8(3)°. These angles are slightly less than the anticipated angle of 120° for an sp<sup>2</sup> hybridized carbon atom. Both Si–C≡C bond angles, observed at 172.2(3)° and 174.9(4)°, are distorted from linearity presumably due to crystal packing effects. The dramatic steric hindrance between the two diphenyl groups prohibit them from achieving co-planarity, forcing them out of the cross-conjugated enediyne plane by 47.7(6)° and 43.0(6)°, respectively. All bond lengths in the enediyne are observed in expected range: C(1)–C(2) at 1.192(5) Å, C(2)–C(3) at 1.458(5) Å, C(3)–C(4) at 1.357(5) Å, C(3)–C(5) at 1.434(5) Å, and C(5)–C(6) at 1.205(5) Å.

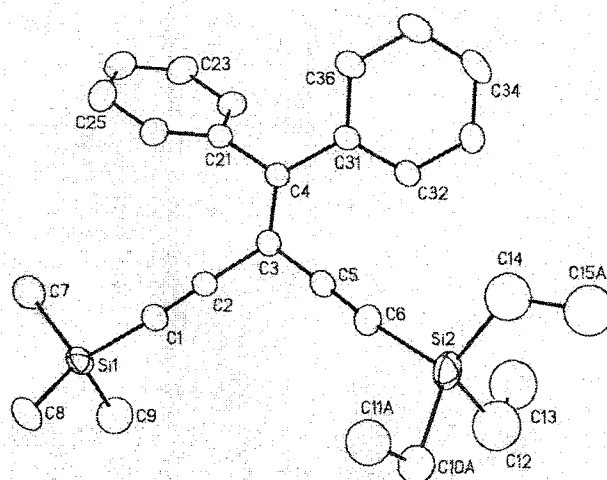


**Fig. 3.3** ORTEP drawing (20% probability level) of **134**. Selected bond lengths (Å) and angles (°): C(1)–C(2) 1.192(5), C(2)–C(3) 1.458(5), C(3)–C(4) 1.357(5), C(3)–C(5) 1.434(5), C(5)–C(6) 1.205(5); Si(1)–C(1)–C(2) 172.2(3), C(1)–C(2)–C(3) 176.9(4), C(2)–C(3)–C(5) 114.3(3), C(3)–C(5)–C(6) 177.5(4), C(21)–C(4)–C(31) 116.8(3), Si(2)–C(6)–C(5) 174.9(4).

Single crystals of dimer **136b** were obtained by slowly crystallization from a cooled saturated THF solution at –4 °C, and the structural data were collected at low temperature. Although adopting a pseudo *s-trans* orientation, the cross-conjugated enyne

framework of **136b** is not completely planar. The dihedral angle between two vinylidene least-squares planes, namely plane 1 (C2, C3, C4, and C5) and plane 2 (C6, C7, C8, and C9), is observed at  $33.70(16)^\circ$ . The two enediyne vinylidene angles show values similar to that of monomer **134** at  $113.9(3)^\circ$  and  $113.6(3)^\circ$ . The bond angles of Si–C≡C are slightly distorted from linearity at  $175.4(3)^\circ$  and  $172.7(3)^\circ$ . The phenyl groups are also twisted out of the vinylidene planes by  $53.7(5)^\circ$ ,  $40.5(5)^\circ$ ,  $40.0(5)^\circ$ , and  $49.5(5)^\circ$ . No observable reduction in bond length alternation is observed in dimer **136b**. Single bonds of the conjugated framework, e.g., C(2)–C(3) and C(6)–C(7) at 1.430(5) and 1.431(5) Å, are in the range expected for single bonds linking sp and sp<sup>2</sup> carbons. The C≡C bond C(5)–C(6) at 1.183(4) Å and the double bond C(3)–C(4) at 1.356(4) Å are also in the range expected. Interestingly, the distance between H(32) and phenyl plane (C41', C42', C43, C44', C45', C46') is observed at 3.26 Å, suggesting an intermolecular  $\pi$ -stacking in a “face to edge” manner, i.e., “T-stacking” (Fig. 3.4b).<sup>13</sup>

Likewise, single crystals of trimer **138** were obtained by slowly crystallization from a cooled saturated THF solution at  $-4^\circ\text{C}$ . Disorder occurred only for the ethyl groups; however, reasonable refinement was obtained to reveal the solid-state properties of this trimeric *iso*-PDA. The cross-conjugated oligoenyne framework does not assume a planar conformation due to the steric interactions between the neighboring phenyl groups. Interestingly, trimer **138** shows a pseudo-*cis-trans* orientation rather than an all *s-trans* orientation; the only *iso*-PDA to date displaying a cisoid orientation for neighboring vinylidene groups. The torsion angles between the three least-squares planes, namely plane 1 (C2, C3, C4, C5), plane 2 (C6, C7, C8, C9), and plane 3 (C10, C11, C12, C13), are observed as  $50.30(15)^\circ$  (plane 1 to 2),  $46.84(14)^\circ$  (plane 1 to 3), and  $11.0(2)^\circ$  (plane 2

to 3), respectively. The distances between H(55) to phenyl plane 4 (C61, C62, C63, C64, C65, C66), and H(56) to phenyl plane 4, are observed at 3.20 and 3.37 Å. The angle between these two phenyl planes is 79°. These results suggest the possibility of a “face to edge”  $\pi$ -stacking, which contribute to stabilizing this pseudo-*cis* orientation in the solid state. The vinylidene angles are also consistent with those observed for monomer **134** and dimer **136b**; that is, C(2)–C(3)–C(5) at 114.4(3)°, C(6)–C(7)–C(9) at 114.2(3)°, and C(10)–C(11)–C(13) at 113.0(3)°. Furthermore, no obvious reduction of bond length alternation is observed in trimer **138**; for instance, C(5)–C(6) and C(9)–C(10) are of similar length at 1.199(4) and 1.187(4) Å, respectively, and in the expected range for C $\equiv$ C bonds. For the three olefinic C=C bonds, C(3)–C(4) at 1.375(4) Å and C(11)–C(12) at 1.363(4) Å are also in the range expected, whereas the central C=C bond, C(7)–C(8) at 1.357(4) Å, is slightly shorter than the others. Single bonds C(3)–C(5) at 1.431(4) Å, C(6)–C(7) at 1.443(4) Å, C(7)–C(9) at 1.437(4) Å, and C(10)–C(11) at 1.432(4) Å, are in the range expected for single bonds linking sp and sp<sup>2</sup> carbons. In addition, the six phenyl rings along the framework are twisted out of the respective enediyne planes by 45.8(5)°, 47.7(4)°, 42.0(4)°, 48.9(4)°, 27.6(5)°, and 61.5(4)°, respectively.

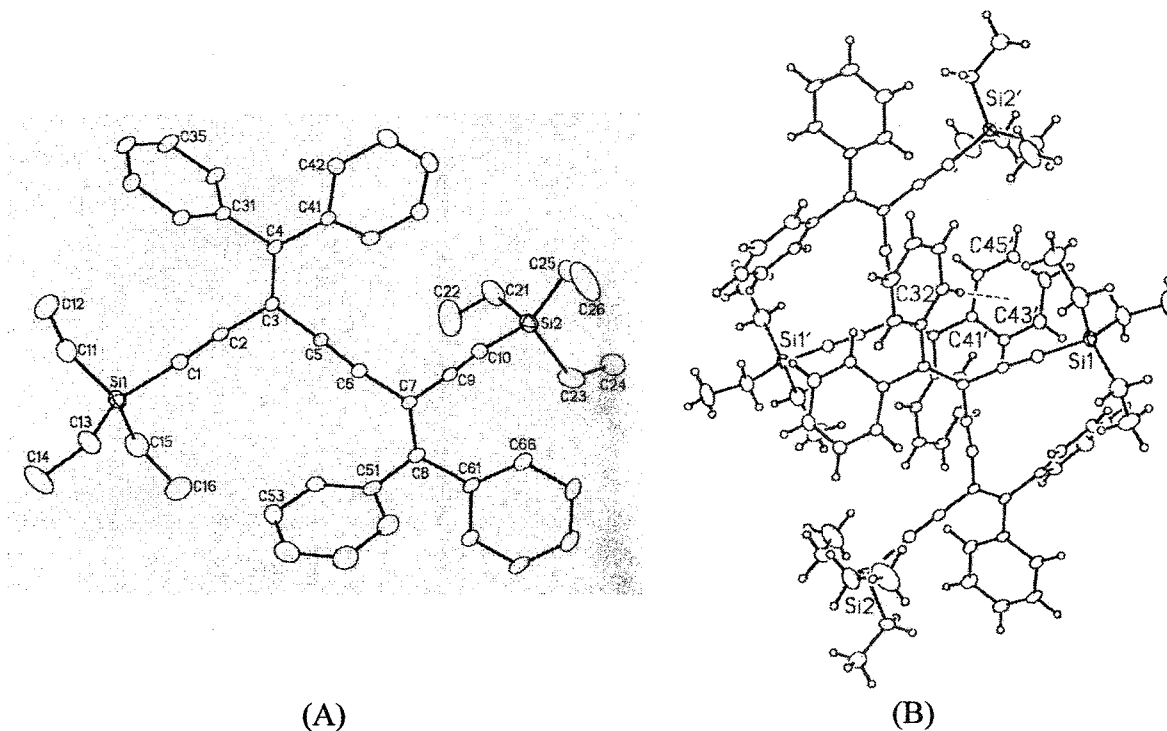


**Fig. 3.4** (a) ORTEP drawing (20% probability level) of **136b**. Selected bond lengths (Å) and angles (°): C(1)–C(2) 1.194(4), C(2)–C(3) 1.430(5), C(3)–C(4) 1.356(4), C(3)–C(5) 1.438(4), C(5)–C(6) 1.183(4), C(6)–C(7) 1.431(5), C(7)–C(8) 1.356(4), C(7)–C(9) 1.437(5), C(9)–C(10) 1.188(5); Si(1)–C(1)–C(2) 175.4(3), C(1)–C(2)–C(3) 175.4(4), C(2)–C(3)–C(5) 113.9(3), C(3)–C(5)–C(6) 176.5(4), C(5)–C(6)–C(7) 171.6(3), C(6)–C(7)–C(9) 113.6(3), C(7)–C(9)–C(10) 176.8(4), Si(2)–C(10)–C(9) 172.7(3). (b) Crystal packing diagram of **136b**.

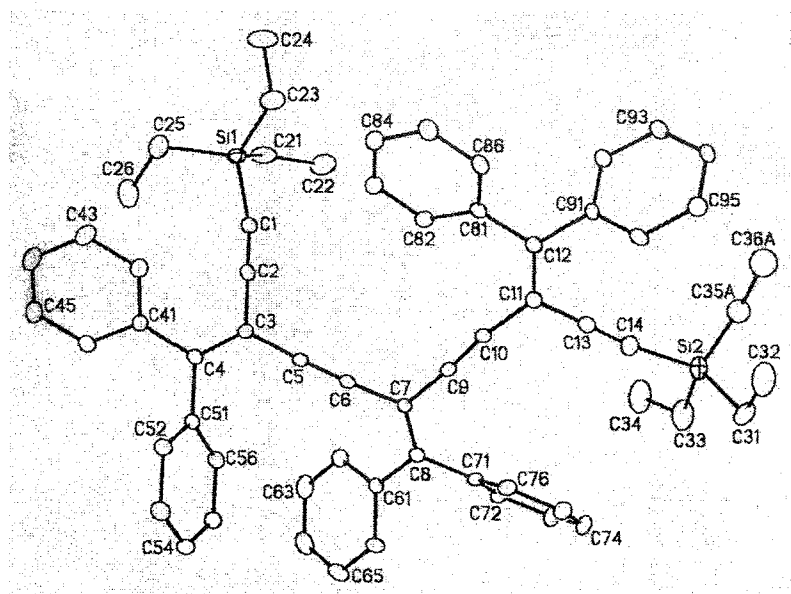


**Fig. 3.5** ORTEP drawing (20% probability level) of **138**. Selected bond lengths (Å) and angles (°): C(1)–C(2) 1.199(4), C(2)–C(3) 1.444(4), C(3)–C(4) 1.375(4), C(3)–C(5) 1.431(4), C(5)–C(6) 1.199(4), C(6)–C(7) 1.443(4), C(7)–C(8) 1.357(4), C(7)–C(9) 1.437(4), C(9)–C(10) 1.187(4), C(10)–C(11) 1.432(4), C(11)–C(12) 1.363(4), C(11)–C(13) 1.439(5) C(13)–C(14) 1.204(5); Si(1)–C(1)–C(2) 168.9(3), C(1)–C(2)–C(3) 176.5(3), C(2)–C(3)–C(5) 114.4(3), C(3)–C(5)–C(6) 176.8(3), C(5)–C(6)–C(7) 175.1(3), C(6)–C(7)–C(9) 114.2(3), C(7)–C(9)–C(10) 174.4(4), C(9)–C(10)–C(11) 170.4(3), C(10)–C(11)–C(13) 113.0(3), C(11)–C(13)–C(14) 177.5(4), Si(2)–C(14)–C(13) 172.2(3).

Single crystals of homocoupled dimeric **137a** were also obtained by diffusion of MeOH into a CH<sub>2</sub>Cl<sub>2</sub> solution at –20 °C. Unlike the aforementioned *iso*-PDA enyne oligomer **138**, the cross-conjugated enyne framework of **137a** (Fig. 3.6) assumes a transoid centrosymmetric and nearly planar conformation (*C*<sub>2h</sub> symmetry), with a maximum deviation of 0.078(2) Å from the least-squares plane (excluding phenyl moieties). It is obvious that the central butadiynyl moiety provides a sufficient distance of the vinylidene moieties such that steric interactions of neighboring phenyl groups are relieved; therefore, a planar conjugated orientation in the crystal is achieved. The

vinylidene angle of C(2)–C(3)–C(5) at 115.13(19)° is found to be slightly greater than those of the *iso*-PDAs **134**, **136b**, and **138**; however, is still less than that of the expected 120° for an sp<sup>2</sup> hybridized carbon center.

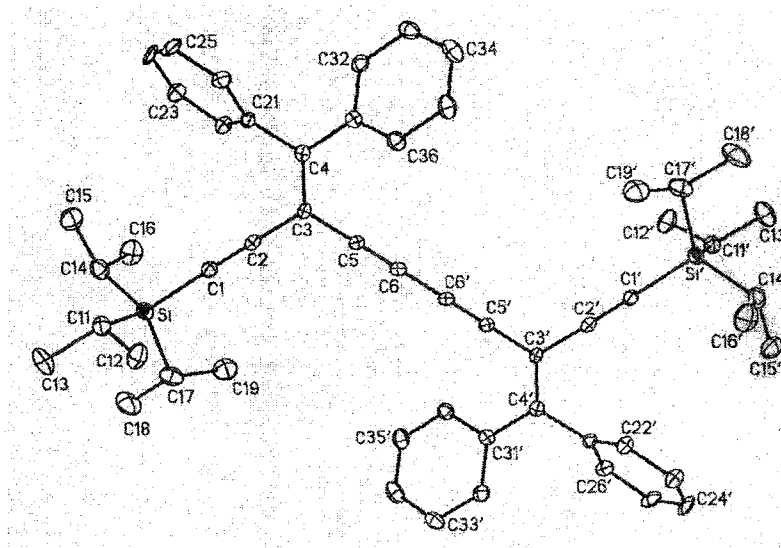


**Fig. 3.6** ORTEP drawing (20% probability level) of **137a**. Selected bond lengths (Å) and angles (°): C(1)–C(2) 1.205(3), C(2)–C(3) 1.445(3), C(3)–C(4) 1.372(3), C(3)–C(5) 1.437(3), C(5)–C(6) 1.197(3), C(6)–C(6′) 1.382(4); Si–C(1)–C(2) 178.2(2), C(1)–C(2)–C(3) 176.2(3), C(2)–C(3)–C(5) 115.13(19), C(3)–C(5)–C(6) 174.4(3), C(5)–C(6)–C(6′) 178.7(3).

Interestingly, **137a** show stacking features of parallel arrangement in the solid state as shown in Fig. 3.7a. The solid-state packing parameters for the central butadiynyl moieties are observed as:  $\Phi = 34.7^\circ$ ,  $R_{1,4} = 6.14 \text{ \AA}$ ,  $d = 8.56 \text{ \AA}$  (Fig. 3.6b). Compared to the optimal geometry parameters for topochemical polymerization of butadiynes in a 1,4-addition fashion, i.e.,  $\Phi = 45^\circ$ ,  $R_{1,4} = 3.5 \text{ \AA}$ ,  $d = 5.0 \text{ \AA}$ ,<sup>14,15</sup> the parameters for **137a** however, do not suggest any possibility for this type of reaction, because of the distance between each molecule is out of the expected range. Such a long distance in molecular stacking is probably due to the great steric interactions between phenyl groups.

Moreover, there is no observation of possible intermolecular and/or intramolecular  $\pi$ -stacking effect in the crystal packing of **137a**.

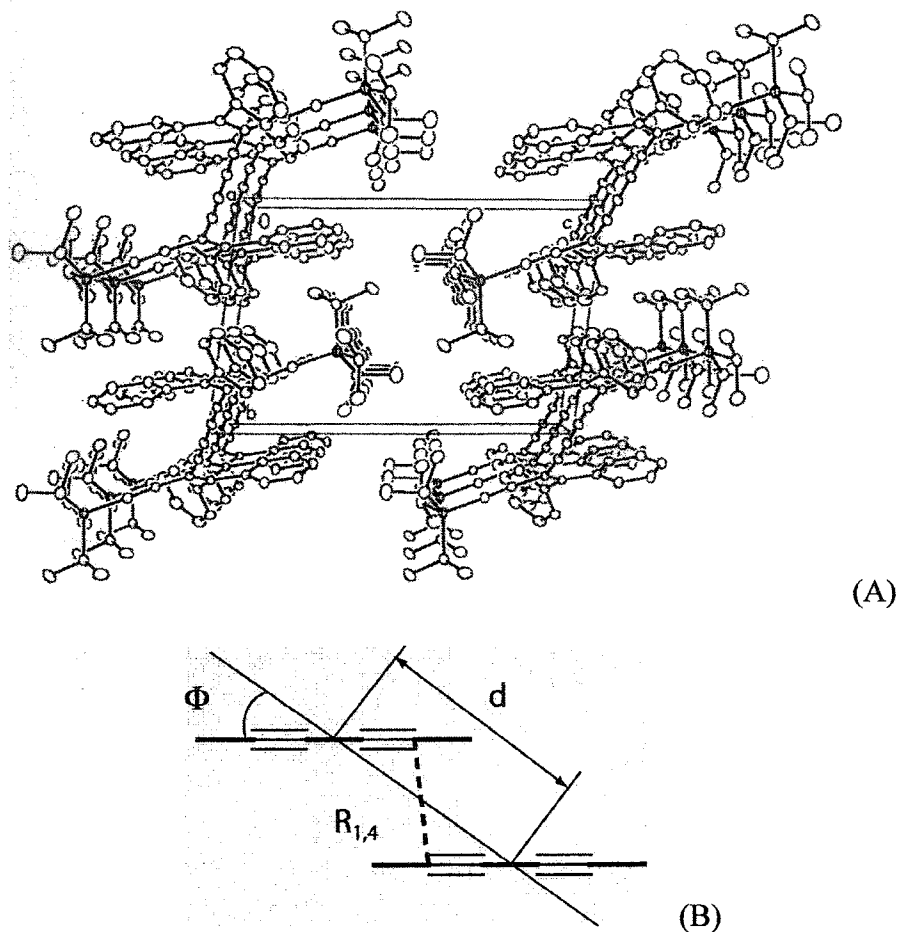


**Fig. 3.7** (a) Crystal packing diagram of **137a** viewed along  $b$ -axis. (b) Geometry parameters:  $\Phi = 34.7^\circ$ ,  $R_{1,4} = 6.14 \text{ \AA}$ ,  $d = 8.56 \text{ \AA}$ . Optimal parameters for 1,4-addition are:  $\Phi = 45^\circ$ ,  $R_{1,4} = 3.5 \text{ \AA}$ ,  $d = 5.0 \text{ \AA}$ .

### 3.2.4 Electronic Absorption and Emission Properties

Electronic absorption behavior of perphenylated *iso*-PDAs, ranging from dimer **136b** to pentadecamer **144**, was investigated by their UV-vis absorption characteristics as measured in  $\text{CHCl}_3$  (Fig. 3.8). As demonstrated in Scheme 3.4, dimer **136b** (shown in bold) contains the longest linearly conjugated segment in this series of *iso*-PDA

oligomers. The electronic absorption of this segment dominates the lowest energy region. Nevertheless, this segment is, in fact, not easily achieved in solution due to steric interactions and preference for the non-planar conformation as alluded to by crystallographic analyses. Accordingly, it could be empirically estimated that the  $\pi$ -delocalization would be, on average, confined within a more limited segment.

To a first approximation, it might be expected that the weak electronic interaction between cross conjugation observed in isopropylidene *iso*-PDA oligomers to be diminished for the phenylated derivatives as a result of steric considerations. That is, the saturation of optical band gap ( $E_g$ ) would then be reached at a shorter chain length, and the  $n_{ECL}$  of perphenylated *iso*-PDAs would be less than that of isopropylidene *iso*-PDA oligomers ( $n = 9$ ). To the contrary, surprisingly, experimental data show a different result from this empirical prediction.

From the spectra of these *iso*-PDAs, a steady increase of molar absorptivity is observed as the oligomeric chain length increases. The electronic absorption spectrum of dimeric **136b** shows two distinct absorptions at 373 and 323 nm, and the low-energy absorptions are assigned to the  $\pi \rightarrow \pi^*$  transition, from HOMO to LUMO. The higher-energy absorption is believed to be from a combination of the HOMO to LUMO and HOMO to LUMO+1 transitions (as described in Chapter 2). Similar UV-vis profile can be observed in the spectrum of trimeric **138**, where two absorption peaks are present at 373 and 324 nm, respectively. In the spectrum of pentameric **139**, the higher-energy absorption peaks at 324 nm merges into the intense, low-energy peak and is a barely distinguishable shoulder; hence, the only notable characteristic is the low-energy absorption at 377 nm. From heptameric **140** to pentadecameric **144**, the electronic

absorption profiles show similar broad and featureless peaks at a maximum absorption energy at  $\lambda_{\max} = 378$  nm. Although the  $\pi$ -electron delocalization along the phenyl-ene-ene-ene-phenyl conjugated segment is expected to be diminished due to the non-planar conformations, a slight lowering of the low-energy cutoff with chain-length increasing is, observed as one progress from dimer **136b** to pentadecamer **144**.

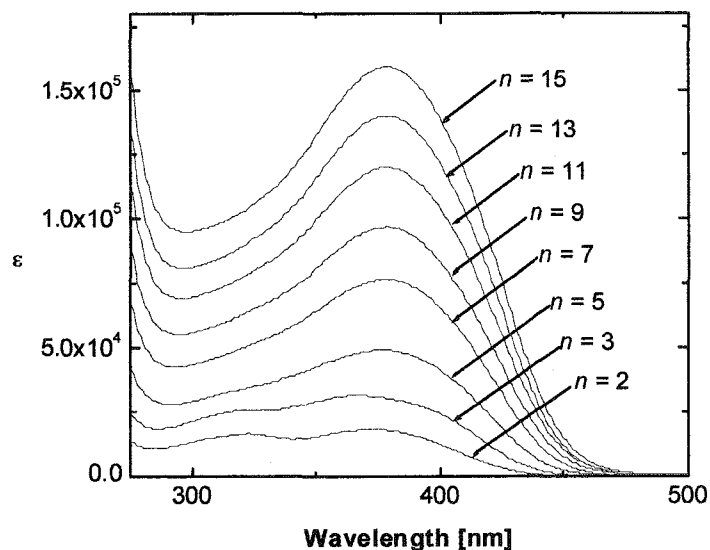


**Fig. 3.8** Electronic absorption spectra ( $\epsilon$  [ $\text{L mol}^{-1} \text{cm}^{-1}$ ]) in  $\text{CHCl}_3$  comparing the effects of oligomer chain length between **136b**, **138–144**.

The optical band gap  $E_g$  of the perphenylated *iso*-PDA oligomers was then approximated using the methods mentioned in Chapter 2. Figure 3.9 shows that plots of estimated band gap ( $E_g$ ) versus the reciprocal of monomer unit number ( $1/n$ ) presents similar characteristics, where the band gap values decrease steadily with the increasing chain length from dimer **136b** to tridecamer **143**. In method B (from maximal wavelength at one-half intensity of maximal absorption), the band gap reaches a constant to pentadecamer **144**. In method A, however, a continued lowering of  $E_g$  from tridecamer to pentadecamer is observed, but by an insignificant amount. It is therefore

suggested that the saturation of  $E_g$  occurs by the pentadecameric stage ( $n = 15$ ). By extrapolation, it is reasonable to assume that any further extension of the oligomer chain length will not appreciably lower  $E_g$ . In other words,  $E_g$  of a polymer containing an infinite number of monomer units should be the same as that of the pentadecamer, 2.76 eV (as measured by method A). Based on this analysis the ECL for this oligomeric series can be estimated as  $n_{\text{ECL}} = 15$ . In addition, the extent of  $E_g$  lowering from dimer **136b** to pentadecamer **144** is trivial (total 0.11 eV by method A), which means a much limited  $\pi$ -electron communication across the *iso*-PDA skeleton.

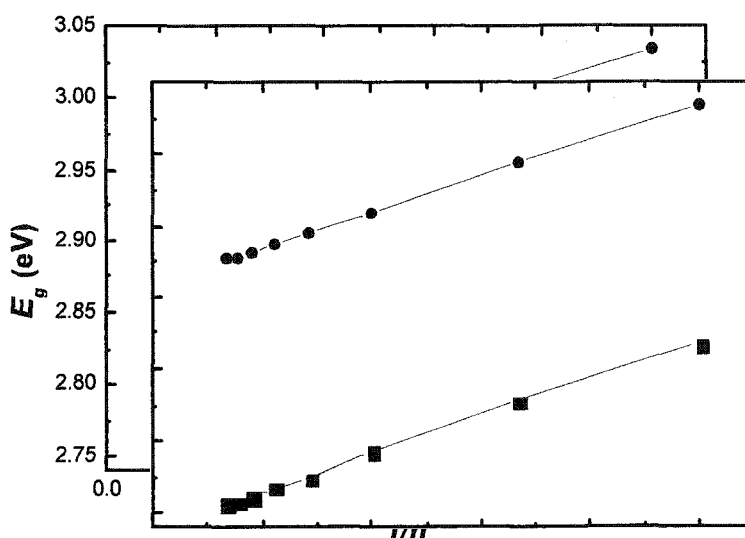


**Fig. 3.9** Plot of estimated optical band gap ( $E_g$ ) versus reciprocal number of monomer unit ( $1/n$ ) of perphenylated *iso*-PDAs via method A (■) and method B (●).

The influence of solvent polarity on the electronic absorptions for nonamer **141** was investigated via measurements in  $\text{CHCl}_3$ , hexanes, benzene,  $\text{Et}_2\text{O}$ , acetonitrile, and THF (Fig. 3.10). The UV-vis spectra of nonamer show only a slight shift of maximum absorptions  $\lambda_{\text{max}}$  toward higher energy region (ca. 3 nm) with the increasing dielectric constants. For example,  $\lambda_{\text{max}}$  in  $\text{CHCl}_3$ , hexanes, and benzene are at 377 nm, whereas the

$\lambda_{\text{max}}$  in Et<sub>2</sub>O and THF are at 374 nm. In addition, the absorption profiles are similar to each other in these solvents. The UV-vis spectrum from acetonitrile, however, shows obvious differences compared to those from the other solvents. The  $\lambda_{\text{max}}$  in acetonitrile (365 nm) has shifted toward higher energy by ca. 12 nm. Furthermore, an additional distinctive absorption peak at 323 nm observable in the spectra of dimer **136b** and trimer **138** from CHCl<sub>3</sub> is also discernible. It is suggested that acetonitrile, a hydrophilic solvent induces a conformational alteration in the longer oligomers ( $n > 7$ ), possibly “folding”, which enhances the second absorption peak at 323 nm. Similar results have been reported by Moore and co-workers.<sup>16-18</sup>

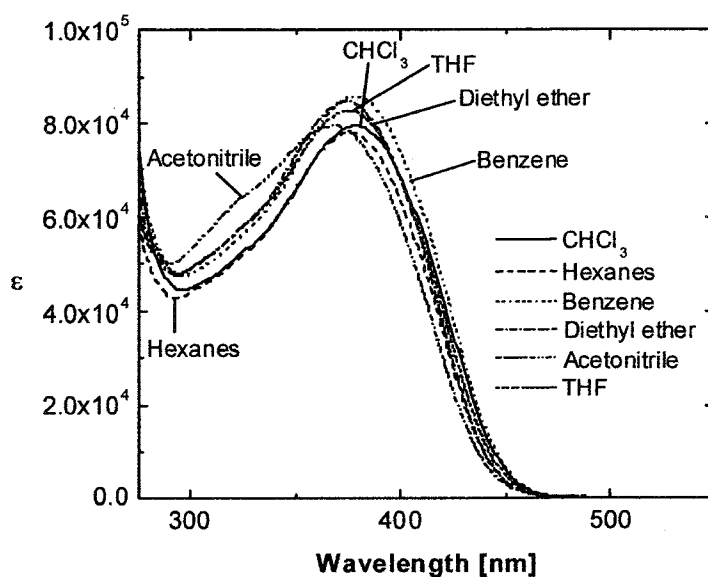
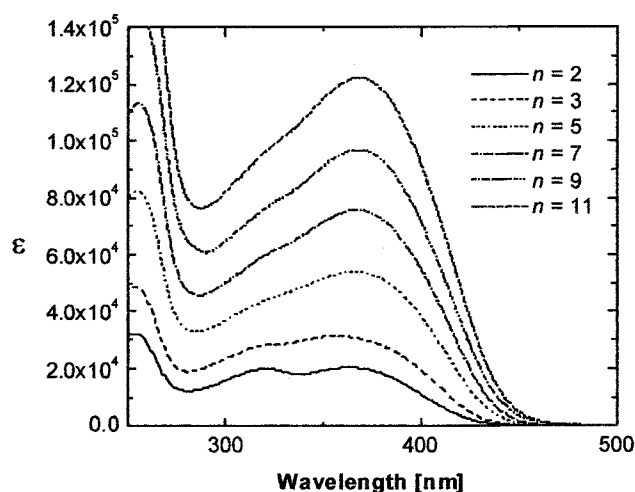


Fig. 3.10 Electronic absorption spectra of **141** in various solvents.

To probe the “solvophobic effect” of acetonitrile on the perphenylated *iso*-PDA series, the electronic absorption spectra of oligomers ( $n = 2-11$ ) were measured as shown in Fig. 3.11 (meaningful UV-vis spectra for **143** and **144** were not successfully measured due to the poor solubility in acetonitrile). Compared to the spectra measured in CHCl<sub>3</sub>,

all of the maximum absorption peaks for the oligomer series are observed to shift bathochromically by approximately 10 nm. It is also noted that acetonitrile indeed induces the higher-energy absorptivity at 323 nm; this absorption is still discernible as a shoulder peak in the spectrum of undecamer **142**. It is believed that this absorption enhancement at 323 nm is attributed to a conformational preference in the oligomers, and this possibility will be outlined later in this chapter.



**Fig. 3.11** Electronic absorption spectra ( $\epsilon$  [ $\text{L mol}^{-1} \text{cm}^{-1}$ ]) in acetonitrile comparing the effects of oligomer chain length between **136b**, **138–142**.

The possible effects of intermolecular aggregation for the *iso*-PDA heptamer **140** and nonamer **141** were measured in  $\text{CHCl}_3$  at varying concentration from  $10^{-5}$  to  $10^{-7}$  M (Fig. 3.12). Generally, the presence of phenyl groups is expected to allow or induce molecular aggregation through  $\pi$ -stacking, in either an intermolecular and/or intramolecular manner. The consistent profiles and molar absorptivity values observed at various concentrations (in the low energy region), however, did not confirm such aggregations in  $\text{CHCl}_3$ . Elaboration on the concentration-dependent study of these

oligomers in acetonitrile, however, is not achieved due to the limited solubility in acetonitrile.

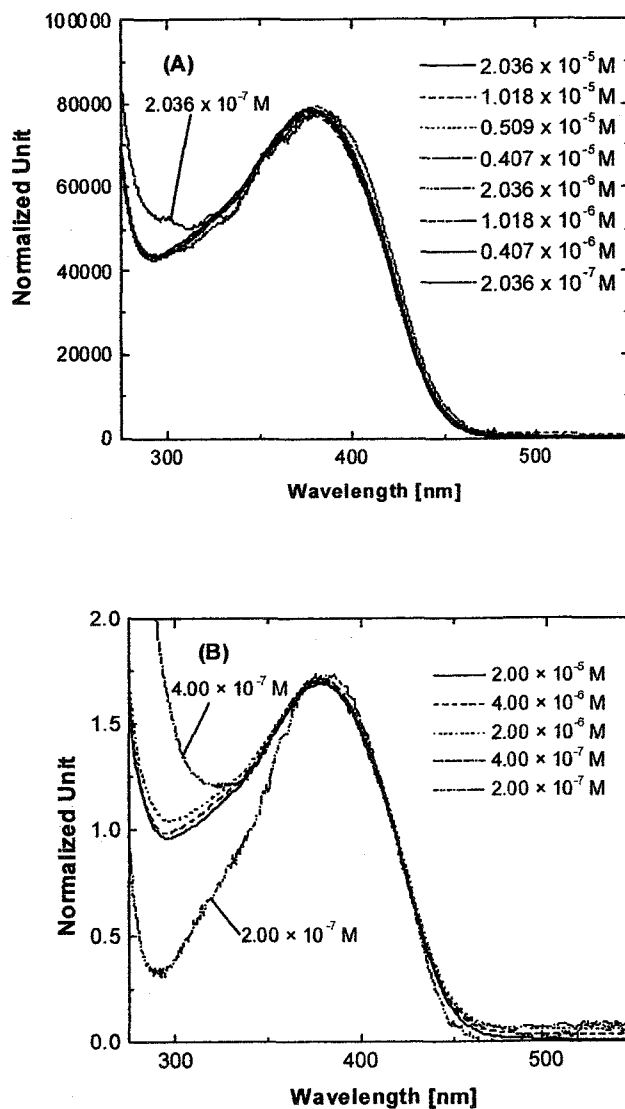


**Fig. 3.12** Electronic absorption spectra of 140 (Fig. A) and 141 (Fig. B) in  $\text{CHCl}_3$  at various concentrations. The absorption scale has been normalized to facilitate comparison (dilution causes variance of higher energy absorption).

The absorption spectra of *iso*-PDA as thin films cast from  $\text{CHCl}_3$  solution onto quartz slides are shown in Fig. 3.13. Interestingly, all perphenylated *iso*-PDA oligomers

can form thin films of good quality. The absorption profiles are similar to those measured in acetonitrile, suggesting that there is no pronounced *intermolecular* aggregation band detectable by solid-film UV-vis spectroscopic analysis. Moreover, a slight random lowering of the low-energy absorption cutoff (i.e., optical  $E_g$ ) is observed in the solid-film UV-vis spectra, presumably due to the scattering effects from cast films and inherent inaccuracies. However, the aggregation effect can not be precluded simply based on absorption spectral analysis, because it is possible that even the aggregated molecules do not show any notable change in absorption spectra.

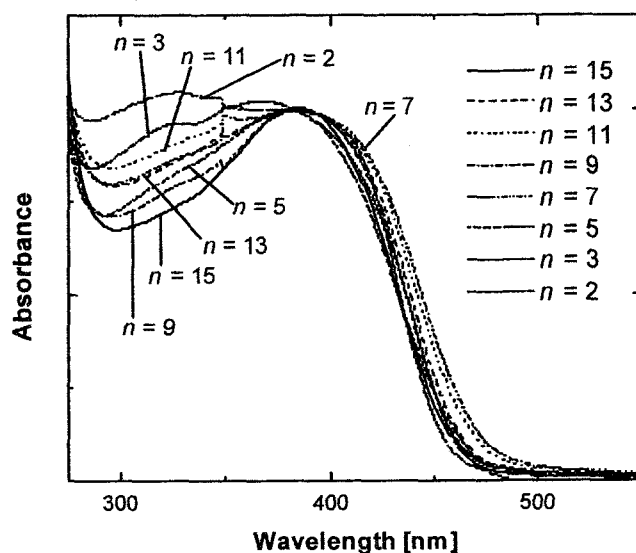
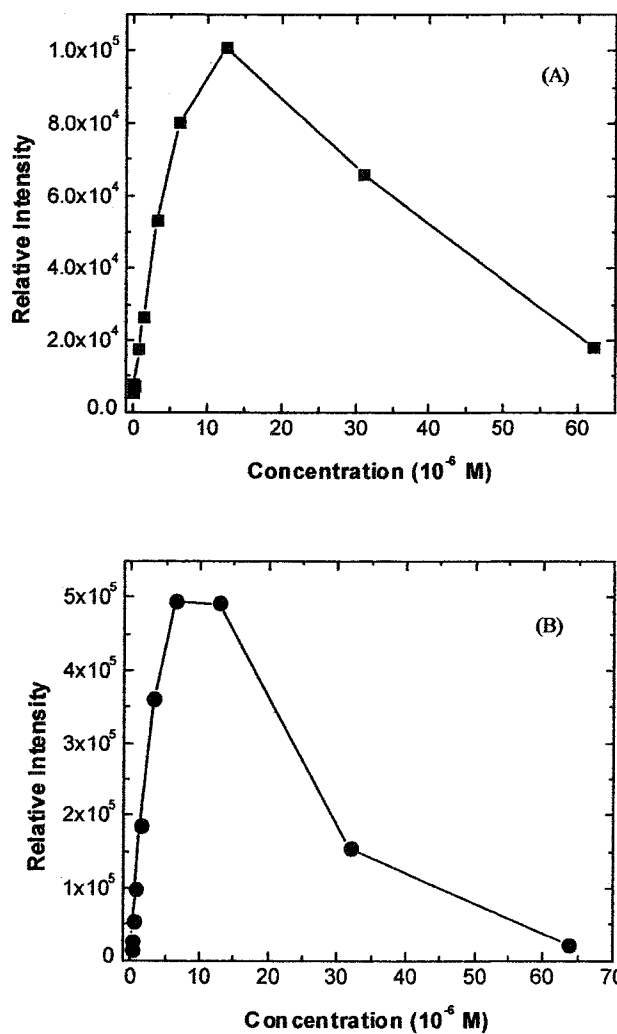


Fig. 3.13 Electronic absorption spectra for thin films of 136b, 138–144.

The perphenylated *iso*-PDAs show enhanced fluorescence properties compared to their isopropylidene analogues, possibly due to the extended conjugation  $\pi$ -system and rigid-backbone conformations. Since the fluorescence intensity is sensitive to concentrations, emission behavior study of pentameric 139 was first carried out at concentrations ranging from  $10^{-5}$  to  $10^{-8}$  M in degassed  $\text{CHCl}_3$  at an excitation

wavelength of 380 nm. At varied concentration, **139** shows consistent profiles with a maximum emission at 501 nm. However, the relative emission intensity (at 501 nm) indeed manifests a non-linear relationship with the concentration (Fig. 3.14a). At low concentrations (less than 15  $\mu\text{M}$ ), the emission intensity shows a linear increase with respect to the increasing concentrations. Moreover, this linear relationship reaches saturation at ca. 1.5  $\mu\text{M}$ . At higher concentrations ( $> 1.5 \mu\text{M}$ ), however, the emission intensity decreases linearly with the concentration increase, possibly due to the intermolecular aggregation, as has often been reported. Similar emission vs. concentration relationship is also observed for nonamer **141** (Fig. 3.14b). Therefore, in order to obtain meaningful concentration-dependent fluorescence spectra for *iso*-PDA oligomers, low concentrations (less than 10  $\mu\text{M}$ ) are necessary.

Emission spectra from dimer **136b** to pentadecamer **144** (shown in Fig. 3.15), were thus measured in degassed  $\text{CHCl}_3$  solutions at low concentrations ( $< 10 \mu\text{M}$ ) with an excitation wavelength of 380 nm. Unlike their UV-vis spectra, all the *iso*-PDA oligomers ( $n = 2-15$ ) consistently show only one broad emission peak, and the maximum emission wavelength  $\lambda_{\text{max}}$  shifts toward the lower-energy region from dimer **136b** (478 nm) to heptamer **140** (504 nm). From heptamer **140** to pentadecamer **144**, the maximum emission, nonetheless, reaches a constant value of  $\lambda_{\text{max}} = 504 \text{ nm}$ . Another notable feature in the fluorescence spectra of these *iso*-PDAs is the steady increase of the molar emission intensity ( $I_{\text{max}}$ ) with increasing chain length  $n$ .



**Fig. 3.14** Plot of relative maximum emission intensity versus concentration in  $\text{CHCl}_3$  for 139 (Fig. A) and 141 (Fig. B) (Maximum emission intensity at 501 nm for 139 and 504 nm for 141).

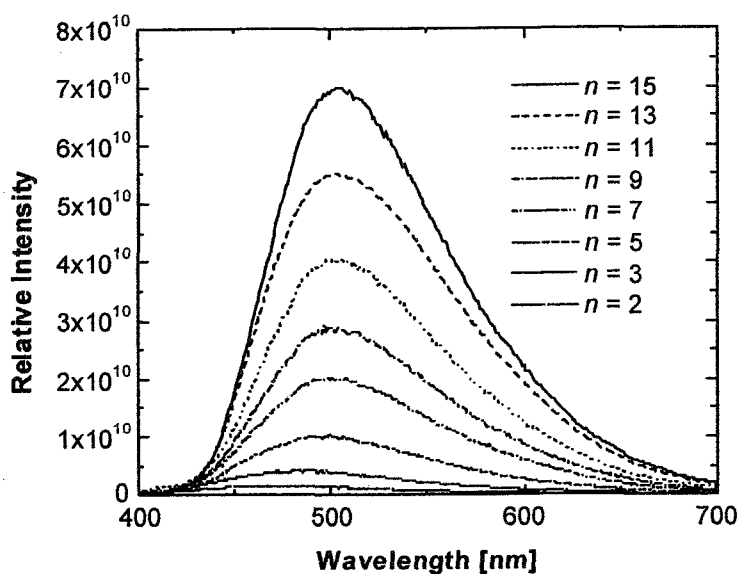


Fig. 3.15 Emission spectra in  $\text{CHCl}_3$  for *iso*-PDA series of 136b, 138–144.

Moreover, another interesting phenomenon observed in the concentration-dependent emission study of pentamer **139** and nonamer **141** in  $\text{CHCl}_3$  is an additional high-energy emission at ca. 423 nm from their reduced concentration spectra (ca. 0.1  $\mu\text{M}$ ). For instance, Fig. 3.16 shows two emission profiles (normalized) of **141** measured in  $\text{CHCl}_3$  at 6.326 and 0.1265  $\mu\text{M}$ . In addition to the consistent emission profiles in low-energy regime, an extra high-energy emission is observable at 423 nm at a reduced concentration of 0.1265  $\mu\text{M}$ . Measurement of emission spectrum for  $\text{CHCl}_3$  only does not show such a peak; therefore, precluding the possibility of solvent and instrumental effects. To date, there is still no explanation for this. However, this phenomenon might be related to molecular aggregation.

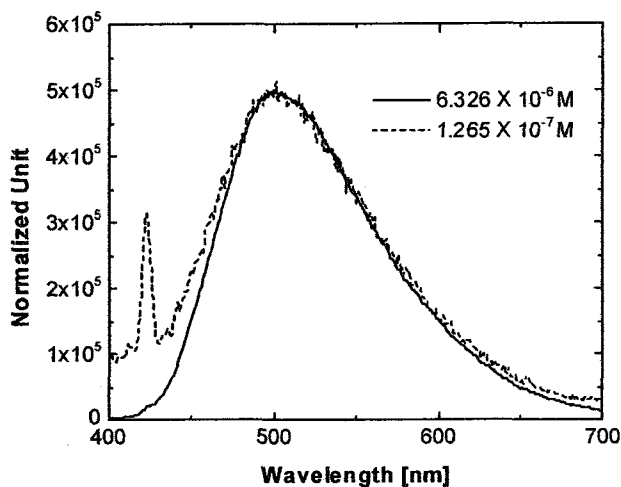
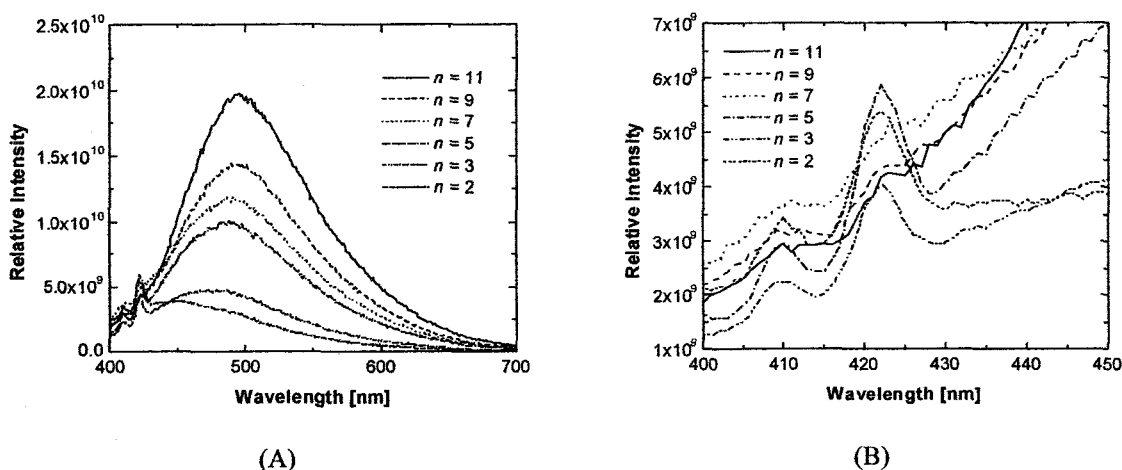


Fig. 3.16 Emission spectra of **141** in  $\text{CHCl}_3$  comparing the effects of concentrations, whereas the relative emission intensities are normalized.

As suggested by UV-vis solvent-dependent analysis, acetonitrile can influence the absorption of *iso*-PDAs by inducing higher-energy absorption(s). The solvophobic effect<sup>16,18,19</sup> on emission properties was subsequently investigated, and the emission spectra for oligomer series ( $n = 2-11$ ) were measured from their degassed acetonitrile solutions at normal concentrations (ca. 4–7  $\mu\text{M}$ ) as shown in Fig. 3.17. Interestingly, in the spectra of dimer **136b** to pentamer **139**, two distinct high-energy emissions are observed at ca. 410 and 422 nm, whereas the low energy peak that shifts from 455 to 490 nm, respectively. However, in the spectra of heptamer **140** to undecamer **142**, the low-energy emissions slightly shift from 492 to 497 nm, whereas the two high-energy emissions merge into an indistinctive shoulder. It is therefore believed that the two distinct high-energy emissions belong to the non-aggregated oligomers. When the oligomer length  $n$  reaches 7, however, aggregation effects become pronounced; as a consequence, the two emissions are quenched. Moreover, this chain length dependent

aggregation phenomenon also suggests a “folding” mechanism for longer oligomers ( $n \geq 7$ ).<sup>16,17,20,21</sup>



**Fig. 3.17** Emission spectra in acetonitrile of *iso*-PDA series **136b**, **138–142**. (A) Spectra in range of 400–700 nm. (B) Expansion spectra in range of 400–450 nm.

### 3.2.5 Nonlinear Optical Properties

To determine the nonlinear optical (NLO) properties of perphenylated *iso*-PDA series, in particular third-order NLO properties, the differential optical Kerr effect (OKE) (detail description see Chapter 1) was utilized to measure third-order nonlinear susceptibilities,  $\chi^{(3)}$ , and second hyperpolarizabilities,  $\gamma$ . In these experiments, samples of the TES-encapped oligomers from monomer **134** to pentadecamer **144** were prepared by dissolving solid oligomers in high-purity THF to give solutions of 0.035–0.23 M.

The molecular second hyperpolarizability of the oligomer samples,  $\gamma_s$ , is obtained using the methods described by Hegmann and co-workers.<sup>22</sup> For purposes of comparison, all the  $\gamma_s$  values are referenced to that of THF. A summary for the entire oligomer series are listed in Table 3.1 and Fig. 3.18.

**Table 3.1** Summary of results for the *iso*-polydiacetylene oligomer series.  $\gamma_s$  and  $\gamma_{THF}$  are the second hyperpolarizabilities of the oligomer samples and THF reference, respectively.  $n$  is the number of repeat units in the oligomer.

Sample	$n$	Concentration (M)	$\gamma_s \times 10^{-36}$ esu	$\frac{\gamma_s}{\gamma_{THF}}$
Monomer	1	0.23	9.2±0.4	17.7±0.8
Dimer	2	0.15	30.3±0.3	58.2±0.5
Trimer	3	0.13	48±4	94±7
Pentamer	5	0.12	70±5	134±9
Heptamer	7	0.10	94±4	181±9
Nonamer	9	0.12	123±8	240±15
Undecamer	11	0.054	177±18	347±35
Tridecamer	13	0.054	208±10	408±20
Pentadecamer	15	0.035	308±8	603±16

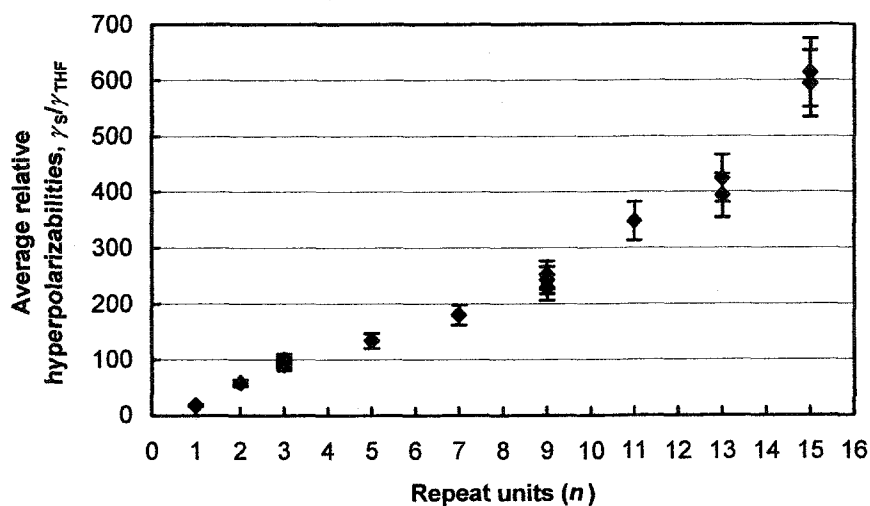


**Fig. 3.18** Molecular second hyperpolarizability of perphenylated *iso*-PDAs,  $\gamma_s$ , relative to the absolute THF hyperpolarizability,  $\gamma_{THF}$ , as a function of monomer repeat units,  $n$ .

As expected, the molecular hyperpolarizability increases as a function of oligomer length. As seen in Fig. 3.18, the *iso*-PDA series shows an order of magnitude increase in  $\gamma$  from the monomer to pentadecamer. This is consistent with the increase in the number

of fixed-length linearly conjugated paths as the number of repeat units in the oligomer is increased. The effect of adding  $\pi$ -delocalization paths is expected to produce a linear increase in  $\gamma$  as a function of  $n$ , the number of repeat unit in molecule. To understand the relationship of second hyperpolarizability  $\gamma$  against chain length  $n$ , three mathematics methods were employed to correlate these data (as shown in Fig. 3.19). As a result of its shorter linearly conjugated segment, the monomer has been excluded from all analyses. In method A, the  $\gamma$  values are linearly correlated with oligomer chain length  $n$ , ranging from dimer to pentadecamer. In method B, two different linear fits are conducted, from  $n = 2$  to 7, and  $n = 9$  to 15, where the second linear fit ( $n = 9-15$ ) shows a slightly greater slope than the first fit ( $n = 2-7$ ). In method C, an exponential correlation of  $\gamma$  versus  $n$  is conducted, ranging from dimer to pentadecamer. The results in Fig. 3.19 clearly show that both method B and C can result in very good correlations, with satisfying root-square errors  $R^2$ , while method A, however, turns out to be more erroneous.

Indeed, the nonlinearities of these samples seem to be governed by  $\pi$ -communication along the linearly conjugated paths. This is seen from the increase trend in second hyperpolarizability as repeat units are added. Empirically, communication along the cross-conjugated backbone might be expected to give a linearly increasing as in Fig. 3.19a, especially in the range of dimer to nonamer. The observed trend is, however, better described as superlinear rather than linear (as shown in Fig. 3.19b and c). It seems more reasonable to assign the two linear-fit relationships in method B rather than method C, because it is unusual to extrapolate physical properties, such as hyperpolarizability, for a polymeric system using an exponential function. Moreover, the increase of slope value from nonamer to pentadecamer (method B) which correlates with the suggestion of a

conformational preference of these oligomers in solution, which will be discussed in later section.

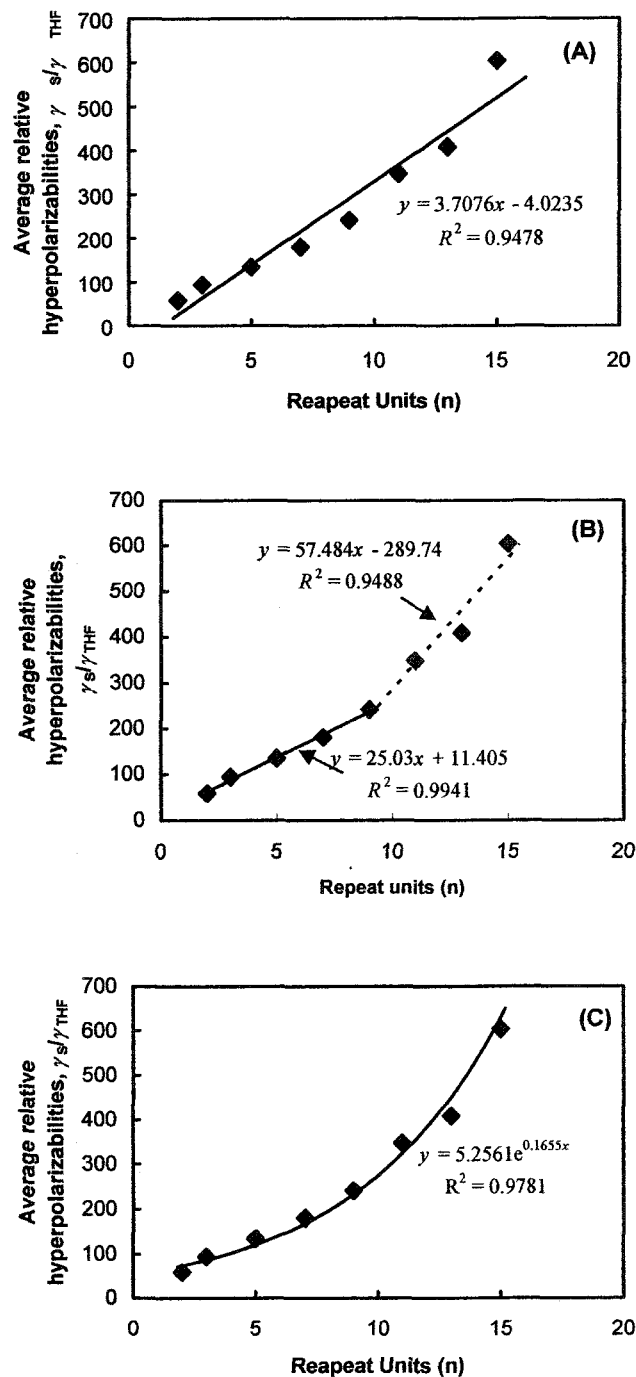


**Fig. 3.19** Correlation of relative molecular second hyperpolarizabilities ( $\gamma_s/\gamma_{THF}$ ) as a function of oligomer length  $n$ . (a) Linear fit ( $n = 1-15$ ). (b) Two linear fits ( $n = 2-9$  and  $n = 9-15$ ). (c) Exponential fit ( $n = 2-15$ ).

As the goal of this study was not necessarily to produce an oligomer with a world record  $\gamma$  value, but rather to probe the possibility of transparent oligomers. A comparison to linearly conjugated enyne oligomers is therefore instructive. For example, a dodecameric (containing 12 C=C and 24 C≡C bonds in the backbone) and hexadecameric polytriacetylene (containing 16 C=C and 32 C≡C bonds in the backbone) showed  $\gamma$  values of  $2570 \times 10^{-36}$  and  $4230 \times 10^{-36}$  esu (measured by THG),<sup>29</sup> respectively, while the pentadecameric *iso*-PDA **144** (containing 15 C=C and 16 C≡C bonds in the backbone) has a  $\gamma$  value of  $308 \times 10^{-36}$  esu. Thus, while transparency is maintained for *iso*-PDAs, when compared with the oligomeric PTAs,<sup>29</sup> it comes at the cost of an order of magnitude reduction in  $\gamma$ .

### 3.2.6 Conformational Studies

As suggested by the crystallographic analysis of trimer **138**, the pseudo-*cis* orientation between each cross-conjugated enediyne segment allows the neighboring phenyl groups to approach close enough to effect  $\pi$ -stacking (Fig. 3.20). For shorter oligomers ( $n < 7$ ), the conformation, however, is not likely dominated by this effect. As a result, their oligomeric backbones show a certain amount of rotational flexibility about the (-C≡C-) groups. For longer oligomers ( $n \geq 7$ ), however, the oligomeric conformations are potentially dominated by the pseudo-*cis*  $\pi$ -stacking; that is, the oligomeric backbone could prefer an all pseudo-*cis* orientation.

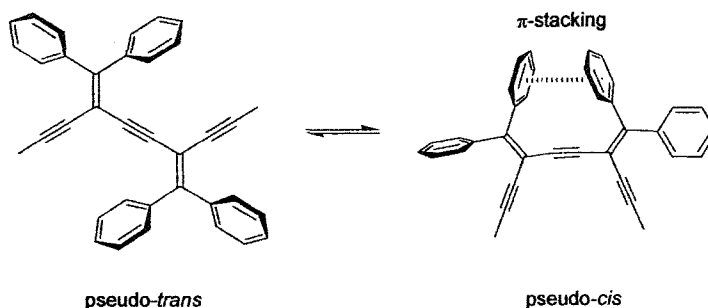


**Fig. 3.20** Schematic illustration of pseudo-*trans* and pseudo-*cis* perphenylated *iso*-PDA.

A theoretical conformational study was accomplished with *Macromodel 7.0* using the implemented MM3\* force field parameters.<sup>23</sup> The calculation results suggest that oligomers start folding from the heptameric stage on up. For example, geometry optimization of tridecamer **143** was carried out, where the silyl protecting groups were replaced by hydrogens, for purposes of saving computation time. A local minimization of **143** based on the all pseudo-*cis* orientation clearly shows a folded backbone with three turns (the pitch angle is calculated at 40°) as illustrated in Fig. 3.21.

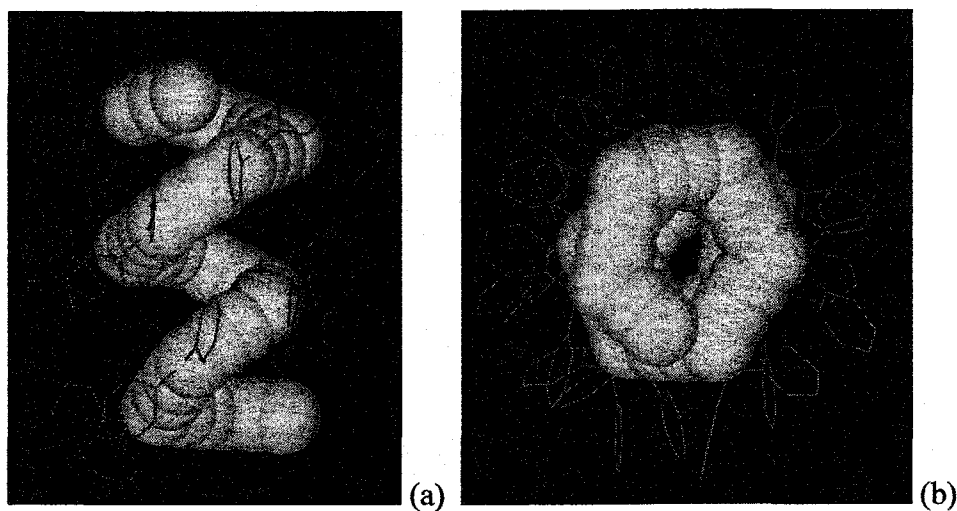


**Fig. 3.21** Minimized structure of tridecameric *iso*-PDA using MM3\* force field parameters. Only backbone carbons are displayed as space-filling representation for clarity. (A) View from side. (B) View from top.

This modeling study is in good agreement with the experimental data from emission spectral study, which suggests an intramolecular aggregation starting from heptamer (see Fig. 3.17). Additional evidence to support the folding mechanism is from UV-vis spectroscopic analysis. As indicated in the UV-vis absorption analyses, two independent absorptions at ca. 323 and 378 nm are attributed to different conformations. A plot of absorbance ratio ( $A_{378}/A_{323}$ ) versus chain length  $n$  is employed to evaluate the conformational characteristics with the increasing chain length in  $\text{CHCl}_3$  and acetonitrile, respectively. As shown in Fig. 3.22, in both solvents the ratios of  $A_{378}/A_{323}$  show a steady increase from dimer **136b** to heptamer **140**, and these ratios reach a constant for longer oligomers ( $n \geq 7$ ), which is consistent with the premise of a “folded” conformation. Unfortunately, this trend is not observed in solid-film UV-vis spectra, possibly due to the inaccuracy from instrumental errors (e.g., scattering).

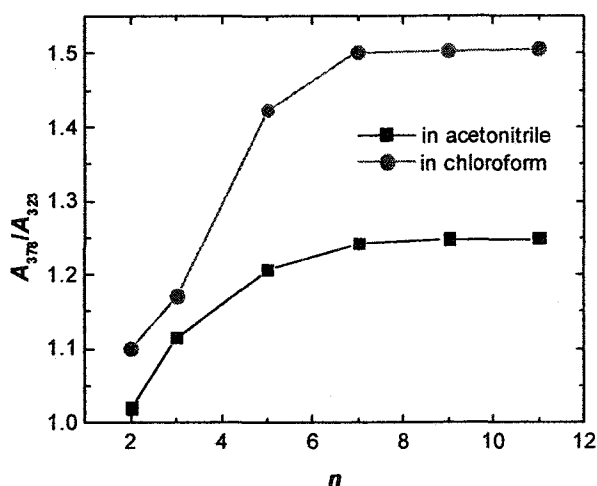


**Fig. 3.22** Plot of absorbance ratio  $A_{378}/A_{323}$  vs. chain length ( $n$ ) in  $\text{CHCl}_3$  (●) and acetonitrile (■).  $A_{378}$  denotes the absorbance intensity at 378 nm, and  $A_{323}$  denotes the absorbance intensity at 323 nm.

Additional evidence supporting the “folding” mechanism comes from the DOKE measurements. First, as shown in Fig. 3.19b, an apparent increase of slope, in the correlation of second hyperpolarizability  $\gamma$  versus chain length  $n$ , suggests that a conformational preference in solution state; in other words, the longer oligomer adopting a “folded” orientation. It is believed that the preferred “folded” conformation in solution state contributes to an additional increase of second hyperpolarizability  $\gamma$ , as a result, causing another linearly increasing trend in Fig. 3.19b, with an enhanced slope value. Moreover, it is also reasonable to assume that, with further chain length extension, the correlation between  $\gamma$  and  $n$  will follow this linear relationship. Second, in a closer inspection of the time-resolved Kerr response of THF reference and oligomer samples, enhanced humps in the response tails can be observed starting from heptamer to pentadecamer. For shorter oligomers ( $n < 7$ ), this feature is quite insignificant, and no hump is observable in solvent THF (Fig. 3.23). It is believed that such a hump is due to a process of molecular dynamics, probably pseudo-*trans* to pseudo-*cis* isomerization (as shown in Fig. 3.20). As revealed by the molecular modeling study, longer oligomers ( $n \geq 7$ ) favor a “folded” conformation (all pseudo-*cis* orientation) in the ground state. In other words, the all pseudo-*cis* conformer is stabilized by a much lower ground state energy compared to the shorter oligomer ( $n < 7$ ), owing to the contribution of “folding” effect. Upon laser pulse excitation, this folded conformation could be “opened” (excited) into an unfolded (pseudo-*trans*) conformation instantaneously, and then it is likely to relax back into its folded ground state after excitation (on a pico-second time scale), since this process is thermodynamically favored. This “folding back” process therefore causes an enhanced hump-shaped response in the tail of the main response peak. In the case of

shorter oligomers ( $n < 7$ ), such a relaxation (i.e., pseudo-*trans* to pseudo-*cis*), however, is less thermodynamically favored due to the relatively smaller energy difference. As a result, only insignificant humps are observed in the main response peak tails.

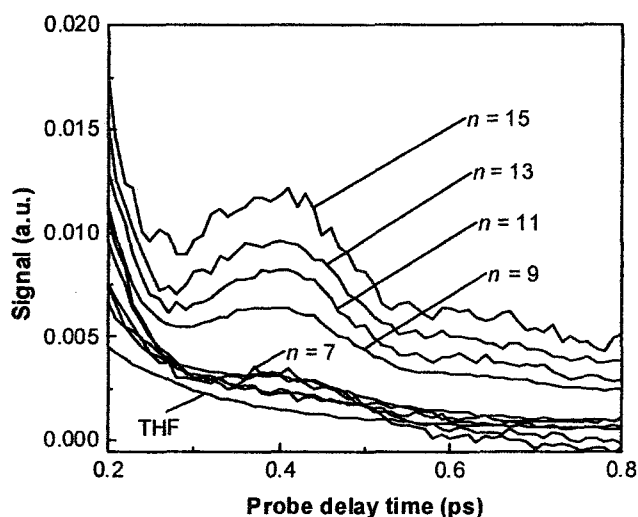


**Fig. 3.23** Zoom in on hump in *iso*-PDA series Kerr response. Signals have been normalized to monomer concentration and THF peak signals. Data series have been averaged.

Unlike the oligo(*m*-phenylene ethynylene) foldamers reported by Moore and co-workers,<sup>17,24-26</sup> it seems the folding/unfolding process of *iso*-PDA foldamers can not be easily controlled by solvation effect, i.e, hydrophobically-driven folding. Furthermore, we have attempted to induce a twist-sense bias in the folded oligomers by incorporating small chiral guest molecules, such as (+) and (-)-pinene, in acetonitrile. However, circular dichromism (CD) spectroscopic results show that no enhanced CD signal is observable after adding the guest molecules. This is not surprising, as molecular modeling study has already shown that the folding cavity (a diameter at *ca.* 3 Å) is likely too small to capture large guest molecules. Further studies on the folding properties

currently target incorporation of chiral auxiliary onto the oligomer chain, on the basis of “Sergeants-and-Soldiers” principle.<sup>27,28</sup>

### 3.3 Conclusions

In this chapter, we have described an efficient synthesis of a modified cross-conjugated *iso*-PDA oligomeric series, namely perphenylated *iso*-PDAs. These oligomers can be synthesized and isolated in reasonable to excellent yields as stable and soluble solids. Solid-state analyses of monomeric **134** to trimeric **138** show that the steric interactions from the phenyl groups prohibits the oligomeric framework from achieving planarity. Electronic absorption and emission spectral analyses were conducted to explore the  $\pi$ -electron delocalization and communication characteristics. The solution state nonlinear optical properties were investigated by the DOKE technique, where the third-order nonlinear optical characteristics, second hyperpolarizability  $\gamma$ , for *iso*-PDA oligomer series were measured. As chain length increases, the perphenylated *iso*-PDAs show a steadily super-linear increment of the  $\gamma$ . Molecular mechanics study on the conformational properties of perphenylated *iso*-PDAs suggests that the oligomers start folding from the stage of heptamer ( $n \geq 7$ ). This conformational preference is also supported by UV-vis and fluorescence spectroscopic analyses, and DOKE experimental results.

### 3.4 References and Notes

- (1) Orfanopoulos, M.; Stratakis, M.; Elemen, Y. *Tetrahedron* **1989**, *30*, 4875-4878.

- (2) Orfanopoulos, M.; Stratakis, M.; Elemen, Y. *J. Am. Chem. Soc.* **1990**, *112*, 6417-6419.
- (3) Stang, P. J.; White, M. R.; Maas, G. *Organometallics* **1983**, *2*, 720-725.
- (4) Zhao, Y.; Campbell, K.; Tykwinski, R. R. *J. Org. Chem.* **2002**, *67*, 336-344.
- (5) Stang, P. J.; Fisk, T. E. *Synthesis* **1979**, 438-440.
- (6) Stang, P. J.; Treptow, W. *Synthesis* **1980**, 283-284.
- (7) Walton, R. M.; Waugh, H. *J. Organomet. Chem.* **1972**, *37*, 45-56.
- (8) Birkofer, L.; Ritter, A.; Uhlenbrauck, H. *Chem. Ber.* **1963**, *96*, 3280-3288.
- (9) Roy, R.; Das, S. K.; Hernández-Mateo, F.; Santoyo-González, F.; Gan, Z. *Synthesis* **2001**, 1049-1052.
- (10) Jones, P. G.; Hopf, H.; Kreutzer, M. *Acta Crystallogr. E* **2002**, *58*, o266-o267.
- (11) Diederich, F. *Chem. Commun.* **2001**, 219-227.
- (12) Nikas, S.; Rodios, N. A.; Varvoglis, A.; Terzis, A.; Raptopoulou, C. P. *J. Heterocycl. Chem.* **1996**, *33*, 997-999.
- (13) (a) Hunter, C. A.; Lawson, K. R.; Perkins, J.; Urch, C. J. *J. Chem. Soc., Perkin Trans 2*, **2001**, 651-669. (b) Carver, F. J.; Hunter, C. A.; Jones, P. S.; Livingston, D. J.; McCabe, J. F.; Seward, E. M.; Tiger, P.; Spey, S. E. *Chem. Eur. J.* **2001**, *7*, 4854-4862. (c) Shannon, R. D. *Acta Cryst.* **1976**, *A32*, 751-767.
- (14) Enkelmann, V. In *Adv. Polym. Sci.*; Springer-Verlag: Berlin Heidelberg, 1984; Vol. 63, pp 91-136.
- (15) Fowler, F. W.; Lauher, J. W. *J. Phys. Org. Chem.* **2000**, *13*, 850-857.
- (16) Nelson, J. C.; Saven, J. G.; Moore, J. S. *Science* **1997**, *277*, 1793-1796.

- (17) Prince, R. B.; Barnes, S. A.; Moore, J. S. *J. Am. Chem. Soc.* **2000**, *122*, 2758-2762.
- (18) Gin, M. S.; Yokozawa, T.; Prince, R. B.; Moore, J. S. *J. Am. Chem. Soc.* **1999**, *121*, 2643-2644.
- (19) Prince, R. B.; Okada, T.; Moore, J. S. *Angew. Chem. Int. Ed.* **1999**, *38*, 233-236.
- (20) Hill, D. J.; Mio, M. J.; Prince, R. B.; Hughes, T. S.; Moore, J. S. *Chem. Rev.* **2001**, *101*, 3893-4011.
- (21) Brunsveld, L.; Prince, R. B.; Meijier, E. W.; Moore, J. S. *Org. Lett.* **2000**, *2*, 1525-1528.
- (22) Slepko, A. D.; Hegemann, F. A.; Zhao, Y.; Tykwinski, R. R.; Kamada, K. *J. Chem. Phys.* **2002**, *116*, 3834-3840.
- (23) *Macromodel*, Version 7.0; Schrödinger Inc.: Portland, OR, 1999.
- (24) Tanatani, A.; Hughes, T. S.; Moore, J. S. *Angew. Chem. Int. Ed.* **2001**, *41*, 325-326.
- (25) Tanatani, A.; Mio, M. J.; Moore, J. S. *J. Am. Chem. Soc.* **2001**, *123*, 1792-1793.
- (26) Hill, D. J.; Mio, M. J.; Hughes, T. S.; Moore, J. S. *Chem. Rev.* **2001**, *101*, 3893-4001.
- (27) Prince, R. B.; Moore, J. S.; Brunsveld, L.; Meijier, E. W. *Chem. Eur. J.* **2001**, *7*, 4150-4154.
- (28) Gin, M. S.; Moore, J. S. *Org. Lett.* **2000**, *2*, 135-138.
- (29) Martin, R. E.; Gubler, U.; Cornil, J.; Balakina, M.; Boudon, C.; Bosshard, C.; Gisselbrecht, J.-P.; Diederich, F.; Günter, P.; Gross, M.; Brédas, J.-L. *Chem. Eur. J.* **2000**, *6*, 3622-3635.

## Chapter 4 Synthesis and Characterization of *iso*-Polytriacetylenes and Related Oligoenynes

### 4.1 Introduction

With the reasoning that bigger is better, our success with the studies of *iso*-PDAs quickly directed our efforts toward other cross-conjugated enynes.<sup>1,2</sup> The next members of the series of expanded dendralenes, the *iso*-polytriacetylenes (*iso*-PTAs, **145**), would result from the insertion of an additional triple bond into the framework of an *iso*-PDA. As the constitutional isomers of polytriacetylenes,<sup>3</sup> the cross-conjugated *iso*-PTAs **145** are expected to show distinctly different electronic properties resulting from  $\pi$ -electron communication.<sup>2,3</sup> Specifically,  $\pi$ -electronic delocalization is not likely to extend along the cross-conjugated carbon backbone to the extent that it would in the analogous linearly conjugated isomer. This structural attribute could be potentially exploited to generate desirable electronic characteristics such as increased “optical transparency”, which is essential for the use of conjugated organic materials in optical applications in the visible region of the spectrum. Furthermore, conjugated oligomers with high energy absorption generally are also of substantial interest as organic materials with high energy (electro)luminescence.

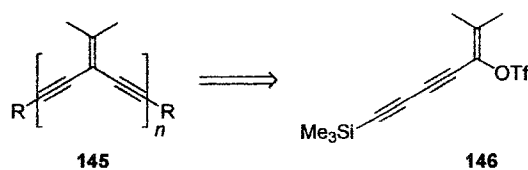


Fig. 4.1 Proposed synthesis of *iso*-PTAs.

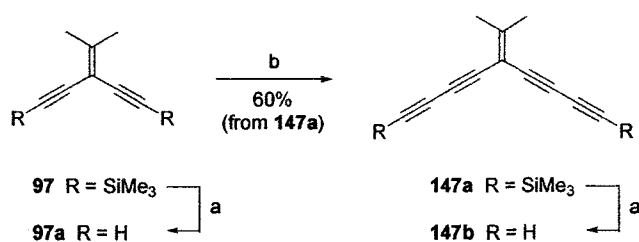
Unlike *iso*-PDAs, there is precedent for *iso*-PTAs. Via the oxidative coupling of appropriately desilylated tetraethynylethenes, Diederich and his group had synthesized the first members of this class of compounds **83** and **84** (see page 67).<sup>3</sup> Rather than a one-pot procedure, however, we envisioned an iterative and divergent sequence for the synthesis of *iso*-PTAs **145** from triflate **146** (Fig. 4.1), similar to what we had achieved for *iso*-PDAs. In addition, a hybrid series of oligoenynes derived directly from *iso*-PTAs, was also synthesized and will be discussed in this chapter.

## 4.2 Results and Discussion

### 4.2.1 Synthesis and Characterization of *iso*-PTAs

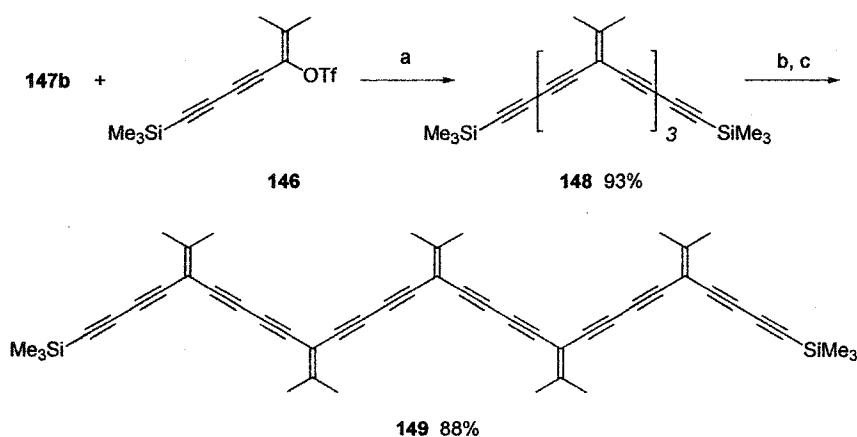
Enetetrayne monomer **147a** was prepared to serve as the central core unit for the divergent construction of *iso*-PTAs (Scheme 4.1). Desilylation of monomer **97** with K<sub>2</sub>CO<sub>3</sub> in THF/MeOH afforded the terminal enediyne **97a**<sup>4</sup> in essentially quantitative yield, which could be used without additional purification after workup.<sup>5</sup> Oxidative acetylenic coupling<sup>6</sup> of **97a** with an excess of trimethylsilylacetylene using *Hay* catalyst in dry acetone for 24 h afforded **147a** in 60% yield as a colorless solid. While **147a** is unstable in the solid state, it can be stored for short periods of time in dilute acetone under refrigeration (4 °C). The reaction in Scheme 4.1 also affords a substantial amount of bis(trimethylsilyl)butadiyne, the other product of homocoupling. The two compounds can, however, be separated by column chromatography, and the bis(trimethylsilyl)butadiyne can subsequently be used as starting material for synthesis of vinyl triflate **146**.<sup>7</sup>

### Scheme 4.1



Reagents and conditions: (a)  $\text{K}_2\text{CO}_3$ , wet MeOH/THF (1:1), rt. (b) Trimethylsilylacetylene, *Hay* catalyst,  $\text{O}_2$ , acetone, rt.

### Scheme 4.2



Reagents and conditions: (a)  $\text{PdCl}_2(\text{PPh}_3)_2$ , CuI, *i*-Pr<sub>2</sub>NH, THF, rt. (b)  $\text{K}_2\text{CO}_3$ , wet MeOH/THF (1:1), rt. (c) 146,  $\text{PdCl}_2(\text{PPh}_3)_2$ , CuI, *i*-Pr<sub>2</sub>NH, THF, rt.

Following isolation, monomer **147a** was quickly subjected to protodesilylation, which proceeds quantitatively to the terminal alkyne **147b**, as judged by TLC analysis. The desilylated enyne **147b** was then taken on directly to the cross-coupling step with two equiv. of vinyl triflate **146** in dry THF, using  $\text{PdCl}_2(\text{PPh}_3)_2$  catalyst, CuI co-catalyst, and diisopropylamine as the base (Scheme 4.2). *iso*-PTA trimer **148** was formed in a yield of 93% and isolated as a relatively stable colorless solid. Using trimeric **148**, a second iteration of the protodesilylation and cross-coupling procedure readily generated *iso*-PTA pentamer **149** in 88% yield. Attempts toward the desilylation of pentamer **149**

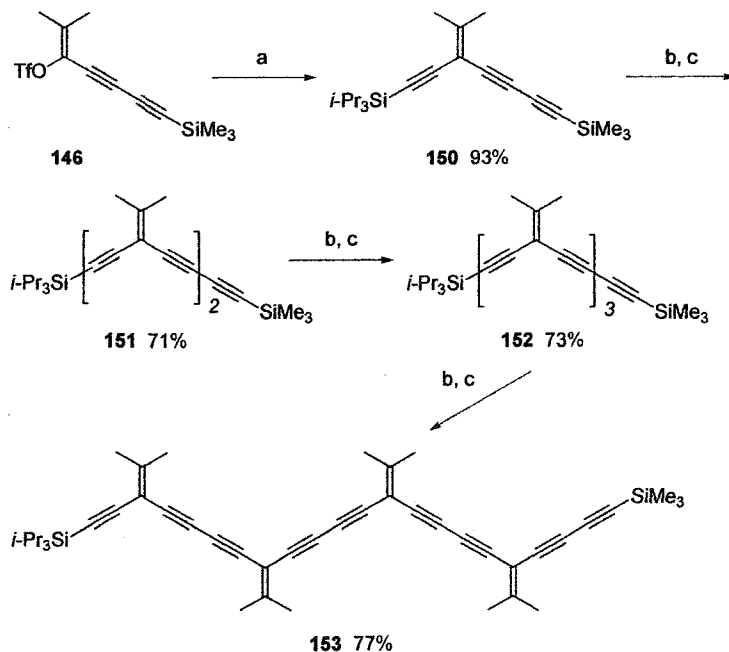
have resulted in only decomposition of the deprotected derivative, and thus far all attempts to extend the chain length of this series beyond that of **149** have been unsuccessful.

A complementary series of *iso*-PTA oligomers was synthesized as illustrated in Scheme 4.3, starting from vinyl triflate **146**. In contrast to the method outlined in Scheme 4.2, this more laborious approach achieved chain extension by only a single unit per protidesilylation/cross-coupling iteration. It was expected, however, that the incorporation of the TIPS group would help to alleviate problems with stability and solubility that had plagued advanced stages of the previous approach in Scheme 4.2. Thus, vinyl triflate **146** was cross-coupled with triisopropylsilylacetylene under standard conditions to afford an enediyne monomer **150** in 93% yield as a stable colorless solid that melts just above room temperature (Mp 30–31 °C). Selective removal of the trimethylsilyl group in monomer **150** with  $K_2CO_3/MeOH$ , followed by cross-coupling with 1 equiv. of vinyl triflate **146** gave dimer **151** in 71% yield as a colorless solid. Employing **151**, a repetition of the protidesilylation and cross-coupling with **146** gave trimer **152** in a yield of 73%, and tetramer **153** was then generated from **152** in 77% yield. Both **152** and **153** were isolated by column chromatography as relatively unstable colorless solids.

The incorporation of the TIPS moiety onto one terminus of the *iso*-PTAs did have the desired result of improving the solubility of these derivatives. Although solubility had been achieved, instability of the desilylated derivatives, even with only monodesilylation, persisted. As had been observed in attempts to extend the chain length

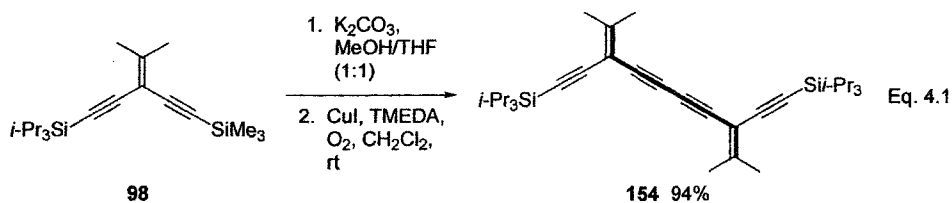
of pentamer **149**, removal of the TMS protecting group of tetramer **153** and attempted cross-coupling failed to produce isolable yields of the next oligomer in the series.

**Scheme 4.3**



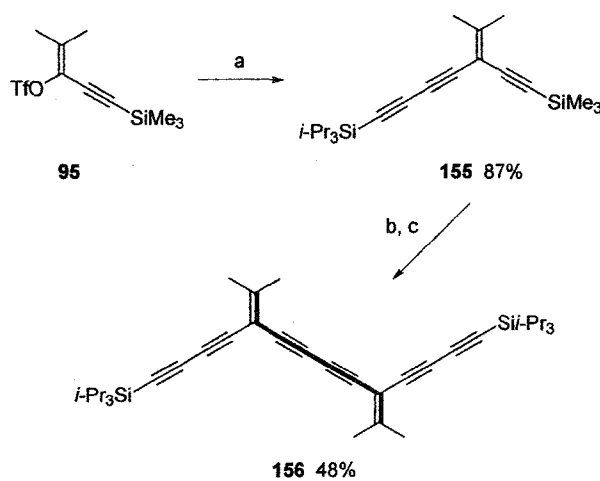
Reagents and conditions: (a)  $i\text{-Pr}_3\text{Si}-\text{C}\equiv\text{CH}$ ,  $\text{PdCl}_2(\text{PPh}_3)_2$ ,  $\text{CuI}$ ,  $i\text{-Pr}_2\text{NH}$ , THF, rt. (b)  $\text{K}_2\text{CO}_3$ , wet MeOH/THF (1:1), rt. (c) **146**,  $\text{PdCl}_2(\text{PPh}_3)_2$ ,  $\text{CuI}$ ,  $i\text{-Pr}_2\text{NH}$ , THF, rt.

For purposes of comparison within the *iso*-PTA series, two dimeric derivatives have also been constructed. The first, dimer **154**, was assembled from monomer **98** via selective removal of the trimethylsilyl group followed by oxidative acetylenic homocoupling (Eq. 4.1). Dimer **154** was isolated as a stable colorless solid in a yield of 94%.



Scheme 4.4 outlines the synthesis of dimer **156**. Triisopropylsilylbutadiyne was cross-coupled with vinyl triflate **95**<sup>8</sup> using palladium-catalyzed coupling conditions to give triyne **155**. Selective removal of the trimethylsilyl group gave the terminal alkyne, which was carried on directly to oxidative dimerization to give hexayne **156** as a stable colorless solid in 48% yield.

**Scheme 4.4**



Reagents and conditions: (a) *i*-Pr<sub>3</sub>Si-C≡C-C≡CH, PdCl<sub>2</sub>(PPh<sub>3</sub>)<sub>2</sub>, CuI, *i*-Pr<sub>2</sub>NH, THF, rt. (b) K<sub>2</sub>CO<sub>3</sub>, wet MeOH/THF (1:1), rt. (c) CuCl/TMEDA, CH<sub>2</sub>Cl<sub>2</sub>, O<sub>2</sub>, rt.

In general, *iso*-PTAs all displayed limited thermal stability. For example, monomer **147a** (64–65 °C), dimer **156** (129–130 °C), and trimer **148** (96–98 °C) all show defined melting points, whereas pentamer **149** decomposes at 85 °C. Relative to the shorter oligomers, the kinetic stability of the longer derivatives (e.g., tetramer **153** and pentamer **149**) was quite diminished, and decomposition was observed even when stored under nitrogen at low temperature.

The stability of all *iso*-PTAs was sufficient for complete characterization, and <sup>1</sup>H and <sup>13</sup>C NMR spectroscopic analyses are consistent with their proposed structures. For

example, the  $^{13}\text{C}$  NMR spectrum of the longest oligomer, pentamer **149**, demonstrates the polarized nature of vinylidene carbons. The three vinyl carbons external to the oligomer chain ( $\text{C}=\text{CMe}_2$ ) are significantly deshielded to  $\delta$  162–163, whereas the endo-chain vinyl carbons ( $\text{C}=\text{CMe}_2$ ) are shifted considerably upfield and resonate in the range of the  $\text{sp}^2$  hybridized carbons at  $\delta$  100. Considering the similar electronic environment for carbons in an individual enyne repeat unit of the *iso*-PTA oligomers, it is noteworthy that all 20 unique  $\text{sp}$  and  $\text{sp}^2$  hybridized carbons are distinguishable in the  $^{13}\text{C}$  NMR spectrum of **152**, and 25 of 26 such carbons are observed in the spectrum of **153**.

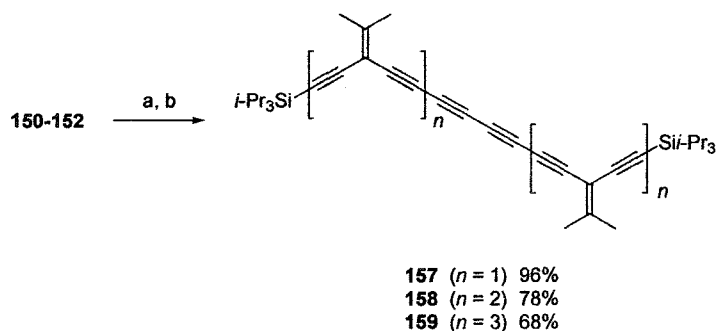
Electronic impact mass spectrometric analysis of longer oligomers **149** and **153** was unsuccessful as a result of their high molecular weight. Electrospray ionization, however, proved quite useful in confirming their mass. Analysis in the positive mode of MeOH/toluene (3:1) solutions of **149** and **153** with AgOTf added to the solution produced well resolved signals at  $m/z$  813.2 and 771.2, consistent with that expected for  $[\mathbf{149} + \text{Ag}^+]^+$  and  $[\mathbf{153} + \text{Ag}^+]^+$ , respectively.

#### 4.2.2 *Synthesis and Characterization of Expanded Enynes.*

Differentially protected enynes **150**–**153** provided the springboard for the realization of a hybrid sequence of oligoenynes based on a tetrayne core, as depicted in Schemes 4.5 and 4.6. Synthesis of the parent member of this series began with triyne **150**, which was desilylated with  $\text{K}_2\text{CO}_3/\text{MeOH}$  and then dimerized via oxidative acetylenic homocoupling with  $\text{CuI}/\text{TMEDA}$  and oxygen in  $\text{CH}_2\text{Cl}_2$  to give **157** in a yield of 96% as a pale yellow solid. An analogous sequence of trimethylsilyl removal followed by dimerization was applied to **151** and **152**, giving decayne **158** and tetradecayne **159** as light yellow solids in 78% and 68% yields, respectively. The longest

member of this series to be achieved, octadecayne **160**, was obtained from tetrameric **153** in 56% yield (Scheme 4.6). This molecule is composed of a contiguous sequence of 44  $sp$  and  $sp^2$  carbons, and, based on molecular modeling of the all *s-trans* orientation, it spans ca. 5.6 nm from silicon atom to silicon atom.<sup>9</sup>

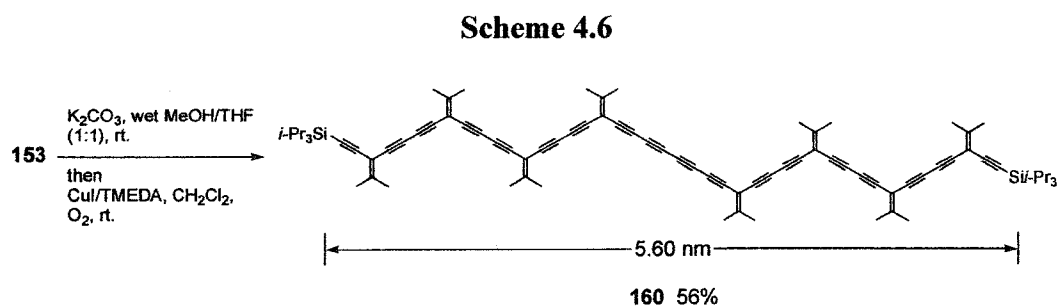
**Scheme 4.5**



Reagents and conditions: (a)  $K_2CO_3$ , wet MeOH/THF (1:1), rt. (b) CuI/TMEDA,  $CH_2Cl_2$ ,  $O_2$ , rt.

Whereas enyne **157** and **158** show reasonable solubility, longer oligomers **159** and **160** have only limited solubility in organic solvents. In addition, the environmental stability of the enynes steadily decreased as the conjugated framework was extended from hexayne **157** to octadecayne **160**. Although octadecayne **160** could be isolated and characterized by  $^1H$  NMR, IR, and UV-vis spectroscopies, it was neither sufficiently soluble nor stable for  $^{13}C$  NMR spectroscopic analysis. In the  $^{13}C$  NMR spectra for tetrayne derived systems **157–159**, the most distinguishable features are: (1) the  $sp^2$  isopropylidene carbons ( $C=CMe_2$ ), which are observed in a range from 160.6 to 167.0 ppm, even more deshielded than for the *iso*-PTAs (*vide supra*), (2) the two interior carbons of the tetrayne moiety, shielded to 68.1 and 64.2 ppm, and (3) the fact that all 28 unique carbons resonances are observable for **159**. ESI MS proved invaluable for

confirming the formation of the desired oligomers. Analysis of **158–160** by ESI in the positive mode with added AgOTf clearly showed signals corresponding to  $[M + Ag^+]^+$  at  $m/z$  879.3, 1083.4, and 1287.6, respectively.



#### 4.2.3 Solid-State Properties of Cross-conjugated *iso*-PTA **156** and Tetrayne **157**

Single crystals of *iso*-PTA dimer **156** were obtained by diffusion of MeOH into a  $\text{CH}_2\text{Cl}_2$  solution at  $-20\text{ }^\circ\text{C}$ , and two geometrically similar but crystallographically independent molecules were observed in the unit cell (Fig. 4.2). Although disorder is present in one of the silyl groups for molecule B of **156**, reasonable refinement was obtained to allow analysis and comparison between molecules A and B. The cross-conjugated enyne frameworks of both molecules A and B, similarly, are non-planar. This non-planar characteristics of both molecules can be depicted via the dihedral angles between the two vinylidene least-squares planes, namely plane 1 and plane 2. In molecule A, the dihedral angle between plane 1 (C14, C15, C16, and C19) and plane 2 (C22, C23, C24, and C27) is  $36.79(19)^\circ$ , whereas such a dihedral angle of  $30.8(2)^\circ$  is observed for molecule B.

Similar to the *iso*-PDA oligomers, there is no observable reduced bond length alternation for **156**. For instance, in molecule A, the  $\text{sp}^2$ - $\text{sp}$  single bonds on the conjugated framework: C(15)–C(19) and C(22)–C(23) at 1.435(4) and 1.433(4) Å, and in

molecule B, C(55)–C(59) and C(62)–C(63) at 1.429(5) and 1.439(5) Å, respectively, are in the expected range for single bonds linking sp<sup>2</sup> carbons. Similar results are found for the sp–sp single bonds: C(20)–C(21) at 1.385(5) Å (molecule A), and C(12)–C(13) at 1.381(4) Å. The two C≡C bonds, C(19)–C(20) and C(21)–C(22) at 1.196(4) and 1.201(4) Å, and the two C=C bonds, C(15)–C(16) and C(23)–C(24) at 1.351 and 1.349 Å, are also in the range expected. In molecule B, similar results can be observed: for C–C bonds, C(55)–C(59), C(60)–C(61), and C(62)–C(63) are at 1.429(5), 1.380(5), and 1.439(5), respectively. For C=C bonds, C(55)–C(56), C(63)–C(64) are at 1.354(5) and 1.361(5) Å, respectively, whereas, C(59)–C(60) and C(61)–C(62) at 1.202(5) and 1.195(5) Å for C≡C bonds. Another noteworthy feature for single crystals of **156** is the consistent vinylidene bond angles, C(14)–C(15)–C(19) and C(22)–C(23)–C(27) at 115.0(3) and 114.9(3)°, respectively (molecule A), and C(54)–C(55)–C(59) and C(62)–C(63)–C(67) at 115.6(3) and 115.4(3)°, respectively (molecule B), which are slightly less than the theoretically predicted angle of 120° for an sp<sup>2</sup>-hybridized carbon center. However, these vinylidene angles are comparable to those observed in *iso*-PDA oligomers.<sup>4,10</sup> The packing parameters for **156** are unsuitable for solid-state topochemical polymerization.

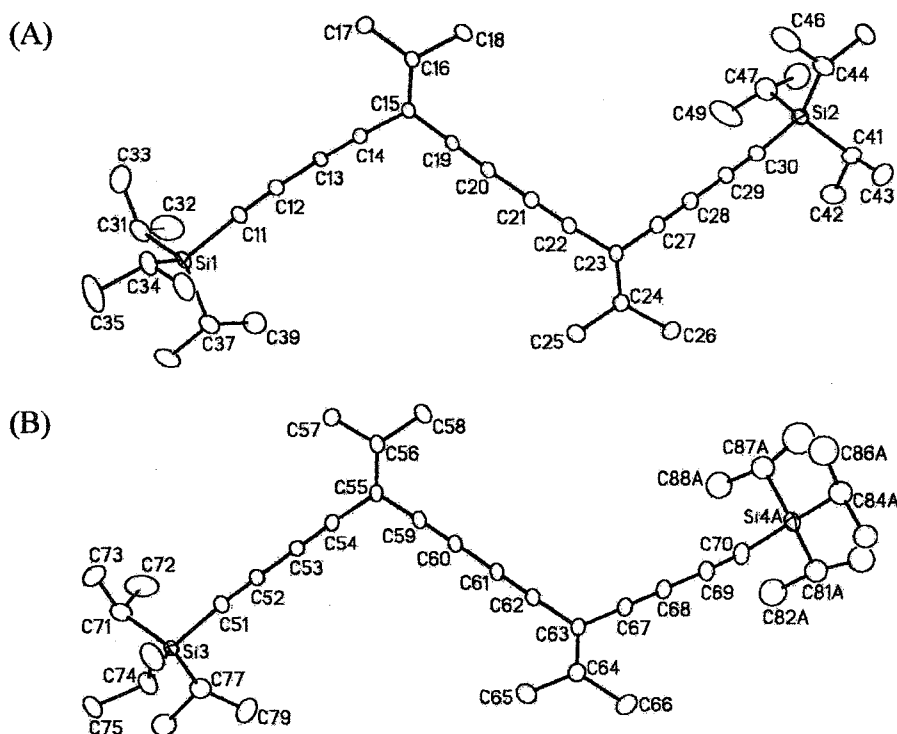


**Fig. 4.2** ORTEP drawings (20% probability level) of **156**. Selected bond lengths (Å) and angles (°) for molecule A: C(11)–C(12) 1.208(4), C(12)–C(13) 1.381(4), C(13)–C(14) 1.197(4), C(14)–C(15) 1.440(4), C(15)–C(16) 1.351(4), C(15)–C(19) 1.435(4), C(19)–C(20) 1.196(4), C(20)–C(21) 1.385(5), C(21)–C(22) 1.201(4), C(22)–C(23) 1.433(4), C(23)–C(24) 1.349(5), C(23)–C(27) 1.437(5), C(27)–C(28) 1.202(5), C(28)–C(29) 1.375(5), C(29)–C(30) 1.195(5); Si(1)–C(11)–C(12) 177.3(3), C(11)–C(12)–C(13) 175.8(4), C(12)–C(13)–C(14) 177.0(4), C(13)–C(14)–C(15) 176.1(3), C(14)–C(15)–C(19) 115.0(3), C(15)–C(19)–C(20) 177.4(4), C(19)–C(20)–C(21) 176.5(4), C(20)–C(21)–C(22) 176.6(4), C(21)–C(22)–C(23) 176.6(4), C(22)–C(23)–C(27) 114.9(3), C(23)–C(27)–C(28) 177.9(4), C(27)–C(28)–C(29) 178.7(4), C(28)–C(29)–C(30) 178.9(5), Si(2)–C(30)–C(29) 175.9(3).

Single crystals of tetrayne **157** were obtained by diffusion of MeOH into a CH<sub>2</sub>Cl<sub>2</sub> solution at –20 °C and provided an excellent opportunity to probe the solid-state properties of this highly unsaturated enyne. Surprisingly, under the same crystallization conditions, two different polymorphs of **157** could be observed. In addition, there

appears to be no way to direct which polymorph will result for a given crystallization attempt.

The two geometrically similar solid-state structures adopt *s-trans* orientation with respect to the octatetrayndiyl moiety (Fig. 4.3). The overall  $\pi$ -framework is virtually planar in both cases, with a maximum deviation of 0.13 Å and 0.02 Å from a least-squares plane for the 16-carbon conjugated skeletons in Structure 1 and 2, respectively. All triple bonds are essentially the same length and are comparable to other reported polyynes.<sup>11-13</sup> The eight tetrayne carbons show only a gradual curvature with bond angles deviating from 180° by less than 3° in all cases. In structure A, the four triple bond lengths of C(4)–C(5), C(6)–C(7), C(8)–C(9), and C(10)–C(11) are found at 1.200(3), 1.209(3), 1.203(3), and 1.200(3) Å, respectively, and no obvious reduction in bond length alternation is observable. Moreover, the two double bonds of C(3)–C(15) at 1.351(3) Å and C(12)–C(18) at 1.350(3) Å, and two vinylidene angles observed at 115.98(17)° and 116.36(17)°, are comparable to other cross-conjugated enyne species.

The major difference between the two structures is the orientation of the individual molecules with respect to each other in the solid state. In the case of structure A, the molecules are aligned parallel to each other in a manner potentially suitable for topochemical polymerization.<sup>1,14-18</sup> In structure B, neighboring molecules are nearly perpendicular to each other, precluding the possibility of solid-state polymerization. The topochemical polymerization of **157** and other related cross-conjugated enynes will be subsequently discussed in Chapter 5.

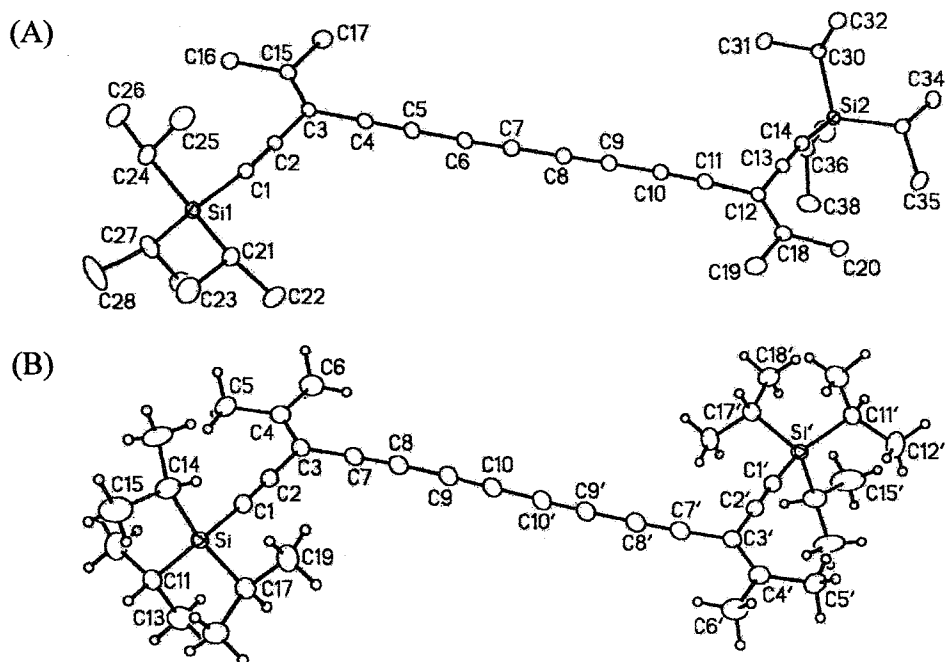


**Fig. 4.3** ORTEP drawings (20% probability level) of **157**. Selected bond lengths (Å) and angles (°): for structure A: C(1)–C(2) 1.204(3), C(2)–C(3) 1.444(3), C(3)–C(15) 1.351(3), C(3)–C(4), 1.433(3), C(4)–C(5) 1.200(3), C(5)–C(6) 1.369(3), C(6)–C(7) 1.209(3), C(7)–C(8) 1.365(3), C(8)–C(9) 1.203(3), C(9)–C(10) 1.373(3), C(10)–C(11) 1.200(3), C(11)–C(12) 1.432(3), C(12)–C(18) 1.350(3), C(12)–C(13) 1.447(3), C(13)–C(14) 1.207(3); Si(1)–C(1)–C(2) 173.32(18), C(1)–C(2)–C(3) 179.0(2), C(2)–C(3)–C(4) 115.98(17), C(3)–C(4)–C(5) 179.1(2), C(4)–C(5)–C(6) 177.8(2), C(5)–C(6)–C(7) 177.5(2), C(6)–C(7)–C(8) 179.4(2), C(7)–C(8)–C(9) 179.5(3), C(9)–C(10)–C(11) 177.1(2), C(11)–C(12)–C(13) 116.36(17), C(12)–C(13)–C(14) 178.2(2), Si(2)–C(14)–C(13) 173.59(19). For structure B: C(1)–C(2) 1.203(4), C(3)–C(4), 1.357(4), C(7)–C(8) 1.199(4), C(9)–C(10) 1.209(4); Si(1)–C(1)–C(2) 175.5(3), C(1)–C(2)–C(3) 178.9(3), C(2)–C(3)–C(7) 114.5(2), C(7)–C(8)–C(9) 178.4(3), C(8)–C(9)–C(10) 178.7(3).

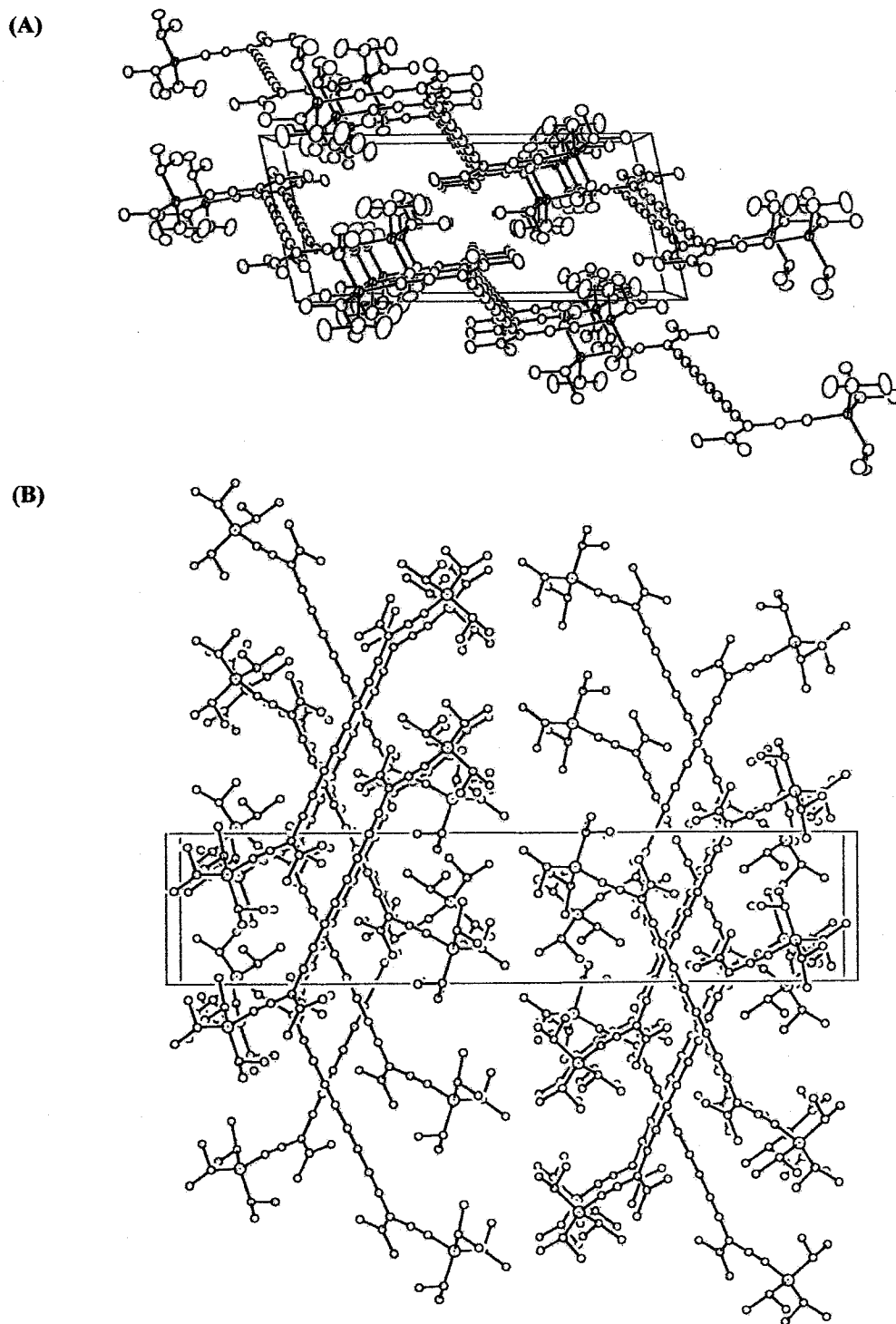


**Fig. 4.4** (a) Crystal packing diagram of structure A of 157, as viewed along  $a$ -axis. (b) Crystal packing diagram of structure B of 157, as viewed along  $a$ -axis.

#### 4.2.4 Electronic Characteristics of Cross-conjugated Oligoenynes

Electronic absorption spectra of cross-conjugated *iso*-PTAs and related oligoenynes were used to survey their  $\pi$ -electronic properties. Dimer **156** provides the basis of comparison with the *iso*-PTA series. It possesses the longest linearly conjugated segment (shown in bold in Scheme 4.4), and contributions via cross-conjugation in the longer oligomers would be manifested in a change in  $\lambda_{\max}$  values for oligomers **148** and **149** vs. **156**. In the progression from dimer **156** to trimer **148** to pentamer **149**, the higher energy region of the electronic absorption spectra shows a steadily augmenting molar absorptivity. The lower energy region of the spectra of all three compounds shows two major absorptions of similar energy at 312 and 334 nm. The spectra for this series of *iso*-PTAs, **148–149** and **156**, thus suggest that chain length extension is of little consequence on  $\lambda_{\max}$  values. This effect is in accord with the previous observations for *iso*-PTAs, but runs contrary to that observed in *iso*-PDAs.

Whereas the spectra of *iso*-PTAs **156**, **148**, and **149** show absorptions of similar energy, a comparison of the three dimeric molecules synthesized in this study, namely **151**, **154**, and **156**, provides an interesting observation. As the terminal functionality are altered from simply ethynyl to 1,3-butadiynyl in the progression from **154**→**151**→**156**, a steady decrease in both the molar absorptivity and energy of  $\lambda_{\max}$  is observed: **154** 329 (22 300) nm to **151** 332 (13 600) nm to **156** 335 (11 100) nm (Fig. 4.5b). This trend demonstrates the ability to influence the electronic communication in cross-conjugated enynes, albeit to only a small extent as measured by UV-vis spectroscopy.

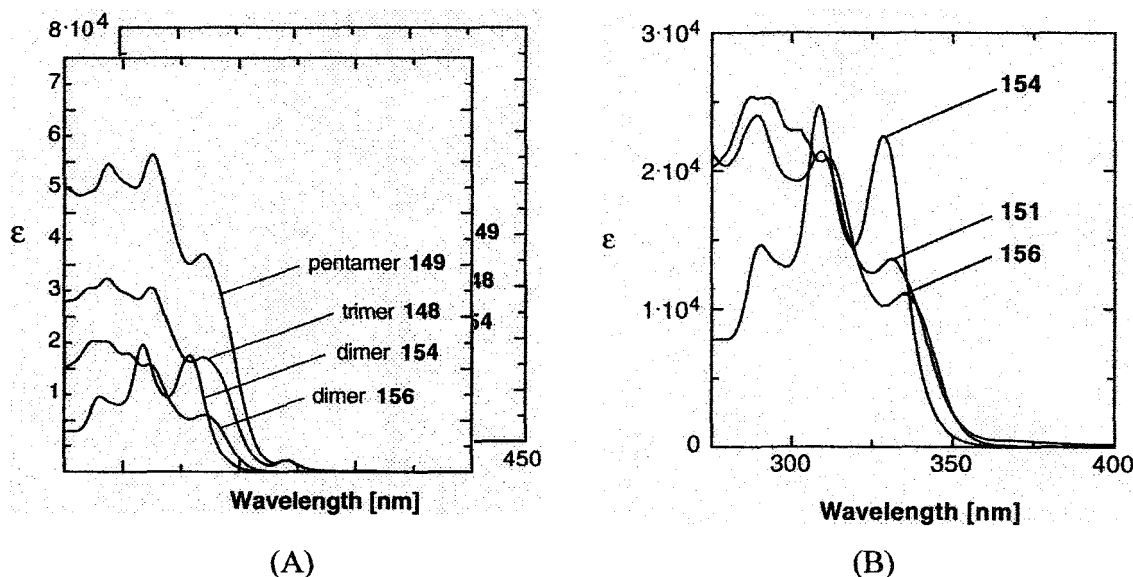


Fig. 4.5 (a) Electronic absorption spectra ( $\epsilon$  [ $\text{L mol}^{-1} \text{cm}^{-1}$ ]) in  $\text{CHCl}_3$  comparing 148, 149, 154, and 156. (b) Electronic absorption spectra ( $\epsilon$  [ $\text{L mol}^{-1} \text{cm}^{-1}$ ]) in  $\text{CHCl}_3$  comparing dimers 151, 154, and 156.

The spectra of tetrayne based oligoenynes **157–160** are shown in Fig. 4.6. As demonstrated for the *iso*-PTAs, the higher energy region shows a steadily increasing molar absorptivity versus the number of enediyne monomer. The lower energy region is dominated by the absorption pattern of the tetrayne moiety. Each tetrayne displays three identical absorption at 405, 374, and 348 nm that are found at virtually identical energies for other tetraynes such as 1,8-bis(4-*t*-butylphenyl)octatetrayne.<sup>2,19</sup> No obvious energy shift (less than 1 nm) can be observed in the tetrayne absorptions as a result of increasing the cross-conjugated chain length from **157**→**160**. To the contrary, however, the higher energy absorptions resulting from the *iso*-PTA segments of the molecules (ca. 330 nm) show a slight bathochromic shift in the longer oligomers. Thus, with chain elongation, this ultimately results in a merging of the *iso*-PTA absorption with that of the tetrayne moiety at 348 nm, affording a single, non-distinctive shoulder for **160**.

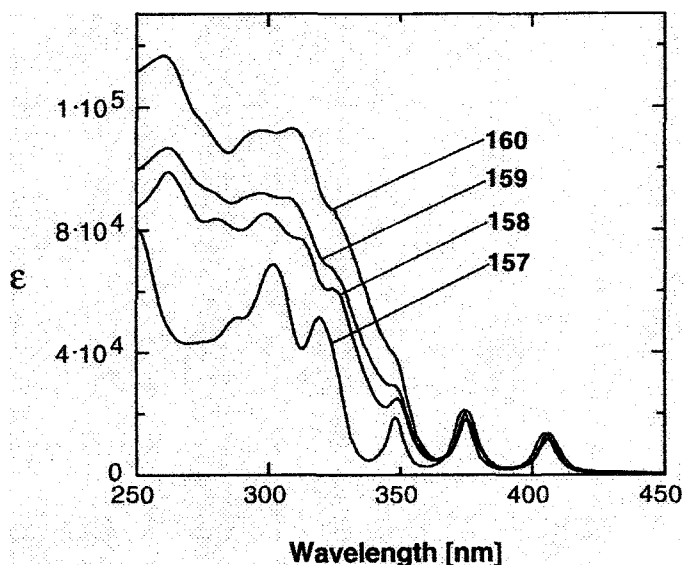


Fig. 4.6 Electronic absorption spectra ( $\epsilon$  [ $\text{L mol}^{-1} \text{cm}^{-1}$ ]) in  $\text{CHCl}_3$  comparing 157–160.

### 4.3 Conclusions

This chapter demonstrated an effective synthesis of highly unsaturated, cross-conjugated enynes. The iterative sequence of palladium-catalyzed cross-coupling of terminal alkynes with vinyl triflates is quite effective for the realization of *iso*-PTA oligomers, combining short reaction times with good to excellent yields. Whereas shorter cross-conjugated oligomers are generally soluble and stable, all of the longer oligomers were less robust and only marginally soluble in organic solvents. Ultimately, these factors both prevented chain length extension beyond that found in pentameric *iso*-PTA **153** and tetrayne derived **160**. There is a minimal electronic effect resulting from cross-conjugation, although in shorter oligomers such as dimers **151**, **154**, and **156** the effect of the end group (ethynyl vs. butadiynyl) is clearly observed.

#### 4.4 References and Notes

- (1) Zhao, Y.; McDonald, R.; Tykwinski, R. R. *Chem. Commun.* **2000**, 77-78.
- (2) Zhao, Y.; McDonald, R.; Tykwinski, R. R. *J. Org. Chem.* **2002**, *67*, 2805-2812.
- (3) Boldi, A. M.; Anthony, J.; Gramlich, V.; Knobler, C. B.; Boudon, C.; Gisselbrecht, J.-P.; Gross, M.; Diederich, F. *Helv. Chim. Acta* **1995**, *78*, 779-796.
- (4) Zhao, Y.; Campbell, K.; Tykwinski, R. R. *J. Org. Chem.* **2002**, *67*, 336-344.
- (5) As a result of their general instability, desilylated derivatives were carried on, following workup, to the subsequent coupling reaction without additional purification. Yields and purities from desilylation are sufficient to accommodate this tactic.
- (6) Siemsen, P.; Livingston, R. C.; Diederich, F. *Angew. Chem. Int. Ed.* **2000**, *39*, 2632-2657.
- (7) Stang, P.; Ladika, M. *Synthesis* **1981**, 29-30.
- (8) Stang, P. J.; Fisk, T. E. *Synthesis* **1979**, 438-440.
- (9) *MacSpartan Plus*, Version 1.1.9; Wavefunction, Inc.: Irvine, CA, 1998.
- (10) Zhao, Y.; Tykwinski, R. R. *J. Am. Chem. Soc.* **1999**, *121*, 458-459.
- (11) Mohr, W.; Stahl, J.; Hampel, F.; Gladysz, J. A. *Inorg. Chem.* **2001**, *40*, 3263-3264.
- (12) Dembinski, R.; Lis, T.; Szafert, S.; Mayne, C. L.; Bartik, T.; Gladysz, J. A. *J. Organomet. Chem.* **1999**, *578*, 229-246.
- (13) Bartik, B.; Dembinski, R.; Bartik, T.; Arif, A. M.; Gladysz, J. A. *New J. Chem.* **1997**, *21*, 739-750.

- (14) Xiao, J.; Yang, M.; Lauher, J. W.; Fowler, F. W. *Angew. Chem. Int. Ed.* **2000**, *39*, 2132-2135.
- (15) Sarkar, A.; Okada, S.; Matsuzawa, H.; Matsuda, H.; Nakanishi, H. *J. Mater. Chem.* **2000**, *10*, 819-828.
- (16) Sarkar, A.; Shuji, O.; Kyoji, K.; Hachiro, N.; Hiro, M. *Macromolecules* **1998**, *31*, 5624-5630.
- (17) Enkelmann, V. In *Adv. Polym. Sci.*; Springer-Verlag: Berlin Heidelberg, 1984; Vol. 63, pp 91-136.
- (18) Baughman, R. H.; Yee, K. C. *J. Polym. Sci.: Macromol. Rev.* **1978**, *13*, 219-239.
- (19) This compound was generously provided by Dr. Michael M. Haley at the University of Oregon. For synthesis of similar tetraynes: Haley, M. M.; Bell, M. L.; Brand, S. C.; Kimball, D. B.; Pak, J. J.; Wan, W. B. *Tetrahedron Lett.* **1997**, *38*, 7483-7486.

## Chapter 5 Synthesis, Characterization, and Solid-State Polymerization of Cross-conjugated Tetrynes

### 5.1 Introduction

As described in Chapter 4, a novel class of cross-conjugated tetrynes **157–160** has readily been synthesized employing a sequence of palladium catalyzed cross-coupling and oxidative homocoupling reactions. Crystallographic analysis of tetryne **157** shows that a planar *s-trans* orientation is adopted by the enyne framework.<sup>1</sup> Moreover, as indicated for structure **A** of **157**, the central tetrynes are parallelly packed with respect to each other. The resulting packing parameters suggest the possibility of a solid-state polymerization (i.e., topochemical polymerization) reaction.<sup>2,3</sup> For example, Fig. 5.1–5.2 illustrates the topochemical polymerizations of tetrynes in both the 1,6- and 1,4-addition fashion.

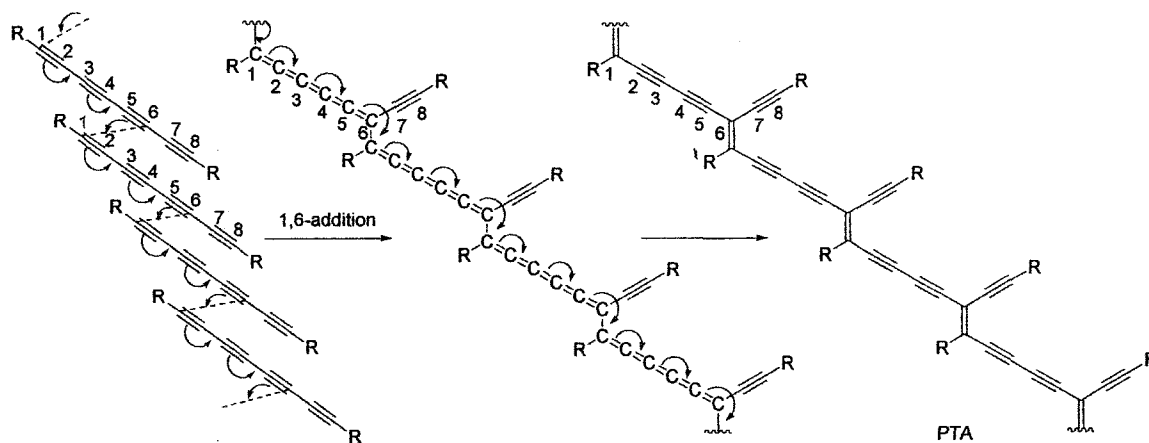
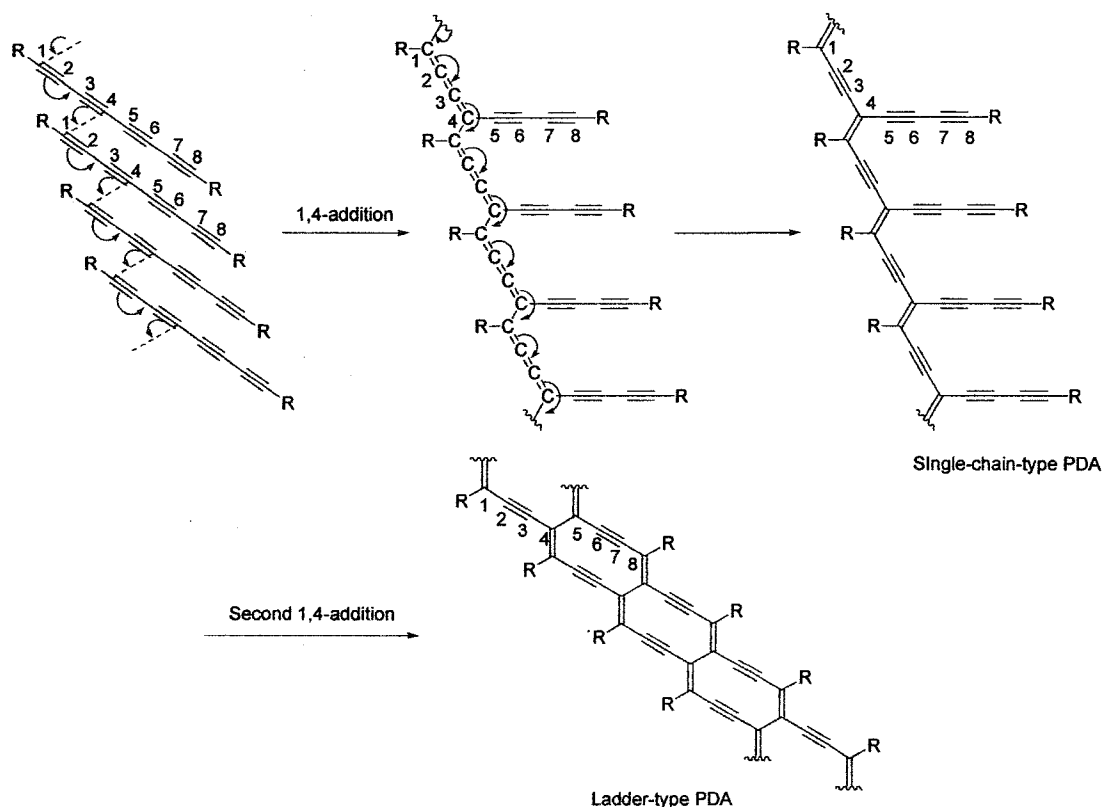


Fig. 5.1 Solid-state topochemical polymerization of tetrynes in 1,6-addition fashion.



**Fig. 5.2** Solid-state topochemical polymerization of tetraynes in 1,4-addition fashion.

Solid-state polymerization has been the subject of considerable research efforts, since it provides a route to large, nearly defect-free polymer crystals.<sup>2,4</sup> In recent years, much attention has been focused on the topochemical polymerization of polyynes monomers into polyenyne polymers. This is due to their potential application as third order non-linear optical (NLO) materials.<sup>5-13</sup> First reported by Wegner in 1969,<sup>14</sup> topochemical polymerizations have been extensively studied employing a variety of polyynes monomers,<sup>15</sup> ranging from butadiyne up to dodecahexaynes under the conditions of heat,<sup>11</sup> UV light,<sup>16</sup> pressures, or  $\gamma$ -rays irradiation.<sup>17</sup> Experimental results have demonstrated that the physical state of the monomer polyynes is crucial to both the kinetic and structural properties of the resulting polymer.<sup>11</sup> In principle, the reactivity in the

solid state is generally dominated by the motional fashion that allows the reactive sites to contact each other. The solid-state topochemical polymerizations can thus be described as a transformation of the parent crystal into the daughter crystal. In an orderly packed monomer crystal, if all the reactive sites can move cooperatively to form another order structure (i.e., phase transition) with a minimal translational requirement, then such a topochemical reaction is favored and likely to occur when energy (heat, light, pressure) is introduced. For instance, a well oriented butadiyne monomer crystal will favor only the 1,4-addition to form a polydiacetylene single crystal,<sup>6,18-24</sup> since this type of topochemical reaction requires a minimal amount of translational motion. For longer polyyne monomers, however, such as triyne,<sup>17,25</sup> tetrayne,<sup>6,7,26</sup> pentayne<sup>27</sup>, and hexayne<sup>28</sup> species, the possibilities of 1,6-, 1,8- and 3,6-addition also exist, in addition to the most commonly observed 1,4-addition. This can hamper the realization of the defect-free single crystal transformation, as well as complicate characterization of reaction products.

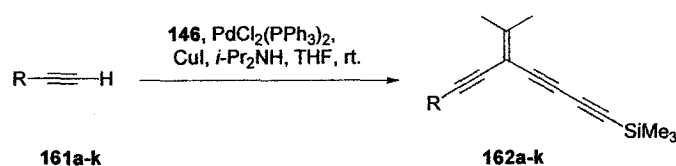
In 2000, Fowler's group first effected a 1,6-addition of a triyne species by elegantly controlling the solid-state crystal packing of a monomeric triyne through modification of pendant side groups (as shown in Scheme 5.1).<sup>17,29</sup> Of similar importance, tetraynes are also central to topochemical polymerization, since it can lead to various polydiacetylenes and "ladder" polymers,<sup>5,9</sup> of significant potential as optical materials. Albeit, direct observation of the 1,6-addition in tetraynes still has not been conclusively demonstrated. Thus, a systematic study of solid-state topochemical polymerization for tetrayne species was undertaken.

In addition to their interesting solid-state properties, cross-conjugated tetraynes can also play important roles, as cross-conjugated linkers or molecular wires, in probing



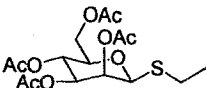
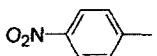
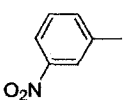
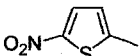
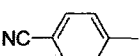
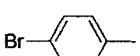
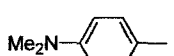
$\text{PdCl}_2(\text{PPh}_3)_2$  as catalyst,  $\text{CuI}$  as co-catalyst,  $i\text{-Pr}_2\text{NH}$  as base in THF solution (Scheme 5.2). Generally, all the cross-coupling reactions proceeded smoothly at room temperature and were complete within 2 h. The resulting enetriyne monomers **162a–k** can be readily purified by a brief aqueous workup, followed by a flash column chromatography over silica gel. The synthetic results of **162a–k** are summarized in Table 5.1.

**Scheme 5.2**

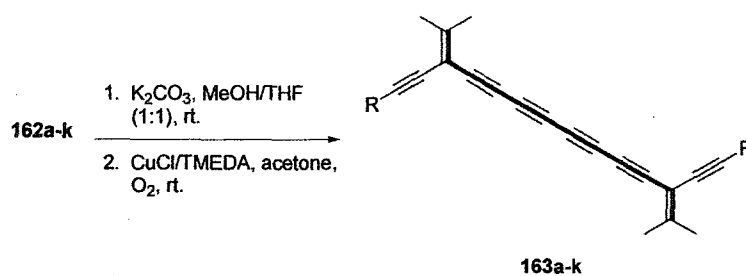


Next, cross-conjugated tetraines **163a–k** were obtained via oxidative homocoupling of the respective deprotected precursors **162a–k**, using Cu-mediated Hay coupling conditions.<sup>31</sup> The reactions proceeded smoothly and completely in 0.5 h at room temperature in the presence of the *Hay* catalyst in acetone solution affording tetraines **163a–k** (Scheme 5.3). The resulting tetraines **163a–k** were extracted with diethyl ether and washed with 10% HCl, saturated  $\text{NaHCO}_3$ , and brine sequentially. Flash column chromatography over silica gel then afforded the pure tetraines. It is worth noting that oxygen is essential to the oxidative homocoupling, and in all cases, exposure to air is sufficient enough for the reaction. The results of homocoupling reactions are listed in Table 5.2.

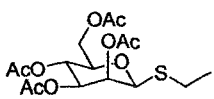
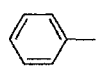
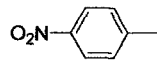
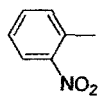
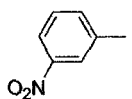
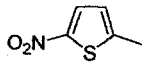
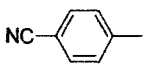
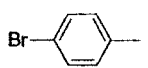
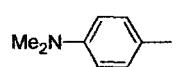
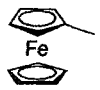
**Table 5.1** Synthesis of enetriyne monomers **162a–k**.

Entry	R	Yield (%)	Description
<b>162a</b>	<i>n</i> -Butyl	98	Unstable oil
<b>162b</b>		65	Colorless solid (Mp 54–57 °C)
<b>162c</b>		96	Colorless solid (Mp 71–72 °C)
<b>162d</b>		90	Yellow solid (Mp 94–95 °C)
<b>162e</b>		87	Yellow solid (Mp 93–94 °C)
<b>162f</b>		92	Yellow solid (Mp 77–78 °C)
<b>162g</b>		36	Light yellow solid (Mp 68–69 °C)
<b>162h</b>		80	Yellow solid (Mp 60–62 °C)
<b>162i</b>		79	Colorless wax
<b>162j</b>		83	Light yellow solid (Mp 82–83 °C)
<b>162k</b>		56	Yellow solid (Mp 84–85 °C)

**Scheme 5.3**



**Table 5.2** Synthesis of cross-conjugated tetraynes **163a–k**.

Entry	R	Yield (%)	Description
<b>163a</b>	<i>n</i> -Butyl	94	Unstable oil
<b>163b</b>		91	Brown solid (Mp 57–62 °C)
<b>163c</b>		64	Yellow waxy solid
<b>163d</b>		94	Yellow solid (Mp >115 °C, dec.)
<b>163e</b>		27	Unstable yellow solid
<b>163f</b>		39	Unstable yellow solid
<b>163g</b>		0	
<b>163h</b>		73	Unstable yellow solid
<b>163i</b>		85	Yellow solid (Mp >110 °C, dec.)
<b>163j</b>		76	Yellow solid (Mp >115 °C, dec.)
<b>163k</b>		74	Orange solid (Mp >120 °C, dec.)

### 5.2.2 Physical Properties

*n*-Butyl protected tetrayne **163a** is a relatively unstable brown oil, which slowly decomposes at room temperature. IR spectroscopic analysis of the decomposed product shows broad featureless peaks at 2100 and 1600  $\text{cm}^{-1}$ , suggesting that the decomposition might result from a topochemical polymerization pathway. Similarly, the nitroaryl functionalized tetraynes **163e**, and **163f** show relatively low kinetic stability even at low temperatures, which results in drastically lower homocoupling yields. This

decomposition is observable by TLC analysis, and these compounds are only stable for days at low temperature ( $-4\text{ }^{\circ}\text{C}$ ) under argon atmosphere. Reasonable characterization, including  $^1\text{H}$  NMR,  $^{13}\text{C}$  NMR, IR spectroscopic, and MS, could be conducted immediately after column chromatographic isolation. In the case of 4-nitrothienyl substituted tetrayne, **163g**, the decomposition occurred so rapidly that no characterizable product could be isolated from the reaction.

The other tetraynes, to the contrary, show much improved kinetic and thermal stability. For instance, a  $\beta$ -thio-mannose functionalized tetrayne **163b** shows a defined melting point at  $57\text{--}62\text{ }^{\circ}\text{C}$ . Compound **163b** is also the first example of cross-conjugated tetrayne bridged (ca. 1.7 nm from sulfur to sulfur atoms) " $\beta$ -sugar rod".<sup>32-34</sup> Most *para*-functionalized phenyl derivatives (**163d, i-j**) are also quite thermally stable, all with decomposition points above  $110\text{ }^{\circ}\text{C}$ . The exception to this trend is **163h**, which is unstable at room temperature. In addition, these compounds can be stored at low temperature ( $-4\text{ }^{\circ}\text{C}$ ) under argon for weeks without substantial decomposition as judged by TLC and NMR spectroscopic analysis.

Among all of the tetraynes, ferrocenyl substituted tetrayne **163k** shows the best stability and crystalline properties. It can be readily crystallized from MeOH/ $\text{CH}_2\text{Cl}_2$  to give orange needle-shaped crystals, which remain thermally stable even at  $120\text{ }^{\circ}\text{C}$  and are stable for months at low temperatures without observable decomposition.

The spectroscopic data for cross-conjugated tetraynes **163** are consistent with their proposed structures. In the  $^{13}\text{C}$  NMR spectra, the resonances of the pendant methyl groups are observed in the range of 22–23 ppm. The vinylidene carbons external to the cross-conjugated backbones ( $\text{Me}_2\text{C}=\text{C}$ ) are quite deshielded, resonating in the range of

159–165 ppm. While the electron-withdrawing groups deshield this vinylidene carbon, electron-donating groups result in a significant upfield shift (ca. 5 ppm). For instance, the vinylidene carbons for electron-withdrawing functionalized **163d**, **e**, **h** are found at  $\delta$  163.9, 165.0, and 163.6, respectively, whereas for electron-rich **163j** and **163k**, these resonances occur at  $\delta$  159.5 and 159.9. The in-chain vinylidene carbons ( $\text{Me}_2\text{C}=\text{C}$ ) are observed in the range of 99–100 ppm, and neither electron-withdrawing nor electron-donating substituents exert a significant influence on these resonances. For the octatetrayne moiety ( $-\text{C}_1\equiv\text{C}_2-\text{C}_3\equiv\text{C}_4-\text{C}\equiv\text{C}-\text{C}\equiv\text{C}-$ ), the central triple bond carbons  $\text{C}_3\equiv\text{C}_4$  are dramatically shielded, resonating at 63–64 and 67–68 ppm, respectively, whereas the adjacent carbons  $\text{C}_1\equiv\text{C}_2$  resonate in the range of  $\delta$  74–76. The resonances of the final acetylenic unit  $\text{C}\equiv\text{C}$ , cross-conjugated with tetrayne segment, are observed between  $\delta$  75–99 dependent upon substitution.

### 5.2.3 *Electronic Properties*

The electronic absorption behavior of stable cross-conjugated tetraynes, **163a**, **c–f**, **h–k**, were analyzed by UV-vis spectroscopy. In these spectra, the most noteworthy feature is the consistent vibrational modes of the tetrayne absorptions in the low energy region. The ene-tetrayne-ene segment (shown in bold in Scheme 5.2) represents the longest  $\pi$ -conjugated segment in these cross-conjugated tetrayne species, and the low energy absorptions are, in fact, dominated by this linearly conjugated moiety as mentioned in earlier.

To this point, however, the effects from electron-donating and accepting functionality pendant on the tetrayne moiety was not clear. To shed light on this issue, comparison of electron-withdrawing and electron-releasing substituted cross-conjugated

tetraynes has been probed. For purposes of comparison, the UV-vis spectrum for a linearly conjugated tetrayne species, bis(4-*tert*-butylphenyl)octatetrayne **164**<sup>35</sup> has also been included.



Figure 5.3 shows the electronic absorption spectra of cross-conjugated tetraynes **163a**, **c**, **i**, which are functionalized with weakly electron-donating or accepting substituents, as well as linearly conjugated tetrayne **164**. In the low energy region of these spectra, the tetrayne species show three identical absorption peaks at 349, 375, and 407 nm, which are consistent with the absorption characteristic of tetrayne **164**.

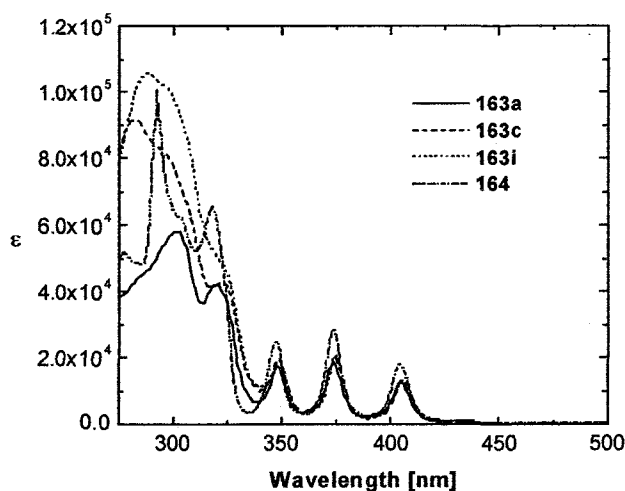


**Fig. 5.3** Electronic absorption spectra ( $\epsilon$  [ $\text{L mol}^{-1} \text{cm}^{-1}$ ]) in  $\text{CHCl}_3$  for **163a**, **163c**, **163i**, and **164**.

The electronic absorption spectra of strongly electron-withdrawing substituted cross-conjugated tetraynes (**136d–f**, **h**, shown in Fig. 5.4) also show three identical low energy absorptions at 349, 374, and 406 nm. The most distinguishable feature is for **163d**, where the molar absorptivity is significantly enhanced. Overall, however, these

results suggest that there is no significant influence on the tetrayne moiety from pendant electron-withdrawing functionality on  $\lambda_{\text{max}}$  values.

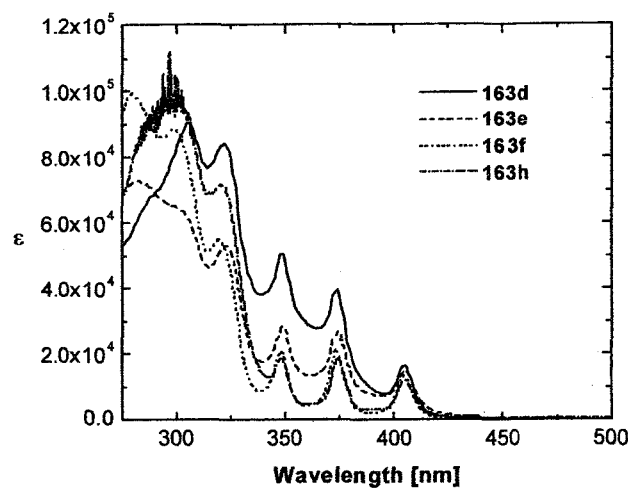


**Fig. 5.4** Electronic absorption spectra ( $\epsilon$  [ $\text{L mol}^{-1} \text{cm}^{-1}$ ]) in  $\text{CHCl}_3$  for **163d**, **163e**, **163f** and **163h**.

Similarly, the UV-vis spectra of the more strongly electron-donating substituted cross-conjugated tetraynes, **163j** and **163k** (Fig. 5.5), also reveal the presence of three low energy absorptions at 349, 375, and 406 nm, respectively, which clearly demonstrates that the electron-donating groups, (ferrocenyl and *N,N*-dimethylamino-phenyl) have little effect on the energy of the electronic characteristics of the central octatetrayn-diyl moiety. The absorption at 349 nm for **163j**, however, merges (as seen a distinguishable shoulder peak) with higher energy absorptions similar to that of **163d**. For **163k** a distinct broad peak at 450 nm is attributed to the absorption characteristics of the ferrocenyl groups.

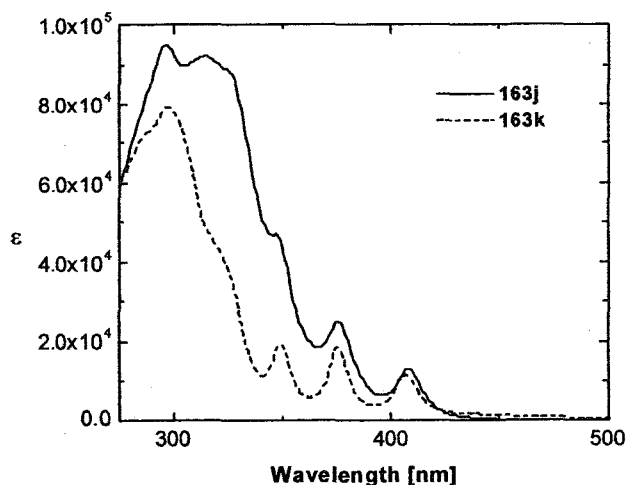


Fig. 5.5 Electronic absorption spectra ( $\epsilon$  [ $\text{L mol}^{-1} \text{cm}^{-1}$ ]) in  $\text{CHCl}_3$  for 163j and 163k.

In summary, based on UV-vis spectral analysis of various functionalized cross-conjugated tetrynes, it is evident that the central tetrayne moiety plays a dominant role on the absorption characteristics in low energy absorption region. In other words, the  $\pi$ -electron delocalization is likely confined to the linearly conjugated tetrayne segment only, and additional extension of conjugation, such as double bonds, has no apparent effect on the degree of  $\pi$ -delocalization. Unlike *iso*-PDA oligomers, there is little or no electron communication between the side groups and tetrayne via cross-conjugation.

#### 5.2.4 Solid-State Properties and Topochemical Polymerization

Crystal packing analysis of tetrayne 157 in polymorph A (see Chapter 4) shows that the individual molecules are aligned in a parallel fashion that is predicted to favor the 1,6-addition polymerization (Fig. 5.6). The packing parameters have been determined as:  $\Phi = 28^\circ$ ,  $R_{1,6} = 3.6 \text{ \AA}$ ,  $R_{1,8} = 4.2 \text{ \AA}$ , and  $d = 7.5 \text{ \AA}$ , which perfectly correspond to those values predicted by Enkleman<sup>2</sup> ( $\Phi = 27^\circ$ ,  $R_{1,6} = 3.6 \text{ \AA}$ , and  $d = 7.7 \text{ \AA}$ ). The possibility of

1,4- or 1,8-addition, however, can not be precluded since the distances  $R_{1,4}$  and  $R_{1,8}$  are also within predicted ranges, which are 3.4 to 5.0 Å.<sup>2,3</sup>

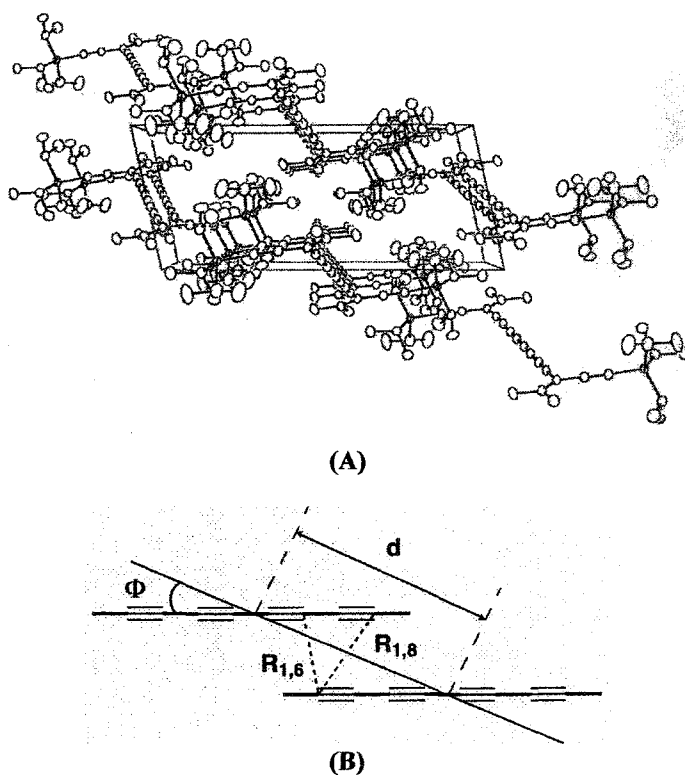


**Fig. 5.6** Crystal packing diagram of **157** (structure A). (a) views along  $a$ -axis. (b) geometry parameters:  $\Phi = 28^\circ$ ,  $R_{1,6} = 3.6 \text{ \AA}$ ,  $R_{1,8} = 4.2 \text{ \AA}$ ,  $d = 7.5 \text{ \AA}$ .

Preliminary efforts to effect the topochemical polymerization of single crystals of TIPS-endcapped tetrayne **157** upon heating, however, have not been successful.<sup>1</sup> One reason for this is due to a low melting point (103–104 °C). As a consequence, the geometrically directed topochemical polymerization can not occur. Employing other methods to effect the polymerization, such as exposure to UV light (280 nm) for 24h, or  $\gamma$ -irradiation ( $54 \pm 3 \text{ krad/h}$ ) for two weeks, yielded dark-colored single crystals. X-ray analysis of these crystals, however, reveals exactly the same diffraction pattern as **157**. Unfortunately, there is to date no efficient way to trigger a solid-state polymerization in

single crystals of **157**, although their crystal packing parameters match the essential requirements predicted for 1,6-addition polymerization. As a consequence, we have realized a structurally diverse series of functionalized cross-conjugated tetraynes in a search for suitable candidates (with reasonable thermal stabilities and crystalline properties) for topochemical polymerization.

Among the functionalized cross-conjugated tetraynes **163a–k**, only 4-nitrophenyl substituted **163d**, *N,N*-dimethylaminophenyl substituted **163j**, and ferrocenyl substituted **163k** showed sufficient kinetic and thermal stability for a detailed solid-state study. Whereas attempts to acquire single crystals of **163d** and **163j** have not been successful, single crystals of **163k** were easily grown from a methanol diffused ethereal solution at  $-4\text{ }^{\circ}\text{C}$ , affording orange/brown translucent needle-shaped crystals. The structural properties of **163k** in the solid-state have been subsequently determined by X-ray crystallographic analysis as outlined in Fig. 5.7. The 16-carbon  $C_{2v}$  symmetrical cross-conjugated enyne skeleton is virtually planar with a maximum deviation of  $0.056(3)\text{ \AA}$  from a least-squares plane. All triple bonds are essentially the same length and are comparable to other reported tetraynes.<sup>36,37</sup> The tetrayne carbons show only a gradual curvature with bond angles deviating from  $180^{\circ}$  by less than  $4^{\circ}$  in all cases. The cyclopentadienyl plane is, nevertheless, twisted out of the enyne plane by an angle of  $30.6(4)^{\circ}$ .

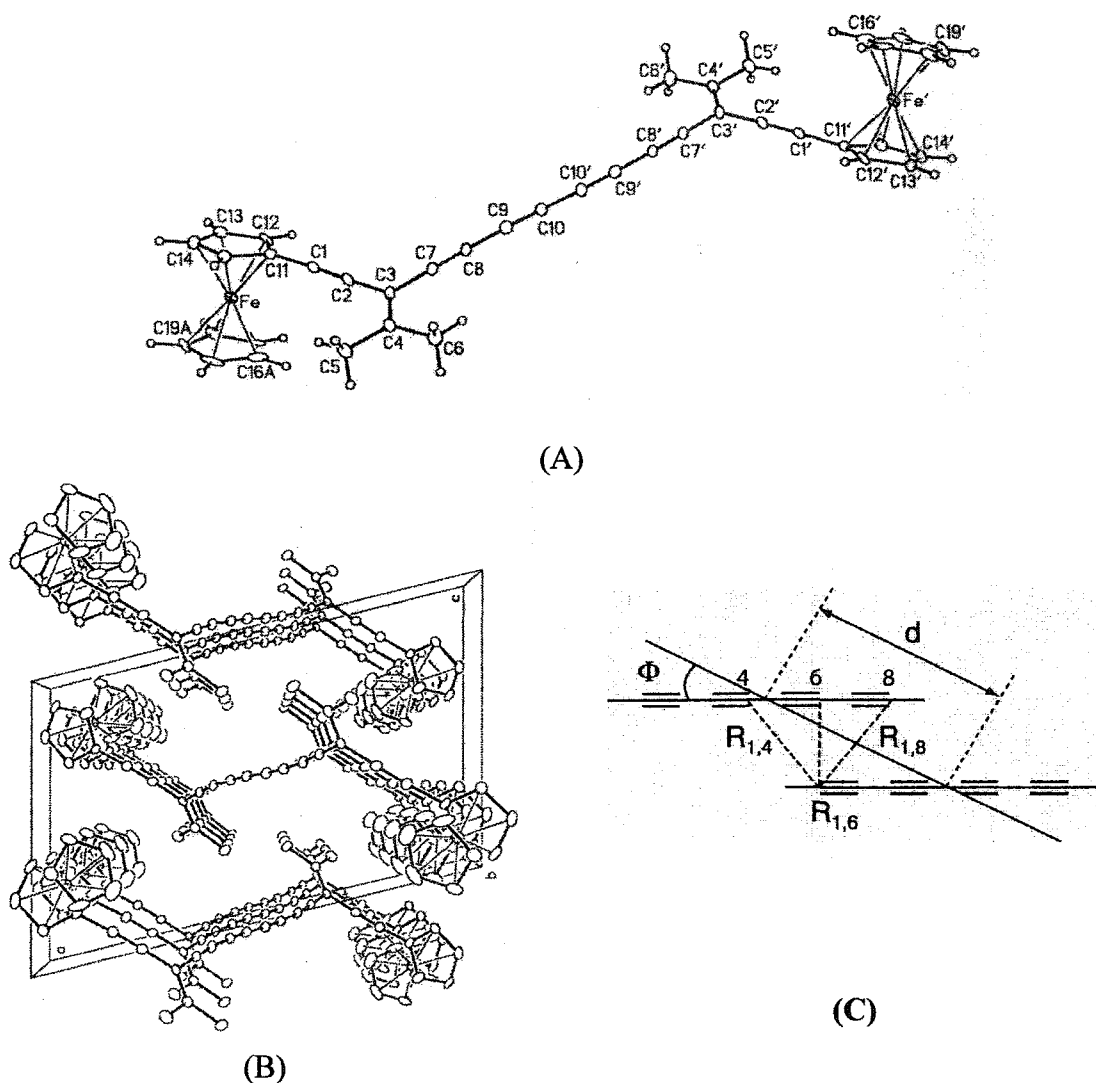


**Fig. 5.7** (a) ORTEP drawing (20% probability level) of **163k**. Selected bond lengths (Å) and angles(°): C(1)–C(2) 1.199(5), C(2)–C(3) 1.431(6), C(3)–C(4) 1.371(5), C(3)–C(7), 1.455(6), C(7)–C(8) 1.185(5), C(8)–C(9) 1.383(6), C(9)–C(10) 1.211(5), C(10)–C(10') 1.355(8); C(2)–C(1)–C(11) 176.3(5), C(1)–C(2)–C(3) 178.3(5), C(2)–C(3)–C(7) 116.2(4), C(3)–C(7)–C(8) 178.9(5), C(7)–C(8)–C(9) 176.6(5), C(8)–C(9)–C(10) 177.1(5), C(9)–C(10)–C(10') 177.5(6). (b) Crystal packing diagram as viewed along *b*-axis. (c) Geometry parameters:  $\Phi = 31^\circ$ ,  $R_{1,4} = 4.5 \text{ \AA}$ ,  $R_{1,6} = 3.7 \text{ \AA}$ ,  $R_{1,8} = 4.5 \text{ \AA}$ ,  $d = 7.4 \text{ \AA}$ .

The most notable feature of the solid-state structure of **163k** is the parallel stacking of tetrayne moieties, suggesting the possibility of a topochemical

polymerization. In the solid-state packing of **163k**, molecules tilt at an angle of  $\Phi = 31^\circ$ , and the distance parameters are observed as  $R_{1,6} = 3.7 \text{ \AA}$  and  $d = 7.4 \text{ \AA}$ . These features correspond well with the optimal parameters ( $\Phi = 27^\circ$ ,  $R_{1,6} = 3.6 \text{ \AA}$ , and  $d = 7.7 \text{ \AA}$ ) for topochemical polymerization in a 1,6-addition manner. However, the possibility of other polymerization pathways, such as 1,4- and 1,8-addition, can not be precluded since the distances between these carbons (e.g.,  $R_{1,4} = 4.5 \text{ \AA}$ , and  $R_{1,8} = 4.5 \text{ \AA}$ ) are also within the predicted range of reactivity (ca. 3.4–5.0  $\text{\AA}$ ).

Various conditions as described in the literature have been utilized to induce the solid-state polymerization of cross-conjugated tetraynes **163d**, **j**, **k**, including heat, monochromic UV light (280 nm for 12 h), and  $^{60}\text{Co}$   $\gamma$ -ray irradiation ( $54 \pm 3 \text{ krad/h}$  for two weeks). Preliminary efforts have focused on the single crystals of **163k**. After exposure to UV light or  $\gamma$ -rays, however, X-ray structural analysis of the resulting crystals show diffraction patterns identical to the original tetrayne, suggesting no polymerization has taken place. Nevertheless, when heated up to  $150 \text{ }^\circ\text{C}$ , the crystal transformed into a black solid that is characterized as amorphous rather than crystalline by X-ray analysis, suggesting that the topochemical polymerization of **163k** could be effected through heating.

To investigate the polymerization behavior of tetraynes under thermal conditions, differential scanning calorimetry (DSC) analysis was consequently carried out.<sup>38</sup> Samples of **163d**, **j**, **k** were sealed in aluminum pellets and then subjected to temperatures scanning from  $50$  to  $400 \text{ }^\circ\text{C}$  at a rate of  $5 \text{ }^\circ\text{C/min}$  under a nitrogen flow. The results of the DSC studies are shown in Fig. 5.8–5.11, respectively. Upon heating, tetrayne **163d** show an apparent exotherm peak at  $192.8 \text{ }^\circ\text{C}$ , giving an enthalpy of  $\Delta H = -349.4 \text{ kJ/mol}$

(Fig. 5.8). Similarly, tetrayne **163k** show an exotherm at 187.5 °C with a  $\Delta H = -348.0$  kJ/mol (Fig. 5.9). Interestingly, in addition to the major exotherm, a distinguishable shoulder peak is observed at ca. 165 °C (Fig. 5.10). Likewise, compound **163j** shows a much sharper exotherm peak at 164.2 °C with a  $\Delta H = -194.8$  kJ/mol. These exotherm characteristics all suggest that significant transitions are occurring at these temperatures, possibly due to topochemical polymerization.

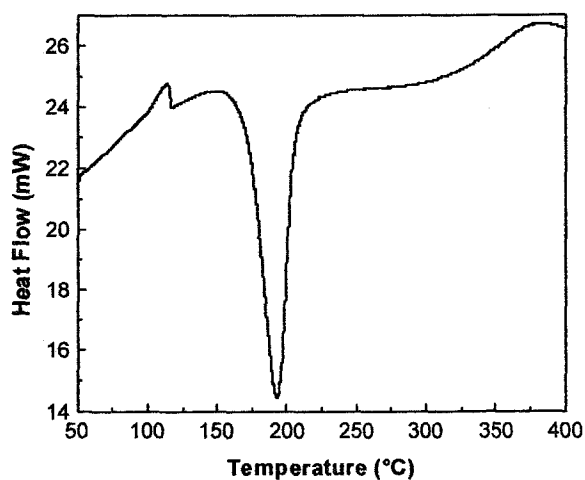


**Fig. 5.8** DSC spectrum for **163d** scanned from 50 to 400 °C at a rate of 5 °C/min (the heat flow fluctuation at 120 °C is due to the instrumental error).

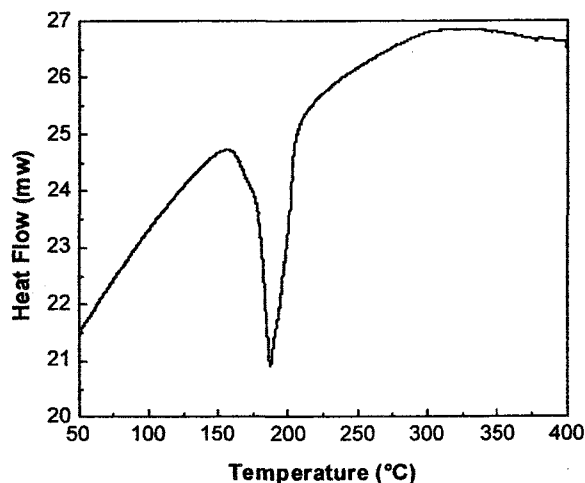


Fig. 5.9 DSC spectrum for **163k** scanned from 50 to 400 °C at a rate of 5 °C/min.

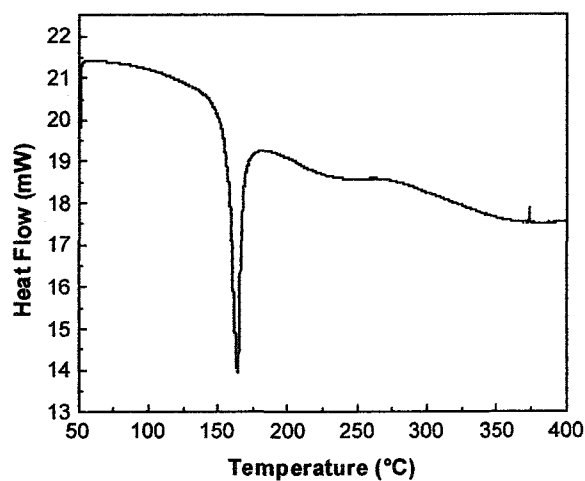


Fig. 5.10 DSC spectrum for **163j** scanned from 50 to 400 °C at a rate of 5 °C/min.

The DSC profile of **163d** is observed as relatively broad and featureless Gaussian-type peak at 192.8 °C, which suggests that the polymerization probably occurs in a random, non-regioselective manner. In the case of **163j**, the sharp peak observed at lower temperature (164.2 °C), suggests that this process is more likely to be regioselective, for example, via 1,6-addition. For ferrocenyl substituted **163k**, the sharp

peak at ca. 165 °C suggests a polymerization in regioselective fashion (i.e., 1,6-addition), whereas the more broad shoulder peak at 187.5 °C is an evidence for random, non-regioselective polymerizations at the higher temperature. In addition, above the polymerization temperatures (> 200 °C), the three tetraynes do not show any further significant transition, even at temperature as high as 400 °C, which suggests that the polymerized products possess thermal stability.

Thermogravimetric analysis (TGA) measurements were also carried out for crystals of tetrayne **163k** from 50 to 600 °C under air, the results of which is shown in Fig. 5.11. At temperatures ranging from 150 to 200 °C there is only 1.5% weight loss, which is in agreement with the proposed topochemical polymerization. The possibility of other processes such as oxidation or decomposition is therefore precluded as a substantial weight loss would be expected. Significant weight loss (25.5%) is observed in the temperature range of 300–600 °C, which is probably due to oxidative decomposition (e.g., pyrolysis or combustion).

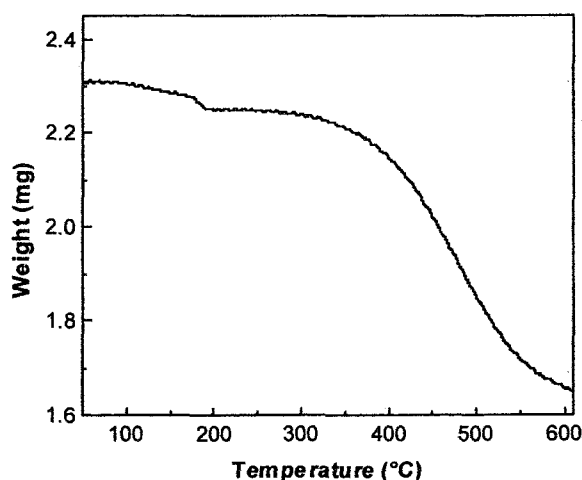


Fig. 5.11 TGA spectrum for **163k** scanned from 50 to 600 °C at a rate of 5 °C/min.

To better understand the kinetics of the solid-state polymerization for cross-conjugated tetrayne species, isothermal scanning studies of **163k** were carried out at various temperatures, ranging from 125 to 160 °C (as shown in Fig. 5.12). A consistent feature of these isotherm profiles (at 145–160 °C) is the apparent exotherm peak in the range of 0 to 150 min, followed by a relative stable phases until 600 min. After 600 min, slow decomposition is observed as endo-thermal processes. It is believed that the first exotherm process corresponds to the solid-state polymerization process, where the peak values of the exotherm ( $\tau$ ) can be deemed as an estimate for the reaction rate. For the isothermal profiles at 135 and 140 °C, the first exotherm peaks are much broader, while still distinguishable, indicating much lower reaction rates. Moreover, the featureless profiles at 125 and 130 °C suggest that no polymerization or extremely slow reaction is occurring at these temperatures.

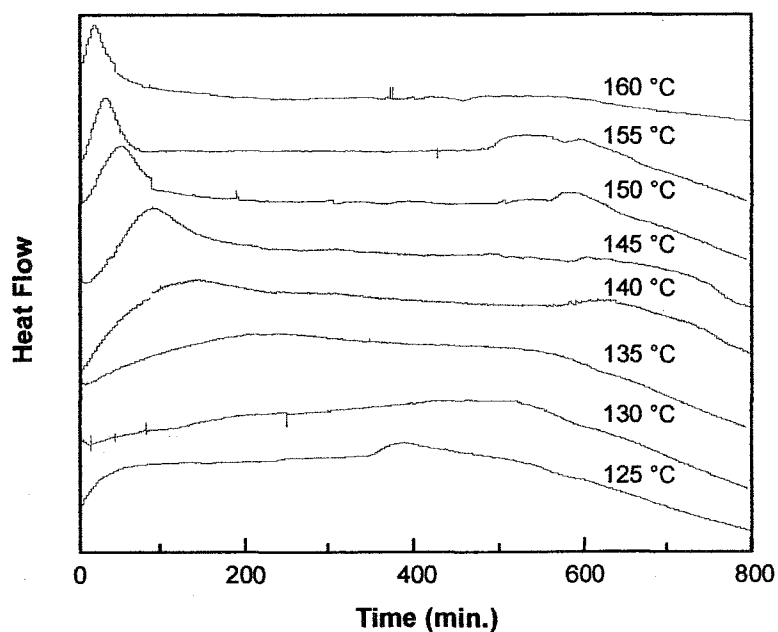


Fig. 5.12 DSC isothermal scanning spectra for **163k** at various temperatures.

Consequently, according to kinetic laws, correlation of reaction time  $\ln(\tau)$  with the reciprocal of temperature ( $1/T$ ) ranging from 140–165 °C gives a linear relationship, yielding an activation energy,  $E_a = 136.7$  kJ/mol (Fig. 5.13). Comparison to values reported in the literature for a 1,4-addition polymerization (ca. 93 KJ/mol)<sup>2</sup> suggests a much higher energy barrier for cross-conjugated tetrynes, likely due to steric effect and an increase demand for translational motion. Additionally, this particularly high energy barrier also explains why there is no polymerization observed under conditions of UV light and  $\gamma$ -ray irradiation.

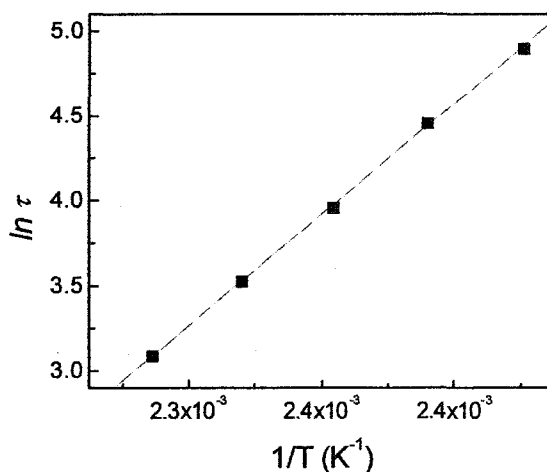


Fig. 5.13 Correlation of  $\ln(\tau)$  versus  $1/T$  obtained from isothermal analysis of 163k.

In addition to thermochemical studies, alternative evidence for topochemical polymerization is provided by UV-vis spectral analysis. As shown in Fig. 5.14, the electronic absorption spectrum for a solid film of 163k on a quartz plate was measured. Three characteristic tetrayne absorptions are observed at 354, 381, and 414 nm, respectively, which are shifted bathochromically by ca. 4 nm relative to the  $\text{CHCl}_3$  solution spectrum. After subjecting the sample to heat at 150 °C for 5 min, the UV-vis spectrum clearly shows loss of the tetrayne absorptions, likely due to topochemical

polymerization. The broad featureless peak at 400–520 nm, however, makes it difficult to identify whether the absorptions are from the resulting polyenyne or ferrocenyl groups.

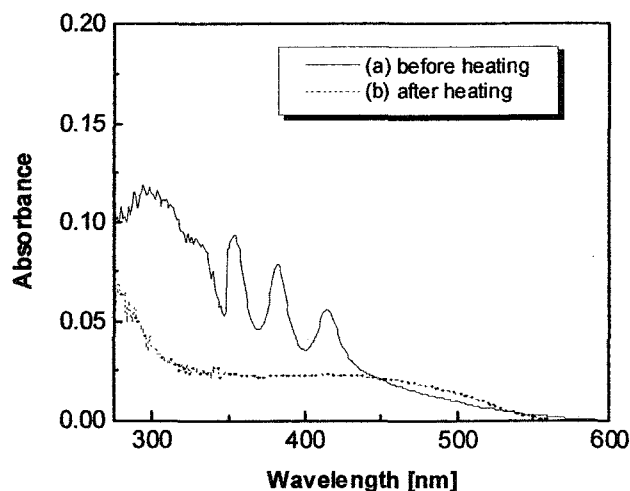
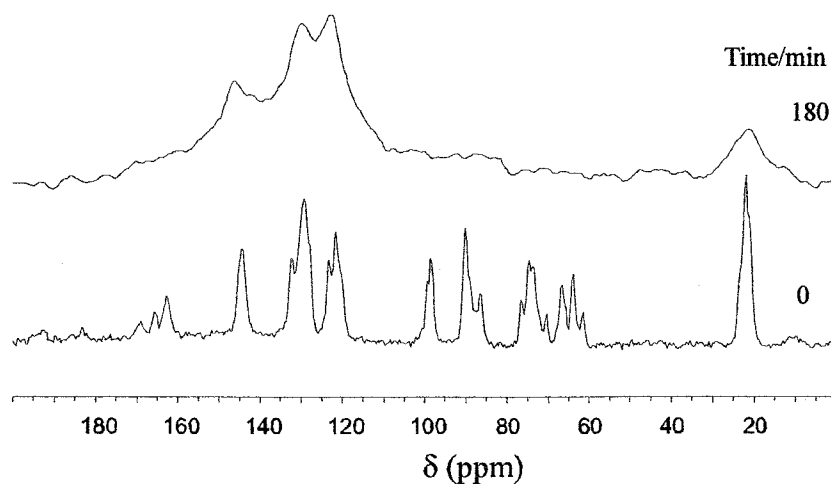


Fig. 5.14 Solid-state UV-vis spectra for 163k comparing the effect of heating.

To study the solid-state structural properties during the process of topochemical polymerization, other spectral analyses, namely solid-state CP-MAS  $^{13}\text{C}$  NMR spectroscopy, were conducted for tetraynes **136d**, **j**, **k**, using a 50 MHz spectrometer. In these experiments, solid-state  $^{13}\text{C}$  NMR spectra of the tetraynes were first recorded at room temperature, and then the samples were subjected to heating at temperatures from 100–160 °C to effect polymerization. The solid-state  $^{13}\text{C}$  NMR spectra for the polymerized products were then measured for purposes of comparison. In the solid-state  $^{13}\text{C}$  NMR spectra of **163d** (Fig. 5.15), the resonances of tetrayne show moderate resolution, whereas the skeleton  $\text{sp}$  carbons and the in-chain vinylidene carbons ( $\text{Me}_2\text{C}=\text{C}$ ) are observed at 64–67 and 87–99 ppm, respectively; consistent with its solution-state  $^{13}\text{C}$  NMR data. The external vinylidene carbon ( $\text{Me}_2\text{C}=\text{C}$ ) is observed at  $\delta$

163.5. Other than the expected resonances, several unidentified peaks are, however, observable possibly due to decomposition or spinning side bands. After heating at 120 °C for 2 h, the sample showed an identical spectrum to the original tetrayne **163d**, indicating that no discernible polymerization occurs at this temperature. Increasing the temperature to 160 °C and heating for another 1 h yielded a black solid, the spectrum of which shows broadened resonances at  $\delta$  100–160 corresponding to olefinic and phenyl carbons. In addition, the resonances of the methyl groups at 22.6 ppm are broadened into a range of 15–30 ppm. Interestingly, the characteristic peaks for interior tetrayne carbons at 64–67 ppm disappear completely after heating, which are in agreement with the proposed polymerized products. Moreover, the broad featureless resonances suggest a random and non-regioselective polymerization rather than the predicted regioselective 1,6-addition.



**Fig. 5.15** Solid-state <sup>13</sup>C NMR spectra for **163d** recorded before and after heating at 160 °C for 3 h.

The solid-state <sup>13</sup>C NMR spectrum of tetrayne **163j** (Fig. 5.16) was acquired at room temperature with reasonable resolution as compared to its solution-state <sup>13</sup>C NMR

spectrum. All of the 7 unique sp and sp<sup>2</sup> carbons on the cross-conjugated enyne skeleton are clearly observed at 64.5, 68.4, 76.9, 82.4, 97.5, 101.7, and 106.2 ppm, respectively. The external vinylidene carbon and two methyl carbons on the vinylidene are also distinctively observed at 160.4, 23.4, and 24.5 ppm, respectively, and the *N,N*-dimethyl carbons resonate at  $\delta$  39.9. After heating at 100 °C for 1 h, the sample turned into a dark brown solid showing an apparent altered NMR resonance pattern with fair resolution. The most significant changes are the two non-equivalent vinylidene peaks at  $\delta$  158.5 and 164.6, and a different resonance pattern at 88–100 ppm. This is possibly due to the 1,6-addition polymerization process that destroys the *C*<sub>2</sub> symmetry of the starting tetrayne. In addition, the interior tetrayne carbon resonances at 64–67 ppm are still present. However, these peaks are of relative low intensity compared to the original spectrum. This spectrum suggests the tetrayne polymerized in a regioselective manner, i.e., 1,6-addition. Heating at 100 °C for another 3 h yielded black solids, the spectrum of which shows broad featureless resonance peaks at 150, 130, 110, 40, and 20 ppm. The tetrayne peaks at 65–88 ppm are no longer observable, suggesting the completion of polymerization. Moreover, it is evident that the polymerization has occurred non-regioselectively in the later stages of the heating process.

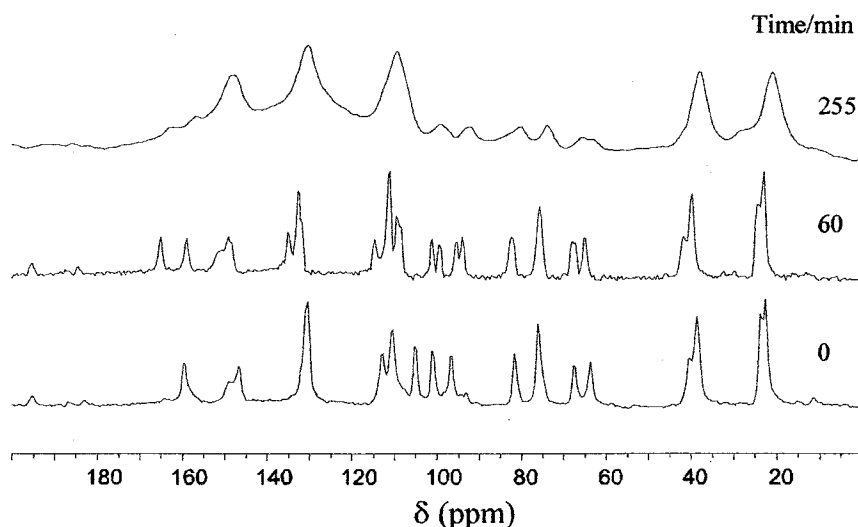


**Fig. 5.16** Solid-state <sup>13</sup>C NMR spectra for **163j** recorded before and after heating at 100 °C for shown times.

In the same manner, solid-state <sup>13</sup>C NMR spectra for **163k** were acquired every 30 minutes at 150 °C from 0 to 300 minutes, and a comparison of the spectra is shown in Fig. 5.17. The spectrum of the original tetrayne shows amazing resolution compared to its solution-state spectrum, and as such, all of the unique skeleton sp and sp<sup>2</sup> carbons are clearly observable. In the spectra of heated sample, gradual peak-broadening can be observed with increasing time, suggesting the occurrence of topochemical polymerization. After heating for 300 min, a broad ferrocenyl carbon peak is observed at 60–80 ppm, which makes it difficult to characterize the tetrayne carbon resonances. Likewise, a broad hump from 120 to 160 ppm, possibly resulting from olefinic carbons, coincidentally overlaps with the external vinylidene carbons; therefore hampering a meaningful analysis. Moreover, unlike **163j**, there is no clear evidence that **163k** polymerizes through a regioselective way, i.e., 1,6-addition, as suggested by its crystallographic analysis.

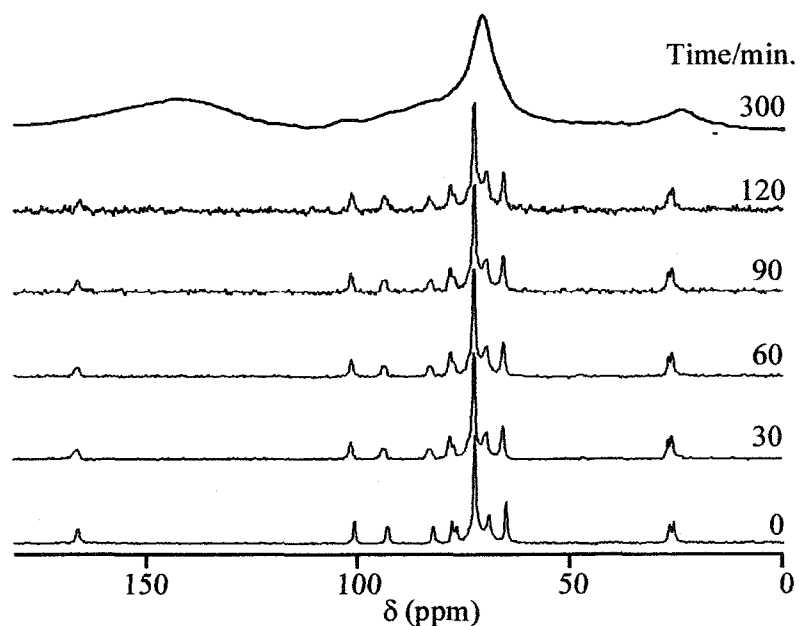


**Fig. 5.17** Solid-state  $^{13}\text{C}$  NMR spectra for **163k** recorded before and after heating at 150  $^{\circ}\text{C}$  for shown times.

### 5.3 Conclusions

In this chapter, we have described the synthesis of a series of functionalized, cross-conjugated tetraines. UV-vis spectroscopic analysis shows that the electronic characteristics of the tetrayne moiety dominate the lower energy absorption region, and the side groups, either electron-donating or electron-withdrawing, have only a marginal influence on the absorption of the central tetrayne. The solid-state structural properties of tetrayne **157** and **163k** were elucidated through X-ray crystallographic analysis. The packing parameters for these two tetraines fall into the predicted range suitable for topochemical polymerization, in particular, the distances between each molecules in solid-state packing well correspond to the optimal parameters for topochemical polymerization in a 1,6-addition manner. Our inability to effect clean polymerization of these crystallized samples shows that these parameters are clearly not the only factors

that influence this process. Other factors such as steric or thermodynamics effect must also play significant roles. Studies toward solid-state polymerization for three stable tetraynes **163d**, **j**, **k** have been accomplished by their thermal analysis (DSC and TGA), solid-state UV-vis, and solid-state CP-MAS <sup>13</sup>C NMR spectroscopies. These results support the premise that topochemical polymerizations takes place upon heating, and for tetrayne **163j**, evidence of 1,6-addition polymerization have been obtained from DSC and solid-state <sup>13</sup>C NMR spectroscopic analyses. But we are still unable to control or limit this process.

#### 5.4 References and Notes

- (1) Zhao, Y.; McDonald, R.; Tykwinski, R. R. *Chem. Commun.* **2000**, 77-78.
- (2) Enkelmann, V. In *Adv. Polym. Sci.*; Springer-Verlag: Berlin Heidelberg, 1984; Vol. 63, pp 91-136.
- (3) Baughman, R. H.; Yee, K. C. *J. Polym. Sci.: Macromol. Rev.* **1978**, *13*, 219-239.
- (4) Baughman, R. H. *J. Polym. Sci.* **1974**, *12*, 1511-1535.
- (5) Matsuzawa, H.; Okada, S.; Sarkar, A.; Nakanishi, H.; Matsuda, H. *J. Polym. Sci.: Part A: Polym. Chem.* **1999**, *37*, 3537-3548.
- (6) Okada, S.; Doi, T.; Mito, A.; Hayamizu, K.; Ticktin, A.; Matsuda, H.; Kikuchi, N.; Masaki, A.; Minami, N.; Haas, K.-H.; Nakanishi, H. *Nonlinear Optics* **1994**, *8*, 121-132.
- (7) Okada, S.; Doi, T.; Kikuchi, N.; Hayamizu, K.; Matsuda, H.; Nakanishi, H. *Mol. Cryst. Liq. Cryst.* **1994**, *247*, 99-109.
- (8) Okada, S.; Nakanishi, H. *Int. J. Nonlinear Opt. Phys.* **1994**, *3*, 501-509.

- (9) Okada, S.; Matsuda, H.; Masaki, A.; Nakanishi, H.; Hayamizu, K. *SPIE* **1991**, *1560*, 25-34.
- (10) Okada, S.; Matsuda, H.; Nakanishi, H.; Kato, M. *Mol. Cryst. Liq. Cryst.* **1990**, *189*, 57-63.
- (11) Paley, M. S.; Frazier, D. O.; Abeledyem, H.; McManus, S. P.; Zutaut, S. E. *J. Am. Chem. Soc.* **1992**, *114*, 3247-3251.
- (12) Kawanami, H.; Okada, S.; Matsuda, H.; Doi, T.; Kikuchi, N.; Hayamizu, K.; Oiawa, H.; Nakanishi, H. *Mol. Cryst. Liq. Cryst.* **1994**, *255*, 103-122.
- (13) Jia, W.; Misawa, K.; Matsuda, H.; Okada, S.; Nakanishi, H.; Kobayashi, T. *Chem. Phys. Lett.* **1996**, *255*, 385-392.
- (14) Wegner, G. *Z. Naturforsch* **1969**, *B24*, 824-832.
- (15) Okada, S.; Hayamizu, K.; Matsuda, H.; Masaki, A.; Nakanishi, H. *Bull. Chem. Soc. Jpn.* **1991**, *64*, 857-863.
- (16) Brit, D. W.; Hofmann, U. G.; Möbius, M.; Hell, S. W. *Langmuir* **2001**, *17*, 3757-3765.
- (17) Xiao, J.; Yang, M.; Lauher, J. W.; Fowler, F. W. *Angew. Chem. Int. Ed.* **2000**, *39*, 2132-2135.
- (18) Matsuzawa, H.; Okada, S.; Sarkar, A.; Matsuda, H.; Nakanishi, H. *Polym. Int.* **2001**, *33*, 182-189.
- (19) Mochizuki, E.; Hibamoto, Y.; Yano, K.; Kanehisa, N.; Kai, Y.; Tagawa, S.; Yamamoto, Y. *J. Chem. Soc., Perkin Trans. 2* **2000**, 155-159.
- (20) Okada, S.; Matsuda, H.; Otsuda, M.; Kikuchi, N.; Hayamizu, K.; Nakanishi, H.; Kato, M. *Bull. Chem. Soc. Jpn.* **1994**, *67*, 455-461.

- (21) Shimada, S.; Masaki, A.; Hayamizu, K.; Matsuda, H.; Okada, S.; Nakanishi, N. *Chem. Commun.* **1997**, 1421-1422.
- (22) Sarkar, A.; Okada, S.; Matsuzawa, H.; Matsuda, H.; Nakanishi, H. *J. Mater. Chem.* **2000**, *10*, 819-828.
- (23) Irngartinger, H.; Skipinski, M. *Tetrahedron* **2000**, *56*, 6781-6794.
- (24) Jonas, U.; Shah, K.; Norvez, S.; Charych, D. H. *J. Am. Chem. Soc.* **1999**, *121*, 4580-4588.
- (25) Shim, S. C.; Lee, T. S. *J. Org. Chem.* **1988**, *53*, 2410-2413.
- (26) Sarkar, A.; Shuji, O.; Kyoji, K.; Hachiro, N.; Hiro, M. *Macromolecules* **1998**, *31*, 5624-5630.
- (27) Rubin, Y.; Lin, S. S.; Knobler, C. B.; Armen, J. A.; Boldi, M.; Diederich, F. *J. Am. Chem. Soc.* **1991**, *113*, 6943-6949.
- (28) Okada, S.; Hayamizu, K.; Matsuda, H.; Masaki, A.; Minami, N.; Nakanishi, H. *Macromolecules* **1994**, *27*, 6259-6266.
- (29) Fowler, F. W.; Lauher, J. W. *J. Phys. Org. Chem.* **2000**, *13*, 850-857.
- (30) Zhao, Y.; McDonald, R.; Tykwinski, R. R. *J. Org. Chem.* **2002**, *67*, 2805-2812.
- (31) Hay, A. S. *J. Org. Chem.* **1962**, *27*, 3320-3321.
- (32) Roy, R.; Das, S. K.; Hernández-Mateo, F.; Santoyo-González, F.; Gan, Z. *Synthesis* **2001**, 1049-1052.
- (33) Charych, D. H.; Nagy, J. O.; Spevak, W.; Bedenarski, M. D. *Science* **1993**, *261*, 585-588.
- (34) Roy, R.; Das, S. K.; Santoyo-González, F.; Hernández-Mateo, F.; Dam, T. K.; Brewer, C. F. *Chem. Eur. J.* **2000**, *6*, 1757-1762.

- (35) Compound **164** was generously provided by Dr. Michael M. Haley at the University of Oregon.
- (36) Mohr, W.; Stahl, J.; Hampel, F.; Gladysz, J. A. *Inorg. Chem.* **2001**, *40*, 3263-3264.
- (37) Eisler, S.; Tykwinski, R. R. *J. Am. Chem. Soc.* **2000**, *122*, 10736-10737.
- (38) Sarkar, A.; Talwar, S. S. *Bull. Chem. Soc. Jpn.* **1999**, *72*, 859-864.

## Chapter 6 Other Related Work and Theoretical Studies

### 6.1 Introduction

This chapter discusses projects involving other cross-conjugated enyne oligomers, which have to date not been completed. Other than the major works discussed in previous chapters, alternative interesting topics have also been explored in this thesis, including (1) modifications of vinyl triflate building blocks, (2) synthesis of strained cross-conjugated tetraynes, (3) donor and acceptor functionalized cross-conjugated enynes, and (4) synthesis of cross-conjugated macrocycles.

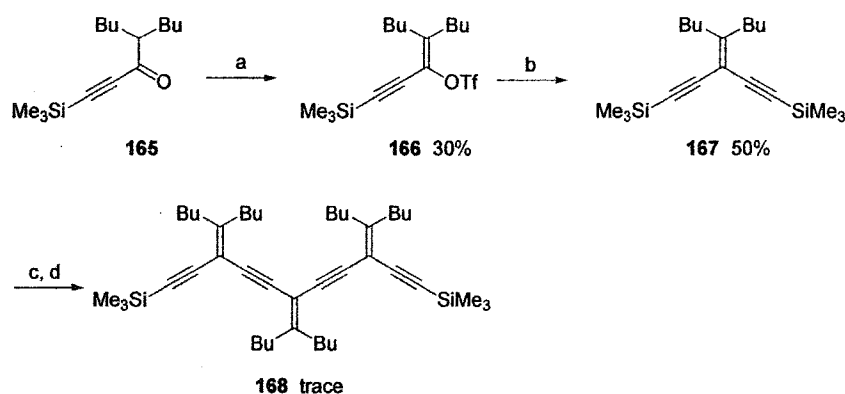
In addition to the many interesting synthetic efforts, theoretical studies of cross-conjugated enynes are also of fundamental importance to the understanding of these novel molecules, in particular, their unique  $\pi$ -delocalization and corresponding structure-property relationships. Recently, the rapid developments in computer technology have allowed us to explore and predict the properties of much more complicated molecules with much faster speeds and more satisfying accuracy. For conjugated organic systems, a number of computational methods, such as semi-empirical (CNDO, AM1, PM3, etc.), *ab initio* Hartree-Fock, and density functional theory (DFT) calculations,<sup>1</sup> have been successfully applied to predict molecular properties and interpret experimental data. Eventually, this will lead to a better understanding of conjugated molecules. In the latter part of this chapter, a thorough theoretical study on a series of cyclic cross-conjugated model compounds, namely expanded radialenes, will be discussed with a main focus on their structural, electronic, and magnetic properties.

## 6.2 Synthesis

### 6.2.1 Synthetic Efforts on Modification of Vinyl Triflate Building Blocks

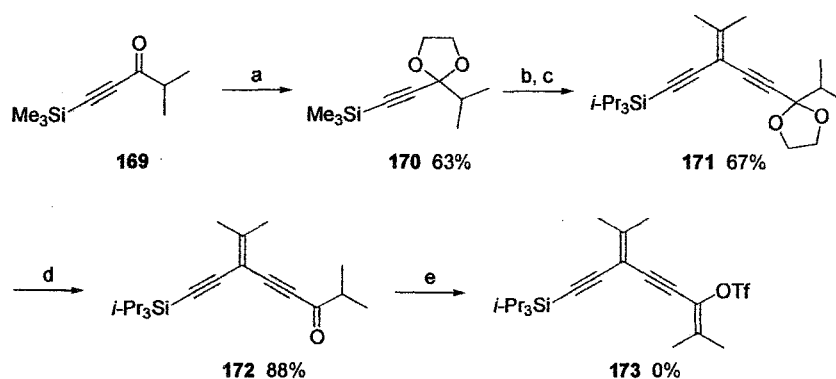
The first synthetic effort to modify the vinyl triflate building blocks targeted on the 5-nonylidene substituted vinyl triflate **166** (Scheme 6.1), in hopes that the auxiliary dibutyl groups could improve the solubility of *iso*-PDA series. Triflate **166** was readily obtained in a manner as described by Stang and co-workers,<sup>2,3</sup> from the respective ketone **165** in 30% yield. Cross-coupling of **166** with trimethylsilylacetylene in the presence of  $\text{PdCl}_2(\text{PPh}_3)_2$  as catalyst,  $\text{CuI}$  as co-catalyst,  $\text{Et}_2\text{NH}$  as base, in DMF under nitrogen atmosphere, afforded a colorless oil, **167**, in a yield of 50%. Monomer **167** shows quite limited kinetic stability, observable as a slow color change at room temperature under exposure to air. It is believed that the decomposition occurs via an oxygen ene reaction at the allylic position.<sup>4,5</sup> Further iteration of the sequence toward trimeric **168** was attempted, but TLC analysis showed only a trace amount of **168**, which decomposed completely before column chromatographic isolation could be accomplished.

Scheme 6.1



Reagents and conditions: (a) triflic anhydride, 2,6-di(*t*-butyl)-4-methylpyridine,  $\text{CH}_2\text{Cl}_2$ , rt. (b) trimethylsilylacetylene,  $\text{PdCl}_2(\text{PPh}_3)_2$ ,  $\text{CuI}$ ,  $\text{Et}_2\text{NH}$ , DMF, rt. (c)  $\text{K}_2\text{CO}_3$ , wet  $\text{MeOH}/\text{THF}$  (1:1), rt. (d) **166**,  $\text{PdCl}_2(\text{PPh}_3)_2$ ,  $\text{CuI}$ ,  $\text{Et}_2\text{NH}$ , DMF, rt.

### Scheme 6.2



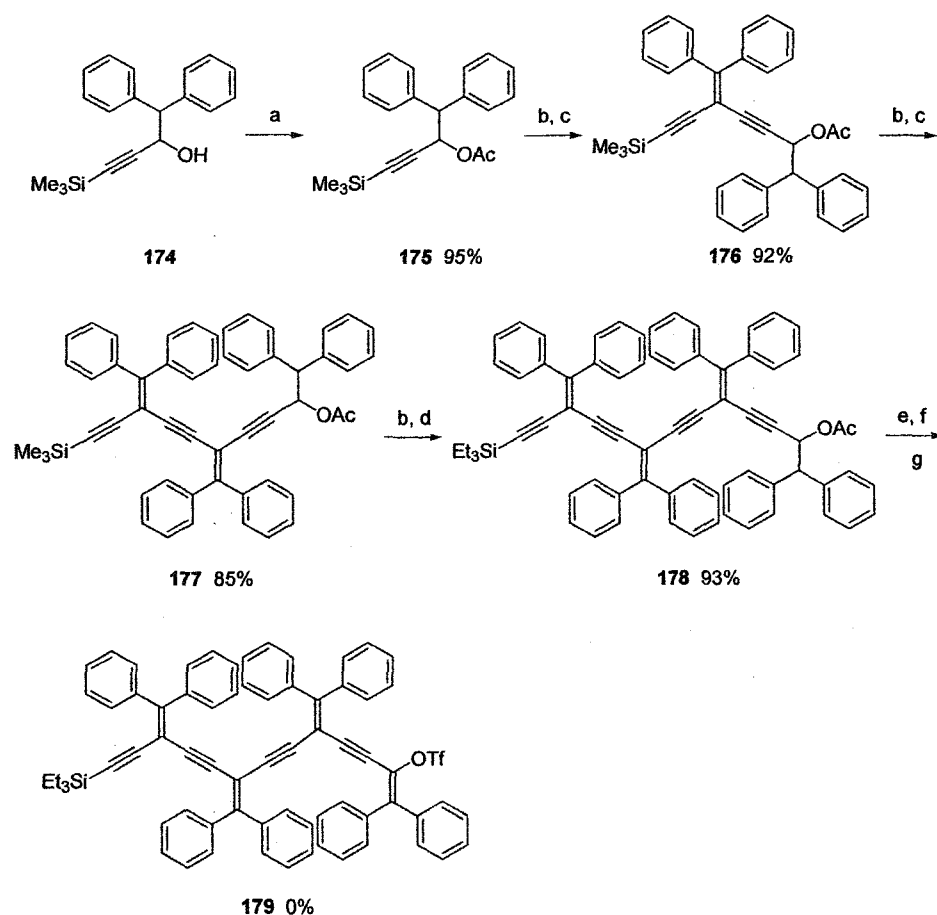
Reagents and conditions: (a) glycerol, TsOH, benzene, reflux. (b)  $\text{K}_2\text{CO}_3$ , wet MeOH/THF (1:1), rt. (c) **96**,  $\text{PdCl}_2(\text{PPh}_3)_2$ , CuI,  $\text{Et}_2\text{NH}$ , DMF, rt. (d) 2,6-lutidinium *p*-toluenesulfonate, THF, reflux. (e) LDA, 2-(*N,N*-bistrifluoromethylsulfonyl)amino-5-chloropyridine,  $-78^\circ\text{C}$ .

As mentioned in previous chapters, extension of the oligomer length, using the sequence of protideprotection and cross-coupling reactions, can only occur by increasing two units in each iteration.<sup>6,7</sup> In order to more rapidly elongate the chain length using fewer synthetic steps, we envisioned the use of “bigger” building blocks, i.e., oligomeric vinyl triflates. The first synthesis toward a dimeric triflate **173** is shown in Scheme 6.2. Since the presence of carbonyl group in ketone **169** complicates Pd-catalyzed cross-coupling reactions, 1,3-dioxane protected **170** was prepared from **169** and glycerol in the presence of TsOH as catalyst in refluxing benzene for 2 h. Column chromatography through  $\text{SiO}_2$  afforded **170** as a colorless oil in 63% yield. Monomer **170** was successfully desilylated with  $\text{K}_2\text{CO}_3$  in MeOH/THF (1:1) to give terminal alkyne, which was then cross-coupled with vinyl triflate **96** to afford protected **171** in a yield of 67%. Dimer **171** can be readily deprotected with 2,6-lutidinium *p*-toluenesulfonate (LPTS) to yield the dimer ketone **172** in 88% yield. Triflation of **172** in

the presence of LDA and 2-(*N,N*-bistrifluoromethylsulfonyl)amino-5-chloropyridine in THF under  $-78\text{ }^{\circ}\text{C}$ ,<sup>8</sup> however, gave only an unidentified black mass resulting from decomposition.

The extreme instability of **173** is believed to arise from the presence of allylic hydrogens (*vide supra*). We, therefore, focused on the diphenylmethylidene substituted derivatives **179** (Scheme 6.3) to prevent this decomposition pathway. A racemic alcohol **174** was reacted with acetic anhydride and a catalytic amount of 4-dimethylamino-pyridine (DMAP) in  $\text{Et}_3\text{N}$ ,<sup>9</sup> giving acetate **175** in 95% yield. Acetate **175** was then desilylated with 1 equiv. of TBAF and subsequently cross-coupled with vinyl triflate **130** in the presence of  $\text{Pd}(\text{PPh}_3)_4$  as catalyst, CuI as co-catalyst, and *i*- $\text{Pr}_2\text{NH}$  as base in THF at  $60\text{ }^{\circ}\text{C}$  for 12 h.  $\text{SiO}_2$  chromatography afforded dimeric **176** in a yield of 92%. A second desilylation/cross-coupling iteration from **176** subsequently gave trimeric **177** as a yellow solid in 85% yield. Trimer **177** was then desilylated with TBAF and cross-coupled with TES-protected vinyl triflate **131** to afford tetrameric acetate **178** in 93% yield. Tetramer **178** was reduced to give the free alcohol with  $\text{LiAlH}_4$  in diethyl ether at  $0\text{ }^{\circ}\text{C}$  in an almost quantitative yield, as analyzed by TLC.<sup>9</sup> The reduced alcohol was then treated with Jones reagent, affording a mixture of unidentified black mass that could not be purified by column chromatography. Altering the oxidation conditions, e.g., PCC,  $\text{MnO}_2$ , and Dess-Martin, resulted in similar black mixtures. Further attempts to generate the ketone *in situ* followed by trapping with a triflation reagent were also unsuccessful.<sup>10</sup> Currently, efforts to elaborate **178** into triflate **179** are still under investigation.

### Scheme 6.3

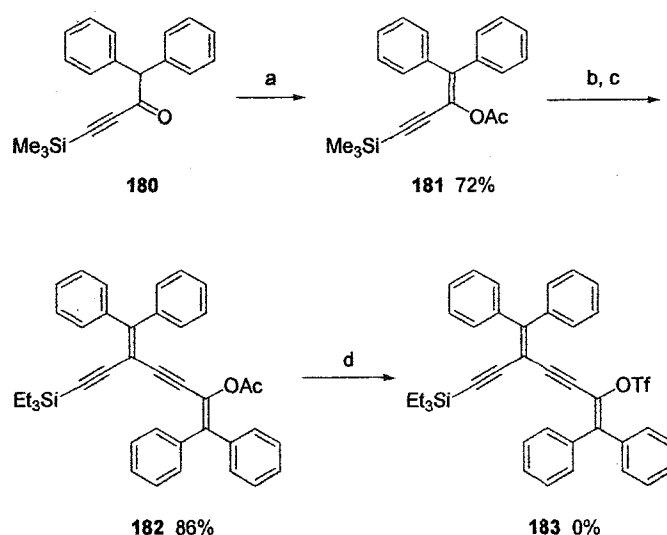


Reagents and conditions: (a)  $\text{Ac}_2\text{O}$ , DMAP,  $\text{Et}_3\text{N}$ , rt. (b) TBAF (1 equiv), THF, rt. (c) **130**,  $\text{Pd}(\text{PPh}_3)_4$ ,  $\text{CuI}$ ,  $i\text{-Pr}_2\text{NH}$ , THF,  $60^\circ\text{C}$ . (d) **131**,  $\text{Pd}(\text{PPh}_3)_4$ ,  $\text{CuI}$ ,  $i\text{-Pr}_2\text{NH}$ , THF,  $60^\circ\text{C}$ . (e)  $\text{LiAlH}_4$ ,  $\text{EtO}_2$ ,  $0^\circ\text{C}$ . (f)  $\text{CrO}_3$ ,  $\text{H}_2\text{SO}_4$ , acetone/ $\text{H}_2\text{O}$ ,  $0^\circ\text{C}$ . (g) LDA, 2-(*N,N*-bistrifluoromethylsulfonyl)amino-5-chloropyridine,  $-78^\circ\text{C}$ .

Since the oxidation step in Scheme 6.3 had become problematic, we consequently envisaged an alternative route to generate dimeric triflate **183** without oxidation (Scheme 6.4). Ketone **180** was transformed into vinyl acetate **181** in the presence of acetic anhydride and potassium bis(trimethylsilyl)amide (KHMDs) in THF at  $-78^\circ\text{C}$  for 0.5 h,<sup>9</sup> providing a colorless solid in a yield of 72%. Compound **181** was desilylated with TBAF

and cross-coupled with triflate **131** yielding dimeric **182** as a yellow solid in 86% yield. Acetate **182** was expected to react to produce triflate **183** in the presence of *t*-BuOK and a triflation reagent, e.g., 2-(*N,N*-bistrifluoromethylsulfonyl)amino-5-chloropyridine. However, preliminary attempts toward **183** were not successful. Optimization of the reaction conditions is continuing.

**Scheme 6.4**



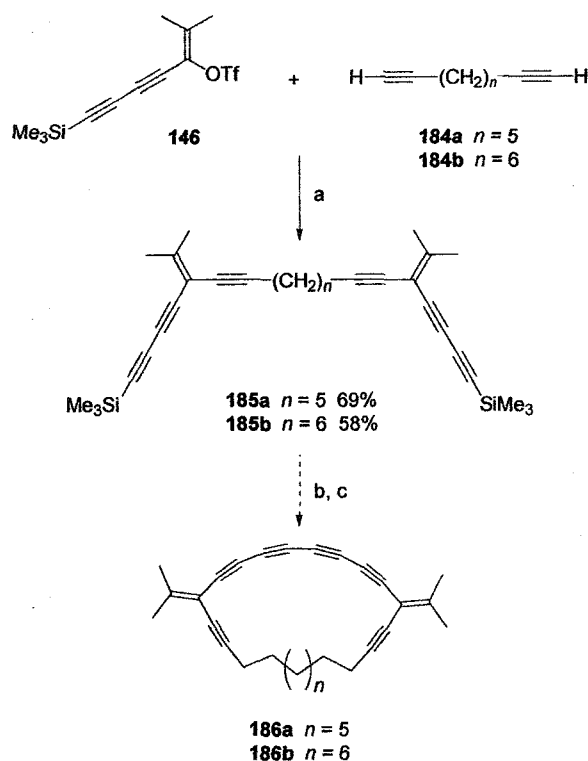
Reagents and conditions: (a) KHMDS, Ac<sub>2</sub>O, THF, -78 °C. (b) TBAF (1 equiv), THF, rt. (c) **131**, Pd(PPh<sub>3</sub>)<sub>4</sub>, CuI, *i*-Pr<sub>2</sub>NH, THF, 60 °C. (d) *t*-BuOK, 2-(*N,N*-bistrifluoromethyl-sulfonyl)amino-5-chloropyridine, -78 °C.

### 6.2.2 Synthesis of Precursors to Strained Cross-conjugated Tetrynes

The synthesis of cyclic strained cross-conjugated tetrynes **186a–b** was attempted and the synthetic approach is as shown in Scheme 6.5.<sup>11</sup> Two precursors, **185a–b**, were synthesized via Pd-catalyzed cross-coupling of vinyl triflate **146** with diynes **184a–b** in yields of 69% and 58%, respectively. Removal of the trimethylsilyl groups with K<sub>2</sub>CO<sub>3</sub> can give the bisterminal alkyne, which can be subsequently homocoupled under Hay

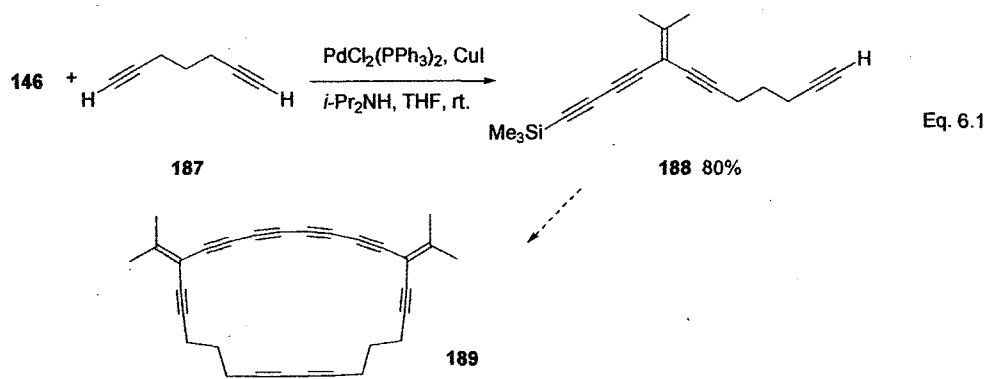
conditions to yield the strained tetraynes **186a–b**. Further elaboration of this sequence to the strained tetrayne species is underway.

**Scheme 6.5**



Reagents and conditions: (a)  $\text{PdCl}_2(\text{PPh}_3)_2$ ,  $\text{CuI}$ ,  $i\text{-Pr}_2\text{NH}$ , THF, rt. (b)  $\text{K}_2\text{CO}_3$ , wet  $\text{MeOH}/\text{THF}(1:1)$ . (c)  $\text{CuCl}/\text{TMEDA}$ ,  $\text{CH}_2\text{Cl}_2$ ,  $\text{O}_2$ , rt.

Another precursor to a strained tetrayne species was synthesized as described in Eq. 6.1. Triflate **146** was cross-coupled with 1,6-heptadiyne **187** (present in excess) in the presence of  $\text{PdCl}_2(\text{PPh}_3)_2$  as catalyst,  $\text{CuI}$  as co-catalyst,  $i\text{-Pr}_2\text{NH}$  as base in THF, yielding **188** in 80% yield. Compound **188** could therefore lead to the strained cross-conjugated tetrayne **189** through two consecutive oxidative homocouplings.

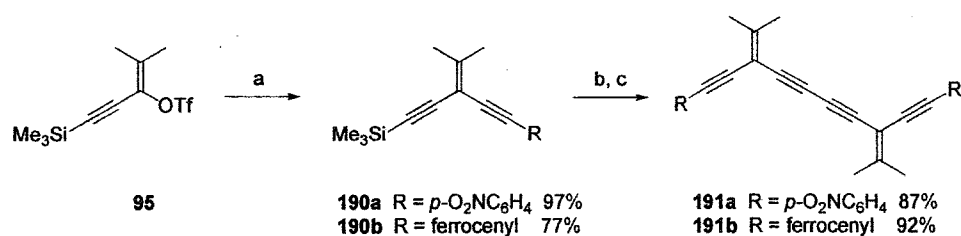


### 6.2.3 Synthesis of Donor/Acceptor Functionalized Cross-conjugated Enynes

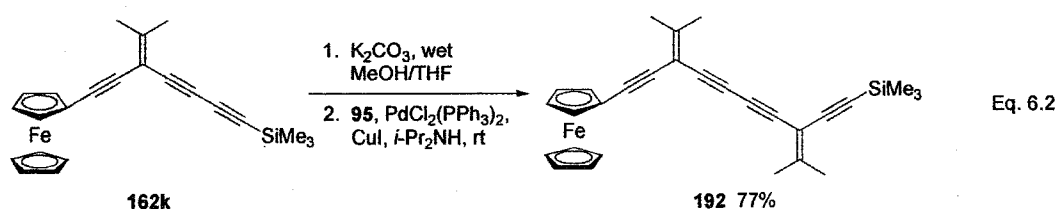
Our exploration of cross-conjugated molecules also focused on the assembly of donor/acceptor enyne derivatives.<sup>12,13</sup> This includes *iso*-PTA dimers with bis-donor/acceptor functionalities, **191–192** (Scheme 6.6 and Eq. 6.2), and bis-donor/acceptor cross-conjugated enetetraynes **193a–b** (Eq. 6.3). Donor/acceptor substituted *iso*-PDA monomers were synthesized via Pd-catalyzed cross-coupling vinyl triflate **95** with donor/acceptor acetylenes (*p*-nitrophenylacetylene and ethynylferrocene) to afford acceptor monomer **190a** and donor monomer **190b** in yields of 97% and 77%, respectively. The monomers were desilylated with K<sub>2</sub>CO<sub>3</sub> in MeOH/THF (1:1) and then oxidatively homocoupled in the presence of *Hay* catalyst, yielding bis(acceptor) and bis(donor) substituted *iso*-PTA dimers **191a** and **191b** as yellow solids in 87% and 92% yields, respectively.

Differentially substituted *iso*-PTA dimer **192** was prepared via cross-coupling desilylated monomer **162k** with triflate **95** in the presence of PdCl<sub>2</sub>(PPh<sub>3</sub>)<sub>2</sub>, CuI and *i*-Pr<sub>2</sub>NH in THF at room temperature for 1 h (Eq. 6.2). Column chromatography through silica gel afforded dimeric **192** as a yellow solid in 77% yield.

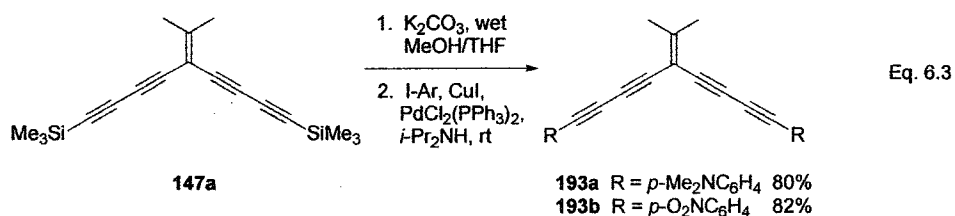
### Scheme 6.6



Reagents and conditions: (a) *p*-nitrophenylacetylene or ethynylferrocene, PdCl<sub>2</sub>(PPh<sub>3</sub>)<sub>2</sub>, CuI, *i*-Pr<sub>2</sub>NH, THF, rt. (b) K<sub>2</sub>CO<sub>3</sub>, wet MeOH/THF (1:1), rt. (c) CuCl/TMEDA, O<sub>2</sub>, acetone, rt.

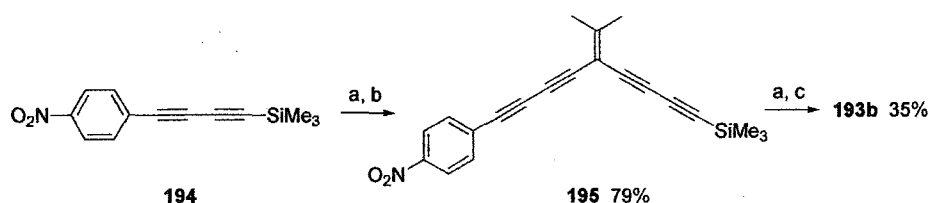


The second series of bis(donor) and bis(acceptor) chromophores was based on an enetetrayne framework (Eq. 6.3). Desilylation of precursor **147a** with K<sub>2</sub>CO<sub>3</sub> in MeOH/THF gave the terminal alkyne, which was then cross-coupled under Sonogashira conditions with either *p*-iodo-*N,N*-dimethylaniline or *p*-iodo-nitrobenzene to give **193a** and **193b** in 80% and 82% yields, respectively. Whereas **193a** could be readily purified by column chromatography, the isolation of **193b** proved problematic. Despite the fact that it was formed in high yield, the isolation of **193b** was always hampered by contamination with side product(s) resulting from oxidative homocoupling reactions of the acetylenic precursor.



As a result, an alternative route was designed, as shown in Scheme 6.7. Coupling of vinyl triflate **146** with desilylated diyne **194** using  $\text{PdCl}_2(\text{PPh}_3)_2/\text{CuI}$  gave tetrayne **195** in 79% yield. Removal of the trimethylsilyl group by methanolic  $\text{K}_2\text{CO}_3$  gave the terminal alkyne, which could be cross-coupled with *p*-iodo-nitrobenzene to give **193b** as a yellow solid that could be effectively purified by column chromatography.

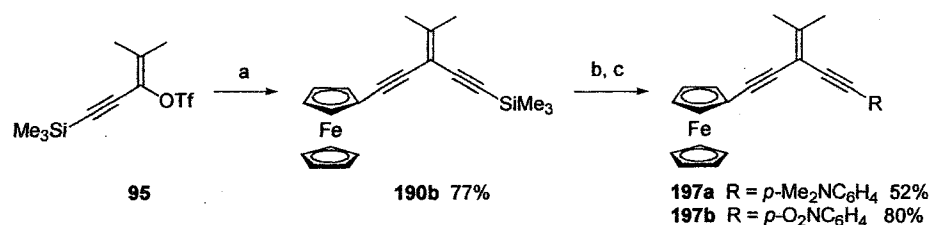
Scheme 6.7



Reagents and conditions: (a)  $\text{K}_2\text{CO}_3$ , wet MeOH/THF (1:1), rt. (b) **146**,  $\text{PdCl}_2(\text{PPh}_3)_2$ , CuI, *i*-Pr<sub>2</sub>NH, THF, rt. (c) *p*-iodo-nitrobenzene,  $\text{PdCl}_2(\text{PPh}_3)_2$ , CuI, *i*-Pr<sub>2</sub>NH, THF, rt.

The last donor/acceptor enyne series focuses on the *iso*-PDA monomeric framework. As a complementary study to Ciulei's project,<sup>12</sup> a Master student in our group, donor/acceptor substituted *iso*-PDA monomers were synthesized as shown in Scheme 6.8. Vinyl triflate **95** was cross-coupled with ethynylferrocene to afford monomer **190b** as a yellow solid in 77% yield. Removal of the trimethylsilyl group from **190b** gave the terminal alkyne, which was cross-coupled with either *p*-iodo-*N,N*-dimethylaniline or *p*-iodo-nitrobenzene under Sonogashira conditions to give **197a** and **197b** in 52% and 80% yields, respectively. In the same manner as described by Ciulei,<sup>12</sup> donor/acceptor *iso*-PDA oligomers could be obtained; however, this work has not yet been pursued.

### Scheme 6.8



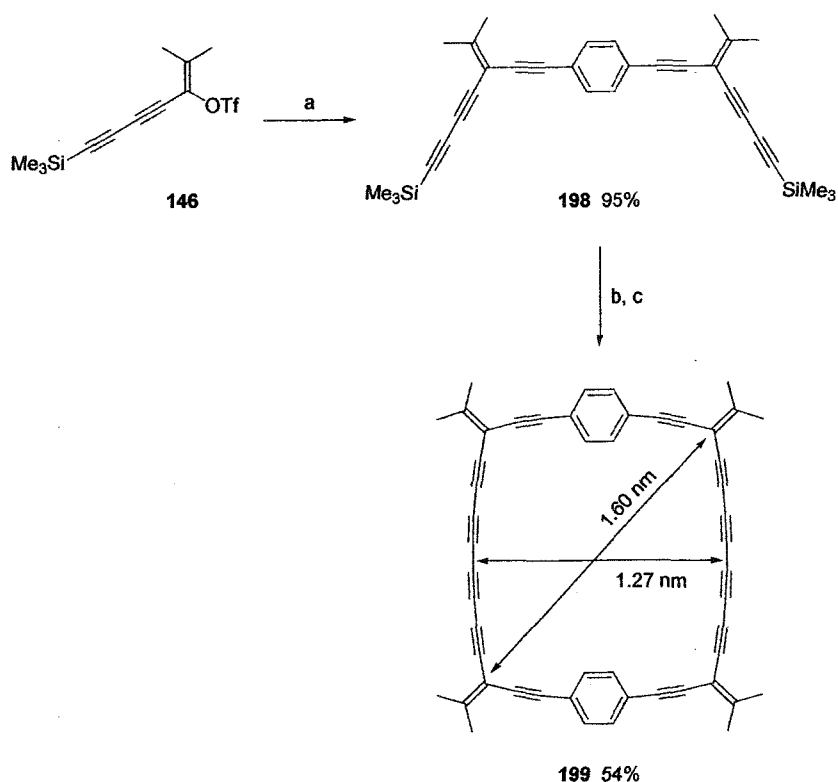
Reagents and conditions: (a) ethynylferrocene, PdCl<sub>2</sub>(PPh<sub>3</sub>)<sub>2</sub>, CuI, *i*-Pr<sub>2</sub>NH, THF, rt. (b) K<sub>2</sub>CO<sub>3</sub>, wet MeOH/THF (1:1), rt. (c) *p*-iodo-*N,N*-dimethylaniline or *p*-iodo-nitrobenzene, PdCl<sub>2</sub>(PPh<sub>3</sub>)<sub>2</sub>, CuI, *i*-Pr<sub>2</sub>NH, THF, rt.

#### 6.2.4 Synthesis of Cross-conjugated Macrocycles

The synthesis of cross-conjugated enynes provided us with a springboard toward the preparation of a series of cross-conjugated macrocycles. Unlike their linearly conjugated and homoconjugated counterparts,<sup>14-19</sup> cross-conjugated macrocycles show interesting electronic properties due to their unique  $\pi$ -delocalization.<sup>20</sup> With only a few examples in the literature, the synthesis of these macrocycles is of ongoing interest from both a theoretical and synthetic perspective.<sup>21</sup>

The first cross-conjugated macrocycle, **199**, was synthesized through the route shown in Scheme 6.9.<sup>15</sup> Precursor **198** was synthesized via cross-coupling 2 equiv. of vinyl triflate **146** with 1,4-diethynylbenzene as a yellow solid in 95% yield. Compound **198** was then desilylated with K<sub>2</sub>CO<sub>3</sub> in MeOH/THF, and a macrocyclization was performed under Hay conditions to give macrocycle **199** in 53% yield. Molecular modeling studies of **199** was accomplished using a molecular mechanics method (MM3\*), and the minimized structure of **199** shows that the cycle has a diameter of ca. 1.3–1.6 nm.

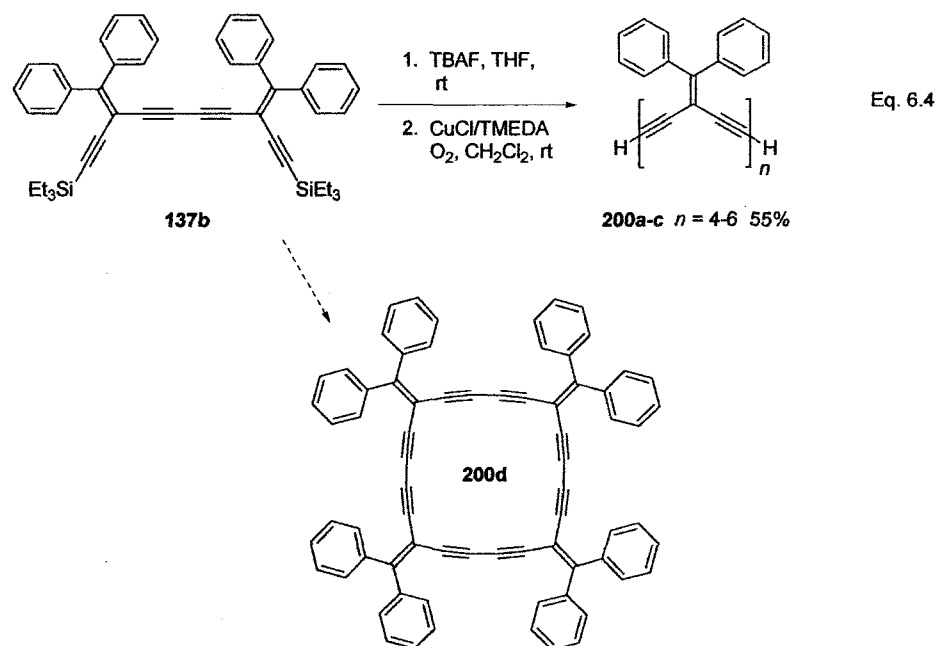
### Scheme 6.9



Reagents and conditions: (a) 1,4-diethynylbenzene,  $\text{PdCl}_2(\text{PPh}_3)_2$ , CuI, *i*-Pr<sub>2</sub>NH, THF, rt. (b)  $\text{K}_2\text{CO}_3$ , wet MeOH/THF (1:1), rt. (c) CuI/TMEDA, O<sub>2</sub>, CH<sub>2</sub>Cl<sub>2</sub>, rt.

A second cross-conjugated macrocycle **200d** has been attempted as outlined in Eq. 6.4. The *iso*-PTA dimer **137b** was desilylated with 2 equiv. of TBAF to give terminal alkynes, which were then homocoupled to each other in the presence of CuCl/TMEDA and oxygen in CH<sub>2</sub>Cl<sub>2</sub>. Column chromatography on SiO<sub>2</sub> gave a yellow solid in 55% yield. However, MALDI-TOF mass spectral analysis shows the  $[\text{M} + \text{Na}]^+$  peaks for acyclic *iso*-PTAs **200a–c** at 929.21, 115.26, and 1381.28, respectively, confirming that this mixture consists of **200a–c**. <sup>1</sup>H and <sup>13</sup>C NMR spectroscopic analyses also supported the formation of these acyclic *iso*-PTA oligomers rather than the cyclized

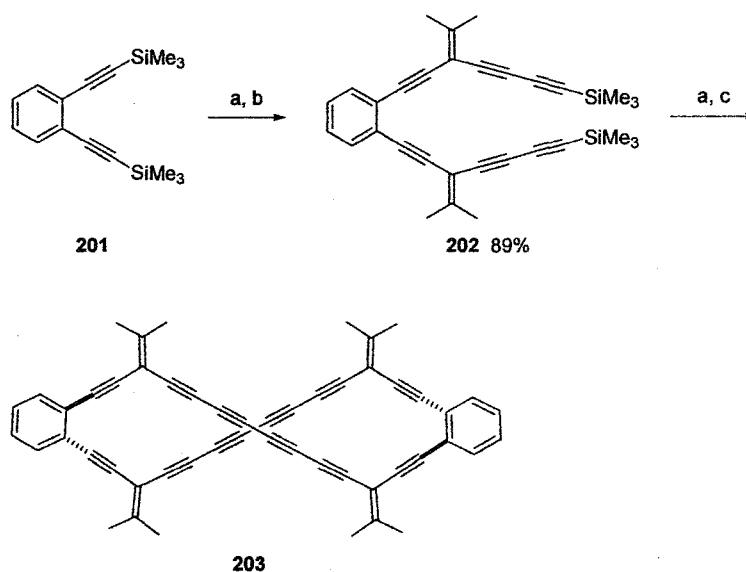
product **200d**. Further chromatography (SiO<sub>2</sub>, Al<sub>2</sub>O<sub>3</sub>, and reverse phase) to isolate each of the individual *iso*-PTA has, however, been problematic. This is due to their annoyingly similar eluting behavior over these columns. Alternative purification method, such as gel permeation chromatography (GPC), is currently under investigation. In addition, effort to elaborate the cyclization reaction is also underway.



The last cross-conjugated macrocyclic target was a twisted molecule **203** (shown in Scheme 6.10), which shows intriguing geometric properties due to its unique topology.<sup>22</sup> Molecular modeling (MM3\*) reveals that compound **203** shows interesting stereogenic characteristic resulting from its twisted non-planar conformation. Precursor **202** was prepared by cross-coupling 1,2-diethynylbenzene with vinyl triflate **146** to give a yellow solid in 89% yield. Removal of the trimethylsilyl groups in **202** gave the terminal alkyne which was homocoupled under Hay conditions in acetone. The resulting yellow product **203** is sparsely soluble in acetone, but is readily soluble in chlorinated solvents. In addition to the problems of insolubility, the limited kinetic stability of **203**

hampered the further chromatographic isolation and spectroscopic characterization of this compound. It was found to decompose immediately after removal of solvent. It is believed that the presence of an allylic hydrogen and the highly unsaturated unstable tetrayne moiety, as well as the possible Bergman cyclization,<sup>23</sup> are the reasons for such rapid decomposition. To prevent the decomposition, we envision an alternative macrocycle with more robust substituents rather than the isopropylidene groups, such as adamantanylidene or diphenylmethylidene derivatives. As well, the incorporation of solubilizing groups pendant to the main framework is likely necessary.

**Scheme 6.10**



Reagents and conditions: (a)  $K_2CO_3$ , wet MeOH/THF (1:1), rt. (b) **146**,  $PdCl_2(PPh_3)_2$ , CuI, *i*-Pr<sub>2</sub>NH, THF, rt. (c) CuCl/TMEDA, O<sub>2</sub>, acetone, rt.

## 6.3 Results and Discussion

### 6.3.1 Physical Characteristics

Complete spectroscopic characterization was accomplished for all isolated compounds discussed above. For the donor/acceptor functionalized enyne oligomers

**191–197**,  $^{13}\text{C}$  NMR spectral analysis provides an indication of the ability of pendant donor or acceptor groups to influence physical properties. For the bis(acceptor) *iso*-PTA **191a**, the external vinylidene carbon ( $\text{Me}_2\text{C}=\text{C}$ ) is deshielded to  $\delta$  160.7, and the other vinylidene carbon is observed at 100.4 ppm. The central butadiynyl carbons are present at 76.1 and 78.5 ppm, respectively, whereas the pendent triple bond carbons are observed at 90.1 and 90.4 ppm. For the bis(donor) *iso*-PTA **191b**, the vinylidene carbons ( $\text{Me}_2\text{C}=\text{C}$ ) are shielded to  $\delta$  156.6, as expected based on resonance. The other vinylidene carbon is observed at 101.4 ppm. The central butadiynyl carbons resonate at 75.7 and 79.3 ppm, whereas the peripheral  $\text{C}\equiv\text{C}$  show resonances at  $\delta$  81.6 and 91.0. For differentially functionalized **192**, interestingly, all 12 of the unique  $\text{sp}$  and  $\text{sp}^2$  carbons on the framework are observable in a 125 MHz spectrum. The two non-equivalent external vinylidene carbons ( $\text{Me}_2\text{C}=\text{C}$ ) show two distinct signals, and this carbon adjacent to the ferrocenyl group is slightly shielded at  $\delta$  156.4. The carbon nearest to the trimethylsilyl group is observed at  $\delta$  159.1. The other two in-chain vinylidene carbons ( $\text{Me}_2\text{C}=\text{C}$ ) show resonances at 101.0 and 101.3 ppm. The central butadiynyl carbons are observed at 75.6, 76.2, 78.6, and 79.3 ppm, respectively, whereas, the other acetylenic carbons are discernible at  $\delta$  81.4, 90.9, 97.1, and 100.4, respectively.

A similar trend is also observable for enynes **147a** and **193a–b**. The external vinylidene carbon in tetrayne **147a**, observed at 163.9 ppm, is even more deshielded than that for **154** (bis(TIPS)-encapped *iso*-PTA dimer), as a result of the increased electron deficiency of the two butadiynyl groups. For bis(donor) **193a**, the external vinylidene carbon ( $\text{Me}_2\text{C}=\text{C}$ ) is shielded by nearly 4 ppm to 159.4 ppm compared to **147a**, whereas for electron deficient **193b**, this type of carbon at  $\delta$  165.0 is slightly more deshielded than

**147a.** The other vinylidene carbons resonate, however, between  $\delta$  99.7 and 100.9. The butadiynyl carbons for bis(donor) **193a** are observed at 72.0, 77.0, 77.1, and 84.0 ppm, whereas the carbons resonate at 76.2, 78.6, 79.2, and 80.2 ppm for bis(acceptor) **193b**.

For ferrocenyl functionalized *iso*-PDA monomers, the external vinylidene carbon ( $\text{Me}_2\text{C}=\text{C}$ ) for donor substituted **197a** is deshielded by ca. 3 ppm at  $\delta$  151.1 than trimethylsilyl substituted **190b** (154.2 ppm), and by ca. 6 ppm versus bis(trimethylsilyl)-derivative **97** (156.9 ppm). The vinylidene carbon for the acceptor substituted **197b** is slightly deshielded at 155.5 ppm. In addition, the other vinylidene carbons are observed at 102.2, 102.2, and 101.4 ppm for **197a**, **190b**, and **197b**, respectively. The triple bond carbons for **197a** resonate at  $\delta$  83.1, 84.7, 89.6, and 92.0, whereas for **190b** they appear at  $\delta$  82.4, 90.2, 95.8, and 102.0, and for **197b** at  $\delta$  81.8, 89.2, 90.0, and 92.3, respectively.

In the  $^{13}\text{C}$  NMR spectrum for macrocycle **199**, the four symmetrical external vinylidene carbons ( $\text{Me}_2\text{C}=\text{C}$ ) are observed as one equivalent resonance at 163.1 ppm, whereas the in-chain carbons are at 100.2 ppm. As expected, the octatetraynl carbons resonate at  $\delta$  64.3, 67.9, 75.2, and 76.4, similar to other tetrayne species. The other  $\text{C}\equiv\text{C}$  carbons adjacent to benzene ring show resonance peaks at 86.5 and 92.7 ppm. The carbons of the benzene ring show two peaks at  $\delta$  123.2, and 131.7, whereas two methyl peaks are observed at  $\delta$  23.5 and 23.6, respectively. In addition to the  $^{13}\text{C}$  NMR data, the  $^1\text{H}$  NMR, IR and UV-vis spectra for **199** also well support the proposed macrocyclic structure; however, mass spectroscopic measurements (ESI and MALDI-TOF) have not been successful.

### 6.3.2 *Solid-State Structures*

Single crystals of enediyne **193a**, ferrocenyl substituted *iso*-PDA monomers **197a** and **197b** were grown by diffusion of MeOH into CH<sub>2</sub>Cl<sub>2</sub> solutions at 4 °C. X-ray analysis for **193a** shows that its solid-state structure incorporates two geometrically similar, but crystallographically independent molecules in the unit cell. The cross-conjugated enyne core, including one of the *N,N*-dimethylaminophenyl groups, is nearly planar (Fig. 6.1). The second aryl moiety, however, is rotated out of this plane by 59.8° in case of molecule A, and 72.3° for molecule B. The vinylidene angles are observed at 115.0(4)° and 113.7(4)° for molecule A and B, respectively, whereas the butadiynyl structures are nearly linear with less than 2° deviation from 180°. No anomalous bond lengths are observed for the conjugated enyne framework; for instance, in molecule A, the bond lengths for C(1)–C(2) at 1.191(5) Å, C(2)–C(3) at 1.373(5) Å, C(3)–C(4) at 1.189(5) Å, C(4)–C(5) at 1.445(5) Å, and C(5)–C(6) at 1.350(5) Å, are all in expected ranges of sp and sp<sup>2</sup> carbon connections.

X-ray crystallographic analysis for single crystals of **197a** shows a nearly planar structure for the enediyne skeleton with a maximum deviation of 0.0070(14) Å from the least-squares plane, whereas the *N,N*-dimethylaminophenyl group is slightly rotated out of this plane by 20.70(10)° (Fig. 6.2). However, the cyclopentadienyl group is significantly twisted out of the enyne plane by an angle of 87.77(7)°. The vinylidene angle, 114.05(15)°, is in line with other enediynes, and the bond angles of C(1)–C(2)–C(3) at 176.10(18)° and C(3)–C(7)–C(8) at 176.07(18)° are slightly deviated from linearity by ca. 4°. Bond lengths are observed as: C(1)–C(2) at 1.196(2) Å, C(2)–C(3) at 1.442(2) Å, C(3)–C(4) at 1.348(2) Å, C(3)–C(7) at 1.433(2) Å, and

C(7)–C(8) at 1.195(3) Å, respectively, which all fall into the expected range of  $sp$  and  $sp^2$  connections.

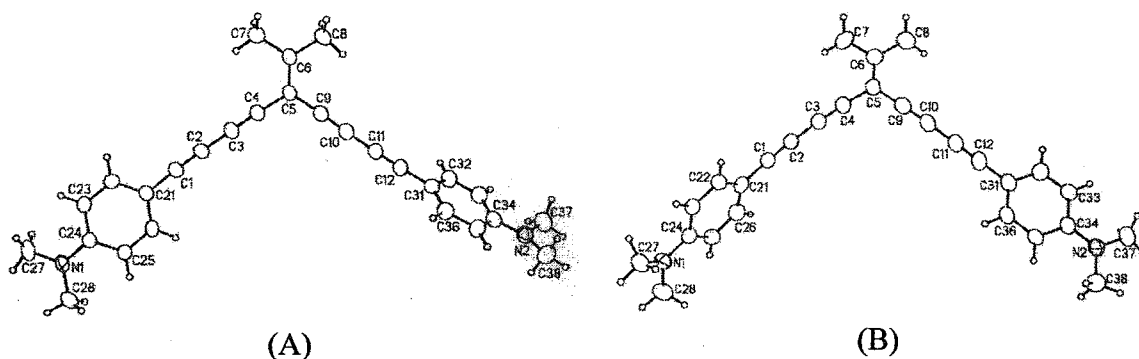


**Fig. 6.1** ORTEP drawings (20% probability level) of two crystallographically independent molecules of **193a**. Selected bond lengths (Å) and angles (°) for molecule A: C(1)–C(21) 1.429(5), C(1)–C(2) 1.191(5), C(2)–C(3) 1.373(5), C(3)–C(4) 1.189(5), C(4)–C(5) 1.445(5), C(5)–C(6) 1.350(5), C(5)–C(9) 1.432(6), C(9)–C(10) 1.196(6), C(10)–C(11) 1.376(6), C(11)–C(12) 1.182(6), C(12)–C(31) 1.447(6); C(2)–C(1)–C(21) 177.1(4), C(1)–C(2)–C(3) 179.4(5), C(2)–C(3)–C(4) 178.8(5), C(3)–C(4)–C(5) 177.3(4), C(4)–C(5)–C(9) 115.0(4), C(5)–C(9)–C(10) 177.7(4), C(9)–C(10)–C(11) 177.6(5), C(10)–C(11)–C(12) 179.1(5), C(11)–C(12)–C(31) 177.1(5).

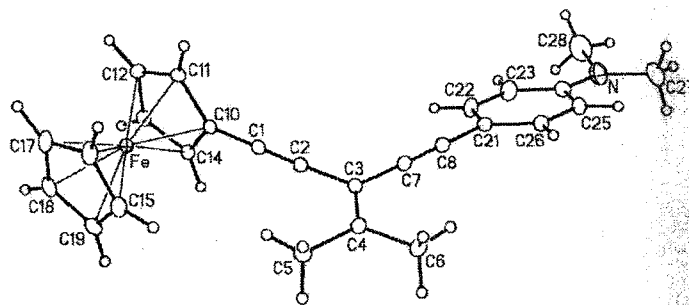


**Fig. 6.2** ORTEP drawings (20% probability level) of **197a**. Selected bond lengths (Å) and angles (°): C(1)–C(2) 1.196(2), C(1)–C(10) 1.422(2), C(2)–C(3) 1.442(2), C(3)–C(4) 1.348(2), C(3)–C(7) 1.433(2), C(7)–C(8) 1.195(3), C(8)–C(21) 1.432(3); C(2)–C(1)–C(10) 178.16(18), C(1)–C(2)–C(3) 176.10(18), C(2)–C(3)–C(7) 114.05(15), C(3)–C(7)–C(8) 176.07(18), C(7)–C(8)–C(21) 177.58(17).

X-ray structural analysis of single crystals of **197b** (Fig. 6.3) shows a similarly planar enediyne framework with a maximum deviation of 0.003(2) Å from the least-squares plane, which is nearly co-planar with the nitrophenyl group at a twisted angle of 1.56(19)°. Likewise, the angle between the cyclopentadienyl group and the enyne plane at 14.70(16)° is much smaller than that for **197a**, suggesting an extended  $\pi$ -conjugation along the ferrocenyl-enediyne-nitrophenyl skeleton. The vinylidene angle is observed as 116.6(2)°, which is slightly greater than that for **197a**. The bond angles of C(1)–C(2)–C(3) at 178.6(3)° and C(3)–C(7)–C(8) at 178.2(3)° are nearly linear with a deviation of less than 2°. The bond lengths observed for C(1)–C(2) at 1.201(4) Å, C(2)–C(3) at 1.434(4) Å, C(3)–C(4) at 1.355(4) Å, C(3)–C(7) at 1.441(4) Å, and C(7)–C(8) at 1.187(4) Å, are also consistent with that expected for  $sp$  and  $sp^2$  hybridized carbon-carbon bonds. In addition, the D/A chromophore **197a** was observed to pack non-centrosymmetrically in the solid state, i.e., monoclinic  $P2_1$  (No.4) space group, suggesting a potential as second-order nonlinear optical materials.

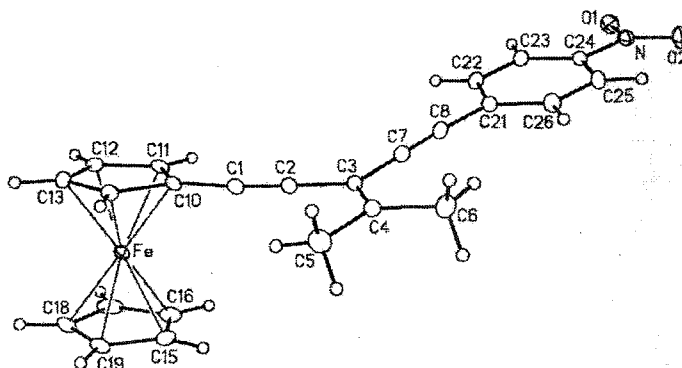


**Fig. 6.3** ORTEP drawings (20% probability level) of **197b**. Selected bond lengths (Å) and angles (°): C(1)–C(2) 1.201(4), C(1)–C(10) 1.420(4), C(2)–C(3) 1.434(4), C(3)–C(4) 1.355(4), C(3)–C(7) 1.441(4), C(7)–C(8) 1.187(4), C(8)–C(21) 1.438(4); C(2)–C(1)–C(10) 175.9(3), C(1)–C(2)–C(3) 178.6(3), C(2)–C(3)–C(7) 116.6(2), C(3)–C(7)–C(8) 178.2(3), C(7)–C(8)–C(21) 175.4(3).

### 6.3.3 Electronic Properties

The electronic absorption spectra for dimeric **191a–b** are shown in Fig. 6.4. Three low energy absorptions at ca. 290, 310, and 330 nm are observed in both derivatives, varying slightly as a result of the different pendant groups. The broad absorption hump at ca. 450 nm for **191b** is due to the ferrocenyl  $\pi \rightarrow \pi^*$  transition. The most surprising observation, however, is found in the spectrum for **191a**, where a significant shoulder absorption is found near 350 nm. Meanwhile, the same shoulder peak is also distinguishable in the spectrum for **191b**, however, it has a much lower absorption intensity. Whereas previous studies have suggested that enhanced communication in cross-conjugated molecules results from increasingly electron rich substitution,<sup>12</sup> in tetraynes **191**, it is clear that the electron poor functionality has the more dramatic effect. In addition, such a trend is also observable in the spectra of *iso*-PTA dimers **151**, **154**, and **156** (See Fig. 4.4b).

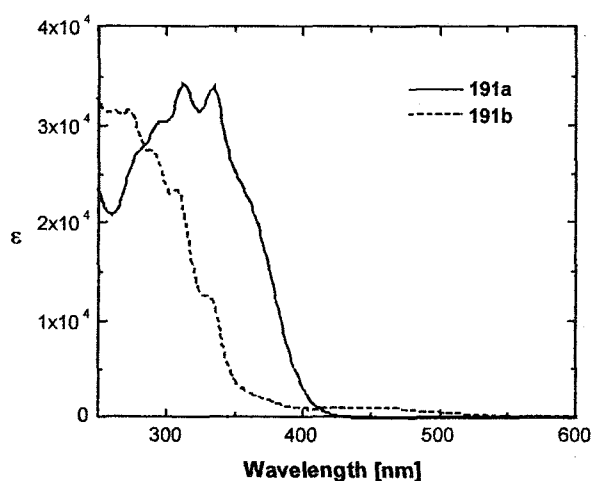


Fig. 6.4 Electronic absorption spectra ( $\epsilon$  [L mol<sup>-1</sup> cm<sup>-1</sup>]) in CHCl<sub>3</sub> for **191a** and **191b**.

The UV-vis spectra for **193a–b** are shown in Fig. 6.5. In both compounds, three low energy absorptions are visible, centered at approximately 327, 346, and 366 nm. Although electron rich **193a** shows a slightly higher molar absorptivity, the overall electronic absorption characteristics for **193a–b** are quite analogous. Thus, the anomalous behavior resulting from  $\pi$ -electron acceptors appears limited to molecules such as **191**.

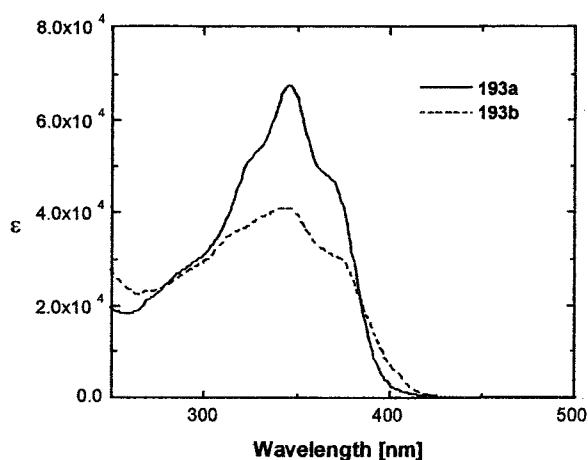


Fig. 6.5 Electronic absorption spectra ( $\epsilon$  [ $\text{L mol}^{-1} \text{cm}^{-1}$ ]) in  $\text{CHCl}_3$  for **193a** and **193b**.

The electronic absorption spectra for the ferrocenyl substituted *iso*-PDA monomer series **190b** and **197** are shown in Fig. 6.6. Two low energy absorptions at ca. 265 and 302 nm are observed for all three derivatives. Meanwhile, in the spectra of donor **190b** and **197a**, an additional lower energy absorption is observed at ca. 330 nm as a shoulder, while this absorption shifts toward lower energy by ca. 20 nm in the spectrum for acceptor **197b**. It is therefore clear that only monomer **197b** is dramatically influenced as a result of incorporation of donor and acceptor groups into the enyne framework. Additionally, in all three spectra, the ferrocenyl absorptions are observed as broad humps centered at 450 nm without obvious shifts.

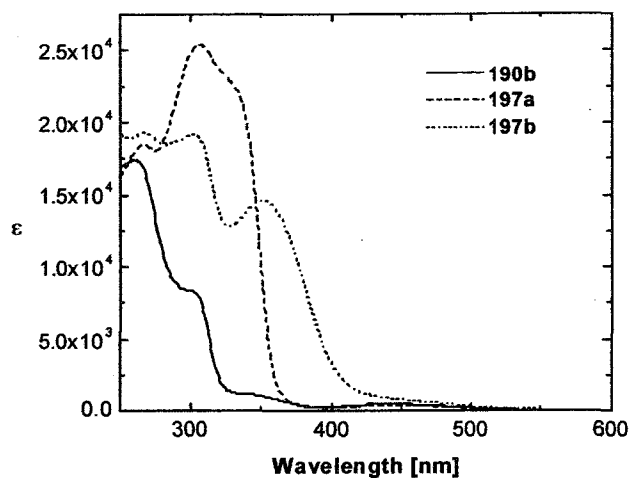


Fig. 6.6 Electronic absorption spectra ( $\epsilon$  [ $\text{L mol}^{-1} \text{cm}^{-1}$ ]) in  $\text{CHCl}_3$  for **190b** and **197a–b**.

The UV-vis spectrum of macrocycle **199** is shown in Fig. 6.7. Like the other tetrayne species, the lower energy region is dominated by the vibrational mode of the octatetraynyl structure, and three characteristic absorptions are observed at 350, 375, and 408 nm, respectively. In addition, two other absorptions at 310 and 327 nm are believed to be due to the enyne and diethynylbenzene moieties.

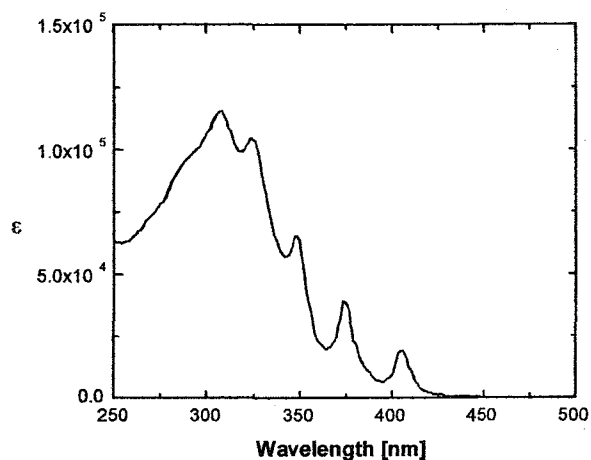


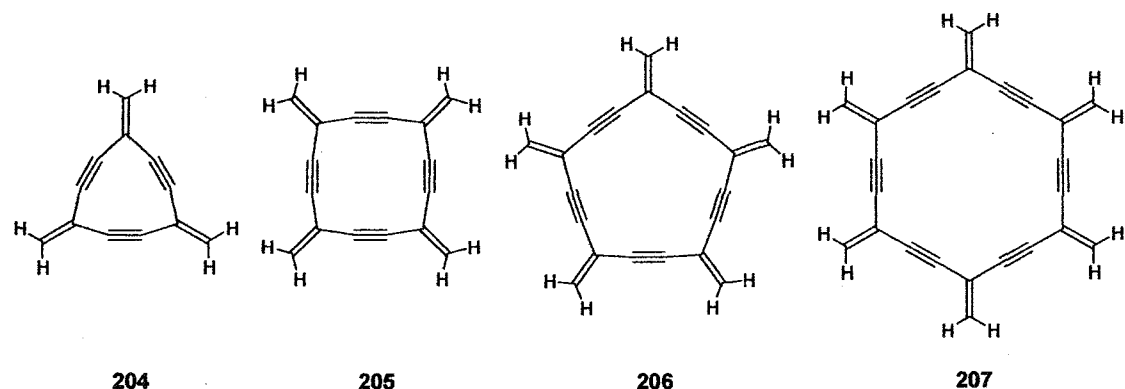
Fig. 6.7 Electronic absorption spectra ( $\epsilon$  [ $\text{L mol}^{-1} \text{cm}^{-1}$ ]) in  $\text{CHCl}_3$  for **199**.

#### 6.4 Density Functional Theory (DFT) Studies of Expanded Radialenes

Cross-conjugated monocyclic molecules, such as [*n*]radialenes and their expanded derivatives, have been of continuous interest in both a theoretical and experimental sense.<sup>24</sup> Although radialenes have been defined and studied for many years, less effort has focused on their expanded analogues, i.e., the cross-conjugated [*n*]radialenes. Our group recently reported the synthesis of a cross-conjugated expanded [6]radialene derivative, a member of the so-called “exploded [*n*]radialenes” family (204–207).<sup>25</sup> Currently, experimental efforts toward a functionalized series are underway. To date, only a few theoretical studies have been performed on this class of molecules.<sup>26</sup> Deeper exploration into the nature of these molecules, such as the structure-property relationship resulting from the cross-conjugated cyclic  $\pi$ -system has not been achieved, due to the lack of sufficient experimental and computational data.

The general Hückel’s rule ( $4n+2$ ) is regarded as applicable only in planar cyclic conjugated systems to predict properties such as aromaticity for various conjugated ring systems. In the particular case of cross-conjugated monocyclic exploded [*n*]radialenes, Hückel’s rule is not viable. According to electronic behavior studies of the cross-conjugated *iso*-polydiacetylenes (expanded dendralenes), electron communication via the oligomeric framework can still be observed despite the fact that cross conjugation limits delocalization of each conjugated segment. In the same manner, electron communication resulting from cross-conjugation in expanded radialene species can also, accordingly, be deemed as possible. Nevertheless, simplifying this unique  $\pi$ -system by Hückel’s rule is questionable. For instance, in expanded [4]radialene 205, there are two sets of orthogonal *p*-orbitals, i.e. in-plane ( $\pi_y$ ) and out-of-plane ( $\pi_z$ ) systems, which are counted

as  $8 e^-$  and  $16 e^-$ , respectively (Fig. 6.8). In principle, they can generate either a diamagnetic or a paramagnetic ring current under exposure to a magnetic field; in other words, aromaticity or antiaromaticity.



A subsequent question therefore arises: Are these molecules aromatic, antiaromatic, or nonaromatic? It is obvious that simple Hückel MO theory can not answer this question because of the complicated  $\pi$ -conjugated system. On the other hand, the more sophisticated quantum mechanics theories, such as DFT and *ab initio* methods, are capable of accounting for these issues with satisfying accuracy and reliability.<sup>27-29</sup>

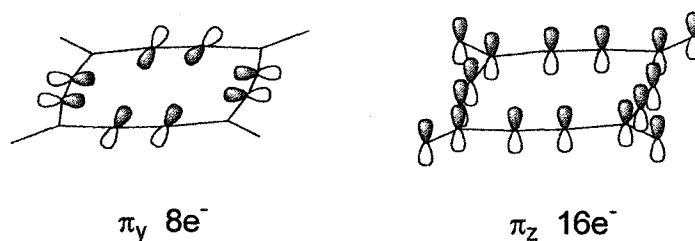


Fig. 6.8 Orthogonal  $\pi$ -systems in expanded radialene.

In the last few years, methods based on Density Functional Theory (DFT) have gained steadily in popularity. The best DFT methods achieve significantly greater accuracy than traditional Hartree-Fock theory at only a modest increase in cost (far less

than MP2 for medium-size and larger molecular systems). They do so by including some of the effects of electron correlation much less expensively than traditional correlated methods. DFT methods compute electron correlation via general functionals of electron density. DFT functionals partition the electronic energy into several components, which are computed separately: the kinetic energy, the electron-nuclear interaction, the Coulomb repulsion, and an exchange-correlation term accounting for the remainder of the electron-electron interaction.

A variety of functionals have been defined, generally distinguished by the way they treat the exchange and correlation components. The traditional functionals includes the local exchange and correlation functionals and gradient-corrected functionals, such as the widely used Vosko, Wilk and Nusair (VWN), the LYP functionals of Lee, Yang and Parr, Perdew 86, and Perdew-Wang 91. There are also several hybrid functionals, which define the exchange functional as a linear combination of Hartree-Fock, local, and gradient-corrected exchange terms; this exchange functional is then combined with a local and/or gradient-corrected correlation functional. The best known of these hybrid functionals is Becke's three-parameter formulation.

In this section, theoretical exploration of exploded [*n*]radialene series **204–207**, will be discussed, and the calculations were carried out using the Becke's three-parameter Lee, Yang and Parr functionals, which are available in the quantum mechanics computational software package, Gaussian 98w,<sup>30</sup> via the B3LYP keyword. Initial structures of **204–207** were generated by *MacSpartan Plus* using the AM1 semi-empirical SCF-MO method. Full geometry optimizations were then accomplished at the B3LYP/6-311G\*\* level and checked by frequency calculation. No imaginary frequency

can be observed from the frequency calculation results indicating that the geometry is in a global minima state. Nucleus-Independent Chemical Shifts (NICSSs) were calculated at B3LYP/6-311G\*\* level using the Gauge-Independent Atomic Orbital (GIAO) method. Calculated structures were generated and plotted by Chem3D program.

#### 6.4.1 Structural and Electronic Properties

The optimized structures and respective geometrical parameters for expanded [*n*]radialenes **204**–**207** are shown in Fig. 6.9, and all of these molecules adopt a planar centrosymmetrical  $D_{nh}$  geometry. It is notable that double-bond lengths increase slightly with ring expansion; that is, from 1.343 Å (**204**) to 1.351 Å (**207**), while the triple- and single-bond lengths show an insignificant decreasing trend. Trimeric **204** has the most strained ring-structure, where the bond angles at  $sp^2$  hybridized C(2) and  $sp$  center C(3) are calculated as 105.3° and 157.4°, respectively. Tetrameric **205** shows an  $sp^2$  vinylidene angle of 111.4° that is obviously smaller than those observed in *iso*-PDAs, whereas the  $sp$  angle of 169.3° at C(3) reveals a relief of ring strain relative to **204**. For pentameric **206** and hexameric **207**, the degree of ring strain becomes insignificant, with the vinylidene angles at 115.0° and 117.7°, and the  $sp$  angles at 176.5° and 178.8°, respectively, all in the range of their acyclic *iso*-PDA counterparts.

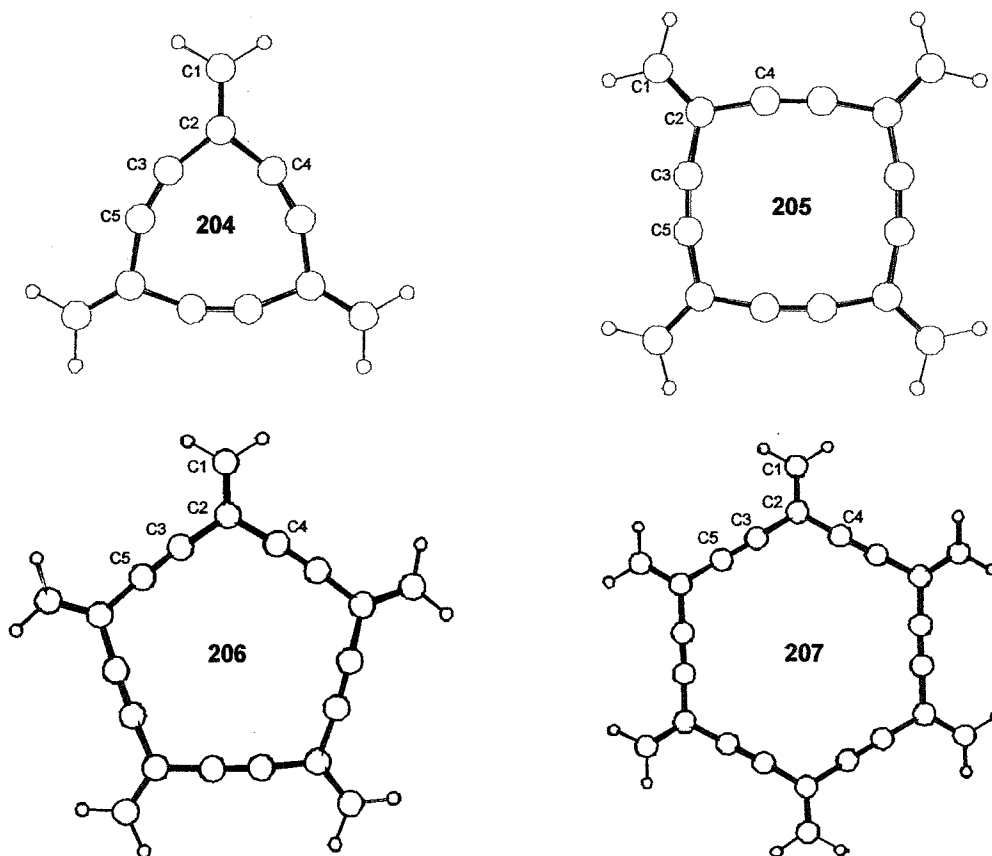


**Fig. 6.9** Optimized structures of **204–207** by B3LYP/6-311G\*\*. Geometry parameters for **204** ( $D_{3h}$ ): C(1)–C(2) 1.343 Å, C(2)–C(3) 1.440 Å, C(3)–C(5) 1.215 Å,  $\angle$ C(3)–C(2)–C(4) 105.3°,  $\angle$ C(2)–C(3)–C(5) 157.4°. For **205** ( $D_{4h}$ ): C(1)–C(2) 1.347 Å, C(2)–C(3) 1.433 Å, C(3)–C(5) 1.209 Å,  $\angle$ C(3)–C(2)–C(4) 111.4°,  $\angle$ C(2)–C(3)–C(5) 169.3°. For **206** ( $D_{3h}$ ): C(1)–C(2) 1.349 Å, C(2)–C(3) 1.430 Å, C(3)–C(5) 1.209 Å,  $\angle$ C(3)–C(2)–C(4) 115.0°,  $\angle$ C(2)–C(3)–C(5) 176.5°. For **207** ( $D_{6h}$ ): C(1)–C(2) 1.351 Å, C(2)–C(3) 1.429 Å, C(3)–C(5) 1.208 Å,  $\angle$ C(3)–C(2)–C(4) 117.7°,  $\angle$ C(2)–C(3)–C(5) 178.8°.

The total energies and the frontier molecular orbital (MO) characteristics are summarized in Table 6.1 and Fig. 6.10.

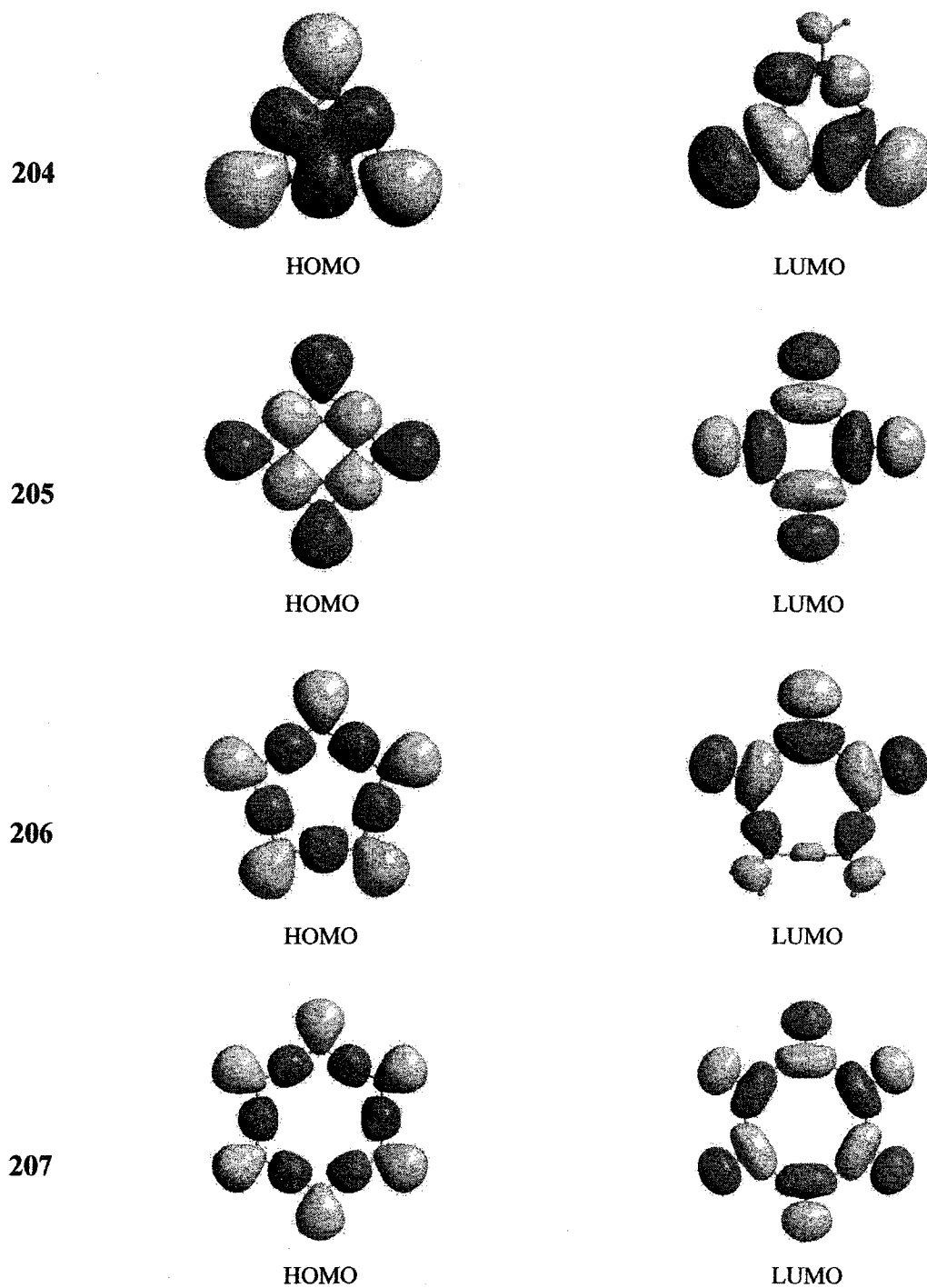


Fig. 6.10 Frontier MOs of 204–207 plotted at isocontour of 0.01000 a.u.

The most significant feature of the HOMO for expanded [3]radialene 204 is the particularly high electron-density at the ring center, which arises from the overlapping of

triple-bond  $\pi$ -electrons. For HOMOs of larger size rings **205–207**, however, the overlapping of triple-bond  $\pi$ -electrons decreases drastically. In addition, all of the HOMO densities for **204–207** are centrosymmetrically distributed along the cyclic enyne frameworks, whereas the LUMO density for only even-numbered cyclic systems, **205** and **207**, are centrosymmetrically distributed.

**Table 6.1** Total energies and frontier MO energies for **204–207**.

Entry	Total Energy $E$ (a.u.)	$E_{\text{HOMO}}$ (Hartree)	$E_{\text{LUMO}}$ (Hartree)	Band gap $\Delta\varepsilon$ (Hartree)
<b>204</b>	-460.716631	-0.234360	-0.075438	0.158922
<b>205</b>	-614.335503	-0.228499	-0.089284	0.139215
<b>206</b>	-767.935513	-0.225539	-0.084004	0.141535
<b>207</b>	-921.524047	-0.223774	-0.088257	0.135517

#### 6.4.2 Aromaticity Study Based on NICS Calculations

As mentioned above, the characteristics of aromaticity/antiaromaticity for expanded  $[n]$ radialenes are of fundamental significance to a deeper understanding of this unique cyclic-conjugated class of molecules. Since the most classic  $(4n+2)$  theory of “aromaticity” proposed by Hückel in 1937, the definition of aromaticity has undergone development mainly incorporating four criteria, i.e., chemical behavior (electrophilic aromatic substitution), structural (bond length equalization due to cyclic delocalization), energetic (enhanced stability), and magnetic (“ring current” effects).<sup>31</sup> Proposed by Schleyer and co-workers<sup>32</sup> in 1996, nucleus independent chemical shielding (NICS) has been widely accepted as one of the most universal and reliable criteria for aromaticity.

In order to shed light on this subject, NICS calculations, at the B3LYP/6-311G\*\* level using Gauge-Independent Atomic Orbital (GIAO) method, were performed for the series **204–207**, where ghost atoms (Bq) were put into the center of the radialene cyclic rings. According to Schleyer's theory, if the ring system is aromatic, a resulting diamagnetic ring-current will cause a dramatic shielding effect at the ring center; therefore, leading to negative NICS values (i.e., a positive value of isotropic shielding tensor in Gaussian 98 output). In addition, to preclude the influence from anisotropic effects, extended NICS tests, i.e., NICS curve,<sup>33</sup> were computed, where the position of the ghost atom above the center of ring is varied from 0 to 2.5 Å. The shape of the NICS curve is diagnostic for aromaticity, where a Gaussian function like negative curve is indicative of aromaticity and vice versa.

The calculated NICS results are shown in Fig 6.11, where the NICS(0) (denoting the NICS value at the ring centeroid position and on the ring plane) values for **204–207** are found as -6.18, 1.17, 0.42, and 0.51, respectively. For comparison purpose, NICS(0) for typical aromatic and antiaromatic model compounds, benzene and cyclobutadiene, were also achieved as -8.88 and 25.16, respectively, at B3LYP/6-311G\*\* level. Although the [3]radialene **204** show an isotropic shielding tensor similar to benzene, it is believed that such a shielding effect is due to the anisotropic effect from the triple bond  $\pi$ -electron density rather than from the ring current. This is evident by the particularly high electron-density at the ring center for the HOMO of **204**. Second, the NICS curve for **204** shows only a consistently decreasing trend rather than a Gaussian-type shape, indicating an anisotropy rather than aromaticity characteristics. Finally, to confirm the anisotropy effect, NICS(0) value in the mirror position of the ring-centeroid ghost atom

versus the  $C\equiv C$  bond was computed at same level as  $-0.22$ . In principle, if there is a “current effect” across the ring backbone, the NICS at this position will be of the same intensity as the ring-center position, however, with an opposite sign. The NICS of  $-0.22$  is the same sign as that at the ring-center ( $-6.18$ ). Therefore, proving that anisotropy effect but current effect occurs in the ring center of **204**. For the other  $[n]$ radialenes **205–207**, the slightly negative isotropic shielding tensors indicate their slight antiaromatic characteristics, showing that the cross-conjugated exapened radialenes are nonaromatic.

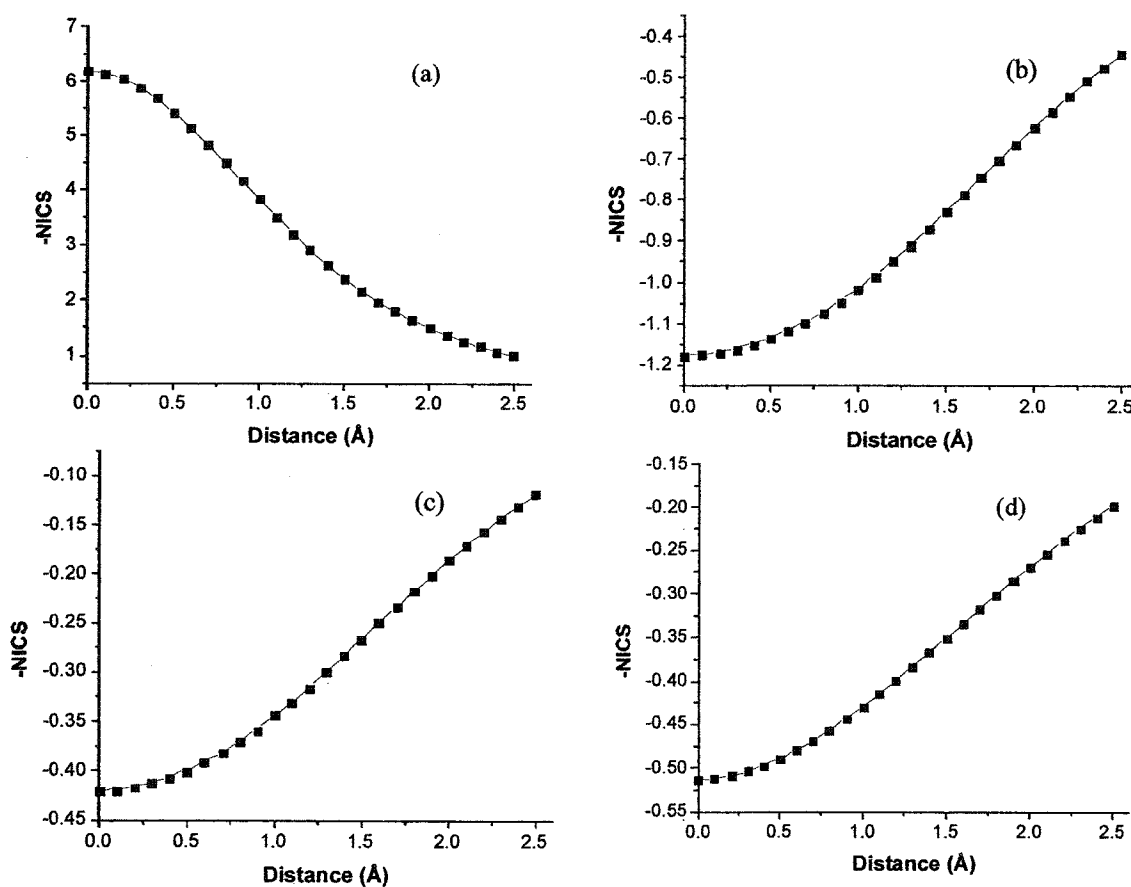


**Fig. 6.11** Plots of  $-NICS$  values versus the distances from ring center, where a positive Gaussian-shape curve denotes aromaticity, and a negative Gaussian-shape curve denotes antiaromaticity. (a) **204**. (b) **205**. (c) **206**. (d) **207**.

In summary, the cross-conjugated expanded  $[n]$ radialenes show insignificant “current effects” along the cyclic enyne framework; in other words, no apparently aromatic or antiaromatic characteristics are proposed by these conjugated cyclic systems.

## 6.5 Conclusions

In this chapter, we have described several projects including: (1) Synthesis of modified vinyl triflate building blocks, where the respective precursor compounds have been prepared effectively. However, to date, the synthesis of the target compounds, oligomeric triflates, has not been successful due to their unexpected instability. (2) Synthesis of precursors toward strained cyclic tetrayne species. Using the Pd-catalyzed cross-coupling protocol between vinyl triflate and terminal alkynes, these precursors can be readily accessed in reasonable yields. (3) Donor/acceptor functionalized cross-conjugated enynes that were efficiently synthesized via Pd-catalyzed cross-coupling. The solid-state structural properties and electronic absorption behaviors of these D/A chromophores have been characterized, as well. (4) Synthesis of cross-conjugated macrocycles. In addition, DFT study of a series of cyclic cross-conjugated enynes, namely expanded  $[n]$ radialenes, was carried out, and structural and electronic properties were elucidated. In addition, the aromatic/antiaromatic characteristics for this class of molecules were evaluated by NICS calculations.

## 6.6 References and Notes

- (1) Hinchliffe, A. *Modelling Molecular Structures*; 2nd ed.; John Wiley & Sons Ltd.: West Sussex, 2000.

- (2) Stang, P. J.; Fisk, T. E. *Synthesis* **1979**, 438-440.
- (3) Stang, P. J.; Treptow, W. *Synthesis* **1980**, 283-284.
- (4) Orfanopoulos, M.; Stratakis, M.; Elemes, Y. *Tetrahedron* **1989**, *30*, 4875-4878.
- (5) Orfanopoulos, M.; Stratakis, M.; Elemes, Y. *J. Am. Chem. Soc.* **1990**, *112*, 6417-6419.
- (6) Zhao, Y.; Campbell, K.; Tykwinski, R. R. *J. Org. Chem.* **2002**, *67*, 336-344.
- (7) Zhao, Y.; McDonald, R.; Tykwinski, R. R. *J. Org. Chem.* **2002**, *67*, 2805-2812.
- (8) Ritter, K. *Synthesis* **1993**, 735-762.
- (9) Greene, T. W. *Protective Groups in Organic Synthesis*; John Wiley & Sons, Inc.: New York, 1981.
- (10) Comins, D. L.; Dehghani, A. *Tetrahedron Lett.* **1992**, *33*, 6299-6302.
- (11) Eisler, S.; McDonald; Loppnow, G. R.; Tykwinski, R. R. *J. Am. Chem. Soc.* **2000**, *122*, 6917-6928.
- (12) Ciulei, S. C.; Tykwinski, R. R. *Org. Lett.* **2000**, *2*, 3607-3610.
- (13) Zhao, Y.; Ciulei, S.; Tykwinski, R. R. *Tetrahedron Lett.* **2001**, *42*, 7721-7723.
- (14) Leibrock, B.; Vostrowsky, O.; Hirsh, A. *Eur. J. Org. Chem.* **2001**, 4401-4409.
- (15) Haley, M. M.; Bell, M. L.; Brand, S. C.; Kimball, D. B.; Pak, J. J.; Wan, W. B. *Tetrahedron Lett.* **1997**, *38*, 7483-7486.
- (16) Diederich, F. *Chem. Commun.* **2001**, 219-227.
- (17) Hopf, H. *Classics in Hydrocarbon Chemistry*; Wiley-VCH: Weinheim, 2000.
- (18) Diederich, F.; Gobbi, L. *Top. Curr. Chem.* **1999**, *201*, 44-79.
- (19) Haley, M. M.; Pak, J. J.; Brand, S. C. *Top. Curr. Chem.* **1999**, *201*, 81-130.

- (20) Tobe, Y.; Utsumi, N.; Nagano, A.; Sonoda, M.; Naemura, K. *Tetrahedron* **2001**, *57*, 8075-8083.
- (21) Schreiber, M.; Tykwinski, R. R.; Diederich, F.; Spreiter, R.; Gubler, U.; Bosshard, C.; Poberaj, I.; Günter, P.; Boudon, C.; Gisselbrecht, J.-P.; Gross, M.; Jonas, U.; Ringsdorf, H. *Adv. Mater.* **1997**, *9*, 339-343.
- (22) Heuft, M. A.; Collins, S. K.; Yap, G. P. A.; Fallis, A. G. *Org. Lett.* **2001**, *3*, 2883-2886.
- (23) Nicolaou, K. C.; Smith, A. L. In *Modern Acetylene Chemistry*; Stang, P., Diederich, F., Eds.; VCH: Weinheim, 1995, pp 203-283.
- (24) Eisler, S.; Tykwinski, R. R. *Angew. Chem. Int. Ed.* **1999**, *38*, 1940-1943.
- (25) Hopf, H. In *Classics in Hydrocarbon Chemistry*; WILEY-VCH: Weinheim, 1999, pp 251-320.
- (26) Rogers, D. W.; MacLafferty, F. J. *J. Phys. Chem. A* **2002**, *106*, 1054-1059.
- (27) Godard, C.; Lepetit, C.; Chauvin, R. *Chem. Commun.* **2000**, 1833-1834.
- (28) Martín-Santamaría, S.; Rzepa, H. S. *J. Chem. Soc., Perkin Trans.* **2000**, 2372-2377.
- (29) Alkorta, I.; Elguero, J. *New J. Chem.* **1999**, *23*, 951-954.
- (30) Gaussian 98 (Revision A.9), M. J. Frisch, G. W. Trucks, H. B. Schlegel, G. E. Scuseria, M. A. Robb, J. R. Cheeseman, V. G. Zakrzewski, J. A. Montgomery, Jr., R. E. Stratmann, J. C. Burant, S. Dapprich, J. M. Millam, A. D. Daniels, K. N. Kudin, M. C. Strain, O. Farkas, J. Tomasi, V. Barone, M. Cossi, R. Cammi, B. Mennucci, C. Pomelli, C. Adamo, S. Clifford, J. Ochterski, G. A. Petersson, P. Y. Ayala, Q. Cui, K. Morokuma, D. K. Malick, A. D. Rabuck, K. Raghavachari, J.

B. Foresman, J. Cioslowski, J. V. Ortiz, A. G. Baboul, B. B. Stefanov, G. Liu, A. Liashenko, P. Piskorz, I. Komaromi, R. Gomperts, R. L. Martin, D. J. Fox, T. Keith, M. A. Al-Laham, C. Y. Peng, A. Nanayakkara, C. Gonzalez, M. Challacombe, P. M. W. Gill, B. G. Johnson, W. Chen, M. W. Wong, J. L. Andres, M. Head-Gordon, E. S. Replogle and J. A. Pople, Gaussian, Inc., Pittsburgh PA, 1998.

- (31) Schleyer, P. v. R.; Jiao, H. *Pure & Appl. Chem.* **1996**, *68*, 209-218.
- (32) Schleyer, P. v. R.; Maercker, A.; Dransfeld, A.; Jiao, H.; Hommes, N. J. R. v. E. *J. Am. Chem. Soc.* **1996**, *118*, 6317-6318.
- (33) Jakins, C.; Lewars, E. *Theochem* **2000**, *531*, 181-192.

## Chapter 7 Conclusions

In this thesis, we have demonstrated a thorough study of cross-conjugated enyne oligomers. First, a sequence of protideprotection and palladium-catalyzed cross-coupling reactions between vinyl triflates and terminal acetylenes has been used to successfully assemble an unprecedented class of oligoenynes, namely *iso*-polydiacetylenes (*iso*-PDAs). This method has been successful up to nonameric stage using an iterative approach. Investigation of structure-property relationship for this oligomer series was then conducted via spectroscopic characterizations and X-ray structural analyses. Electronic absorption spectroscopic analysis shows a steadily bathochromic shift of  $\lambda_{\text{max}}$  with the progression of oligomeric chain length  $n$ , and this shift saturates at the nonameric stage. This result clearly indicates  $\pi$ -electronic communication across the *iso*-PDA oligomeric framework. Extrapolation of the optical bandgap ( $E_g$ ) versus the chain length  $n$  shows that this value reaches a constant at the stage of nonamer, indicating an effective conjugation length (ECL) of  $n_{\text{ECL}} = 9$ . In addition, in the electronic absorption cutoff for this oligomer series reaches saturation at 3.75 eV (331 nm); resulting in the so called “electronic transparency”. The presence of allylic hydrogens on the oligomer chains, however, reduces the stability of *iso*-PDAs, and as a result, limits their potential for applications. Although these isopropylidene substituted *iso*-PDAs are ideal models for the investigation of properties, they are not of usefulness and interest to us because of their moderately poor stability and solubility.

In an attempt to improve the stability and solubility of *iso*-PDA oligomers, a series of perphenylated *iso*-PDA oligomers ( $n = 2-15$ ) were constructed as the next

generation of *iso*-PDAs. The structural and electronic properties of these oligomers were characterized by various spectroscopic analyses and X-ray crystallography. To probe their third-order nonlinear optical properties, a new technique, namely DOKE, was employed to determine the second hyperpolarizabilities  $\gamma$  for this oligomer series ( $n = 2-15$ ). Interestingly, with the increase of chain length  $n$ , a superlinearly increase  $\gamma$  is observed as a function of oligomer length. Furthermore, incorporation of the diphenylmethyldene substituents onto the oligomeric chain not only enhances the stability and solubility, but also induces a conformational preference in solution state for longer oligomers ( $n > 7$ ). To date, the second hyperpolarizability for this oligomer series is about one order of magnitude lower than their linearly conjugated enyne oligomeric counterparts, however, the potential of improving  $\gamma$  by modifying the structures is still promising. In addition, molecular modeling study suggests that a longer oligomer favors a folded conformation, and this result is supported by studies using UV-vis and fluorescence spectroscopies, as well as the DOKE measurements. This unique folding property is sparsingly observed in the synthetic enyne oligomers, and will become one of the major research focuses in the future.

By introducing an additional carbon-carbon triple bond into each *iso*-PDA repeat unit, an extended series of cross-conjugated oligoenynes, namely *iso*-polytriacetylenes (*iso*-PTAs), was designed and realized. Utilizing a similar iterative strategy as employed for *iso*-PDA synthesis, the *iso*-PTA oligomers were prepared up to the length of pentamer. Poor stability and solubility for these highly unsaturated species, however, prohibited further elongation of the oligomeric chain. Characterization using spectroscopic and X-ray crystallographic methods has been conducted toward elucidating

structure-property relationships. UV-vis spectroscopic analyses show that there is insignificant  $\pi$ -electronic communication across the *iso*-PTA framework. This result confirms the fact that extending the length of each linearly conjugated segment leads to more localized electronic properties. As a result, electronic communication between each cross-conjugated segment is dramatically reduced. This is not completely unexpected in light of the limited delocalization potential of sp hybridized carbons.

The *iso*-PTA oligomers also provided a springboard toward a series of tetrayne-based oligoenyne hybrid molecules. Using the Cu-catalyzed oxidative homocoupling reactions, specifically Hay coupling, this series of oligomers was synthesized in satisfying yields. Electronic absorption spectroscopic analysis again showed that the pendant enyne moieties have no influence on the electronic characteristics of the tetrayne moiety via cross conjugation.

X-ray crystallographic analysis of the packing of tetrayne **157** in solid state suggests the possibility of a solid-state topochemical polymerization in preference of a 1,6-addition manner. This led to a project focused on the synthesis and properties of cross-conjugated tetrayne species with various pendant functionalities. Using Pd-catalyzed cross-coupling and Cu-catalyzed homocoupling reactions, these tetraynes have been successfully synthesized and characterized. Electronic absorption spectroscopic analysis shows that the pendant functionalities, ranging from strong electron donating to strong electron withdrawing groups, have little influence on the electronic characteristics of the central tetrayne moiety. X-ray structural analysis of tetrayne **163k** also suggests a possibility of 1,6-addition topochemical polymerization in the solid state. To deepen our understand of the solid-state polymerization behavior for these cross-conjugated

tetraynes, in depth studies on three tetraynes **163d**, **j**, **k** were conducted using various methods, such as DSC and TGA, solid-state UV-vis, and solid-state CP-MAS  $^{13}\text{C}$  NMR spectroscopies. These spectroscopic results supported the occurrence of predicted solid-state topochemical polymerizations. In particular, for tetrayne **163j**, evidences of regioselective topochemical polymerization were obtained from the DSC and solid-state  $^{13}\text{C}$  NMR spectroscopic analyses. These results also suggest, however, that geometrical parameters alone are not successful for predicting successful polymerization of tetraynes, since it can be readily complicated by numerous polymerization pathways.

In the last section of this thesis, other related works on cross-conjugated molecules have been included, which are: 1) modification of vinyl triflate building blocks, 2) the synthesis of strained cross-conjugated tetraynes, and 3) D/A functionalized cross-conjugated enynes. Although these works are not yet complete, they provide promise and potential as directions for this work. In addition to this experimental work, theoretical studies of cross-conjugated molecular systems, in particular, expanded radialenes, have also been performed using the density functional theory (DFT) method. Nucleus independent chemical shielding (NICS) calculations for this radialene series show that these molecules are nonaromatic.

## Chapter 8 Experimental

**General Experimental Details.** Column chromatography: *silica gel-60* (230-400 mesh) from *General Intermediates of Canada*. Size-exclusion chromatography (SEC): *Bio-Beads S-X1 Beads* from *Bio-Rad Laboratories*. Thin layer chromatography (TLC): aluminum sheet coated with *silica gel F<sub>254</sub>* from *Whatman*; visualization by UV light or  $\text{KMnO}_4$  stain. Melting point: *Fisher-Johns* or *Gallenkamp* apparatus; uncorrected. UV-Vis spectra: *Pharmacia Biotech Ultrospec 300* or *Varian Cary 400* at rt;  $\lambda$  in nm ( $\epsilon$  in  $\text{L mol}^{-1} \text{cm}^{-1}$ ). Fluorescence spectra: *PTI LPS-220B*; IR spectra ( $\text{cm}^{-1}$ ): *Nicolet Magna-IR 750* (neat) or *Nic-Plan IR Microscope* (solids).  $^1\text{H}$  and  $^{13}\text{C}$  NMR: *Varian Gemini-300*, -400, or -500 and *Bruker AM-300* instruments, at rt in  $\text{CDCl}_3$ ; solvent peaks (7.24 ppm for  $^1\text{H}$  and 77.0 ppm for  $^{13}\text{C}$ ) as reference. For simplicity, the coupling constants of the aryl protons for have been reported as pseudo first-order, even though they are second-order spin systems. EI MS ( $m/z$ ): *Kratos MS 50* instrument. ESI MS ( $m/z$ ): *Micromass Zabspec oaTOF* or *PE Biosystems Mariner TOF* instruments; solvent: MeOH or MeOH/toluene 3:1. Elemental analyses were performed by the Microanalytical Service, Department of Chemistry-University of Alberta. Differential scanning calorimetry (DSC): *Perkin Elmer Pyris 1 Differential Scanning Calorimeter*, and thermogravimetric analysis (TGA): *Perkin Elmer Pyris 1 Thermogravimetric Analyzer*.

**General Methods.** Reagents and solvents were purchased reagent grade and used without further purification. Compounds **95**,<sup>1</sup> **96**,<sup>3</sup> **130**,<sup>1</sup> **146**,<sup>2</sup> **124–126**,<sup>5</sup> **174**<sup>6</sup> were prepared as previously described. Compounds **161c–k** were obtained from cross-coupling of corresponding aryl iodide and trimethylsilylacetylene following by

desilylation under the general cross-coupling/desilylation conditions described below. Anhydrous  $\text{MgSO}_4$  was used as the drying agent after aqueous workup. Evaporation and concentration *in vacuo* was done at  $\text{H}_2\text{O}$ -aspirator pressure. All reactions were performed in standard glassware under an inert atmosphere of Ar or  $\text{N}_2$ . A positive pressure of Ar or  $\text{N}_2$  was essential to the success of all Pd-catalyzed reactions. Degassing of solvents was accomplished by vigorously bubbling Ar or  $\text{N}_2$  through the solution for at least 45 min. Flash chromatography was conducted on silica gel using the eluent system defined in the individual experimental procedures. EI MS were conducted at high resolution with  $\text{M}^+$  as the base peak unless otherwise noted in the respective experimentals. ESI spectra were done in MeOH or MeOH/toluene with added AgOTf in some cases.

X-Ray crystal data for **99**:<sup>7</sup> triclinic space group  $P\bar{1}$  (No. 2),  $D_c = 0.973 \text{ g cm}^{-3}$ ,  $Z = 4$ ,  $a = 14.440(3)$ ,  $b = 14.464(3)$ ,  $c = 15.314(2) \text{ \AA}$ ,  $\alpha = 111.702(3)^\circ$ ,  $\beta = 105.415(4)^\circ$ ,  $\gamma = 90.142(3)^\circ$ ,  $V = 2846.6(8) \text{ \AA}^3$ . Final  $R(F) = 0.0911$ ,  $wR^2(F^2) = 0.2607$  for 522 variables and 11521 data with  $F_o^2 \geq -3\sigma(F_o^2)$  (3980 observations [ $F_o^2 \geq 2\sigma(F_o^2)$ ]).

X-Ray crystal data for **101** (CCDC number: 86882): monoclinic space group  $C2/c$  (No. 15),  $D_c = 0.998 \text{ g cm}^{-3}$ ,  $Z = 4$ ,  $a = 21.0638(8)$ ,  $b = 15.4221(7)$ ,  $c = 11.8055(5) \text{ \AA}$ ,  $\beta = 95.757(4)^\circ$ ,  $V = 3815.7(3) \text{ \AA}^3$ . Final  $R(F) = 0.0709$ ,  $wR^2(F^2) = 0.1747$  for 182 variables and 2572 data with  $F_o^2 \geq -3\sigma(F_o^2)$  (2064 observations [ $F_o^2 \geq 2\sigma(F_o^2)$ ]).

X-Ray crystal data for **134**:<sup>7</sup> triclinic space group  $P\bar{1}$  (No. 2),  $D_c = 1.053 \text{ g cm}^{-3}$ ,  $Z = 2$ ,  $a = 10.4407(10)$ ,  $b = 10.7950(11)$ ,  $c = 13.3995(12) \text{ \AA}$ ,  $\alpha = 109.883(2)^\circ$ ,  $\beta = 110.009(2)^\circ$ ,  $\gamma = 93.3621(18)^\circ$ ,  $V = 1308.0(2) \text{ \AA}^3$ . Final  $R(F) = 0.0798$ ,  $wR^2(F^2) = 0.2684$  for 244 variables and 5319 data with  $F_o^2 \geq -3\sigma(F_o^2)$  (2202 observations [ $F_o^2 \geq 2\sigma(F_o^2)$ ]).

X-Ray crystal data for **136b**:<sup>7</sup> triclinic space group  $P\bar{1}$  (No. 2),  $D_c = 1.098 \text{ g cm}^{-3}$ ,  $Z = 2$ ,  $a = 9.4863(11)$ ,  $b = 15.3985(19)$ ,  $c = 15.4984(19) \text{ \AA}$ ,  $\alpha = 63.595(2)^\circ$ ,  $\beta = 83.603(2)^\circ$ ,  $\gamma = 79.586(2)^\circ$ ,  $V = 1993.1(4) \text{ \AA}^3$ . Final  $R(F) = 0.0782$ ,  $wR^2(F^2) = 0.2126$  for 433 variables and 8045 data with  $F_o^2 \geq -3\sigma(F_o^2)$  (4031 observations [ $F_o^2 \geq 2\sigma(F_o^2)$ ]).

X-Ray crystal data for **138**:<sup>7</sup> triclinic space group  $P\bar{1}$  (No. 2),  $D_c = 1.124 \text{ g cm}^{-3}$ ,  $Z = 2$ ,  $a = 12.5176(8)$ ,  $b = 14.7430(9)$ ,  $c = 16.0604(10) \text{ \AA}$ ,  $\alpha = 117.1350(10)^\circ$ ,  $\beta = 90.8121(12)^\circ$ ,  $\gamma = 103.0660(12)^\circ$ ,  $V = 2545.8(3) \text{ \AA}^3$ . Final  $R(F) = 0.0732$ ,  $wR^2(F^2) = 0.2133$  for 573 variables and 10250 data with  $F_o^2 \geq -3\sigma(F_o^2)$  (5688 observations [ $F_o^2 \geq 2\sigma(F_o^2)$ ]).

X-Ray crystal data for **137a**:<sup>7</sup> triclinic space group  $P\bar{1}$  (No. 2),  $D_c = 1.087 \text{ g cm}^{-3}$ ,  $Z = 1$ ,  $a = 8.5646(7)$ ,  $b = 9.4803(8)$ ,  $c = 14.5851(14) \text{ \AA}$ ,  $\alpha = 97.6378(16)^\circ$ ,  $\beta = 92.8192(17)^\circ$ ,  $\gamma = 90.452(2)^\circ$ ,  $V = 1172.19(18) \text{ \AA}^3$ . Final  $R(F) = 0.0594$ ,  $wR^2(F^2) = 0.1543$  for 253 variables and 4747 data with  $F_o^2 \geq -3\sigma(F_o^2)$  (2868 observations [ $F_o^2 \geq 2\sigma(F_o^2)$ ]).

X-Ray crystal data for **156**:<sup>7</sup> triclinic space group  $P\bar{1}$  (No. 2),  $D_c = 1.009 \text{ g cm}^{-3}$ ,  $Z = 4$ ,  $a = 14.1472(11)$ ,  $b = 15.3588(12)$ ,  $c = 17.4878(13) \text{ \AA}$ ,  $\alpha = 92.9484(15)^\circ$ ,  $\beta = 96.4437(15)^\circ$ ,  $\gamma = 97.6664(14)^\circ$ ,  $V = 3733.5(5) \text{ \AA}^3$ . Final  $R(F) = 0.0823$ ,  $wR^2(F^2) = 0.2466$  for 722 variables and 15141 data with  $F_o^2 \geq -3\sigma(F_o^2)$  (8508 observations [ $F_o^2 \geq 2\sigma(F_o^2)$ ]).

X-Ray crystal data for **157** (Structure A) (CCDC number: 88550): monoclinic space group  $P2_1/n$  (an alternative setting of  $P2_1/c$  [No. 14]),  $D_c = 0.993 \text{ g cm}^{-3}$ ,  $Z = 2$ ,  $a = 8.1266(9)$ ,  $b = 12.8068(13)$ ,  $c = 18.6241(19) \text{ \AA}$ ,  $\beta = 101.987(2)^\circ$ ,  $V = 1896.1(3) \text{ \AA}^3$ . Final

$R(F) = 0.0679$ ,  $wR_2(F^2) = 0.2053$  for 183 variables and 3863 data with  $F_o^2 \geq -3\sigma(F_o^2)$  (2397 observations [ $F_o^2 \geq 2\sigma(F_o^2)$ ]).

X-Ray crystal data for **157** (Structure B):<sup>7</sup> monoclinic space group  $P2_1/c$  (No. 14),  $D_c = 1.018 \text{ g cm}^{-3}$ ,  $Z = 4$ ,  $a = 13.5571(8)$ ,  $b = 7.7132(5)$ ,  $c = 35.616(2) \text{ \AA}$ ,  $\beta = 96.5990(10)^\circ$ ,  $V = 3699.7(4) \text{ \AA}^3$ . Final  $R(F) = 0.0472$ ,  $wR_2(F^2) = 0.1366$  for 365 variables and 7039 data with  $F_o^2 \geq -3\sigma(F_o^2)$  (4842 observations [ $F_o^2 \geq 2\sigma(F_o^2)$ ]).

X-Ray crystal data for **163k**:<sup>7</sup> monoclinic space group  $P2_1/c$  (No. 14),  $D_c = 1.355 \text{ g cm}^{-3}$ ,  $Z = 2$ ,  $a = 18.075(3)$ ,  $b = 7.4082(11)$ ,  $c = 11.7293(16) \text{ \AA}$ ,  $\beta = 103.751(3)^\circ$ ,  $V = 1525.6(4) \text{ \AA}^3$ . Final  $R(F) = 0.0562$ ,  $wR^2(F^2) = 0.0901$  for 212 variables and 3133 data with  $F_o^2 \geq -3\sigma(F_o^2)$  (1455 observations [ $F_o^2 \geq 2\sigma(F_o^2)$ ]).

X-Ray crystal data for **193a**:<sup>7</sup> monoclinic space group  $P2_1/c$  (No. 14),  $D_c = 1.133 \text{ g cm}^{-3}$ ,  $Z = 8$ ,  $a = 15.9322(15)$ ,  $b = 24.877(2)$ ,  $c = 11.8608(11) \text{ \AA}$ ,  $\beta = 103.1956(19)^\circ$ ,  $V = 4576.8(7) \text{ \AA}^3$ . Final  $R(F) = 0.0739$ ,  $wR^2(F^2) = 0.2045$  for 533 variables and 9396 data with  $F_o^2 \geq -3\sigma(F_o^2)$  (2703 observations [ $F_o^2 \geq 2\sigma(F_o^2)$ ]).<sup>7</sup>

X-Ray crystal data for **197a**:<sup>7</sup> monoclinic space group  $P2_1/c$  (No. 14),  $D_c = 1.326 \text{ g cm}^{-3}$ ,  $Z = 4$ ,  $a = 19.3515(17)$ ,  $b = 10.0900(9)$ ,  $c = 10.4497(9) \text{ \AA}$ ,  $\beta = 90.5693(18)^\circ$ ,  $V = 2040.3(3) \text{ \AA}^3$ . Final  $R(F) = 0.0321$ ,  $wR^2(F^2) = 0.0986$  for 257 variables and 4182 data with  $F_o^2 \geq -3\sigma(F_o^2)$  (3666 observations [ $F_o^2 \geq 2\sigma(F_o^2)$ ]).<sup>7</sup>

X-Ray crystal data for **197b**:<sup>7</sup> monoclinic space group  $P2_1$  (No. 4),  $D_c = 1.420 \text{ g cm}^{-3}$ ,  $Z = 2$ ,  $a = 12.4819(9)$ ,  $b = 6.0734(5)$ ,  $c = 12.6720(10) \text{ \AA}$ ,  $\beta = 94.7813(14)^\circ$ ,  $V = 957.29(13) \text{ \AA}^3$ . Final  $R(F) = 0.0330$ ,  $wR^2(F^2) = 0.0769$  for 255 variables and 3883 data with  $F_o^2 \geq -3\sigma(F_o^2)$  (3526 observations [ $F_o^2 \geq 2\sigma(F_o^2)$ ]).

**General Desilylation and Palladium-catalyzed Cross-coupling Procedure.** A mixture of the appropriate trimethylsilyl- or triisopropylsilyl-protected polyynes and  $K_2CO_3$  (ca. 0.2 equiv.) or TBAF (2.2 equiv.) in wet THF/MeOH (1:1, 20 mL) or THF (20 mL), respectively, was stirred at rt for 2 h. Ether and satd. aq.  $NH_4Cl$  were added, the organic phase separated, washed with satd. aq.  $NH_4Cl$  ( $2 \times 50$  mL), dried, reduced to ca. 1 mL, and added to a degassed solution of vinyl triflate in THF or DMF (20 mL).  $Pd(PPh_3)_4$  or  $PdCl_2(PPh_3)_2$  (ca. 0.05 equiv.) and *i*-Pr<sub>2</sub>NH or Et<sub>2</sub>NH were sequentially added, the solution stirred for 5 min, CuI (ca. 0.15 equiv.) was added and the solution stirred under conditions described in the individual procedures, until TLC analysis no longer showed the presence of the deprotected polyynes starting material. Ether and H<sub>2</sub>O were added, the organic phase separated, washed with satd. aq.  $NH_4Cl$  ( $2 \times 50$  mL), dried and the solvent removed *in vacuo*. Flash column chromatography or size-exclusion chromatography, and/or precipitation from MeOH gave the desired enyne oligomer.

**General Copper-catalyzed Oxidative Acetylenic Coupling Procedure.** The appropriate trimethylsilyl protected oligomer was desilylated in methanolic  $K_2CO_3$  as described above. Following workup, the solution of the deprotected product was reduced to ca. 1 mL and added to  $CH_2Cl_2$  or acetone (40 mL). A solution of the catalyst mixture [CuI (50 mg) and TMEDA (75 mg) added to  $CH_2Cl_2$  (2 mL) and stirred until homogeneous] or Hay catalyst<sup>4</sup> was then added. The mixture was stirred at rt under air until TLC analysis no longer showed the deprotected polyynes (generally less than 0.5 h). The reaction solution was concentrated *in vacuo* to ca. 5 mL and diethyl ether added (50 mL). The ethereal solution was consecutively washed with 10% HCl soln (25 mL), satd. aq.  $NaHCO_3$  (25 mL) and satd. aq. NaCl (25 mL), dried, and the solvent removed. Flash

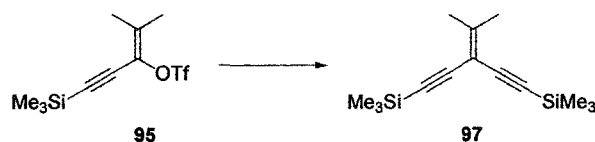
column chromatography and precipitation from MeOH gave the desired homo-coupled oligomer.

**Trifluoromethanesulfonic acid 2-methyl-1-triisopropylsilylethynylpropenyl ester (96).**



Reaction of 4-methyl-1-triisopropylsilylpent-1-yn-3-one with trifluoromethanesulfonic anhydride (4.53 g, 16.1 mmol) and 2,6-di-*t*-butyl-4-methylpyridine (2.72 g, 13.2 mmol) in CH<sub>2</sub>Cl<sub>2</sub> (50 mL) was conducted under argon for 24 h. The CH<sub>2</sub>Cl<sub>2</sub> was removed *in vacuo* and the residue extracted with pentane. The organic solution was washed with 10% HCl, satd. aq. NaHCO<sub>3</sub>, and brine. Evaporation followed by flash chromatography (hexane/CH<sub>2</sub>Cl<sub>2</sub> 2:1) gave **96** (2.72 g, 66%) as a clear light yellow oil. *R<sub>f</sub>* = 0.8 (hexane/CH<sub>2</sub>Cl<sub>2</sub> 2:1). IR (neat): 2946, 2868, 2150 cm<sup>-1</sup>. <sup>1</sup>H NMR (300 MHz, CDCl<sub>3</sub>): δ 1.99 (s, 3H), 1.90 (s, 3H), 1.07 (m, 21H). <sup>13</sup>C NMR (125 MHz, CDCl<sub>3</sub>): δ 138.1, 126.6, 118.3 (q, *J* = 263.4 Hz), 100.1, 96.2, 21.1, 18.7, 18.5, 11.2. EI HRMS: calcd for C<sub>16</sub>H<sub>27</sub>F<sub>3</sub>O<sub>3</sub>SSi (M<sup>+</sup>), 384.1402; found, 384.1404.

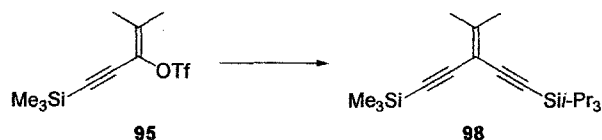
**1-Trimethylsilyl-3-trimethylsilylethynyl-4-methylpent-3-en-1-yne (97).**



Triflate **95** (0.300 g, 1.00 mmol) was cross-coupled with trimethylsilylacetylene (0.200 g, 2.04 mmol) in degassed THF (20 mL) in the presence of PdCl<sub>2</sub>(PPh<sub>3</sub>)<sub>2</sub> (35 mg, 0.05 mmol), diisopropylamine (3 mL), and CuI (20 mg, 0.11 mmol) for 2 h as described

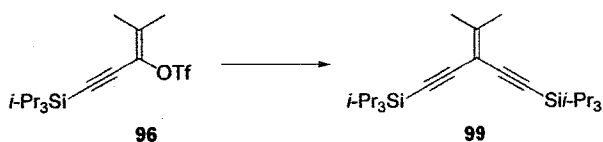
in the general procedure. Flash chromatography (hexane/CH<sub>2</sub>Cl<sub>2</sub> 5:1) afforded **97** (0.228 g, 92%) as a light yellow oil.  $R_f = 0.7$  (hexane/CH<sub>2</sub>Cl<sub>2</sub> 5:1). IR (neat): 2960, 2153, 1593 cm<sup>-1</sup>. <sup>1</sup>H NMR (300 MHz, CDCl<sub>3</sub>): δ 1.99 (s, 6H), 0.18 (s, 18H). <sup>13</sup>C NMR (75 MHz, CDCl<sub>3</sub>, APT): δ 156.9, 101.9, 101.5, 96.4, 22.8, 0.0. EI MS  $m/z$  (rel. intensity): 248.1 (M<sup>+</sup>, 76), 233.1 ([M - Me]<sup>+</sup>, 100). EI HRMS: calcd. for C<sub>14</sub>H<sub>24</sub>Si<sub>2</sub> (M<sup>+</sup>), 248.1417; found, 248.1417. Anal. Calcd for C<sub>14</sub>H<sub>24</sub>Si<sub>2</sub>: C, 67.66; H, 9.73. Found: C, 67.28; H, 9.88.

**1-Triisopropylsilyl-3-trimethylsilylethynyl-4-methylpent-3-en-1-yne (98).**



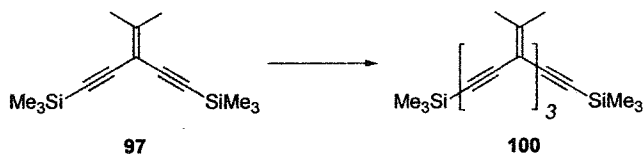
Triflate **95** (0.300 g, 1.00 mmol) was cross-coupled with triisopropylsilylacetylene (0.364 g, 2.00 mmol) in degassed DMF (20 mL) in the presence of Pd(PPh<sub>3</sub>)<sub>4</sub> (58 mg, 0.054 mmol), diethylamine (3 mL), and CuI (29 mg, 0.15 mmol) for 2 h as described in the general procedure. Flash chromatography (hexane/CH<sub>2</sub>Cl<sub>2</sub> 5:1) afforded **98** (0.280 g, 84%) as a colorless oil.  $R_f = 0.7$  (hexane/CH<sub>2</sub>Cl<sub>2</sub> 5:1). IR (neat): 2959, 2944, 2153, 1464 cm<sup>-1</sup>. <sup>1</sup>H NMR (300 MHz, CDCl<sub>3</sub>): δ 2.01 (s, 3H), 1.99 (s, 3H), 1.07 (s, 21H), 0.17 (s, 9H). <sup>13</sup>C NMR (75 MHz, CDCl<sub>3</sub>, APT): δ 155.6, 103.5, 102.3, 101.9, 96.1, 92.8, 22.7 (2×), 18.7, 11.4, 0.0. EI MS  $m/z$  (rel. intensity): 332.2 (M<sup>+</sup>, 24), 289.2 ([M - *i*-Pr]<sup>+</sup>, 100). EI HRMS: calcd for C<sub>20</sub>H<sub>36</sub>Si<sub>2</sub> (M<sup>+</sup>), 332.2356; found, 332.2354. Anal. Calcd for C<sub>20</sub>H<sub>36</sub>Si<sub>2</sub>: C, 72.21; H, 10.91. Found: C, 72.25; H, 10.77.

### 1-Triisopropylsilyl-3-triisopropylsilylethynyl-4-methylpent-3-en-1-yne (99).



Triflate **96** (0.770 g, 2.00 mmol) was cross-coupled with triisopropylsilylacetylene (0.730 g, 4.00 mmol) in degassed THF (40 mL) in the presence of PdCl<sub>2</sub>(PPh<sub>3</sub>)<sub>2</sub> (70 mg, 0.10 mmol), diisopropylamine (6 mL), and CuI (58 mg, 0.30 mmol) for 2 h as described in the general procedure. Flash chromatography (hexane/CH<sub>2</sub>Cl<sub>2</sub> 5:1) afforded **99** (0.816 g, 98%) as a colorless solid. *R<sub>f</sub>* = 0.7 (hexane/CH<sub>2</sub>Cl<sub>2</sub> 5:1). Mp: 52.5 °C. IR (μscope): 2956, 2941, 2891, 2865, 2151, 1461 cm<sup>-1</sup>. UV-vis (CHCl<sub>3</sub>): λ<sub>max</sub> (ε) 265 (16 500). <sup>1</sup>H NMR (300 MHz, CDCl<sub>3</sub>): δ 2.02 (s, 6H), 1.06 (s, 42 H). <sup>13</sup>C NMR (75 MHz, CDCl<sub>3</sub>, APT): δ 154.9, 103.8, 102.6, 92.5, 22.7, 18.7, 11.4. EI MS *m/z* (rel. intensity): 416.3 (M<sup>+</sup>, 63), 373.3 ([M - *i*-Pr]<sup>+</sup>, 100). EI HRMS: calcd for C<sub>26</sub>H<sub>48</sub>Si<sub>2</sub> (M<sup>+</sup>), 416.3295; found, 416.3306. X-ray.

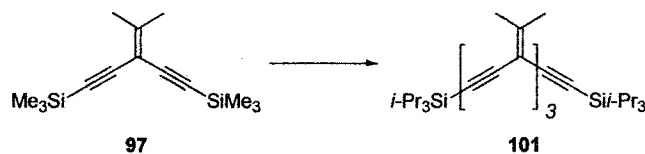
### 3,9-Bis(trimethylsilylethynyl)-2-10-dimethyl-6-isopropylidene-2,9-undecadiene-4,7-diyne (100).



Enediyne **97** (0.146 g, 0.590 mmol) was desilylated with K<sub>2</sub>CO<sub>3</sub>/MeOH and cross-coupled with triflate **8** (0.360 g, 1.20 mmol) in degassed DMF (20 mL) in the presence of Pd(PPh<sub>3</sub>)<sub>4</sub> (69 mg, 0.06 mmol), diisopropylamine (3 mL), and CuI (35 mg, 0.18 mmol) for 2 h as described in the general procedure. Flash chromatography (hexane/CH<sub>2</sub>Cl<sub>2</sub> 5:1)

afforded **100** (0.220 g, 92%) as a colorless solid.  $R_f = 0.5$  (hexane/CH<sub>2</sub>Cl<sub>2</sub> 5:1). Mp: 136 °C. IR (μscope): 2958, 2907, 2147, 1605 cm<sup>-1</sup>. UV-vis (CHCl<sub>3</sub>): λ<sub>max</sub> (ε) 286 (25 900), 309 (18 000). <sup>1</sup>H NMR (300 MHz, CDCl<sub>3</sub>): δ 1.87 (s, 6H), 1.84 (s, 6H), 1.82 (s, 6H), 0.19 (s, 18H). <sup>13</sup>C NMR (75 MHz, CDCl<sub>3</sub>, APT): δ 154.6, 152.8, 101.8, 101.7, 95.7, 88.7, 88.0, 22.8, 22.7 (2×), 0.0 (one coincident peak not observed). EI MS  $m/z$  (rel. intensity): 404.2 (M<sup>+</sup>, 50), 73.0 (Me<sub>3</sub>Si<sup>+</sup>, 100). EI HRMS: calcd for C<sub>26</sub>H<sub>36</sub>Si<sub>2</sub> (M<sup>+</sup>), 404.2356; found, 404.2354.

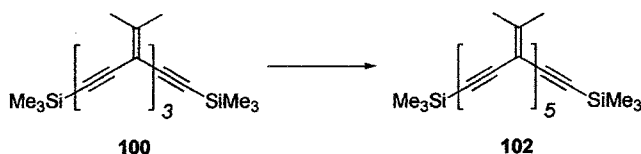
**3,9-Bis(triisopropylsilylethynyl)-2-10-dimethyl-6-isopropylidene-2,9-undecadiene-4,7-diyne (101).**



Enediyne **97** (0.279 g, 1.12 mmol) was desilylated with K<sub>2</sub>CO<sub>3</sub>/MeOH and cross-coupled with triflate **96** (0.870 g, 2.26 mmol) in degassed DMF (40 mL) in the presence of Pd(PPh<sub>3</sub>)<sub>4</sub> (0.13 g, 0.11 mmol), diisopropylamine (6 mL), and CuI (63 mg, 0.33 mmol) for 2 h as described in the general procedure. Flash chromatography (hexane/CH<sub>2</sub>Cl<sub>2</sub> 5:1) followed by precipitation from MeOH gave **101** (0.338 g, 53%) as a colorless solid.  $R_f = 0.7$  (hexane/CH<sub>2</sub>Cl<sub>2</sub> 5:1). Mp: 70–71 °C. IR (μscope): 2944, 2864, 2146, 1604 cm<sup>-1</sup>. UV-vis (CHCl<sub>3</sub>): λ<sub>max</sub> (ε) 286 (29 100), 312 (20 200). <sup>1</sup>H NMR (300 MHz, CDCl<sub>3</sub>): δ 2.07 (s, 6H), 2.05 (s, 6H), 2.03 (s, 6H), 1.09 (s, 42 H). <sup>13</sup>C NMR (75 MHz, CDCl<sub>3</sub>, APT): δ 153.7, 152.7, 103.8, 102.2, 101.6, 92.2, 88.6, 88.4, 22.8, 22.6 (2×), 18.7, 11.4. EI MS  $m/z$  (rel. intensity):

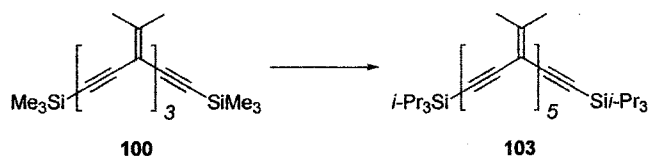
572.4 ( $M^+$ , 73), 157.1 ( $i\text{-Pr}_3\text{Si}^+$ , 100). EI HRMS: calcd for  $C_{38}H_{60}Si_2$  ( $M^+$ ), 572.4233; found, 572.4223. X-ray.

**3,15-Bis(trimethylsilylethynyl)-2,16-dimethyl-6,9,12-triisopropylidene-2,15-heptadecadiene-4,7,10,13-tetrayne (102).**



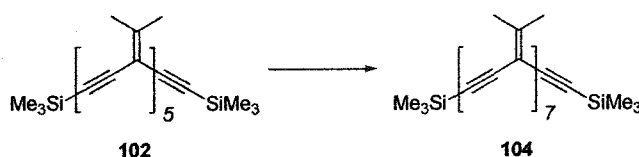
Trimer **100** (0.171 g, 0.42 mmol) was desilylated with  $K_2CO_3/MeOH$  and cross-coupled with triflate **95** (0.255 g, 0.85 mmol) in degassed DMF (20 mL) in the presence of  $Pd(PPh_3)_4$  (50 mg, 0.043 mmol), diethylamine (3 mL), and  $CuI$  (20 mg, 0.10 mmol) for 2 h as described in the general procedure. Flash chromatography (hexane/ $CH_2Cl_2$  5:1) and subsequent recrystallization from MeOH gave **102** (0.163 g, 69%) as a colorless solid.  $R_f = 0.3$  (hexane/ $CH_2Cl_2$  5:1). Mp: 196 °C (dec.). IR ( $\mu$ scope): 2958, 2906, 2147, 1605  $cm^{-1}$ . UV-vis ( $CHCl_3$ ):  $\lambda_{max}$  ( $\epsilon$ ) 281 (41 300).  $^1H$  NMR (300 MHz,  $CDCl_3$ ):  $\delta$  2.02 (s br, 24H), 1.99 (s, 6H), 0.17 (s, 18H).  $^{13}C$  NMR (125 MHz,  $CDCl_3$ ):  $\delta$  154.5, 152.6, 152.5, 101.9, 101.8 (2 $\times$ ), 95.8, 94.8, 88.7, 88.4, 88.3, 88.0, 22.8, 22.7 (4 $\times$ ), 0.1. EI HRMS: calcd for  $C_{38}H_{48}Si_2$  ( $M^+$ ), 560.3295; found, 560.3299.

**3,15-Bis(triisopropylsilylethynyl)-2,16-dimethyl-6,9,12-triisopropylidene-2,15-heptadecadiene-4,7,10,13-tetrayne (103).**



Trimer **100** (80 mg, 0.20 mmol) was desilylated with  $K_2CO_3/MeOH$  and cross-coupled with triflate **96** (0.152 g, 0.40 mmol) in degassed DMF (20 mL) in the presence of  $Pd(PPh_3)_4$  (23 mg, 0.020 mmol), diethylamine (3 mL), and CuI (11 mg, 0.058 mmol) for 2 h as described in the general procedure. Flash chromatography (hexane/ $CH_2Cl_2$  5:1) and recrystallization from MeOH gave **103** (0.120 g, 82%) as a colorless solid.  $R_f = 0.5$  (hexane/ $CH_2Cl_2$  5:1). Mp: 115–116 °C (dec.). IR ( $\mu$ scope): 2943, 2865, 2147, 1602  $cm^{-1}$ . UV–vis ( $CHCl_3$ ):  $\lambda_{max}$  ( $\epsilon$ ) 286 (43 600).  $^1H$  NMR (360 MHz,  $CDCl_3$ ):  $\delta$  2.03 (s, 6H), 2.01 (s, 18H), 2.00 (s, 6H), 1.08 (s, 42 H).  $^{13}C$  NMR (75 MHz,  $CDCl_3$ , APT):  $\delta$  153.8, 152.5, 152.4, 103.8, 102.2, 101.8, 92.2, 88.7, 88.4, 88.3, 22.8, 22.7, 22.6, 18.7, 11.4 (four coincident peaks not observed). EI HRMS: calcd for  $C_{50}H_{72}Si_2$  ( $M^+$ ), 728.5173; found, 728.5164.

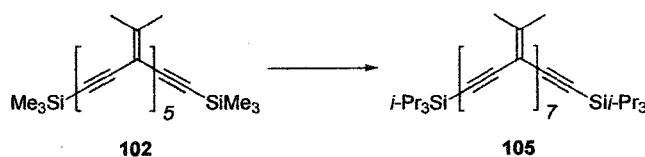
**3,21-Bis(trimethylsilylethynyl)-2,22-dimethyl-6,9,12,15,18-pentaisopropylidene-2,21-tricosadiene-4,7,10,13,16,19-hexayne (104).**



Pentamer **102** (56 mg, 0.10 mmol) was desilylated with  $K_2CO_3/MeOH$  and cross-coupled with triflate **95** (61 mg, 0.20 mmol) in degassed DMF (20 mL) in the presence of  $Pd(PPh_3)_4$  (23 mg, 0.020 mmol), diethylamine (3 mL), and CuI (11 mg, 0.058 mmol) for 2 h as described in the general procedure. Flash chromatography (hexane/ $CH_2Cl_2$  5:1) and recrystallization from MeOH gave **104** (54 mg, 75%) as a colorless solid.  $R_f = 0.2$  (hexane/ $CH_2Cl_2$  5:1). Mp: >170 °C (dec.). IR ( $\mu$ scope): 2959, 2906, 2148, 1606  $cm^{-1}$ . UV–vis ( $CHCl_3$ ):  $\lambda_{max}$  ( $\epsilon$ ) 282 (59 200).  $^1H$  NMR (300 MHz,  $CDCl_3$ ):  $\delta$  2.02 (s, 36H),

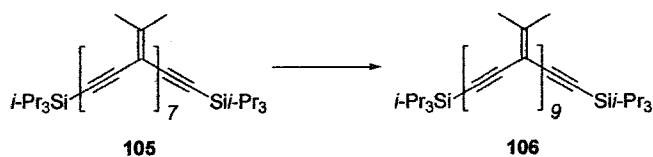
1.99 (s, 6H), 0.17 (s, 18H). EI HRMS: calcd for  $C_{50}H_{60}Si_2$  ( $M^+$ ), 716.4233; found, 716.4236. This oligomer was insufficiently soluble for meaningful  $^{13}C$  NMR spectroscopic analysis.

**3,21-Bis(triisopropylsilylethynyl)-2,22-dimethyl-6,9,12,15,18-pentaisopropylidene-2,21-tricosadiene-4,7,10,13,16,19-hexayne (105).**



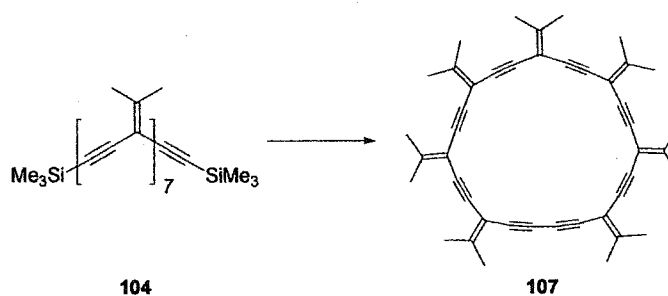
Pentamer **102** (83 mg, 0.15 mmol) was desilylated with  $K_2CO_3/MeOH$  and cross-coupled with triflate **96** (0.114 g, 0.304 mmol) in degassed DMF (20 mL) in the presence of  $Pd(PPh_3)_4$  (17 mg, 0.015 mmol), diethylamine (3 mL), and  $CuI$  (9 mg, 0.05 mmol) for 2 h as described in the general procedure. Flash chromatography (hexane/ $CH_2Cl_2$  5:1) and recrystallization from MeOH gave **105** (58 mg, 44%) as a colorless solid.  $R_f = 0.4$  (hexane/ $CH_2Cl_2$  5:1). Mp: 148 °C (dec.). IR ( $\mu$ scope): 2943, 2905, 2146, 1606  $cm^{-1}$ . UV-vis ( $CHCl_3$ ):  $\lambda_{max}$  ( $\epsilon$ ) 284 (62 900).  $^1H$  NMR (300 MHz,  $CDCl_3$ ):  $\delta$  2.03 (s, 6H), 2.01 (s, 30H), 2.00 (s, 6H), 1.06 (s, 42 H).  $^{13}C$  NMR (75 MHz,  $CDCl_3$ ):  $\delta$  153.8, 152.5, 152.4, 152.2, 103.8, 102.2, 101.9, 101.8, 92.2, 88.7, 88.4, 22.8, 22.7, 22.6, 18.7, 11.4 (nine coincident peaks not observed). EI HRMS: calcd for  $C_{62}H_{84}Si_2$  ( $M^+$ ), 884.6111; found, 884.6111.

**3,27-Bis(triisopropylsilylethynyl)-2,28-dimethyl-6,9,12,15,18,21,24-heptaisopropylidene-2,27-nonacosadiene-4,7,10,13,16,19,22,25-octayne (106).**



Heptamer **105** (19 mg, 0.021 mmol) was desilylated with TBAF and cross-coupled with triflate **96** (20 mg, 0.052 mmol) in degassed DMF (20 mL) in the presence of Pd(PPh<sub>3</sub>)<sub>4</sub> (28 mg, 0.024 mmol), diethylamine (0.6 mL), and CuI (14 mg, 0.073 mmol) for 15 min as described in the general procedure. The crude reaction solid was recrystallized from MeOH to give **106** (8 mg, 37%) as a colorless solid. Mp: >190 °C (dec.). IR (μscope): 2943, 2905, 2146, 1605 cm<sup>-1</sup>. UV-vis (CHCl<sub>3</sub>): λ<sub>max</sub> (ε) 283 (80 800). <sup>1</sup>H NMR (300 MHz, CDCl<sub>3</sub>): δ 2.04, (s, 6H), 2.02 (s, 42 H), 2.00 (s, 6H), 1.06 (s, 42 H). <sup>13</sup>C NMR (125.7 MHz, CDCl<sub>3</sub>): δ 153.8, 152.6, 152.4, 103.8, 102.2, 101.8 (3×), 92.2, 88.7, 88.4, 22.8, 22.7 (2×), 22.6 (2×), 18.7, 11.4 (thirteen coincident peaks not observed). Attempts for MS analyses were unsuccessful.

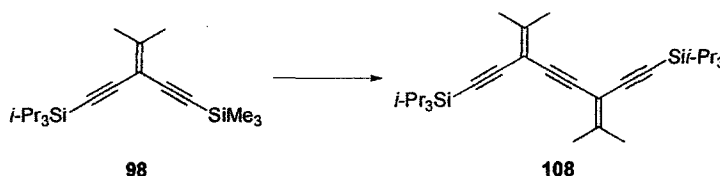
**5,8,11,14,17,20,23-Heptaisopropylidencyclotricosa-1,3,6,9,12,15,18,21-octayne (107).**



Heptamer **104** (20 mg, 0.028 mmol) was desilylated with K<sub>2</sub>CO<sub>3</sub>/MeOH as described in the general procedure and then oxidatively homocoupled in the presence of CuI (16 mg, 0.084 mmol), TMEDA (4.9 mg, 0.042 mmol), and THF (10 mL) under air

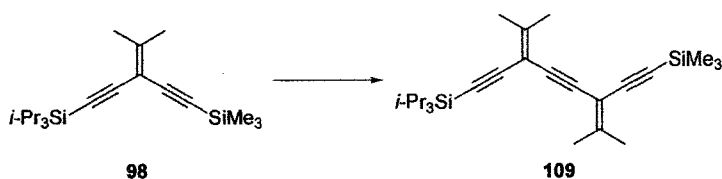
for 2 h. Flash chromatography (hexane/CH<sub>2</sub>Cl<sub>2</sub> 5:1) gave **107** (5 mg, 31%) as a colorless solid.  $R_f$  = 0.3 (hexane/CH<sub>2</sub>Cl<sub>2</sub> 5:1). Mp: >115 °C (dec.). UV-vis (CHCl<sub>3</sub>):  $\lambda_{\max}$  ( $\epsilon$ ) 280 (44 400), 336 (6 200). <sup>1</sup>H NMR (300 MHz, CDCl<sub>3</sub>):  $\delta$  2.07 (s, 12H), 2.04 (m, 30H). <sup>13</sup>C NMR (125 MHz, CDCl<sub>3</sub>, APT):  $\delta$  155.1, 152.8, 152.5, 152.4, 102.2, 101.8, 101.7 (2 $\times$ ), 100.7, 88.8, 88.4 (2 $\times$ ), 88.3, 88.2, 87.8, 80.6, 78.8, 22.9, 22.8, 22.7 (five coincident peaks not observed). EI HRMS: calcd for C<sub>44</sub>H<sub>42</sub> (M<sup>+</sup>), 570.3287; found, 570.3289.

### 3,6-Bis(triisopropylsilylethynyl)-2,7-dimethyl-2,6-octadiene-4-yne (**108**).



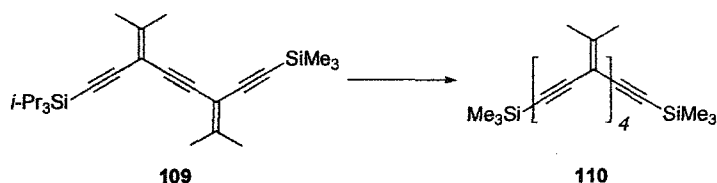
Enediyne **98** (79 mg, 0.24 mmol) was mono-desilylated with K<sub>2</sub>CO<sub>3</sub>/MeOH and cross-coupled with triflate **96** (91 mg, 0.24 mmol) in degassed DMF (20 mL) in the presence of Pd(PPh<sub>3</sub>)<sub>4</sub> (27 mg, 0.023 mmol), diethylamine (3 mL), and CuI (14 mg, 0.074 mmol) for 2 h as described in the general procedure. Flash chromatography (hexane/CH<sub>2</sub>Cl<sub>2</sub> 5:1) gave **108** (0.104 g, 88%) as a colorless solid.  $R_f$  = 0.8 (hexane/CH<sub>2</sub>Cl<sub>2</sub> 5:1). Mp: 65–66 °C. IR ( $\mu$ scope): 2943, 2865, 2145, 1463 cm<sup>-1</sup>. UV-vis (CHCl<sub>3</sub>):  $\lambda_{\max}$  ( $\epsilon$ ) 256 (23 400), 291 (18 700), 306 (16 100). <sup>1</sup>H NMR (300 MHz, CDCl<sub>3</sub>):  $\delta$  2.04, (s, 6H), 1.99 (s, 6H), 1.06 (s, 42H). <sup>13</sup>C NMR (75 MHz, CDCl<sub>3</sub>):  $\delta$  153.8, 103.7, 102.2, 92.2, 88.6, 22.8, 22.5, 18.7, 11.4. EI HRMS: calcd for C<sub>32</sub>H<sub>54</sub>Si<sub>2</sub> (M<sup>+</sup>), 494.3764; found, 494.3768.

**3-(Triisopropylsilylethynyl)-6-(trimethylsilylethynyl)-2,7-dimethyl-2,6-octadiene-4-yne (109).**



Enediyne **98** (0.140 g, 0.421 mmol) was desilylated with  $\text{K}_2\text{CO}_3/\text{MeOH}$  and cross-coupled with triflate **95** (0.127 g, 0.423 mmol) in degassed DMF (20 mL) in the presence of  $\text{Pd}(\text{PPh}_3)_4$  (24 mg, 0.021 mmol), diethylamine (3 mL), and  $\text{CuI}$  (12 mg, 0.063 mmol) for 40 min as described in the general procedure. Flash chromatography (hexane/ $\text{CH}_2\text{Cl}_2$  5:1) gave **109** (0.140 g, 81%) as a yellow oil.  $R_f = 0.7$  (hexane/ $\text{CH}_2\text{Cl}_2$  5:1). IR ( $\text{CH}_2\text{Cl}_2$ , cast): 2943, 2865, 2149, 1601  $\text{cm}^{-1}$ .  $^1\text{H}$  NMR (300 MHz,  $\text{CDCl}_3$ ):  $\delta$  2.32 (s, 3H), 2.30 (s, 3H), 2.29 (s, 3H), 2.27 (s, 3H), 1.35 (s, 21H), 0.46 (s, 9H).  $^{13}\text{C}$  NMR (75 MHz,  $\text{CDCl}_3$ ):  $\delta$  154.4, 153.8, 103.8, 102.2, 101.9, 101.8, 95.8, 92.2, 88.8, 88.3, 22.8 (2 $\times$ ), 22.6 (2 $\times$ ), 18.7, 11.4, 0.0. EI HRMS: calcd for  $\text{C}_{26}\text{H}_{42}\text{Si}_2$  ( $\text{M}^+$ ), 410.2825; found, 410.2829.

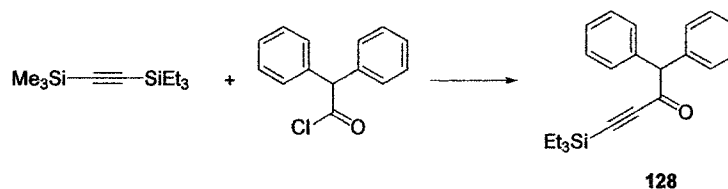
**3,12-Bis(trimethylsilylethynyl)-2,13-dimethyl-6,9-diisopropylidene-2,12-tetradecadiene-4,7,10-triyne (110).**



Dimer **109** (88 mg, 0.21 mmol) was desilylated with TBAF and cross-coupled with triflate **95** (0.128 g, 0.428 mmol) in degassed DMF (20 mL) in the presence of  $\text{Pd}(\text{PPh}_3)_4$  (25 mg, 0.022 mmol), diethylamine (3 mL), and  $\text{CuI}$  (12 mg, 0.063 mmol) for

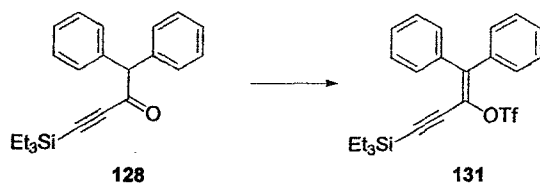


**1,1-Diphenyl-4-triethylsilylbut-3-yn-2-one (128).**



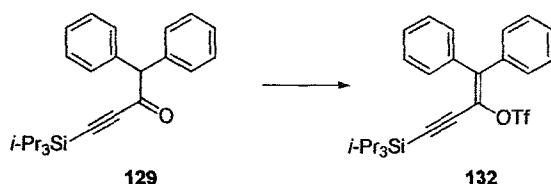
1-Triethylsilyl-2-trimethylsilylacetylene (2.12 g, 0.0100 mol) and diphenylacetyl chloride (2.31 g, 0.0100 mol) in  $\text{CH}_2\text{Cl}_2$  (200 mL) were placed into a flask at 0 °C under nitrogen atmosphere. Aluminium chloride (1.33 g, 0.0100 mol) was slowly added in portions, while the solution was stirred at 0 °C. The solution was kept stirring at 0 °C for 30 min, then poured into a mixture of 10% HCl soln (200 mL) and ice (200 g). The aqueous layer was extracted with ethyl acetate (3 × 50 mL) and the combined organic phases were subsequently washed with satd. aq.  $\text{NaHCO}_3$  and brine, and then dried with  $\text{MgSO}_4$ . Removal of the solvents *in vacuo* and followed by a flash column chromatography (hexanes/ $\text{CH}_2\text{Cl}_2$  2:1) over  $\text{SiO}_2$  afforded **128** (2.37 g, 71%) as a yellow oil.  $R_f = 0.4$  (hexanes/ $\text{CH}_2\text{Cl}_2$  2:1). IR ( $\text{CH}_2\text{Cl}_2$ , cast): 3062, 3029, 2957, 2912, 2875, 2146, 1680, 1600, 1495, 1453  $\text{cm}^{-1}$ .  $^1\text{H}$  NMR (300 MHz,  $\text{CDCl}_3$ ):  $\delta$  7.32-7.21 (m, 10H), 5.13 (s, 1H), 0.83 (t,  $J = 8.1$  Hz, 9H), 0.50 (q,  $J = 8.1$  Hz, 6H).  $^{13}\text{C}$  NMR (75 MHz,  $\text{CDCl}_3$ , APT):  $\delta$  185.5, 137.6, 129.4, 128.7, 127.5, 103.4, 99.6, 66.3, 7.2, 3.8. EI MS  $m/z$  (rel. intensity): 334.2 ( $\text{M}^+$ , 3.23), 167.1 ( $[\text{Ph}_2\text{CH}]^+$ , 100). EI HRMS: calcd for  $\text{C}_{22}\text{H}_{26}\text{Si}_2$  ( $\text{M}^+$ ), 334.1753; found, 334.1754.

**Trifluoromethanesulfonic acid 1-diphenylmethylidene-3-triethylsilyl-prop-2-ynyl ester (131).**



Reaction of **128** (2.30 g, 6.88 mmol) with trifluoromethanesulfonic anhydride (2.31 mL, 13.8 mmol) and 2,6-di-*t*-butyl-4-methylpyridine (2.12 g, 10.3 mmol) in CH<sub>2</sub>Cl<sub>2</sub> (50 mL) was conducted under argon for 3 days. The CH<sub>2</sub>Cl<sub>2</sub> was removed *in vacuo* and the residue extracted with pentane. The organic solution was washed with 10% HCl, satd. aq. NaHCO<sub>3</sub>, and brine. Evaporation followed by flash chromatography (hexane/CH<sub>2</sub>Cl<sub>2</sub> 2:1) gave **131** (2.55 g, 79%) as a clear light yellow oil.  $R_f = 0.6$  (hexanes/CH<sub>2</sub>Cl<sub>2</sub> 2:1). IR (CH<sub>2</sub>Cl<sub>2</sub>, cast): 3060, 2958, 2913, 2877, 2149, 1600, 1424 cm<sup>-1</sup>. <sup>1</sup>H NMR (400 MHz, CDCl<sub>3</sub>): δ 7.46–7.43 (m, 2H), 7.35–7.30 (m, 6H), 7.26–7.24 (m, 2H), 0.91 (t,  $J = 8.4$  Hz, 9H), 0.57 (q,  $J = 8.4$  Hz, 6H). <sup>13</sup>C NMR (100 MHz, CDCl<sub>3</sub>, APT): δ 143.7, 136.7, 135.9, 130.3, 129.9, 129.1, 129.0, 128.2, 127.9, 126.2, 118.1 (q,  $J = 255.8$  Hz), 103.0, 97.3, 7.2, 4.2. EI HRMS: calcd for C<sub>23</sub>H<sub>25</sub>F<sub>3</sub>O<sub>3</sub>SSi (M<sup>+</sup>), 466.1246; found, 466.1253.

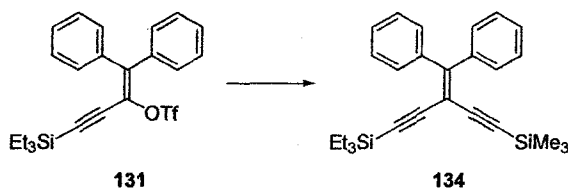
**Trifluoromethanesulfonic acid 1-diphenylmethylidene-3-triisopropylsilyl-prop-2-ynyl ester (132).**



Reaction of **129** (1.30 g, 3.45 mmol) with trifluoromethanesulfonic anhydride (1.46 mL, 5.17 mmol) and 2,6-di-*t*-butyl-4-methyl pyridine (1.00 g, 4.87 mmol) in

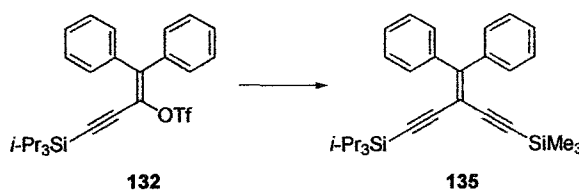
CH<sub>2</sub>Cl<sub>2</sub> (50 mL) was conducted under argon for 2 weeks. The CH<sub>2</sub>Cl<sub>2</sub> was removed *in vacuo* and the residue extracted with pentane. The organic solution was washed with 10% HCl, satd. aq. NaHCO<sub>3</sub>, and brine. Evaporation followed by flash chromatography (hexane/CH<sub>2</sub>Cl<sub>2</sub> 2:1) gave **132** (562 mg, 32%) as a clear light yellow oil. *R<sub>f</sub>* = 0.7 (hexanes/CH<sub>2</sub>Cl<sub>2</sub> 2:1). IR (CH<sub>2</sub>Cl<sub>2</sub>, cast): 3060, 3025, 2945, 2892, 2867, 2148, 1601, 1494, 1424 cm<sup>-1</sup>. <sup>1</sup>H NMR (300 MHz, CDCl<sub>3</sub>): δ 7.47–7.43 (m, 2H), 7.40–7.32 (m, 6H), 7.29–7.26 (m, 2H), 1.02 (s, 21H). EI HRMS: calcd for C<sub>26</sub>H<sub>31</sub>F<sub>3</sub>O<sub>3</sub>SSi (M<sup>+</sup>), 508.1715; found, 508.1714.

### 3-Diphenylmethylidene-1-triethylsilyl-5-trimethylsilyl-1,4-pentadiyne (**134**).



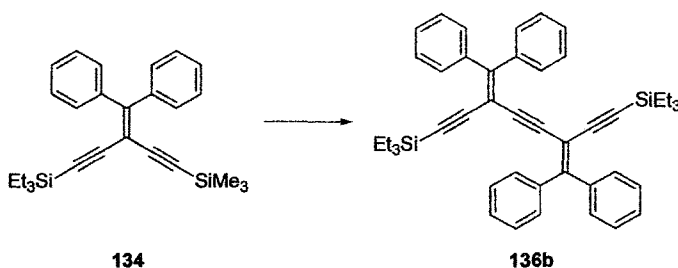
Triflate **131** (466 mg, 1.00 mmol) was cross-coupled with trimethylsilylacetylene (150 mg, 1.53 mmol) in degassed THF (20 mL) in the presence of PdCl<sub>2</sub>(PPh<sub>3</sub>)<sub>2</sub> (35 mg, 0.05 mmol), diisopropylamine (3 mL), and CuI (17 mg, 0.09 mmol) for 12 h under reflux as described in the general procedure. Flash chromatography (hexane/CH<sub>2</sub>Cl<sub>2</sub> 2:1) afforded **134** (392 mg, 95%) as a pale yellow solid. *R<sub>f</sub>* = 0.5 (hexanes/CH<sub>2</sub>Cl<sub>2</sub> 2:1). Mp: 61–62 °C. IR (μscope): 3053, 2957, 2146, 1442 cm<sup>-1</sup>. <sup>1</sup>H NMR (300 MHz, CDCl<sub>3</sub>): δ 7.43–7.38 (m, 4H), 7.29–7.24 (m, 6H), 0.89 (t, *J* = 7.5 Hz, 9H), 0.52 (q, *J* = 7.5 Hz, 6H), 0.09 (s, 9H). <sup>13</sup>C NMR (75 MHz, CDCl<sub>3</sub>, APT): δ 157.6, 140.2, 140.1, 130.4, 130.3, 128.5, 128.4, 127.6, 127.5, 104.4, 103.5, 102.2, 97.7, 95.8, 7.4, 4.3, -0.4. EI HRMS: calcd for C<sub>27</sub>H<sub>34</sub>Si<sub>2</sub> (M<sup>+</sup>), 414.2199; found, 414.2206. X-ray.

### 3-Diphenylmethylidene-1-triethylsilyl-5-trimethylsilyl-1,4-pentadiyne (135).



Triflate **132** (102 mg, 0.201 mmol) was cross-coupled with trimethylsilyl-acetylene (39 mg, 0.21 mmol) in degassed THF (20 mL) in the presence of  $\text{PdCl}_2(\text{PPh}_3)_2$  (7 mg, 0.01 mmol), diisopropylamine (1 mL), and CuI (4 mg, 0.02 mmol) for 12 h under reflux as described in the general procedure. Flash chromatography (hexane/ $\text{CH}_2\text{Cl}_2$  2:1) afforded **135** (82 mg, 90%) as a pale yellow solid.  $R_f = 0.6$  (hexanes/ $\text{CH}_2\text{Cl}_2$  2:1). Mp: 79–81 °C. IR ( $\mu$ scope): 3056, 2959, 2151, 1443  $\text{cm}^{-1}$ .  $^1\text{H}$  NMR (300 MHz,  $\text{CDCl}_3$ ):  $\delta$  7.46–7.38 (m, 4H), 7.34–7.29 (m, 6H), 1.01 (s, 21H), 0.12 (s, 9H).  $^{13}\text{C}$  NMR (75 MHz,  $\text{CDCl}_3$ , APT):  $\delta$  157.4, 140.6, 140.3, 130.6 (2 $\times$ ), 128.9, 128.8, 128.1, 127.9, 105.4, 103.9, 102.6, 98.1, 95.4, 19.5, 11.7,  $-0.4$ . EI HRMS: calcd for  $\text{C}_{30}\text{H}_{46}\text{Si}_2$  ( $\text{M}^+$ ), 456.2669; found, 456.2670.

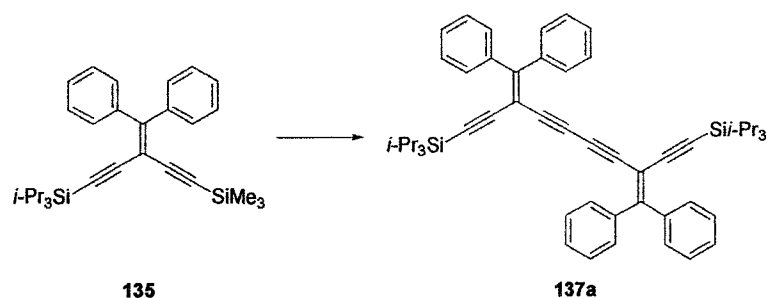
### 3,6-Bis(diphenylmethylidene)-1,8-bis(trimethylsilyl)-1,6,7-octatriyne (136b).



Monomer **134** (100 mg, 0.241 mmol) was selectively desilylated with  $\text{K}_2\text{CO}_3$  in MeOH/THF (1:1) and cross-coupled with triflate **131** (112 mg, 0.241 mmol) in degassed

THF (20 mL) in the presence of Pd(PPh<sub>3</sub>)<sub>4</sub> (12 mg, 0.010 mmol), diisopropylamine (1 mL), and CuI (6 mg, 0.03 mmol) for 12 h under reflux as described in the general procedure. Flash chromatography (hexane/CH<sub>2</sub>Cl<sub>2</sub> 2:1) gave **136b** (148 mg, 93%) as a yellow solid. *R<sub>f</sub>* = 0.6 (hexanes/CH<sub>2</sub>Cl<sub>2</sub> 2:1). Mp: 67–69 °C. IR (CH<sub>2</sub>Cl<sub>2</sub>, cast): 3054, 2955, 2874, 2143, 1442 cm<sup>-1</sup>. UV–vis (CHCl<sub>3</sub>): λ<sub>max</sub> (ε) 324 (16 800), 373 (18 500). <sup>1</sup>H NMR (500 MHz, CDCl<sub>3</sub>): δ 7.39–7.34 (m, 8H), 7.28–7.18 (m, 12H), 0.87 (t, *J* = 8.0 Hz, 18H), 0.51 (q, *J* = 8.0 Hz, 12H). <sup>13</sup>C NMR (125 MHz, CDCl<sub>3</sub>, APT): δ 156.3, 140.4, 139.8, 130.3, 130.1, 128.4, 128.2, 127.5, 127.4, 103.9, 102.1, 95.1, 90.5, 7.5, 4.3. EI HRMS: calcd for C<sub>46</sub>H<sub>50</sub>Si<sub>2</sub> (M<sup>+</sup>), 658.3451; found, 658.3449. ESI MS *m/z* (MeOH/toluene 3:1, AgOTf added): 767.2 ([M + Ag<sup>+</sup>]<sup>+</sup>). X-ray.

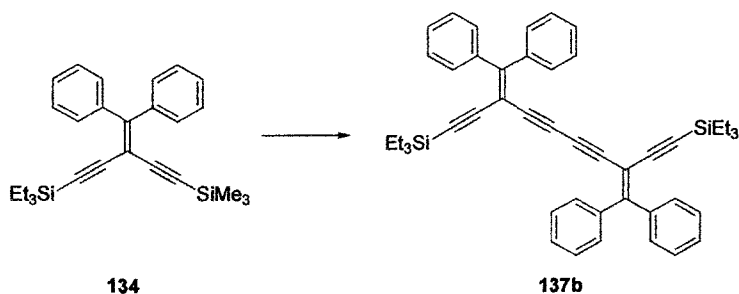
### 3,8-Bis(diphenylmethylidene)-1,10-bis(triisopropylsilyl)-1,4,6,9-decatetrayne (**137a**).



Monomer **135** (89 mg, 0.195 mmol) was selectively desilylated with K<sub>2</sub>CO<sub>3</sub> in MeOH/THF (1:1) and cross-coupled with triflate **132** (99 mg, 0.20 mmol) was attempted in degassed THF (20 mL) in the presence of PdCl<sub>2</sub>(PPh<sub>3</sub>)<sub>2</sub> (7 mg, 0.01 mmol), diisopropylamine (2 mL), and CuI (3.5 mg, 0.018 mmol) for 12 h under reflux as described in the general procedure. Flash chromatography (hexane/CH<sub>2</sub>Cl<sub>2</sub> 2:1) gave homocoupled product **137a** (50 mg, 70%) as a yellow solid. *R<sub>f</sub>* = 0.4 (hexanes/CH<sub>2</sub>Cl<sub>2</sub> 2:1). Mp: 127–131 °C. IR (CHCl<sub>3</sub>, cast): 3054, 2942, 2864, 2146, 1442 cm<sup>-1</sup>. UV–vis (CHCl<sub>3</sub>): λ<sub>max</sub> (ε) 338

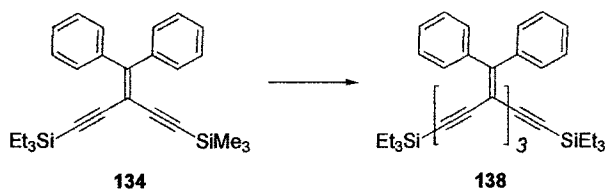
(23 100), 379 (24 600).  $^1\text{H}$  NMR (300 MHz,  $\text{CD}_2\text{Cl}_2$ ):  $\delta$  7.43-7.28 (m, 20H), 1.01 (s, 42H).  $^{13}\text{C}$  NMR (75 MHz,  $\text{CD}_2\text{Cl}_2$ , APT):  $\delta$  160.0, 140.2, 140.2, 130.6, 130.4, 129.4, 129.2, 128.2 (2 $\times$ ), 104.1, 101.5, 96.2, 82.2, 76.4, 18.7, 11.7. EI HRMS: calcd for  $\text{C}_{54}\text{H}_{62}\text{Si}_2$  ( $\text{M}^+$ ), 766.4390; found, 766.4381. X-ray.

**3,8-Bis(diphenylmethylidene)-1,10-bis(triethylsilyl)-1,4,6,9-decatetrayne (137b).**



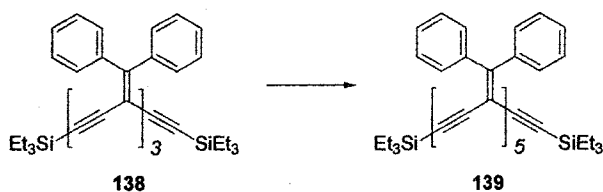
Homocoupled dimer **137b** was isolated from the synthesis of **136b** as a yellow solid in < 3% yield.  $R_f = 0.5$  (hexanes/ $\text{CH}_2\text{Cl}_2$  2:1). Mp: 89–91 °C. IR ( $\text{CDCl}_3$ , cast): 3054, 2954, 2874, 2148, 1442  $\text{cm}^{-1}$ .  $^1\text{H}$  NMR (500 MHz,  $\text{CDCl}_3$ ):  $\delta$  7.43–7.36 (m, 8H), 7.35–7.26 (m, 12H), 0.88 (t,  $J = 7.5$  Hz, 18H), 0.53 (q,  $J = 7.5$  Hz, 12H).  $^{13}\text{C}$  NMR (125 MHz,  $\text{CDCl}_3$ , APT):  $\delta$  159.4, 139.8, 139.6, 130.3, 130.1, 128.8, 128.6, 127.7, 127.5, 103.2, 101.1, 96.4, 81.6, 76.8, 7.4, 4.3. EI HRMS: calcd for  $\text{C}_{48}\text{H}_{50}\text{Si}_2$  ( $\text{M}^+$ ), 682.3451; found, 682.3472.

**1,11-Bis(triethylsilyl)-3,6,9-tri(diphenylmethylidene)-1,4,7,10-undecatetrayne (138).**



Monomer **134** (100 mg, 0.241 mmol) was desilylated with 2 equiv. of TBAF and cross-coupled with triflate **131** (224 mg, 0.480 mmol) in degassed THF (20 mL) in the presence of Pd(PPh<sub>3</sub>)<sub>4</sub> (28 mg, 0.024 mmol), diisopropylamine (2 mL), and CuI (14 mg, 0.074 mmol) for 12 h under refluxing, as described in the general procedure. Flash chromatography (hexane/CH<sub>2</sub>Cl<sub>2</sub> 2:1) gave **138** (168 mg, 81%) as a yellow solid. *R<sub>f</sub>* = 0.8 (hexanes/CH<sub>2</sub>Cl<sub>2</sub> 2:1). Mp: 60–61 °C. IR (μscope): 3054, 2954, 2910, 2874, 2143, 1492, 1442 cm<sup>-1</sup>. UV-vis (CHCl<sub>3</sub>): λ<sub>max</sub> (ε) 324 (26 200), 375 (31 100). <sup>1</sup>H NMR (500 MHz, CD<sub>2</sub>Cl<sub>2</sub>): δ 7.44–7.24 (m, 30H), 0.92 (t, *J* = 8.0 Hz, 18H), 0.57 (q, *J* = 8.0 Hz, 12H). <sup>13</sup>C NMR (125 MHz, CD<sub>2</sub>Cl<sub>2</sub>, APT): δ 157.5, 155.6, 140.7, 140.4, 140.3, 130.7, 130.6, 129.1, 129.0, 128.9, 128.2, 128.1, 128.0, 104.2, 102.3, 102.2, 96.0, 90.9, 90.2, 7.6, 4.6 (one coincident peak not observed). ESI MS *m/z* (MeOH/toluene 3:1): 883.4 ([M + Na<sup>+</sup>]<sup>+</sup>). X-ray.

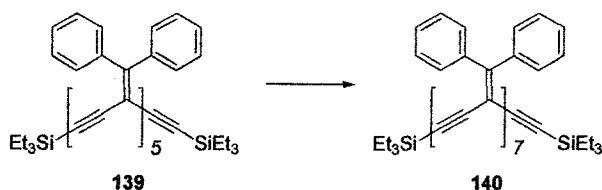
**1,17-Bis(triethylsilyl)-3,6,9,12,15-penta(diphenylmethylidene)-1,4,7,10,13,16-heptadecahexayne (139).**



Trimer **138** (140 mg, 0.162 mmol) was desilylated with 2 equiv. of TBAF and cross-coupled with triflate **131** (154 mg, 0.330 mmol) in degassed THF (20 mL) in the presence of Pd(PPh<sub>3</sub>)<sub>4</sub> (19 mg, 0.016 mmol), diisopropylamine (2 mL), and CuI (10 mg, 0.053 mmol) for 12 h under refluxing, as described in the general procedure. Flash chromatography (hexane/CH<sub>2</sub>Cl<sub>2</sub> 2:1) gave **139** (148 mg, 72%) as a yellow solid. *R<sub>f</sub>* = 0.8 (hexanes/CH<sub>2</sub>Cl<sub>2</sub>

2:1). Mp: 85–86 °C. IR (CHCl<sub>3</sub>, cast): 3053, 2954, 2932, 2873, 2141, 1492, 1442 cm<sup>-1</sup>. UV–vis (CHCl<sub>3</sub>): λ<sub>max</sub> (ε) 377 (49 300). <sup>1</sup>H NMR (500 MHz, CDCl<sub>3</sub>): δ 7.40–7.13 (m, 50H), 0.88 (t, *J* = 7.5 Hz, 18H), 0.52 (q, *J* = 7.5 Hz, 12H). <sup>13</sup>C NMR (125 MHz, CDCl<sub>3</sub>, APT): δ 156.8, 154.8 (2×), 140.4, 140.0 (2×), 139.8, 130.3, 130.2, 130.1, 128.6, 128.4 (2×), 128.2, 127.7, 127.6, 127.5, 127.4, 104.0, 102.1, 102.0, 95.2, 90.7, 90.3, 90.1 (2×), 7.5, 4.4 (six coincident peaks not observed). ESI MS *m/z* (MeOH/toluene 3:1, AgOTf added): 1373.5 ([M + Ag<sup>+</sup>]<sup>+</sup>). MALDI-TOF MS *m/z* (matrix, retinoic acid): 1264.5 (M<sup>+</sup>).

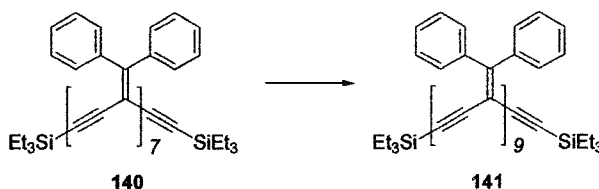
**1,12-Bis(triethylsilyl)-3,6,9,12,15,18,21-hepta(diphenylmethylidene)-  
1,4,7,10,13,16,19,22-tricosaoctayne (140).**



Pentamer **139** (148 mg, 0.117 mmol) was desilylated with 2 equiv. of TBAF and cross-coupled with triflate **131** (109 mg, 0.234 mmol) in degassed THF (20 mL) in the presence of Pd(PPh<sub>3</sub>)<sub>4</sub> (14 mg, 0.012 mmol), diisopropylamine (2 mL), and CuI (7 mg, 0.04 mmol) for 12 h under reflux as described in the general procedure. Flash chromatography (hexane/CH<sub>2</sub>Cl<sub>2</sub> 2:1) gave **140** (190 mg, 97%) as a yellow solid. *R<sub>f</sub>* = 0.8 (hexanes/CH<sub>2</sub>Cl<sub>2</sub> 2:1). Mp: 124–126 °C. IR (μscope): 3054, 2954, 2932, 2910, 2874, 2141, 1598, 1492, 1442 cm<sup>-1</sup>. UV–vis (CHCl<sub>3</sub>): λ<sub>max</sub> (ε) 378 (76 800). <sup>1</sup>H NMR (400 MHz, CDCl<sub>3</sub>): δ 7.44–7.16 (m, 70H), 0.91 (t, *J* = 8.0 Hz, 18H), 0.55 (q, *J* = 8.0 Hz, 12H). <sup>13</sup>C NMR (100 MHz, CDCl<sub>3</sub>, APT): δ 156.9, 155.4, 155.1, 154.9, 140.5, 140.1, 140.0 (2×), 139.9, 139.8, 130.4, 130.3, 130.2, 128.7 (2×), 128.6, 128.5, 128.4, 128.3, 127.7

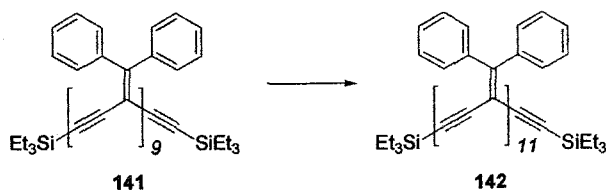
(3×), 127.6, 127.5, 104.0, 102.1, 102.0 (2×), 95.2, 90.8, 90.4, 90.2 (2×), 90.1, 7.4, 4.2 (eight coincident peaks not observed). ESI MS  $m/z$  (MeOH/toluene 3:1, AgOTf added): 1778.6 ( $[M + Ag^{++}]^+$ ).

**1,29-Bis(triethylsilyl)-3,6,9,12,15,18,21,24,27-nona(diphenylmethylidene)-1,4,7,10,13,16,19,22,25,28-nonacosadecayne (141).**



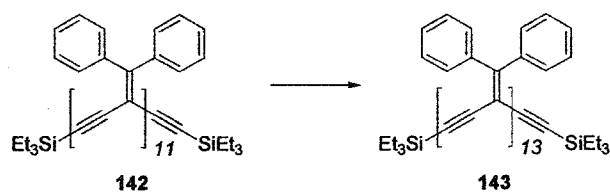
Heptamer **140** (39 mg, 0.023 mmol) was desilylated with 2 equiv. of TBAF and cross-coupled with triflate **131** (22 mg, 0.047 mmol) in degassed THF (20 mL) in the presence of Pd(PPh<sub>3</sub>)<sub>4</sub> (3 mg, 0.003 mmol), diisopropylamine (2 mL), and CuI (1.5 mg, 0.0079 mmol) for 12 h under refluxing, as described in the general procedure. Size-exclusion chromatography (CH<sub>2</sub>Cl<sub>2</sub>) gave **141** (36 mg, 74%) as a yellow solid. Mp: 134–135 °C. IR (CH<sub>2</sub>Cl<sub>2</sub>, cast): 3053, 2954, 2873, 2140, 1599, 1492, 1442 cm<sup>-1</sup>. UV-vis (CHCl<sub>3</sub>): λ<sub>max</sub> (ε) 378 (96 900). <sup>1</sup>H NMR (400 MHz, CDCl<sub>3</sub>): δ 7.43–7.14 (m, 90H), 0.90 (t,  $J = 8.0$  Hz, 18H), 0.54 (q,  $J = 8.0$  Hz, 12H). <sup>13</sup>C NMR (100 MHz, CDCl<sub>3</sub>, APT): δ 156.9, 155.4, 155.1, 154.9, 140.5, 140.1, 140.0, 139.9, 139.8, 130.4 (2×), 130.2, 128.7, 128.5 (2×), 128.3, 127.7, 127.6, 127.5, 104.0, 102.1, 102.0 (3×), 95.2, 90.8, 90.4, 90.3, 90.2, 90.1, 7.4, 4.2 (26 coincident peaks not observed). ESI MS  $m/z$  (MeOH/toluene 3:1, AgOTf added): 2183 ( $[M + Ag^{++}]^+$ ).

**1,35-Bis(triethylsilyl)-3,9,12,15,18,21,24,27,30,33-undeca(diphenylmethylidene)-  
1,4,7,10,13,16,19,22,25,28,31,34-pentatricontadodecayne (142).**



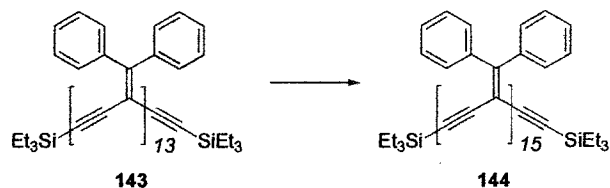
Nonamer **141** (57 mg, 0.028 mmol) was desilylated with 2 equiv. of TBAF and cross-coupled with triflate **131** (26 mg, 0.056 mmol) in degassed THF (20 mL) in the presence of Pd(PPh<sub>3</sub>)<sub>4</sub> (3 mg, 0.003 mmol), diisopropylamine (2 mL), and CuI (1.5 mg, 0.0079 mmol) for 12 h under reflux as described in the general procedure. Size-exclusion chromatography (CH<sub>2</sub>Cl<sub>2</sub>) gave **142** (55 mg, 81%) as a yellow solid. Mp: 140–142 °C. IR (CH<sub>2</sub>Cl<sub>2</sub>, cast): 3053, 2954, 2873, 2140, 1597, 1492, 1442 cm<sup>-1</sup>. UV-vis (CHCl<sub>3</sub>): λ<sub>max</sub> (ε) 378 (119 800). <sup>1</sup>H NMR (400 MHz, CDCl<sub>3</sub>): δ 7.42–7.14 (m, 110H), 0.91 (t, *J* = 8.0 Hz, 18H), 0.56 (q, *J* = 8.0 Hz, 12H). <sup>13</sup>C NMR (100 MHz, CDCl<sub>3</sub>, APT): 157.6, 156.2, 156.1, 156.0, 155.8, 140.7, 140.4 (2×), 140.3, 130.7 (2×), 130.6, 130.5, 129.2, 129.0, 128.8, 128.2, 128.1, 128.0, 104.2, 102.3, 102.2, 95.9, 91.0, 90.7, 90.6, 90.5, 90.4, 90.3, 7.6, 4.6 (39 coincident peaks not observed). ESI MS *m/z* (MeOH/toluene 3:1, AgOTf added): 2584 ([M + Ag<sup>+</sup>]<sup>+</sup>), 2610 ([M + Cs<sup>+</sup>]<sup>+</sup>).

**1,41-Bis(triethylsilyl)-3,9,12,15,18,21,24,27,30,33,36,39-  
trideca(diphenylmethylidene)-1,4,7,10,13,16,19,22,25,28,31,34,37,40-  
hentetracontatetradecayne (143).**



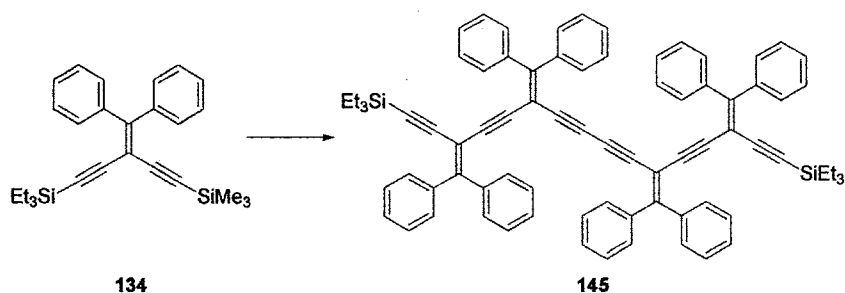
Undecamer **142** (29 mg, 0.012 mmol) was desilylated with 2 equiv. of TBAF and cross-coupled with triflate **131** (10.9 mg, 0.0234 mmol) in degassed THF (20 mL) in the presence of Pd(PPh<sub>3</sub>)<sub>4</sub> (3 mg, 0.003 mmol), diisopropylamine (2 mL), and CuI (1.5 mg, 0.0079 mmol) for 12 h under reflux as described in the general procedure. Size-exclusion chromatography (CH<sub>2</sub>Cl<sub>2</sub>) gave **143** (26 mg, 77%) as a yellow solid. Mp: 148–150 °C (dec.). IR (CH<sub>2</sub>Cl<sub>2</sub>, cast): 3053, 2954, 2873, 2140, 1575, 1492, 1442 cm<sup>-1</sup>. UV-vis (CHCl<sub>3</sub>): λ<sub>max</sub> (ε) 378 (139 900). <sup>1</sup>H NMR (400 MHz, CD<sub>2</sub>Cl<sub>2</sub>): δ 7.42–7.15 (m, 130H), 0.91 (t, *J* = 7.6 Hz, 18H), 0.56 (q, *J* = 7.6 Hz, 12H). <sup>13</sup>C NMR (100 MHz, CDCl<sub>3</sub>, APT): 157.6, 156.2, 156.1, 156.0, 155.8, 140.7, 140.4 (2×), 140.3, 130.7, 130.5, 129.2, 129.0, 128.8, 128.2, 128.0, 104.2, 102.3, 102.2, 95.9, 91.0, 90.7, 90.6, 90.5, 90.4, 90.3, 7.6, 4.6 (54 coincident peaks not observed). ESI MS *m/z* (MeOH/toluene 3:1, AgOTf added): 2991 ([M + Ag<sup>+</sup>]<sup>+</sup>).

**1,47-Bis(triethylsilyl)-3,9,12,15,18,21,24,27,30,33,36,39,42,45-pentadeca(diphenylmethylidene)-1,4,7,10,13,16,19,22,25,28,31,34,37,40,43,46-heptatetracontahexadecayne (144).**



Tridecamer **143** (41 mg, 0.015 mmol) was desilylated with 2 equiv. of TBAF and cross-coupled with triflate **131** (14 mg, 0.030 mmol) in degassed THF (20 mL) in the presence of Pd(PPh<sub>3</sub>)<sub>4</sub> (3 mg, 0.003 mmol), diisopropylamine (2 mL), and CuI (1.5 mg, 0.0079 mmol) for 12 h under reflux as described in the general procedure. Size-exclusion chromatography (CH<sub>2</sub>Cl<sub>2</sub>) gave **144** (35.8 mg, 73%) as a yellow solid. Mp: 155–159 °C (dec.). IR (CH<sub>2</sub>Cl<sub>2</sub>, cast): 3053, 2956, 2872, 2140, 1491, 1442 cm<sup>-1</sup>. UV–vis (CHCl<sub>3</sub>): λ<sub>max</sub> (ε) 378 (159 500). <sup>1</sup>H NMR (400 MHz, CD<sub>2</sub>Cl<sub>2</sub>): δ 7.42–7.16 (m, 150H), 0.91 (t, *J* = 7.6 Hz, 18H), 0.56 (q, *J* = 7.6 Hz, 12H). <sup>13</sup>C NMR (100 MHz, CD<sub>2</sub>Cl<sub>2</sub>, APT): 157.6, 156.1, 156.0, 155.8, 140.7, 140.4, 140.3, 130.7, 130.5, 129.2, 129.0, 128.8, 128.2, 128.0, 104.2, 102.3, 102.2, 95.9, 91.0, 90.7, 90.6, 90.5, 90.4, 90.3, 7.6, 4.6 (68 coincident peaks not observed). ESI MS *m/z* (MeOH/toluene 3:1, AgOTf added): 3309 ([M + Na]<sup>+</sup>), 3392 ([M + Ag]<sup>+</sup>).

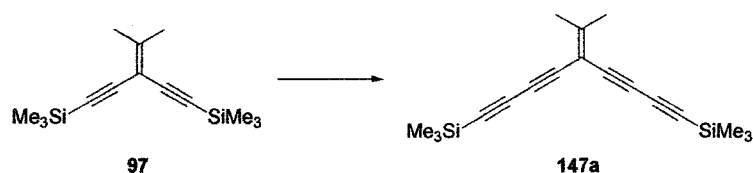
**1,16-Bis(triethylsilyl)-3,6,11,14-tetra(diphenylmethylidene)-1,4,7,9,12,15-hexadecahexayne (145).**



Homocoupled tetramer **145** was isolated from the synthesis of **138** as a yellow solid in 8% yield. *R<sub>f</sub>* = 0.7 (hexanes/CH<sub>2</sub>Cl<sub>2</sub> 2:3). Mp: 57–59 °C. IR (CHCl<sub>3</sub>, cast): 3053, 2954, 2873, 2141, 1442 cm<sup>-1</sup>. UV–vis (CHCl<sub>3</sub>): λ<sub>max</sub> (ε) 325 (33 100), 384 (46 600). <sup>1</sup>H NMR (300 MHz, CDCl<sub>3</sub>): δ 7.42–7.16 (m, 40H), 0.87 (t, *J* = 8.1 Hz, 18H), 0.51 (q, *J* = 8.1 Hz,

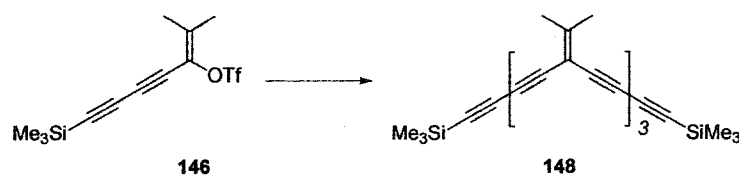
12H).  $^{13}\text{C}$  NMR (125 MHz,  $\text{CD}_2\text{Cl}_2$ , APT):  $\delta$  158.7, 158.0, 140.5, 140.2, 140.1, 140.0, 130.7, 130.6 (2 $\times$ ), 130.4, 129.5 (2 $\times$ ), 129.2, 128.9, 128.3 (2 $\times$ ), 128.2, 128.0, 103.8, 102.0, 101.3, 96.1, 91.9, 89.6, 81.5, 76.9, 7.6, 4.5. ESI MS  $m/z$  (MeOH/toluene 3:1): 1110.5 ( $[\text{M} + \text{Na}^+]$ ).

**1,9-Bis(trimethylsilyl)-5-isopropylidene-1,3,6,8-nonatetrayne (147a).**



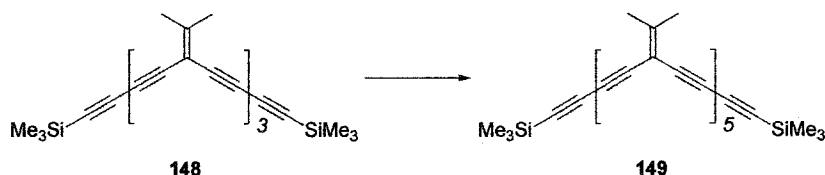
Enediyne **97** (200 mg, 0.805 mmol) was desilylated with  $\text{K}_2\text{CO}_3/\text{MeOH}$  to give **97a**, which was directly subjected to oxidative coupling with trimethylsilylacetylene (1.0 g, 10 mmol) using *Hay* catalyst (4 mL) in dry acetone (100 mL). The mixture was stirred at rt under air for 24 h. The solution was extracted with pentane, sequentially washed with 10% HCl (25 mL), satd.  $\text{NaHCO}_3$  (25 mL) and brine (25 mL), and then dried. Solvent removal and flash chromatography (pentane) afforded **147a** (142 mg, 60%) as a colorless solid.  $R_f = 0.5$  (pentane). Mp: 64–65 °C. IR ( $\text{CH}_2\text{Cl}_2$ , cast): 2960, 2901, 2202, 2094, 1588  $\text{cm}^{-1}$ .  $^1\text{H}$  NMR (300 MHz,  $\text{CDCl}_3$ ):  $\delta$  2.04 (s, 6H), 0.18 (s, 18).  $^{13}\text{C}$  NMR (75 MHz,  $\text{CDCl}_3$ ):  $\delta$  163.3, 99.7, 91.6, 87.7, 77.0, 72.5, 23.3, -0.4. EI HRMS: calcd for  $\text{C}_{18}\text{H}_{24}\text{Si}_2$  ( $\text{M}^+$ ), 296.1417; found, 296.1415. Anal. Calcd for  $\text{C}_{18}\text{H}_{24}\text{Si}_2$ : C, 72.90; H, 8.16. Found: C, 72.61; H, 7.98.

**1,19-Bis(trimethylsilyl)-5,10,15-tri(isopropylidene)-1,3,6,8,11,13,16,18-nonadecaoyne (148).**



Compound **147a** (30 mg, 0.10 mmol) was desilylated to give **147b**, which was directly cross-coupled with triflate **146** (77 mg, 0.24 mmol) in degassed THF (10 mL) in the presence of  $\text{PdCl}_2(\text{PPh}_3)_2$  (7 mg, 0.01 mmol), diisopropylamine (0.5 mL), and CuI (4 mg, 0.02 mmol) for 20 min as described in the general procedure. Flash chromatography (hexane/ $\text{CH}_2\text{Cl}_2$  5:1) afforded **148** (47 mg, 93%) as a light yellow solid.  $R_f = 0.8$  (hexane/ $\text{CH}_2\text{Cl}_2$  5:1). Mp: 96–98 °C. IR ( $\text{CHCl}_3$ , cast): 2960, 2906, 2200, 2096, 1584  $\text{cm}^{-1}$ . UV–vis ( $\text{CHCl}_3$ ):  $\lambda_{\text{max}}$  ( $\epsilon$ ) 284 (35 100), 294 (37 400), 312 (35 600), 334 (22 200).  $^1\text{H}$  NMR (300 MHz,  $\text{CDCl}_3$ , APT):  $\delta$  2.06 (s, 9H), 2.05 (s, 9H), 0.18 (s, 18H).  $^{13}\text{C}$  NMR (125 MHz,  $\text{CDCl}_3$ ):  $\delta$  162.5, 162.0, 100.1, 99.9, 91.4, 87.7, 78.1, 78.0, 76.8, 76.5, 76.4, 72.5, 23.3, –0.3 (two coincidental peaks not observed). EI HRMS: calcd for  $\text{C}_{34}\text{H}_{36}\text{Si}_2$  ( $\text{M}^+$ ), 500.2356; found, 500.2347.

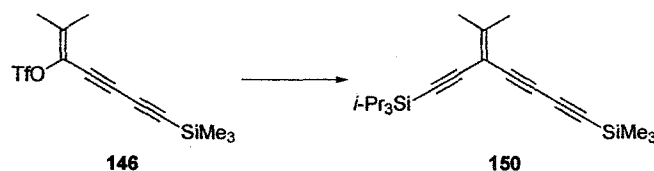
**1,29-Bis(trimethylsilyl)-5,10,15,20,25-penta(isopropylidene)-  
1,3,6,8,11,13,16,18,21,23,26,28-nonacosadodecayne (149).**



Compound **148** (50 mg, 0.10 mmol) was desilylated and cross-coupled with triflate **146** (65 mg, 0.20 mmol) in degassed THF (10 mL) in the presence of  $\text{PdCl}_2(\text{PPh}_3)_2$  (7 mg, 0.01 mmol), diisopropylamine (80 mg, 0.79 mmol), and CuI (4 mg, 0.02 mmol) for 2 h as described in the general procedure. Flash chromatography

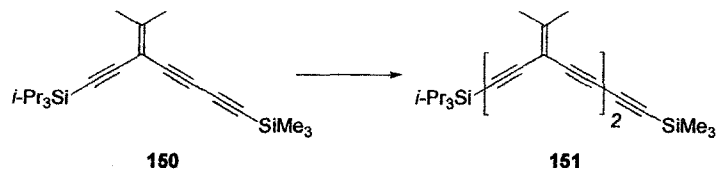
(hexane/CH<sub>2</sub>Cl<sub>2</sub> 5:1) afforded **149** (62 mg, 88%) as a light yellow solid.  $R_f = 0.6$  (hexane/CH<sub>2</sub>Cl<sub>2</sub> 5:1). Mp: 85 °C (dec.). IR (CH<sub>2</sub>Cl<sub>2</sub>, cast): 2958, 2923, 2849, 2201, 2095, 1584 cm<sup>-1</sup>. UV-vis (CHCl<sub>3</sub>):  $\lambda_{\max}$  ( $\epsilon$ ) 294 (59 000), 313 (62 000), 334 (42 300). <sup>1</sup>H NMR (300 MHz, CDCl<sub>3</sub>):  $\delta$  2.07 (s, 15H), 2.06 (s, 15H), 0.19 (s, 18H). <sup>13</sup>C NMR (125 MHz, CDCl<sub>3</sub>, APT):  $\delta$  162.5, 161.6, 100.2, 99.5, 91.4, 87.7, 78.1 (3 $\times$ ), 78.0, 76.8, 76.5, 76.4 (3 $\times$ ), 72.5, 23.4, 23.3, -0.3 (four coincidental peaks not observed). ESI MS (MeOH/toluene 3:1, AgOTf added): 813.2 ([M + Ag<sup>+</sup>]<sup>+</sup>).

### 2-Methyl-7-trimethylsilyl-3-triisopropylsilylethynylhepta-2-ene-4,6-diyne (**150**).



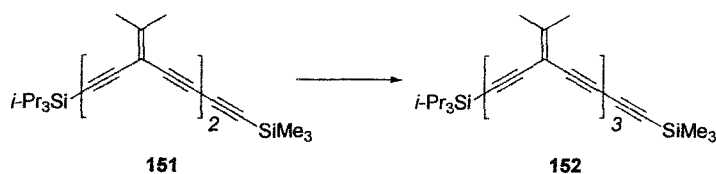
Triflate **146** (100 mg, 0.308 mmol) was cross-coupled with triisopropylsilylacetylene (112 mg, 0.616 mmol) in degassed THF (20 mL) in the presence of PdCl<sub>2</sub>(PPh<sub>3</sub>)<sub>2</sub> (11 mg, 0.016 mmol), diisopropylamine (93 mg, 0.92 mmol), and CuI (6 mg, 0.03 mmol) for 1.3 h as described in the general procedure. Flash chromatography (hexane/CH<sub>2</sub>Cl<sub>2</sub> 2:1) afforded **150** (102 mg, 93%) as a colorless solid.  $R_f = 0.8$  (hexane/CH<sub>2</sub>Cl<sub>2</sub> 2:1). Mp: 30–31 °C. IR (CH<sub>2</sub>Cl<sub>2</sub>, cast): 2943, 2866, 2202, 2144, 2098, 1587 cm<sup>-1</sup>. <sup>1</sup>H NMR (300 MHz, CDCl<sub>3</sub>):  $\delta$  2.05 (s, 3H), 2.04 (s, 3H), 1.07 (s, 21H), 0.20 (s, 9H). <sup>13</sup>C NMR (75 MHz, CDCl<sub>3</sub>, APT):  $\delta$  160.0, 101.9, 101.1, 93.9, 90.6, 88.1, 76.0, 73.9, 23.2, 23.0, 18.7, 11.3, -0.3. EI MS  $m/z$  (rel. intensity): 356 (M<sup>+</sup>, 46), 313 ([M - *i*-Pr]<sup>+</sup>, 100). EI HRMS: calcd for C<sub>22</sub>H<sub>36</sub>Si<sub>2</sub> (M<sup>+</sup>), 356.2356; found, 356.2357. Anal. Calcd for C<sub>22</sub>H<sub>36</sub>Si<sub>2</sub>: C, 74.08; H, 10.17. Found: C, 74.05; H, 10.41.

**2-Methyl-8-isopropylidene-12-trimethylsilyl-3-triisopropylsilylethynyl-dodeca-2-ene-4,6,9,11-tetrayne (151).**



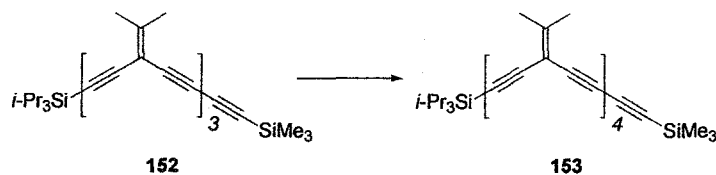
Enetriyne **150** (151 mg, 0.423 mmol) was desilylated and cross-coupled with triflate **146** (137 mg, 0.423 mmol) in degassed THF (20 mL) in the presence of  $\text{PdCl}_2(\text{PPh}_3)_2$  (18 mg, 0.026 mmol), diisopropylamine (130 mg, 1.28 mmol), and CuI (6 mg, 0.03 mmol) for 20 min as described in the general procedure. Flash chromatography (hexane/ $\text{CH}_2\text{Cl}_2$  5:1) afforded **151** (138 mg, 71%) as a pale yellow solid.  $R_f = 0.5$  (hexane/ $\text{CH}_2\text{Cl}_2$  5:1). Mp: 82-83 °C. IR (neat): 2943, 2865, 2202, 2149, 2095, 1581  $\text{cm}^{-1}$ . UV-vis ( $\text{CHCl}_3$ ):  $\lambda_{\text{max}}$  ( $\epsilon$ ) 290 (23 900), 310 (21 300), 332 (13 600).  $^1\text{H}$  NMR (300 MHz,  $\text{CDCl}_3$ ):  $\delta$  2.06 (s, 9H), 2.04 (s, 3H), 1.07 (s, 21H) 0.18 (s, 9H).  $^{13}\text{C}$  NMR (125 MHz,  $\text{CDCl}_3$ ):  $\delta$  162.3, 159.3, 102.1, 101.4, 100.1, 93.8, 91.4, 87.8, 79.5, 77.4, 76.9, 76.8, 75.5, 72.7, 23.3 (2 $\times$ ), 23.2, 23.0, 18.7, 11.3, -0.4. EI HRMS: calcd for  $\text{C}_{30}\text{H}_{42}\text{Si}_2$  ( $\text{M}^+$ ), 458.2825; found, 458.2830. Anal. Calcd for  $\text{C}_{30}\text{H}_{42}\text{Si}_2$ : C, 78.53; H, 9.23. Found: C, 78.89; H, 9.33.

**2-Methyl-8,13-di(isopropylidene)-17-trimethylsilyl-3-triisopropylsilylethynyl-heptadeca-2-ene-4,6,9,11,14,16-hexayne (152).**



Dimer **151** (92 mg, 0.20 mmol) was desilylated and cross-coupled with triflate **146** (65 mg, 0.20 mmol) in degassed THF (20 mL) in the presence of PdCl<sub>2</sub>(PPh<sub>3</sub>)<sub>2</sub> (10 mg, 0.014 mmol), diisopropylamine (60 mg, 0.59 mmol), and CuI (5 mg, 0.02 mmol) for 15 min as described in the general procedure. Flash chromatography (hexane/CH<sub>2</sub>Cl<sub>2</sub> 2:1) afforded **152** (82 mg, 73%) as a pale yellow solid. *R<sub>f</sub>* = 0.6 (hexane/CH<sub>2</sub>Cl<sub>2</sub> 2:1). Mp: 40–44 °C. IR (CH<sub>2</sub>Cl<sub>2</sub>, cast): 2943, 2865, 2200, 2147, 2096, 1585 cm<sup>-1</sup>. <sup>1</sup>H NMR (300 MHz, CDCl<sub>3</sub>): δ 2.072 (s, 3H), 2.065 (s, 3H), 2.055 (s, 6H), 2.040 (s, 3H), 2.038 (s, 3H), 1.07 (s, 21H) 0.18 (s, 9H). <sup>13</sup>C NMR (125 MHz, CDCl<sub>3</sub>, APT): δ 162.4, 161.6, 159.0, 102.0, 101.3, 100.3, 100.0, 93.7, 91.4, 87.7, 79.5, 78.3, 77.9, 77.5, 76.8 (2×), 76.6, 76.3, 75.5, 72.5, 23.4, 23.3 (2×), 23.2, 23.0, 18.7, 11.4, -0.3 (one coincident signal not observed). EI HRMS: calcd for C<sub>38</sub>H<sub>48</sub>Si<sub>2</sub> (M<sup>+</sup>), 560.3295; found, 560.3286.

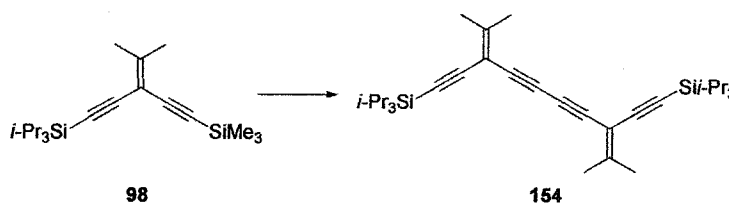
**2-Methyl-8,13,18-tri(isopropylidene)-22-trimethylsilyl-3-triisopropylsilylethynyl-dososa-2-ene-4,6,9,11,14,16,19,21-octayne (153).**



Timer **152** (67 mg, 0.12 mmol) was desilylated and cross-coupled with triflate **146** (39 mg, 0.12 mmol) in degassed THF (20 mL) in the presence of PdCl<sub>2</sub>(PPh<sub>3</sub>)<sub>2</sub> (4 mg, 0.006 mmol), diisopropylamine (40 mg, 0.40 mmol), and CuI (2 mg, 0.01 mmol) for 15 min as described in the general procedure. Flash chromatography (hexane/CH<sub>2</sub>Cl<sub>2</sub> 2:1) afforded **153** (61 mg, 77%) as a pale yellow solid. *R<sub>f</sub>* = 0.6 (hexane/CH<sub>2</sub>Cl<sub>2</sub> 2:1). Mp: 82–85 °C. IR (CHCl<sub>3</sub>, cast): 2942, 2865, 2195, 2147, 2097, 1584 cm<sup>-1</sup>. <sup>1</sup>H NMR

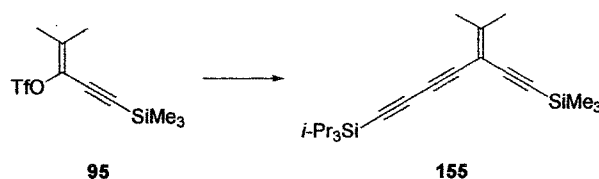
(500 MHz, CDCl<sub>3</sub>, APT):  $\delta$  2.074 (s, 3H), 2.067 (s, 9H), 2.06 (s, 9H), 2.04 (s, 3H), 1.07 (s, 21H), 0.19 (s, 9H). <sup>13</sup>C NMR (125 MHz, CDCl<sub>3</sub>, APT):  $\delta$  162.5, 162.0, 161.6, 159.0, 102.0, 101.3, 100.3, 100.2, 99.9, 93.7, 91.4, 87.7, 79.4, 78.27, 78.15, 78.05, 78.0, 77.5, 76.8, 76.53, 76.47, 76.37, 76.32, 75.5, 72.5, 23.35, 23.34, 23.32, 23.2, 23.0, 18.7, 11.3, -0.3 (four coincident peaks not observed). ESI MS *m/z* (MeOH/toluene 3:1, AgOTf added): 771.2 ([M + Ag<sup>+</sup>]<sup>+</sup>).

**3,8-Bis(trimethylsilylethynyl)-2,9-dimethyl-deca-2,8-diene-4,6-diyne (154).**



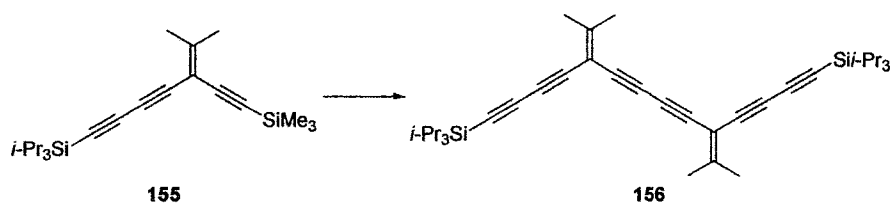
The trimethylsilyl group of enediyne **98** (60 mg, 0.18 mmol) was removed with methanolic K<sub>2</sub>CO<sub>3</sub> according to the general procedure. Homocoupling as described in general procedure followed by flash chromatography (hexane/CH<sub>2</sub>Cl<sub>2</sub> 2:1) afforded **154** (44 mg, 94%) as a colorless solid. *R<sub>f</sub>* = 0.7 (hexane/CH<sub>2</sub>Cl<sub>2</sub> 2:1). Mp: 117 °C. IR (CHCl<sub>3</sub>, cast): 2943, 2866, 2150, 2096 cm<sup>-1</sup>. UV-vis (CHCl<sub>3</sub>):  $\lambda_{\text{max}}$  ( $\epsilon$ ) 290 (14 600), 309 (24 600), 329 (22 300). <sup>1</sup>H NMR (300 MHz, CDCl<sub>3</sub>):  $\delta$  2.06 (s, 6H), 2.04 (s, 6H), 1.07 (s, 42H). <sup>13</sup>C NMR (125 MHz, CDCl<sub>3</sub>):  $\delta$  158.8, 102.3, 101.5, 93.6, 79.0, 75.9, 23.1, 23.0, 18.7, 11.4. EI HRMS: calcd for C<sub>34</sub>H<sub>54</sub>Si<sub>2</sub> (M<sup>+</sup>), 518.3764; found, 518.3744.

**2-Methyl-3-trimethylsilylethynyl-7-triisopropylsilyl-hepta-2-ene-4,6-diyne (155).**



1-Triisopropylsilylbuta-1,3-diyne (89 mg, 0.43 mmol) was protidesilylated and cross-coupled with triflate **95** (109 mg, 0.363 mmol in degassed THF (20 mL) in the presence of  $\text{PdCl}_2(\text{PPh}_3)_2$  (12 mg, 0.017 mmol), diisopropylamine (93 mg, 0.92 mmol), and CuI (6 mg, 0.032 mmol) for 2h as described in the general procedure. Flash chromatography (hexane/ $\text{CH}_2\text{Cl}_2$  2:1) afforded **155** (113 mg, 87%) as a pale yellow oil.  $R_f = 0.8$  (hexane/ $\text{CH}_2\text{Cl}_2$  2:1). IR ( $\text{CH}_2\text{Cl}_2$  cast): 2944, 2866, 2201, 2147, 2095, 1587  $\text{cm}^{-1}$ .  $^1\text{H}$  NMR (500 MHz,  $\text{CDCl}_3$ ):  $\delta$  2.04 (s, 3H), 2.03 (s, 3H), 1.07(s, 21H), 0.18 (s, 9H).  $^{13}\text{C}$  NMR (125 MHz,  $\text{CDCl}_3$ , APT):  $\delta$  160.1, 100.6, 100.2, 97.2, 89.6, 88.0, 76.6, 72.2, 23.1 (2 $\times$ ), 18.6, 11.4, 0.0. EI MS  $m/z$  (rel. intensity): 356 ( $\text{M}^+$ , 50), 313 ( $[\text{M} - i\text{-Pr}]^+$ , 100). EI HRMS: calcd for  $\text{C}_{22}\text{H}_{36}\text{Si}_2$  ( $\text{M}^+$ ), 356.2356; found 356.2355.

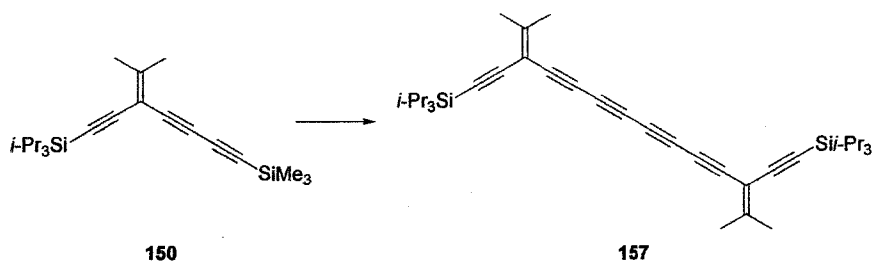
**1,14-Bis(trimethylsilyl)-5,10-di(isopropylidene)-1,3,6,8,11,13-tetradeca-hexayne (156).**



Enetriyne **155** (70 mg, 0.20 mmol) was selectively protidesilylated with  $\text{K}_2\text{CO}_3$  as described in general procedure and homo-coupled in the presence of *Hay* catalyst under air in  $\text{CH}_2\text{Cl}_2$  (10 mL) for 4h. Flash chromatography (hexane/ $\text{CH}_2\text{Cl}_2$  2:1) afforded **156** (26 mg, 48%) as a pale yellow solid.  $R_f = 0.6$  (hexane/ $\text{CH}_2\text{Cl}_2$  2:1). Mp: 129–130

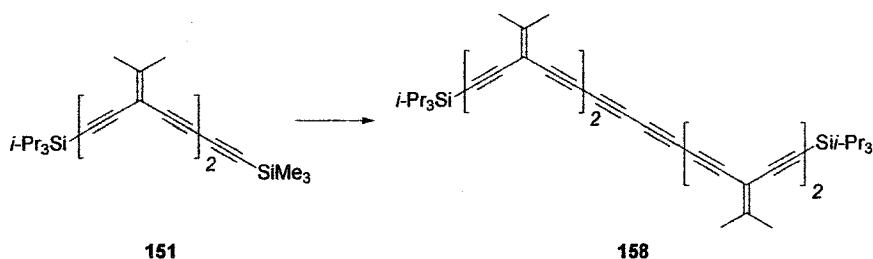
°C. IR (CH<sub>2</sub>Cl<sub>2</sub>, cast): 2943, 2865, 2199, 2092 cm<sup>-1</sup>. UV-vis (CHCl<sub>3</sub>): λ<sub>max</sub> (ε) 289 (25 200), 310 (20 700), 335 (11 100). <sup>1</sup>H NMR (500 MHz, CDCl<sub>3</sub>): δ 2.08 (s, 6H), 2.06 (s, 6H), 1.07 (s, 42H). <sup>13</sup>C NMR (125 MHz, CDCl<sub>3</sub>, APT): δ 162.4, 100.0, 89.3, 88.7, 78.2, 76.4, 71.2, 23.41, 23.35, 18.6, 11.4 (one coincident peak not observed). EI HRMS: calcd for C<sub>38</sub>H<sub>54</sub>Si<sub>2</sub> (M<sup>+</sup>), 566.3764; found, 566.3753. X-ray.

**3,12-Bis(triisopropylsilylethynyl)-2,13-dimethyl-tetradeca-2,12-diene-4,6,8,10-tetrayne (157).**



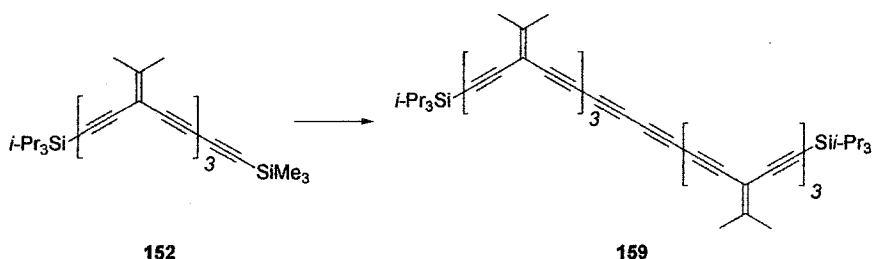
Enetriyne **150** (42 mg, 0.12 mmol) was desilylated and homo-coupled in CH<sub>2</sub>Cl<sub>2</sub> (20 mL) in the presence of CuI (50 mg, 0.26 mmol), TMEDA (75 mg, 0.65 mmol) and air for 20 min as described in the general procedure. Flash chromatography (hexane/CH<sub>2</sub>Cl<sub>2</sub> 2:1) afforded **157** (32 mg, 96%) as a yellow solid. *R<sub>f</sub>* = 0.7 (hexane/CH<sub>2</sub>Cl<sub>2</sub> 2:1). Mp: 103–104 °C. IR (μscope): 2943, 2865, 2194, 2143, 1586 cm<sup>-1</sup>. UV-vis (CHCl<sub>3</sub>): λ<sub>max</sub> (ε) 288 (51 400), 300 (67 900), 319 (51 700), 348 (18 600), 374 (20 200), 405 (13 400). <sup>1</sup>H NMR (300 MHz, CDCl<sub>3</sub>): δ 2.07 (s, 6H), 2.05 (s, 6H), 1.07 (s, 42H). <sup>13</sup>C NMR (75 MHz, CDCl<sub>3</sub>): δ 162.4, 101.2, 100.9, 94.8, 76.3, 75.0, 67.8, 64.1, 23.4, 23.2, 18.7, 11.3. EI HRMS: calcd for C<sub>38</sub>H<sub>54</sub>Si<sub>2</sub> (M<sup>+</sup>), 566.3764; found, 566.3774. X-Ray.

**3,22-Bis(triisopropylsilylethynyl)-8,17-di(isopropylidene)-2,23-dimethyl-tetracos-2,22-diene-4,6,9,11,13,15,18,20-octayne (158).**



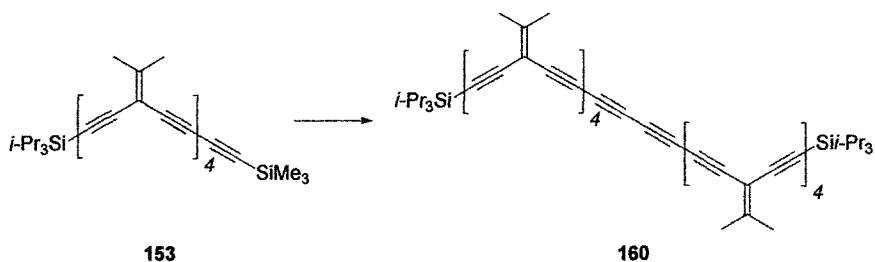
Dimer **151** (29 mg, 0.063 mmol) was desilylated and homo-coupled in  $\text{CH}_2\text{Cl}_2$  (20 mL) in the presence of  $\text{CuI}$  (50 mg, 0.26 mmol),  $\text{TMEDA}$  (75 mg, 0.65 mmol) and air for 0.5h as described in the general procedure. Flash chromatography (hexane/ $\text{CH}_2\text{Cl}_2$  2:1) afforded **158** (19 mg, 78%) as a waxy yellow solid.  $R_f = 0.4$  (hexane/ $\text{CH}_2\text{Cl}_2$  2:1). IR ( $\mu\text{scope}$ ): 2942, 2864, 2200, 2145, 1580  $\text{cm}^{-1}$ . UV-vis ( $\text{CHCl}_3$ ):  $\lambda_{\text{max}}$  ( $\epsilon$ ) 262 (98 700), 299 (85 300), 312 (77 100), 324 (61 000), 349 (25 000), 375 (20 900), 406 (13 500).  $^1\text{H}$  NMR (300 MHz,  $\text{CH}_2\text{Cl}_2$ ):  $\delta$  2.11 (s, 12H), 2.09 (s, 6H), 2.06 (s, 6H), 1.10 (s, 42H).  $^{13}\text{C}$  NMR (125 MHz,  $\text{CH}_2\text{Cl}_2$ ):  $\delta$  166.6, 160.8, 102.3, 101.2, 99.7, 94.3, 80.2, 77.5, 77.0, 76.9, 75.4, 74.4, 68.1, 64.2, 23.7, 23.6, 23.3, 23.1, 18.8, 11.7. ESI MS  $m/z$  (MeOH/toluene 3:1,  $\text{AgOTf}$  added): 879.3 ( $[\text{M} + \text{Ag}^+]^+$ ).

**3,32-Bis(triisopropylsilylethynyl)-8,13,22,27-tetra(isopropylidene)-2,33-dimethyl-tetratricula-2,32-diene-4,6,9,11,14,16,18,20,23,25,28,30-dodecayne (159).**



Trimer **152** (37 mg, 0.066 mmol) was desilylated and homo-coupled in CH<sub>2</sub>Cl<sub>2</sub> (20 mL) in the presence of CuI (50 mg, 0.26 mmol), TMEDA (75 mg, 0.65 mmol) and air for 15 min as described in the general procedure. Flash chromatography (hexane/CH<sub>2</sub>Cl<sub>2</sub> 2:1) afforded **159** (22 mg, 68%) as a light yellow solid. Mp 85 °C (dec.). *R<sub>f</sub>* = 0.2 (2:1 hexane/CH<sub>2</sub>Cl<sub>2</sub>). IR (neat): 2941, 2849, 2195, 2146, 1582 cm<sup>-1</sup>. UV-vis (CHCl<sub>3</sub>): λ<sub>max</sub> (ε) 262 (107 000), 297 (91 800), 307(90 300), 324 (67 700), 348 (29 200), 375 (18 100), 406 (11 900). <sup>1</sup>H NMR (400 MHz, CDCl<sub>3</sub>): δ 2.09 (s, 12H), 2.08 (s, 6H), 2.07 (s, 6H), 2.06 (s, 6H), 2.04 (s, 6H), 1.07 (s, 42H). <sup>13</sup>C NMR (100 MHz, CDCl<sub>3</sub>, APT): δ 165.3, 162.0, 159.2, 102.0, 101.3, 100.3, 99.8, 93.7, 79.5, 78.7, 77.4, 77.2, 77.1, 77.0, 76.9, 76.1, 75.5, 73.7, 68.1, 63.9, 23.5, 23.4, 23.3, 23.2, 23.1, 22.9, 18.8, 11.7. ESI MS *m/z* (MeOH/toluene 3:1, AgOTf added): 1083.4 ([M + Ag<sup>+</sup>]).

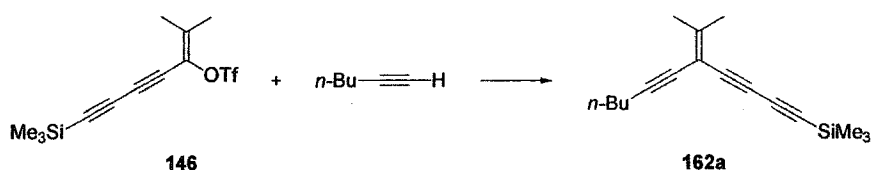
**3,42-Bis(triisopropylsilylethynyl)-8,13,18,27,32,37-hexa(isopropylidene)-2,43-dimethyl-tetratetraconta-2,42-diene-4,6,9,11,14,16,19,21,23,25,28,30,33,35,38,40-hexadecayne (160).**



Tetramer **153** (10 mg, 0.015 mmol) was desilylated and homo-coupled in CH<sub>2</sub>Cl<sub>2</sub> (20 mL) in the presence of CuI (50 mg, 0.26 mmol), TMEDA (75 mg, 0.65 mmol) and air for 15 min as described in the general procedure. Flash chromatography (hexane/CH<sub>2</sub>Cl<sub>2</sub> 1:1) afforded **160** (5 mg, 56%) as a light yellow solid. *R<sub>f</sub>* = 0.6 (hexane/CH<sub>2</sub>Cl<sub>2</sub> 1:1).

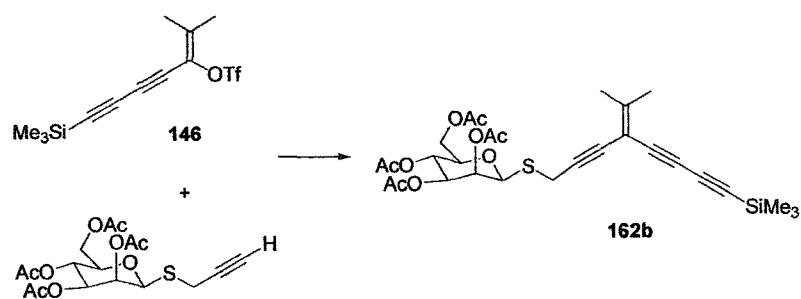
Mp: >98 °C (dec.). IR (μscope): 2942, 2865, 2196, 2145, 1578 cm<sup>-1</sup>. UV-vis (CHCl<sub>3</sub>): λ<sub>max</sub> (ε) 260 (137 000), 308 (113 000), 375 (18 200), 406 (11 500). <sup>1</sup>H NMR (400 MHz, CDCl<sub>3</sub>): δ 2.08 (s, 18H), 2.07 (s, 24H), 2.06 (s, 6H), 2.04 (s, 6H), 1.07 (s, 42H). This sample was insufficiently soluble and stable for meaningful <sup>13</sup>C NMR spectroscopic analysis. ESI MS *m/z* (MeOH/toluene 3:1, AgOTf added): 1287.6 ([M + Ag<sup>+</sup>]<sup>+</sup>).

**5-Isopropylidene-1-trimethylsilyl-undeca-1,3,6-triyn (162a).**



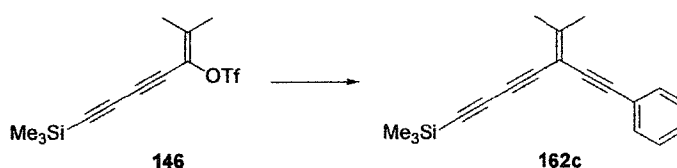
Triflate **146** (108 mg, 0.333 mmol) was cross-coupled with 1-hexyne (30 mg, 0.36 mmol) in degassed THF (20 mL) in the presence of PdCl<sub>2</sub>(PPh<sub>3</sub>)<sub>2</sub> (12 mg, 0.017 mmol), diisopropylamine (2 mL), and CuI (6 mg, 0.03 mmol) for 3 h as described in the general procedure. Flash chromatography (hexane/CH<sub>2</sub>Cl<sub>2</sub> 2:1) afforded **150** (102 mg, 93%) as a colorless oil. *R<sub>f</sub>* = 0.7 (hexane/CH<sub>2</sub>Cl<sub>2</sub> 2:1). IR (CH<sub>2</sub>Cl<sub>2</sub>, cast): 2959, 2933, 2873, 2198, 2097 cm<sup>-1</sup>. <sup>1</sup>H NMR (300 MHz, CDCl<sub>3</sub>): δ 2.32 (t, *J* = 7.2 Hz, 2H), 2.00 (s, 3H), 1.98 (s, 3H), 1.56–1.36 (m, 4H), 0.90 (t, *J* = 6.9 Hz, 3H). <sup>13</sup>C NMR (125 MHz, CDCl<sub>3</sub>, APT): δ 157.0, 100.5, 93.3, 90.5, 88.1, 76.1, 75.4, 74.6, 30.8, 22.8, 22.7, 22.0, 19.1, 13.6, -0.4. EI MS *m/z* (rel. intensity): 256 (M<sup>+</sup>, 100), 241 ([M - Me]<sup>+</sup>, 88). EI HRMS: calcd for C<sub>17</sub>H<sub>24</sub>Si (M<sup>+</sup>), 256.1647; found, 256.1642.

**3-Isopropylidene-7-trimethylsilyl-1,4,6-heptatriynyl 2,3,4,6-tetra-*O*-acetylc-1-thio-β-D-mannopyranoside (162b).**



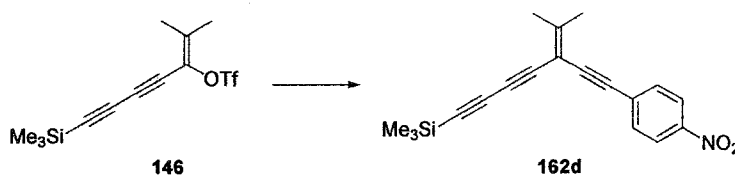
Triflate **146** (32 mg, 0.099 mmol) was cross-coupled with 2-propynyl 2,3,4,6-*O*-acetyl-1-thio- $\beta$ -D-mannopyranoside (40 mg, 0.099 mmol) in degassed THF (20 mL) in the presence of  $\text{PdCl}_2(\text{PPh}_3)_2$  (3 mg, 0.004 mmol), diisopropylamine (2 mL), and CuI (1.5 mg, 0.0079 mmol) for 1 h as described in the general procedure. Flash chromatography (hexane/ethyl acetate 3:1) afforded **162b** (37 mg, 65%) as a colorless solid.  $R_f = 0.3$  (hexane/ethyl acetate 3:1). Mp: 54–57 °C. IR ( $\mu$ scope): 2961, 2916, 2849, 2199, 2098, 1744, 1592, 1433  $\text{cm}^{-1}$ .  $^1\text{H}$  NMR (600 MHz,  $\text{CDCl}_3$ ):  $\delta$  5.51 (d,  $J = 3.5$  Hz, 1H), 5.28 (t,  $J = 10.0$  Hz, 1H), 5.09 (dd,  $J_1 = 10.0$  Hz,  $J_2 = 3.6$  Hz, 1H), 5.02 (s, 1H), 4.29 (dd,  $J_1 = 10.0$  Hz,  $J_2 = 0.6$  Hz, 1H), 4.13 (dd,  $J_1 = 10.0$  Hz,  $J_2 = 0.2$  Hz, 1H), 3.72 (d,  $J = 16.7$  Hz, 1H), 3.70 (m, 1H), 3.42 (d,  $J = 16.7$  Hz, 1H), 2.16 (s, 3H), 2.07 (s, 3H), 2.05 (s, 3H), 2.023 (s, 3H), 2.020 (s, 3H), 1.96 (s, 3H), 0.18 (s, 9H).  $^{13}\text{C}$  NMR (75 MHz,  $\text{CD}_2\text{Cl}_2$ , APT):  $\delta$  170.8, 170.4, 170.2, 169.9, 160.4, 99.9, 91.6, 87.8, 87.5, 81.3, 79.8, 77.1, 76.3, 74.0, 72.3, 70.5, 65.9, 62.7, 30.0, 23.2, 23.0, 20.9, 20.7, 19.6, -0.4 (three coincident peaks not observed). ESI MS  $m/z$  (MeOH): 599.17 ( $[\text{M} + \text{Na}]^+$ ).

#### 6-Methyl-5-phenylethynyl-1-trimethylsilylhept-5-ene-1,3-diyne (**162c**).



Trimethylphenylethyne (60 mg, 0.34 mmol) was desilylated with  $K_2CO_3$  in THF/MeOH (1:1) and cross-coupled with triflate **146** (109 mg, 0.336 mmol) in degassed THF (20 mL) in the presence of  $PdCl_2(PPh_3)_2$  (12 mg, 0.017 mmol), diisopropylamine (2 mL), and CuI (6 mg, 0.03 mmol) for 50 min as described in the general procedure. Flash chromatography (hexane/ $CH_2Cl_2$  2:1) afforded **162c** (90 mg, 96%) as a colorless solid.  $R_f = 0.6$  (hexane/ $CH_2Cl_2$  2:1). Mp: 71–72 °C. IR ( $CH_2Cl_2$ , cast): 2960, 2904, 2199, 2094, 1594, 1489  $cm^{-1}$ .  $^1H$  NMR (400 MHz,  $CDCl_3$ ):  $\delta$  7.45–7.42 (m, 2H), 7.31–7.27 (m, 3H), 2.10 (s, 3H), 2.09 (s, 3H), 0.20 (s, 9H).  $^{13}C$  NMR (100 MHz,  $CDCl_3$ , APT):  $\delta$  158.8, 131.4, 128.2 (2 $\times$ ), 123.1, 100.5, 92.1, 90.9, 88.0, 85.0, 76.0, 73.8, 23.0 (2 $\times$ ), –0.4. EI MS  $m/z$  (rel. intensity): 276.1 ( $M^+$ , 100), 261.1 ( $[M - Me]^+$ , 88). EI HRMS: calcd for  $C_{19}H_{20}Si$  ( $M^+$ ), 276.1334; found, 276.1334.

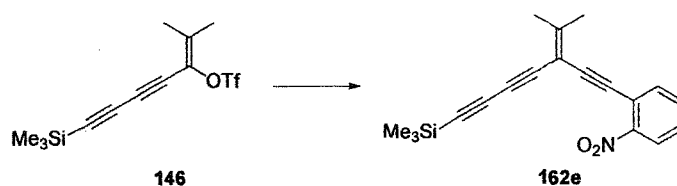
**6-Methyl-5-(4-nitrophenylethynyl)-1-trimethylsilylhept-5-ene-1,3-diyne (162d).**



Trimethyl(4-nitrophenylethynyl)silane (75 mg, 0.34 mmol) was desilylated with  $K_2CO_3$  in THF/MeOH (1:1) and cross-coupled with triflate **146** (109 mg, 0.336 mmol) in degassed THF (20 mL) in the presence of  $PdCl_2(PPh_3)_2$  (12 mg, 0.017 mmol), diisopropylamine (2 mL), and CuI (6 mg, 0.03 mmol) for 50 min as described in the general procedure. Flash chromatography (hexane/ $CH_2Cl_2$  1:1) afforded **162d** (97 mg, 90%) as a yellow solid.  $R_f = 0.4$  (hexane/ $CH_2Cl_2$  1:1). Mp: 94–95 °C. IR ( $CHCl_3$ , cast): 2960, 2199, 2095, 1595, 1519, 1491, 1433, 1342  $cm^{-1}$ .  $^1H$  NMR (400 MHz,  $CDCl_3$ ):  $\delta$

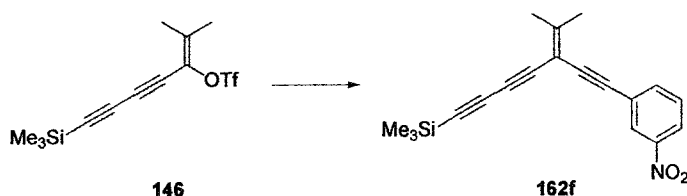
8.15 (d,  $J = 8.9$  Hz, 2H), 7.54 (d,  $J = 8.9$  Hz, 2H), 2.11 (s, 6H), 0.19 (s, 9H).  $^{13}\text{C}$  NMR (100 MHz,  $\text{CDCl}_3$ , APT):  $\delta$  161.2, 146.9, 132.0, 129.9, 123.5, 100.1, 91.5, 90.3, 90.2, 87.6, 76.6, 72.8, 23.2 (2 $\times$ ), -0.5. EI MS  $m/z$  (rel. intensity): 321.1 ( $\text{M}^+$ , 100), 306.1 ( $[\text{M} - \text{Me}]^+$ , 58). EI HRMS: calcd for  $\text{C}_{19}\text{H}_{19}\text{NO}_2\text{Si}$  ( $\text{M}^+$ ), 321.1185; found, 321.1180.

**6-Methyl-5-(2-nitrophenylethynyl)-1-trimethylsilylhept-5-ene-1,3-diyne (162e).**



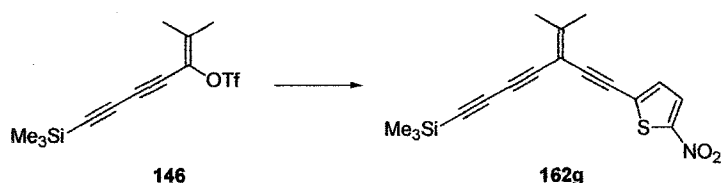
Trimethyl(2-nitrophenylethynyl)silane (75 mg, 0.34 mmol) was desilylated with  $\text{K}_2\text{CO}_3$  in THF/MeOH (1:1) and cross-coupled with triflate **146** (109 mg, 0.336 mmol) in degassed THF (20 mL) in the presence of  $\text{PdCl}_2(\text{PPh}_3)_2$  (12 mg, 0.017 mmol), diisopropylamine (2 mL), and CuI (6 mg, 0.032 mmol) for 2 h as described in the general procedure. Flash chromatography (hexane/ $\text{CH}_2\text{Cl}_2$  1:1) afforded **162e** (95 mg, 87%) as a yellow solid.  $R_f = 0.4$  (hexane/ $\text{CH}_2\text{Cl}_2$  1:1). Mp: 93–94 °C. IR ( $\text{CH}_2\text{Cl}_2$ , cast): 2960, 2199, 2094, 1607, 1526, 1480, 1438, 1343  $\text{cm}^{-1}$ .  $^1\text{H}$  NMR (400 MHz,  $\text{CDCl}_3$ ):  $\delta$  8.02 (d,  $J = 11.2$  Hz, 1H), 7.62 (d,  $J = 10.2$  Hz, 1H), 7.54 (dd,  $J_1 = 11.2$  Hz,  $J_2 = 10.2$  Hz, 1H), 7.41 (dd,  $J_1 = 11.2$  Hz,  $J_2 = 10.2$  Hz, 1H), 2.17 (s, 3H), 2.11 (s, 3H), 0.19 (s, 9H).  $^{13}\text{C}$  NMR (100 MHz,  $\text{CDCl}_3$ , APT):  $\delta$  162.4, 148.9, 134.6, 132.8, 128.5, 124.6, 118.6, 100.2, 93.0, 91.2, 87.9, 87.3, 76.3, 73.1, 23.3, 23.2, -0.4. EI MS  $m/z$  (rel. intensity): 321.1 ( $\text{M}^+$ , 35), 73.0 ( $\text{Me}_3\text{Si}^+$ , 100). EI HRMS: calcd for  $\text{C}_{19}\text{H}_{19}\text{NO}_2\text{Si}$  ( $\text{M}^+$ ), 321.1185; found 321.1182. Anal. Calcd for  $\text{C}_{19}\text{H}_{19}\text{NO}_2\text{Si}$ : C, 70.99; H, 5.96; N, 4.36. Found: C, 71.00; H, 5.95; N, 4.29.

### 6-Methyl-5-(3-nitrophenylethynyl)-1-trimethylsilylhept-5-ene-1,3-diyne (162f).



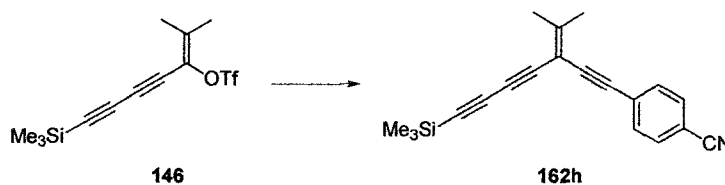
Trimethyl(3-nitrophenylethynyl)silane (75 mg, 0.34 mmol) was desilylated with  $K_2CO_3$  in THF/MeOH (1:1) and cross-coupled with triflate **146** (109mg, 0.336mol) in degassed THF (20 mL) in the presence of  $PdCl_2(PPh_3)_2$  (12 mg, 0.017 mmol), diisopropylamine (2 mL), and CuI (6 mg, 0.032 mmol) for 10 min as described in the general procedure. Flash chromatography (hexane/ $CH_2Cl_2$  1:1) afforded **162f** (98 mg, 92%) as a yellow solid.  $R_f = 0.5$  (hexane/ $CH_2Cl_2$  1:1). Mp: 77–78 °C. IR ( $CH_2Cl_2$ , cast): 3084, 2960, 2904, 2200, 2095, 1572, 1532, 1477, 1433, 1351  $cm^{-1}$ .  $^1H$  NMR (400 MHz,  $CDCl_3$ ):  $\delta$  8.26 (s, 1H), 8.13 (d,  $J = 10.8$  Hz, 1H), 7.72 (d,  $J = 10.0$  Hz, 1H), 7.48 (dd,  $J_1 = 10.8$  Hz,  $J_2 = 10.0$  Hz, 1H), 2.12 (s, 3H), 2.11 (s, 3H), 0.19 (s, 9H).  $^{13}C$  NMR (75 MHz,  $CDCl_3$ , APT):  $\delta$  160.7, 148.2, 137.1, 129.4, 126.2, 125.0, 122.9, 100.1, 91.5, 89.6, 87.8, 87.7, 76.6, 73.1, 23.3, 23.2, -0.4. EI MS  $m/z$  (rel. intensity): 321.1 ( $M^+$ , 100), 306.1 ( $[M - Me]^+$ , 48). EI HRMS: calcd for  $C_{19}H_{19}NO_2Si$  ( $M^+$ ), 321.1185; found, 321.1176.

### 6-Methyl-5-(5-nitrothienyl-2-ylethynyl)-1-trimethylsilylhept-5-ene-1,3-diyne (162g).



Trimethyl(5-nitrothienyl-2-ylethynyl)silane (76 mg, 0.34 mmol) was desilylated with  $K_2CO_3$  in THF/MeOH (1:1) and cross-coupled with triflate **146** (109 mg, 0.336 mmol) in degassed THF (20 mL) in the presence of  $PdCl_2(PPh_3)_2$  (12 mg, 0.017 mmol), diisopropylamine (2 mL), and CuI (6 mg, 0.03 mmol) for 1 h as described in the general procedure. Flash chromatography (hexane/ $CH_2Cl_2$  2:1) afforded **162g** (40 mg, 36%) as a yellow solid.  $R_f = 0.2$  (hexane/ $CH_2Cl_2$  2:1). Mp: 68–69 °C. IR ( $CH_2Cl_2$ , cast): 3084, 3108, 2960, 2196, 2097, 1587, 1531, 1503, 1430, 1332  $cm^{-1}$ .  $^1H$  NMR (400 MHz,  $CDCl_3$ ):  $\delta$  7.77 (d,  $J = 4.4$  Hz, 1H), 7.06 (d,  $J = 4.4$  Hz, 1H), 2.11 (s, 3H), 2.09 (s, 3H), 0.20 (s, 9H).  $^{13}C$  NMR (100 MHz,  $CDCl_3$ , APT):  $\delta$  162.4, 150.8, 130.8, 130.6, 128.5, 99.8, 93.8, 91.9, 87.5, 83.6, 72.1, 23.4, 23.3, -0.5 (one coincident peak not observed). EI MS  $m/z$  (rel. intensity): 327.1 ( $M^+$ , 100), 312.0 ( $[M - Me]^+$ , 29). EI HRMS: calcd for  $C_{17}H_{17}NO_2SSi$  ( $M^+$ ), 327.0749; found, 327.0733. Anal. Calcd for  $C_{17}H_{17}NO_2SSi$ : C, 62.35; H, 5.23; N, 4.28. Found: C, 62.91; H, 5.22; N, 4.28.

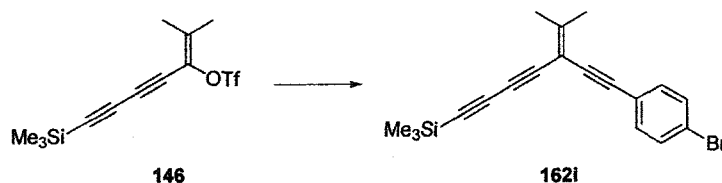
**6-Methyl-5-(4-cyanophenylethynyl)-1-trimethylsilylhept-5-ene-1,3-diyne (162h).**



4-Trimethylsilylanylethynylbenzonitrile (43 mg, 0.22 mmol) was desilylated with  $K_2CO_3$  in THF/MeOH (1:1) and cross-coupled with triflate **146** (70 mg, 0.22 mmol) in degassed THF (20 mL) in the presence of  $PdCl_2(PPh_3)_2$  (6 mg, 0.009 mmol), diisopropylamine (2 mL), and CuI (3 mg, 0.02 mmol) for 1.5 h as described in the general procedure. Flash chromatography (hexane/ $CH_2Cl_2$  1:1) afforded **162g** (52 mg,

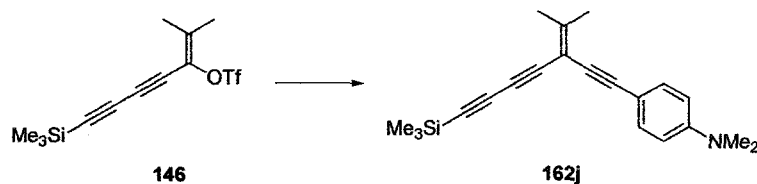
80%) as a yellow solid.  $R_f = 0.5$  (hexane/ $\text{CH}_2\text{Cl}_2$  1:1). Mp: 60–62 °C. IR ( $\text{CH}_2\text{Cl}_2$ , cast): 2960, 2904, 2229, 2198, 2095, 1604, 1499, 1433  $\text{cm}^{-1}$ .  $^1\text{H}$  NMR (400 MHz,  $\text{CDCl}_3$ ):  $\delta$  7.59 (d,  $J = 1.2$  Hz, 2H), 7.50 (d,  $J = 1.2$  Hz, 2H), 2.10 (s, 6H), 0.20 (s, 9H).  $^{13}\text{C}$  NMR (75 MHz,  $\text{CDCl}_3$ , APT):  $\delta$  160.9, 132.0, 131.9, 128.1, 118.5, 111.6, 100.2, 91.5, 90.4, 89.5, 87.7, 73.0, 23.3,  $-0.4$  (two coincident peaks not observed). EI MS  $m/z$  (rel. intensity): 301.1 ( $\text{M}^+$ , 92), 286.1 ( $[\text{M} - \text{Me}]^+$ , 100). EI HRMS: calcd for  $\text{C}_{20}\text{H}_{19}\text{NSi}$  ( $\text{M}^+$ ), 301.1287; found, 301.1292.

#### 6-Methyl-5-(4-bromophenylethynyl)-1-trimethylsilylhept-5-ene-1,3-diyne (162i).



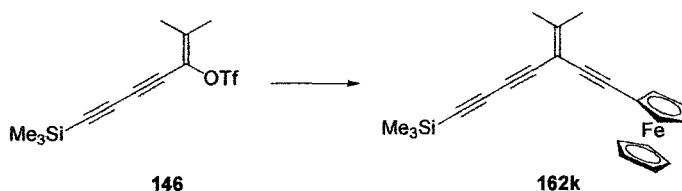
(4-Bromophenylethynyl)trimethylsilane (101 mg, 0.399 mmol) was desilylated with  $\text{K}_2\text{CO}_3$  in THF/MeOH (1:1) and cross-coupled with triflate **146** (130 mg, 0.401 mmol) in degassed THF (20 mL) in the presence of  $\text{PdCl}_2(\text{PPh}_3)_2$  (14 mg, 0.020 mmol), diisopropylamine (2 mL), and CuI (7 mg, 0.04 mmol) for 2 h as described in the general procedure. Flash chromatography (hexane/ $\text{CH}_2\text{Cl}_2$  1:1) afforded **162i** (112 mg, 79%) as a colorless waxy solid.  $R_f = 0.8$  (hexane/ $\text{CH}_2\text{Cl}_2$  1:1). IR ( $\text{CHCl}_3$ , cast): 2959, 2198, 2094, 1484, 1421  $\text{cm}^{-1}$ .  $^1\text{H}$  NMR (400 MHz,  $\text{CDCl}_3$ ):  $\delta$  7.42 (d,  $J = 8.4$  Hz, 2H), 7.28 (d,  $J = 8.4$  Hz, 2H), 2.08 (s, 6H), 0.20 (s, 9H).  $^{13}\text{C}$  NMR (75 MHz,  $\text{CDCl}_3$ , APT):  $\delta$  159.3, 132.8, 131.5, 122.5, 122.0, 100.4, 91.1, 91.0, 87.9, 86.2, 76.2, 73.5, 23.1, 23.0,  $-0.4$ . EI MS  $m/z$  (rel. intensity): 356.0 ( $\text{M}^+$ , 100), 341.0 ( $[\text{M} - \text{Me}]^+$ , 78). EI HRMS: calcd for  $\text{C}_{19}\text{H}_{19}^{81}\text{BrSi}$  ( $\text{M}^+$ ), 356.0419; found, 356.0419.

**6-Methyl-5-(4-*N,N*-dimethylaminophenylethynyl)-1-trimethylsilylhept-5-ene-1,3-diyne (162j).**



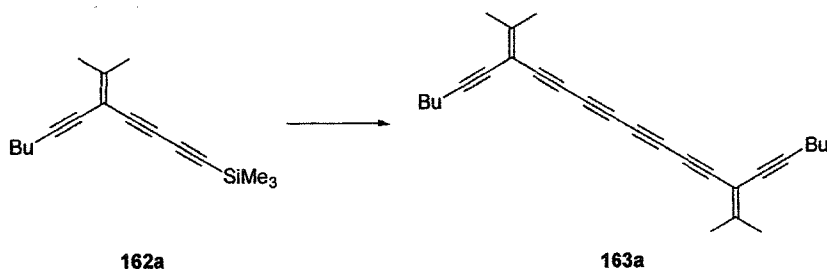
*N,N*-Dimethyl(4-trimethylsilylethynylphenyl)amine (109 mg, 0.501 mmol) was desilylated with  $K_2CO_3$  in THF/MeOH (1:1) and cross-coupled with triflate **146** (162 mg, 0.501 mmol) in degassed THF (20 mL) in the presence of  $PdCl_2(PPh_3)_2$  (18 mg, 0.026 mmol), diisopropylamine (2 mL), and CuI (9 mg, 0.05 mmol) for 1.5 h as described in the general procedure. Flash chromatography (hexane/ $CH_2Cl_2$  2:1) afforded **162j** (133 mg, 83%) as a yellow solid.  $R_f = 0.5$  (hexane/ $CH_2Cl_2$  2:1). Mp: 82–83 °C. IR ( $CHCl_3$ , cast): 2959, 2902, 2200, 2094, 1609, 1521, 1481, 1445  $cm^{-1}$ .  $^1H$  NMR (400 MHz,  $CDCl_3$ ):  $\delta$  7.30 (d,  $J = 8.8$  Hz, 2H), 7.60 (d,  $J = 8.8$  Hz, 2H), 2.96 (s, 6H), 2.09 (s, 3H), 2.07 (s, 3H), 0.22 (s, 9H).  $^{13}C$  NMR (100 MHz,  $CDCl_3$ , APT):  $\delta$  156.9, 150.0, 132.5, 111.7, 109.8, 100.8, 93.3, 90.5, 88.2, 82.9, 75.6, 74.4, 40.1, 22.9, 22.8,  $-0.4$ . EI MS  $m/z$  (rel. intensity): 319.2 ( $M^+$ , 100), 304.1 ( $[M - Me]^+$ , 20). EI HRMS: calcd for  $C_{21}H_{25}NSi$  ( $M^+$ ), 319.1756; found, 319.1750.

**6-Methyl-5-(ferrocenylethynyl)-1-trimethylsilylhept-5-ene-1,3-diyne (162k).**



Ethynyl ferrocene (76 mg, 0.36 mmol) was cross-coupled with triflate **146** (117 mg, 0.362 mmol) in degassed THF (20 mL) in the presence of PdCl<sub>2</sub>(PPh<sub>3</sub>)<sub>2</sub> (13 mg, 0.018 mmol), diisopropylamine (2 mL), and CuI (7 mg, 0.04 mmol) for 2 h as described in the general procedure. Flash chromatography (hexane/CH<sub>2</sub>Cl<sub>2</sub> 2:1) afforded **162k** (78 mg, 56%) as a yellow solid. *R<sub>f</sub>* = 0.8 (hexane/CH<sub>2</sub>Cl<sub>2</sub> 2:1). Mp: 84–85 °C. IR (μscope): 3099, 2964, 2908, 2214, 2191, 2091, 1593, 1426, 1410 cm<sup>-1</sup>. <sup>1</sup>H NMR (300 MHz, CDCl<sub>3</sub>): δ 4.42 (s, 2H), 4.21 (s, 7H), 2.06 (s, 3H), 2.05 (s, 3H), 0.19 (s, 9H). <sup>13</sup>C NMR (75 MHz, CDCl<sub>3</sub>, APT): δ 157.6, 100.9, 91.1, 90.7, 88.1, 81.2, 74.2, 71.4, 70.0, 68.8, 65.1, 23.1, 22.9, -0.3 (one coincident peak not observed). EI HRMS: calcd for C<sub>23</sub>H<sub>24</sub>FeSi (M<sup>+</sup>), 384.0997; found, 384.1001.

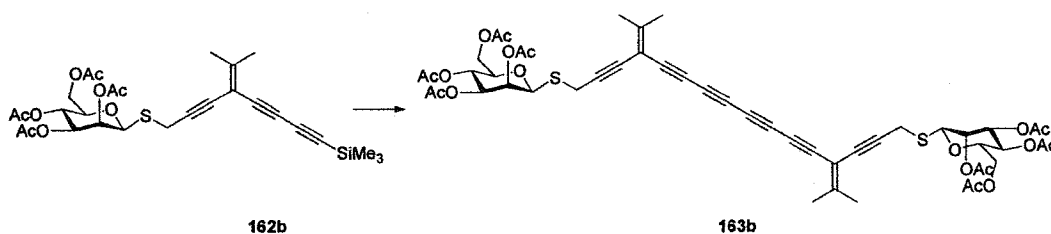
**3,12-Bis(1-pentynyl)-2,13-dimethyltetradeca-2,12-diene-4,6,8,10-tetrayne (163a).**



Compound **162a** (66 mg, 0.26 mmol) was desilylated with K<sub>2</sub>CO<sub>3</sub> in MeOH/THF (1:1) and homo-coupled in acetone (10 mL) in the presence of *Hay* catalyst (1 mL) and air for 1 h as described in the general procedure. Flash chromatography (hexane/CH<sub>2</sub>Cl<sub>2</sub> 2:1) afforded **163a** (45 mg, 94%) as a brown oil. *R<sub>f</sub>* = 0.8 (hexane/CH<sub>2</sub>Cl<sub>2</sub> 2:1). IR (CHCl<sub>3</sub>, cast): 2958, 2932, 2872, 2193, 2125, 1587 cm<sup>-1</sup>. UV-vis (CHCl<sub>3</sub>): λ<sub>max</sub> (ε) 303 (57 800), 321 (41 700), 349 (17 100), 374 (18 800), 406 (11 800). <sup>1</sup>H NMR (300 MHz, CDCl<sub>3</sub>): δ 2.33 (t, *J* = 6.6 Hz, 4H), 2.02 (s, 6H), 2.01 (s, 6H), 1.54–1.36 (m, 8H), 0.90 (t,

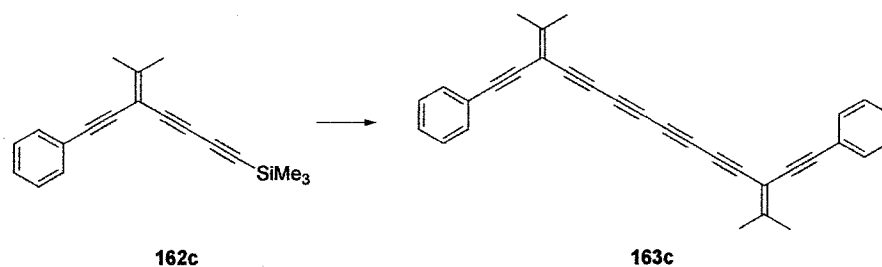
$J = 7.2$  Hz, 6H).  $^{13}\text{C}$  NMR (75 MHz,  $\text{CDCl}_3$ , APT):  $\delta$  159.7, 100.5, 94.2, 75.7, 75.5, 67.7, 64.0, 30.8, 23.1, 23.0, 22.0, 19.2, 13.6 (one coincident peak not observed). EI HRMS: calcd for  $\text{C}_{28}\text{H}_{30}$  ( $\text{M}^+$ ), 366.2347; found, 366.2349.

**1,16-Bis(2,3,4,6-tetra-*O*-acetyl- $\beta$ -D-mannopyranosylmecarpto)-4,13-diisopropylidene-2,5,7,9,11,14-hexadecaheptyne (163b).**



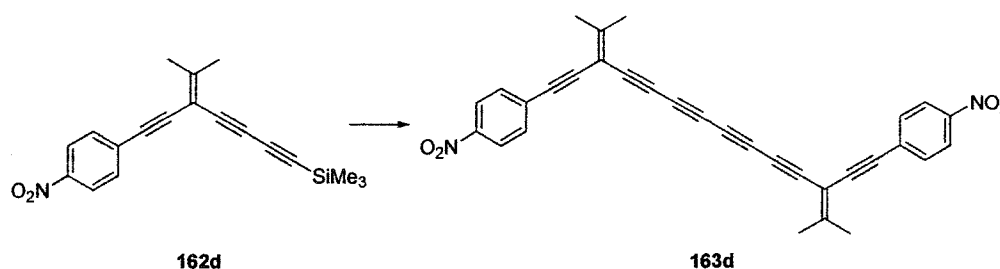
Compound **162b** (20 mg, 0.035 mmol) was desilylated with  $\text{K}_2\text{CO}_3$  in MeOH/THF (1:1) and homo-coupled in acetone (10 mL) in the presence of *Hay* catalyst (1 mL) and air for 0.5 h as described in the general procedure. Flash chromatography (hexane/ethyl acetate 1:5) afforded **163b** (16 mg, 91%) as a brown solid.  $R_f = 0.6$  (hexane/ethyl acetate 1:5). Mp: 57–62 °C. IR ( $\text{CH}_2\text{Cl}_2$ , cast): 2934, 2193, 1750, 1587, 1432  $\text{cm}^{-1}$ .  $^1\text{H}$  NMR (600 MHz,  $\text{CDCl}_3$ ):  $\delta$  5.51 (d,  $J = 3.5$  Hz, 2H), 5.28 (t,  $J = 10.1$  Hz, 2H), 5.09 (dd,  $J_1 = 10.1$  Hz,  $J_2 = 3.5$  Hz, 2H), 5.02 (s, 2H), 4.29 (dd,  $J_1 = 12.3$  Hz,  $J_2 = 5.7$  Hz, 2H), 4.13 (dd,  $J_1 = 12.3$  Hz,  $J_2 = 2.4$  Hz, 2H), 3.73 (d,  $J = 17.0$  Hz, 4H), 3.71 (m, 2H), 3.43 (d,  $J = 17.0$  Hz, 4H), 2.16 (s, 6H), 2.07 (s, 12 H), 2.04 (s, 12H), 1.97 (s, 6H).  $^{13}\text{C}$  NMR (75 MHz,  $\text{CDCl}_3$ , APT):  $\delta$  170.7, 170.1, 170.0, 169.7, 162.3, 99.7, 87.6, 80.9, 76.9, 76.4, 75.1, 72.1, 70.2, 69.6, 68.1, 65.8, 62.6, 31.8, 29.3, 23.4, 23.2, 20.8, 20.7 (2 $\times$ ), 20.6. ESI MS  $m/z$  (MeOH): 1029.3 ( $[\text{M} + \text{Na}]^+$ ).

**3,12-Bis(1-phenylethynyl)-2,13-dimethyltetradeca-2,12-diene-4,6,8,10-tetrayne  
(163c).**



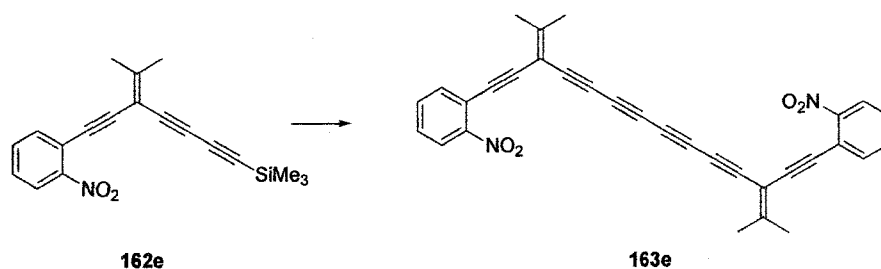
Compound **162c** (68 mg, 0.24 mmol) was desilylated with  $K_2CO_3$  in MeOH/THF (1:1) and homo-coupled in acetone (10 mL) in the presence of *Hay* catalyst (1 mL) and air for 0.5 h as described in the general procedure. Flash chromatography (hexane/ $CH_2Cl_2$  2:1) afforded **163c** (32 mg, 64%) as a yellow waxy solid.  $R_f = 0.6$  (hexane/ $CH_2Cl_2$  2:1). IR ( $\mu$ scope): 3056, 2930, 2906, 2194, 2127, 1598, 1583, 1489, 1442  $cm^{-1}$ . UV-vis ( $CHCl_3$ ):  $\lambda_{max}$  ( $\epsilon$ ) 284 (91 200), 296 (82 100), 325 (41 900), 350 (18 600), 375 (19 900), 407 (11 800).  $^1H$  NMR (300 MHz,  $CDCl_3$ ):  $\delta$  7.46–7.42 (m, 4H), 7.32–7.28 (m, 6H), 2.13 (s, 6H), 2.12 (s, 6H).  $^{13}C$  NMR (75 MHz,  $CDCl_3$ , APT):  $\delta$  161.5, 131.5, 128.4, 128.3, 122.9, 100.4, 92.8, 84.4, 76.4, 75.0, 67.9, 64.1, 23.4, 23.3. EI HRMS: calcd for  $C_{32}H_{22}$  ( $M^+$ ), 406.1722; found, 406.1728.

**3,12-Bis(4-nitrophenylethynyl)-2,13-dimethyltetradeca-2,12-diene-4,6,8,10-tetrayne  
(163d).**



Compound **162d** (88 mg, 0.27 mmol) was desilylated with  $K_2CO_3$  in MeOH/THF (1:1) and homo-coupled in acetone (10 mL) in the presence of *Hay* catalyst (1 mL) and air for 0.5 h as described in the general procedure. Flash chromatography (hexane/ $CH_2Cl_2$  2:1) afforded **163d** (64 mg, 94%) as a yellow solid.  $R_f = 0.6$  (hexane/ $CH_2Cl_2$  2:1). Mp: > 115 °C (dec.). IR ( $\mu$ scope): 3104, 2932, 2847, 2198, 2128, 1594, 1520, 1491, 1432, 1343  $cm^{-1}$ . UV-vis ( $CHCl_3$ ):  $\lambda_{max}$  ( $\epsilon$ ) 287 (66 700), 306 (90 400), 323 (83 700), 349 (50 200), 374 (39 800), 406 (15 900).  $^1H$  NMR (400 MHz,  $CDCl_3$ ):  $\delta$  8.17 (d,  $J = 8.8$  Hz, 4H), 7.57 (d,  $J = 8.8$  Hz, 4H), 2.149 (s, 6H), 2.146 (s, 6H).  $^{13}C$  NMR (100 MHz,  $CDCl_3$ , APT):  $\delta$  163.9, 147.1, 132.1, 129.7, 123.6, 99.9, 90.8, 89.5, 76.7, 74.2, 68.1, 63.9, 23.5 (2 $\times$ ). EI HRMS: calcd for  $C_{32}H_{20}N_2O_4$  ( $M^+$ ), 496.1423; found, 496.1424.

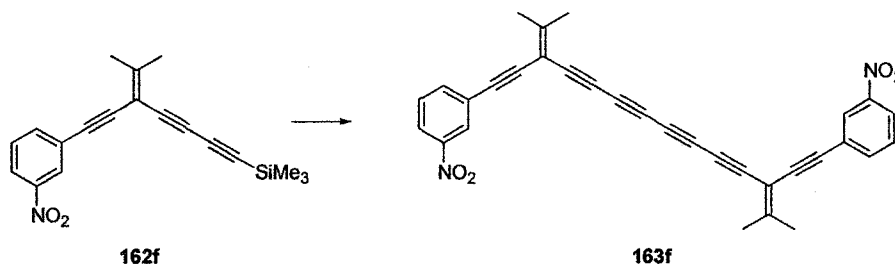
**3,12-Bis(2-nitrophenylethynyl)-2,13-dimethyltetradeca-2,12-diene-4,6,8,10-tetrayne (163e).**



Compound **162e** (53 mg, 0.16 mmol) was desilylated with  $K_2CO_3$  in MeOH/THF (1:1) and homo-coupled in acetone (10 mL) in the presence of *Hay* catalyst (1 mL) and air for 2 h as described in the general procedure. Flash chromatography (hexane/ $CH_2Cl_2$  2:1) afforded **163e** (11 mg, 27%) as a yellow waxy solid.  $R_f = 0.3$  (hexane/ $CH_2Cl_2$  2:1). IR ( $\mu$ scope): 2927, 2200, 1607, 1567, 1528, 1479, 1438, 1336  $cm^{-1}$ . UV-vis ( $CHCl_3$ ):

$\lambda_{\max}$  ( $\epsilon$ ) 285 (72 300), 304 (63 000), 324 (52 600), 349 (28 500), 374 (27 000), 406 (14 700).  $^1\text{H}$  NMR (400 MHz,  $\text{CDCl}_3$ ):  $\delta$  8.06 (d,  $J = 8.0$  Hz, 2H), 7.66 (d,  $J = 8.0$  Hz, 2H), 7.57 (t,  $J = 8.0$  Hz, 2H), 7.44 (t,  $J = 8.0$  Hz, 2H), 2.21 (s, 6H), 2.15 (s, 6H).  $^{13}\text{C}$  NMR (100 MHz,  $\text{CDCl}_3$ , APT):  $\delta$  165.0, 149.0, 134.7, 132.9, 128.6, 124.7, 118.5, 100.1, 92.2, 88.0, 76.6, 74.3, 68.0, 64.0, 23.6, 23.5. EI HRMS: calcd for  $\text{C}_{32}\text{H}_{20}\text{N}_2\text{O}_4$  ( $\text{M}^+$ ), 496.1423; found, 496.1419.

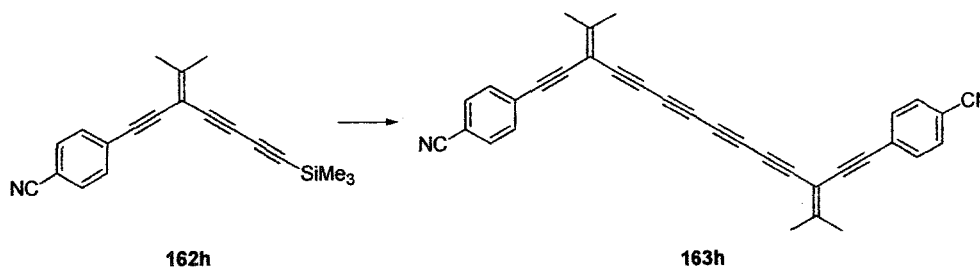
**3,12-Bis(3-nitrophenylethynyl)-2,13-dimethyltetradeca-2,12-diene-4,6,8,10-tetrayne (163f).**



Compound **162f** (77 mg, 0.24 mmol) was desilylated with  $\text{K}_2\text{CO}_3$  in MeOH/THF (1:1) and homo-coupled in acetone (10 mL) in the presence of *Hay* catalyst (1 mL) and air for 0.5 h as described in the general procedure. Flash chromatography (hexane/ $\text{CH}_2\text{Cl}_2$  2:1) afforded **163f** (23 mg, 39%) as a yellow waxy solid.  $R_f = 0.4$  (hexane/ $\text{CH}_2\text{Cl}_2$  2:1). IR ( $\text{CH}_2\text{Cl}_2$ , cast): 3087, 2926, 2197, 1576, 1536, 1475, 1427, 1346  $\text{cm}^{-1}$ . UV-vis ( $\text{CHCl}_3$ ):  $\lambda_{\max}$  ( $\epsilon$ ) 282 (98 100), 301 (87 500), 321 (54 200), 349 (20 100), 374 (21 400), 405 (13 300).  $^1\text{H}$  NMR (300 MHz,  $\text{CDCl}_3$ ):  $\delta$  8.28 (s, 2H), 8.15 (d,  $J = 8.1$  Hz, 2H), 7.73 (d,  $J = 8.1$  Hz, 2H), 7.49 (t,  $J = 8.1$  Hz, 2H), 2.152 (s, 6H), 2.146 (s, 6H).  $^{13}\text{C}$  NMR (75 MHz,  $\text{CDCl}_3$ , APT):  $\delta$  163.4, 148.2, 137.1, 129.4, 126.3, 124.8, 123.1, 99.9, 90.2, 86.9,

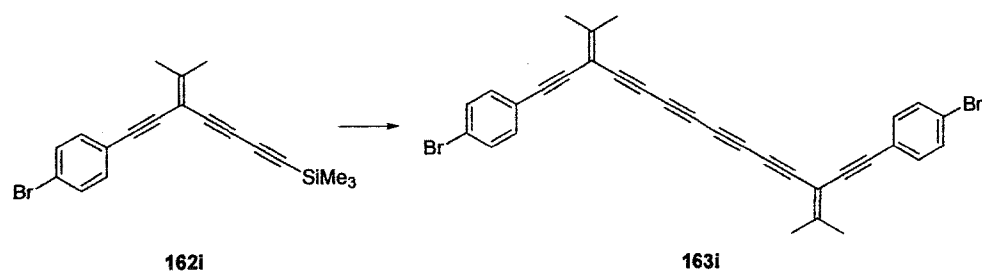
74.3, 68.1, 64.0, 23.6, 23.5 (one coincident peak not observed). EI HRMS: calcd for  $C_{32}H_{20}N_2O_4$  ( $M^+$ ), 496.1423; found, 496.1409.

**3,12-Bis(4-cyanophenylethynyl)-2,13-dimethyltetradeca-2,12-diene-4,6,8,10-tetrayne (163h).**



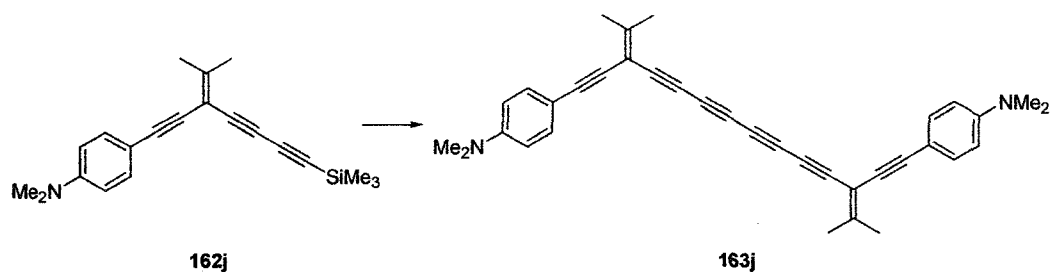
Compound **162h** (40 mg, 0.13 mmol) was desilylated with  $K_2CO_3$  in MeOH/THF (1:1) and homo-coupled in acetone (10 mL) in the presence of *Hay* catalyst (1 mL) and air for 0.5 h as described in the general procedure. Flash chromatography (hexane/ $CH_2Cl_2$  2:1) afforded **163h** (22 mg, 73%) as a yellow waxy solid.  $R_f = 0.6$  (hexane/ $CH_2Cl_2$  2:1). IR ( $CH_2Cl_2$ , cast): 2907, 2228, 2194, 2126, 1603, 1450, 1432  $cm^{-1}$ . UV-vis ( $CHCl_3$ ):  $\lambda_{max}$  ( $\epsilon$ ) 300 (104 400), 323 (69 600), 349 (17 600), 375 (17 700), 407 (9 700).  $^1H$  NMR (300 MHz,  $CDCl_3$ ):  $\delta$  7.59 (d,  $J = 8.4$  Hz, 4H), 7.51 (d,  $J = 8.4$  Hz, 4H), 2.14 (s, 12H).  $^{13}C$  NMR (75 MHz,  $CDCl_3$ , APT):  $\delta$  163.6, 132.1, 132.0, 127.8, 118.5, 111.8, 100.0, 91.1, 88.7, 76.7, 74.3, 68.1, 64.0, 23.6, 23.5. EI HRMS: calcd for  $C_{34}H_{20}N_2$  ( $M^+$ ), 456.1627; found, 456.1629.

**3,12-Bis(4-bromophenylethynyl)-2,13-dimethyltetradeca-2,12-diene-4,6,8,10-tetrayne (163i).**



Compound **162i** (93 mg, 0.26 mmol) was desilylated with  $K_2CO_3$  in MeOH/THF (1:1) and homo-coupled in acetone/ $CH_2Cl_2$  (1:1) (10 mL) in the presence of *Hay* catalyst (1 mL) and air for 0.5 h as described in the general procedure. Flash chromatography (hexane/ $CH_2Cl_2$  2:1) afforded **163i** (63 mg, 85%) as a yellow solid.  $R_f = 0.2$  (hexane/ $CH_2Cl_2$  2:1). Mp:  $>110$  °C (dec.). IR ( $CH_2Cl_2$ , cast): 2904, 2198, 1589, 1485, 1425  $cm^{-1}$ . UV-vis ( $CHCl_3$ ):  $\lambda_{max}$  ( $\epsilon$ ) 285 (104 300), 322 (49 000), 347 (17 600), 374 (20 100), 404 (12 200).  $^1H$  NMR (400 MHz,  $CDCl_3$ , APT):  $\delta$  7.43 (d,  $J = 8.8$  Hz, 4H), 7.29 (d,  $J = 8.8$  Hz, 4H), 2.11 (s, 12H).  $^{13}C$  NMR (100 MHz,  $CDCl_3$ ):  $\delta$  162.0, 132.8, 131.6, 122.7, 121.8, 100.2, 91.7, 85.4, 76.4, 74.7, 67.9, 64.0, 23.4, 23.3. ESI HRMS (MeOH/toluene, 1:1): calcd for  $C_{32}H_{20}^{79}Br_2$  ( $M^+$ ), 561.9926; found, 561.9928.

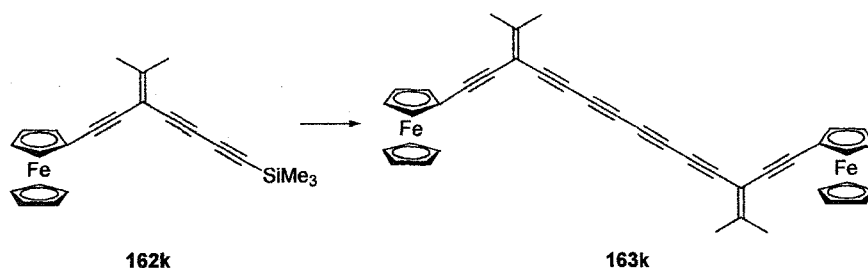
**3,12-Bis[4-*N,N*-(dimethylamino)phenylethynyl]-2,13-dimethyltetradeca-2,12-diene-4,6,8,10-tetrayne (163j).**



Compound **162j** (73 mg, 0.23 mmol) was desilylated with  $K_2CO_3$  in MeOH/THF (1:1) and homo-coupled in acetone/ $CH_2Cl_2$  (1:1) (10 mL) in the presence of *Hay* catalyst

(1 mL) and air for 20 min as described in the general procedure. Flash chromatography (hexane/CH<sub>2</sub>Cl<sub>2</sub> 2:1) afforded **163j** (43 mg, 76%) as a yellow solid.  $R_f = 0.5$  (hexane/CH<sub>2</sub>Cl<sub>2</sub> 2:1). Mp: >115 °C (dec.). IR (CHCl<sub>3</sub>, cast): 2902, 2194, 2122, 1608, 1520, 1480, 1444 cm<sup>-1</sup>. UV-vis (CHCl<sub>3</sub>):  $\lambda_{\max}$  ( $\epsilon$ ) 295 (94 600), 312 (92 000), 346 (46 900), 374 (24 000), 407 (12 800). <sup>1</sup>H NMR (400 MHz, CDCl<sub>3</sub>):  $\delta$  7.31 (d,  $J = 9.2$  Hz, 4H), 6.61 (d,  $J = 9.2$  Hz, 4H), 2.96 (s, 12H), 2.10 (s, 6H), 2.09 (s, 6H). <sup>13</sup>C NMR (100 MHz, CDCl<sub>3</sub>, APT):  $\delta$  159.5, 150.2, 132.6, 111.7, 109.6, 100.7, 94.1, 82.3, 75.9, 75.5, 67.8, 64.1, 40.1, 23.2, 23.1. ESI HRMS (MeOH/toluene, 1:1): calcd for C<sub>36</sub>H<sub>32</sub>N<sub>2</sub> (M<sup>+</sup>), 492.2565; found, 492.2560.

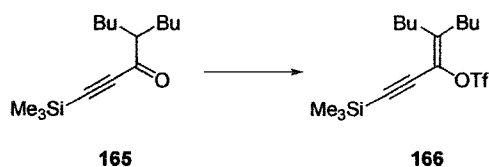
**3,12-Bis(ferrocenylethynyl)-2,13-dimethyltetradeca-2,12-diene-4,6,8,10-tetrayne (163k).**



Compound **162k** (70 mg, 0.18 mmol) was desilylated with K<sub>2</sub>CO<sub>3</sub> in MeOH/THF (1:1) and homo-coupled in acetone/CH<sub>2</sub>Cl<sub>2</sub> (1:1) (10 mL) in the presence of *Hay* catalyst (1 mL) and air for 0.5 h as described in the general procedure. Flash chromatography (hexane/CH<sub>2</sub>Cl<sub>2</sub> 2:1) afforded **163k** (42 mg, 74%) as an orange solid.  $R_f = 0.4$  (hexane/CH<sub>2</sub>Cl<sub>2</sub> 2:1). Mp: >120 °C (dec.). IR ( $\mu$ scope): 3097, 2987, 2932, 2904, 2214, 2191, 1577, 1424 cm<sup>-1</sup>. UV-vis (CHCl<sub>3</sub>):  $\lambda_{\max}$  ( $\epsilon$ ) 296 (78 800), 349 (19 400), 375 (18 400), 406 (11 500). <sup>1</sup>H NMR (500 MHz, CDCl<sub>3</sub>):  $\delta$  4.42 (m, 4H), 4.20 (m, 14H), 2.08 (s,

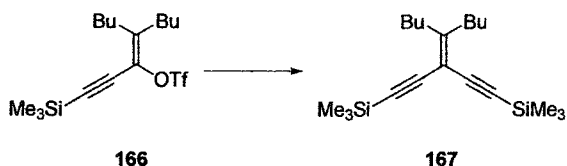
6H), 2.07 (s, 6H).  $^{13}\text{C}$  NMR (125 MHz,  $\text{CDCl}_3$ , APT):  $\delta$  159.9, 100.7, 91.9, 80.5, 76.0, 75.3, 71.4, 69.9, 68.9, 67.8, 64.8, 64.1, 23.4, 23.2. ESI HRMS (MeOH/toluene, 3:1): calcd for  $\text{C}_{40}\text{H}_{30}\text{Fe}_2$  ( $\text{M}^+$ ), 622.1046; found, 622.1043. X-ray.

**Trifluoromethanesulfonic acid 2-butyl-1-trimethylsilylethynylhex-1-enyl ester (166).**



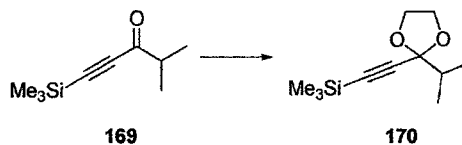
Reaction of 4-butyl-1-trimethylsilyl-oct-1-yn-3-one **165** (174 mg, 0.689 mmol) with trifluoromethane-sulfonic anhydride (243 mg, 0.861 mmol) and 2,6-di-*t*-butyl-4-methyl pyridine (212 mg, 1.03 mmol) in  $\text{CH}_2\text{Cl}_2$  (25 mL) was conducted under argon for 24 h. The  $\text{CH}_2\text{Cl}_2$  was removed *in vacuo* and the residue extracted with pentane. The organic solution was washed with 10% HCl, satd. aq.  $\text{NaHCO}_3$ , and brine, and dried. Evaporation followed by flash chromatography (hexane/ $\text{CH}_2\text{Cl}_2$  2:1) gave **166** (80 mg, 30%) as a clear light yellow oil.  $R_f$  = 0.8 (2:1 hexane/ $\text{CH}_2\text{Cl}_2$ ). IR ( $\text{CH}_2\text{Cl}_2$ , cast): 2961, 2934, 2864, 2153, 1467, 1419  $\text{cm}^{-1}$ .  $^1\text{H}$  NMR (300 MHz,  $\text{CDCl}_3$ ):  $\delta$  2.29 (t,  $J$  = 7.2 Hz, 2H), 2.23 (t,  $J$  = 6.9 Hz, 2H), 1.52–1.23 (m, 8H), 0.91 (t,  $J$  = 7.5 Hz, 3H), 0.89 (t,  $J$  = 7.2 Hz, 3H), 0.19 (s, 9H).  $^{13}\text{C}$  NMR (75 MHz,  $\text{CDCl}_3$ , APT):  $\delta$  146.4, 126.7, 113.8, 110.6, 31.7, 29.7, 29.5, 29.4, 22.7, 22.4, 13.8, -0.6 (one coincident peak and  $\text{CF}_3$  peak not observed). EI HRMS: calcd for  $\text{C}_{16}\text{H}_{27}\text{F}_3\text{O}_3\text{SSi}$  ( $\text{M}^+$ ), 384.1402; found, 384.1400.

**4-Butyl-1-trimethylsilyl-3-trimethylsilylethynyl-oct-3-en-1-yne (167).**



Triflate **166** (89 mg, 0.23 mmol) was cross-coupled with trimethylsilylacetylene (46 mg, 0.46 mmol) in degassed DMF (10 mL) in the presence of  $\text{PdCl}_2(\text{PPh}_3)_4$  (13 mg, 0.019 mmol), diethylamine (2 mL), and CuI (6.6 mg, 0.035 mmol) for 2 h as described in the general procedure. Flash chromatography (hexane/ $\text{CH}_2\text{Cl}_2$  2:1) afforded **167** (38 mg, 50%) as a colorless oil.  $R_f = 0.8$  (hexane/ $\text{CH}_2\text{Cl}_2$  2:1). IR ( $\text{CH}_2\text{Cl}_2$ , cast): 2958, 2929, 2873, 2860, 2151, 1574, 1465  $\text{cm}^{-1}$ .  $^1\text{H}$  NMR (300 MHz,  $\text{CDCl}_3$ ):  $\delta$  2.36 (t,  $J = 6.9$  Hz, 4H), 1.46-1.23 (m, 8H), 0.89 (t,  $J = 7.2$  Hz, 6H), 0.17 (s, 18H). EI HRMS: calcd for  $\text{C}_{20}\text{H}_{36}\text{Si}_2$  ( $\text{M}^+$ ), 332.2356; found, 332.2352.

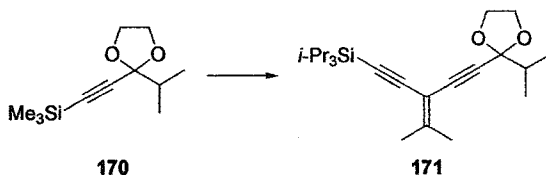
**(2-Isopropyl-[1,3]dioxolan-2-ylethynyl)trimethylsilane (170).**



4-Methyl-1-trimethylsilyl-pent-1-yn-3-one **169** (1.10 g, 6.54 mmol) and glycerol (1.10 g, 17.7 mmol) were added to benzene (10 mL) in the presence of TsOH (5 mg, 0.03 mmol). The mixture were refluxed for 2 h, and then washed with satd.  $\text{NaHCO}_3$ , brine and dried with  $\text{MgSO}_4$ . Removal of the solvent *in vacuo* followed by column chromatography (hexanes/ethyl acetate 2:1) afforded **170** (0.881 g, 63%) as a colorless liquid.  $R_f = 0.6$  (hexane/ethyl acetate 2:1). IR (neat): 2967, 2893, 2168, 1472, 1118  $\text{cm}^{-1}$ .  $^1\text{H}$  NMR (300 MHz,  $\text{CDCl}_3$ ):  $\delta$  4.07 (m, 2H), 3.93 (m, 2H), 1.97 (m, 1H), 1.03 (d,  $J = 6.6$  Hz, 6H), 0.16 (s, 9H).  $^{13}\text{C}$  NMR (75 MHz,  $\text{CDCl}_3$ , APT):  $\delta$  106.4, 101.8, 89.4,

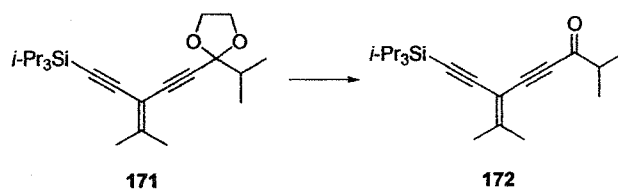
64.8, 36.6, 17.1, -0.1 (one coincident peak not observed). EI HRMS: calcd for  $C_{11}H_{20}O_2Si$  ( $M^+$ ), 212.1233; found, 212.1222.

**[3-(2-Isopropyl-[1,3]dioxolan-2-ylethynyl)-4-methylpent-3-en-1-ynyl]triisopropylsilane (171).**



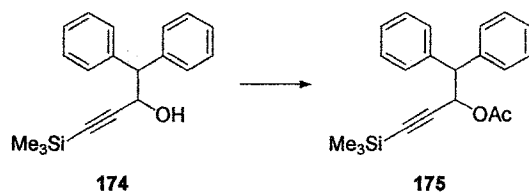
Compound **170** (42 mg, 0.20 mmol) was desilylated with  $K_2CO_3$  in MeOH/THF (1:1) and cross-coupled with triflate **96** (77 mg, 0.20 mmol) in degassed DMF (10 mL) in the presence of  $Pd(PPh_3)_4$  (12 mg, 0.010 mmol), diethylamine (2 mL), and CuI (6 mg, 0.03 mmol) for 1.5 h as described in the general procedure. Flash chromatography (hexane/ $CH_2Cl_2$  2:1) afforded **171** (50 mg, 67%) as a colorless waxy solid.  $R_f = 0.2$  (hexane/ $CH_2Cl_2$  2:1). IR ( $CH_2Cl_2$ , cast): 2962, 2944, 2892, 2866, 2147, 1464, 1116  $cm^{-1}$ .  $^1H$  NMR (300 MHz,  $CDCl_3$ ):  $\delta$  4.08 (m, 2H), 3.96 (m, 2H), 2.02 (s, 3H), 1.99 (s, 3H), 1.06 (s, 21H).  $^{13}C$  NMR (75 MHz,  $CDCl_3$ , APT):  $\delta$  155.0, 107.1, 103.5, 101.3, 92.7, 87.7, 81.8, 64.7, 36.8, 22.7 (2 $\times$ ), 18.7, 17.29, 11.3 (one coincident peak not observed). EI MS  $m/z$  (rel. intensity): 374.3 ( $M^+$ , 6), 331.2 ( $[M - i-Pr]^+$ , 100). EI HRMS: calcd for  $C_{23}H_{38}O_2Si$  ( $M^+$ ), 374.2641; found, 374.2633.

**2,7-Dimethyl-6-triisopropylsilylethynyl-oct-6-en-4-yn-3-one (172).**



Compound **171** (100 mg, 0.34 mmol) and 2,6-lutidium *p*-toluenesulfonate (10 mg, 0.036 mmol) were added into THF (10 mL). The mixture was refluxed for 8 h, and then diethyl ether (15 mL) was added. The organic phase was washed with satd. NaHCO<sub>3</sub> and brine, and dried with MgSO<sub>4</sub>. Removal of solvents *in vacuo* afforded **172** (74.6 mg, 88%) as a light yellow oil. IR (CH<sub>2</sub>Cl<sub>2</sub>, cast): 2943, 2866, 2190, 2148, 1672 cm<sup>-1</sup>. <sup>1</sup>H NMR (300 MHz, CDCl<sub>3</sub>): δ 2.64 (m, 1H), 2.10 (s, 3H), 2.09 (s, 3H), 1.20 (d, *J* = 6.9 Hz, 6H), 1.07 (s, 21H). <sup>13</sup>C NMR (75 MHz, CDCl<sub>3</sub>, APT): δ 192.1, 162.1, 101.8, 100.7, 94.4, 89.2, 89.1, 43.3, 23.4, 23.2, 18.7, 18.1, 11.3. EI MS *m/z* (rel. intensity): 330.2 (M<sup>+</sup>, 12), 287.2 ([M - *i*-Pr]<sup>+</sup>, 100). EI HRMS: calcd for C<sub>21</sub>H<sub>34</sub>OSi (M<sup>+</sup>), 330.2379; found, 330.2376.

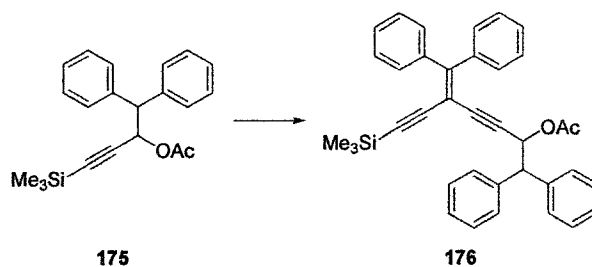
#### Acetic acid 1-diphenylmethyl-3-trimethylsilyl-2-propynyl ester (**175**).



1,1-Diphenyl-4-trimethylsilylbut-3-yn-2-ol **174** (294 mg, 1.00 mmol), acetic anhydride (153 mg, 1.50 mmol), trimethyl amine (152 mg, 1.50 mmol), and 4-dimethylaminopyridine (5 mg, 0.04 mmol) were added into CH<sub>2</sub>Cl<sub>2</sub> (20 mL). The reaction mixture was kept stirring at rt for 24 h, and then washed with 10% HCl, satd. NaHCO<sub>3</sub> and brine, dried with MgSO<sub>4</sub>. The organic solution was filtered through a short

silica gel plug and evaporated under reduced pressure to afford **175** (320 mg, 95%) as a yellow oil. IR (CH<sub>2</sub>Cl<sub>2</sub>, cast): 3029, 2959, 2899, 2182, 1748, 1600, 1496, 1452 cm<sup>-1</sup>. <sup>1</sup>H NMR (400 MHz, CDCl<sub>3</sub>): δ 7.28–7.13 (m, 10H), 6.02 (d, *J* = 8.4 Hz, 1H), 4.31 (d, *J* = 8.4 Hz, 1H), 1.88 (s, 3H), 0.02 (s, 9H). <sup>13</sup>C NMR (100 MHz, CDCl<sub>3</sub>, APT): δ 169.7, 140.0, 129.0, 128.5, 128.3, 128.2, 126.9, 126.8, 101.7, 92.8, 66.2, 55.6, 20.8, -0.5 (one coincident peak not observed). EI MS *m/z* (rel. intensity): 336.2 (M<sup>+</sup>, 1.5), 167.1 (Ph<sub>2</sub>CH<sup>+</sup>, 100). EI HRMS: calcd for C<sub>21</sub>H<sub>24</sub>O<sub>2</sub>Si (M<sup>+</sup>), 336.1546; found, 336.1548.

**Acetic acid 1-diphenylmethyl-4-diphenylmethylidene-6-trimethylsilyl-2,5-hexadiynyl ester (176).**

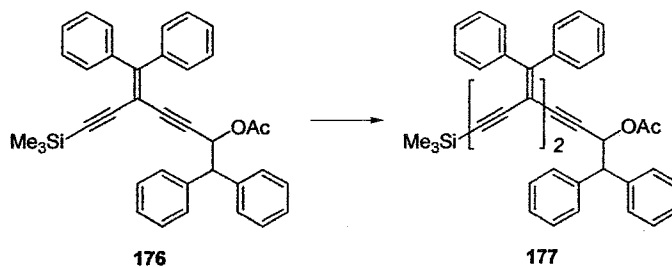


Compound **175** (237 mg, 0.704 mmol) was desilylated with 1 equiv. of TBAF in THF and cross-coupled with triflate **130** (299 mg, 0.704 mmol) in degassed THF (20 mL) in the presence of Pd(PPh<sub>3</sub>)<sub>4</sub> (35 mg, 0.030 mmol), diisopropylamine (2 mL), and CuI (17 mg, 0.089 mmol) under reflux for 12 h as described in the general procedure. Flash chromatography (hexane/CH<sub>2</sub>Cl<sub>2</sub> 1:1) afforded **176** (349 mg, 92%) as a yellow solid. *R<sub>f</sub>* = 0.4 (hexane/CH<sub>2</sub>Cl<sub>2</sub> 1:1). Mp: 86–87 °C. IR (CH<sub>2</sub>Cl<sub>2</sub>, cast): 3028, 2958, 2143, 1745, 1660, 1599 cm<sup>-1</sup>. <sup>1</sup>H NMR (400 MHz, CDCl<sub>3</sub>, APT): δ 7.41–7.21 (m, 20H), 6.17 (d, *J* = 8.4 Hz, 1H), 4.37 (d, *J* = 8.4 Hz, 1H), 1.89 (s, 3H), 0.13 (s, 9H). <sup>13</sup>C NMR (100 MHz, CDCl<sub>3</sub>) δ 169.4, 157.6, 140.1, 139.8 (3×), 130.2, 130.1, 128.9, 128.6, 128.5, 128.4, 128.3,

128.2, 127.6, 127.4, 126.8 (2×), 102.9, 100.9, 97.6, 88.1, 85.3, 66.3, 54.9, 20.7, -0.5. EI

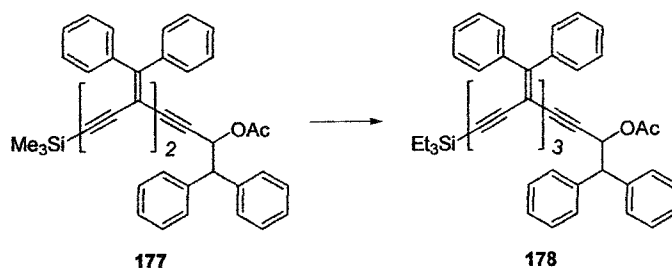
HRMS: calcd for  $C_{37}H_{34}O_2Si$  ( $M^+$ ), 538.2328; found, 538.2330.

**Acetic acid 1-diphenylmethyl-4,7-bis(diphenylmethylidene)-9-trimethylsilyl-2,5,8-nonatriynyl ester (177).**



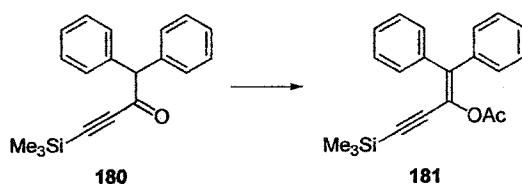
Compound **176** (349 mg, 0.648 mmol) was desilylated with 1 equiv. of TBAF in THF and cross-coupled with triflate **130** (275 mg, 0.648 mmol) in degassed THF (20 mL) in the presence of Pd(PPh<sub>3</sub>)<sub>4</sub> (38 mg, 0.033 mmol), diisopropylamine (2 mL), and CuI (19 mg, 0.10 mmol) under reflux for 12 h as described in the general procedure. Flash chromatography (hexane/CH<sub>2</sub>Cl<sub>2</sub> 1:1) afforded **177** (408 mg, 85%) as a yellow solid.  $R_f$  = 0.6 (hexane/CH<sub>2</sub>Cl<sub>2</sub> 1:1). Mp: 64–67 °C. IR (CHCl<sub>3</sub>, cast): 3057, 2958, 2143, 1745 cm<sup>-1</sup>. <sup>1</sup>H NMR (400 MHz, CDCl<sub>3</sub>, APT): δ 7.43–7.12 (m, 30H), 6.13 (d,  $J$  = 8.4 Hz, 1H), 4.31 (d,  $J$  = 8.4 Hz, 1H), 1.89 (s, 3H), 0.11 (s, 9H). <sup>13</sup>C NMR (100 MHz, CDCl<sub>3</sub>): δ 169.4, 156.8, 156.4, 140.2, 140.1, 140.0, 139.9, 139.8 (2×), 130.4, 130.2, 130.0, 129.0, 128.6 (2×), 128.4, 128.3, 128.2, 127.7, 127.6 (2×), 127.4, 126.9, 126.8, 102.9, 101.8, 100.9, 97.4, 90.5, 90.3, 87.8, 85.2, 66.3, 55.0, 20.8, -0.4 (three coincident peak not observed). EI HRMS: calcd for  $C_{53}H_{44}O_2Si$  ( $M^+$ ), 740.3110; found, 740.3132.

**Acetic acid 1-diphenylmethyl-4,7,10-tri(diphenylmethylidene)-12-trimethylsilyl-2,5,8,11-dodecatetraynyl ester (178).**



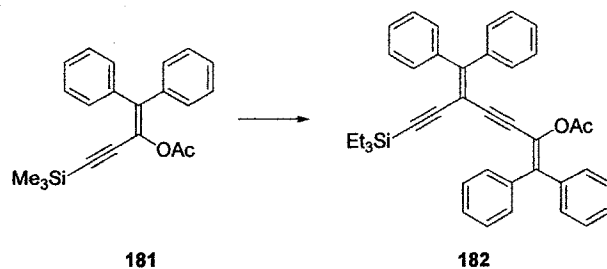
Compound **177** (330 mg, 0.445 mmol) was desilylated with 1 equiv. of TBAF in THF and cross-coupled with triflate **131** (208 mg, 0.446 mmol) in degassed THF (20 mL) in the presence of Pd(PPh<sub>3</sub>)<sub>4</sub> (26 mg, 0.023 mmol), diisopropylamine (2 mL), and CuI (13 mg, 0.068 mmol) under reflux for 12 h as described in the general procedure. Flash chromatography (hexane/CH<sub>2</sub>Cl<sub>2</sub> 1:1) afforded **178** (408 mg, 93%) as a yellow solid. *R<sub>f</sub>* = 0.7 (hexane/CH<sub>2</sub>Cl<sub>2</sub> 1:1). Mp: 73–75 °C. IR (μscope): 3056, 2954, 2873, 2141, 1746, 1661, 1599 cm<sup>-1</sup>. <sup>1</sup>H NMR (500 MHz, CDCl<sub>3</sub>): δ 7.44–7.14 (m, 40H), 6.15 (d, *J* = 8.5 Hz, 1H), 4.31 (d, *J* = 8.5 Hz, 1H), 1.86 (s, 3H), 0.90 (t, *J* = 8.0 Hz, 9H), 0.54 (q, *J* = 8.0 Hz, 6H). <sup>13</sup>C NMR (125 MHz, CDCl<sub>3</sub>, APT): δ 169.3, 156.7, 156.1, 154.6, 140.3, 140.0 (2×), 139.9 (2×), 139.7 (2×), 139.6, 130.3 (2×), 130.2 (2×), 129.9, 128.8, 128.5 (2×), 128.4, 128.3 (2×), 128.2 (2×), 127.6 (2×), 127.5, 127.4, 126.8, 126.7, 103.9, 102.1, 101.9, 100.9, 95.3, 90.8, 90.2, 90.1, 87.9, 85.2, 66.3, 55.1, 20.8, 7.5, 4.3 (six coincident peak not observed). ESI MS *m/z* (MeOH/toluene 3:1, AgOTf added): 1093 ([M + Ag<sup>+</sup>]<sup>+</sup>).

**Acetic acid 1-diphenylmethylidene-3-trimethylsilyl-2-propynyl ester (181).**



1,1-Diphenyl-4-trimethylsilylbut-3-yn-2-one **180** (934 mg, 3.19 mmol) and potassium bis(trimethylsilyl) amide (0.5 M, 10 mL) were added to THF (20 mL) at  $-78$  °C. Acetic anhydride (0.5 mL) was then added, and the mixture was stirred at  $-78$  °C for 0.5 h. The mixture was extracted with diethyl ether (40 mL) and washed with 10% HCl, satd.  $\text{NaHCO}_3$ , and brine, then dried with  $\text{MgSO}_4$ . Removal of the solvents *in vacuo* followed by a flash chromatography (hexane/ $\text{CH}_2\text{Cl}_2$  1:1) afforded **181** (773 mg, 72%) as a colorless solid.  $R_f = 0.5$  (hexane/ $\text{CH}_2\text{Cl}_2$  1:1). Mp:  $82-83$  °C. IR ( $\text{CHCl}_3$ , cast): 3056, 2959, 2146, 1768, 1599  $\text{cm}^{-1}$ .  $^1\text{H}$  NMR (400 MHz,  $\text{CDCl}_3$ ):  $\delta$  7.48 (m, 2H), 7.29 (m, 6H), 7.19 (m, 2H), 1.98 (s, 3H), 0.12 (s, 9H).  $^{13}\text{C}$  NMR (100 MHz,  $\text{CDCl}_3$ , APT):  $\delta$  168.4, 140.5, 137.9, 137.8, 130.3, 129.3, 128.3, 128.2, 128.0, 127.9, 127.6, 100.3, 99.2, 20.7,  $-0.6$ . EI HRMS: calcd for  $\text{C}_{21}\text{H}_{22}\text{O}_2\text{Si}$  ( $\text{M}^+$ ), 334.1389; found, 334.1384.

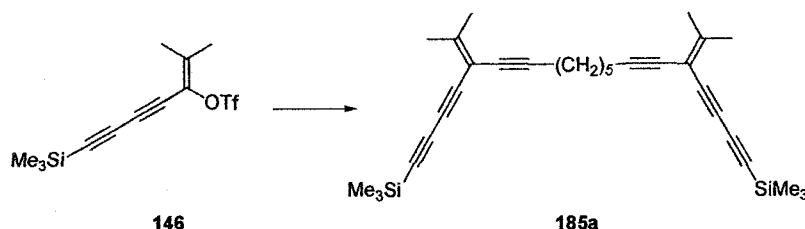
**Acetic acid 1,4-bis(diphenylmethylidene)-6-trimethylsilyl-2,5-hexadiynyl ester (182).**



Compound **181** (38 mg, 0.11 mmol) was desilylated with 1 equiv. of TBAF in THF and cross-coupled with triflate **131** (54 mg, 0.12 mmol) in degassed THF (20 mL) in

the presence of Pd(PPh<sub>3</sub>)<sub>4</sub> (6 mg, 0.005 mmol), diisopropylamine (2 mL), and CuI (3 mg, 0.02 mmol) under reflux for 12 h as described in the general procedure. Flash chromatography (hexane/CH<sub>2</sub>Cl<sub>2</sub> 1:1) afforded **182** (57 mg, 86%) as a yellow waxy solid. *R<sub>f</sub>* = 0.7 (hexane/CH<sub>2</sub>Cl<sub>2</sub> 1:1). IR (CHCl<sub>3</sub>, cast): 3054, 2954, 2873, 2142, 1769, 1661, 1598 cm<sup>-1</sup>. <sup>1</sup>H NMR (400 MHz, CDCl<sub>3</sub>): δ 7.43–7.15 (m, 20H), 1.87 (s, 3H), 0.89 (t, *J* = 8.4 Hz, 9H), 0.52 (q, *J* = 8.4 Hz, 6H). <sup>13</sup>C NMR (100 MHz, CDCl<sub>3</sub>, APT): δ 168.3, 157.3, 140.0, 139.9, 139.5, 138.0, 137.8, 130.3, 130.2, 130.1, 130.0, 129.5, 128.5, 128.2 (2×), 127.9, 127.8, 127.7, 127.5, 103.2, 101.5, 95.8, 92.5, 86.9, 20.6, 7.4, 4.2. EI HRMS: calcd for C<sub>40</sub>H<sub>38</sub>O<sub>2</sub>Si (M<sup>+</sup>), 578.2641; found, 578.2628.

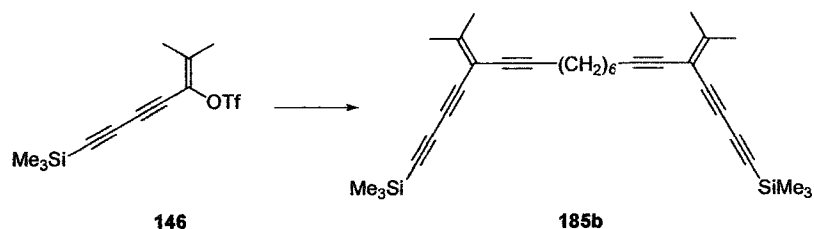
**5,15-Diisopropylidene-1,19-bis(trimethylsilyl)-1,3,6,13,16,18-nonadecahexayne (185a).**



1,8-Nonadiyne (60 mg, 0.50 mmol) was cross-coupled with triflate **146** (330 mg, 1.02 mmol) in degassed THF (20 mL) in the presence of PdCl<sub>2</sub>(PPh<sub>3</sub>)<sub>2</sub> (20 mg, 0.028 mmol), diisopropylamine (1 mL), and CuI (10 mg, 0.052 mmol) for 1.5 h as described in the general procedure. Flash chromatography (hexane/CH<sub>2</sub>Cl<sub>2</sub> 2:1) afforded **185a** (162 mg, 69%) as a colorless oil. *R<sub>f</sub>* = 0.4 (hexane/CH<sub>2</sub>Cl<sub>2</sub> 2:1). IR (CH<sub>2</sub>Cl<sub>2</sub>, cast): 2937, 2860, 2198, 2098, 1591 cm<sup>-1</sup>. <sup>1</sup>H NMR (300 MHz, CDCl<sub>3</sub>): δ 2.33 (m, 4H), 2.00 (s, 6H), 1.98 (s, 6H), 1.53 (m, 6H), 0.18 (s, 18H). <sup>13</sup>C NMR (75 MHz, CDCl<sub>3</sub>): δ 157.2, 100.6,

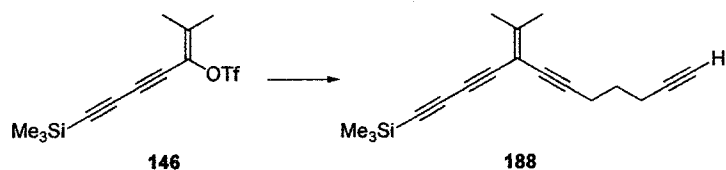
93.1, 90.6, 88.2, 76.4, 75.5, 74.7, 28.3, 28.2, 22.9, 22.8, 19.4, -0.3. EI HRMS: calcd for  $C_{31}H_{40}Si_2$  ( $M^+$ ), 468.2669; found, 468.2665.

**5,16-Diisopropylidene-1,20-bis-trimethylsilyl-1,3,6,14,17,19-eicosahexayne (185b).**



1,9-Decadiyne (67 mg, 0.50 mmol) was cross-coupled with triflate **146** (330 mg, 1.02 mmol) in degassed THF (20 mL) in the presence of  $PdCl_2(PPh_3)_2$  (20 mg, 0.028 mmol), diisopropylamine (1 mL), and CuI (10 mg, 0.052 mmol) for 1.5 h as described in the general procedure. Flash chromatography (hexane/ $CH_2Cl_2$  2:1) afforded **185b** (140 mg, 58%) as a colorless oil.  $R_f = 0.4$  (hexane/ $CH_2Cl_2$  2:1). IR ( $CH_2Cl_2$ , cast): 2935, 2858, 2198, 2096, 1592  $cm^{-1}$ .  $^1H$  NMR (300 MHz,  $CDCl_3$ ):  $\delta$  2.33 (t,  $J = 6.6$  Hz, 4H), 2.00 (s, 6H), 1.98 (s, 6H), 1.55 (m, 4H), 1.41 (m, 4H), 0.18 (s, 18H).  $^{13}C$  NMR (75 MHz,  $CDCl_3$ , APT):  $\delta$  157.2, 100.6, 93.3, 90.5, 88.2, 76.3, 75.5, 74.7, 28.6, 28.4, 22.9, 22.8, 19.4, -0.3. EI HRMS: calcd for  $C_{32}H_{42}Si_2$  ( $M^+$ ), 482.2825; found, 468.2824.

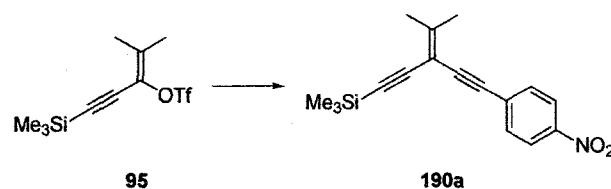
**5-Isopropylidene-1-trimethylsilyl-1,3,6,11-dodecatetrayne (188).**



1,6-Heptadiyne **187** (60 mg, 0.65 mmol) was cross-coupled with triflate **146** (130 mg, 0.40 mmol) in degassed THF (10 mL) in the presence of  $PdCl_2(PPh_3)_2$  (15 mg, 0.021

mmol), diisopropylamine (1 mL), and CuI (8 mg, 0.04 mmol) for 1 h as described in the general procedure. Flash chromatography (hexane/CH<sub>2</sub>Cl<sub>2</sub> 2:1) afforded **188** (86 mg, 80%) as a colorless oil.  $R_f = 0.6$  (hexane/CH<sub>2</sub>Cl<sub>2</sub> 2:1). IR (CH<sub>2</sub>Cl<sub>2</sub>, cast): 3300, 2958, 2906, 2198, 2097, 1591, 1431 cm<sup>-1</sup>. <sup>1</sup>H NMR (300 MHz, CDCl<sub>3</sub>): δ 2.46 (t,  $J = 7.2$  Hz, 2H), 2.31 (td,  $J_1 = 6.9$  Hz,  $J_2 = 2.7$  Hz, 2H), 2.00 (s, 3H), 1.98 (s, 3H), 1.95 (t,  $J = 2.7$  Hz, 1H), 1.75 (m, 2H), 0.18 (s, 9H). <sup>13</sup>C NMR (125 MHz, CDCl<sub>3</sub>, APT): δ 157.6, 100.4, 91.9, 90.7, 88.1, 76.8, 76.4, 75.6, 74.5, 68.9, 27.6, 22.9, 22.8, 18.6, 17.7, -0.3. EI HRMS: calcd for C<sub>18</sub>H<sub>22</sub>Si (M<sup>+</sup>), 266.1491; found, 266.1492.

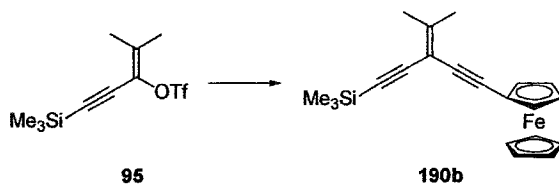
#### 4-Methyl-3-(4-nitrophenylethynyl)-1-trimethylsilylpent-3-en-1-yne (**190a**).



Trimethyl(4-nitrophenylethynyl)silane (110 mg, 0.50 mmol) was desilylated with K<sub>2</sub>CO<sub>3</sub> in THF/MeOH (1:1) and cross-coupled with triflate **95** (150 mg, 0.50 mmol) in degassed THF (20 mL) in the presence of PdCl<sub>2</sub>(PPh<sub>3</sub>)<sub>2</sub> (18 mg, 0.016 mmol), diisopropylamine (2 mL), and CuI (9 mg, 0.047 mmol) for 20 min as described in the general procedure. Flash chromatography (hexane/diethyl ether 3:1) afforded **190a** (144 mg, 97%) as a yellow solid.  $R_f = 0.7$  (hexane/diethyl ether 3:1). Mp: 66–67 °C. IR (μscope): 3079, 2957, 2843, 2204, 2150, 1594, 1511, 1492, 1433 cm<sup>-1</sup>. <sup>1</sup>H NMR (400 MHz, CDCl<sub>3</sub>): δ 8.15 (d,  $J = 9.2$  Hz, 2H), 7.56 (d,  $J = 9.2$  Hz, 2H), 2.09 (s, 6H), 0.21 (s, 9H). <sup>13</sup>C NMR (100 MHz, CDCl<sub>3</sub>, APT): δ 158.0, 146.8, 132.0, 130.4, 123.5, 101.1,

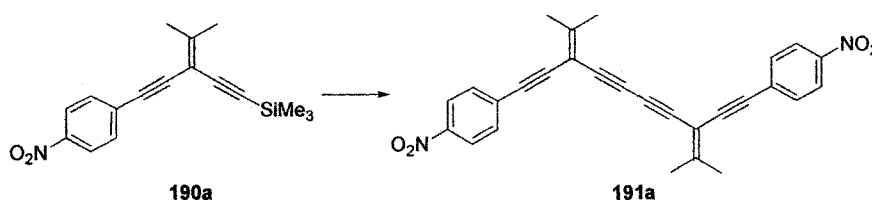
100.7, 97.0, 91.6, 89.6, 23.0, 22.9, 0.0. EI MS  $m/z$  (rel. intensity): 297.1 ( $M^+$ , 94), 282.1 ( $[M - Me]^+$ , 100). EI HRMS: calcd for  $C_{17}H_{19}NO_2Si$  ( $M^+$ ), 297.1185; found, 297.1191.

#### 4-Methyl-3-ferrocenylethynylpent-3-en-1-yne (190b).



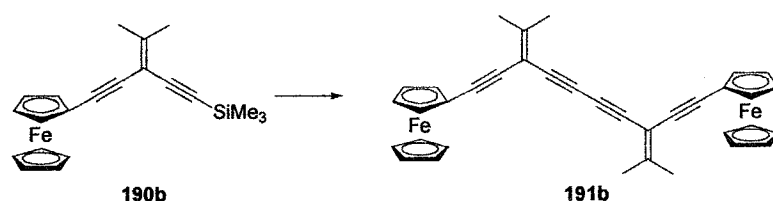
Ethynyl ferrocene (135 mg, 0.643 mmol) was cross-coupled with triflate **95** (193 mg, 0.643 mmol) in degassed THF (20 mL) in the presence of  $PdCl_2(PPh_3)_2$  (22 mg, 0.031 mmol), diisopropylamine (2 mL), and CuI (11 mg, 0.058 mmol) for 1.5 h as described in the general procedure. Flash chromatography (hexane/ $CH_2Cl_2$  2:1) afforded **190b** (178 mg, 77%) as a yellow solid.  $R_f = 0.4$  (hexane/ $CH_2Cl_2$  2:1). Mp: 66–67 °C. IR ( $\mu$ scope): 3095, 2960, 2903, 2207, 2146  $cm^{-1}$ . UV-vis ( $CHCl_3$ ):  $\lambda_{max}$  ( $\epsilon$ ) 260 (17 400), 299 (8 400), 341 (1 200), 447 (500).  $^1H$  NMR (300 MHz,  $CDCl_3$ ):  $\delta$  4.45 (s, 2H), 4.22 (m, 7H), 2.04 (s, 3H), 2.03 (s, 3H), 0.20 (s, 9H).  $^{13}C$  NMR (75 MHz,  $CDCl_3$ , APT):  $\delta$  154.2, 102.2, 102.0, 95.8, 90.2, 82.4, 71.4, 69.9, 68.7, 65.5, 22.8, 0.1 (one coincident peak not observed). EI HRMS: calcd for  $C_{21}H_{24}FeSi$  ( $M^+$ ), 360.0997; found, 360.0994.

#### 1,10-Bis(4-nitrophenyl)-3,8-diisopropylidene-1,4,6,9-decatetrayne (191a).



Compound **190a** (88 mg, 0.30 mmol) was desilylated with  $K_2CO_3$  in MeOH/THF (1:1) and homo-coupled in acetone (10 mL) in the presence of *Hay* catalyst (1 mL) and air for 12 h as described in the general procedure. Flash chromatography (hexane/diethyl ether 3:1) afforded **191a** (58 mg, 87%) as a yellow solid.  $R_f = 0.5$  (hexane/diethyl ether 3:1). Mp: > 185 °C (dec.). IR ( $\mu$ scope): 3104, 2910, 2840, 2209, 1595, 1515, 1491, 1432  $cm^{-1}$ . UV-vis ( $CHCl_3$ ):  $\lambda_{max}$  ( $\epsilon$ ) 277 (26 800), 291 (29 800), 310 (33 900), 331 (33 300).  $^1H$  NMR (300 MHz,  $CDCl_3$ ):  $\delta$  8.16 (d,  $J = 9.0$  Hz, 4H), 7.57 (d,  $J = 9.0$  Hz, 4H), 2.14 (s, 12H).  $^{13}C$  NMR (100 MHz,  $CDCl_3$ , APT):  $\delta$  160.7, 147.0, 132.0, 129.9, 123.6, 100.4, 90.4, 90.2, 78.5, 76.1, 23.2 (one coincident peak not observed). EI HRMS: calcd for  $C_{28}H_{20}N_2O_4$  ( $M^+$ ), 448.1423; found, 448.1419.

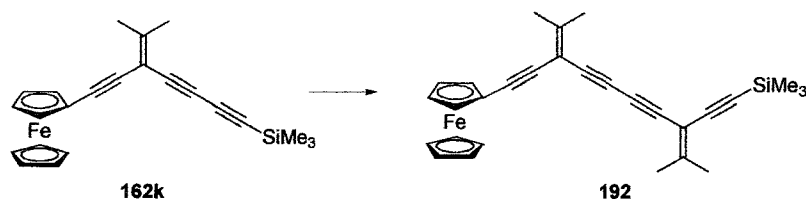
**1,10-Bis(ferrocenyl)-3,8-diisopropylidene-1,4,6,9-decatetrayne (191b).**



Compound **190b** (72 mg, 0.20 mmol) was desilylated with  $K_2CO_3$  in MeOH/THF (1:1) and homo-coupled in acetone (10 mL) in the presence of *Hay* catalyst (1 mL) and air for 12 h as described in the general procedure. Flash chromatography (hexane/ $CH_2Cl_2$  1:1) afforded **191b** (53 mg, 92%) as a yellow solid.  $R_f = 0.5$  (hexane/ $CH_2Cl_2$  1:1). Mp: 173–174 °C (dec.). IR ( $\mu$ scope): 3105, 2992, 2842, 2215, 1585, 1425  $cm^{-1}$ . UV-vis ( $CHCl_3$ ):  $\lambda_{max}$  ( $\epsilon$ ) 271 (31 400), 287 (27 500), 306 (23 300), 330 (12 500), 360 (2 600), 449 (1 000).  $^1H$  NMR (300 MHz,  $CDCl_3$ ):  $\delta$  4.43 (s, 4H), 4.20 (m, 14H), 2.073 (s, 6H), 2.069 (s, 6H).  $^{13}C$  NMR (75 MHz,  $CDCl_3$ , APT):  $\delta$  156.6, 101.4, 91.0, 81.6, 79.3, 75.7,

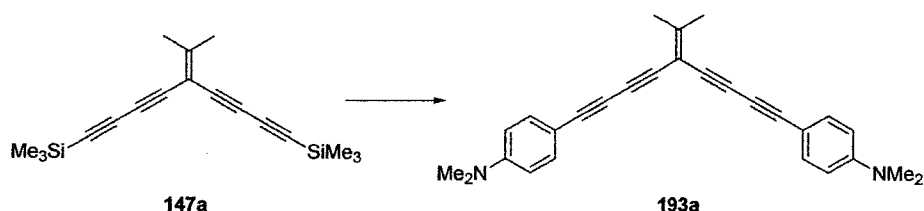
71.4, 70.0, 68.8, 65.2, 23.1, 23.0. EI HRMS: calcd for  $C_{36}H_{30}Fe_2$  ( $M^+$ ), 574.1046; found, 574.1051.

**1-ferrocenyl-3,8-diisopropylidene-10-trimethylsilyl-1,4,6,9-decatetrayne (192).**



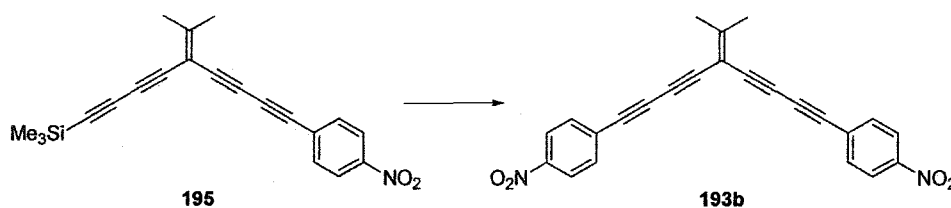
Compound **162k** (77 mg, 0.20 mmol) was desilylated with  $K_2CO_3$  in MeOH/THF (1:1) and was cross-coupled with triflate **95** (60 mg, 0.20 mmol) in degassed THF (20 mL) in the presence of  $PdCl_2(PPh_3)_2$  (7 mg, 0.010 mmol), diisopropylamine (2 mL), and CuI (3 mg, 0.02 mmol) for 1 h as described in the general procedure. Flash chromatography (hexane/ $CH_2Cl_2$  1:1) afforded **192** (71 mg, 77%) as a yellow solid.  $R_f$  = 0.5 (hexane/ $CH_2Cl_2$  1:1). Mp: 110–111 °C. IR ( $CHCl_3$ , cast): 3095, 2959, 2904, 2210, 2147, 1588, 1432  $cm^{-1}$ .  $^1H$  NMR (500 MHz,  $CDCl_3$ ):  $\delta$  4.42 (m, 2H), 4.20 (s, 5H), 4.17 (m, 2H), 2.07 (s, 3H), 2.06 (s, 3H), 2.043 (s, 3H), 2.038 (s, 3H), 0.18 (s, 9H).  $^{13}C$  NMR (125 MHz,  $CDCl_3$ , APT):  $\delta$  159.2, 156.5, 101.3, 101.1, 100.4, 97.1, 91.0, 81.5, 79.4, 78.7, 76.2, 75.6, 71.4, 70.0, 68.8, 65.3, 23.2, 23.1 (2 $\times$ ), 0.1 (one coincident peak not observed). EI HRMS: calcd for  $C_{29}H_{30}FeSi$  ( $M^+$ ), 462.1466; found, 462.1466.

**1,9-Bis(4-*N,N*-dimethylaminophenyl)-5-isopropylidene-1,3,6,8-nonatetrayne (193a).**



Compound **147a** (64 mg, 0.22 mmol) was desilylated with  $K_2CO_3$  in MeOH/THF (1:1) and cross-coupled with 4-iodo-*N,N*-dimethyl aniline (107 mg, 0.433 mmol) in degassed THF (20 mL) in the presence of  $PdCl_2(PPh_3)_2$  (25 mg, 0.036 mmol), diisopropylamine (2 mL), and CuI (14 mg, 0.074 mmol) for 2 h as described in the general procedure. Flash chromatography (hexane/ $CH_2Cl_2$  1:1) afforded **193a** (67 mg, 80%) as a yellow solid.  $R_f = 0.4$  (hexane/ $CH_2Cl_2$  1:1). Mp: 148 °C (dec.). IR ( $\mu$ scope): 2903, 2198, 2134, 1522  $cm^{-1}$ . UV-vis ( $CHCl_3$ ):  $\lambda_{max}$  ( $\epsilon$ ) 323 (50 400), 345 (67 400), 366 (48 100).  $^1H$  NMR (500 MHz,  $CDCl_3$ ):  $\delta$  7.36 (d,  $J = 9.0$  Hz, 4H), 6.59 (d,  $J = 9.0$  Hz, 4H), 2.97 (s, 12H), 2.09 (s, 6H).  $^{13}C$  NMR (125 MHz,  $CDCl_3$ , APT):  $\delta$  159.4, 150.4, 133.6, 111.6, 108.0, 100.8, 84.0, 77.1, 77.0, 72.2, 40.1, 23.3. EI HRMS: calcd for  $C_{28}H_{26}N_2$  ( $M^+$ ), 390.2096; found, 390.2099. X-ray.

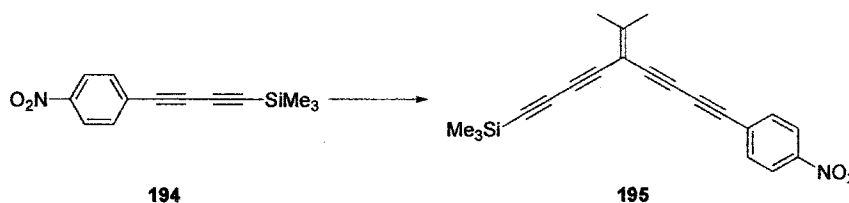
**1,9-Bis(4-nitrophenyl)-5-isopropylidene-1,3,6,8-nonatetrayne (193b).**



Compound **195** (55 mg, 0.16 mmol) was desilylated with  $K_2CO_3$  in MeOH/THF (1:1) and cross-coupled with 4-iodo-1-nitrobenzene (40 mg, 0.16 mmol) in degassed THF (20 mL) in the presence of  $PdCl_2(PPh_3)_2$  (6 mg, 0.009 mmol), diisopropylamine (2 mL), and CuI (3 mg, 0.02 mmol) for 0.5 h as described in the general procedure. Flash chromatography (hexane/diethyl ether 3:1) afforded **193b** (22 mg, 35%) as a yellow solid.  $R_f = 0.4$  (hexane/diethyl ether 3:1). Mp: 117 °C (dec.). IR ( $\mu$ scope): 3103, 2931, 2201, 1343  $cm^{-1}$ . UV-vis ( $CHCl_3$ ):  $\lambda_{max}$  ( $\epsilon$ ) 311 (34 300), 342 (41 000), 372 (30 400).

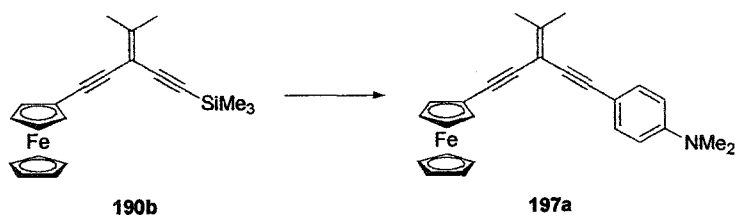
$^1\text{H}$  NMR (400 MHz,  $\text{CDCl}_3$ ):  $\delta$  8.18 (d,  $J = 8.6$  Hz, 4H), 7.62 (d,  $J = 8.6$  Hz, 4H), 2.15 (s, 6H).  $^{13}\text{C}$  NMR (100 MHz,  $\text{CDCl}_3$ , APT):  $\delta$  165.0, 147.5, 133.2, 128.6, 123.7, 99.8, 80.2, 79.6, 78.6, 76.2, 23.5. EI HRMS: calcd for  $\text{C}_{24}\text{H}_{14}\text{N}_2\text{O}_4$  ( $\text{M}^+$ ), 394.0954; found, 394.0954.

**[5-Isopropylidene-1-(4-nitrophenyl)-9-trimethylsilyl-1,3,6,8-nonatetrayne (195).**



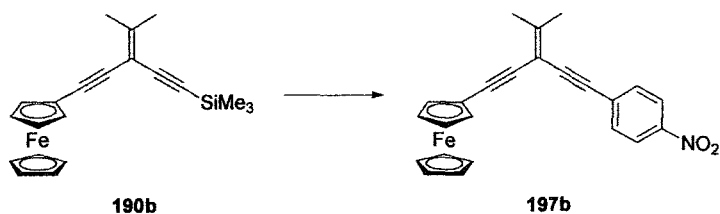
1-(4-Nitrophenyl)-4-trimethylsilyl-1,3-butadiyne **194** (102 mg, 0.419 mmol) was desilylated with  $\text{K}_2\text{CO}_3$  in MeOH/THF (1:1) and cross-coupled with triflate **146** (135 mg, 0.419 mmol) in degassed THF (20 mL) in the presence of  $\text{PdCl}_2(\text{PPh}_3)_2$  (17 mg, 0.015 mmol), diisopropylamine (2 mL), and CuI (8 mg, 0.04 mmol) for 1 h as described in the general procedure. Flash chromatography (hexane/diethyl ether 5:1) afforded **195** (113 mg, 79%) as a yellow solid.  $R_f = 0.7$  (hexane/diethyl ether 5:1). Mp: 114–117 °C. IR ( $\text{CHCl}_3$ , cast): 2960, 2205, 2097, 1592, 1521, 1342  $\text{cm}^{-1}$ .  $^1\text{H}$  NMR (400 MHz,  $\text{CDCl}_3$ ):  $\delta$  8.17 (d,  $J = 8.8$  Hz, 2H), 7.60 (d,  $J = 8.8$  Hz, 2H), 2.097 (s, 3H), 2.093 (s, 3H), 0.19 (s, 9H).  $^{13}\text{C}$  NMR (100 MHz,  $\text{CDCl}_3$ , APT):  $\delta$  164.1, 147.4, 133.1, 128.7, 123.6, 99.7, 91.9, 87.5, 80.0 (2  $\times$ ), 78.8, 77.2, 75.9, 72.0, 23.4,  $-0.5$  (one coincident peak not observed). EI HRMS: calcd for  $\text{C}_{21}\text{H}_{19}\text{NO}_2\text{Si}$  ( $\text{M}^+$ ), 345.1185; found, 345.1187.

**1-Ferrocenylethynyl-4-methyl-3-(4-*N,N*-dimethylaminophenylethynyl)pent-3-ene-1-yne (197a).**



Compound **190b** (102 mg, 0.28 mmol) was desilylated with  $K_2CO_3$  in MeOH/THF (1:1) and was cross-coupled with 4-iodo-*N,N*-dimethyl aniline (74 mg, 0.30 mmol) in degassed THF (20 mL) in the presence of  $PdCl_2(PPh_3)_2$  (10 mg, 0.014 mmol), diisopropylamine (2 mL), and CuI (5 mg, 0.03 mmol) for 1.5 h as described in the general procedure. Flash chromatography (hexane/diethyl ether 5:1) afforded **197a** (60 mg, 52%) as a yellow solid.  $R_f = 0.4$  (hexane/diethyl ether 5:1). Mp: 174–175 °C. IR (CHCl<sub>3</sub>, cast): 3084, 2925, 2197, 1612, 1526, 1441, 1369  $cm^{-1}$ . UV-vis (CHCl<sub>3</sub>):  $\lambda_{max}$  ( $\epsilon$ ) 305 (25 400), 330 (22 600). <sup>1</sup>H NMR (300 MHz, CDCl<sub>3</sub>):  $\delta$  7.34 (d,  $J = 8.4$  Hz, 2H), 6.62 (d,  $J = 8.4$  Hz, 2H), 4.45 (m, 2H), 4.21 (s, 5H), 4.18 (m, 2H), 2.96 (s, 6H), 2.08 (s, 6H). <sup>13</sup>C NMR (75 MHz, CDCl<sub>3</sub>, APT):  $\delta$  151.1, 150.0, 132.5, 111.9, 110.6, 102.2, 92.0, 89.6, 84.7, 83.1, 71.4, 69.9, 68.6, 65.8, 40.3, 22.8, 22.7. EI HRMS: calcd for C<sub>26</sub>H<sub>25</sub>FeN (M<sup>+</sup>), 407.1336; found, 407.1350. X-ray.

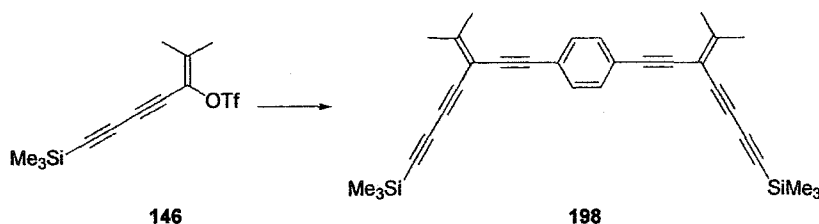
#### 1-Ferrocenyl-4-methyl-3-(4-nitrophenylethynyl)pent-3-ene-1-yne (**197b**).



Compound **190b** (52 mg, 0.14 mmol) was desilylated with  $K_2CO_3$  in MeOH/THF (1:1) and was cross-coupled with 4-iodo-1-nitrobenzene (54 mg, 0.22 mmol) in degassed THF (20 mL) in the presence of  $PdCl_2(PPh_3)_2$  (10 mg, 0.014 mmol), diisopropylamine (2

mL), and CuI (5 mg, 0.03 mmol) for 1.5 h as described in the general procedure. Flash chromatography (hexane/diethyl ether 5:1) afforded **197b** (47 mg, 80%) as a yellow solid.  $R_f = 0.5$  (hexane/diethyl ether 5:1). Mp: 113–114 °C. IR (CH<sub>2</sub>Cl<sub>2</sub>, cast): 3102, 2905, 2844, 2202, 1591, 1516, 1342 cm<sup>-1</sup>. UV-vis (CHCl<sub>3</sub>):  $\lambda_{\max}$  ( $\epsilon$ ) 302 (19 200), 352 (14 700). <sup>1</sup>H NMR (300 MHz, CDCl<sub>3</sub>):  $\delta$  8.17 (d,  $J = 9.0$  Hz, 2H), 7.58 (d,  $J = 9.0$  Hz, 2H), 4.49 (s, 2H), 4.24 (s, 7H), 2.13 (s, 3H), 2.13 (s, 3H). <sup>13</sup>C NMR (75 MHz, CDCl<sub>3</sub>, APT):  $\delta$  155.5, 146.9, 132.0, 130.6, 123.6, 101.4, 92.3, 90.9, 89.2, 81.8, 71.8, 70.4, 69.4, 65.7, 23.1, 23.0. EI HRMS: calcd for C<sub>24</sub>H<sub>19</sub>FeNO<sub>2</sub> (M<sup>+</sup>), 409.0765; found, 409.0768. X-ray.

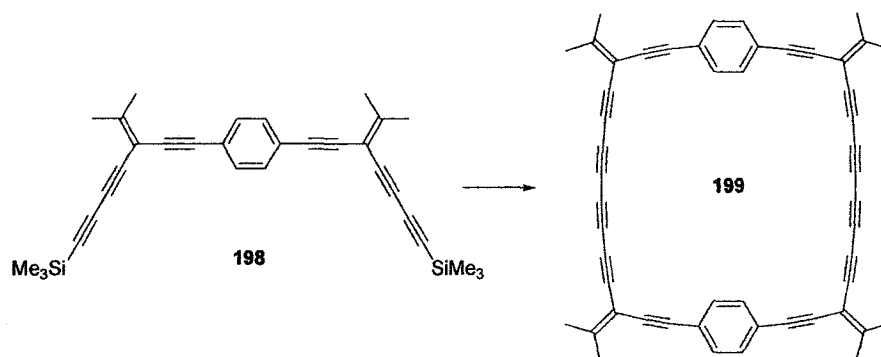
**1,4-Bis-(3-isopropylidene-7-trimethylsilyl-1,4,6-heptatriynyl)benzene (198).**



1,4-Bis(trimethylsilylethynyl)benzene (50 mg, 0.18 mmol) was desilylated with K<sub>2</sub>CO<sub>3</sub> in MeOH/THF (1:1) and cross-coupled with triflate **146** (120 mg, 0.370 mmol) in degassed THF (20 mL) in the presence of PdCl<sub>2</sub>(PPh<sub>3</sub>)<sub>2</sub> (14 mg, 0.020 mmol), diisopropylamine (2 mL), and CuI (7 mg, 0.04 mmol) for 1 h as described in the general procedure. Flash chromatography (hexane/CH<sub>2</sub>Cl<sub>2</sub> 2:1) afforded **198** (83 mg, 95%) as a yellow solid.  $R_f = 0.5$  (hexane/CH<sub>2</sub>Cl<sub>2</sub> 2:1). Mp: 186–187 °C (dec.). IR ( $\mu$ scope): 2957, 2200, 2096, 1506 cm<sup>-1</sup>. <sup>1</sup>H NMR (300 MHz, CD<sub>2</sub>Cl<sub>2</sub>):  $\delta$  7.41 (s, 4H), 2.12 (s, 6H), 2.10 (s, 6H), 0.21 (s, 18H). <sup>13</sup>C NMR (75 MHz, CD<sub>2</sub>Cl<sub>2</sub>, APT):  $\delta$  160.6, 131.7, 123.3, 100.4, 92.0, 91.6, 87.9, 87.2, 76.3, 73.8, 23.3, 23.2, -0.4. EI HRMS: calcd for C<sub>32</sub>H<sub>34</sub>Si<sub>2</sub> (M<sup>+</sup>),

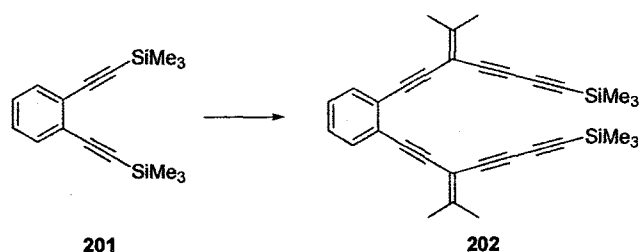
474.2199; found, 474.2194. Anal. Calcd for  $C_{32}H_{34}Si_2$ : C, 80.95; H, 7.22. Found: C, 80.97; H, 7.07.

**4,13,19,28-Tetraisopropylidene-1,16-bis(1,4-benzenediyl)cyclotriacontane-2,5,7,9,11,14,17,20,22,24,26,29-dodecayne (199).**



Compound **198** (35 mg, 0.074 mmol) was desilylated with  $K_2CO_3$  in MeOH/THF (1:1) and homo-coupled in  $CH_2Cl_2$  (10 mL) in the presence of CuI (10 mg, 0.053 mmol), TMEDA (150 mg, 1.29 mmol) and air for 0.5 h as described in the general procedure. Flash chromatography (hexane/ $CH_2Cl_2$  2:1) afforded **199** (10 mg, 54%) as a yellow solid.  $R_f = 0.4$  (hexane/ $CH_2Cl_2$  2:1). Mp:  $> 169$  °C (dec.). IR ( $\mu$ scope): 3038, 2927, 2905, 2192, 2124, 2083, 1584, 1506, 1431  $cm^{-1}$ . UV-vis ( $CHCl_3$ ):  $\lambda_{max}$  ( $\epsilon$ ) 309 (114 500), 326 (103 400), 349 (65 800), 375 (39 000), 407 (18 900).  $^1H$  NMR (300 MHz,  $CD_2Cl_2$ ):  $\delta$  7.42 (s, 8H), 2.15 (s, 12H), 2.14 (s, 12H).  $^{13}C$  NMR (75 MHz,  $CD_2Cl_2$ ):  $\delta$  163.2, 131.7, 123.1, 100.2, 92.7, 86.5, 76.4, 75.2, 67.9, 64.3, 23.6, 23.5. Attempts for MS analyses were unsuccessful.

**1,2-Bis(3-isopropylidene-7-trimethylsilyl-1,4,6-heptatriynyl)benzene (202).**



1,2-Bis(trimethylsilyl)ethynyl-benzene **201** (81 mg, 0.30 mmol) was desilylated with  $K_2CO_3$  in MeOH/THF (1:1) and was cross-coupled with triflate **146** (194 mg, 0.60 mmol) in degassed THF (20 mL) in the presence of  $PdCl_2(PPh_3)_2$  (21 mg, 0.030 mmol), diisopropylamine (2 mL), and CuI (10 mg, 0.052 mmol) for 2 h as described in the general procedure. Flash chromatography (hexane/ $CH_2Cl_2$  2:1) afforded **202** (126 mg, 89%) as a yellow oil.  $R_f = 0.4$  (hexane/ $CH_2Cl_2$  2:1). IR ( $CH_2Cl_2$ , cast): 3061, 2960, 2904, 2198, 2097, 1645, 1594, 1480, 1422  $cm^{-1}$ .  $^1H$  NMR (400 MHz,  $CDCl_3$ ):  $\delta$  7.44 (dd,  $J_1 = 6.0$  Hz,  $J_2 = 3.6$  Hz, 2H), 7.23 (dd,  $J_1 = 6.0$  Hz,  $J_2 = 3.6$  Hz, 2H), 2.14 (s, 6H), 2.10 (s, 6H), 0.20 (s, 18H).  $^{13}C$  NMR (100 MHz,  $CDCl_3$ , APT):  $\delta$  159.9, 131.9, 127.9, 125.2, 100.5, 90.8 (2 $\times$ ), 88.9, 88.1, 76.1, 73.7, 23.3, 23.1, -0.4. EI HRMS: calcd for  $C_{32}H_{34}Si_2$  ( $M^+$ ), 474.2199; found, 474.2186.

## References and Notes

- (1) Stang, P. J.; Fisk, T. E. *Synthesis* **1979**, 438-440.
- (2) Stang, P.; Ladika, M. *Synthesis* **1981**, 29-30.
- (3) Zhao, Y.; Campbell, K.; Tykwinski, R. R. *J. Org. Chem.* **2002**, *67*, 336-344.
- (4) Hay, A. S. *J. Org. Chem.* **1962**, *27*, 3320-3321.
- (5) Brandsma, L. *Preparative Acetylene Chemistry*; 2nd ed.; Elsevier Science: Amsterdam, 1998.

- (6) Hearn, M. T. W. *Tetrahedron* **1976**, *32*, 115-120.
- (7) For coordinates of unpublished data, contact Dr. Robert McDonald at the Department of Chemistry, University of Alberta.

# Appendix Selected $^1\text{H}$ and $^{13}\text{C}$ NMR Spectra

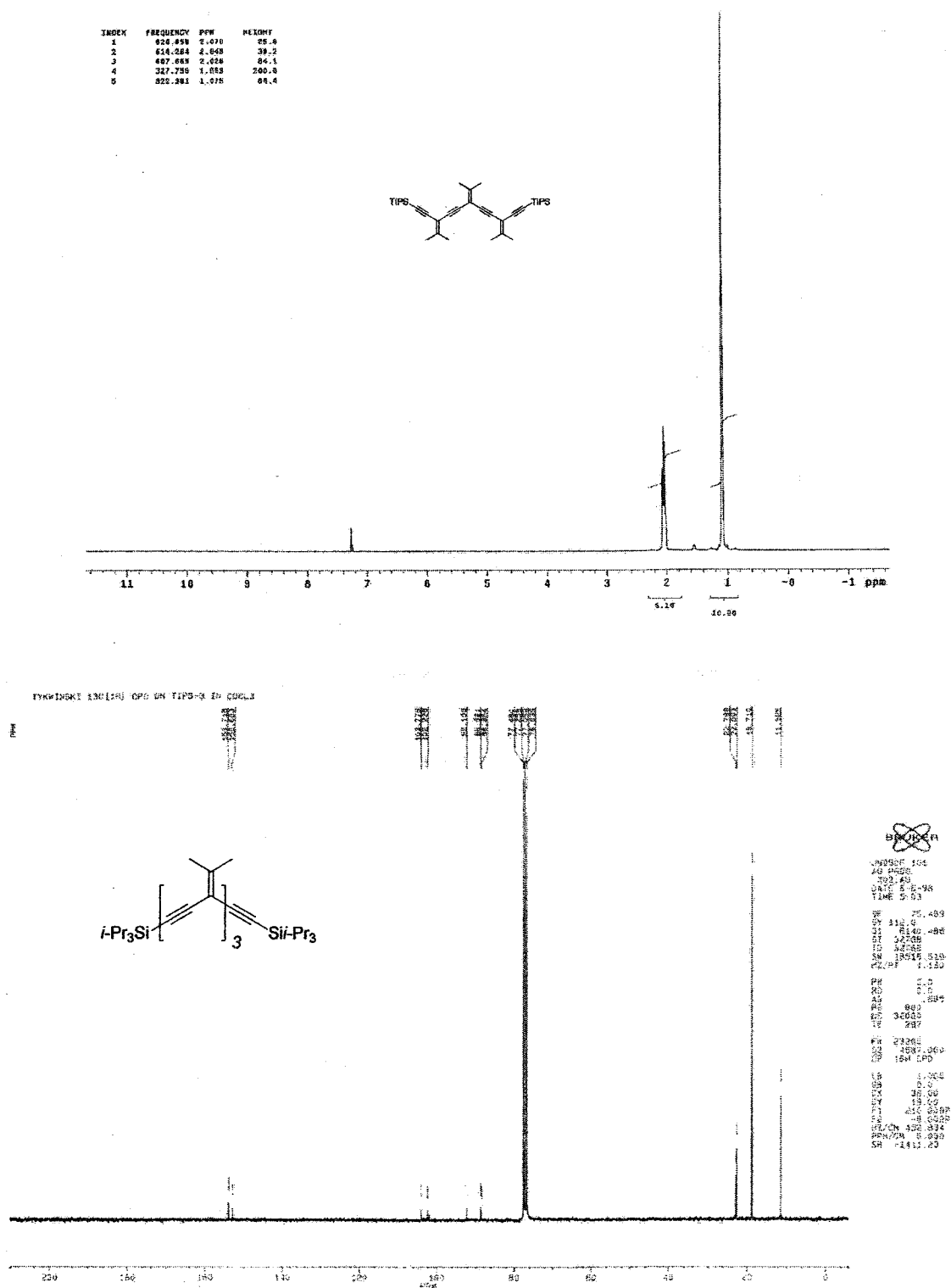


Fig. A-1  $^1\text{H}$  and  $^{13}\text{C}$  NMR spectra of compound 101.





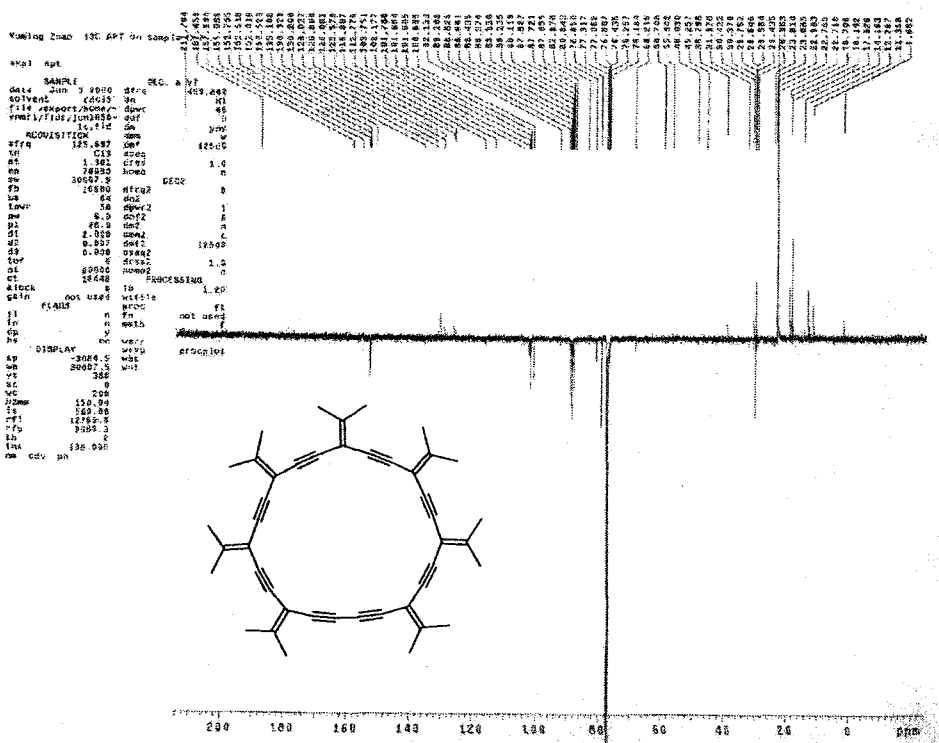
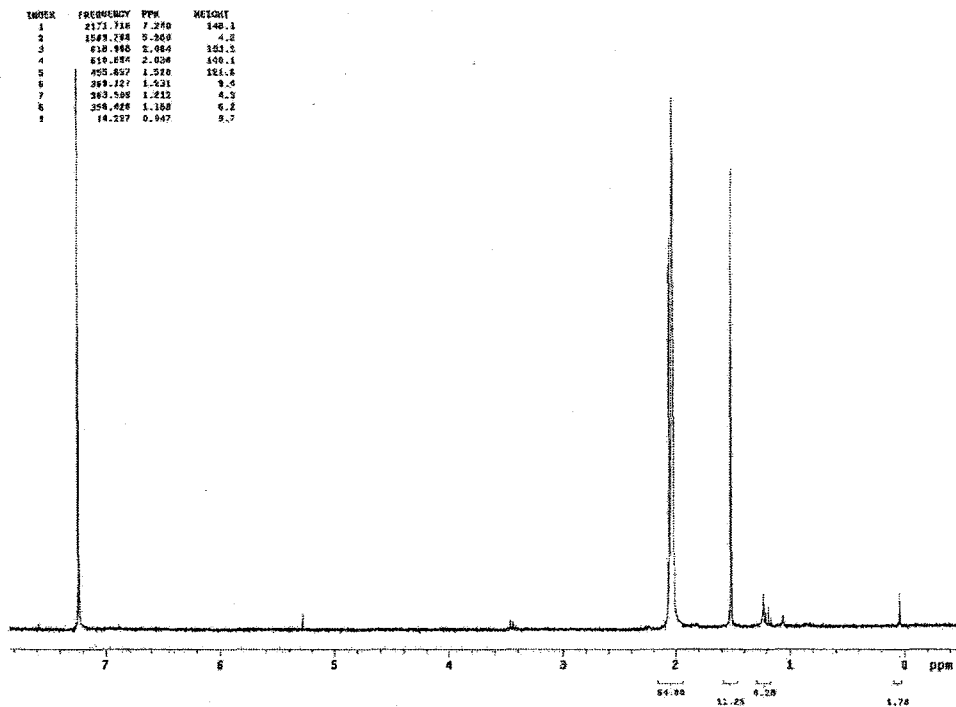
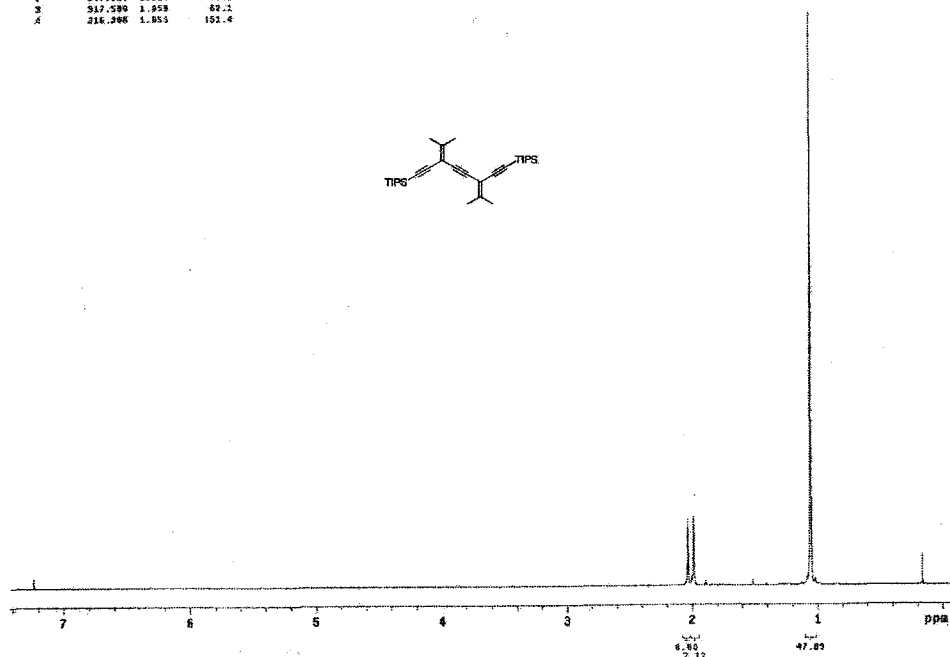


Fig. A-4 <sup>1</sup>H and <sup>13</sup>C NMR spectra of compound 107.

FRQ#	FREQUENCY PPM	WEXONY
1	616.449	2.485
2	597.915	1.889
3	517.399	1.858
4	216.266	1.855



STANDARD CARBON PARAMETERS  
Tuning 2000 carbon on sample TIPS-4

```

exp1 szgul
=====
SAMPLE          DEC. & VF
Date            Jul 21 88  dfr  445.502
Solvent         CDCl3  dn   40
File /export/home/v/gur  40
vnmr1/f14s/j012188-001  0
=====
ACQUISITION
pfrq            2c  dn   jyy
=====
pfrq           125.897  dn   12500
In             C13  dseq
st             1.350  dseq  1.0
sp            100000  homo  n
su            40000.0  DECC  0
fu            20000  ofu2
In             16  dcs
Lmr           50  dpr2  i
SI             0  dpr2  0
Sof            0  dpr2  0
st            10000  ofu2  10000
of            450  ofu2
Stack         0  ofu2  1.0
Gain          not used  homo2  n
=====
PLMB          n  ib  PROCESSING  1.20
In            0  vflie
Sp            y  ofoc  pt
Ns            on  fu  not used  r
=====
DISPLAY      on  meth
=====
sp           -600.5
vp           5000.8  werr
vs           200  wamp
vc           2  wds
wc           200  wnt
=====
p3mm        200.26
fa          500.00
f2f         17700.0
rfp         1668.0
lh           0
lwr         1.000
re  cdc  ph  1.000

```

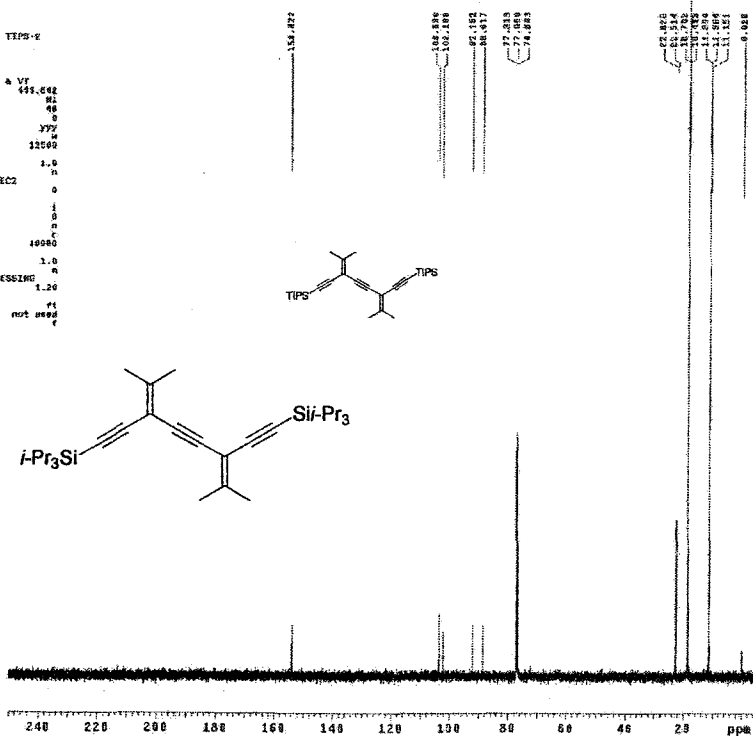


Fig. A-5 <sup>1</sup>H and <sup>13</sup>C NMR spectra of compound 108.

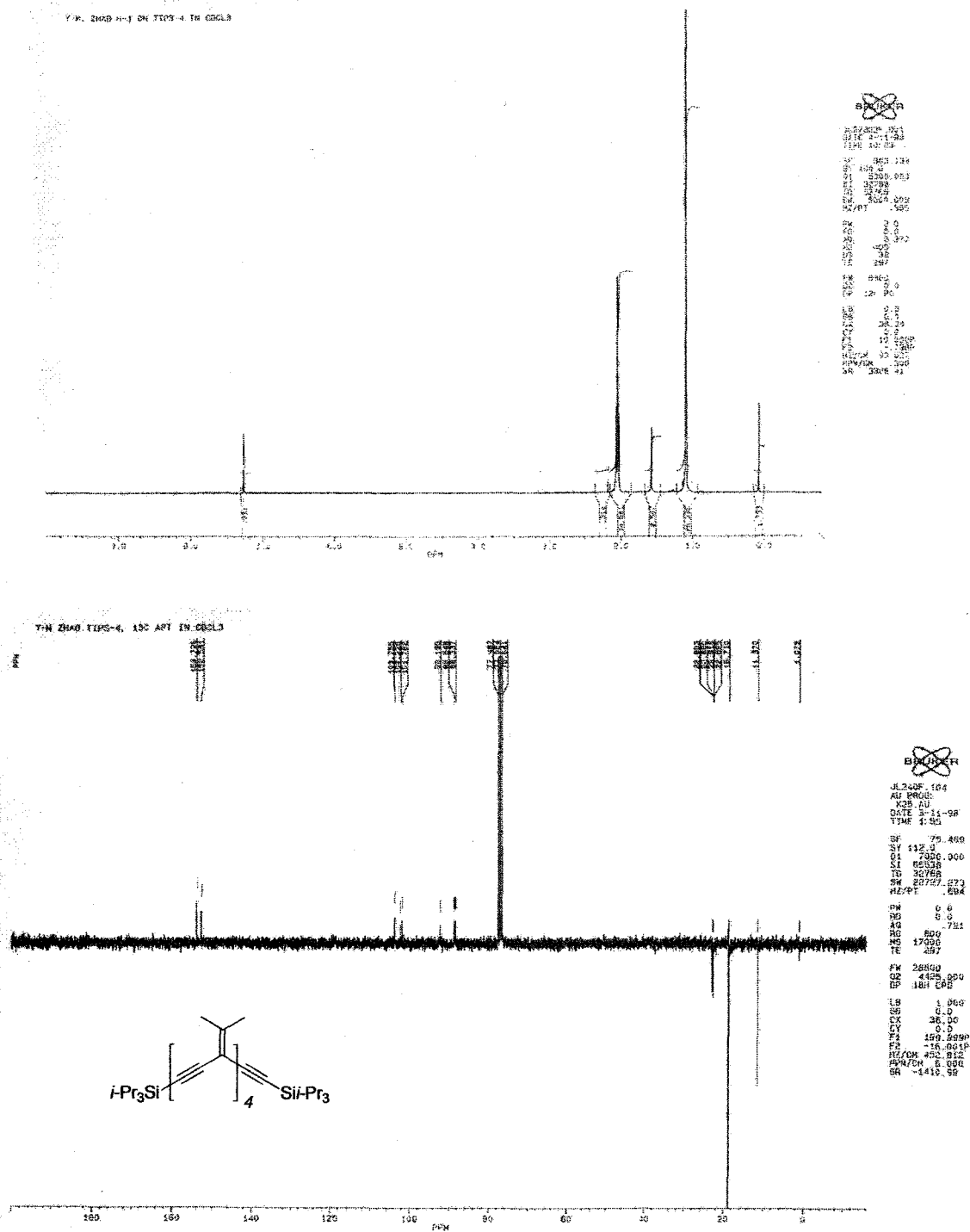


Fig. A-6 <sup>1</sup>H and <sup>13</sup>C NMR spectra of compound 111.

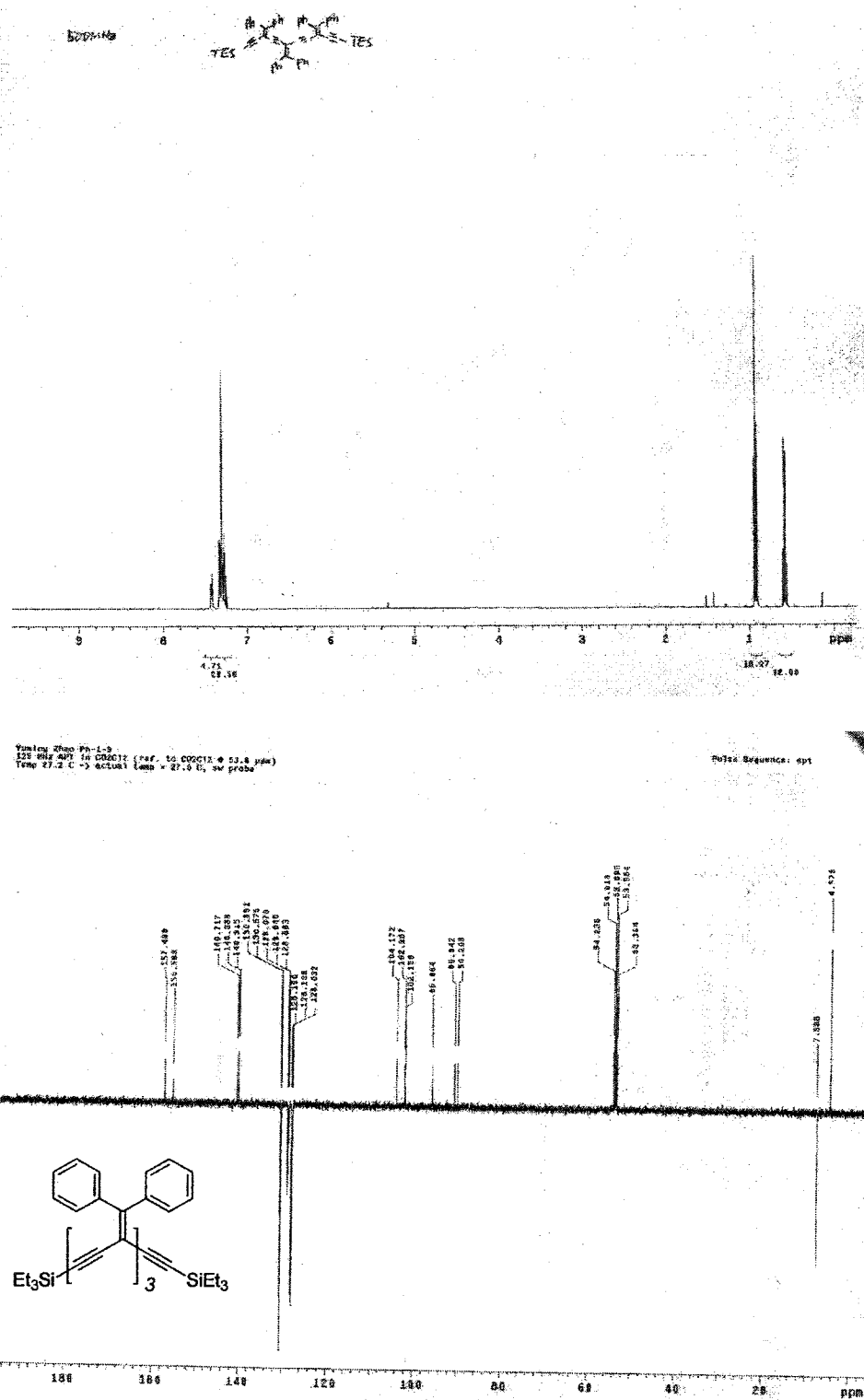
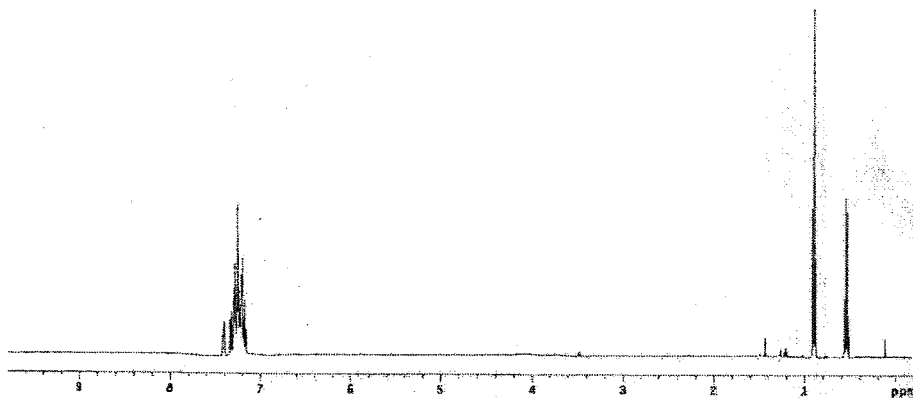
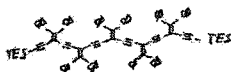


Fig. A-7 <sup>1</sup>H and <sup>13</sup>C NMR spectra of compound 138.

600 MHz 1D in CDCl3 (ref. to CDCl3 @ 7.26 ppm), temp 27.2 C -> actual temp = 27.0 C, 4w probe  
 Pulse Sequence: zgpg30

Solvent: dms-d6  
 Temp: 27.2 C / 262.4 K  
 INOVA-800 \*1HDS\*

PULSE SEQUENCE  
 Acq - delay 3.000 sec  
 Pulse 77.1 degrees  
 Acq. time 1.938 sec  
 Width 5000.2 Hz  
 18 - acquisitions  
 OBSERVE CH: gac.130656 MHz  
 DATA PROCESSING  
 FT SIZE 65528  
 Total time 1 min, 48 sec



125 MHz 1D in CDCl3 (ref. to CDCl3 @ 77.0 ppm), temp 27.2 C -> actual temp = 27.0 C, 3v probe  
 CH, CH2 positive; C, CD2 negative

Pulse Sequence: zgpg30

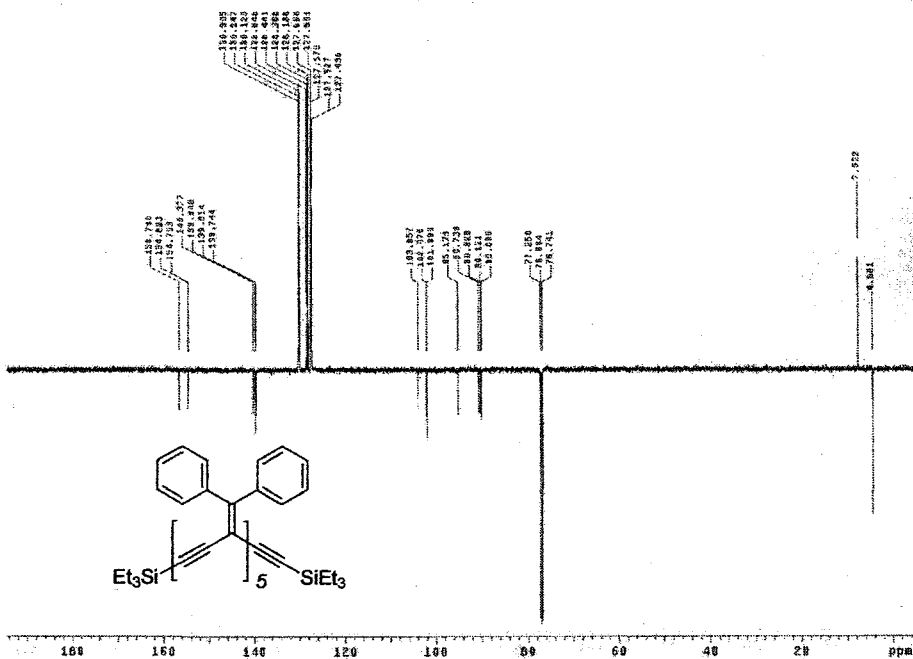


Fig. A-8 <sup>1</sup>H and <sup>13</sup>C NMR spectra of compound 139.



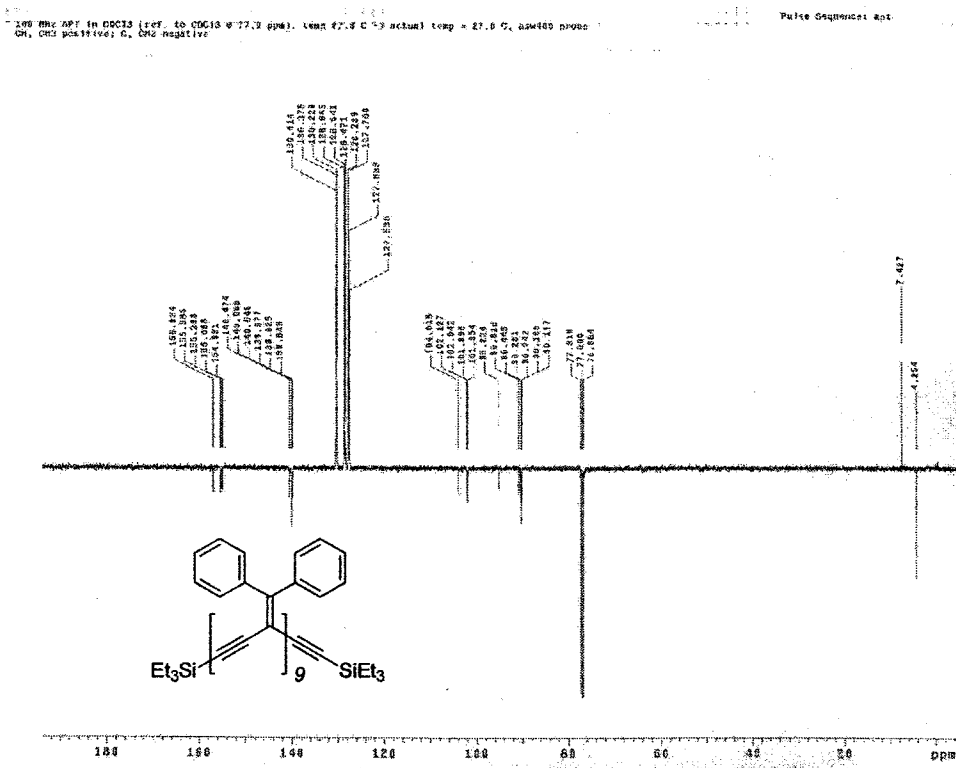
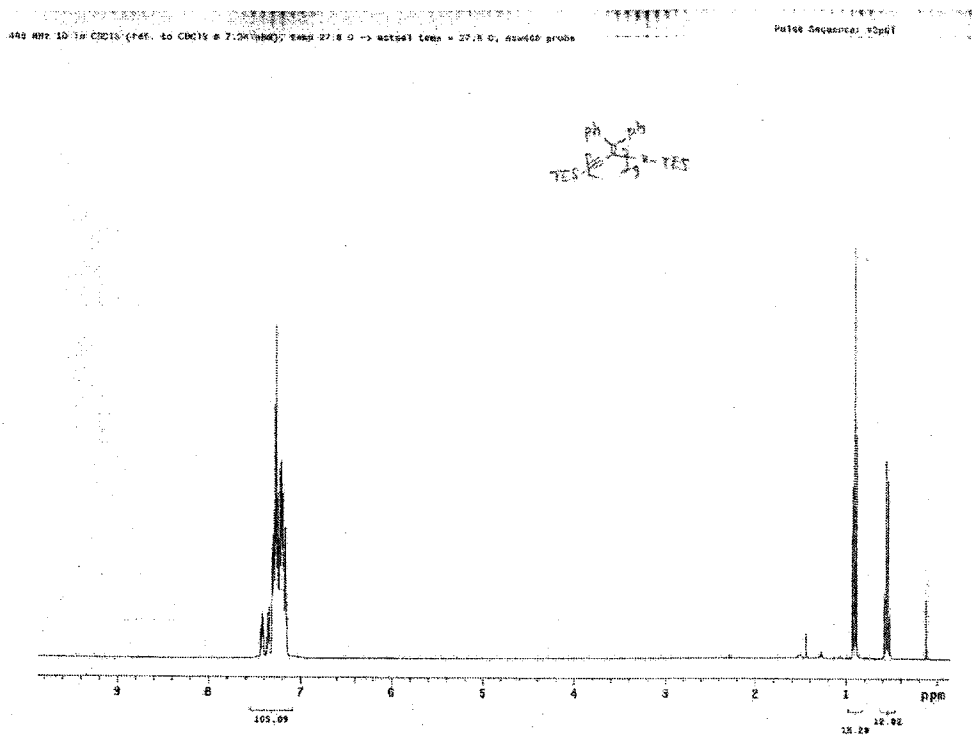
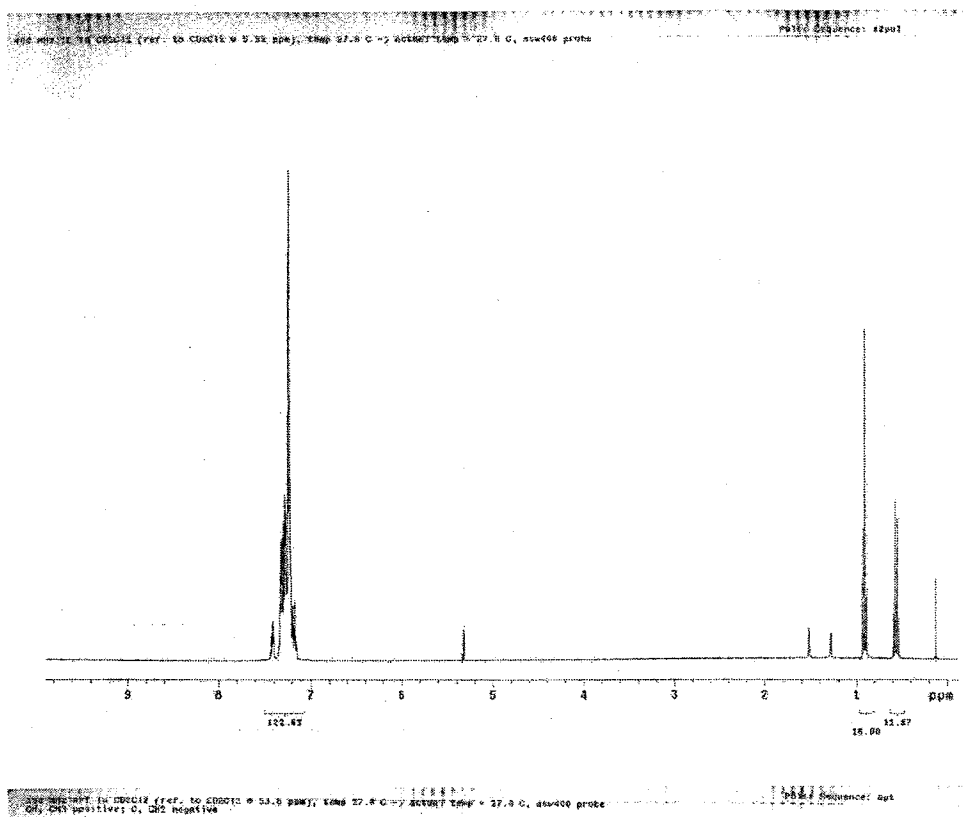
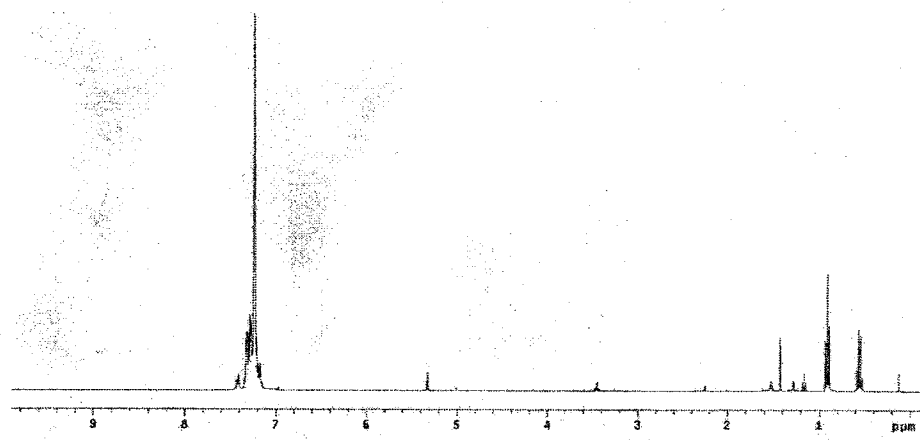


Fig. A-10  $^1\text{H}$  and  $^{13}\text{C}$  NMR spectra of compound 141.



400 MHz  $^1\text{H}$  NMR (ref. to TMS at 0 ppm), temp 27.5 C -> actual temp = 27.0 C, axiess probe Pb-13 Pulse Sequence: zgpg30

Solvent: CDCl<sub>3</sub>  
 Temp: 27.5 C, 300.4 K  
 INOVA-400 400MHz  
 PULSE: zgpg30  
 Pulse: 9.000 sec  
 Pulse: 9.000 sec  
 Acc: 3180.1318 sec  
 Width: 4001.4 Hz  
 16 Scans  
 OBSERVE: M1 400.773000 MHz  
 P1: 9.000000  
 FT size: 151392  
 Total time: 1 min, 39 sec



100 MHz  $^{13}\text{C}$  NMR (ref. to CDCl<sub>3</sub> @ 77.0 ppm), temp 27.0 C -> actual temp = 27.0 C, axiess probe Pulse Sequence: hpt  
 DR: 0.00 positive; 0, 0.02 negative

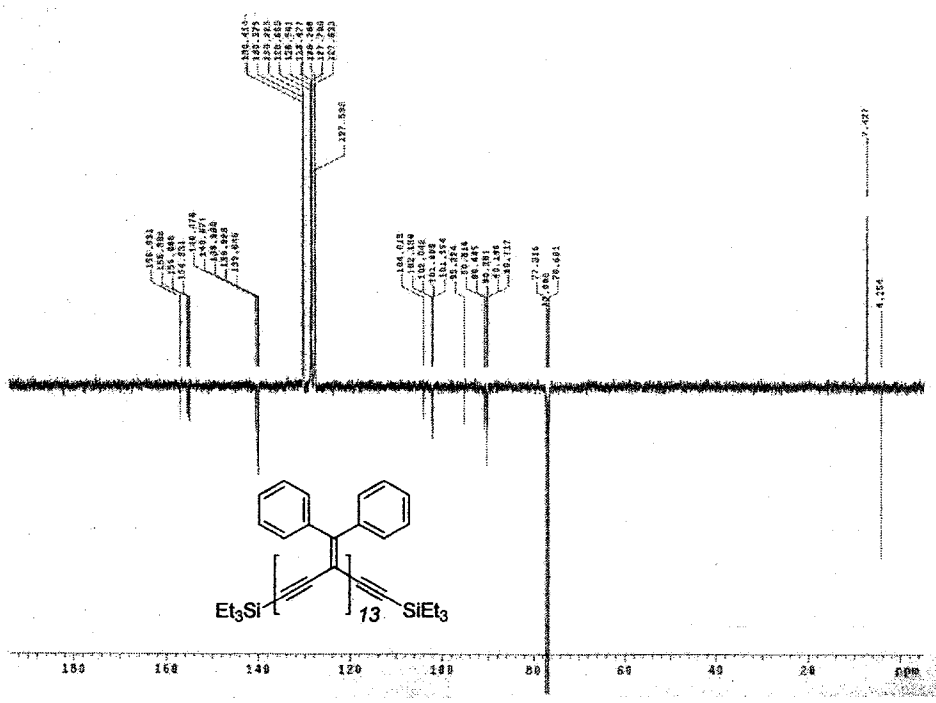


Fig. A-12  $^1\text{H}$  and  $^{13}\text{C}$  NMR spectra of compound 143.



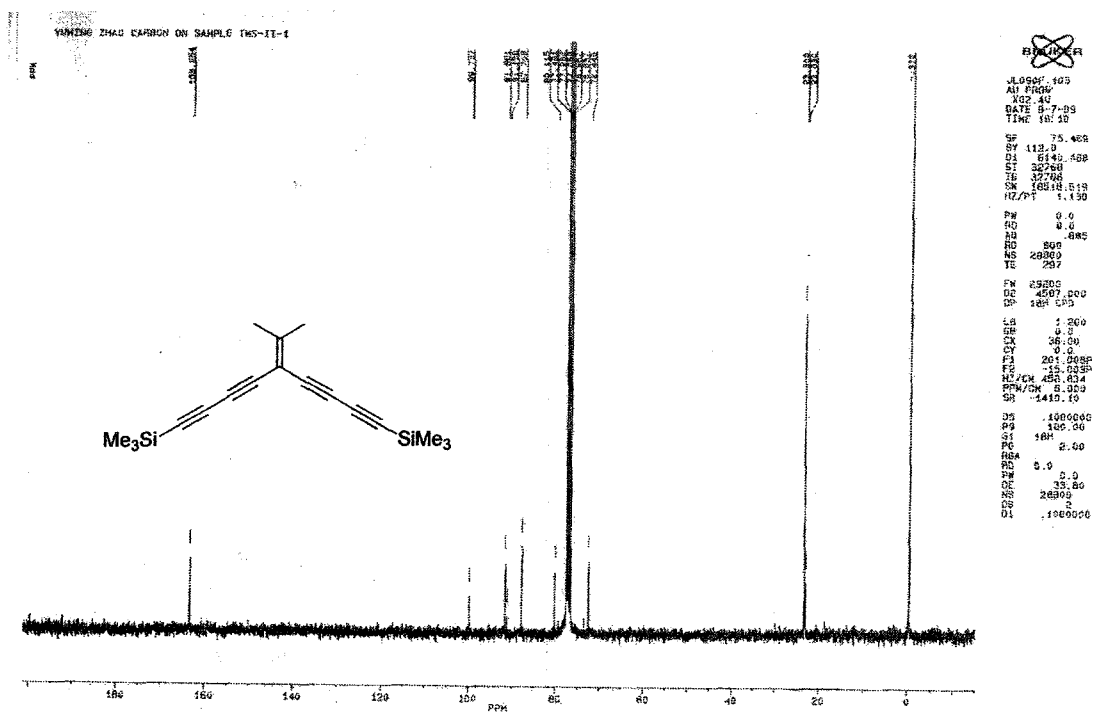
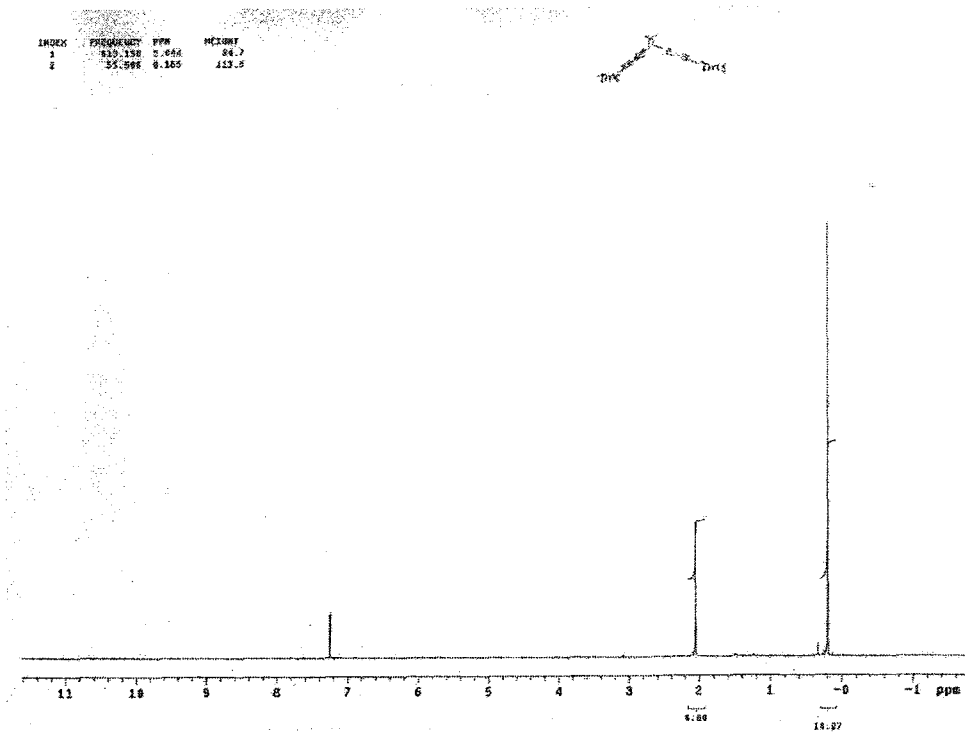
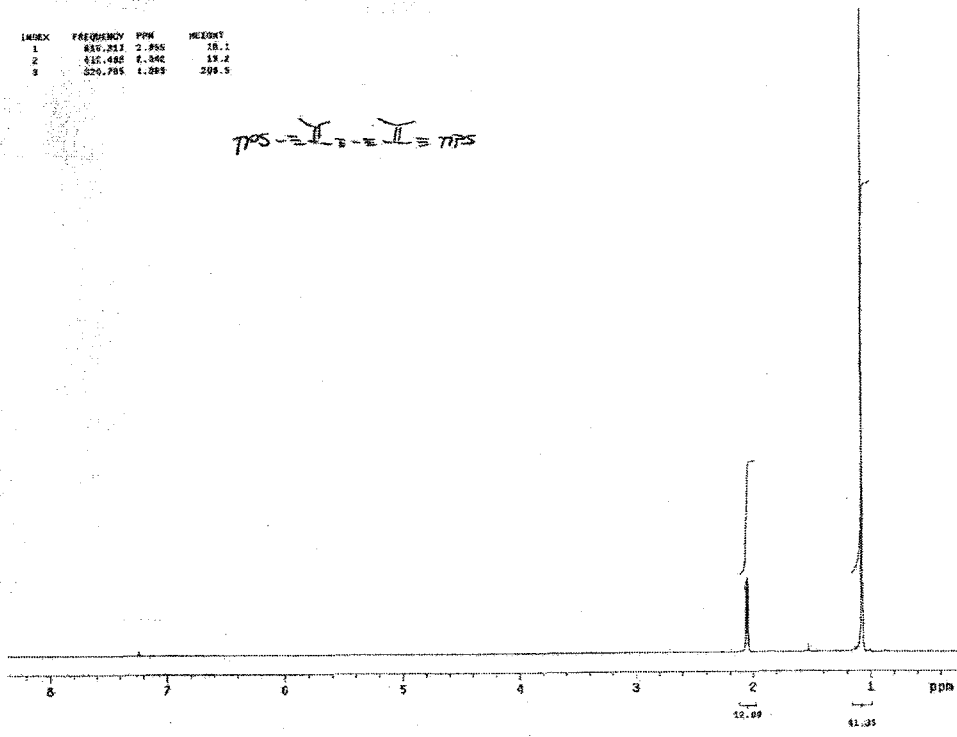
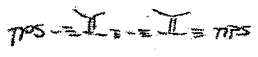


Fig. A-14  $^1\text{H}$  and  $^{13}\text{C}$  NMR spectra of compound 147a.





INDEX	FREQUENCY	PPM	HEIGHT
1	816.813	2.965	18.1
2	816.485	1.866	19.2
3	820.785	1.293	208.5



STANDARD NMR PARAMETERS  
 File: 154.nmr  
 Date: Nov 13 80  
 Time: 10:00  
 Name: 154

NAME	TYPE	VALUE
NUC1	13C	125.00
NUC2	1H	1.00
NUC3	13C	100.62
NUC4	1H	1.00
NUC5	13C	100.62
NUC6	1H	1.00
NUC7	13C	100.62
NUC8	1H	1.00
NUC9	13C	100.62
NUC10	1H	1.00
NUC11	13C	100.62
NUC12	1H	1.00
NUC13	13C	100.62
NUC14	1H	1.00
NUC15	13C	100.62
NUC16	1H	1.00
NUC17	13C	100.62
NUC18	1H	1.00
NUC19	13C	100.62
NUC20	1H	1.00
NUC21	13C	100.62
NUC22	1H	1.00
NUC23	13C	100.62
NUC24	1H	1.00
NUC25	13C	100.62
NUC26	1H	1.00
NUC27	13C	100.62
NUC28	1H	1.00
NUC29	13C	100.62
NUC30	1H	1.00
NUC31	13C	100.62
NUC32	1H	1.00
NUC33	13C	100.62
NUC34	1H	1.00
NUC35	13C	100.62
NUC36	1H	1.00
NUC37	13C	100.62
NUC38	1H	1.00
NUC39	13C	100.62
NUC40	1H	1.00
NUC41	13C	100.62
NUC42	1H	1.00
NUC43	13C	100.62
NUC44	1H	1.00
NUC45	13C	100.62
NUC46	1H	1.00
NUC47	13C	100.62
NUC48	1H	1.00
NUC49	13C	100.62
NUC50	1H	1.00
NUC51	13C	100.62
NUC52	1H	1.00
NUC53	13C	100.62
NUC54	1H	1.00
NUC55	13C	100.62
NUC56	1H	1.00
NUC57	13C	100.62
NUC58	1H	1.00
NUC59	13C	100.62
NUC60	1H	1.00
NUC61	13C	100.62
NUC62	1H	1.00
NUC63	13C	100.62
NUC64	1H	1.00
NUC65	13C	100.62
NUC66	1H	1.00
NUC67	13C	100.62
NUC68	1H	1.00
NUC69	13C	100.62
NUC70	1H	1.00
NUC71	13C	100.62
NUC72	1H	1.00
NUC73	13C	100.62
NUC74	1H	1.00
NUC75	13C	100.62
NUC76	1H	1.00
NUC77	13C	100.62
NUC78	1H	1.00
NUC79	13C	100.62
NUC80	1H	1.00
NUC81	13C	100.62
NUC82	1H	1.00
NUC83	13C	100.62
NUC84	1H	1.00
NUC85	13C	100.62
NUC86	1H	1.00
NUC87	13C	100.62
NUC88	1H	1.00
NUC89	13C	100.62
NUC90	1H	1.00
NUC91	13C	100.62
NUC92	1H	1.00
NUC93	13C	100.62
NUC94	1H	1.00
NUC95	13C	100.62
NUC96	1H	1.00
NUC97	13C	100.62
NUC98	1H	1.00
NUC99	13C	100.62
NUC100	1H	1.00

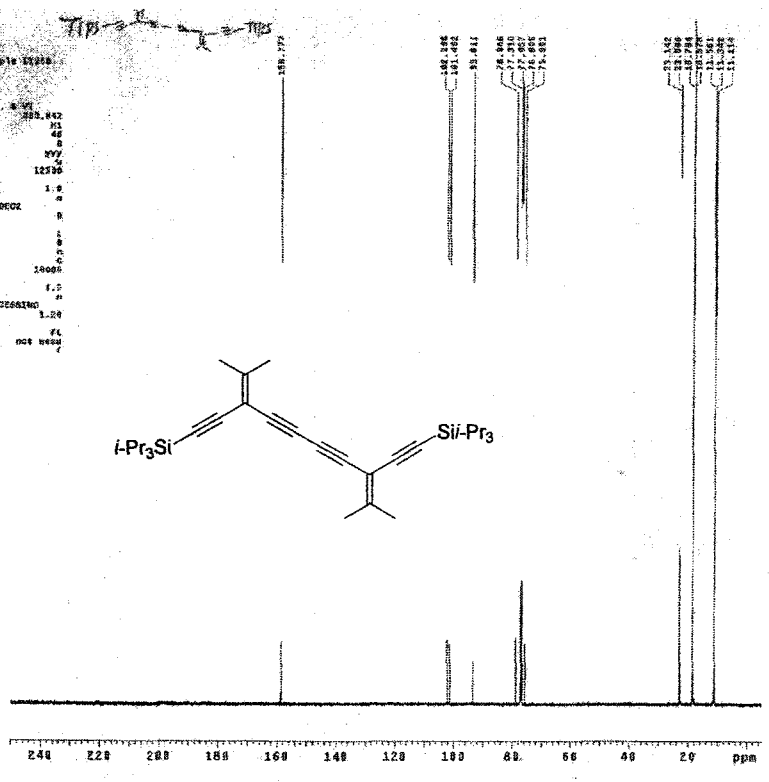


Fig. A-17 <sup>1</sup>H and <sup>13</sup>C NMR spectra of compound 154.

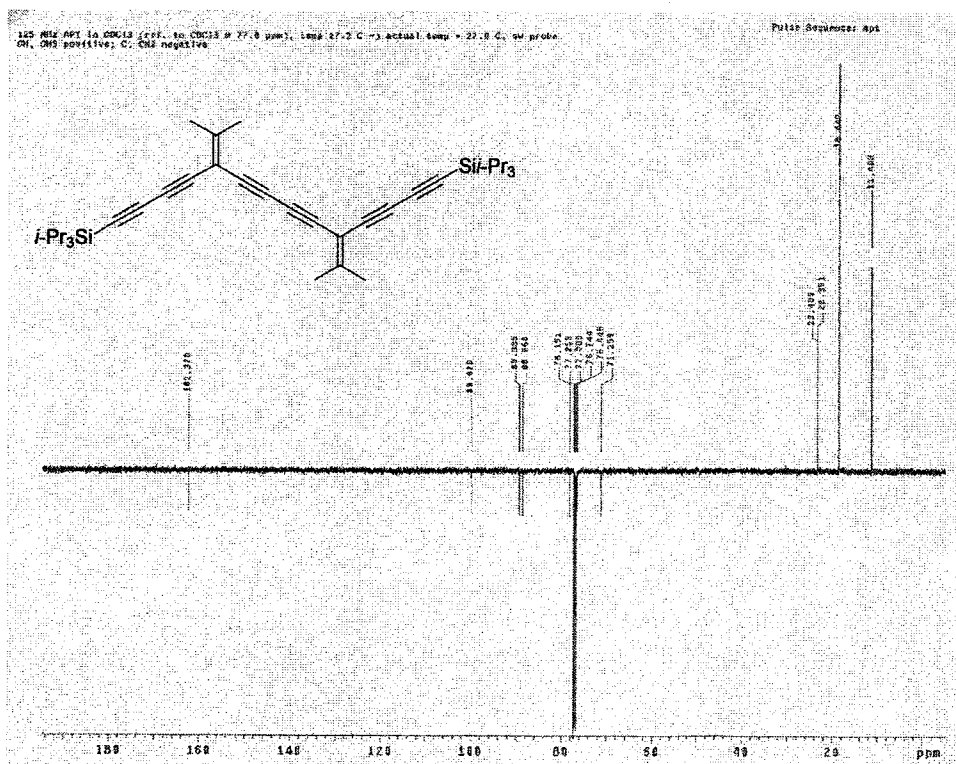
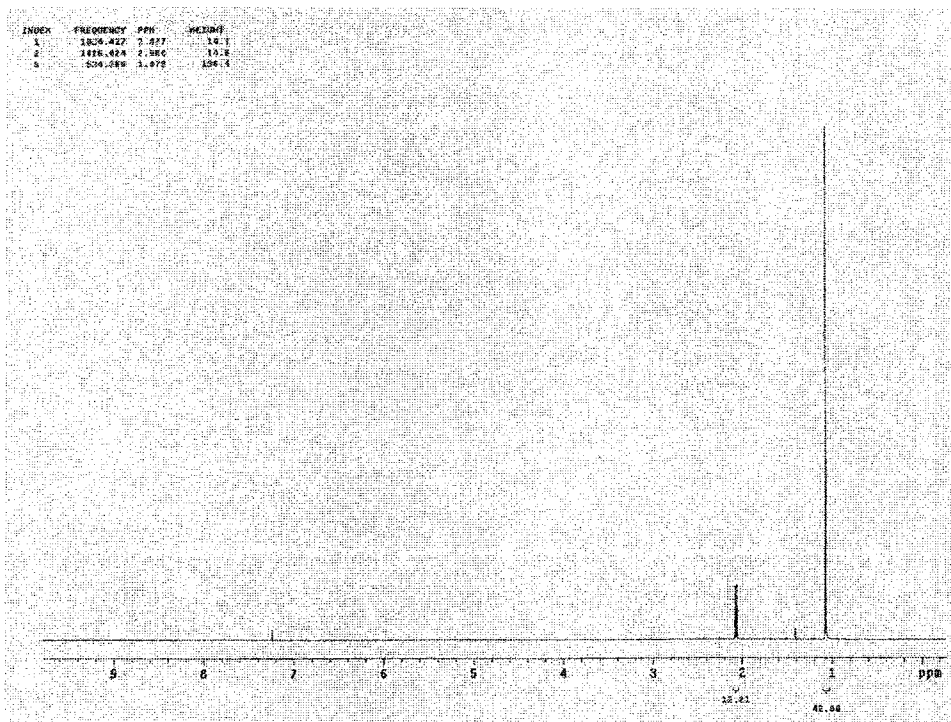
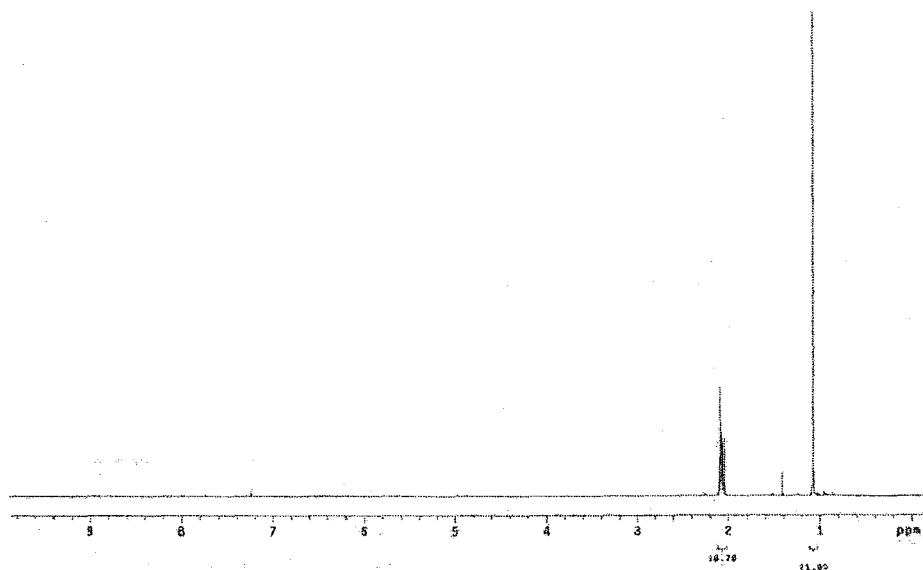


Fig. A-18 <sup>1</sup>H and <sup>13</sup>C NMR spectra of compound 156.

INDEX	FREQUENCY	PPM	HEIGHT
1	304.267	2.086	28.3
2	331.498	2.077	16.4
3	336.859	2.072	15.0
4	323.549	2.080	15.7
5	311.749	2.046	14.8
6	327.160	1.075	120.5



150 MHz APT 13 C NMR (ref. to CDCl3 @ 77.0 ppm), temp 27.8 C -> actual temp = 27.0 C, ezw600 probe  
 CH, CH2 positive; C, CH3 negative

Pulse Sequence: apf

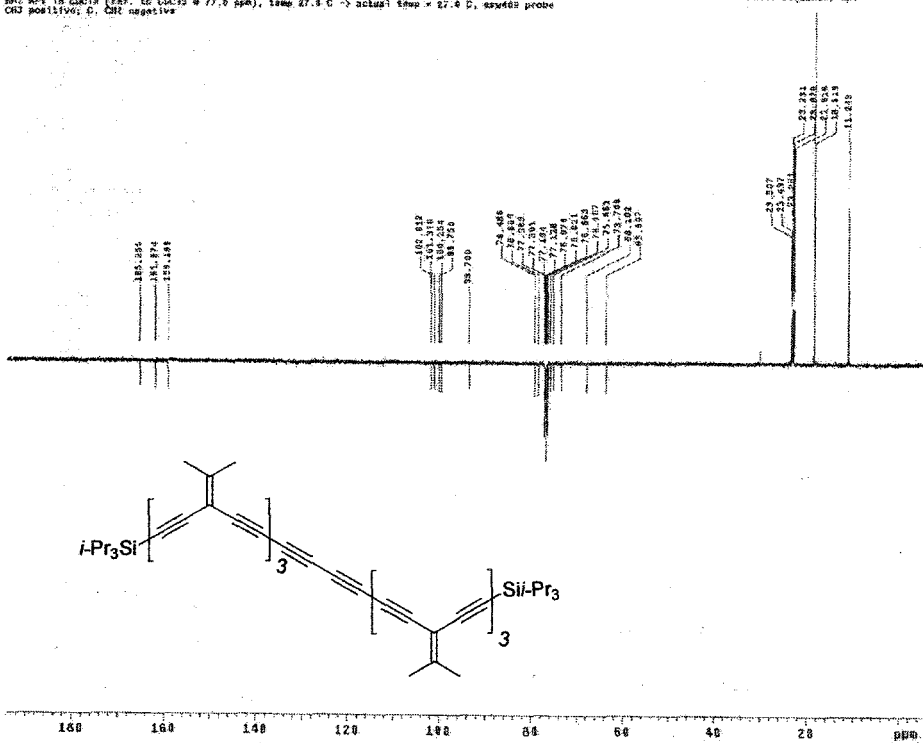
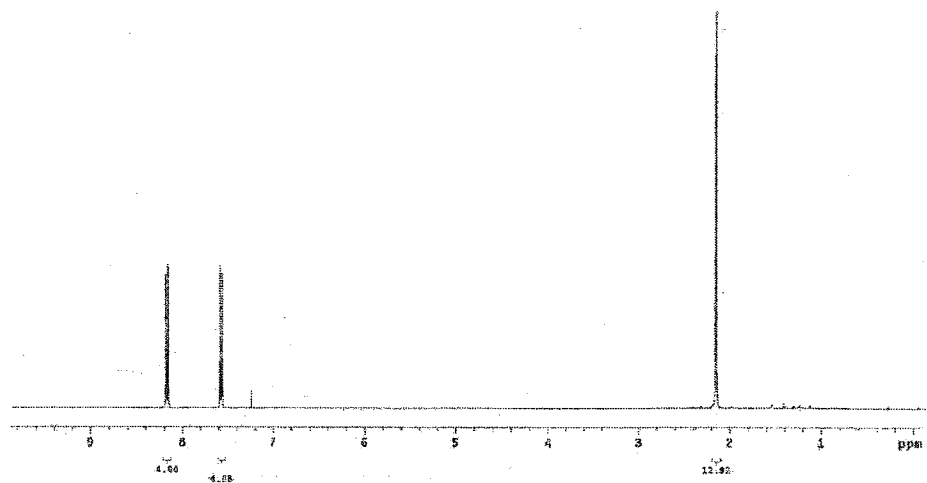


Fig. A-19 <sup>1</sup>H and <sup>13</sup>C NMR spectra of compound 159.



INDEX	FREQUENCY	PPM	HEIGHT
1	3270.418	8.156	84.8
2	3241.594	8.136	37.4
3	2870.852	7.831	85.9
4	3021.655	7.558	35.1
5	855.847	2.349	92.8
6	857.891	2.198	194.2



160 MHz APT in CDCl<sub>3</sub> 1 rev. 50 CDCl<sub>3</sub> @ 77.8 ppm, temp 27.8 C -> detcal temp = 27.8 C, NUS300 probe  
 CH: CH3 positive, C, CH2 negative

Pulse Sequence: aqt

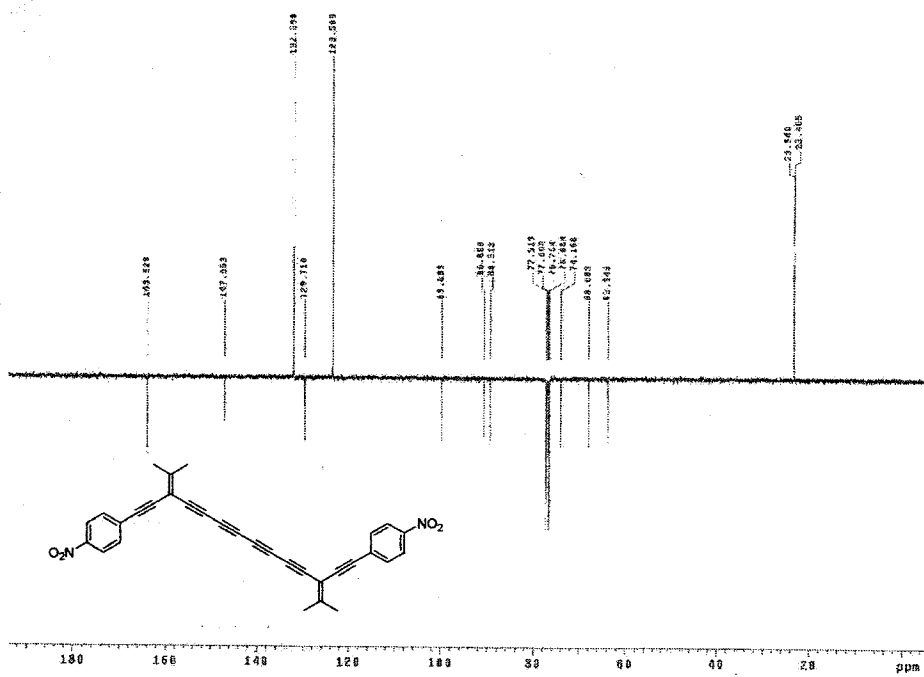
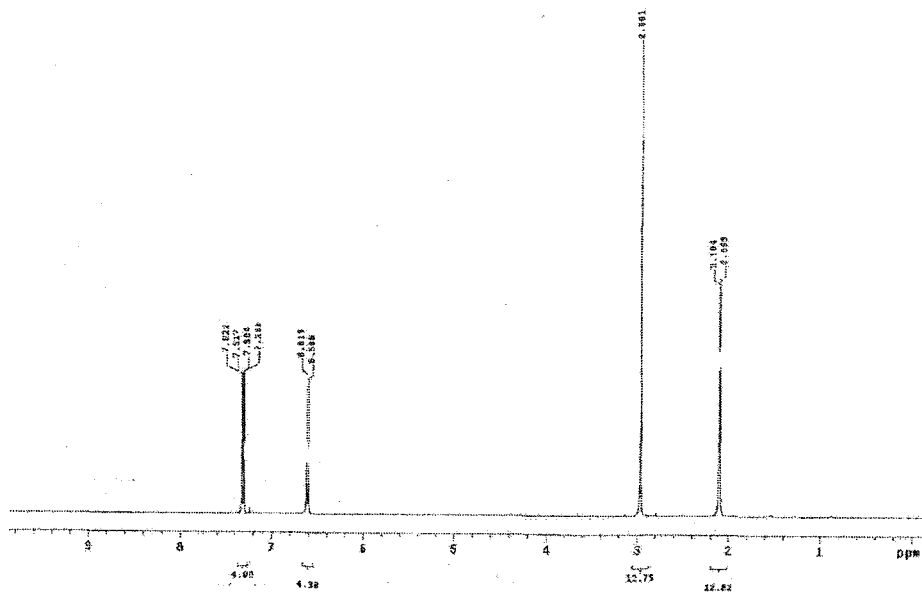


Fig. A-21 <sup>1</sup>H and <sup>13</sup>C NMR spectra of compound 163d.

400 MHz 1D 1H CDCl3 (ref. to CDCl3 @ 7.26 ppm), temp 27.8 C -> AcqIn: 1amp = 27.0 C, acq400 probe

Pulse Sequence: zgpg30



100 MHz 1D 13C CDCl3 (ref. to CDCl3 @ 77.0 ppm), temp 27.8 C -> AcqIn: 1amp = 27.0 C, acq400 probe  
Or: CD3 positive; C, CHC negative

Pulse Sequence: zgpg30

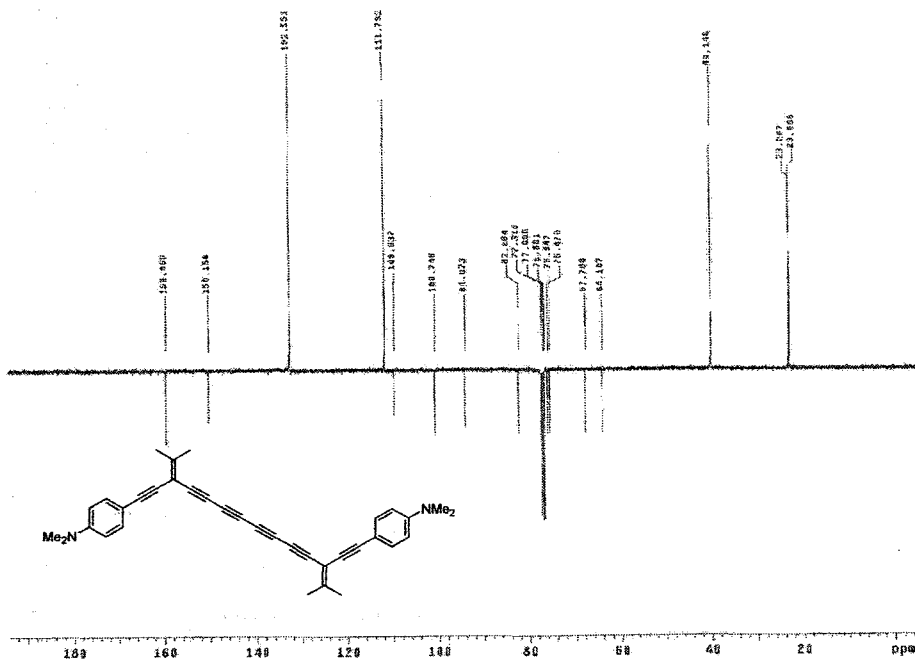


Fig. A-22 <sup>1</sup>H and <sup>13</sup>C NMR spectra of compound 163j.

INDEX	FREQUENCY	PPM	INTEGRATION
1	5605.385	7.202	5.9
2	4220.512	4.428	18.1
3	2245.352	4.424	18.8
4	2531.846	4.420	18.0
5	1092.828	4.285	14.0
6	1001.526	4.189	15.4
7	2092.184	4.186	13.0
8	1837.625	2.083	27.2
9	1652.748	2.070	31.0

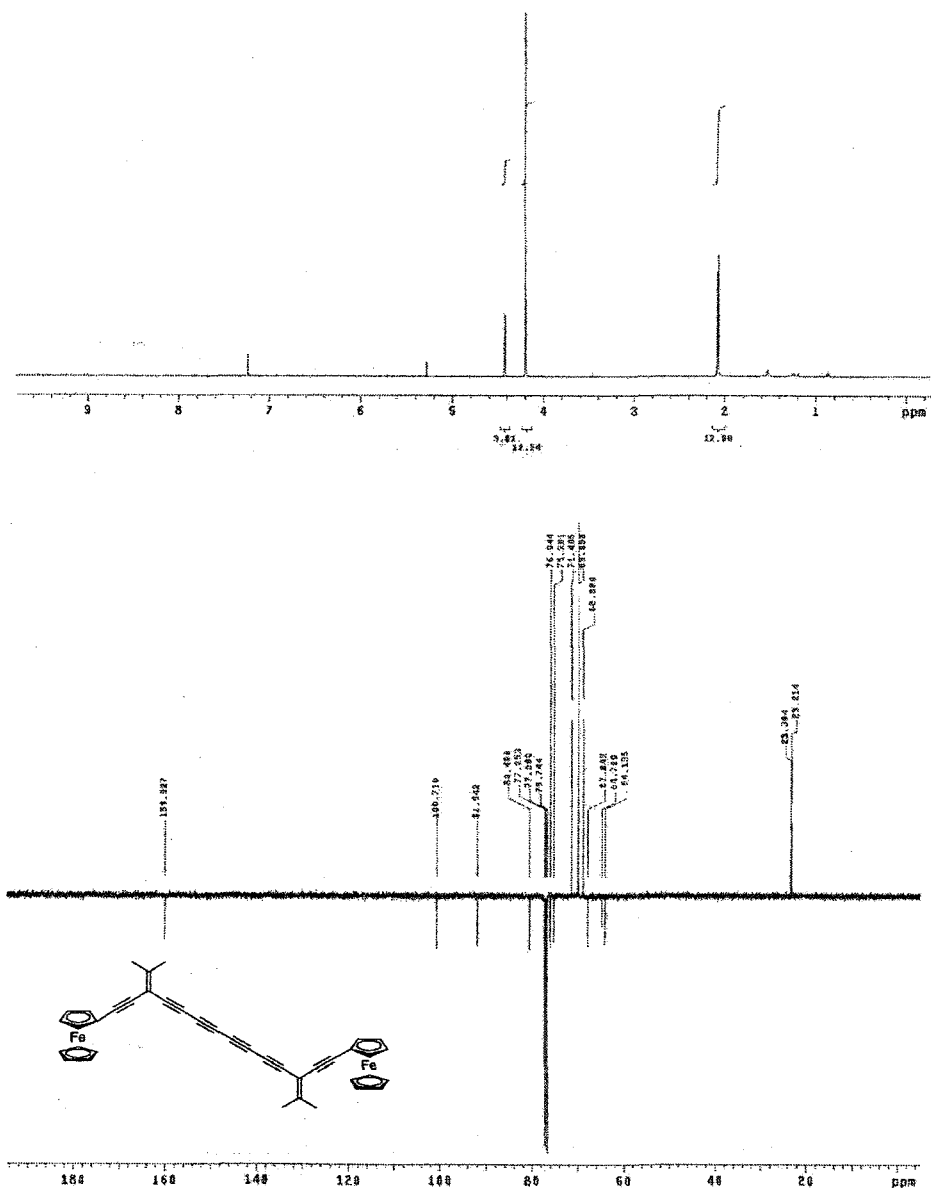


Fig. A-23 <sup>1</sup>H and <sup>13</sup>C NMR spectra of compound 163k.





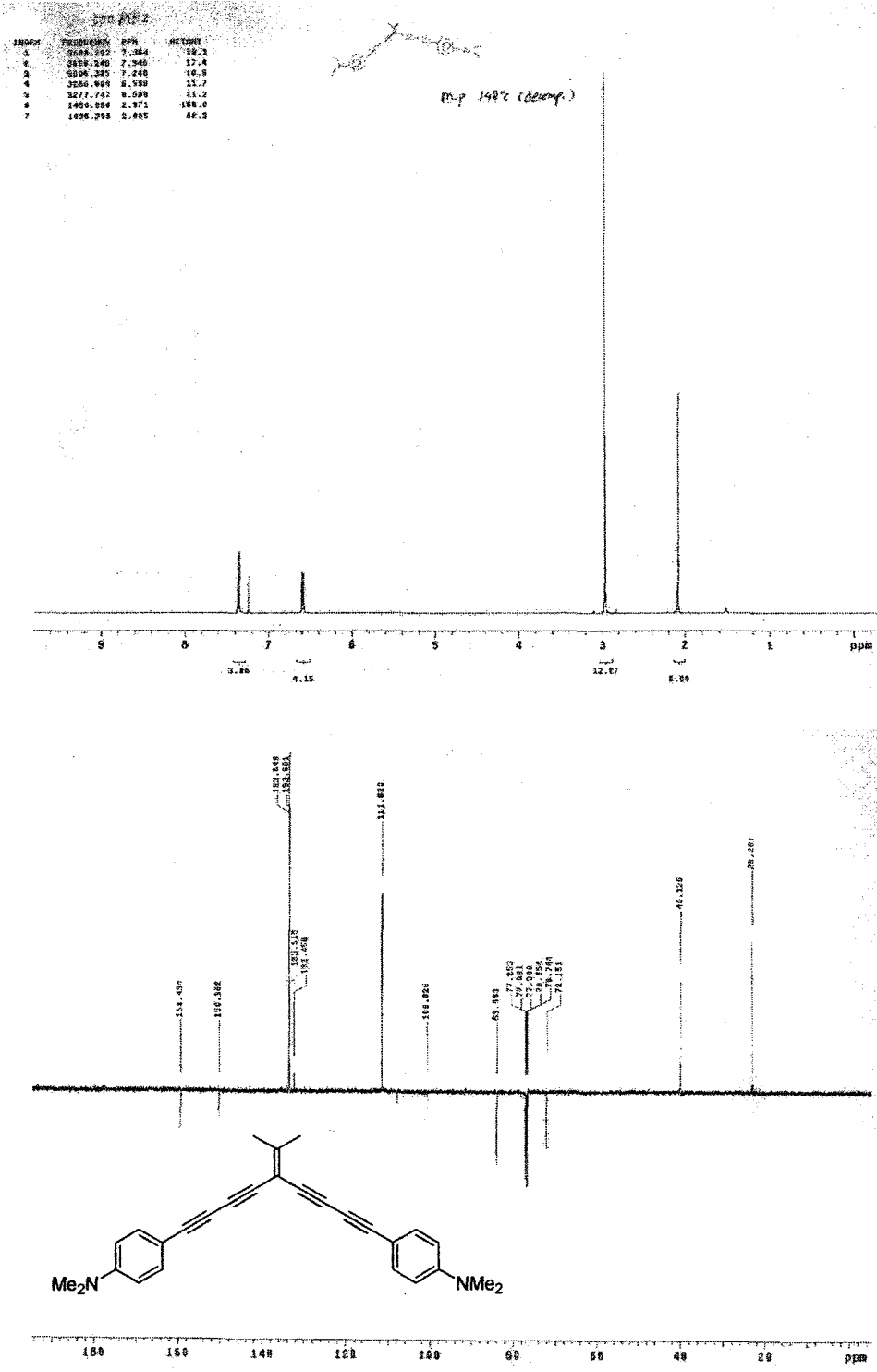
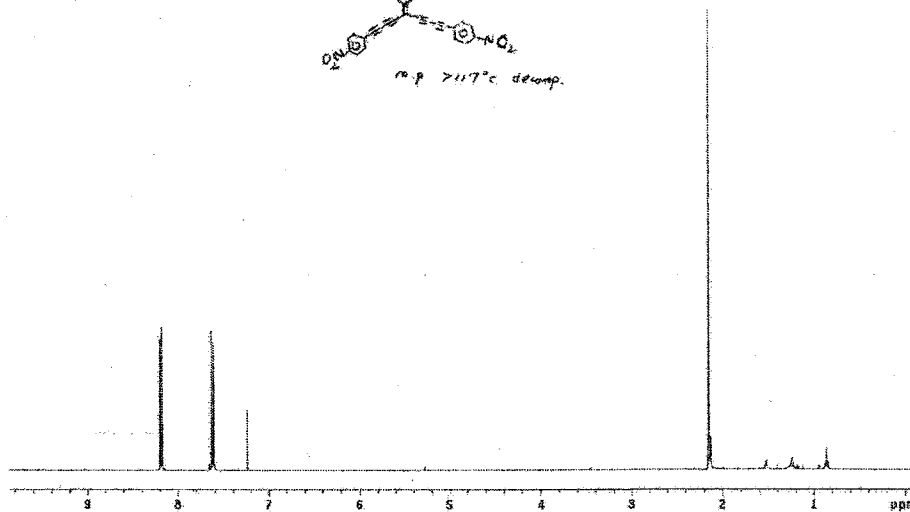


Fig. A-26 <sup>1</sup>H and <sup>13</sup>C NMR spectra of compound 193a.

400 MHz <sup>1</sup>H in CDCl<sub>3</sub> (ref. to CDCl<sub>3</sub> @ 7.24 ppm), temp 27.0 C -> actual temp = 27.0 D, acq400 ppp04

Pulse Sequence: zgpg30

Software: zgpg30  
Temp: 27.0 C / 350.5 K  
INSTR: spect  
PULPROG: zgpg30  
RG: 655.5  
Acq. Time: 1.055 sec  
Width: 4001.8 Hz  
IS: 400 MHz  
DSSNAME: H<sub>2</sub>O  
DETA: 0.000000  
F2: 400.146000  
Total Time: 1 min, 56 sec



100 MHz <sup>13</sup>C NMR in CDCl<sub>3</sub> (ref. to DMSO-d<sub>6</sub> @ 77.0 ppm), temp 27.0 C -> actual temp = 27.0 D, acq100 probe  
CH, CH2 positive; C, CH2 negative

Pulse Sequence: zgpg30

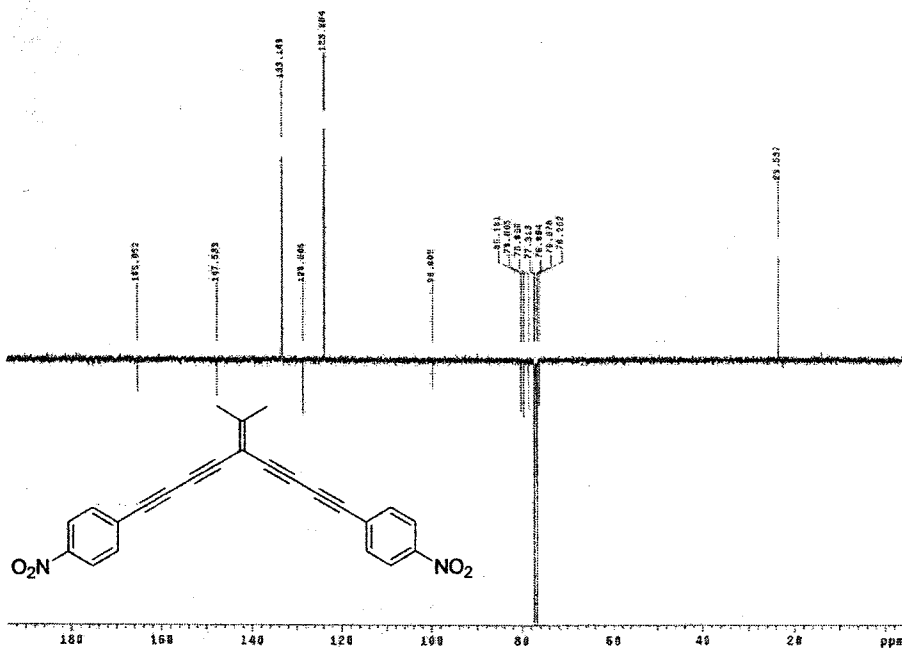


Fig. A-27 <sup>1</sup>H and <sup>13</sup>C NMR spectra of compound 193b.

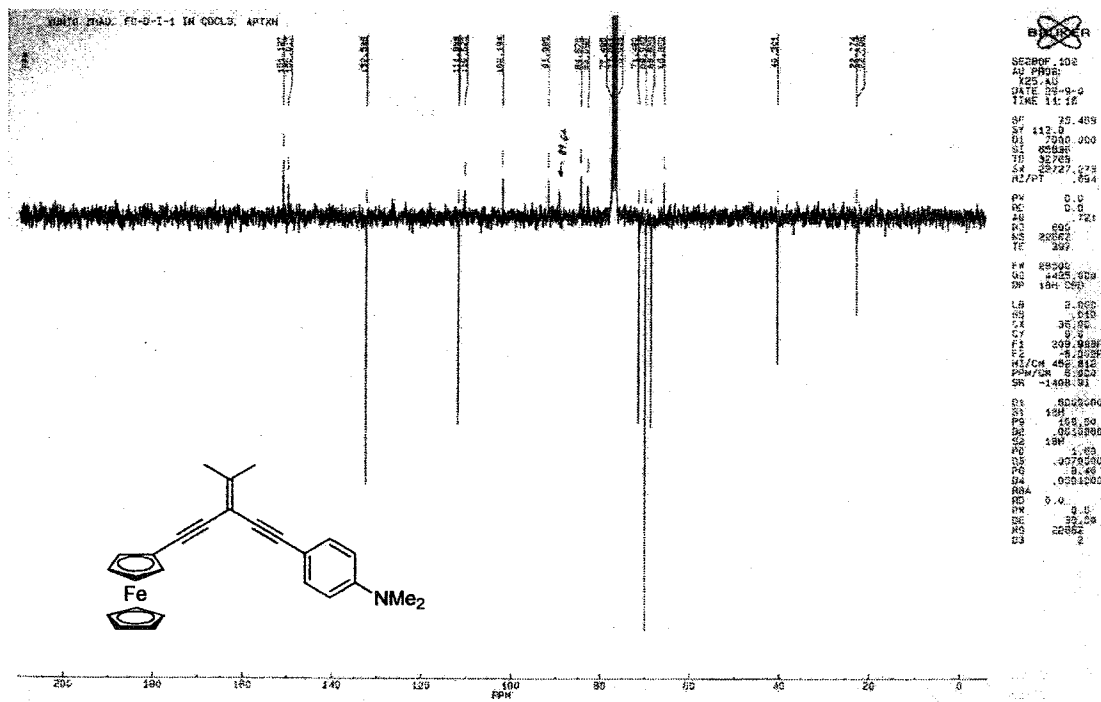
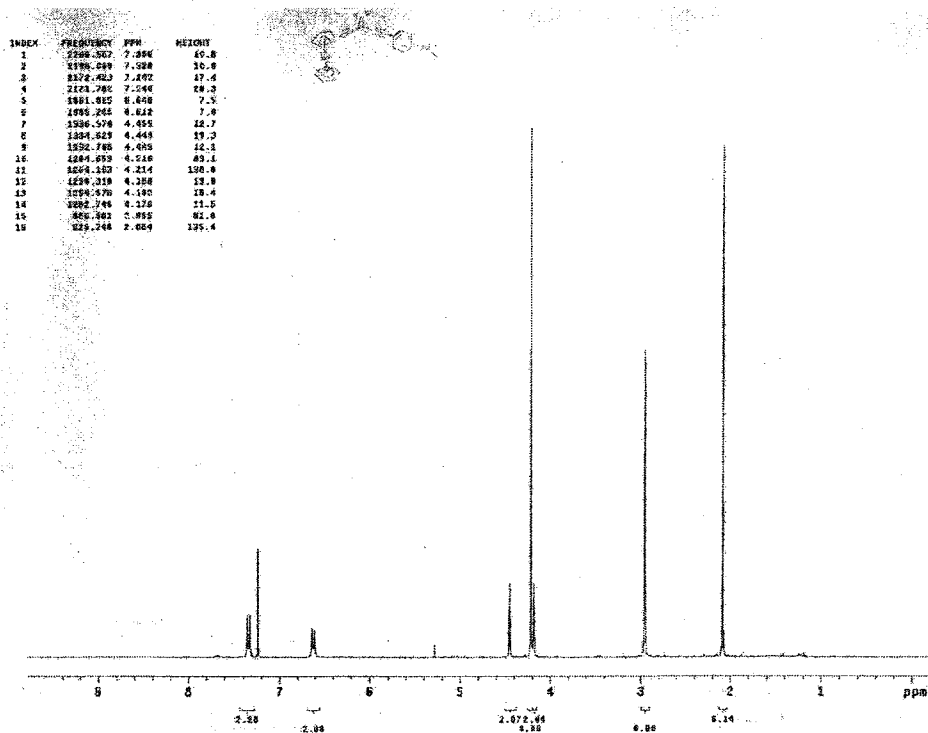


Fig. A-28  $^1\text{H}$  and  $^{13}\text{C}$  NMR spectra of compound 197a.



